Bioactive constituents from the Ghanaian medicinal plant *Chlorophora regia* and its root endophytic fungus JK10

A THESIS SUBMITTED IN FULFILLMENT OF THE REQUIREMENTS FOR THE DEGREE OF

DOCTOR OF PHILOSOPHY

in the

Department of Pharmaceutical Chemistry,

Faculty of Pharmacy and Pharmaceutical Sciences

College of Health Sciences

by

JAMES OPPONG KYEKYEKU

KWAME NKRUMAH UNIVERSITY OF SCIENCE AND TECHNOLOGY, KUMASI

AUGUST, 2016

DECLARATION

I wish to declare that this thesis is my own work. To the best of my knowledge, this work does not contain any material previously accepted for the award of any other degree of a University.

KNUST

…… …….

James Oppong Kyekyeku Date

……. …….

Prof. Reimmel Adosraku Date

(Supervisor)

……. …….

Dr. Isaac Ayensu Date

(Head of Department)

NYANSAPƆ WƆ SANE NO BADWENMA

ABSTRACT

The extracts of the Ghanaian medicinal plant *Chlorophora regia* A. Chev (Moraceae) has been used for the treatment of various ailments in traditional medicine including burns, wounds, snake bite, wasp bite. A search through the literature, however, revealed there were no available data on the phytochemical composition of the plant. Therefore, the main objective of this study was to isolate, characterize and evaluate some biological activities of secondary metabolites from the stem bark of the plant and further investigate the endophytic community harbored in the inner tissues of the plant. Extensive phytochemical investigation of the stem bark resulted in the isolation and characterization of four new metabolites, regiafuran A–C and 6–prenylated–3,5,7,4′–tetrahydroxy–2′–methoxyflavonol in addition to fifteen known compounds. The isolated compounds were tested for their free radical scavenging activities. Regiafuran A–B, mulberrofuran Y, kuwanol E and 5,7,4′–trihydroxy– 2′–methoxyflavanone demonstrated significant free radical scavenging activities with IC_{50} values of 1.9 µg/ml, 2.4 µg/ml, 2.2 µg/ml, 2.1 µg/ml and 1.8 µg/ml respectively. An unidentified endophytic fungus, JK10, was isolated from the root of *C. regia*. Twelve compounds including seven new 7–desmethyl derivatives of fusarin C and five known compounds were isolated from the endophytic fungus, JK10. The planar and relative configurations of the new compounds were elucidated by combined spectroscopic analyses of their UV, IR, HRESI–MS^n, ECD and NMR data. The absolute configuration of solaniol was established for the first time by X–ray diffraction analysis of a single crystal. The antibacterial activities of the isolated compounds were evaluated. 7–desmethyl fusarin C–22/23 and 7– desmethyl fusarin C–25 exhibited remarkable activity at concentrations of 10.0 μg/mL against the soil bacterium *Acinetobacter* sp. BD4 comparable to the reference standard streptomycin. All the tested compounds demonstrated activity against the environmental strain of *E. coli*. Based on the results it could be proposed that the endophytic

fungus, whose origin is from the roots, contributes a chemical–mediated defensive mechanism to the host plant against invading specific soil and environmental bacterial pathogens. This may confirm the existence of a unique cost–benefit endophyte–plant association. The spatial distribution of three kaurane diterpenes, xylopic acid, ent–kaur–16–en–19–oic acid and 15–oxo–ent–kaur–16–en–19–oic acid, in the fruits of *Xylopia aethiopica* (Dunal) A. Rich (Annonaceae) were visualized by MALDI–HRMS imaging techniques. The distribution of the compounds was predominantly

in the pericarp region of the fruit with non-detectable levels in the seed.

KNUST

DEDICATION

Dedicated to my wife Mrs. Joycelyn Oppong Kyekyeku and my sons Kojo Kwarteng Oppong–Kyekyeku and Nana Kwaku Oppong–Kyekyeku

KNUST



ACKNOWLEDGEMENT

''I will extol the LORD at all times; His praise will always be on my lips'' Ps. 34:1 Indeed the race is not to the swift nor the battle to the strong but time and season happen to them all. I am most grateful to the Almighty God for life, grace and strength in successfully completing this programme.

I am eternally grateful to my wife who had to endure so much taking care of our children in my absence.

I am grateful to **Prof. R. K. Adosraku** for his timely counsel and encouragement. I could not have come this far but for his mentorship and immense assistance. My profound gratitude goes to **Prof. Dr. Dr. h.c. Michael Spiteller** for granting me the rare opportunity in using state-of-the-art equipment for my work at INFU, TU-Dortmund and for his valuable supervision, support and critical reviews of my PhD research. My sincere appreciation goes to **Prof. Abraham Yeboah Mensah** for his invaluable assistance and timely motivation. I am also grateful to my co-workers at INFU especially **Dr. Souvik Kusari**, **Dr. Ferdinand Talontsi** (formerly of INFU), **Dr. Sebastian** , **Dr. Remy Teponno** (formerly of INFU) and **Dr. Li Gang** (formerly of INFU) for priceless discussions and suggestions, **Anke Bullach**, **Dennis Ecklemann** and **Selahaddin Sezgin** for LC-MS and MALDI measurements. I acknowledge **Prof. Dr. Carsten Strohmann** and **Mr. Christopher Golz** for the X-ray diffraction measurement. And to my project mate **Evelyn Afua Mireku** I say a very special thank you. I appreciate the wonderful contributions of **Dr. Samuel Asare-Nkansah**, **Dr. Isaac Ayensu** (Head of Department) and **Dr. Samuel Oppong-Bekoe** during my PhD programme. I would like to acknowledge the immense assistance of **Mr. Clifford Kofi Asare**, a herbalist and **Dr. Kwasi Boadu Mensah** with the collection of the plant samples for this research project.

Special mention is made of German Academic Exchange Services (DAAD) for funding my project and my stay in TU–Dortmund, Germany for a period of two years under the Sandwich-

model programme. I am again grateful to Kwame Nkrumah University of Science and Technology (KNUST) for granting me the permission and study leave throughout my stay in Germany.

KNUST



KNUST

TABLE OF CONTENT

DECLARATION ..... **i**
ABSTRACT ..... **ii**
ACKNOWLEDGEMENT ..... **iv**
TABLE OF CONTENT ..... **vii**
LIST OF TABLES ..... **xi**
LIST OF FIGURES ..... **xiii**
LIST OF ABBREVIATIONS ..... **xx**
CHAPTER 1: INTRODUCTION **1**
1.1 General introduction 1
1.2 Background of study 1
1.2.1 *Chlorophora regia* 1
1.2.2 *Xylopia aethiopica* 3
1.3 Problem statement 4
1.4 Justification 4
1.5 Aims and objectives 5
CHAPTER 2: LITERATURE REVIEW **7**
2.1 Bioactive secondary metabolites from natural sources as drugs 7
2.2 Natural products from endophytic micro-organisms 12
2.2.1 Endophytic fungal products as antibiotics 12

2.2.2 Endophytic fungal and bacterial products as anticancer 13
2.3 Free radicals and natural antioxidants 15
2.3.1 Measurement of antioxidant activity 16
2.4 Inflammation 17
2.4.1 Anti–inflammatory agents 17
2.3 Imaging mass spectroscopy of natural products in space 18
CHAPTER 3: MATERIALS AND METHODS 20
3.1 Materials 20
3.1.1 Media for cultivation 20
3.1.2 Bacteria used for antibacterial assay 21
3.1.3 Chemicals 21
3.1.4 Plant collection, authentication and preparation 21
3.2 Methodology 23
3.2.1 Extraction of plant materials 23
3.2.1.1 Extraction and isolation of constituents from *Chlorophora regia* 23
3.2.1.2 Extraction and isolation of xylopic acid from *Xylopia aethiopica* 24
3.2.1.3 Fruit extraction of *X. aethiopica* for HPLC–HRESI–MS^n 25
3.2.2 Isolation, cultivation and storage of endophytic fungi from *C. regia* 25
3.2.3 Pre–screening, selection and large–scale fermentation 26
3.2.4 Fungal extraction, isolation and purification of secondary metabolites 27
3.2.5 General experimental procedures 28
3.2.5.1 NMR 28
3.2.5.2 Chromatography 29
3.2.5.3 HPLC 29
3.2.5.4 LC–$HRMS^n$ 29
3.2.5.5 X–ray diffraction analysis 30
3.2.5.6 MALDI–HRMS imaging of kaurane diterpenes in the fruits of *X. aethiopica* 30
3.2.5.7 Other methods 31
3.2.6 Bioassay 31
3.2.6.1 DPPH free radical scavenging assay of metabolites isolated from *C. regia* 31
3.2.6.2 Anti–inflammatory assay 32
3.2.6.3 Antibacterial assay of metabolites isolated from the endophytic fungus 33

CHAPTER 4: RESULTS AND DISCUSSION 4.1 Isolation and characterization of secondary metabolites from the stem bark of **33**
Chlorophora regia 33
4.1.1 Structure elucidation of Regiafuran A (**1**, new compound) 35
4.1.2 Structure elucidation of Regiafuran B (**2**, new compound) 39
4.1.3 Structure elucidation of Regiafuran C (**3**, new compound) 42
4.1.4 Structure elucidation of mulberrofuran Y (**4**, known compound) 45
4.1.5 Structure elucidation of moracin N (**5**, known compound) 49
4.1.6 Structure elucidation of moracin O (**6**, known compound) 51
4.1.7 Structure elucidation of sanggenon C (**7**, known compound) 54
4.1.8 Structure elucidation of kuwanol E (**8**, known compound) 58
4.1.9 Structure elucidation of chalcomoracin (**9**, known compound) 62
4.1.10 Structure elucidation of chlorophorin (**10**, known compound) 65
4.1.11 Structure elucidation of isochlorophorin (**11**, known compound) 67
4.1.12 Structure elucidation of 6–prenylated–3,7,5,4′–tetrahydroxy–2′–methoxyflavonol (**12**, new compound) 70
4.1.12.1 Proposed biosynthesis of compound **12** 73
4.1.13 Structure elucidation of gancaonin P (**13**, known compound) 74
4.1.14 Structure elucidation of 3,7,5,4′–tetrahydroxy–2′–methoxyflavonol (**14**, known compound) 77
4.1.15 Structure elucidation of quercetin (**15**, known compound) 79
4.1.16 Structure elucidation of kaempferol (**16**, known compound) 81
4.1.17 Structure elucidation of 5,7,4′–trihydroxy–2′–methoxyflavanone (**17**, known compound) 83
4.1.18 Structure elucidation of 5,7,3′,5′–tetrahydroxyflavanone (**18**, known compound) 85
4.1.19 Structure elucidation of naringenin (**19**, known compound) 87
4.2 Secondary metabolites isolated and characterized from the endophytic fungus JK10 .. 89
4.2.1 Structure elucidation of 7–desmethyl fusarin C–**20**/**21** (new compounds) 90
4.2.2 Structure elucidation of 7–desmethyl fusarin C–**22**/**23** (new compounds) 94
4.2.3 Structure elucidation of 7–desmethyl fusarin C–**24** (new compound) 98
4.2.4 Structure elucidation of 7–desmethyl fusarin C–**25** (new compound) 101
4.2.5 Structure elucidation of 7–desmethyl fusarin C–**26** (new compound) 105
4.2.6 Structure elucidation of NG–391/NG–393 (**27**/**28**, known compounds) 108
4.2.7 Structure elucidation of (+)–(S)–Solaniol (**29**, known compound) 111

4.2.8 Structure elucidation of 2,3–dihydro–5–hydroxy–8–methoxy–2,4–dimethylnaphtho[1,2–b]furan–6,9–dione (**30**, known compound)..... 114

4.2.9 Structure elucidation of N_b–acetyltryptamine (**31**, known compound)..... 116

4.3 Imaging and Characterization studies on the fruits of *X. aethiopica*4.3.1 MALDI–HRMS imaging and HPLC–HRESI–MS^n characterization of kaurane 118

diterpenoids (**32**–**34**) in the fruits of *Xylopia aethiopica* (Dunal) A. Rich (Annonaceae)..... 118

4.3.1.1 MALDI–HRMS imaging of compounds **32**–**34** 119

4.3.2 HPLC–HRESI–MS^n characterization of compounds **32**–**34** 121

4.4 Biological activities..... 123

4.4.1 DPPH free radical scavenging assay 123

4.4.2 Anti–inflammatory assay..... 124

4.4.3 Antibacterial assay and possible ecological role of endophytic fungus JK10..... 125

CHAPTER 5: CONCLUSIONS AND RECOMMENDATIONS..... 127

5.1 CONCLUSIONS **..... 127**

5.2 RECOMMENDATIONS**..... 129**

REFERENCES..... 130

APPENDICES..... 142

KNUST

LIST OF TABLES

Table 2.1: Drugs and derivatives from natural products, natural sources and medicinal indication(s)……10

Table 2.2: Bioactive compounds from endophytic microorganisms, natural sources and medicinal indication(s)……14

Table 3.1: Selected plants for the study……..22

Table 4.1: NMR spectral data for Compound **1** in CD_3OD……...39

Table 4.2: NMR spectral data for Compound **2** in CD_3OD……...42

Table 4.3: NMR spectral data for Compound **3** in CD_3OD……...45

Table 4.4: NMR spectral data for compound **4** in CD_3OD……49

Table 4.5: NMR spectral data for Compound **5** in CD_3OD……...52

Table 4.6: NMR spectral data for Compound **6** in CD_3OD……...55

Table 4.7: NMR spectral data for Compound **7** in CD_3OD……...58

Table 4.8: NMR spectral data for Compound **8** in CD_3OD……...62

Table 4.9: NMR spectral data for Compound **9** in CD_3OD (at 500 MHz)…….66

Table 4.10: NMR spectral data for Compound **10** in CD_3OD……...68

Table 4.11: NMR spectral data for Compound **11** in CD_3OD……...71

Table 4.12: NMR spectral data for Compound **12** in CD_3OD……...74

Table 4.13: NMR spectral data for Compound **13** in CD_3OD……...78

Table 4.14: NMR spectral data for Compound **14** in DMSO-d_6……80
Table 4.15: NMR spectral data for Compound **15** in CD_3OD…… ……83

Table 4.16: NMR spectral data for Compound **16** in CD_3OD……..84

Table 4.17: NMR spectral data for Compound **17** in CD_3OD……..86

Table 4.18: NMR spectral data for Compound **18** in CD_3OD……..88

Table 4.19: NMR spectral data for Compound **19** in CD_3OD……..90

Table 4.20: NMR spectral data for Compounds **20**/**21** in CD_3OD……95

Table 4.21: NMR spectral data for Compounds **22**/**23** in CD_3OD……99

Table 4.22: NMR spectral data for Compounds **24** in CD_3OD……102

Table 4.23: NMR spectral data for compound **25** in $CDCl_3$……..106

Table 4.24: NMR spectral data for compound **26** in $CDCl_3$……..109

Table 4.25: NMR spectral data for Compounds **27**/**28** in CD_3OD…….....112

Table 4.26: NMR spectral data for compound **29** in $CDCl_3$……..115

Table 4.27: NMR spectral data for compound **30** in $CDCl_3$……..118

Table 4.28: NMR spectral data for compound **31** in $CDCl_3$……..120

Table 4.29: Free radical scavenging effects of tested compounds……127

Table 4.30: Minimum inhibitory concentrations (MIC) of compounds **20□28** and the crude extract (**CrE**) against Gram–positive and Gram–negative bacteria compared to standard references (streptomycin and gentamicin)……..129

LIST OF FIGURES

Figure 1.2: Representative structures of compounds isolated from the genus *Chlorophora*…3

Figure 2.1: Chemical structures of representative drugs and derivatives from natural sources……...11

Figure 2.2: Structures of representative bioactive natural products from endophytes……15

Figure 2.3: Schematic representation of MALDI–HRMS imaging process……19

Figure 3.1: Two Ghanaian medicinal plants……23

Figure 3.2: Schematic diagram of isolation of secondary metabolites from the stem bark of *C. regia*……..25

Figure 3.3: The isolation of the endophytic fungus JK10……...27

Figure 3.4: Schematic diagram of isolation of secondary metabolites from the endophytic fungus JK10…….29

Figure 4.1: Chemical structures of 2-arylbenzofuran derivatives from *C. regia*……35

Figure 4.2: Chemical structures of Diels-Alder adducts from *C. regia*……..…35

Figure 4.3: Chemical structures of stilbene derivatives from *C. regia*……...36

Figure 4.4: Chemical structures of flavonoids from *C. regia*…….36

Figure 4.5: Chemical structure of compound **1**……...37

Figure 4.6: Selected HMBC and COSY correlations of compound **1**…….39

Figure 4.7: Proposed collision–induced mass spectral fragmentation pattern of compound **1** in

positive ESI mode……40

KNUST

Figure 4.
8: Chemical structure of compound **2**……..40

Figure 4.9: Selected HMBC and COSY correlations of compound **2**……42

Figure 4.10: Proposed collision–induced mass spectral fragmentation pattern of compound **2** in positive ESI mode……43

Figure 4.11: Chemical structure of compound **3**……43

Figure 4.12: Selected HMBC and COSY correlations of compound **3**……...46

Figure 4.13: Proposed collision–induced mass spectral fragmentation pattern of compound **3** in positive ESI mode……46

Figure 4.14: Chemical structure of compound **4**……47

Figure 4.15: Selected HMBC and COSY correlations of compound **4**……...50

Figure 4.16: Proposed collision–induced mass spectral fragmentation pattern of compound **4** in positive ESI mode……50

Figure 4.17: Chemical structure of compound **5**……51

Figure 4.18: Selected HMBC and COSY correlations of compound **5**……..52

Figure 4.19: Proposed collision–induced mass spectral fragmentation pattern of compound **5** in positive ESI mode……53

Figure 4.20: Chemical structure of compound **6**……53

Figure 4.21: Selected HMBC and COSY correlations of compound **6**……..55

KNUST

Figure 4.

Figure 4.
Figure 4.22: Proposed collision–induced mass spectral fragmentation pattern of compound **6**

in positive ESI mode……...56
23: Chemical structure of compound **7**……...56

24: Selected HMBC and COSY correlations of compound **7**…….59

Figure 4.25: Proposed collision–induced mass spectral fragmentation pattern of compound **7**

in positive ESI mode……...60

Figure 4.26: Chemical structure of compound **8**.....60

Figure 4.27: Selected HMBC and COSY correlations of compound **8**…….63

Figure 4.28: Proposed collision–induced mass spectral fragmentation pattern of compound **8**

in positive ESI mode……...64

Figure 4.29: Chemical structure of compound **9**……....65

Figure 4.30: Proposed collision–induced mass spectral fragmentation pattern of compound **9**

in positive ESI mode……66

Figure 4.31: Chemical structure of compound **10**……..67

Figure 4.32: Selected HMBC and COSY correlations of compound **10**……69

Figure 4.33: Proposed collision–induced mass spectral fragmentation pattern of compound **10**

in positive ESI mode……69

Figure 4.34: Chemical structure of compound **11**……..70

Figure 4.

Figure 4.
Figure 4.35: Selected HMBC and COSY correlations of compound **11**……72

Figure 4.36: Proposed collision–induced mass spectral fragmentation pattern of compound **11** in positive ESI mode……72

Figure 4.37: Chemical structure of compound **12**……..73
38: Selected HMBC and COSY correlations of compound **12**……74

39: Proposed collision–induced mass spectral fragmentation pattern of compound **12** in positive ESI mode……75

Figure 4.40: Chemical structure of compound **13**……...77

Figure 4.41: Selected HMBC and COSY correlations of compound **13**……78

Figure 4.42: Chemical structure of compound **14**……...79

Figure 4.43: Selected HMBC and COSY correlations of compound **14**……81

Figure 4.44: Retrocyclization cleavage of the C–ring of compound **14**……..……81

Figure 4.45: Chemical structure of compound **15**……...82

Figure 4.46: Retrocyclization cleavage of the C–ring of compound **15**……83

Figure 4.47: Chemical structure of compound **16**……...84

Figure 4.48: Retrocyclization cleavage of the C–ring of compound **16**……85

Figure 4.49: Chemical structure of compound **17**……...85

KNUST

Figure 4.

Figure 4.
Figure 4.50: Retrocyclization cleavage of the C–ring of compound **17**…….87

Figure 4.51: Chemical structure of compound **18**……..87

Figure 4.52: Retrocyclization cleavage of the C–ring of compound **18**…….89

Figure 4.53: Chemical structure of compound **19**……..89

Figure 4.54: Retrocyclization cleavage of the C–ring of compound **19**…….91

Figure 4.55: Chemical structures of novel metabolites from the endophytic fungus…….92
56: Chemical structures of known metabolites from the endophytic fungus……...92

57: Chemical structures of compounds **20**/**21**……...93

Figure 4.58: Selected HMBC and COSY correlations of compounds **20/21**……..95

Figure 4.59: Experimental ECD spectrum of **20**/**21** and **27**/**28**……..…….96

Figure 4.60: Proposed collision–induced mass spectral fragmentation pattern of compounds **20**/**21** in positive ESI mode……..96

Figure 4.61: Chemical structures of compounds **22**/**23**……...97

Figure 4.62: Selected HMBC and COSY correlations of compounds **22/23**……..99

Figure 4.63: Key NOESY correlations of **22**…….100

Figure 4.64: Chemical structure of compound **24**…….100

Figure 4.65: Selected HMBC and COSY correlations of compounds **24**…….103

Figure 4.

Figure 4.
Figure 4.66: Key NOESY correlations of **24**…….....103

Figure 4.67: Chemical structure of compound **25**…….....104

Figure 4.68: Selected HMBC and COSY correlations of compound **25**……..107

Figure 4.69: Key NOESY correlations of compound **25**……..107

Figure 4.70: Proposed collision–induced mass spectral fragmentation pattern of compound **25** in positive ESI mode……..107

Figure 4.71: Chemical structure of compound **26**……108

Figure 4.72: Selected HMBC and COSY correlations of compound **26**……..110

KNUST

Figure 4.

73: Proposed collision–induced mass spectral fragmentation pattern of compound **26** in positive ESI mode…….110

Figure 4.74: Chemical structure of compounds **27**/**28**…….111

Figure 4.75: Selected HMBC and COSY correlations of compounds **27**/**28**……...112

Figure 4.76: Proposed collision-induced mass spectral fragmentation pattern of compound **27**/**28** in positive ESI mode……...113

Figure 4.77: Planar and X-ray crystal structures of compound **29**……...114

Figure 4.78: Selected HMBC and COSY correlations of compound **29**……..116

Figure 4.79: Chemical structure of compound **30**……117

Figure 4.80: Selected HMBC and COSY correlations of compound **30**……..118

Figure 4.81: Chemical structure of compound **31**……119

Figure 4.82: Selected HMBC and COSY correlations of compound **31**……..120

Figure 4.83: Chemical structures of compounds **32**–**34**……...121

Figure 4.84: Localization of target compounds by MALDI–HRMS imagining in *X. aethiopica*……..123

Figure 4.85: Observed ZOIs of compounds **22**/**23** (a, 10 μg/mL), **25** (b, 10 μg/mL) against *Acinetobacter* sp and compound **24** against *E. coli* (c, 5 μg/mL)…….129

LIST OF ABBREVIATIONS

AP–SMALDI	Atmospheric pressure–scanning matrix assisted laser desorption ionization
$CDCl_3$	Deuterated chloroform

CD_3OD	Deuterated methanol
CE	Cotton effect
CID	Collision induced dissociation
COX	Cyclooxygenase
COSY	Correlation spectroscopy
DBE	Double bond equivalent
DMSO	Dimethyl sulfoxide
DMSO–d_6	Deutrated dimethyl sulfoxide
DPPH	1,1–diphenyl–2–picrylhydrazyl
ECD	Electronic circular dichroism
ESI	Electrospray ionization
EtOAc	Ethylacetate
HCCA	α–Cyano–4–hydroxycinnamic acid
HESI	Heated electrospray
HMBC	Heteronuclear multiple bond correlation
HPLC	High performance liquid chromatography
HRESI–MS	High resolution electrospray ionization–mass spectrometry
H_2SO_4	Sulfuric acid
HSQC	Heteronuclear single quantum correlation
IR	Infra red
LC–HRMS	Liquid chromatography–high resolution mass spectrometry
MALDI–HRMS	Matrix assisted laser desorption ionization–high resolution mass spectrometry
MeOH	Methanol
NOESY	Nuclear overhauser enhancement spectroscopy
t_R	Retention time
MS	Mass spectrometry
MS/MS	Tandem mass spectrometry
NMR	Nuclear magnetic resonance
PDA (HPLC)	Photodiode array

KNUST

PDA	Potato dextrose agar
PDB	Potato dextrose broth
PGE_2	Prostaglandin E_2
RDA	retro Diels–Alder
rpm	Revolutions per minute
TLC	Thin layer chromatography
UV	Ultra violet
UV–Vis	Ultraviolet–visible
WA	Water agar
WHO	World Health Organization
ZOI	Zone of inhibition

KNUST

CHAPTER 1 INTRODUCTION

1.1 General introduction

Interest in traditional systems of medicine and, in particular, herbal medicines, has increased substantially in both developed and developing countries over the past two decades. More than half of the world's population utilize some form of medicinal herbal preparations in search of relief for painful or unpleasant symptoms (WHO, 2002). Medicinal plants have been utilized as medicines for years immemorial. As a consequence of this development, establishing the bioactivity of the secondary metabolites of medicinal plants has become increasingly essential. In this study, the anti–oxidant and the anti–inflammatory activities of the secondary metabolites isolated from the stem bark of *Chlorophora regia* A. Chev (Moraceae) were investigated. The ecological role of the endophytic fungal community harbored in the inner tissues of *C. regia* was examined based of the biological activity of the metabolites isolated from the endophytic fungus. Additionally, the spatial distribution of kaurane diterpenes in the fruits of the medicinal plant *Xylopia aethiopica* (Dunal) A. Rich (Annonaceae) was investigated by MALDI–HRMS imaging.

1.2 Background of study

1.2.1 *Chlorophora regia*

Chlorophora regia A. Chev is a large dioecious tree belonging to the family Moraceae. The tree is widely distributed across the entire width of tropical Africa, indigenous to the forest zone of West Africa (Senegal, Gambia and Ghana). It grows to about 35–45 metres (m) tall. The bole is normally straight and cylindrical usually branchless for more than 20 m, up to 2 m in diameter, without buttresses but spurs may become very large and extend into long surface roots (Louppe *et al*., 2008; Kyekyeku *et al*., 2016). Locally, it is called *Odum–nua* (Akan dialect) in Ghana. *C. regia* is a largely important commercial timber in Africa and the timber is commonly used for making furniture (Abbiw, 1990). It is also used by indigenes for producing charcoal and as

fire wood (Louppe *et al*., 2008). In traditional medicine, extracts of the stem bark are used for the treatment of burns and wounds, snake bite, wasp bite and syphilis. The root bark extract has been reported to be active against *Staphylococcus aureus* (Magassouba *et al*., 2007). Although the phytochemical profile of some species in the genus have been investigated, there was no report in literature, before this study of the phytochemical profile of this medicinal plant (Kyekyeku *et al*., 2016). Most genera in the Moraceae family are rich sources of phenolic compounds (Royer *et al*., 2010; Naik *et al*.,

2015) and the *Chlorophora* genus is no exception (Kyekyeku *et al*., 2016). The genus *Chlorophora* is also referred to as *Maclura* by some reports (Cioffi *et al*., 2003; Li *et al*., 2002; Minn *et al*., 1996). Many phenolic compounds isolated from species in the genus have been reported to be biologically active. Isoflavones from *Maclura pomifera* demonstrated antioxidant activity (Tsao *et al*., 2003) whereas xanthones from *Maclura tinctoria* exhitibed HIV–inhibitory activity (Groweiss *et al*., 2000). Phenols from *Chlorophora excelsa* were shown to exhibit antibacterial, anti–fungal activities (Padayachee and Odhav, 2013), tyrosinase inhibitory activity (Shimizu *et al*., 2003) and chalcone glycosides and flavanones isolated from *Maclura* (*Chlorophora*) *tinctoria* were reported to demonstrate antioxidant activities (Cioffi *et al*., 2003). Isoflavones from *Maclura tinctoria* were further reported to be fatty acid synthase inhibitors (Li *et al*., 2002).

KNUST

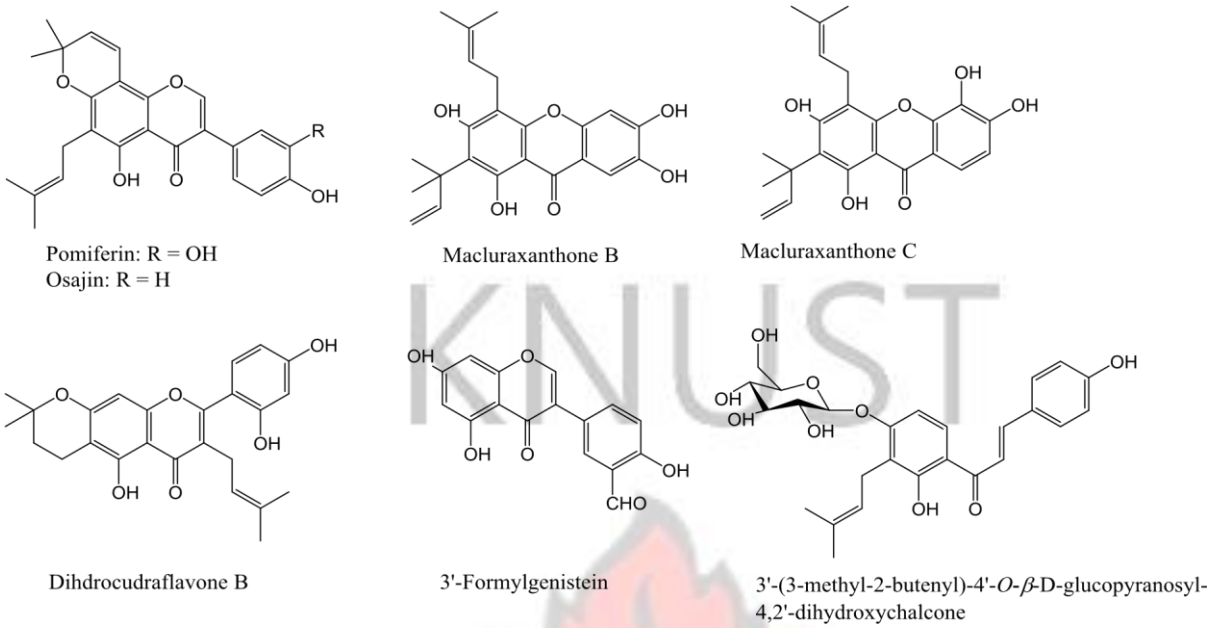


Figure 1.2: Representative structures of compounds isolated from the genus *Chlorophora*

1.2.2 *Xylopia aethiopica*

Xylopia aethiopica (Dunal) A. Rich (Annonaceae) is an evergreen, aromatic plant that grows up to 15 m high with the bark of the plant slightly ridged. The leaves are oblong–anceolate, have round base, glaucous, with lateral nerves. The flowers appear in clusters of 2–4 and the fruits consist of 20–30 capsules. *X. aethopica* is native to the lowland rainforest, deciduous forest in the savannah zones in Africa. It is largely located in West, Central and Southern Africa. The dried fruits of *X. aethiopica* is used traditionally as carminative, stimulant, antifungal, broad–spectrum anti–bacterial, post–partum tonic and lactation aid (Busia, 2007).

Extracts of the fruits and one of its major diterpene constituents in the fruits, xylopic acid (Ekong and Ogan, 1968), have been demonstrated to exhibit interesting biological activities. Biological activities reported include analgesic activity (Woode *et al*., 2013), anti–allodynic activity (Ameyaw *et al*., 2014), antimicrobial activity (Asekun and Adeniyi, 2004; BoakyeYiadom *et al*., 1977), cytotoxic activity (Asekun and Adeniyi, 2004; Adaramoye *et al*., 2011), termite antifeedant activity (Lajide *et al*., 1995), intraocular pressure lowering effect (Igwe *et al*., 2003), hypotensive and diuretic activity (Somova *et al*., 2001), hypolipidaemic and

anti– oxidant activities (Karioti *et al*., 2004; Nwozo *et al*., 2011). In addition to xylopic acid, a number of diterpenes isolated from the fruits of *X. aethiopica* have been reported including ent–kaur–16–en–19–oic acid, 15–oxo–ent–kaur–16–en–19–oic acid (Hutchison *et al*., 1984), 16,17–epoxy–15–oxo–ent–kauran–19–oic acid (Désiré *et al*., 2013).

KNUST

1.3 Problem statement

Many herbal preparations and extracts of medicinal plants are used in the treatment of various ailments traditionally without any established scientific basis for their use. The need to provide scientific credence to the use of these medicinal plants is therefore important. The isolation and characterization of the secondary metabolites responsible for their use would aid in the identification and standardization of these herbal preparations. Moreover, the isolation of novel metabolites could serve as drugs or lead compounds for further drug development.

Emerging evidence have shown that certain microorganisms, example fungi and bacteria, living in the inner tissues of plants have become important source of metabolites with diverse biological activities (Strobel *et al.*, 2004). It has been reported by some authors that these microorganisms are the primary producers of metabolites previously attributed to plants (Kusari *et al*., 2009; Kusari *et al*., 2014; Li *et al*., 2003). The investigation of the relationship between the plant and the associated microorganisms would be beneficial in providing novel lead compounds.

1.4 Justification

Chlorophora regia is used in folklore medicine to treat various disease conditions including burns and wounds. An extensive search through literature revealed the existence of no scientific report on the phytochemical profile of this important medicinal plant. There are several reports on various genera in the Moraceae family of being rich sources of polyphenolic compounds.

These polyphenolic compounds have demonstrated very interesting biological activities (Royer *et al*., 2010; Naik *et al*., 2015). The presence of polyphenolic compounds and their derivatives in *Chlorophora regia*, if found, may be responsible for the traditional use in the treatment of burns, wounds among others. The quest to establish a comprehensive phytochemical composition, possibily identify novel bioactive compounds, contribute to chemotaxonomy, investigate secondary metabolites from the endophytic community harbored in the inner tissues of the Ghanaian medicinal plant *C. regia* and their possible ecological role motivated this study. The phytochemical composition data obtained would assist in the standardization of herbal preparations containing extracts of *C. regia* for traditional medical practice in Ghana. Additionally, the HRESI–MS^n characterization of kaurane diterpenes in the fruit of *X. aethiopica* and their spatial distribution which have not been previously reported further motivated this study.

1.5 Aims and objectives

The aim of this study involves the isolation, characterization and the evaluation of biological activities of secondary metabolites from the Ghanaian medicinal plant *Chlorophora regia* and the endophytic community haboured in the plant. The study also focuses on the investigation of the possible ecological role of the endophytic community in the plant and the investigation of the spatial distribution of kaurane diterpenes in the fruits of *Xylopia aethiopica*.

The specific objectives of this thesis are as follows;

1. Sampling of *C. regia* from Asakraka forest in the Eastern Region of Ghana.
2. Isolation of endophytic fungi from the leaves, stem bark and root of *C. regia*.
3. Pre–screening and identification of endophytic fungi using the OSMAC (One Strain MAny Compounds) approach.
4. Large scale fermentation of selected endophytic fungi.

5. Fractionation, isolation and structure elucidation of secondary metabolites from the stem bark of *C. regia* and the endophytic fungi
6. Evaluation of the biological activity of the isolated and characterized compounds.
7. Isolation and purification of xylopic acid from the fruits of *X. aethiopica*.
8. MALDI mass spectrometry imaging of kaurane diterpenes in fresh fruits of *X. aethiopica* using xylopic acid as reference standard.
9. HRESI–MS^n analysis of kaurane diterpenes in the fruit extract of *X. aethiopica*.

KNUST

CHAPTER 2 LITERATURE REVIEW

2.1 Bioactive secondary metabolites from natural sources as drugs

Medicinal products from natural sources, such as plants, are usually used in dosage forms such as powders, teas, poultices and tinctures in the treatment of various ailments. (Balick and Cox, 1996; Samuelsson, 1992). The use of plants as medicines has involved the isolation and characterization of the bioactive compounds. A typical example includes the isolation of morphine from opium in the early nineteenth century as a typical example (Samuelsson, 1992; Balunas and Kinghorn, 2005). Natural products, particularly medicinal plants, remain an important source of new drugs, new drug leads and new chemical entities (NCEs) (Newman *et al*., 2000; Newman *et al*., 2003; Butler, 2004). Approximately one quarter of the best– selling drugs worldwide in 2001 and 2002, were natural products (Butler, 2004). A number of anti–infective, anti–diabetic, anti–cancer, anti–hypertensive, anti–inflammatory and anti– oxidant agents are from plant sources or derivatives of lead compounds from plant sources.

Arteether, a potent anti–*falciparum* drug for the treatment of malaria is a derivative of artemisinin, a sesquiterpene lactone from *Artemisia annua* L. (Asteraceae), a Chinese medicinal plant. Various derivatives of artemisinin are in use or in clinical trials as antimalarial drugs in Europe (Van Agtmael *et al*., 1999; Graul, 2001). Recently, a new drug for the treatment of chronic obstructive pulmonary disease (COPD), Tiotropium was released to the United States market. Tiotropium is an inhaled anticholinergic bronchodilator, based on ipratropium which is a derivative of the natural product atropine isolated from *Atropa belladonna* L. (Solanaceae) (Barnes *et al*., 1995; Dewick, 2002; Mundy and Kirkpatrick, 2004). Morphine–6–glucuronide which is a metabolite of morphine from *Papaver somniferum* L. (Papaveraceae) is under development as an alternative pain medication with fewer side effects than the parent compound (Lötsch and Geisslinger, 2001).

In the treatment of cancer, medicinal plants have played an important role. Most new clinical applications of secondary metabolites and their derivatives from plants over the last half century have been applied towards combating cancer (Newman *et al*., 2000; Newman *et al*., 2003; Butler, 2004). Anti–cancer agents from plant sources currently in use clinically can be classified into four main groups of compounds: vinca (or *Catharanthus*) alkaloids, epipodophyllotoxins, taxanes and camptothecins. Vinblastine and vincristine, examples of vinca alkaloids, were isolated from *Catharanthus roseus* (L) G. Don (Apocyanaceae)

(formerly *Vinca rosea* L.) and have been in clinical use for over four decades (Balunas and Kinghorn, 2005; Jacobs *et al*., 2004). Podophyllotoxin, an example of the

epipodophyllotoxins, was isolated from *Podophyllum peltatum* L. (Berberidaceae). Due to its toxicity in mice, various derivatives were synthesized and investigated. Etopoisde was the first clinically approved derivative (Gordaliza *et al*., 2004). Paclitaxel, an example of the taxanes, a natural product from *Taxus brevifolia* Nutt. (Taxaceae), was clinically introduced in the early 1990s and has continued to be in use (Wall and Wani, 1996; Oberlies and Kroll, 2004). An example of the last class of natural anti–cancer agents is camptothecin which was isolated from *Camptotheca acuminate* Decne. (Nyssaceae). Several derivatives of each of the four classes have been synthesized and some have been approved for clinical use currently (Balunas and Kinghorn, 2005).

Several anti–microbial agents in use as drugs for treatment of various infections have been isolated or derived from natural sources (notably from bacteria and fungi). Very important lead compounds for designing potent antibiotics have come from microbiological sources.

The ‗Golden Age of Antibiotics' in the early twentieth century had its beginning in the serendipitous discovery of penicillin by the Scottish scientist Alexander Fleming in 1928 (Newman *et al*., 2000). Nearly all the penicillins used as drugs today started from the fermentation-derived product of 6–amino–penicillanic acid (6–APA) including Amoxycillin, Penicillin G, Penicillin V, Flucloxacillin. In 1948, the expanded ring molecule, cephalosporin

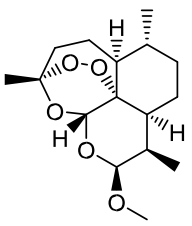
C, was isolated from *Cephalosporium acremonium*, a marine fungus. Cephalosporin C was used as a lead compound to produce modified cephalosporins which were even more potent and resistant to β–lactamase decomposition than the penicillins. Cephalexin, a derivative of cephalosporin C, was the first orally–available cephalosporin (Newman *et al*., 2000; Abraham and Newton, 1961; Newton and Abraham, 1956). Other important antibiotics derived from natural sources include tetracyclines, aminoglycosides (streptomycin), macrolides (erythromycin) (Newman *et al*., 2000).

KNUST

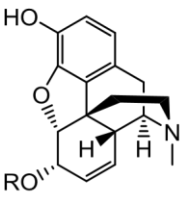
Table 2.1: Drugs and derivatives from natural products, natural sources and medicinal indication(s)

Compound	Lead compound	Natural source	Indication

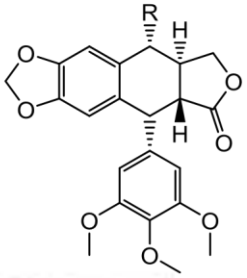
Arteether	Artemisinin	*Artemisia annua* L. (Asteraceae)	Anti–malarial
Tiotropium	Atropine	*Atropa belladonna* L. (Solanaceae)	Treatment of chronic obstructive pulmonary disease (COPD)
Morphine–6–glucuronide	Morphine	*Papaver somniferum* L. (Papaveraceae)	Analgesic
Vinblastine	–	*Catharanthus roseus* (L) G. Don (Apocyanaceae)	Anti–cancer
Vincristine	–	*Catharanthus roseus* (L) G. Don (Apocyanaceae)	Anti–cancer
Etoposide	Podophyllotoxin	*Podophyllum peltatum* L. (Berberidaceae)	Anti–cancer
Paclitaxel	–	*Taxus brevifolia* Nutt. (Taxaceae)	Anti–cancer
Camptothecin	–	*Camptotheca acuminate* Decne. (Nyssaceae)	Anti–cancer
Penicillin	–	*Penicillium* sp. (Trichocomaceae)	Anti–bacterial
Amoxycillin	6–amino–penicillanic acid (6–APA)	*Penicillium* sp. (Trichocomaceae)	Anti–bacterial
Penicillin G	6–amino–penicillanic acid (6–APA)	*Penicillium* sp. (Trichocomaceae)	Anti–bacterial
Penicillin V	6–amino–penicillanic acid (6–APA)	*Penicillium* sp. (Trichocomaceae)	Anti–bacterial
Flucloxacillin	6–amino–penicillanic acid (6–APA)	*Penicillium* sp. (Trichocomaceae)	Anti–bacterial
Cephalexin	Cephalosporin C	*Cephalosporium acremonium* (Hypocreaceae))	Anti–bacterial
Tetracycline	–	*Streptomyces* sp.	Anti–bacterial
Streptomycin	–	*Streptomyces griseus* (Streptomytaceae)	Anti–mycobacterial
Erythromycin	–	*Streptomyces* sp.	Anti–bacterial



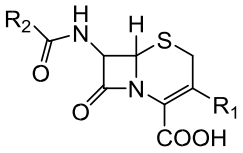
Arteether



Morphine: R = H
Morphine-6-glucoronide: R = glucose

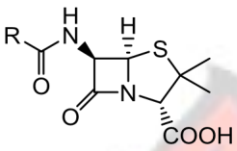


Podophyllotoxin: R = OH
Deoxypodophyllotoxin: R = H



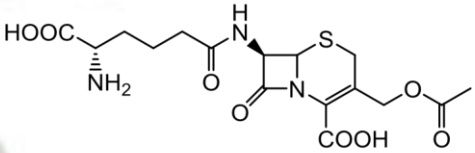
R_1 and R_2 = the variable group

Cephalosporin

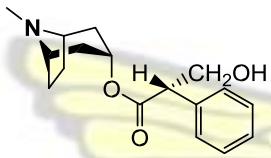


R = the variable group

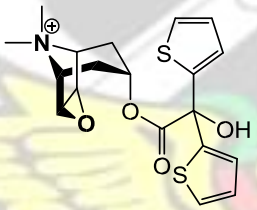
Penicillin



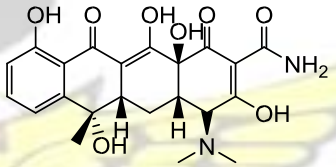
Cephalosporin C



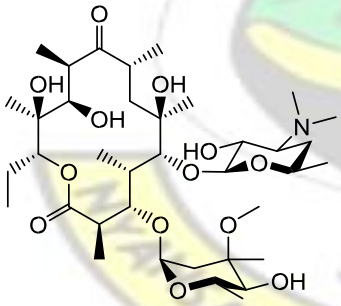
Atropine



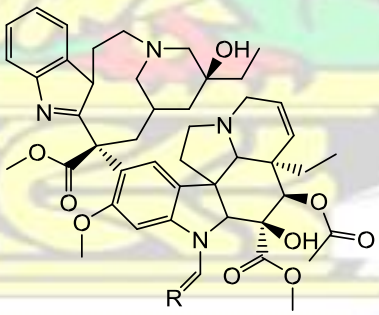
Tiotropium



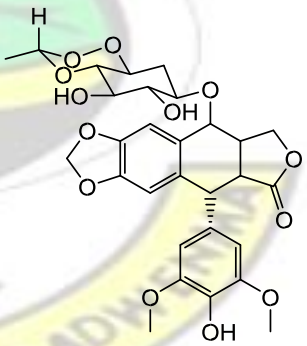
Tetracycline



Erythromycin



Vinblastine: R = H_2
Vincristine: R = O



Etoposide

Figure 2.1: Chemical structures of representative drugs and derivatives from natural sources

2.2 Natural products from endophytic micro-organisms

Endophytes are microorganisms that colonise living tissues of healthy plants without causing any visible manifestation of disease (Stone *et al*., 2000). Endophytic microorganisms are virtually found in every plant. (Strobel *et al*., 2004). ‗Endophytism' is a unique cost–benefit plant–microbe association that is transiently symptomless and established entirely inside the living host plant tissues (Kusari and Spiteller, 2012; Kusari *et al*., 2012). The existence of endophytic fungi living inside the tissues of asymptomatic plants has been known since the nineteenth century (Kusari *et al*., 2012; Guérin, 1898). The term ‗endophyte' was first coined in 1866 (Bary, 1866; Kusari *et al*., 2012). Endophytes may contribute to the total survival of their host plant by producing a myriad of compounds that provide protection to the plant against invading pathogens. These compounds, isolated and characterized, have been shown to have extreme potential for use in modern medicine, agriculture and industry (Strobel *et al*., 2004). The production of bioactive compounds by endophytes, especially compounds exclusive to their host plants, is not only significant from an ecological standpoint but also from a molecular and biochemical perspective. Interesting possibilities for exploiting endophytic fungi exist for the production of novel bioactive secondary metabolites. For example, under controlled fermentation conditions, altering the accessible culture and process parameters (such as media type and composition, aeration, pO_2, pCO_2, pH, temperature, agitation, sampling and harvest points), bioactive compounds produced by endophytes might be optimized (Kusari *et al*., 2012).

2.2.1 Endophytic fungal products as antibiotics

Fungi constitute the most commonly isolated endophytic microbes. They usually appear, when cultivated under axenic conditions, as fine filaments growing from the inner tissues of the plant material on the agar surface. Secondary metabolites from endophytic fungi have been shown to inhibit or kill a wide range of harmful microorganisms such as phytopathogens, as well as bacteria, fungi, viruses and protozoans that affect humans and animals (Strobel *et al*., 2004).

Cryptocandin, a unique peptide antimycotic was isolated from *Cryptosporiopsis* cf. *quercina* has demonstrated excellent antifungal activity against *Candida albicans* and *Trichophyton* spp. *Cryptosporiopsis* cf. *quercina* was isolated as an endophyte from the medicinal plant *Tripterigeum wilfordii* (Strobel *et al*., 1999). The unique tetramic acid, cryptocin, was also isolated from this fungus. This unusual compound was shown to possess potent activity against the causal organism of one of the worst plant diseases, *Pyricularia oryzae* (Li *et al*., 2000; Strobel *et al*., 1999). Cryptocin is under investigation as a natural chemical control agent for rice blast disease (Strobel *et al*., 2004). Colletotric acid is a metabolite of the endophytic fungus *Colletotrichum gloeosporioides* isolated from the medicinal plant *Artemisia mongolica*. It demonstrated antimicrobial activity against bacteria and the fungus *Helminthsporium sativum* (Zou *et al*., 2000). A strain of *Pestalotiopsis microspora*, isolated from the endangered tree *Torreya taxifolia* produced several compounds having antifungal activity including pestaloside and pestalopyrone (Strobel *et al*., 1999; Lee *et al*., 1995).

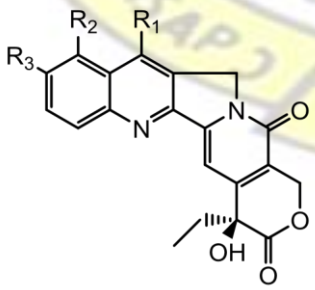
2.2.2 Endophytic fungal and bacterial products as anticancer

Paclitaxel and some of its derivatives represent the first major class of anticancer agents that are produced by endophytes. Paclitaxel or Taxol was originally isolated from *Taxus brevifolia*. Several years later, endophytic fungus, *Taxomyces andreanae* isolated from *Taxus brevifolia* was discovered to produce the anticancer agent Taxol (Strobel *et al*., 1993). Again from the endophytic fungus *Pestalotiopsis microspora,* Torreyanic acid, a selectively cytotoxic quinine dimer and potential anticancer, was isolated. Torreyanic acid was tested against many cancer cell lines and it demonstrated 5–10 times more cytotoxic potency in the lines that are sensitive to protein kinase C agonist and causes cell death by apoptosis (Strobel *et al*., 2004; Li *et al*., 2003). The anticancer agent, camptothecin and two of its analogues 9– methoxycamptothecin and 10–hydroxycamptothecin, have been discovered to be produced by an endophytic fungus *Fusarium solani*, which habours the inner tissues of the plant *Camptotheca acuminata* (Kusari

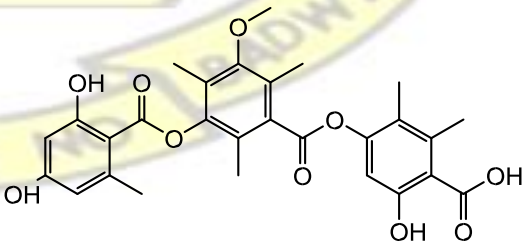
et al., 2009). More recently the endophytic bacterial community living in the roots of *Putterlickia verrucosa* and *P. retrospinosa* has been found to be the hidden producers of the important anticancer and cytotoxic compound maytansine (Kusari *et al*., 2014).

Table 2.2: Bioactive compounds from endophytic microorganisms, natural sources and medicinal indication(s)

Compound	Endophyte	Plant	Indication
Cryptocandin	*Cryptosporiopsis* cf. *quercina*	*Tripterigeum wilfordii* (Celastraceae)	Antifungal
Cryptocin	*Cryptosporiopsis* cf. *quercina*	*Tripterigeum wilfordii* (Celastraceae)	Antifungal
Colletotric acid	*Colletotrichum gloeosporioides*	*Artemisia mongolica* (Asteraceae)	Antibacterial, antifungal
Pestaloside	*Pestalotiopsis microspora*	*Torreya taxifolia* (Taxaceae)	Antifungal
Pestalopyrone	*Pestalotiopsis microspora*	*Torreya taxifolia* (Taxaceae)	Antifungal
Torreyanic acid	*Pestalotiopsis microspora*	*Torreya taxifolia* (Taxaceae)	Anticancer
Camptothecin	*Fusarium solani*	*Camptotheca acuminata* (Nyssaceae)	Anticancer
9–methoxycamptothecin	*Fusarium solani*	*Camptotheca acuminata* (Nyssaceae)	Anticancer
10–hydroxycamptothecin	*Fusarium solani*	*Camptotheca acuminata* (Nyssaceae)	Anticancer
Maytansine	Endophytic bacterial community	*Putterlickia verrucosa P. retrospinosa* (Celastraceae)	Anticancer



Camptothecin: R_1, R_2, R_3 = H
9-methoxycamptothecin: R_1, R_3 = H; R_2 = OCH3
10-hydroxycamptothecin: R_1, R_2 = H; R_3 = OH



Colletotric acid

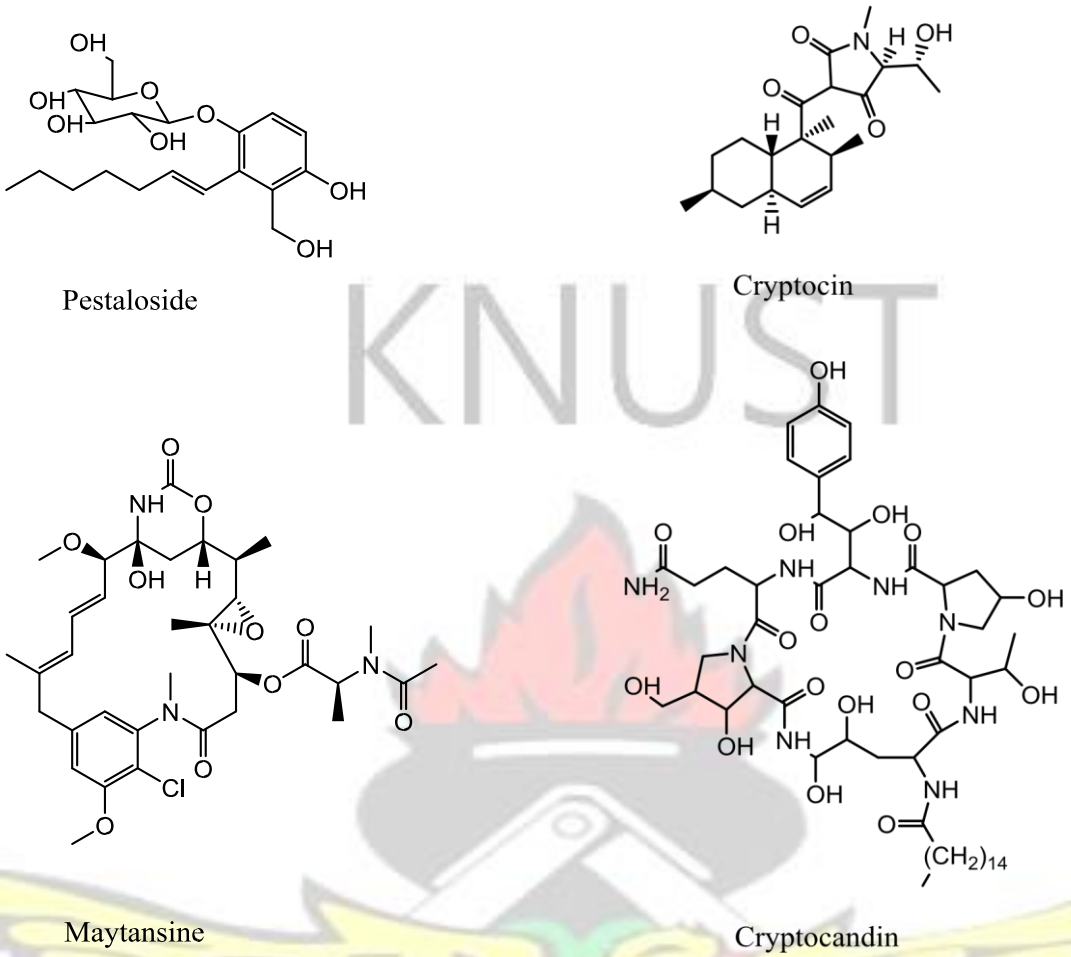


Figure 2.2: Structures of representative bioactive natural products from endophytes.

2.3 Free radicals and natural antioxidants

The normal biochemical processes in the body, higher exposure to the environment in addition to increased levels of dietary xenobiotics result in the generation of reactive oxygen species (ROS) (Nimse and Pal, 2015). ROS are responsible for the oxidative stress in different pathophysiological conditions such as cancer, coronary heart disease, osteoporosis and rheumatoid arthritis. Cellular constituents of the body are affected in oxidative stress conditions, thus resulting in various disease states (Kim and Byzova, 2014). The oxidative stress can be effectively controlled by boosting cellular defenses in the form of antioxidants (Sies, 1997; Pal and Nimse, 2006; Nimse and Pal, 2015). Non–enzymatic antioxidants such as natural phenolic compounds exert their effects by interrupting free radical chain reactions in a process called radical scavenging (Nimse and Pal, 2015).

2.3.1 Measurement of antioxidant activity

Measurement of antioxidant activity cannot be achieved directly but rather antioxidant activity can be measured based on the effects of the antioxidant in controlling the extent of oxidation. Most test methods use accelerated oxidation involving an initiator to manipulate one or more variables in the test system (Antolovich *et al*., 2002).

Various methods have been developed for the evaluation of antioxidant activity, including the ferric reducing antioxidant power (FRAP) assay (Benzie and Strain, 1996), the 2,2′–azino–bis(3–ethylbenzothiazoline–6–sulphonate) radical cation ($ABTS^{*+}$) assay (Miller *et al*., 1993), the oxygen radical absorbance capacity (ORAC) assay (Cao *et al*., 1993; Glazer, 1989), the cupric reducing antioxidant capacity (CUPRAC) assay (Apak *et al*., 2004), the electrochemical estimation of total reducing capacity (Chevion *et al*., 2000) and the 1,1– diphenyl–2–picrylhydrazyl radical ($DPPH^{*}$) assay (Bondet *et al*., 1997; Brand-Williams *et al*., 1995).

The $DPPH^{*}$ method, among the aforementioned methods, is one of the most extensively used for the evaluation of antioxidant activity of natural products due to its stability (Krishnaiah *et al*., 2011; Chen *et al*., 2013). The $DPPH^{*}$ assay is based on the measurement of the reducing capability of the antioxidants toward $DPPH^{*}$ radical, through electron spin resonance (EPR) detection or by the measurement of the decrease of its absorbance(Prior *et al*., 2005; Chen *et al*., 2013). $DPPH^{*}$ reacts with hydrogen/electron donor compounds and has a maximum UV–Vis absorption within the range of 515–520 nm. The radical solution is discoloured after reduction according to the number of paired electrons and the progress of the reaction is effectively monitored by a spectrophotometer (Gil *et al*., 2000; Chen *et al*., 2013). The result is normally expressed as the IC_{50} value, defined as the concentration of antioxidant that causes a 50% decrease in the $DPPH^{*}$ absorbance (Chen *et al*., 2013).

2.4 Inflammation

Inflammation is a normal biological cascade activated in response to tissue injury, microbial infection or chemical irritation and it involves the innate and adaptive immune systems. Inflammation, at the site of injury, is initiated by migration of immune cells from blood vessels and secretion of mediators, followed by recruitment of inflammatory cells and release of reactive oxygen species (ROS), reactive nitrogen species (RNS) and proinflammatory cytokines to eliminate foreign pathogens, and repairing injured tissues (Medzhitov, 2008; Pan *et al*., 2009). The major function of inflammation is beneficial for a host‘s defense. Generally, normal inflammation is rapid and self–limiting but prolonged inflammation is connected to various progressive diseases such as cancer (Balkwill and Mantovani, 2001; Coussens and Werb, 2002; Mantovani *et al*., 2008), neurological disease (Glass *et al*., 2010), metabolic disorders (Hotamisligil, 2006), cardiovascular diseases (Ridker and Silvertown, 2008; Pan *et al*., 2009).

2.4.1 Anti–inflammatory agents

Inflammation is suggested to be a multifaceted and complex process implicated in infiltration and activation of various immune and inflammatory cells, signal transduction, cytokine production and molecular mechanism that results in a widespread physiological state in organ and tissue (Pan *et al*., 2009). There exist several clinical drugs and dietary natural compounds that have shown to possess the ability to protect by different mechanisms, on a number of pathological aspects through targeted interference with chronic inflammatory response. Anti–inflammatory drugs, such as nonsteroidal anti–inflammatory drugs (NSAIDS), in addition to being effective COX–1 and COX–2 inhibitors, are found to have some neuro–protective effects (Hirohata *et al*., 2008; Pan *et al*., 2009). Using monoclonal antibodies against B cells function, TNF–α and IL–6 signaling are beneficial for autoimmune diseases, including rheumatoid arthritis and inflammatory bowel disease (Pan *et al*., 2009). Thus blocking the activity of the

proinflammatory cytokines IL–1, TNF, IL–6, IL–12, IL–17, IL–18, or IL–23 reduces inflammation and suppresses specific pathways that activate T cells (Dinarello, 2010).

2.3 Imaging mass spectroscopy of natural products in space

Mass spectrometry imaging generally, refers to the acquisition of the spatial distribution of the chemical composition of analytes within a sample (Esquenazi *et al*., 2009; Römpp and Spengler, 2013). The spatial distribution can provide useful additional information about the function and properties of an analyte. The first spatially resolved measurements in mass spectrometry were achieved with laser desorption ionization (LDI) in the 1970s (Hillenkamp *et al*., 1975a; Hillenkamp *et al*., 1975b; Römpp and Spengler, 2013). This was however, limited to the analysis of smaller ions, mainly inorganic compounds. The investigation of larger biomolecules was made possible by the introduction of _soft ionization methods‘; electrospray (ESI) and matrix–assisted laser desorption/ionization (MALDI) (Karas and Hillenkamp, 1988; Fenn *et al*., 1989; Römpp and Spengler, 2013). The first major imaging application of MALDI was described in 1994 (Spengler *et al*., 1994).

KNUST

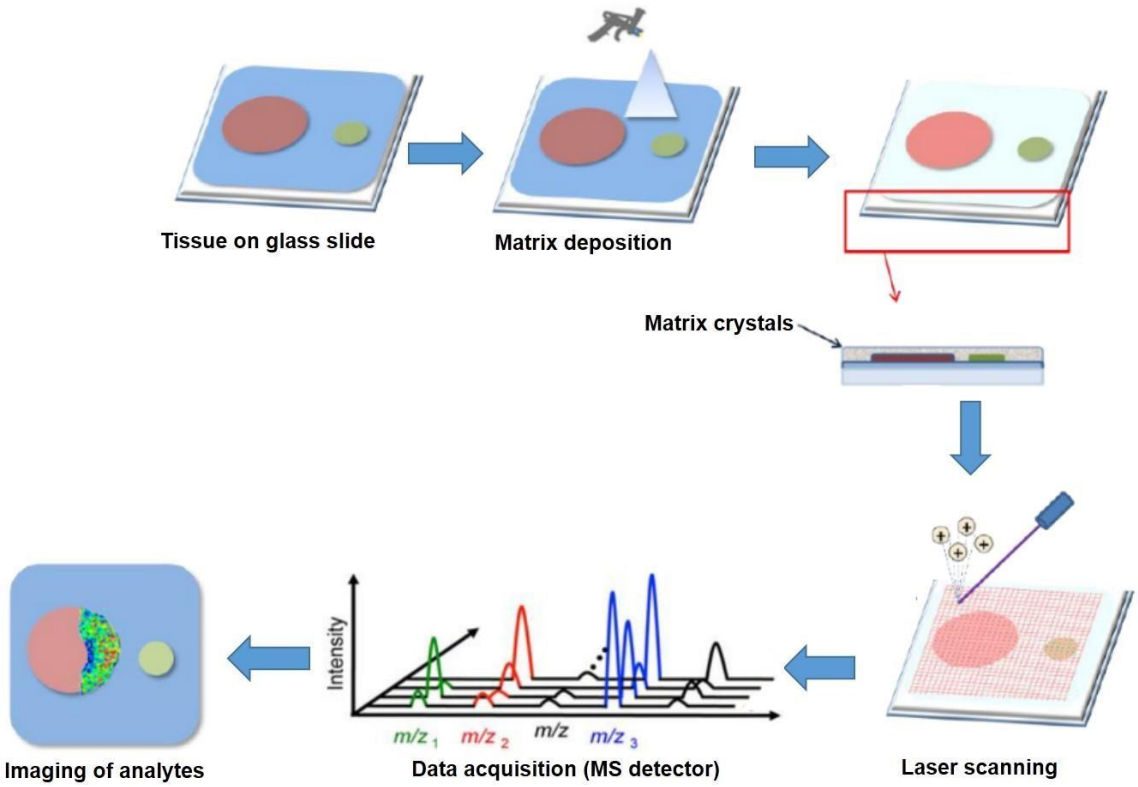


Figure 2.3: Schematic representation of MALDI–HRMS imaging process.

A graphical representation of a MALDI mass spectrometry imaging experiment is as shown in Figure 2.3. The sample (tissue section) is covered with matrix to allow desorption and ionization of the analytes. A laser beam illuminates a specified area of the sample and desorbs and ionizes molecules from the surface. The resulting ions are transferred to the mass spectrometer, and a mass spectrum is obtained. The sample is moved, subsequently, by a specified distance, and the next position on the sample is similarly analyzed. Several thousand spectra are typically obtained sequentially in this manner. MS images of a selected analyte peak are generated by extracting the signal intensity within a certain *m/z* window after the measurement. The signal intensities are plotted as gray scale values for each pixel in a grid representing the corresponding positions on the sample. These _MS images‘ or _selected ion images‘ represent the spatial intensity distribution of a certain *m/z* signal, which can be assigned to a certain molecule. Separate MS images can be generated for each signal in the mass spectrum. Thus, mass spectrometry imaging is an _untargeted‘ and multiplexed method. All desorbed and ionized

compounds in the sample are detected, irrespective of being known or unknown, expected or unexpected (Römpp and Spengler, 2013).

Compounds usually employed as matrix in MALDI experiments for positive mode studies include 2,5–dihydroxybenzoic acid (DHB), α–cyano–4–hydroxycinnamic acid (HCCA), sinapic acid (SA, 3,5–dimethoxy–4–hydroxycinnamic acid), for negative mode studies 9aminoacridine (9AA), 4–nitroaniline, for both positive and negative mode studies 1,5–diaminonapthalene.

CHAPTER 3 MATERIALS AND METHODS

3.1 Materials

3.1.1 Media for cultivation

Potato dextrose agar (DIFCO, cat. no. 213400), potato dextrose broth (Carl Roth Co. GmbH) and water agar (DIFCO, cat. no. 214530) were employed as growth media for the isolation and cultivation of endophytic fungi. Composition of the Potato dextrose broth (PDB) was potato extracts 4 g, dextrose 20 g, in 1 L and that of the potato dextrose agar (PDA), potato extracts 4 g, dextrose 20 g, agar 15 g, in 1 L. Nutrient agar (Carl Roth Co. GmbH) and nutrient broth (Sigma–Aldrich Chemie, GmbH) were used as growth media for the antibacterial assay.

3.1.2 Bacteria used for antibacterial assay

The in–vitro antibacterial activities of the tested compounds were carried out against a panel of standard pathogenic control strains (obtained from Leibanz Institute DSMZ, German Collection of Microorganisms and Cell Cultures, Braunschweig, Germany). The selected organisms were clinically important Gram–positive *Staphylococcus aureus* (DSM 799), Gram–positive *Bacillus subtilis* (DSM 1088), Gram–negative environmental strain of *Escherichia coli* (DSM 1116) and Gram–negative soil bacterium *Acinetobactor* sp. (DSM 586).

3.1.3 Chemicals

All the chemicals employed were sourced from Sigma–Aldrich Chemie GmbH, Germany. The organic solvents (methanol, cyclohexane, ethylacetate, chlorophorm, acetone, dichloromethane, Petroleum ether) used were all of analytical grade and purchased from BDH Laboratory Supplies (Merck Ltd, Lutterworth, UK).

3.1.4 Plant collection, authentication and preparation

Two medicinal plants namely, *Chlorophora regia* and *Xylopia aethiopica* (Dunal) A. Rich (Annonaceae) (Table 3.1; Figure 3.1) were selected for this study.

Chlorophora regia A. Chev (Moraceae) was collected from Asakraka forest (6º37′48,39″N0º41′6,87″W) in the Eastern Region of Ghana in June 2014 by a local herbalist and authenticated by Mr. Clifford Asare at the Department of Herbal Medicine, Kwame Nkrumah University of Science and Technology, Kumasi, Ghana. The stem bark for the phytochemical screening was air–dried, powdered, sealed in plastic bags and transported to Institut für Umweltforschung (INFU), Techniche Universität (TU) Dortmund, Germany. In the case of endophytic investigation, different parts of the plant were collected and washed under running tap water to remove any dirt. The fresh tissues were sealed carefully in aluminium foil and transported to INFU, TU Dortmund, Germany within 48 h of collection. The fruits of *Xylopia aethiopica* were collected from the Physic garden of the Department of

Pharmacognosy, Kwame Nkrumah University of Science and Technology, Kumasi, Ghana in October 2015. The fruits were sealed and transported to INFU, TU Dortmund, Germany for the isolation of xylopic acid as standard and subsequently the MALDI–HRMS measurements.

Table 3.1: Selected plants for the study

Plant name	Family	Location of collection	Voucher number
Chlorophora regia	Moraceae	Asakraka, Eastern Region, Ghana	KNUST/HM/CR1/2014/R002
Xylopia aethiopica	Annonaceae	Physic garden, Kumasi, Ghana	KNUST/HMT/2015/F001

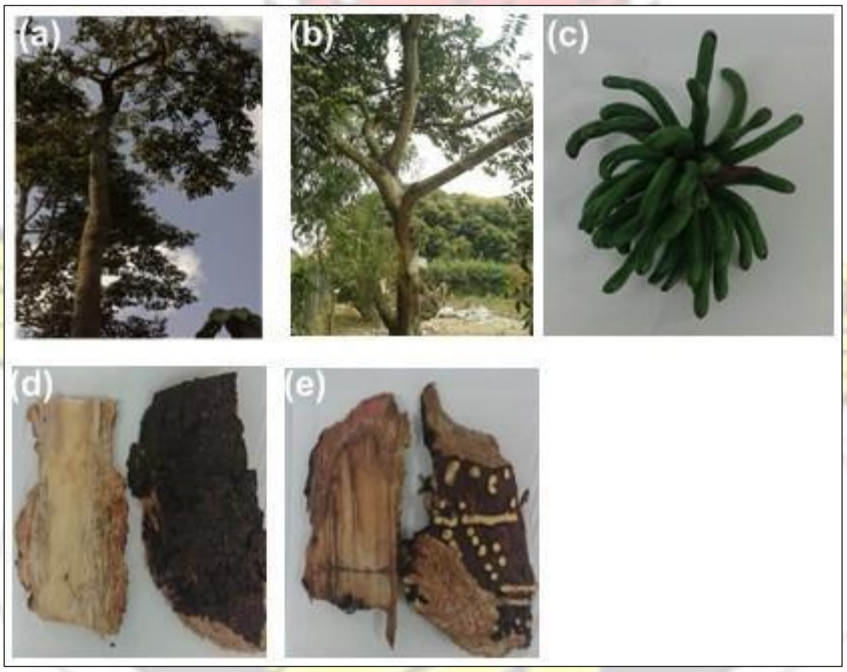


Figure 3.1: Two Ghanaian medicinal plants: (a) *C. regia* (b) *X. aethiopica* (c) Fruit of *X. aethiopica* (d) Stem bark of *C. regia* (e) root of *C. regia*.

3.2 Methodology

3.2.1 Extraction of plant materials

3.2.1.1 Extraction and isolation of constituents from *Chlorophora regia*

The air–dried and powdered stem bark (2 kg) was extracted with methanol–chloroform (80:20) mixture twice by cold maceration. The crude extract obtained was concentrated under vacuum to yield a brownish residue (140 g). The yielded residue was sequentially partitioned in cyclohexane, dichloromethane and methanol. The methanolic fraction (110 g) was subjected to column chromatography on silica gel eluting with varying polarities of cyclohexane–ethyl acetate and ethyl acetate–methanol to afford fourteen major fractions (A– N) after high resolution mass spectrometry (HR–MS) and thin layer chromatography (TLC) profiling. Fraction A, from 95:5 (cyclohexane–ethyl acetate) elution, was subjected to sephadex LH–20 column chromatography using methanol to obtain twenty subfractions (A1– A20). Four subfractions (A13–A16) were purified by *semi-preparative* HPLC (MeOH–H_2O, 80/20, 2.0 mL/min) to afford **9** (4 mg, t_R = 18 min), **10** (1 mg, t_R = 25 min) and **8** (15 mg, t_R = 14.0 min). Fraction G, from 80:20 (cyclohexane–ethyl acetate) elution, was subjected to column chromatography on silica gel using varying polarities of cylohexane–ethyl acetate to obtain four subfractions (G1–G4). **14** (7 mg) crystallised out of G1. G2 was further fractionated by sephadex LH–20 column chromatography using methanol to obtain eight subfractions (G21–G28). **16** (13 mg) and **17** (3 mg) crystallized out of G25 and G26 respectively. G23 was purified by *semi-preparative* HPLC (MeOH–H_2O, 70/30, 2.0 mL/min) to afford **15** (5 mg, t_R = 5 min), **2** (20 mg, t_R = 11 min) and **5** (8 mg, t_R = 14 min). G22 was also purified by *semi-preparative* HPLC (MeOH–H_2O, 70/30, 2.0 mL/min) to afford **18** (7 mg, t_R = 4 min), **19** (15 mg, t_R = 6 min) and **3** (1 mg, t_R = 12 min). Fraction H, from 70:30 (cyclohexane–ethyl acetate) elution, following a similar procedure to that used for Fraction G, yielded ten subfractions (H1–H10). H6 was subjected to column chromatography on sephadex LH–20 to obtain five subfractions (H61–H65) followed by purification of H63 by *semipreparative* HPLC (MeOH–H_2O, 70/30,

2.0 mL/min) to afford **7** (2 mg, t_R = 6 min), **1** (30 mg, t_R = 10 min), **4** (8 mg, t_R = 13 min) and **13** (10 mg, t_R = 16 min). H64 was treated by a similar procedure to that of H63 (MeOH–H_2O, 60/40, 2.0 mL/min) to afford **6** (2 mg, t_R = 12 min), **11** (9 mg, t_R = 17 min) and **12** (10 mg, t_R = 19 min) (Kyekyeku *et al*., 2016).

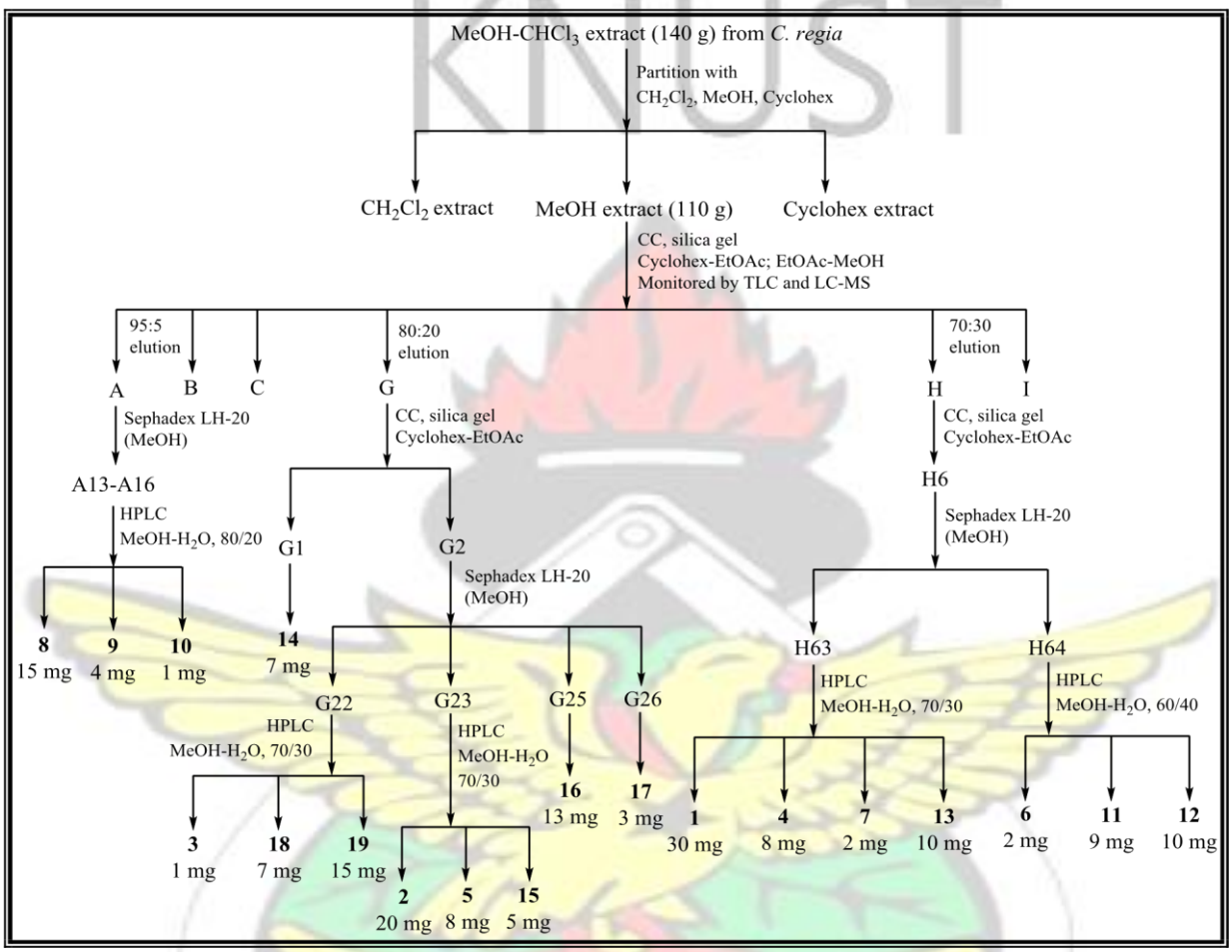


Figure 3.2: Schematic diagram of isolation of secondary metabolites from the stem bark of *C. regia*.

3.2.1.2 Extraction and isolation of xylopic acid from *Xylopia aethiopica*

The extraction and isolation of xylopic acid followed the procedure as previously described (Woode *et al*., 2012). The powdered dried fruit of *X. aethiopica* was extracted with petroleum ether (40–60 ^oC) by cold maceration. The crude extract was concentrated under vacuum and ethyl acetate added to the concentrate to aid crystallization. The mixture was allowed to stand

for three days and the crystallized xylopic acid filtered and washed with petroleum ether (40–60 ^{o}C). The crude xylopic acid crystals obtained were purified by recrystallization in ethanol (96 %).

3.2.1.3 Fruit extraction of *X. aethiopica* for HPLC–HRESI–MS^{n}

Fresh fruits (10 g) were air–dried at room temperature and macerated to powder. The powder was extracted with methanol–chloroform (1:1, *v*/*v*) three times. The crude extracts were pooled, filtered using a Whatman® filter and dried under vacuum. The residue was dissolved in methanol (analytical grade) and centrifuged to separate the clear supernatant from any insoluble component. The supernatant was transferred into LC–MS glass vials after suitable dilution with methanol.

3.2.2 Isolation, cultivation and storage of endophytic fungi from *C. regia*

The endophyte isolation was carried out following a previously established and reported procedure (Kusari *et al*., 2008). The plant tissues were washed with tap water to remove any dirt sticking to them. The tissues were then cut into small sizes, approximately 10 mm (length) x 5 mm (breadth). Surface sterilization of the tissues was achieved by sequentially immersing in 70% ethanol for 1 min, 1.3 M sodium hypochlorite (4% available chlorine) for 3 min, 70% ethanol for 30 s and sterile double–distilled water for 1 min to prevent any possible contamination. The surface–sterilised tissues were then put on sterile paper to remove excess water. The tissues were finally placed evenly on water agar (WA) medium containing 100 mg/L streptomycin in Petri dishes (Greiner Bio–One GmbH, Germany) (Figure 3.3.1). Parafilm (Bemis Company Inc., Neenah, WI, U.S.A) was used to seal the petri dishes and kept at 28 ± 2 ^{o}C in an incubator. The petri dishes with cultures were inspected daily to observe the growth of endophytic fungi. Fungal hyphal tips growing out after 1–2 weeks from the tissues, were selected and subcultured on potato dextrose agar in Petri dishes. The subcultured fungal strains

were incubated at 28 ± 2 ^{o}C in an incubator. After further purification processes, pure cultures of the endophytic fungi were obtained and labeled appropriately. For long–term storage, the isolated endophytic fungi were cryopreserved with

20% (v/v) glycerol at –80 ^{o}C in the internal culture library at INFU, TU Dortmund, Germany.

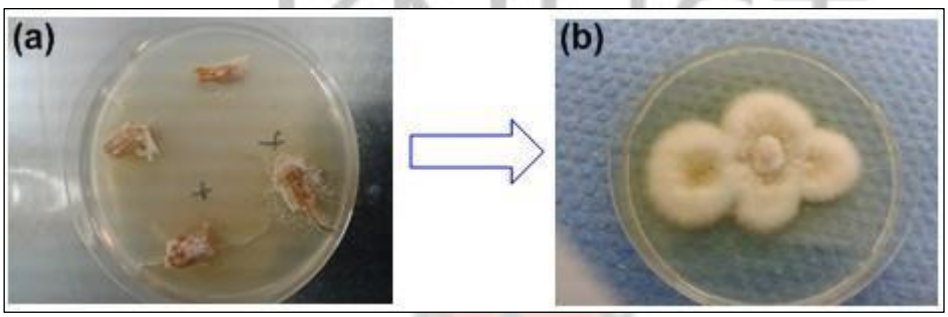


Figure 3.3: The isolation of the endophytic fungus JK10. (a) The surface–sterilized roots of *C. regia* cultured on WA showing the growth of endophytic fungal colonies from tissue (b) The purified endophytic fungus JK10 cultured on PDA media.

3.2.3 Pre–screening, selection and large–scale fermentation

The isolated endophytic fungi were pre–screened following the OSMAC (One Strain MAny Compounds) approach to study the secondary metabolite profile and identify known as well as novel phytochemical constituents. The pure subcultured endophytic fungi on PDA were cut aseptically into small pieces. The cut pieces of each endophytic fungus were used to inoculate a 250 mL flask containing previously sterilized 100 mL potato dextrose broth (PDB). This step was repeated in a different flask containing 40 g rice and 60 mL water. The inoculated flasks containing the PDB medium were incubated at 28 ± 2 ^{o}C for 30 days in a shaker incubator (150 rpm) (INFORS HT Multitron 2, Einsbach, Germany). The flasks with the rice medium were incubated at room temperature for 30 days (or more depending on the rate of growth of the cultures). The fermented cultures after the incubation period, were extracted with EtOAc, dried under vacuum and redissolved in MeOH. The MeOH extracts were analysed by liquid chromatography–high resolution mass spectrometry (LC–HRMS) for secondary metabolite

profiling. The LC–HRMS data in addition to sophisticated databases such as Antibase (Laatsch, 2010) and SciFinder®, assisted the dereplication, identification and analysis of the metabolite profiling of the investigated endophytic fungi. The endophytic fungus labeled JK10 was selected for the purposes of large-scale fermentation after an extensive metabolite profiling. Large–scale fermentation of the fungal strain was carried out by first culturing on PDA at room temperature for 7 days. The agar plugs from the cultivated plate was cut into small pieces aseptically, inoculated on solid rice medium in 20 flasks (1000 mL) each containing 80 g of rice, 120 mL of water and 0.3% peptone and incubated for 60 days.

3.2.4 Fungal extraction, isolation and purification of secondary metabolites

The fermented media, after the large–scale fermentation, was extracted three times with ethyl acetate (EtOAc) at room temperature by sonication. The filtrate was concentrated under vacuum to obtain 15.7 g of crude extract. The residue was subjected to silica gel column chromatography and eluted with a gradient of cyclohexane–EtOAc from 1:0 to 0:1. Six fractions (A–F) were obtained after TLC and LC–HRMS analyses. Fraction C was subjected to silica gel column chromatography with cyclohexane–EtOAc to yield five subfractions (C1– C5). Subfraction C3 was purified by *semi–preparative* HPLC (MeOH–H_2O, 60:40, 2.0 mL/min) to afford solaniol (**29**, 8 mg, t_R = 15 min). Subfraction C4 was subjected to a similar method to that of C3 (MeOH–H_2O, 70:30, 2.0 mL/min) to afford 2,3–dihydro–5–hydroxy–8– methoxy–2,4–dimethylnaphtho[1,2–b]furan–6,9–dione (**30**, 8 mg, t_R = 18 min). Fraction E was separated by column chromatography on silica gel using varying polarities of cyclohexane–EtOAc into five subfractions (E1–E5). E4 was further subjected to column chromatography on sephadex LH–20 using MeOH to obtain three subfractions (E41–E43). Purification of fraction E42 by *semi–preparative* HPLC (MeOH–H_2O, 70:30, 2.0 mL/min) afforded NG–391/NG–393 (**27**/**28**, 13 mg, t_R = 14 min). Fraction E43 was purified by *semi– preparative* HPLC (MeOH–H_2O, 80:20,

2.0 mL/min) to afford **25** (1.5 mg, t_R = 16 min) and N_b–acetyltryptamine (**31**, 5 mg, t_R = 7 min). Fraction E5 was fractionated by silica gel column chromatography (cyclohexane–EtOAc) to yield six subfractions (E51–E56). Fraction E54 was purified by *semi–preparative* HPLC (MeOH–H_2O, 60:40, 2.0 mL/min) to afford **20**/**21** (11 mg, t_R = 22 min) and **26** (4.5 mg, t_R = 37 min). Fraction E55 afforded **22**/**23** (2.7 mg, t_R = 23 min) after purification by *semi–preparative* HPLC (MeOH–H_2O, 40/60, 2.5 mL/min) purification. Fraction E56 was purified by *semi–preparative* HPLC (MeOH–H_2O, 40/60, 2.5 mL/min) to afford **24** (5.2 mg, t_R = 26 min).

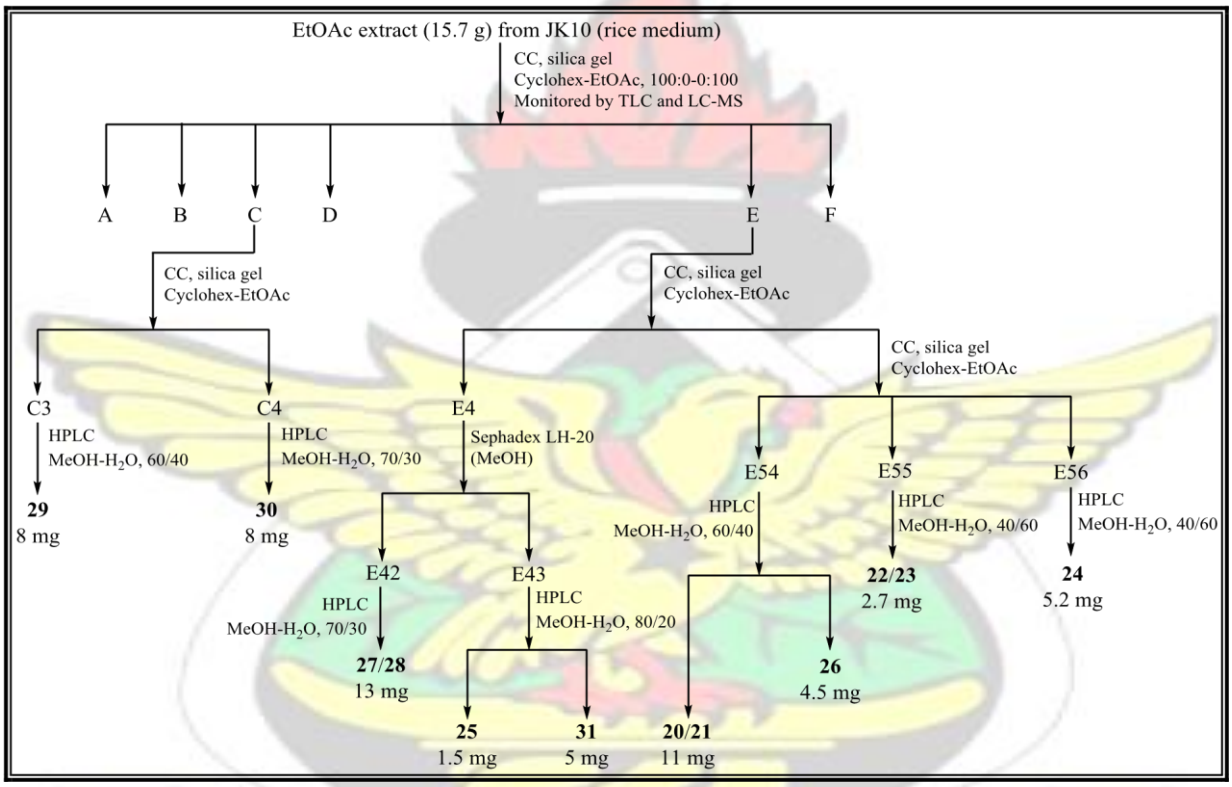


Figure 3.4: Schematic diagram of isolation of secondary metabolites from the endophytic fungus JK10

3.2.5 General experimental procedures

3.2.5.1 NMR

NMR spectra were recorded on a Bruker DRX–500 spectrometer operating at 500 MHz (^{1}H) and 125 MHz (^{13}C) and Bruker Avance III spectrometer operating at 600 MHz (^{1}H) and 150

MHz (^{13}C), Bruker Avance III HDX–700 spectrometer operating at 700 (^{1}H) and 176 (^{13}C) MHz using deutrated methanol–d_4 (CD_3OD) (Deutero GmbH, Kastellaun, Germany), deutrated chloroform ($CDCl_3$) (Deutero GmbH, Kastellaun, Germany) and DMSO–d_6 (Sigma–Aldrich Chemie GmbH) as solvents with TMS as internal standard. Chemical shifts (δ) were quoted in parts per million (ppm) from internal standard tetramethylsilane (TMS).

KNUST

3.2.5.2 Chromatography

For column chromatography, Silica gel 60 (70–230 mesh; AppliChem, GmBH, Darmstadt, Germany) and Sephadex LH–20 (25–100µm, Amersham Biosciences) were used. TLC was carried out on pre–coated silica gel 60 plates (0.25 mm; Merck, Darmstadt, Germany). Compounds were visualized under UV light and further by spraying with H_2SO_4–EtOH (1:9, v/v).

3.2.5.3 HPLC

Semi–preparative HPLC was performed on Gynkotek pump equipped with a Dionex DG– 1210 degasser, a Dionex UVD 340S detector, a Dionex Gina 50 auto–sampler and a Phenomenex Gemini C18 column (10 x 250 mm, 10µm particle size) using a Chromeleon software system.

3.2.5.4 LC–HRMS^n

The HPLC–HRMS^n experiments were performed on an LTQ–Orbitrap spectrometer (Thermo Fisher, USA) equipped with an HESI–II source. The spectrometer was equipped with an Agilent 1200 HPLC system (Santa Clara, USA) including pump, PDA detector, column oven (30°C), and auto–sampler (injection volume 5 µL for Fullscan, 7 µL for MS^n). The spectrometer was operated in a positive mode with nominal mass resolving power of 60,000 at *m/z* 400 with a scan rate of 1 Hz. The following parameters were employed for the HESI–II source; spray

voltage 5 kV, capillary temperature 300 ^{o}C, tube lens 100 V. Argon was used as the collision gas and N_2 as the sheath gas (55 arbitrary units) and auxiliary gas (8 arbitrary units. MS/MS experiments were measured by CID (collision–induced decay, 35eV) mode. HPLC analyses were carried out on a Luna C18 (2) column (50 x 3 mm, 3 µm particle size) from Phenomenex (Torrance, USA) with a water (+ 0.1% formic acid) (A) and methanol (B) gradient (flow rate 350 µL/min). The gradient parameters were set as follows: linear gradient from 95% A to 100% B over 14 min, 100% B isocratic for 4 min, the system returned to initial conditions within 0.5 min of 95% A and was equilibrated for 4.5 min.

KNUST

3.2.5.5 X–ray diffraction analysis

The X–ray diffraction experiment was performed on a Bruker Apex Duo, which was integrated with the Bruker SAINT software package using a narrow-frame algorithm. Data was obtained at 100(2) K with graphite–monochromated Cu–Kα radiation (λ = 1.54178 Å). The multi–scan method (SADABS) was employed on absorption effects for data correction.

The structure of the crystal was solved with intrinsic phasing using SHELXT2014 (Sheldrick, 2015) and refined with the SHELXL2014/7 (Sheldrick, 2008) refinement program by the full–matrix least–squares on F2 method. Molecular graphics were achieved using Ortep–3 (for Windows, Version 2014.1) (Farrugia, 2012).

3.2.5.6 MALDI–HRMS imaging of kaurane diterpenes in the fruits of *X. aethiopica*

Transverse section of the fresh fruit material of *X. aethiopica* was cut at a thickness of 20 µm and fixed onto the surface of a glass slide in a Thermo Scientific HM550 cryostat at a box temperature of –20 ^{o}C and at a sample temperature of –10 ^{o}C. The matrix employed comprised a solution of HCCA (7 mg/mL) in acetonitrile-water 1:1 (*v*:*v*) with an addition of TFA (0.2%). The matrix solution was sprayed on the sample using a SMALDI Prep spray device (TransMIT

GmBH, Gießen, Germany). The spray application was performed according to the following parameters; 15 µL/min matrix flow rate, 4.5 L/min gas (N_2) flow rate and sample plate revolution speed of 100 rpm. Image of the scanned area selected was captured with an optical microscope Leica S8AP0 (Leica Microsystems GmBH, Wetzlar, Germany). MALDI–HRMS measurements of the sample were carried out on an atmospheric pressure scanning microprobe matrix–assisted laser desorption/ionization source (AP– SMALDI) (TransMIT GmBH, Gießen, Germany) coupled with a Q Extractive high-resolution mass spectrometer (Thermo Scientific Inc., Bremen, Germany). A nitrogen laser (337.1 nm) at a pulse frequency of 60 Hz was employed as the ion source. Laser beam attenuation was set at 20°. Full scan measurements, in positive mode, were carried out within the mass range *m/z* 100–800 at a mass resolution of 140,000 at *m/z* 200. The source spray voltage was set at 2000

V. The internal mass calibration used was the lock mass *m/z* 379.09246 $[M + 2H]^+$ of HCCA. Further measurement parameters were a lateral scan (pixel) resolutions in the range 10–15 µm and a maximum injection time of 300 ms. IMS data obtained were analyzed with the ImageQuest (v. 1.1.0) software package (Thermo Scientific GmBH, Bremen, Germany) (Kusari *et al*., 2015b; Wang *et al*., 2015).

3.2.5.7 Other methods

Optical rotations were recorded on A–Krüss Optronic ploarimeter at a wavelength of 589 nm. Electronic circular dichroism (ECD) was measured on a Jasco J–715 spectrometer and Infra–red (IR) spectrum was recorded on a Bruker IR spectrometer TENSOR27.

3.2.6 Bioassay

3.2.6.1 DPPH free radical scavenging assay of metabolites isolated from *C. regia*

The DPPH radical scavenging assay was carried out according to the previously established procedure with suitable modifications (Bondet *et al*., 1997; Moein *et al*., 2008; Wu *et al*., 2010).

The first step of the DPPH assay was to optimize on a Biotek Synergy HT Multi–mode Microplate reader over a series of DPPH concentrations (in MeOH) ranging from 0.2 to 1.0 mM, using the reference standard (Trolox) with a final concentration range of 0.25 µg/ml to 0.5 mg/ml. 200 µL of DPPH solution was briefly added to 10 µL of the reference to reach a desired concentration in a 96–well microplate, and the resulting solution was allowed to react for 30 min in the dark at ambient temperature. The absorbance was then read at OD490, OD517 and OD525, respectively, in order to determine the optimum wavelength for measurements under the tested conditions. Compounds **1**–**5**, **7**–**10** and **15** were tested at concentrations of 0.25 mg/mL, 0.5 mg/mL, 0.75 mg/mL and 1.0 mg/mL in MeOH, using the optimized DPPH assay employing 1.0 mM DPPH solution and read at OD490. The

experiment was carried out in triplicate. The radical scavenging capacity was expressed as percentage inhibition (I %) and calculated using the following equation (Bedane *et al*., 2015):

$$I\% = \frac{Abs_{control} - Abs_{sample}}{Abs_{control}} \times 100$$

3.2.6.2 Anti–inflammatory assay

The anti–inflammatory assay of the metabolites isolated from the stem bark of *C. regia* was performed using a Parameter PGE_2 forward sequential competitive enzyme immunoassay (R&D Systems Europe Ltd., Abingdon, United Kingdom) using cortisone (≥98%) as a reference standard according to the previously established procedure (Mireku *et al*., 2015; Hevesi *et al*., 2009). Compounds **1**–**4**, **11**–**12** and **15,** whose anti-inflammatory activities have not previously been tested, were evaluated at concentrations of 1.0 μM, 5.0 μM, 10 μM, 20 μM and 40 μM in DMSO. The experiment was repeated three times.

3.2.6.3 Antibacterial assay of metabolites isolated from the endophytic fungus

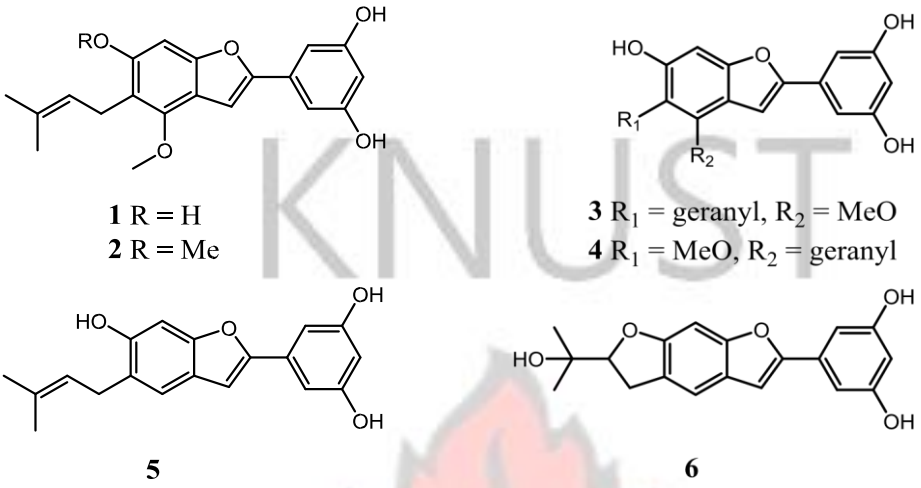
The antibacterial activities were determined using the disk diffusion method. The assay was performed as previously described (Li *et al*., 2014). Nutrient agar was poured into sterile Petri dishes (TPP, Trasadingen, Switzerland) to obtain a depth of 4 mm. 200 μL of inoculum suspension of the test organisms was spread evenly on the surface of the agar in the plates. The plates were allowed to stand for 2 hours at 4 ^{o}C. The compounds to be evaluated (**20–28**) were prepared at concentrations of 0.1 μL/mL, 1.0 μL/mL, 2.0 μL/mL, 5.0 μL/mL and 10.0 μL/mL using HPLC–grade methanol as solvent. The reference standards were similarly prepared using sterile double–distilled water. Sterile paper discs (Schleicher & Schuell GmBH, Dassel, Germany; 6.0 mm in diameter) were soaked with 40 μL of the test compounds, air-dried aseptically and put on the seeded plates. The plates were incubated for 24 hours at 37 ^{o}C. A positive control and two sets of negative control were employed. The positive control consisted of a seeded plate without sample. The first negative control was unseeded plates with samples and the second negative control comprised seeded plates with discs impregnated with HPLC–grade methanol or sterile double-distilled water to check solvent effect. The plates, after incubation, were monitored for zones of inhibition. The minimum inhibitory concentrations (MIC) of each compound tested, including the reference standards, were computed according to the guidelines of Clinical and Laboratory Standards Institute (CLSI) (Wikler, 2006). Each of the tests was carried out in triplicate.

CHAPTER 4 RESULTS AND DISCUSSION 4.1 Isolation and characterization of secondary metabolites from the stem bark of

Chlorophora regia

Extensive phytochemical investigation of the stem bark of the Ghanaian medicinal plant *C. regia*, resulted in the isolation and characterization of three new 2–arylbenzofuran derivatives,

regiafuran A–C (**1**–**3**), together with three known 2–arylbenzofuran derivatives, mulberrofuran Y (**4**), moracin N (**5**) and moracin O (**6**). (Kyekyeku *et al*., 2016).



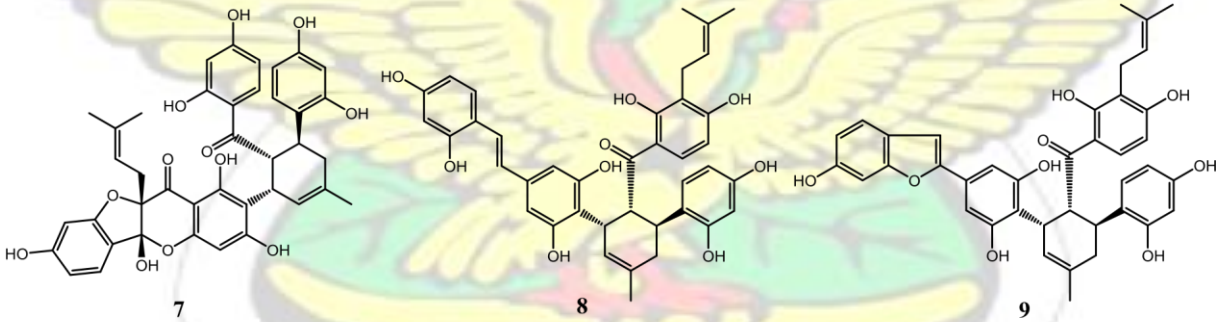
1 R = H
2 R = Me

3 R_1 = geranyl, R_2 = MeO
4 R_1 = MeO, R_2 = geranyl

5 **6**

Figure 4.1: Chemical structures of 2-arylbenzofuran derivatives from *C. regia*.

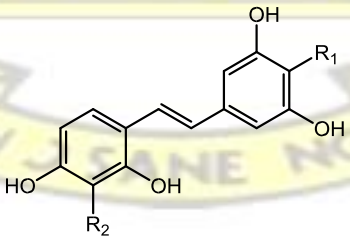
Additionally, three known Diels–Alder adducts sanggenon C (**7**), kuwanol E (**8**) and chalcomoracin (**9**) were isolated.



7 **8** **9**

Figure 4.2: Chemical structures of Diels-Alder adducts from *C. regia*.

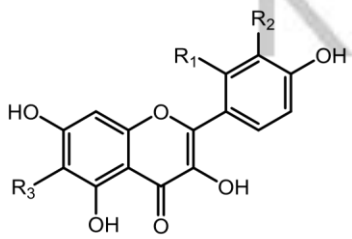
Furthermore, two stilbene derivatives chlorophorin (**10**) and isochlorophorin (**11**) were obtained.

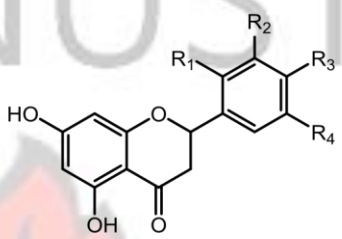


10 R_1 = geranyl, R_2 = H
11 R = H, R_2 = geranyl

Figure 4.3: Chemical structures of stilbene derivatives from *C. regia*.

Finally, one new flavonoid, 6–prenylated–3,5,7,4′–tetrahydroxy–2′–methoxyflavonol (**12**) together with seven known flavonoids, gancaonin P (**13**), 3,5,7,4′–tetrahydroxy–2′–methoxyflavonol (**14**), quercetin (**15**), kaempferol (**16**), 5,7,4′–trihydroxy–2′–methoxyflavanone (**17**), 5,7,3′,5′–tetrahydroxyflavanone (**18**) and naringenin (**19**) were successfully isolated (Kyekyeku *et al*. 2016).





12 R_1 = MeO, R_2 = H, R_3 = prenyl
13 R_1=H, R_2=OH, R_3=prenyl
14 R_1=MeO, R_2=H, R_3=H
15 R_1=H, R_2=OH, R_3=H
16 R_1=H, R_2=H, R_3=H

17 R_1=MeO, R_2=H, R_3=OH, R_4=H
18 R_1=H, R_2=OH, R_3=H, R_4=OH
19 R_1=H, R_2=H, R_3=OH, R_4=H

Figure 4.4: Chemical structures of flavonoids from *C. regia*.

4.1.1 Structure elucidation of Regiafuran A (1, new compound)

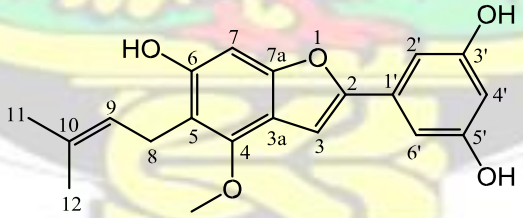


Figure 4.5: Chemical structure of compound **1**.

Regiafuran A (**1**) (Kyekyeku *et al*., 2016), was obtained as yellow amorphous solid and the molecular formula was determined to be as $C_{20}H_{20}O_5$ based on the ion *m/z* 341.1386 $[M + H]^+$ (calcd. for 341.1384) in the HRESI–MS spectrum (Appendix 1). The HRESI–MS/MS (Appendix 2), in positive mode, showed fragments at *m/z* 285.0758 $[M + H–C_4H_8]^+$, *m/z* 257.0809 $[M + H–C_5H_8O]^+$, *m/z* 229.0859 $[M + H–C_6H_8O_2]^+$, *m/z* 273.0757 $[M + H–C_5H_8]^+$,

m/z 211.0752 $[M + H–C_6H_{10}O_3]^+$. In the ^1H NMR spectrum (Table 4.1 and Appendix 3), two nonequivalent methyl protons at δ_H 1.89 (3H, s, H–12) and δ_H 1.71 (3H, s, H–11) along with an olefinic triplet at δ_H 5.39 (1H, t, *J* = 7.5 Hz, H–9) were observed suggesting the presence of an isoprenyl moiety. Methylene protons were observed as a doublet at δ_H 3.60 (2H, d, *J* = 7.5 Hz, H–8) in addition to an olefinic proton at δ_H 6.86 (1H, s, H–3) which appeared not fully resolved from an aromatic proton signal at δ_H 6.85 (1H, s, H–7). Furthermore, two equivalent aromatic protons at δ_H 6.79 (2H, d, *J* = 2 Hz, H–2′ and H–6′) and an aromatic proton as a triplet at δ_H 6.27 (1H, t, *J* = 2 Hz, H–4′) resulting from the *meta* coupling with H–2′/6′ indicated compound **1** was a 2-arylbenzofuran derivative. The spectrum showed a signal at δ_H 3.82 (3H, s, 4–MeO) typical of methoxy protons. The position of the methoxy group was confirmed by the presence of HMBC correlation (Figure 4.6) between the methoxy protons and δ_C 143.9 (C–4). Interpretation of HMBC correlations from 11–Me/12–Me to δ_C 16.7 (C– 12)/ δ_C 24.5 (C–11), δ_C 122.1 (C–9) and δ_C 131.5 (C–10) and δ_H 3.60 (H–8) to C–9, C–10, δ_C 143.9 (C–4), δ_C 118.3 (C–5) and δ_C 147.6 (C–6) established the connection of the isoprenyl group to the 2–arylbenzofuran moiety at C–5 and confirms the positions of the hydroxyl and methoxy groups at C–6 and C–4 respectively. The ^1H–^1H COSY NMR (Appendix 5) showed a proton spin system between δ_H 3.60 (H–8) and δ_H 5.39 (H–9), establishing the presence of the isoprenyl moiety in the structure. Finally, HMBC correlation from δ_H 6.86 (H–3) to δ_C 156.0 (C–2) and δ_C 132.4 (C–1′) and H–2′/H–6′ to C–1′ and C–2 further confirmed compound **1** to be a 2–arylbenzofuran derivative. Based on the analysis of 1D and 2D NMR data, the structure of compound **1** was unambiguously elucidated as 5–(6–hydroxy–4–methoxy–5–(3–methylbut–2–enyl)benzofuran–2–yl)benzene–3′,5′–diol and trivially named Regiafuran A.

KNUST

Table 4.1: NMR spectral data for Compound **1** in CD_3OD (see Appendix 3–7)

Position	δ_H[a] multi. (*J* in Hz)	δ_{Cb}	COSY[a]	HMBC[a]
2		156.0		
3	6.86, s	100.9		2, 3a, 4, 7a,1′
3a		124.6		
4		143.9		
5		118.3		
6		147.6		
7	6.85, s	103.2		3a, 5, 7a
7a		146.8		
8	3.60, d (7.5)	23.0	9	4, 5, 6, 9, 10
9	5.39 t, (7.5)	122.1	8	11, 12
10		131.5		
11	1.71, s	24.5		9, 10, 12

12	1.89, s	16.7		9, 10, 11
1′		132.4		
2′	6.79, d (2.0)	102.7		2, 1′, 3′, 4′, 6′
3′		158.5		
4′	6.27, t (2.0)	102.3	6′/2′	2′, 3′
5′		158.5		
6′	6.79, d (2.0)	102.7		2, 1′, 2′, 4′, 5′
4–MeO	3.82, s	60.2		4

[a]Recorded at 500 MHz; [b]Recorded at 125 MHz

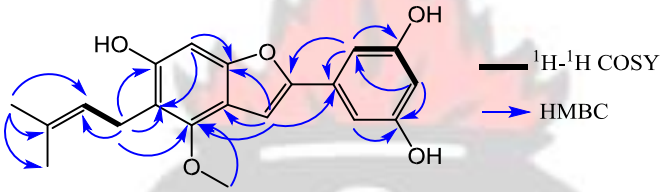


Figure 4.6: Selected HMBC and COSY correlations of compound **1**

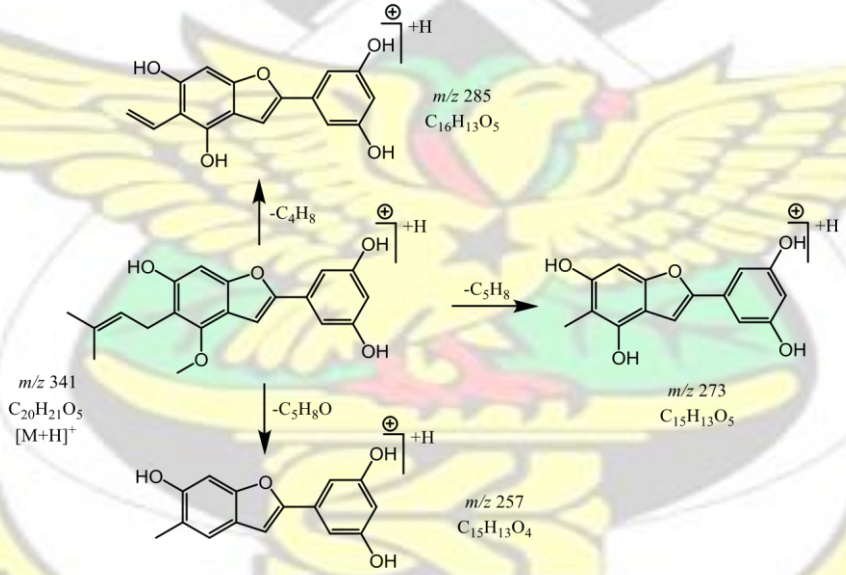


Figure 4.7: Proposed collision–induced mass spectral fragmentation pattern of compound **1** in positive ESI mode.

Regiafuran A (1): Yellow amorphous solid; LC–UV [MeOH–H_2O (0.1% HCOOH)] λ_{max} 318 nm. ^{1}H NMR (500 MHz in CD_3OD) and ^{13}C NMR (125MHz in CD_3OD) data, see Table 4.1.

Positive HRESI–MS: *m/z* 341.1386 $[M + H]^+$ (calcd. for $C_{20}H_{21}O_5$, 341.1384), *m/z* 363.1201 $[M + Na]^+$ (calcd. for $C_{20}H_{20}O_5Na$, 363.1203) (Kyekyeku *et al*., 2016).

4.1.2 Structure elucidation of Regiafuran B (2, new compound)

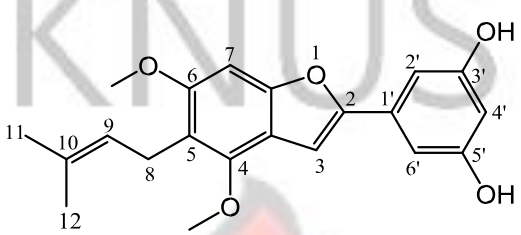


Figure 4.8: Chemical structure of compound **2**.

Regiafuran B (**2**) (Kyekyeku *et al*., 2016) was isolated as yellow amorphous solid with molecular formula of $C_{21}H_{22}O_5$ as determined by HRESI–MS spectrum (Appendix 8) showing a quasi-molecular ion peak at *m/z* 355.1541 $[M + H]^+$ (calcd. for 355.1540). The HRESI–MS/MS profile (Appendix 9), in positive mode, showed fragments at *m/z* 284.0681 [M + H–C_5H_{11}], *m/z* 299.0917 [M + H–C_4H_8], *m/z* 272.0680 [M + H–C_6H_{11}]. The ^{1}H (Table 4.2 and Appendix 10) and ^{13}C NMR spectra (Table 4.2 and Appendix 11) were comparable to that of compound **1** except for the appearance of an additional methoxy group signal at δ_H 3.85 (3H, s, 6–MeO). The attachment of the additional methoxy group to the 2– arylbenzofuran nucleus was determined by the presence of HMBC correlations (Figure 4.9) between δ_C 150.6 (C–6) and the methoxy protons; δ_H 6.95 (1H, s, H–7) and C–6. The difference in the structures indicates compounds **1** and **2** could share the same biosynthetic origin. The pseudo-molecular ions of **1** and **2** were identified in the HRESI–MS spectrum of the crude extract ruling out the possibility of them being artefacts of each other. Thus, the structure of compound **2** was concluded as 5–(4,6–dimethoxy–5–(3–methylbut–2–enyl)benzofuran–2–yl)benzene–3′,5′–diol and trivially named Regiafuran B.

KNUST

Table 4.2: NMR spectral data for Compound **2** in CD_3OD (see Appendix 10–14)

Position	δ_H[a] multi. (*J* in Hz)	δ_{Cb}	COSY[a]	HMBC[a]
2		156.4		
3	6.91, s	101.8		2, 3a, 4, 7a,1′
3a		124.6		
4		145.2		
5		119.1		
6		150.6		
7	6.95, s	100.8		3a, 5, 6, 7a
7a		148.3		
8	3.61, d (7.0)	23.3	9	4, 5, 6, 9, 10
9	5.36, t (7.0)	122.3	8	11, 12
10		131.9		
11	1.69, s	24.9		9, 10, 12
12	1.88, s	17.1		9, 10, 11
1′		132.8		
2′	6.82, d (2.5)	103.2		2, 1′, 3′, 4′, 6′

3′		159.0		
4′	6.31, t (2.0)	102.8	6′/2′	2′, 3′
5′		159.0		
6′	6.82, d (2.5)	103.2		2, 1′, 2′, 4′, 5′
4–MeO	3.81, s	60.7		4
6–MeO	3.85, s	55.6		6

[a]Recorded at 500 MHz; [b]Recorded at 125 MHz

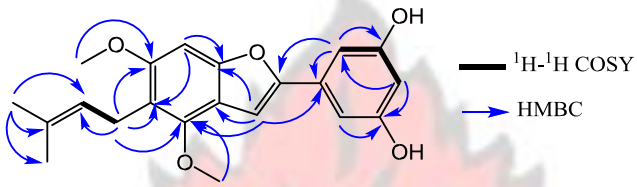


Figure 4.9: Selected HMBC and COSY correlations of compound **2**

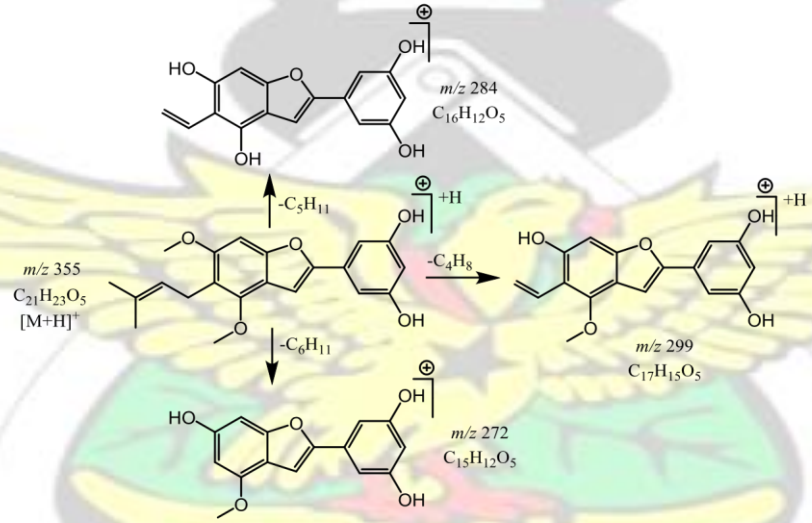


Figure 4.10: Proposed collision–induced mass spectral fragmentation pattern of compound **2** in positive ESI mode.

Regiafuran B (2): Yellow amorphous solid; LC–UV [MeOH–H_2O (0.1% HCOOH)] λ_{max} 316 nm. ^{1}H NMR (500 MHz in CD_3OD) and ^{13}C NMR (125 MHz in CD_3OD) data, see Table 4.2. Positive HRESI–MS: *m/z* 355.1541 $[M + H]^+$ (calcd. for $C_{21}H_{23}O_5$, 355.1540) data, *m/z* 377.1358 $[M + Na]^+$ (calcd. for $C_{21}H_{22}O_5Na$, 377.1359) (Kyekyeku *et al.*, 2016).

4.1.3 Structure elucidation of Regiafuran C (3, new compound)

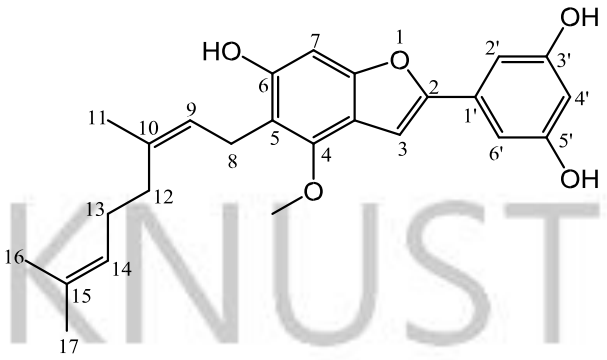


Figure 4.11: Chemical structure of compound **3**.

Regiafuran C (**3**) (Kyekyeku *et al*., 2016) was obtained as yellow oil with a molecular formula of $C_{25}H_{28}O_5$, determined by HRESI–MS (Appendix 15), in which a quasi-molecular ion peak was shown at *m/z* 409.2009 $[M + H]^+$ (calcd. for 409.2010). The HRESI–MS/MS fragmentation, in positive mode, resulted in a spectrum (Appendix 16) with ions at *m/z* 285.0760 $[M + H–C_9H_{16}]^+$, *m/z* 229.0860 $[M + H–C_{11}H_{16}]^+$, *m/z* 257.0808 $[M + H–C_{10}H_{16}O]^+$, *m/z* 377.1747 $[M + H–CH_3OH]^+$, *m/z* 391.1903 $[M + H–H_2O]^+$ *m/z* 299.0913 $[M + H– C_8H_{14}]^+$. The ^{1}H NMR spectrum (Table 4.3 and Appendix 17) was closely related to that of mulberrofuran Y **(4)**. The ^{1}H NMR together with the HSQC spectrum (Appendix 20)

indicated the presence of three methyls at δ_H 1.92 (3H, s, H–11), δ_H 1.55 (3H, s, H–17) and δ_H 1.51 (3H, s, H–16); three methylene groups at δ_H 3.65 (2H, d, *J* = 6.0 Hz, H–8), δ_H 2.09 (2H, m, H–13) and δ_H 2.03 (2H, m, H–12); one olefinic proton typical of 2–arylbenzofuran derivatives at δ_H 6.88 (1H, s, H–3); four aromatic protons at δ_H 6.87 (1H, s, H–7), δ_H 6.80 (2H, d, *J* = 1.8 Hz, H–2′/6′) and δ_H 6.27 (1H, t, *J* = 2.4 Hz, H–4′); and one methoxy group at δ_H 3.84 (3H, s, 4–MeO). The ^{13}C NMR spectrum (Table 4.3 and Appendix 18) displayed 25 signals; the eleven carbons left after excluding the fourteen carbons corresponding to the 2– arylbenzofuran moiety, indicated that compound **3** was substituted by geranyl and methoxy moieties. The ^{13}C NMR spectrum was similar to that of **4**, except at δ_C 143.9 (C–4) and δ_C 118.4 (C–5). The apparent differences in chemical shifts observed at C–4 and C–5 were due to the differences in

substitution at these positions. The structure of compound **3** was finally confirmed by analysis of the HMBC spectrum (Appendix 21). The most important correlations establishing the structure were correlations of H–8 with C–4, C–5 and δ_C 147.6 (C–6) which clearly suggested **3** was an isomer of **4** with the geranyl and methoxy groups attached to C–5 and C–4 respectively. Compound **3** was successfully elucidated as 4– methoxy–5–geranyl–3′,5′,6–trihyroxy–2–arylbenzofuran and trivially named Regiafuran C.

Table 4.3: NMR spectral data for Compound **3** in CD_3OD (see Appendix 17–21)

Position	δ_H[a] multi. (*J* in Hz)	δ_{Cb}	COSY[a]	HMBC[a]
2		156.0		
3	6.88, s	100.9		2, 3a, 1′
3a		124.6		
4		143.9		
5		118.4		
6		147.6		
7	6.87, s	103.2		3a, 5, 7a
7a		146.8		
8	3.65, d (6.0)	22.9	9	4, 5, 6, 9, 10
9	5.41, tm	122.2	8	8, 11, 12
10		135.1		
11	1.92, s	15.1		9, 10, 12
12	2.03, m	39.4	13	9, 10, 11, 13, 14
13	2.09, m	26.2	12, 14	10, 12, 14, 15
14	5.03, tm	123.8	13	13, 16, 17
15		130.8		
16	1.51, s	16.3		14, 15, 17

17	1.55, s	24.4		14, 15, 16
1′		132.4		
2′	6.80, d (1.8)	102.7	4′	2, 3′, 4′, 6′
3′		158.6		
4′	6.27, t (2.4)	102.2	2′/6′	2′, 3′, 5′, 6′
5′		158.6		
6′	6.80, d (1.8)	102.7	4′	2, 2′, 4′, 5′
4–MeO	3.84, s	60.2		4

[a]Recorded at 600 MHz; [b]Recorded at 150 MHz

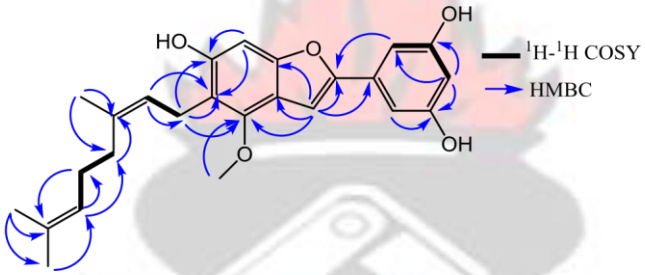


Figure 4.12: Selected HMBC and COSY correlations of compound **3**

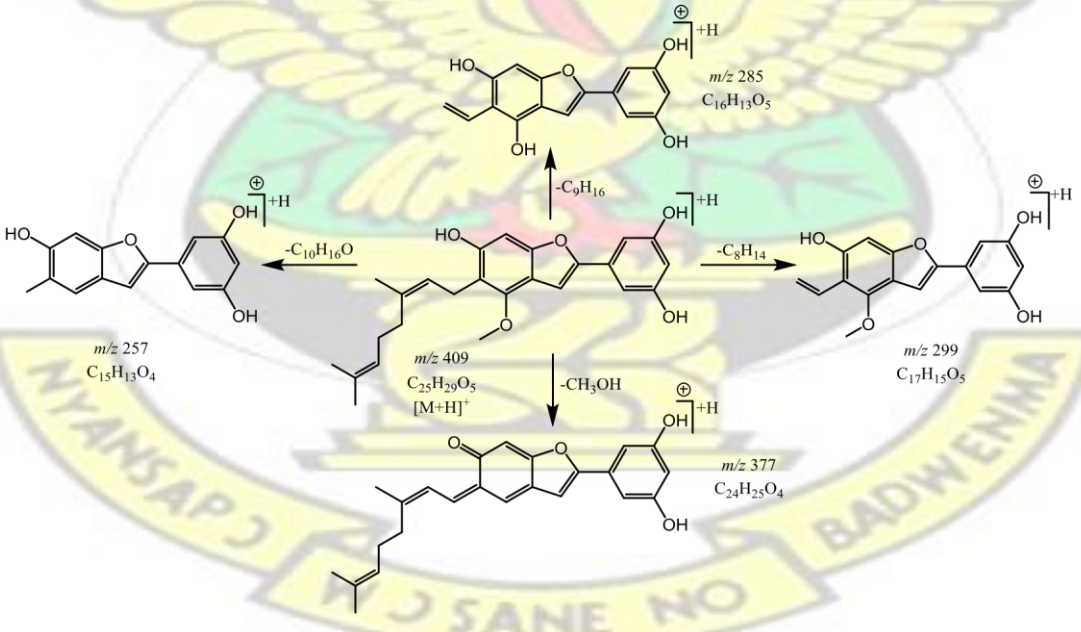


Figure 4.13: Proposed collision–induced mass spectral fragmentation pattern of compound **3** in positive ESI mode.

KNUST
NYANSAPO SANE NO BADWENIMA

Regiafuran C (3): Yellow oil; LC–UV [MeOH–H_2O (0.1% HCOOH)] λ_{max} 318 nm. ^{1}H NMR (600 MHz in CD_3OD) and ^{13}C NMR (150 MHz in CD_3OD) data, see Table 4.3. Positive HRESI–MS: *m/z* 409.2009 $[M + H]^+$ (calcd. for $C_{25}H_{29}O_5$, 409.2010), *m/z* 431.1827 $[M + Na]^+$ (calcd. for $C_{25}H_{28}O_5Na$, 431.1829) (Kyekyeku *et al*., 2016).

KNUST

4.1.4 Structure elucidation of mulberrofuran Y (4, known compound)

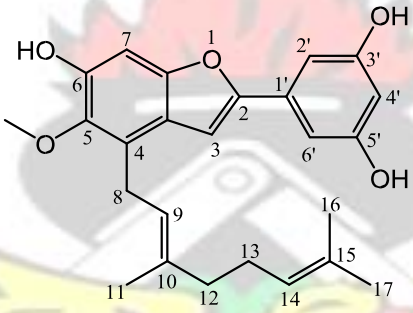


Figure 4.14: Chemical structure of compound **4**.

Mulberrofuran Y (**4)** was isolated as yellow oil with a molecular formula of $C_{25}H_{28}O_5$ as determined by HRESI–MS (Appendix 22), in which a pseudo–molecular ion peak was shown at *m/z* 409.2009 $[M + H]^+$ (calcd. for 409.2010). HRESI–MS/MS fragmentation (Appendix 23), in positive mode, gave fragments similar to that of compound **3** with the same base peak at *m/z* 285.0759 $[M + H–C_9H_{16}]^+$. Further fragments appeared at *m/z* 229.0859 $[M + H– C_{11}H_{16}]^+$, *m/z* 257.0808 $[M + H–C_{10}H_{16}O]^+$, *m/z* 377.1744 $[M + H–CH_3OH]^+$ and *m/z* 299.0913 $[M + H–C_8H_{14}]^+$. The ^{1}H NMR spectrum (Table 4.4 and Appendix 24) exhibited three methyl protons at δ_H 1.86 (3H, s, H–11), δ_H 1.57 (3H, s, H–17) and δ_H 1.55 (3H, s, H– 16); three methylene groups at δ_H 3.59 (2H, d, *J* = 6.5 Hz, H–8), δ_H 2.11 (2H, m, H–13) and δ_H 2.05 (2H, m, H–12); two olefinic protons at δ_H 5.29 (1H, t, *J* = 7.0 Hz, H–9) and δ_H 5.06 (1H, t, *J* = 6.5 Hz, H–14)

indicating the presence of a geranyl moiety. The presence of an olefinic proton signal at δ_H 6.90 (1H, s, H–3) and four aromatic protons at δ_H 6.87 (1H, s, H– 7), δ_H 6.76 (2H, d, *J* = 2.0 Hz, H–2′/6′), δ_H 6.26 (1H, t, *J* = 1.5 Hz, H–4′), with meta coupling (A_2M type) between H–4′ and H–2′/6′, suggested compound **4** had a 2–arylbenzofuran nucleus. Furthermore, protons of a methoxy group at δ_H 3.80 (3H, s, 5–MeO) were observed in the spectrum. The position of the geranyl moiety to the 2–arylbenzofuran nucleus was confirmed by the presence of HMBC correlations (Appendix 28) between H–8 and δ_C 121.2 (C–3a), δ_C 126.6 (C–4) and δ_C 142.8 (C–5) to be at position C–4. The methoxy group was also confirmed to be at position C–5 by observing HMBC correlations between the methoxy protons and C–5. The structure of compound **4** was unequivocally elucidated as 4–geranyl–5– methoxy–3′,5′,6–trihydroxy–2–arylbenzofuran trivially named as mulberrofuran Y. Mulberrofuran Y was first isolated from *Morus mongolica* (Moraceae) and has been reported to possess cytotoxic and anti-inflammatory activity (Shi *et al*., 2001; elov *et al*., 2014). This is the first report, however, of mulberrofuran Y in *C. regia*.

KNUST

KNUST

Table 4.4: NMR spectral data for compound **4** in CD_3OD (see Appendix 24–28)

Position	δ_H[a] multi. (*J* in Hz)	δ_{Cb}	COSY[a]	HMBC[a]
2		154.7		
3	6.90, s	100.3		2, 3a, 7a, 1′
3a		121.2		
4		126.6		
5		142.8		
6		148.7		
7	6.87, s	96.1		3a, 5, 6, 7a
7a		151.6		
8	3.59, d (6.0)	25.9	9	3a, 4, 5, 9, 10
9	5.29, t (7.0)	123.2	8	4, 8, 11, 12
10		135.1		
11	1.87, s	15.3		9, 10, 12
12	2.05, m	39.5	13	9, 10, 11, 13, 14
13	2.11, m	26.3	12, 14	10, 12, 14, 15
14	5.06, tm	124.0	13	12, 13, 16, 17
15		131.1		
16	1.55, s	16.5		14, 15, 17
17	1.57, s	24.6		14, 15, 16
1′		132.6		
2′	6.76, d (1.8)	102.7	4′	2, 3′, 4′, 6′

3′		158.7		
4′	6.26, t (2.4)	102.2	2′/6′	2′, 5′, 6′
5′		158.7		
6′	6.76, d (1.8)	102.7	4′	2, 2′, 4′, 5′
5–MeO	3.80, s	60.4		5

[a]Recorded at 500 MHz; [b]Recorded at 125 MHz

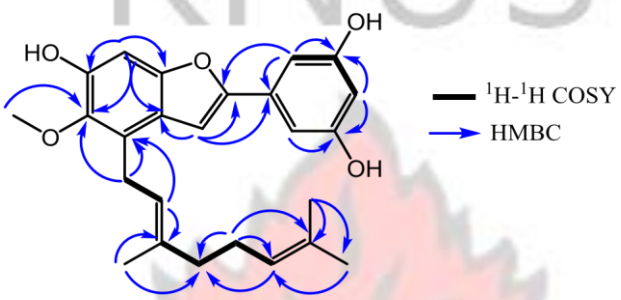


Figure 4.15: Selected HMBC and COSY correlations of compound **4**

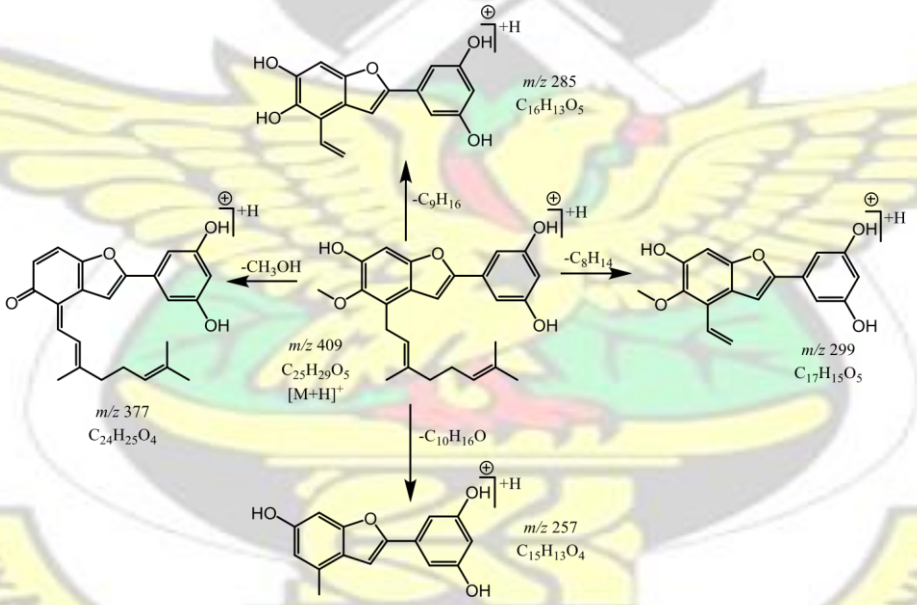


Figure 4.16: Proposed collision–induced mass spectral fragmentation pattern of compound **4** in positive ESI mode.

Mulberrofuran Y (4): Yellow oil; LC–UV [MeOH–H_2O (0.1% HCOOH)] λ_{max} 320 nm. ^{1}H NMR (500 MHz in CD_3OD) and ^{13}C NMR (125 MHz in CD_3OD) data, see Table 4.4.

Positive HRESI–MS: *m/z* 409.2009 $[M + H]^+$ (calcd. for $C_{25}H_{29}O_5$, 409.2010), *m/z* 431.1827 $[M + Na]^+$ (calcd. for $C_{25}H_{28}O_5Na$, 431.1829).

KNUST

4.1.5 Structure elucidation of moracin N (5, known compound)

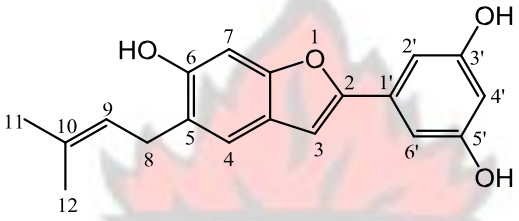


Figure 4.17: Chemical structure of compound **5**.

Compound **5** was obtained as yellow oil with molecular formula of $C_{19}H_{18}O_4$. HRESI–MS (Appendix 29), showed a pseudo-molecular ion peak at *m/z* 311.1278 $[M + H]^+$ (calcd. for 311.1279). The HRESI–MS/MS profile (Appendix 30), in positive mode, gave fragments at *m/z* 255.0652 $[M + H–C_4H_8]^+$, *m/z* 283.1328 $[M + H–CO]^+$, *m/z* 243.0652 $[M + H–C_5H_8]^+$, *m/z* 227.0703 $[M + H–C_5H_8O]^+$, *m/z* 202.0989 $[M + H–C_6H_5O_2]^+$. The ^1H (Table 4.5 and Appendix 31) and ^{13}C (Table 4.5 and Appendix 32) NMR spectra of compound **5** were similar to that of compound **1** with notable exception being the absence of a methoxy group signal and the presence of an aromatic proton signal at δ_H 7.12 (1H, s, H–4). In the ^1H NMR spectrum, two methyls were observed at δ_H 1.68 (3H, d, *J* = 1.2 Hz, H–11) and δ_H 1.65 (3H, br s, H–12) along with an olefinic proton signal at δ_H 5.29 (1H, tm, H–9) suggesting the presence of an isoprenyl moiety. In addition, another olefinic proton at δ_H 6.79 (1H, d, *J* = 0.6 Hz, H–3) and methylene protons at δ_H 3.27 (2H, br s, H–8) were also found. The remaining signals were aromatic protons at δ_H 6.81 (1H, br s, H–7), δ_H 6.67 (2H, d, *J* = 1.8 Hz, H–2'/6') and a triplet at δ_H 6.15 (1H, t, *J*

= 2.4 Hz, H–4') indicating compound **5** was a 2– arylbenzofuran derivative. Based on the analysis of the 2D NMR data and comparing the 1D

NMR data to reported literature, **5** was unambiguously elucidated as moracin N (Yang *et al*., 2012). This is the first report of moracin N in *C. regia*.

Table 4.5: NMR spectral data for Compound **5** in CD_3OD (see Appendix 31–35)

Position	δ_H[a] multi. (*J* in Hz)	δ_{Cb}	COSY[a]	HMBC[a]
2		156.0		
3	6.79, d (0.6)	102.5		2, 3a, 1′
3a		123.0		
4		121.7		3, 3a, 6, 7a, 8
5		126.5		
6		154.9		
7	6.81, br s	98.1		3a, 5, 7a
7a		155.9		
8	3.27, br s	29.8	9	4, 5, 6, 9, 10
9	5.29, tm	124.7	8	8, 11, 12
10		133.1		
11	1.68, d (1.2)	26.3		9, 10, 12
12	1.65, br s	18.1		9, 10, 11
1′		134.3		
2′	6.67, d (1.8)	104.1	4′	2, 3′, 4′, 6′
3′		160.2		
4′	6.15, t (2.4)	103.6	6′/2′	2′, 3′
5′		159.0		
6′	6.67, d (1.8)	104.1	4′	2, 1′, 2′, 4′, 5′

[a]Recorded at 600 MHz; [b]Recorded at 150 MHz

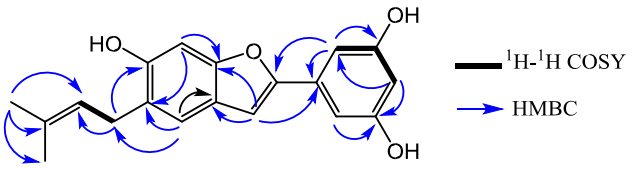


Figure 4.18: Selected HMBC and COSY correlations of compound **5**

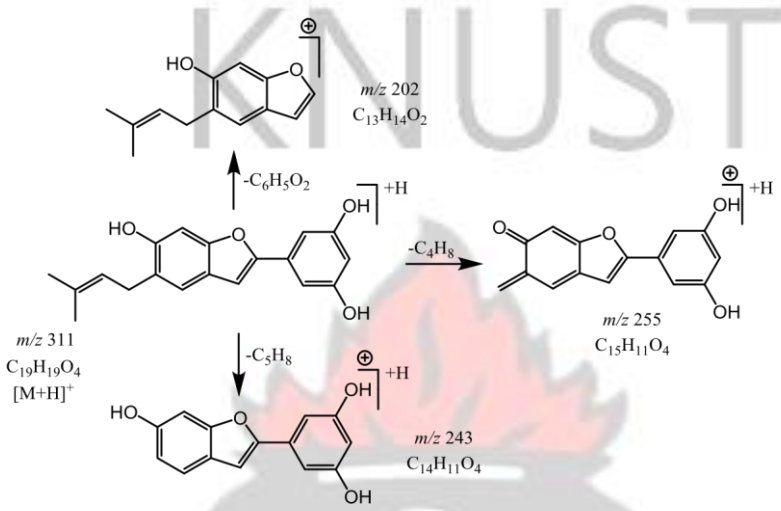


Figure 4.19: Proposed collision–induced mass spectral fragmentation pattern of compound **5** in positive ESI mode.

Moracin N (5): Yellow oil; LC–UV [MeOH–H_2O (0.1% HCOOH)] λ_{max} 320 nm. ^{1}H NMR (600 MHz in CD_3OD) and ^{13}C NMR (150 MHz in CD_3OD) data, see Table 4.5. Positive HRESI–MS: *m/z* 311.1278 $[M + H]^+$ (calcd. for $C_{19}H_{19}O_4$, 311.1279).

4.1.6 Structure elucidation of moracin O (6, known compound)

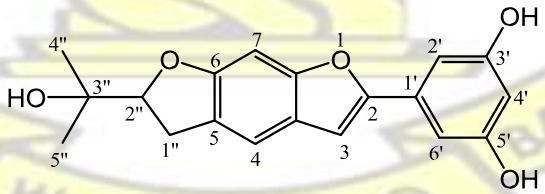


Figure 4.20: Chemical structure of compound **6**.

Compound **6** was brown amorphous solid with molecular formula $C_{19}H_{18}O_5$ based on the quasi-molecular ion *m/z* 327.1226 $[M + H]^+$ (calcd. for 327.1228) in the HRESI–MS spectrum

(Appendix 36). HRESI–MS/MS fragmentation, in positive mode, showed fragments at *m/z* 281.1172 $[M + H–CH_2O_2]^+$, *m/z* 255.0653 $[M + H–C_4H_8O]^+$, *m/z* 309.1121 $[M + H–H_2O]^+$, *m/z* 267.0651 $[M + H–C_3H_8O]^+$, *m/z* 239.0701 $[M + H–C_4H_8O_2]^+$, *m/z* 299.1275 $[M + H– CO]^+$. In the ^{1}H NMR spectrum (Table 4.6 and Appendix 38), a set of ABX type aromatic protons at δ_H 7.24 (1H, s, H–4), δ_H 6.80 (1H, s, H–7) along with an olefinic singlet at δ_H 6.84 (1H, s, H–3); another set of ABX coupling system at δ_H 6.69 (1H, d, *J* = 2.0 Hz, H–2′/6'), and triplet at δ_H 6.18 (1H, t, *J* = 2.0 Hz, H–4') were observed which were assigned to the 2– arylbenzofuran nucleus. Additionally, two nonequivalent methyl protons at δ_H 1.22 (3H, s, H– 4"), and δ_H 1.19 (3H, s, H–5"), methylene protons at δ_H 3.17 (2H, t, *J* = 6.5 Hz, H–1") and a triplet at δ_H 4.59 (1H, t, *J* = 9.0 Hz, H–2") were observed. The ^{13}C NMR (Table 4.6 and Appendix 39) and HSQC spectra (Appendix 41) revealed δ_H 125.4 (C–5) was a quaternary carbon and δ_H 160.2 (C–6) was a secondary carbon bonded to an oxygen functional group. The oxygen functionality was suspected to be an alcoholic moiety due to the loss of water observed at *m/z* 309.1121 in the HRESI–MS/MS spectrum. This indicated that the 2– arylbenzofuran moiety was substituted at C–5 and C–6. Analysis of the HMBC correlations (Appendix 42) confirmed the 2–arylbenzofuran moiety was substituted at C–5 and C–6 by tetrahydrofuran derivative. Important correlations indicating the tetrahydrofuran substitution were from H–4 to δ_H 31.5 (C–1"); H-1" to C–6, δ_H 91.7 (C–2") and δ_H 72.8 (C–3"); H–2" to δ_H 25.5 (C–5"). The structure of compound **6**, after comparing 1D NMR data to literature and by analysis of the 2D NMR spectra, was confirmed to be Moracin O (Ferrari *et al*., 1998). This is, however, the first report of moracin O in *C. regia*.

Table 4.6: NMR spectral data for Compound **6** in CD_3OD (see Appendix 38–42)

Position	δ_H[a] multi. (*J* in Hz)	δ_{Cb}	COSY[a]	HMBC[a]
2		156.6		
3	6.84, s	102.7		3a, 4, 7a, 1'
3a		124.3		
4	7.24, s	117.3		3, 6, 7a, 1"
5		125.4		
6		160.2		
7	6.80, s	93.5		3a, 5, 6, 7a
7a		156.7		
1′		134.1		
2′	6.69, d (2.0)	104.1	4′	2, 3', 4', 6'
3′		160.3		
4′	6.18, t (2.0)	26.3	2′/6′	2', 3'
5′		160.3		
6′	6.69, d (2.0)	104.1	4'	2, 2', 3', 4'
1″	3.17, t (6.5)	31.5	2"	5, 6, 2", 3"
2″	4.59, t (9.0)	91.7	1"	5"
3″		72.8		
4″	1.22, s	25.7		2", 3", 5"
5″	1.19, s	25.5		2", 3", 4"

[a]Recorded at 500 MHz; [b]Recorded at 125 MHz

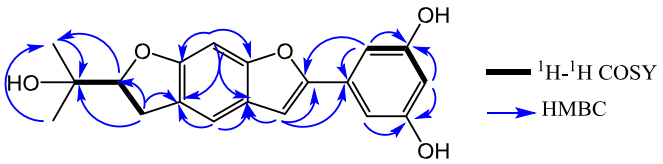


Figure 4.21: Selected HMBC and COSY correlations of compound **6**

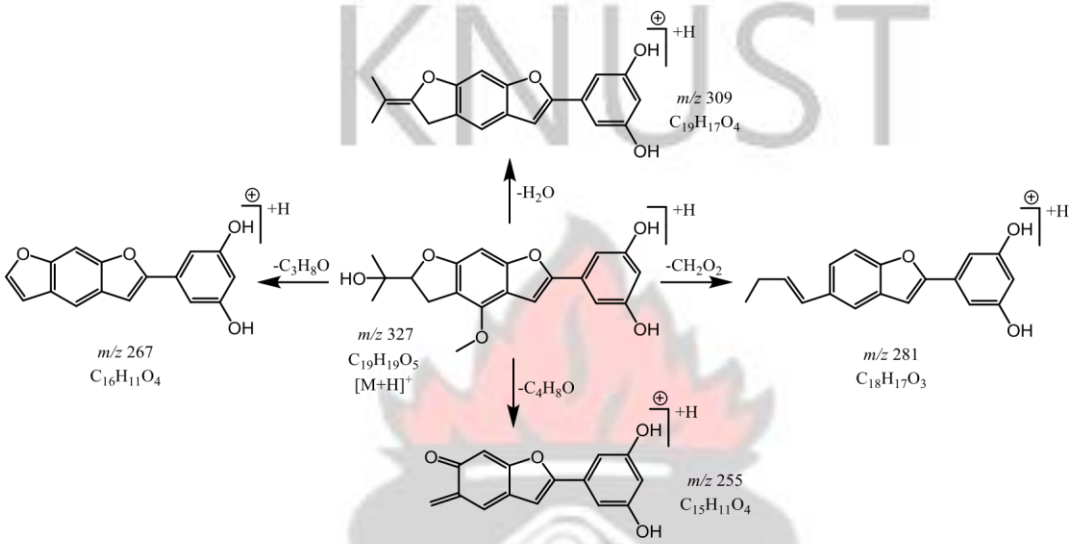


Figure 4.22: Proposed collision–induced mass spectral fragmentation pattern of compound **6** in positive ESI mode.

Moracin O (6): Brown amorphous solid; LC–UV [MeOH–H_2O (0.1% HCOOH)] λ_{max} 324 nm. ^{1}H NMR (500 MHz in CD_3OD) and ^{13}C NMR (125 MHz in CD_3OD) data, see Table 4.6. Positive HRESI–MS: *m/z* 327.1226 $[M + H]^+$ (calcd. for $C_{19}H_{19}O_5$, 327.1228), *m/z* 349.1047 $[M + Na]^+$ (calcd. for $C_{19}H_{18}O_5Na$, 349.1049).

4.1.7 Structure elucidation of sanggenon C (7, known compound)

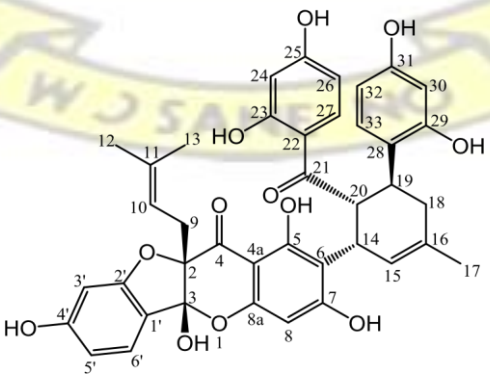


Figure 4.23: Chemical structure of compound **7**.

Compound **7** was obtained as yellow amorphous solid with molecular formula of $C_{40}H_{36}O_{12}$, HRESI–MS (Appendix 43), showed a pseudo–molecular ion at *m/z* 709.2283 $[M + H]^+$ (calcd. for 709.2279). The HRESI–MS/MS study of the **7** produced fragments at *m/z* 641.1646 $[M + H–C_5H_8]^+$, *m/z* 623.1542 $[M + H–C_5H_8\text{-}H_2O]^+$, *m/z* 339.1225 $[M + H–C_{20}H_{18}O_7]^+$, *m/z* 491.1332 $[M + H–C_{13}H_{14}O_3]^+$, *m/z* 573.2114 $[M + H–C_7H_4O_3]^+$. The ^{1}H NMR spectrum (Table 4.7 and Appendix 45) revealed signals typical of Diels–Alder type adducts. The spectrum showed three sets of ABX type aromatic protons at δ_H 6.79 (1H, d, *J* = 8.5 Hz, H– 33), δ_H 6.21 (1H, d, *J* = 1.5 Hz, H–30), δ_H 6.11 (1H, dd, *J* = 8.5, 2.0 Hz, H–32), δ_H 8.01 (1H, d, *J* = 9.0 Hz, H–27), δ_H 6.23 (1H, d, *J* = 2.5 Hz, H–26), δ_H 6.05 (1H, d, *J* = 2.5 Hz, H–24), δ_H 7.14 (1H, d, *J* = 8.5 Hz, H–6′), δ_H 6.35 (1H, dd, *J* = 8.5, 2.0 Hz, H–5′) and δ_H 6.24 (1H, d, *J* = 1.5 Hz, H–3′). Furthermore, protons of an isoprenyl group was observed at δ_H 1.51 (3H, s, H–12), 1.48 (3H, s, H–13), δ_H 2.94 (1H, dd, *J* = 14.5, 9.0 Hz, H–9a), δ_H 2.62 (1H, dd, *J* = 14.5, 6.0 Hz, H–9b) and δ_H 5.12 (1H, t, *J* = 6.5 Hz, H–10). The spectrum showed signals of a trisubstituted methylcyclohexene ring at δ_H 1.75 (3H, s, H–17), δ_H 2.32 (1H, dd, *J* = 17.5, 5.0 Hz, H–18a), δ_H 2.21 (1H, dd, *J* = 18.5, 4.5 Hz, H–18b), δ_H 4.10 (1H, br s, H–14), δ_H 3.80 (1H, dd, *J* = 13.5, 6.5 Hz, H–19), δ_H 4.42 (1H, t, *J* = 6.5 Hz, H–20) and an aromatic proton at δ_H 5.57 (1H, s, H–8). The ^{13}C NMR data (Table 4.7 and Appendix 46) and HMBC correlations (Appendix 49) indicated the methylcyclohexene ring was connected to δ_C 109.5 (C–6) through δ_C 34.3 (C–14) with further substitution at δ_C 49.1 (C–20) and δ_C 36.1 (C–19). Detailed analysis of the 1D and 2D NMR data and comparing to literature confirmed compound **7** to be sanggenon C (Shi *et al*., 2001). This is the first report of sanngenon C in *C. regia*.

Table 4.7: NMR spectral data for Compound **7** in CD_3OD (see Appendix 45–49)

Position	δ_H[a] multi. (*J* in Hz)	δ_C[b]	COSY[a]	HMBC[a]	
2		92.4			
3		103.7			
4		189.1			
4a		100.9			
5		161.7			
6		109.5			
7		168.4			
8		5.57, s	96.3	4a, 6, 7, 8	
8a		162.5			
9	a. 2.94, dd (14.5, 9.0)		32.7	10	2, 10, 11
	b. 2.62, dd (14.5, 6.0)				
10		5.12, t (6.5)	119.1	9	9, 12, 13
11		137.5			
12		1.51, s	18.4	10, 11, 13	
13		1.48, s	26.3	10, 11, 12	
14		4.10, br s	34.3	15, 20	
15		5.38, br s	123.4	14	14, 17, 20
16		134.9			
17		1.75, s	24.1	15, 16, 18	
18		2.32, dd (17.5, 5.0)	35.8	19	16, 20
	2.21, dd (18.5, 4.5)				
19		3.80, dd (13.5, 6.5)	36.1	18 29, 33	14, 16, 18, 20, 21, 28,
20		4.42, t (6.5)	49.1	14, 19	6, 14, 15, 18, 19, 21
21		209.2			
22		115.2			

23		166.3			
24		6.05, d (2.5)	103.7		22, 23, 25, 26
25		166.7			
26		6.23, d (2.5)	108.9	27	22
27		8.01, d (9.0)	135.1	26	21, 25
28		124.0			
29		157.2			
30		6.21, d (1.5)	104.2		28, 31, 32
31		157.7			
32		6.11, dd (8.5, 2.0)	107.8	33	28, 30, 31
33		6.79, d (8.5)	130.0	32	19, 29, 31
1′		121.9			
2′		161.8			
3′	6.24, d (1.5)	99.9		1', 4', 5'	
4′		161.8			
5′	6.35, dd (8.5, 2.0)	110.1	6′	1', 3', 4'	
6′		125.9	5′	2', 4'	

[a]Recorded at 500 MHz; [b]Recorded at 125 MHz

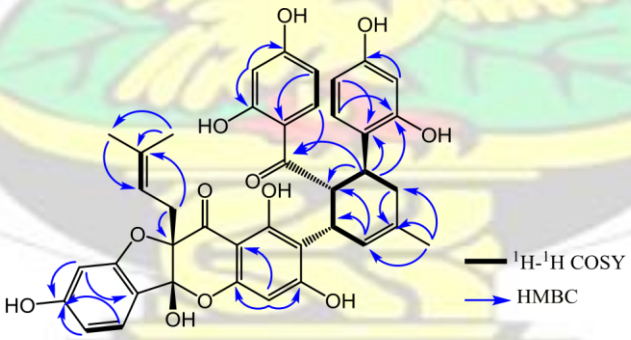


Figure 4.24: Selected HMBC and COSY correlations of compound **7**

KNUST
NYANSAPOW SANE NO BADWENHWA

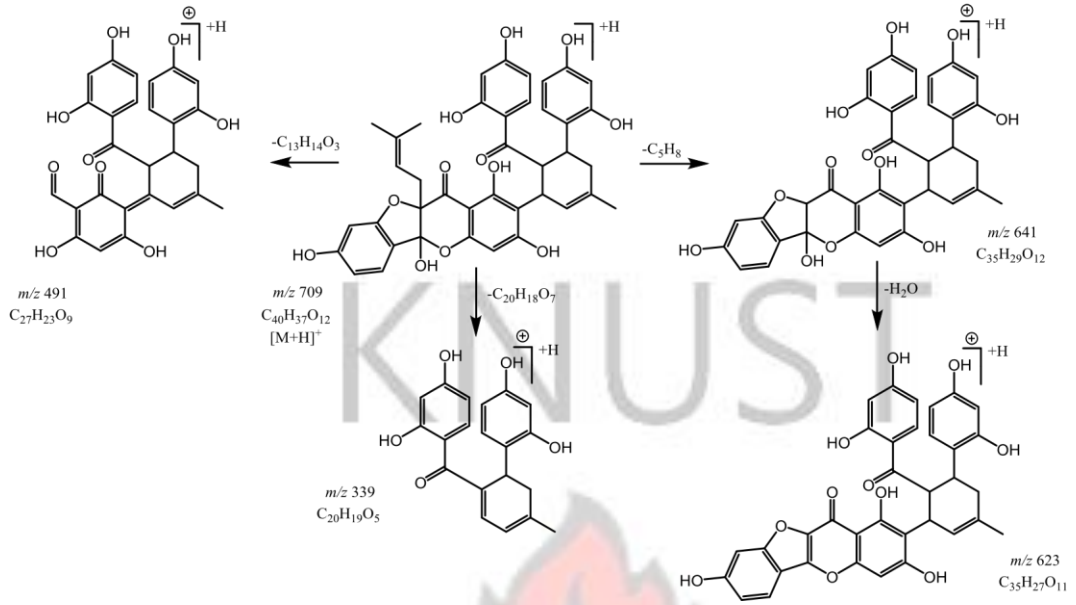


Figure 4.25: Proposed collision–induced mass spectral fragmentation pattern of compound **7** in positive ESI mode.

Sanggenon C (7): Yellow amorphous solid; LC–UV [MeOH–H_2O (0.1% HCOOH)] λ_{max} 284 and 310 nm. ^{1}H NMR (500 MHz in CD_3OD) and ^{13}C NMR (125 MHz in CD_3OD) data, see Table 4.7. Positive HRESI–MS: *m/z* 709.2283 $[M + H]^+$ (calcd. for $C_{40}H_{37}O_5$, 709.2279), *m/z* 731.2099 $[M + Na]^+$ (calcd. for $C_{40}H_{36}O_{12}Na$, 731.2097).

4.1.8 Structure elucidation of kuwanol E (8, known compound)

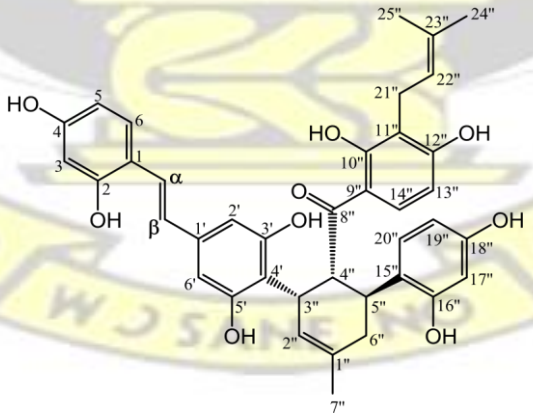


Figure 4.26: Chemical structure of compound **8**.

Compound **8** was isolated as yellow amorphous solid and the molecular formula was assigned as $C_{39}H_{38}O_9$ based on the ion *m/z* 651.2592 $[M + H]^+$ (calcd. for 651.2590) in the HRESI–MS

spectrum (Appendix 50). The HRESI–MS/MS, in positive mode, gave fragment ions at *m/z* 407.1853 [M + H–$C_{14}H_{12}O_4$]$^+$, *m/z* 271.1329 [M + H–$C_{22}H_{20}O_6$]$^+$, *m/z* 205.0861 [M + H–$C_{27}H_{26}O_6$]$^+$, *m/z* 473.1599 [M + H–$C_{11}H_{14}O_2$]$^+$, *m/z* 633.2476 [M + H–H_2O]$^+$. Similar to compound **7**, the ^{1}H NMR spectrum (Table 4.8 and Appendix 52) of **8** showed signals typical of Diels–Alder type adducts. Two sets of ABX type aromatic protons were observed at δ_H 7.21 (1H, d, *J* = 9.0 Hz, H–6), δ_H 6.29 (1H, d, *J* = 3.5 Hz, H–3), δ_H 6.22 (1H, d, *J* = 2.5 Hz, H–5), δ_H 6.86 (1H, d, *J* = 8.5 Hz, H–20″), δ_H 6.27 (1H, d, *J* = 3.0 Hz, H–17″) and δ_H 6.16 (1H, dd, *J* = 8.5, 2.5 Hz, H–19″). Also observed were four aromatic protons at δ_H 8.28 (1H, d, *J* = 9.0 Hz, H–14″), δ_H 6.21 (1H, d, *J* = 2.0 Hz, H–13″), δ_H 6.33 (2H, s, H–2′/6′) and olefinic protons at δ_H 7.12 (1H, d, *J* = 16.5 Hz, H–α), δ_H 6.66 (1H, d, *J* = 16.5 Hz, H–β). In addition, the spectrum indicated the presence of an isprenyl moiety with proton signals at δ_H 5.11 (1H, t, *J* = 7.0 Hz, H–22″), δ_H 3.18 (2H, d, *J* = 7.0 Hz, H–21″), δ_H 1.67 (1H, s, H–24″) and δ_H 1.56 (1H, s, H–25″). Proton signals of the trisubstituted methylcyclohexene ring were observed at δ_H 5.65 (1H, br s, H–2″), δ_H 4.47 (1H, t, *J* = 5.0 Hz, H–4″), δ_H 3.96 (1H, br s, H–3″), δ_H 3.62 (1H, m, H–5″), δ_H 2.39 (1H, d, *J* = 18.0 Hz, H–6″a), δ_H 2.09 (1H, d, *J* = 18.0 Hz, H–6″b) and δ_H 1.85 (1H, s, H–7″). The ^{13}C NMR spectrum (Table 4.8 and Appendix 53) showed signals confirming **8** was a Diels–Alder type adduct. Based on the analyses of the 1D, 2D and comparing the data to reported literature, the structure of **8** was elucidated as kuwanol E (Hano *et al*., 1989). This is the first report of kuwanol E in *C. regia*.

Position	δ_H[a] multi. (*J* in Hz)	δ_C[b]	COSY[a]	HMBC[a]

Table 4.8: ^{1}H NMR spectral data for

1		118.3		
2		158.1		
3	6.29*, d (3.5)	103.8*	2	
4		159.4		
5	6.22**, d (2.5)	108.3**	6	1, 3, 4
6	7.21, d (9.0)	128.6	5	4, 5, α
α	7.12, d (16.5)	124.5	β	1, 6, 1′, β
β	6.66, d (16.5)	126.7	α	1, 1′, 6′, α
1′		140.0		
2′	6.33, s	107.0		3′, 4′, 6′, β
3′		157.9		
4′		116.0		
5′		157.9		
6′	6.33, s	107.0		4′, 5′, β
1″		134.2		
2″	5.65, br s	125.6	3″	4″, 6″, 7″
3″	3.96, br s	33.9	2″, 4″	
4″	4.47, t (5.0)	48.9	3″, 5″	2″, 3″, 5″, 6″, 8″, 15″
5″	3.62, m	37.4	4″, 6″	
6″	a. 2.39, d (18.0)	33.2	5″	1″, 2″, 5″, 7″, 15″
	b. 2.09, d (18.0)			
7″	1.85, s	24.1		1″, 2″, 6″
8″		210.6		
9″		114.1		
10″		164.9		
11″		116.5		
12″		164.1		
13″	6.21**, d (2.0)	108.6**	14″	9″, 11″

Compound **8** in CD_3OD (see Appendix 52–56)

KNUST

14″	8.28, d (9.0)	132.9	13″	8″, 9″, 12″
15″		123.1		
16″		157.5		
17″	6.27*, d (3.0)	103.9*		15″, 19″
18″		157.3		
19″	6.16, dd (8.5, 2.5)	107.5	20″	15″, 17″
20″	6.86, d (8.5)	129.2	19″	5″, 16″, 18″
21″	3.18, d (7.0)	22.7	22″	11″, 12″, 22″, 23″
22″	5.11, t, (7.0)	123.9	21″	21″, 24″, 25″
23″		132.1		
24″	1.67, s	18.2		22″, 23″, 25″
25″	1.56, s	26.2		22″, 23″, 24″

[a]Recorded at 500 MHz; [b]Recorded at 125 MHz; *Interchangeable

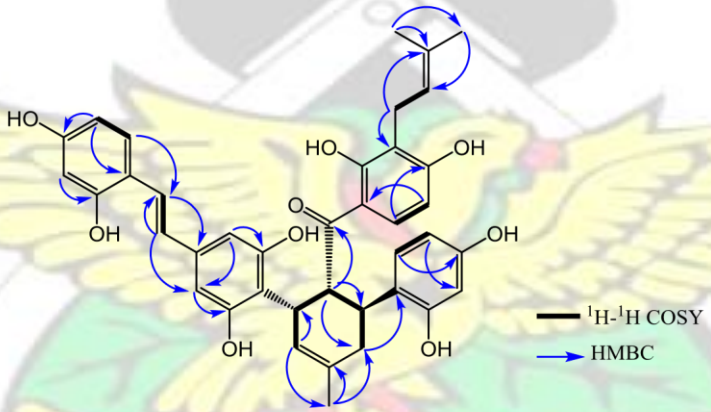


Figure 4.27: Selected HMBC and COSY correlations of compound **8**

KNUST

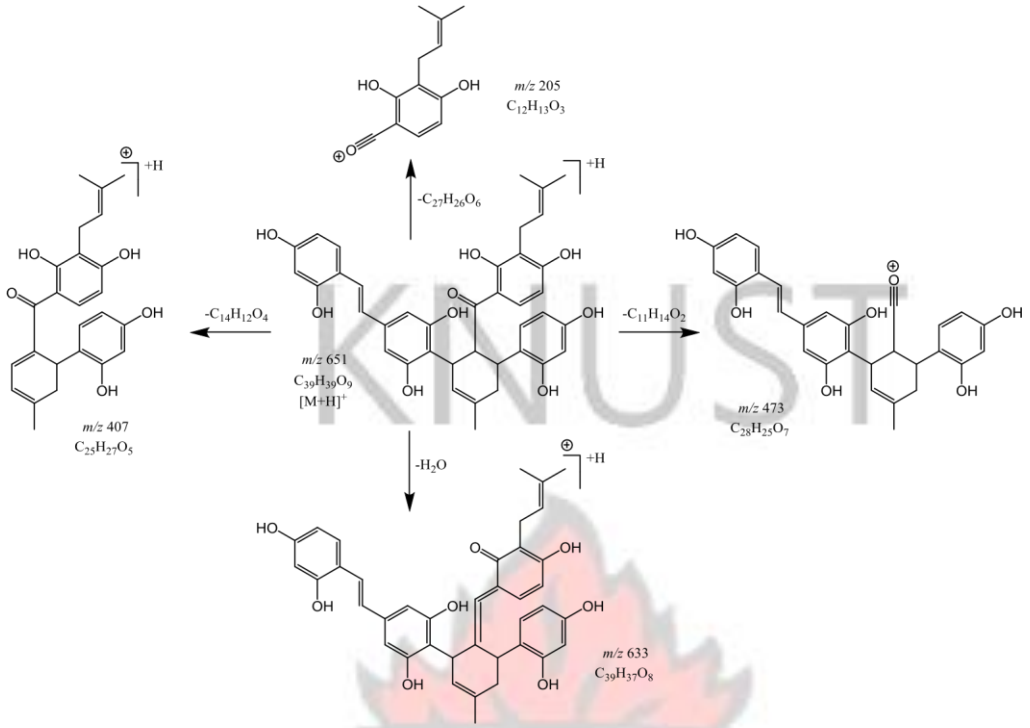


Figure 4.28: Proposed collision–induced mass spectral fragmentation pattern of compound **8** in positive ESI mode.

Kuwanol E (8): Yellow amorphous solid; LC–UV [MeOH–H_2O (0.1% HCOOH)] λ_{max} 294 and 328 nm. ^{1}H NMR (500 MHz in CD_3OD) and ^{13}C NMR (125 MHz in CD_3OD) data, see Table 4.8. Positive HRESI–MS: *m/z* 651.2592 $[M + H]^+$ (calcd. for $C_{39}H_{39}O_9$, 651.2590), *m/z* 673.2412 $[M + Na]^+$ (calcd. for $C_{39}H_{38}O_9Na$, 673.2010).

4.1.9 Structure elucidation of chalcomoracin (9, known compound)

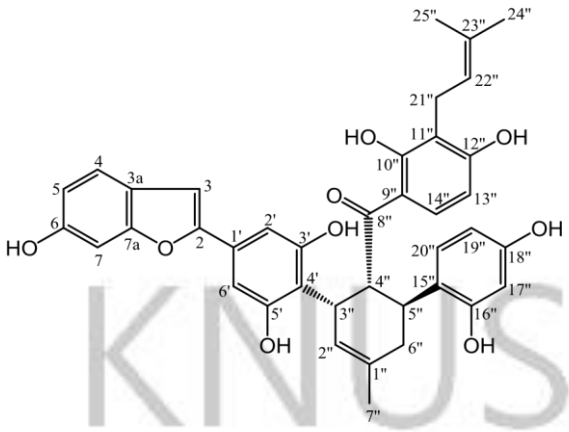


Figure 4.29: Chemical structure of compound **9**.

Compound **9** was yellow amorphous powder with a molecular formula of $C_{39}H_{36}O_9$ determined by HRESI–MS spectrum (Appendix 57) showing a pseudo-molecular ion at *m/z* 649.2437 $[M + H]^+$ (calcd. for 649.2439). The ^{1}H NMR spectrum (Table 4.9 and Appendix 59) were similar to that of compound **8** except for the absence of the olefinic proton signal at δ_H 6.66 and the broad singlet appearance at δ_H 6.84 (1H, br s, H–3) indicating H–3 was not closer to any proton. This observation together with the double bond equivalent (DBE) of twenty–two in **9** suggested the difference in structure between **8** and **9** was an additional ring system. The HRESI–MS/MS spectrum (Appendix 58) of **9** showed fragment losses similar to that of **8**. Detailed analysis of the ^{1}H NMR, HRESI–MS^n, comparing to reported literature confirmed compound **8** to be the Diels–Alder type adduct chalcomoracin (Takasugi *et al*., 1980). This is the first report of chalcomoracin in *C. regia*.

Table 4.9: NMR spectral data for Compound **9** in CD_3OD (at 500 MHz) (see Appendix 59)

Position	δ_H multi. (*J* in Hz)	Position	δ_H multi. (*J* in Hz)
3	6.76, br s	7″	1.86, s

4	7.24, d (8.5)	13″	6.29, d (2.5)
5	6.64, dd (8.0, 2.0)	14″	8.28, d (9.0)
7	6.79, br s	17″	6.27, d (3.5)
2′	6.64, s	19″	6.17, dd (8.5, 2.5)
6′	6.64, s	20″	6.87, d (8.5)
2″	5.66, s	21″	3.17, d (7.0)
3″	4.00, br s	22″	5.10, t, (7.0)
4″	4.50, br s	24″	1.66, s
5″	3.65, m	25″	1.55, s
6″	a. 2.40, d (18.0) b. 2.12, d (17.5)		

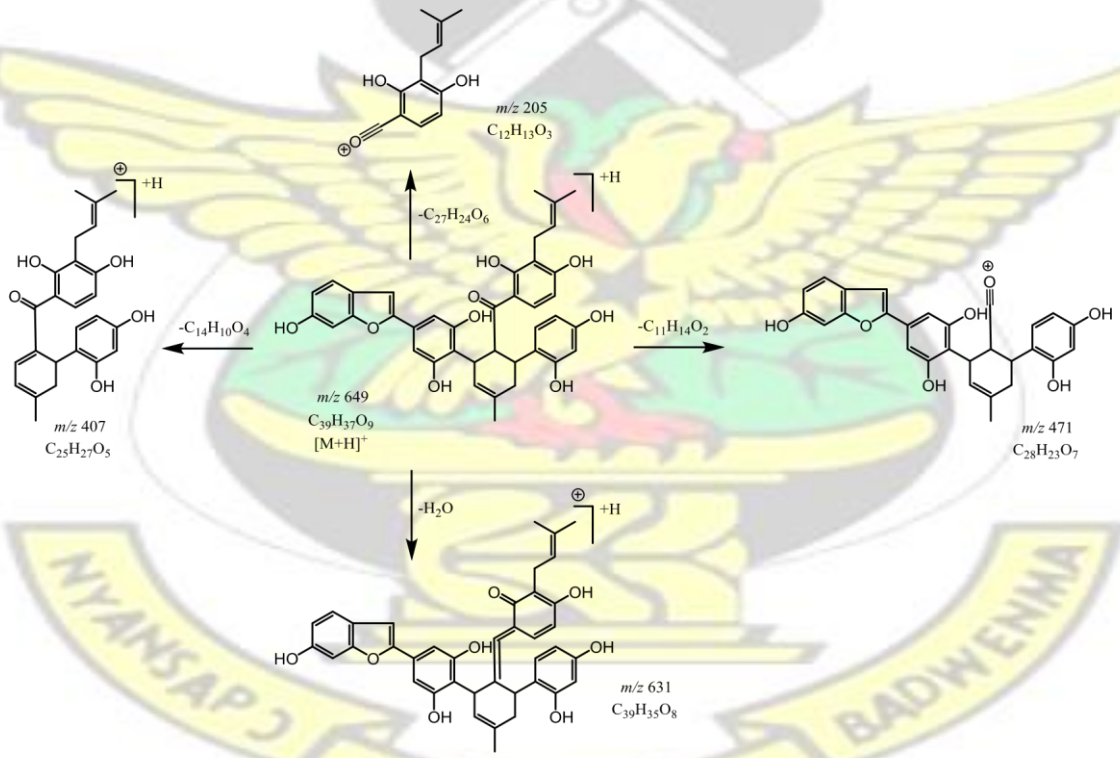


Figure 4.30: Proposed collision–induced mass spectral fragmentation pattern of compound **9** in positive ESI mode.

Chalcomoracin (9): Yellow amorphous solid; LC–UV [MeOH–H_2O (0.1% HCOOH)] λ_{max} 318 nm. ^{1}H NMR (500 MHz in CD_3OD) data, see Table 4.9. Positive HRESI–MS: *m/z*

649.2437 $[M + H]^+$ (calcd. for $C_{39}H_{37}O_9$, 649.2439), *m/z* 671.2256 $[M + Na]^+$ (calcd. for $C_{39}H_{36}O_9Na$, 671.2258).

4.1.10 Structure elucidation of chlorophorin (10, known compound)

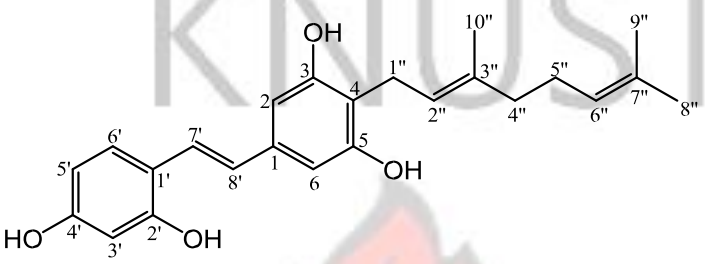


Figure 4.31: Chemical structure of compound **10**.

Compound **10** was obtained as a yellow amorphous solid. The molecular formula was assigned as $C_{24}H_{28}O_4$ based on the quasi–molecular ion peak at *m/z* 381.2061 $[M + H]^+$ (calcd. for 381.2060) in the HRESI–MS spectrum (Appendix 60). The fragmentation profile in the HRESI–MS/MS spectrum (Appendix 61) showed an abundant fragment at *m/z* 257.0808 $[M + H–C_9H_{16}]^+$ and further fragments at *m/z* 271.0963 $[M + H–C_8H_{14}]^+$ and *m/z* 239.0702 $[M + H–C_9H_{16}–H_2O]^+$. Analysis of the ^{1}H NMR spectrum (Table 4.10 and Appendix 62) revealed the presence of a symmetrically substituted aromatic ring at δ_H 6.39 (2H, br s, H–2/6), an ABX pattern aromatic protons at δ_H 7.23 (1H, d, *J* = 9.0 Hz, H–6′), δ_H 6.23 (1H, m, H–5′), δ_H 6.21 (1H, m, H–3′) and a *trans*–stilbene at δ_H 7.14 (1H, d, *J* = 16.8 Hz, H–7′), δ_H 6.69 (1H, d, *J* = 16.8 Hz, H–8′). Proton signals typical of a geranyl moiety were observed at δ_H 5.17 (1H, m, H–2″), δ_H 5.00 (1H, tm, H–6″), δ_H 1.99 (2H, m, H–5″), δ_H 3.28 (2H, d, *J* = 7.2 Hz, H–1″), δ_H 1.88 (2H, m, H–4″), δ_H 1.70 (3H, d, *J* = 12.6 Hz, H–10″), δ_H 1.55 (3H, br s, H–8″) and δ_H 1.49 (3H, br s, H–9″). The ^{13}C NMR spectrum (Table 4.10 and Appendix 63) together with HMBC correlations (Appendix 66) from H–1″ to δ_C 157.5 (C– 3/5) and δ_C 115.9 (C–4) confirmed the geranyl is connected to the symmetrically substituted aromatic ring at C–4. Based on the NMR data and comparing to reported data, the structure of

10 was elucidated as chlorophorin (Christensen *et al*., 1988). Chlorophorin is reported here from *C. regia* for the first time.

Table 4.10: NMR spectral data for Compound **10** in CD_3OD (see Appendix 62–66)

Position	δ_H[a] multi. (*J* in Hz)	δ_C[b]	COSY[a]	HMBC[a]
1		138.8		
2	6.39, br s	105.9		1, 3, 4, 6, 8′
3		157.5		
4		115.9		
5		157.5		
6	6.39, br s	105.9		1, 2, 4, 5, 8′
1′		118.4		
2′		157.4		
3′	6.21*, m	103.8		1′, 2′, 4′, 5′
4′		159.3		
5′	6.23*, m	108.6	6′	1′, 3′, 4′
6′	7.23, d (9.0)	128.5	5′	1′, 2′, 4′, 7′
7′	7.14, d (16.8)	124.0	8′	1, 1′, 2′, 6′, 8′
8′	6.69, d (16.8)	127.0	7′	1, 2, 6, 1′, 7′
1″	3.28, d (7.2)	23.5	2″	3, 4, 5, 3″
2″	5.17, tm	125.0	1″	4, 1″, 4″, 10″
3″		135.1		
4″	1.88, m	41.3	5″	2″, 3″, 5″, 10″
5″	1.99, m	28.1	4″, 6″	3″, 4″, 6″, 7″
6″	5.00, tm	125.9	5″	4″, 5″, 8″, 9″
7″		132.3		
8″	1.55, br s	26.2		6″, 7″, 9″
9″	1.49, br s	18.0		6″, 7″, 8″
10″	1.69, br s	16.6		2″, 3″, 4″

[a]Recorded at 600 MHz; [b]Recorded at 150 MHz; *Overlapping signals

KNUST

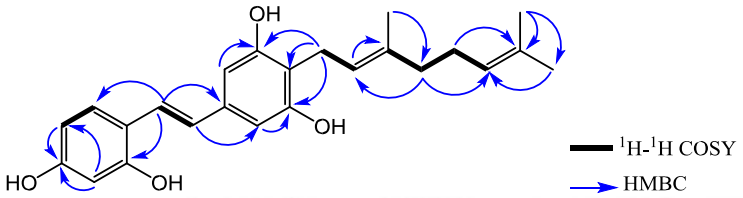


Figure 4.32: Selected HMBC and COSY correlations of compound **10**

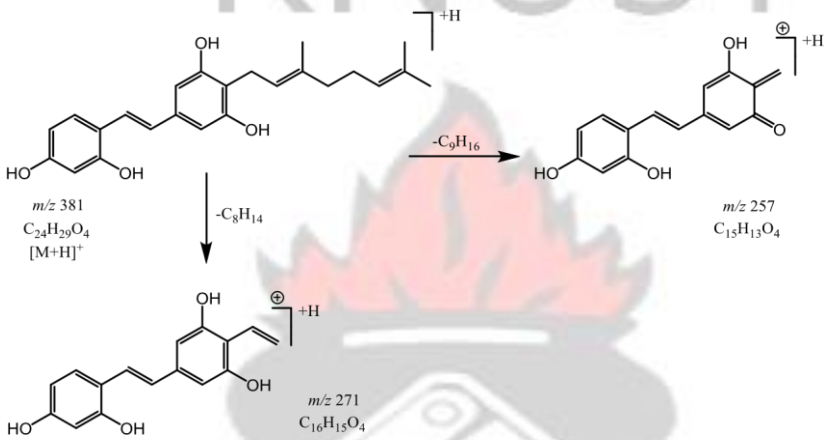


Figure 4.33: Proposed collision–induced mass spectral fragmentation pattern of compound **10** in positive ESI mode.

Chlorophorin (10): Yellow amorphous solid; LC–UV [MeOH–H_2O (0.1% HCOOH)] λ_{max} 328 nm. ^{1}H NMR (600 MHz in CD_3OD) and ^{13}C NMR (150 MHz in CD_3OD) data, see Table 4.10. Positive HRESI–MS: *m/z* 381.2061 $[M + H]^+$ (calcd. for $C_{24}H_{29}O_4$, 381.2060), *m/z* 403.1877 $[M + Na]^+$ (calcd. for $C_{24}H_{28}O_4Na$, 403.1875).

4.1.11 Structure elucidation of isochlorophorin (11, known compound)

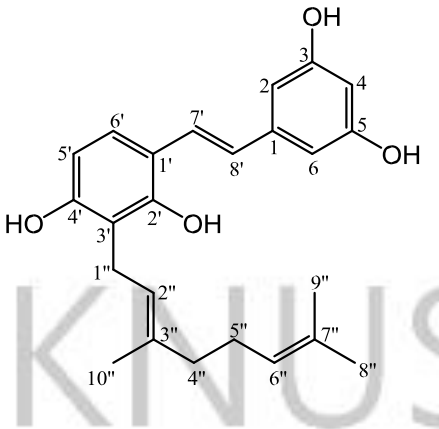


Figure 4.34: Chemical structure of compound **11**.

Compound **11** showed the same molecular formaula, $C_{24}H_{28}O_4$, as that of **10** in the HRESI– MS spectrum (Appendix 67). This indicated compounds **10** and **11** were isomers. The HRESI–MS/MS (Appendix 68) spectrum was closely related to that of 10 with the main fragment at *m/z* 257.0808 $[M + H–C_9H_{16}]^+$ and additional fragments at *m/z* 271.0963 $[M + H– C_8H_{14}]^+$ and *m/z* 239.0702 $[M + H–C_9H_{16}–H_2O]^+$. The ^{1}H NMR spectrum (Table 4.11 and Appendix 69) displayed signals and chemical shifts similar to the ^{1}H NMR spectrum of **10**. HMBC connectivities (Appendix 73) from δ_H 3.36 (2H, d, *J* = 7.2 Hz, H–1″) to δ_C 155.8 (C–4′), δ_C 153.3 (C–2′) and δ_C 116.3 confirmed the geranyl moiety was connected to C–3′. Compound **11** was thus elucidated as isochlorophorin (Maneechai *et al*., 2012). This is the first report of isochlorophorin in the genus *Chlorophora*.

Table 4.11: NMR spectral data for Compound **11** in CD_3OD (see Appendix 69–73)

Position	δ_H[a] multi. (*J* in Hz)	δ_{Cb}	COSY[a]	HMBC[a]

1		142.3		
2	6.38, d (2.4)	106.1	4	3, 4, 6, 8′
3		159.8		
4	6.06, t (2.4)	102.6	2, 6	2, 3, 5, 6
5		159.8		
6	6.38, d (2.4)	106.1	4	1, 2, 4, 5, 8′
1′		119.4		
2′		154.8		
3′		117.8		
4′		157.3		
5′	6.31, d (8.4)	109.4	6′	1′, 3′, 4′
6′	7.13, d (8.4)	125.1	5′	2′, 4′, 7′
7′	7.25, d (16.2)	125.3	8′	1, 1′, 2′, 6′, 8′
8′	6.67, d (16.2)	127.3	7′	1, 2, 6, 1′, 7′
1″	3.29, d (7.2)	23.7	2″	2′, 3′, 4′, 2″, 3″
2″	5.15, tm	124.6	1″	3′, 1″, 4″, 10″
3″		136.1		
4″	1.90, m	41.2	5″	2″, 3″, 5″, 6″, 10″
5″	1.99, m	28.0	4″, 6″	3″, 4″, 6″, 7″
6″	4.99, tm	125.7	5″	4″, 5″, 8″, 9″
7″		132.4		
8″	1.55, br s	26.2		6″, 7″, 9″
9″	1.49, br s	18.0		6″, 7″, 8″
10″	1.71, br s	16.6		2″, 3″, 4″

[a]Recorded at 600 MHz; [b]Recorded at 150 MHz

KNUST

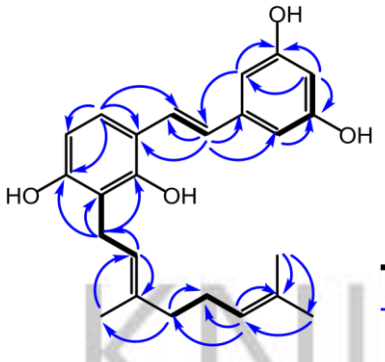


Figure 4.35: Selected HMBC and COSY correlations of compound **11**.

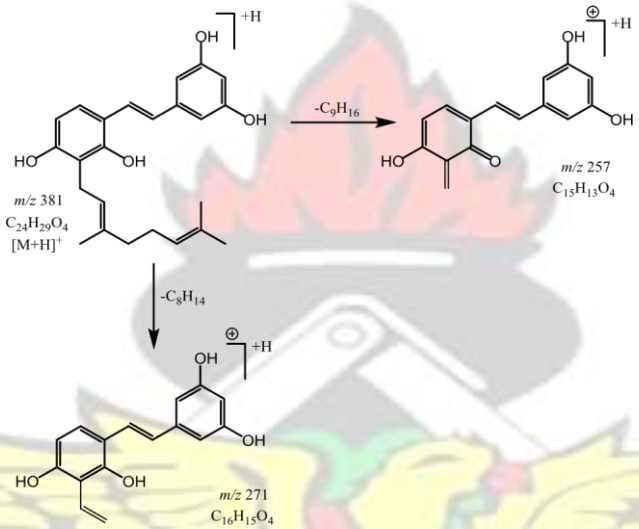


Figure 4.36: Proposed collision–induced mass spectral fragmentation pattern of compound **11** in positive ESI mode.

Isochlorophorin (11): Yellow amorphous solid; LC–UV [MeOH–H_2O (0.1% HCOOH)] λ_{max} 326 nm. ^{1}H NMR (600 MHz in CD_3OD) and ^{13}C NMR (150 MHz in CD_3OD) data, see Table 4.11. Positive HRESI–MS: *m/z* 381.2061 $[M + H]^+$ (calcd. for $C_{24}H_{29}O_4$, 381.2060), *m/z* 403.1877 $[M + Na]^+$ (calcd. for $C_{24}H_{28}O_4Na$, 403.1875).

4.1.12 Structure elucidation of 6–prenylated–3,7,5,4′–tetrahydroxy–2′–methoxyflavonol (12, new compound)

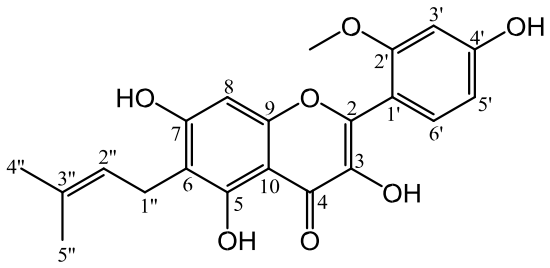


Figure 4.37: Chemical structure of compound **12**.

6–prenylated–3,7,5,4′–tetrahydroxy–2′–methoxyflavonol (**12**) (Kyekyeku *et al*., 2016) was isolated as yellow amorphous solid. The molecular formula was assigned as $C_{21}H_{20}O_7$ based on the quasi-molecular ion *m/z* 385.1284 $[M + H]^+$ (calcd. for 385.1282) in the HRESI–MS spectrum (Appendix 74). HRESI–MS/MS fragmentation, in positive mode, gave a principal fragment at *m/z* 329.0654 [M + H–C_4H_8] and an additional fragment at *m/z* 301.0704 [M + H–C_5H_8O]. Analysis of the ^{1}H NMR spectrum (Table 4.12 and Appendix 76) revealed the spectrum was comparable to that of compound **14** (Figure 4.42) except for the presence of methylene protons at δ_H 3.36 (2H, d, *J* = 7 Hz, H–1″), an olefinic proton at δ_H 5.16 (1H, t, *J* = 7 Hz, H–2″) and two methyl protons at δ_H 1.60 (3H, s, H–4″) and δ_H 1.61 (3H, s, H–5″). These signals typically indicated the presence of an isoprenyl group. The position of the isoprenyl group to the flavonol basic structure was confirmed to be at position δ_C 106.5 (C–6) based on the HMBC correlations (Appendix 80) between H–1″ and δ_C 155.2 (C–5), C–6 and δ_C 161.5 (C–7). The ^{13}C NMR spectrum (Table 4.12 and Appendix 77) was closely related to that of compound **14** with additional signals corresponding to the isoprenyl group. Compound **12** was thus successfully elucidated as 6–prenylated–3,7,5,4′–tetrahydroxy–2′– methoxyflavonol.

Table 4.12: NMR spectral data for Compound **12** in CD_3OD (see Appendix 76–80)

Position	δ_H[a] multi. (*J* in Hz)	δ_C[b]	COSY[a]	HMBC[a]
2		148.7		
3		136.6		

4		177.2		
5		155.2		
6		106.5		
7		161.5		
8	6.23, s	97.7		6, 7, 9, 10
9		159.1		
10		104.1		
1′		111.5		
2′		159.4		
3′	6.56, d (1.5)	93.3		1′, 2′, 4′, 5′
4′		161.3		
5′	6.50, dd (8.0, 2.0)	107.3	6′	1′, 3′, 4′, 6′
6′	7.36, d (8.0)	132.1	5′	2, 2′, 4′
1″	3.36, d (7.0)	21.3	2″	5, 6, 7, 2″, 3″
2″	5.16, t (7.0)	122.6	1″	6, 1″, 4″, 5″
3″		131.0		
4″	1.60, s	24.9		2″, 3″, 5″
5″	1.61, s	16.8		2″, 3″, 4″
2′–MeO	3.83, s	55.2		2′

[a]Recorded at 500 MHz; [b]Recorded at 125 MHz

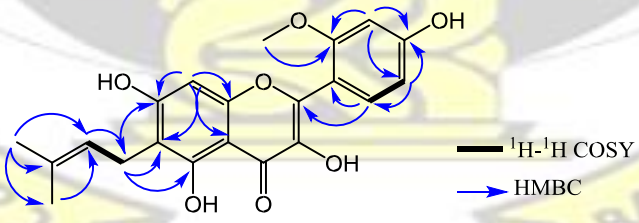


Figure 4.38: Selected HMBC and COSY correlations of compound **12**.

KNUST

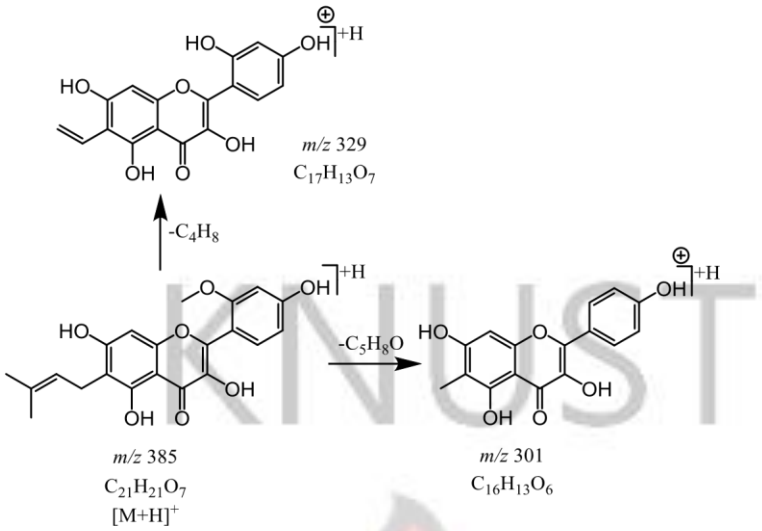
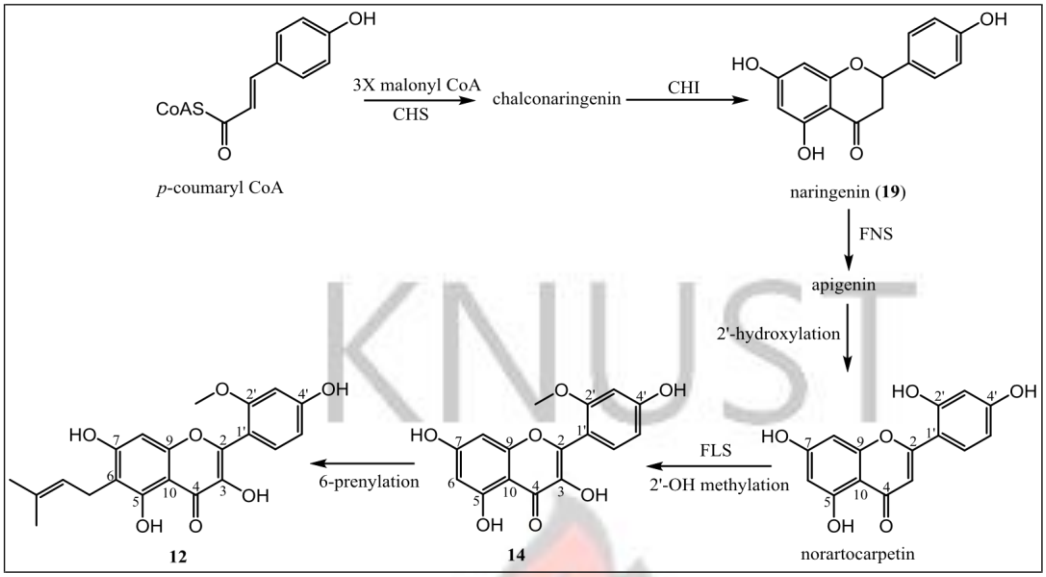


Figure 4.39: Proposed collision–induced mass spectral fragmentation pattern of compound **12** in positive ESI mode.

4.1.12.1 Proposed biosynthesis of compound 12

The biosynthesis of flavonoids in plants has been extensively investigated and documented (Koes *et al*., 1994; Turnbull *et al*., 2004; Maneechai *et al*., 2012). Based on the biosynthesis of flavonols, a tentative biosynthetic pathway of compound **12** was proposed (Scheme 1). The proposed biosynthetic pathway of **12** begins with the condensation of one molecule of *p*–coumaryl CoA and three molecules of malonyl CoA yielding chalconaringenin catalysed by the enzyme chalcone synthase (CHS). Chalconaringenin is converted to naringenin (**19**) by the enzyme chalcone isomerase (CHI). Through further enzyme catalysis, hydroxylation and methylation, naringenin is converted to 3,7,5,4′–tetrahydroxy–2′–methoxyflavonol (**14**). The final step involves prenylation of **14** at C–6 to form 6–prenylated–3,7,5,4′–tetrahydroxy–2′–methoxyflavonol (**12**).



Scheme 1: Proposed biosynthetic pathway of 6–prenylated–3,7,5,4′–tetrahydroxy–2′–methoxyflavonol (**12**) with (**14**) and (**19**) as intermediate metabolites. *CHS*, chalcone synthase; *CHI*, chalcone isomerase; *FNS*, flavones synthase; *FLS*, flavonol synthase.

6–prenylated–3,7,5,4′–tetrahydroxy–2′–methoxyflavonol (**12**): Yellow amorphous solid; LC–UV [MeOH–H_2O (0.1% HCOOH)] λ_{max} 358 nm. ^1H NMR (500 MHz in CD_3OD) and ^{13}C NMR (125 MHz in CD_3OD) data, see Table 4.12. Positive HRESI–MS: *m/z* 385.1284 $[M + H]^+$ (calcd. for $C_{21}H_{21}O_7$, 385.1282), *m/z* 407.1099 $[M + Na]^+$ (calcd. for $C_{21}H_{20}O_7Na$, 407.1101).

4.1.13 Structure elucidation of gancaonin P (13, known compound)

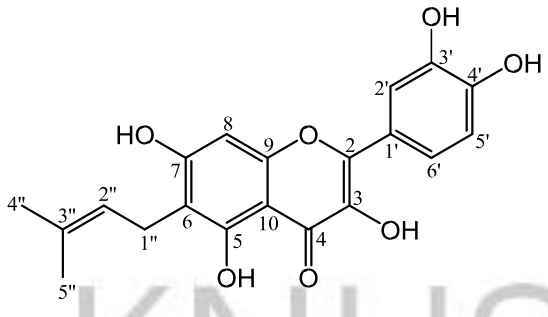


Figure 4.40: Chemical structure of compound **13**.

Compound **13** was yellow amorphous solid with molecular formula $C_{20}H_{18}O_7$ from the quasimolecular ion at *m/z* 371.1128 $[M + H]^+$ (calcd. for 371.1126) in the HRESI–MS spectrum (Appendix 81). HRESI–MS/MS spectrum (Appendix 82) showed a key fragment at *m/z* 315.0498 $[M + H–C_4H_8]^+$. The ^{1}H NMR spectrum (Table 4.13 and Appendix 83) was similar to that of compound **15** (Figure 4.44) with further signals revealing the presence of an isoprenyl moiety. The isoprenyl moiety was exhibited as an olefinic proton at δ_H 5.13 (1H, t, *J* = 6.6 Hz, H–2″), methylene protons at δ_H 3.40 (2H, d, *J* = 6.6 Hz, H–1″), two methyl protons at δ_H 1.70 (3H, s, H–5″) and δ_H 1.57 (3H, s, H–4″). Analysis of the ^{13}C NMR data (Table 4.13 and Appendix 84) and HMBC correlations (Appendix 87) from H–1″ to δ_C 155.7 (C–5), δ_C 108.0 (C–6) and δ_C 163.2 (C–7) confirmed the position of the isoprenyl moiety at C-6. Comparing the 1D and 2D NMR data to reported literature, the structure of compound **13** was elucidated as gancaonin P (Fukai *et al*., 1990). This is the first report of gancaonin P in the genus *Chlorophora*.

Table 4.13: NMR spectral data for Compound **13** in CD_3OD (see Appendix 83–87)

Position	δ_H[a] multi. (*J* in Hz)	δ_C[b]	COSY[a]	HMBC[a]

2		149.0		
3		137.3		
4		177.8		
5		155.7		
6		108.0		
7		163.2		
8	6.12, s	99.1		6, 7, 9, 10
9		160.3		
10		104.7		
1′		124.8		
2′	7.69, d (1.8)	116.6	6′	2, 1′ 3′, 4′, 6′
3′		146.6		
4′		148.3		
5′	6.77, d (8.4)	116.4	6′	1′, 3′, 4′
6′	7.51, dd (8.4, 1.8)	121.8	5′	2, 1′, 2′, 4′
1″	3.40, d (6.6)	22.8	2″	5, 6, 7, 2″, 3″
2″	5.13, t (6.6)	124.2	1″	6, 1″, 4″, 5″
3″		132.8		
4″	1.57, s	26.2		2″, 3″, 5″
5″	1.70, s	18.5		2″, 3″, 4″

[a]Recorded at 600 MHz; [b]Recorded at 150 MHz

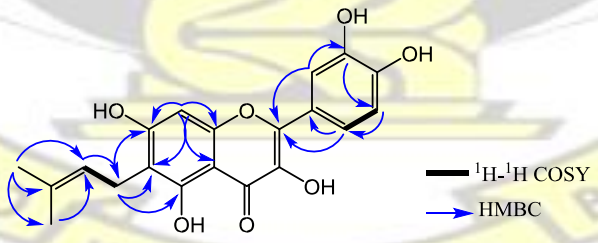


Figure 4.41: Selected HMBC and COSY correlations of compound **13**.

Gancaonin P (**13**): Yellow amorphous solid; LC–UV [MeOH–H_2O (0.1% HCOOH)] λ_{max} 378 nm. ^{1}H NMR (600 MHz in CD_3OD) and ^{13}C NMR (150 MHz in CD_3OD) data, see Table

4.13. Positive HRESI–MS: *m/z* 371.1128 $[M + H]^+$ (calcd. for $C_{20}H_{19}O_7$, 371.1126), *m/z* 393.0945 $[M + Na]^+$ (calcd. for $C_{20}H_{18}O_7Na$, 393.0947).

4.1.14 Structure elucidation of 3,7,5,4′–tetrahydroxy–2′–methoxyflavonol (14, known compound)

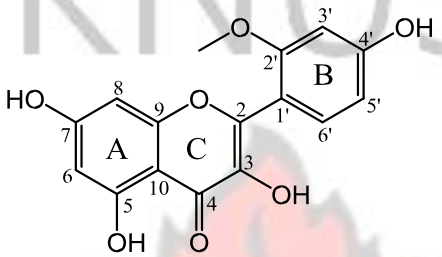


Figure 4.42: Chemical structure of compound **14**.

Compound **14** was obtained as yellow amorphous solid with a molecular formula of $C_{16}H_{12}O_7$ based on the pseudo-molecular ion at *m/z* 317.0657 $[M + H]^+$ (calcd. for 317.0656) in the HRESI–MS spectrum (Appendix 88). The ^1H NMR spectrum (Table 4.14 and Appendix 91) showed the presence of methoxy protons at δ_H 3.70 (3H, s, 2′–MeO), three aromatic protons attached to ring B at δ_H 7.23 (1H, d, *J* = 8.5 Hz, H–6′), δ_H 6.50 (1H, d, *J* = 2.0 Hz, H–3′), δ_H 6.45 (1H, dd, *J* = 8.5, 2.0 Hz, H–5′), and two aromatic protons attached to ring A at δ_H 6.27 (1H, d, *J* = 2.0 Hz, H–8), δ_H 6.17 (1H, d, *J* = 2.0 Hz, H–6). The position of the methoxy moiety was confirmed through HMBC correlation (Appendix 95) between the methoxy protons and δ_C 158.9 (C–2′). Based on detailed analysis of the 1D and 2D NMR and comparing to reported data, the structure of **14** was elucidated as 3,5,7,4′–Tetrahydroxy–2′– methoxyflavonol (Gonda *et al*., 2000; Kyekyeku *et al*., 2016). The HRESI–MS/MS fragmentation of **14** which had not been previously reported follows the fragmentation pattern typical of flavonol aglycones (Cuyckens and Claeys, 2004; Tsimogiannis *et al*., 2007). The main fragment was observed at *m/z* 261 $[M + H–2CO]^+$ which corresponds to a loss of two molecules of carbon monoxide. Subsequent losses of CH_3OH and CO was observed at *m/z* 257

[M + H–CH_3OH–CO]$^+$. Retro Diels–Alder (RDA) cleavage of the C–ring resulted in further fragments which are described based on the nomenclature of Ma *et al*. (Ma *et al*., 1997). Retrocyclization cleavage of the protonated molecule of **14** produced RDA fragments $^{0,2}A^+$ at *m/z* 165, $^{0,2}B^+$ at *m/z* 151, [$^{0,2}B^+$–CH_3] at 139, $^{1,3}A^+$ at *m/z* 153 and $^{1,3}B^+$ at *m/z* 163 (Figure 4.44).

Table 4.14: NMR spectral data for Compound **14** in DMSO-d_6 (see Appendix 91–95)

Position	δ_H[a] multi. (*J* in Hz)	δ_{Cb}	COSY[a]	HMBC[a]
2		148.6		
3		136.9		
4		176.9		
5		160.9		
6	6.17, d (2.0)	98.3		8, 10
7		163.8		
8	6.27, d (2.0)	93.7		6, 10
9		157.1		
10		103.8		
1′		110.7		
2′		158.9		
3′	6.50, d (2.5)	99.7		1′, 5′
4′		160.8		
5′	6.45, dd (8.5, 2.0)	107.4	6′	1′, 3′
6′	7.23, d (8.5)	132.2	5′	2, 2′, 4′
2′–MeO	3.70, s	55.9		2′

[a]Recorded at 500 MHz; [b]Recorded at 125 MHz

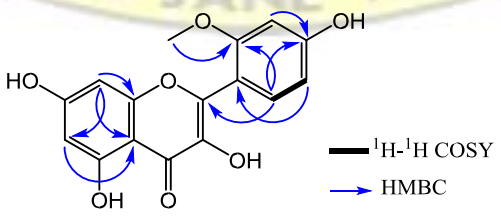


Figure 4.43: Selected HMBC and COSY correlations of compound **14**.

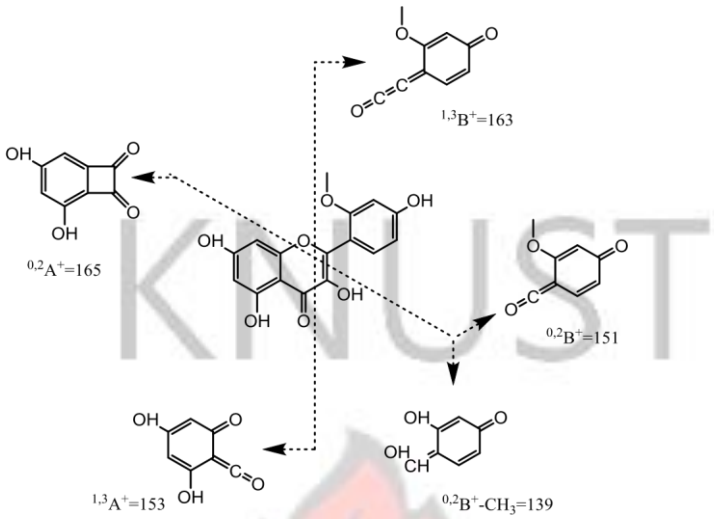


Figure 4.44: Retrocyclization cleavage of the C–ring of compound **14**.

3,7,5,4′–tetrahydroxy–2′–methoxyflavonol (**14**): Yellow amorphous solid; LC–UV [MeOH–H_2O (0.1% HCOOH)] λ_{max} 250 and 350 nm. ^{1}H NMR (500 MHz in DMSO–d_6) and ^{13}C NMR (125 MHz, DMSO–d_6) data, see Table 4.14. Positive HRESI–MS: *m/z* 317.0657 [M + H]$^+$ (calcd. for $C_{16}H_{13}O_7$, 317.0656), *m/z* 339.0478 [M + Na]$^+$ (cald. for $C_{16}H_{12}O_7Na$, 339.0475).

4.1.15 Structure elucidation of quercetin (15, known compound)

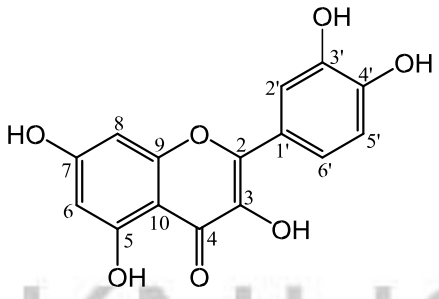


Figure 4.45: Chemical structure of compound **15**.

Compound **15** was isolated as yellow needles with a molecular formula of $C_{15}H_{10}O_7$, determined by HRESI–MS spectrum (Appendix 96) showing a quasi-molecular ion peak at *m/z* 303.0501 $[M + H]^+$ (calcd. for 303.0499). The ^{1}H NMR spectrum (Table 4.15 and Appendix 99) indicated the presence of two aromatic protons attached to ring A at δ_H 6.33 (1H, d, *J* = 2.0 Hz, H–8), δ_H 6.12 (1H, d, *J* = 2.0 Hz, H–6) and three aromatic protons attached to ring B at δ_H 7.67 (1H, d, *J* = 2.0 Hz, H–2′), δ_H 7.57 (1H, d, *J* = 2.0, 8.5 Hz H–6′), δ_H 6.83 (1H, d, *J* = 8.5 Hz, H–5′). The absence of higher upfield proton signals reveals there are no protons attached to ring C. The structure of **15** was concluded to be quercetin, after analysis of the ^{1}H and ^{13}C NMR data and comparing same to reported data (Zhou *et al*., 2013). HRESI– MS/MS fragmentation profile of **15**, expectedly, showed RDA fragments similar to that of **14** which are generally typical of flavonol aglycones (Tsimogiannis *et al*., 2007; Cuyckens and Claeys, 2004). Dehydration of the protonated molecular ion gave a peak at *m/z* 285 $[M + H– H_2O]^+$. Loss of water followed by a loss of carbon monoxide gave the principal fragment at *m/z* 257 $[M + H–H_2O–CO]^+$. A further loss of one molecule of carbon monoxide was observed at *m/z* 229 $[M + H–CH_3OH–2CO]^+$. RDA fragments observed following fission of the C–ring were $^{0,2}A^+$ at *m/z* 165, $^{1,3}A^+$ at *m/z* 153, $^{0,2}B^+$ at *m/z* 137 and $^{1,3}B^+$ at *m/z* 149 (Figure 4.46).

Table 4.15: NMR spectral data for Compound **15** in CD_3OD (see Appendix 99–100)

Position	δ_H[a] multi. (*J* in Hz)	δ_C[b]	Position	δ_H[a] multi. (*J* in Hz)	δ_C[b]
2		149.1	10		104.8
3		137.5	1′		124.5

4		177.6	2′	7.67, d (2.0)	116.3
5		162.8	3′		146.5
6	6.12, d (2.0)	99.6	4′		148.3
7		165.9	5′	6.83, d (8.5)	116.5
8	6.33, d (2.0)	94.7	6′	7.57, dd (8.5, 2.0)	122.0
9		158.5			

[a]Recorded at 500 MHz; [b]Recorded at 125 MHz

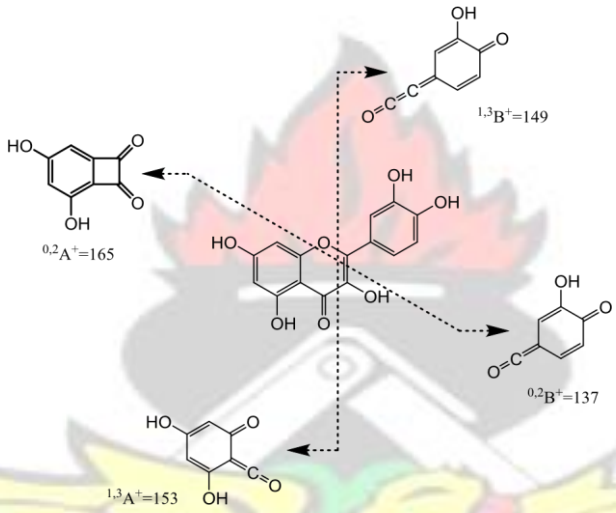


Figure 4.46: Retrocyclization cleavage of the C–ring of compound **15**.

Quercetin (15): Yellow needles; LC–UV [MeOH–H_2O (0.1% HCOOH)] λ_{max} 254 and 370 nm. ^1H NMR (500 MHz in CD_3OD) and ^{13}C NMR (125 MHz, CD_3OD) data, see Table 4.15.

Positive HRESI–MS: *m/z* 303.0501 $[M + H]^+$ (calcd. for $C_{15}H_{11}O_7$, 303.0499).

4.1.16 Structure elucidation of kaempferol (16, known compound)

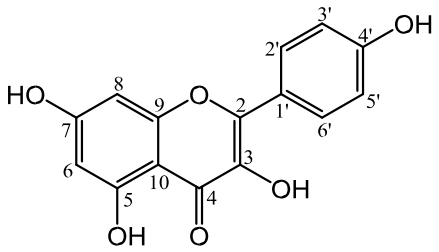


Figure 4.47: Chemical structure of compound **16**.

Compound **16** was obtained as yellow amorphous solid with a molecular formula of $C_{15}H_{10}O_6$, determined by HRESI–MS spectrum (Appendix 101) showing an ion at *m/z* 287.0550 $[M + H]^+$ (calcd. for 287.0550). In the ^1H NMR spectrum (Table 4.16 and Appendix 104), two aromatic protons assigned to ring A at δ_H 6.33 (1H, br s, H–8), δ_H 6.12 (1H, d, *J* = 1.5 Hz, H–6) and two sets of equivalent aromatic protons assigned to ring B at δ_H 8.02 (2H, d, *J* = 8.5 Hz, H–3′/5′), δ_H 6.85 (1H, d, *J* = 9.0 Hz, H–2′/6′) were observed. The structure of **16** was elucidated as kaempferol based on analysis of the ^1H and ^{13}C NMR data and in comparison with reported literature (Markham *et al*., 1978). The HRESI–MS/MS fragmentation of **16** produced fragments similar to that of **14** and **15** (Figure 4.48).

Table 4.16: NMR spectral data for Compound **16** in CD_3OD (see Appendix 104–105)

Position	δ_H[a] multi. (*J* in Hz)	δ_C[b]	Position	δ_H[a] multi. (*J* in Hz)	δ_C[b]
2		148.4	10		104.9
3		137.4	1′		124.0
4		177.7	2′	6.85, d (9.0)	131.0
5		162.8	3′	8.02, d (8.5)	116.6
6	6.12, d (1.5)	99.6	4′		160.8
7		165.9	5′	8.02, d (8.5)	116.6
8	6.33, br s	94.8	6′	6.85, d (9.0)	131.0
9		158.6			

[a]Recorded at 500 MHz; [b]Recorded at 125 MHz

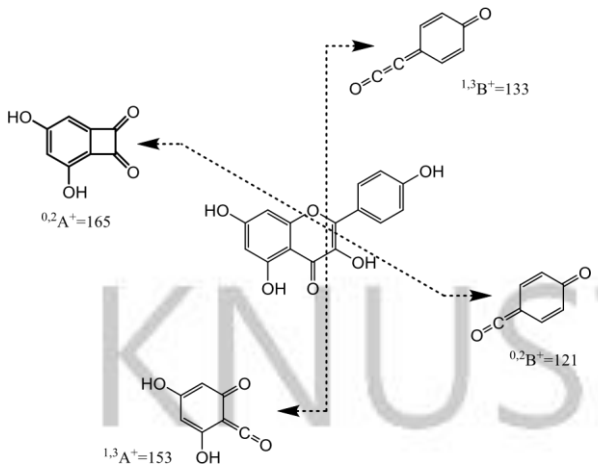


Figure 4.48: Retrocyclization cleavage of the C–ring of compound **16**.

Kaempferol (16): Yellow amorphous solid; LC–UV [MeOH-H_2O (0.1% HCOOH)] λ_{max} 265 and 366 nm. ^{1}H NMR (500 MHz in CD_3OD) and ^{13}C NMR (125 MHz, CD_3OD) data, see Table 4.16. Positive HRESI–MS: *m/z* 287.0550 $[M + H]^+$ (calcd. for $C_{15}H_{11}O_6$, 287.0550), *m/z* 309.0369 $[M + Na]^+$ (cald. for $C_{15}H_{10}O_6Na$, 309.0370).

4.1.17 Structure elucidation of 5,7,4′–trihydroxy–2′–methoxyflavanone (17, known compound)

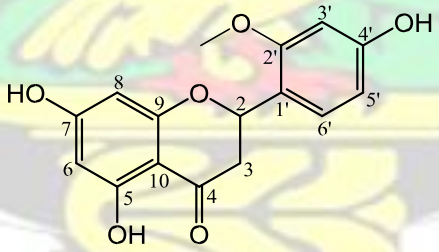


Figure 4.49: Chemical structure of compound **17**.

Compound **17** was obtained as yellow needles. The molecular formula was assigned as $C_{16}H_{14}O_6$ based on the quasi–molecular ion *m/z* 303.0864 $[M + H]^+$ (calcd. for 303.0863) in the HRESI–MS spectrum (Appendix 106). The presence of methoxy protons at δ_H 3.83 (3H, s, 2′–MeO) were observed in the ^{1}H NMR spectrum (Table 4.17 and Appendix 108). The spectrum further showed the presence of five aromatic protons, two were assigned to ring A at δ_H 5.83

(1H, d, *J* = 2.0 Hz, H–6), δ_H 5.81 (1H, d, *J* = 2.0 Hz, H–8) and three assigned to ring B at δ_H 7.23 (1H, d, *J* = 8.5 Hz, H–6′), δ_H 6.39 (1H, d, *J* = 2.0 Hz, H–3′), δ_H 6.36 (1H, dd, *J* = 8.5, 2.0 Hz, H–5′). The observation of two proton signals upfield which were absent in **14** and comparing the Double Bond Equivalent (DBE), indicated a loss of the usual double bond between δ_H 75.9 (C–2) and δ_H 43.5 (C–3). Thus three protons were successfully assigned to ring C at δ_H 5.54 (1H, dd, *J* = 13.0, 3.0 Hz, H–2), δ_H 2.95 (1H, dd, *J* = 17.0, 13.0 Hz, H–3a), δ_H 2.59 (1H, dd, *J* = 13.0, 3.0 Hz, H–3b). A further comparison of the ^{13}C NMR data (Table 4.17 and Appendix 109) to that of **14**, assisted in successfully assigning the position of the methoxy group to δ_H 54.9 (C–2′). The structure of **17** was determined to be 5,7,4′– Trihydroxy–2′–methoxyflavanone (Wollenweber and Roitman, 1991). The fragmentation pattern of **17** in the HRESI–MS/MS was characteristic of flavanone aglycones (Tsimogiannis *et al.*, 2007; Cuyckens and Claeys, 2004). A loss of a CH_2CO group $[M + H–CH_2CO]^+$ was observed at *m/z* 261. Retrocyclization cleavage of **17** produced the following RDA fragments $^{0,4}B^+$ at *m/z* 177, $^{1,3}A^+$ at *m/z* 153, $[M + H–B–ring]^+$ at *m/z* 179 (Figure 4.50).

Table 4.17: NMR spectral data for Compound **17** in CD_3OD (see Appendix 108–109)

Position	δ_H[a] multi. (*J* in Hz)	δ_C[b]	Position	δ_H[a] multi. (*J* in Hz)	δ_C[b]
2	5.54, dd (13.0, 3.0)	75.9	10		103.6
3	2.95, dd (17.0, 13.0) 2.59, dd (17.0, 3.0)	43.5	1′		119.6
4		198.6	2′		159.3
5		165.8	3′	6.39, d (2.0)	100.2
6	5.83, d (2.0)	97.3	4′		160.5
7		168.6	5′	6.36, dd (8.5, 2.0)	108.5
8	5.81, d (2.0)	96.4	6′	7.23, d (8.5)	129.1
9		165.6	2′–MeO	3.73, s	56.2

[a]Recorded at 500 MHz; [b]Recorded at 125 MHz

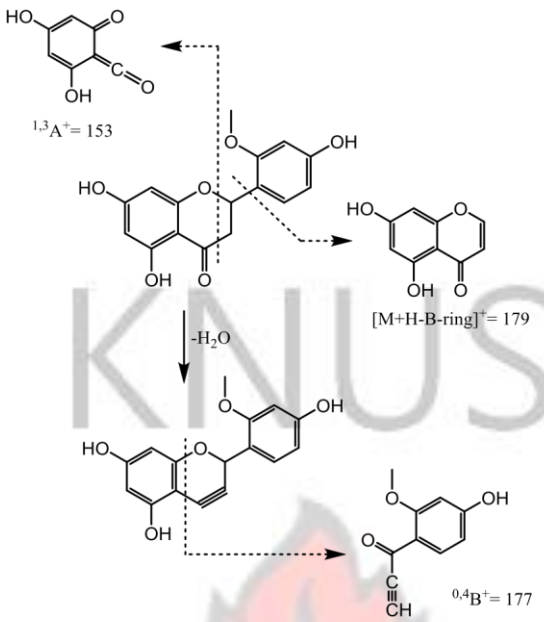


Figure 4.50: Retrocyclization cleavage of the C–ring of compound **17**.

5,7,4′–Trihydroxy–2′–methoxyflavanone (17): Yellow needles; LC–UV [MeOH-H_2O (0.1% HCOOH)] λ_{max} 225 and 288 nm. ^{1}H NMR (500 MHz in CD_3OD) and ^{13}C NMR (125 MHz, CD_3OD) data, see Table 4.17. Positive HRESI–MS: *m/z* 303.0864 $[M + H]^+$ (calcd. for $C_{16}H_{15}O_6$, 303.0863), *m/z* 325.0680 $[M + Na]^+$ (cald. for $C_{16}H_{14}O_6Na$, 325.0683).

4.1.18 Structure elucidation of 5,7,3′,5′–tetrahydroxyflavanone (18, known compound)

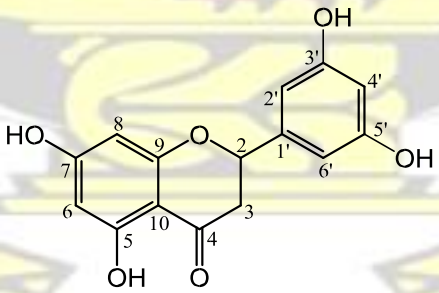


Figure 4.51: Chemical structure of compound **18**.

Compound **18** was isolated as a colourless amorphous solid. The molecular formula was determined as $C_{15}H_{12}O_6$ based on the pseudo–molecular ion *m/z* 289.0708 $[M + H]^+$ (calcd. for 289.0707) in the HRESI–MS spectrum (Appendix 110). The ^{1}H NMR spectrum (Table

4.18 and Appendix 113) indicated the presence of two aromatic protons attached to ring A at δ_H 5.84 (1H, d, *J* = 2.0 Hz, H–6), δ_H 5.82 (1H, d, *J* = 2.5 Hz, H–8) and three aromatic protons attached to ring B at δ_H 6.73 (1H, s, H–2′/6′), δ_H 6.86 (1H, s, H–4′). Two proton signals at δ_H 5.22 (1H, dd, *J* = 13.0, 3.0 Hz, H–2), δ_H 3.01 (1H, dd, *J* = 17.0, 12.5 Hz, H–3a), δ_H 2.64 (1H, dd, *J* = 17.0, 3.0 Hz, H–3b) were observed indicating the absence of the usual unsaturation in ring C characteristic of flavanones. The structure of **18** was confirmed to be 5,7,3′,5′–Tetrahydroxyflavonone after comparing ^{1}H and ^{13}C NMR data (Table 4.18 and Appendix 114) to reported literature (Hashmi *et al*., 2014). The HRESI–MS/MS profile of **18** followed a fragmentation pattern typical of flavanone aglycones. A stepwise loss of two H_2O molecules gave ions at *m/z* 271 $[M + H–H_2O]^+$ and *m/z* 253 $[M + H–2H_2O]^+$. CH_2CO group loss was observed at *m/z* 247 $[M + H–CH_2CO]^+$. Retro Diels–Alder fission of ring C resulted in the fragments $^{0,4}B^+$ at *m/z* 163, $^{1,3}A^+$ at *m/z* 153 and $[M + H–B–ring]^+$ at *m/z* 179 (Figure 4.52).

Table 4.18: NMR spectral data for Compound **18** in CD_3OD (see Appendix 113–114)

Position	δ_H[a] multi. (*J* in Hz)	δ_C[b]	Position	δ_H[a] multi. (*J* in Hz)	δ_C[b]
2	5.22, dd (13.0, 3.0)	80.8	10		103.7
3	3.01, dd (17.0, 12.5) 2.64, dd (17.0, 3.0)	44.4	1′		119.5
4		198.0	2′	6.73, s	116.6
5		165.7	3′		147.2
6	5.84, d (2.0)	97.3	4′	6.86, s	132.1
7		168.7	5′		146.8
8	5.82, d (2.5)	96.5	6′	6.73, s	115.0
9		165.1			

[a]Recorded at 500 MHz; [b]Recorded at 125 MHz

KNUST
NYANSAPOR W J SANE NO BADWENHWA

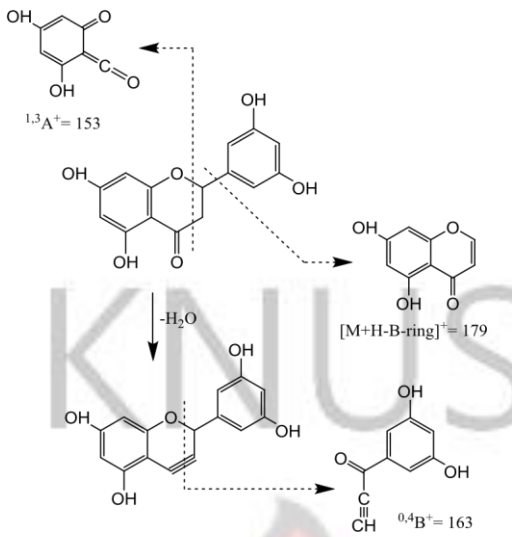


Figure 4.52: Retrocyclization cleavage of the C–ring of compound **18**.

5,7,3′,5′–Tetrahydroxyflavonone (18): Colourless amorphous solid; LC–UV [MeOH–H_2O (0.1% HCOOH)] λ_{max} 228 and 288 nm. ^{1}H NMR (500 MHz in CD_3OD) and ^{13}C NMR (125 MHz, CD_3OD) data, see Table 4.18. Positive HRESI–MS: *m/z* 289.0708 $[M + H]^+$ (calcd. for $C_{15}H_{13}O_6$, 289.0707).

4.1.19 Structure elucidation of naringenin (19, known compound)

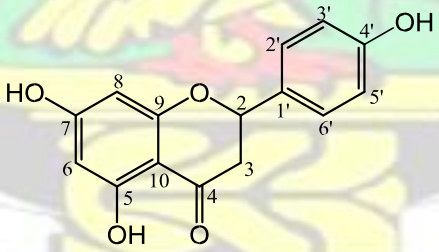


Figure 4.53: Chemical structure of compound **19**.

Compound **19** was obtained as yellow amorphous solid with a molecular formula of $C_{15}H_{12}O_5$ based on the ion *m/z* 273.0754 $[M + H]^+$ (calcd. for 273.0758). The ^{1}H NMR spectrum (Table 4.19 and Appendix 117) indicated the presence of two aromatic protons attached to ring A at δ_H 5.83 (1H, d, *J* = 2.5 Hz, H–6), δ_H 5.82 (1H, d, *J* = 2.0 Hz, H–8), four aromatic protons attached to ring B at δ_H 7.25 (2H, d, *J* = 8.5 Hz, H–2′/6′), δ_H 6.75 (2H, d, *J* = 8.5 Hz, H–3′/5′)

and three saturated protons attached to ring C at δ_H 5.27 (1H, dd, *J* = 13.0, 3.0 Hz, H–2), δ_H 3.04 (1H, dd, *J* = 17.0, 13.0 Hz, H–3a), δ_H 2.63 (1H, dd, *J* = 17.0, 3.0 Hz, H–3b). The structure of **19** was elucidated as 5,7,4′–Trihydroxyflavanone (Naringenin) after comparing the ^{1}H and ^{13}C NMR data (Table 4.19 and Appendix 118) with reported literature (Silva *et al*., 2013). The HRESI–MS/MS fragmentation information confirmed **19** was a flavanone type flavonoid. A loss of CH_2CO was observed at *m/z* 231 $[M + H–CH_2CO]^+$. Retrocyclization cleavage of ring C produced RDA fragments $^{0,4}B^+$ at *m/z* 147, $^{1,3}A^+$ at *m/z* 153 and $[M + H– B–ring]^+$ at *m/z* 179 of the protonated molecular ion (Figure 4.54).

Table 4.19: NMR spectral data for Compound **19** in CD_3OD (see Appendix 117–118)

Position	δ_H[a] multi. (*J* in Hz)	δ_C[b]	Position	δ_H[a] multi. (*J* in Hz)	δ_C[b]
2	5.27, dd (13.0, 3.0)	80.8	10		103.7
3	3.04, dd (17.0, 13.0) 2.63, dd (17.0, 3.0)	44.3	1′		131.4
4		198.1	2′	7.25, d (8.5)	129.3
5		165.2	3′	6.75, d (8.5)	116.6
6	5.83, d (2.5)	97.4	4′		159.3
7		168.7	5′	6.75, d (8.5)	116.6
8	5.82, d (2.0)	96.5	6′	7.25, d (8.5)	129.3
9		165.8			

[a]Recorded at 500 MHz; [b]Recorded at 125 MHz

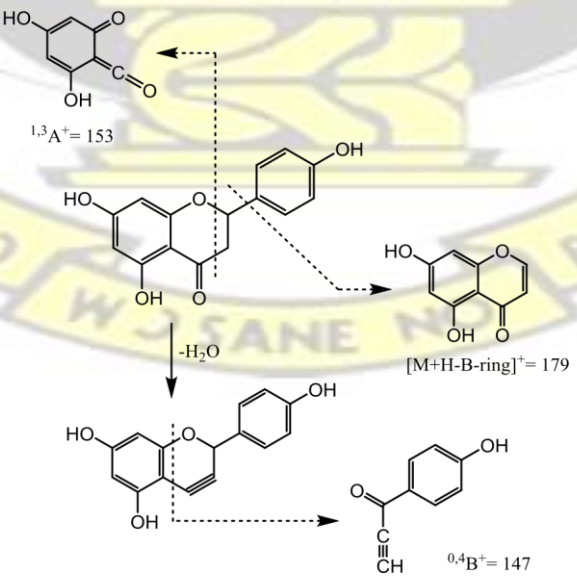


Figure 4.54: Retrocyclization cleavage of the C–ring of compound **19**.

Naringenin, 5,7,4′–Trihydroxyflavanone, (19): Yellow amorphous solid; LC–UV [MeOH–H_2O (0.1% HCOOH)] λ_{max} 214 and 289 nm. ^1H NMR (500 MHz in CD_3OD) and ^{13}C NMR (125 MHz, CD_3OD) data, see Table 4.19. Positive HRESI–MS: *m/z* 273.0754 $[M + H]^+$ (calcd. for $C_{15}H_{13}O_5$, 273.0758), *m/z* 295.0571 $[M + Na]^+$ (cald. for $C_{15}H_{12}O_5Na$, 295.0577).

4.2 Secondary metabolites isolated and characterized from the endophytic fungus JK10

The unidentified endophytic fungus labelled JK10, was isolated from the root of the Ghanaian medicinal plant C. regia. The endophytic strain was prescreened for important metabolites using the OSMAC approach. Large–scale fermentation was finally carried out on solid rice media and the mycelia extracted with ethylacetate. Comprehensive investigation led to the isolation and characterization of seven new 7–desmethyl derivatives of fusarin C (**20**–**26**).

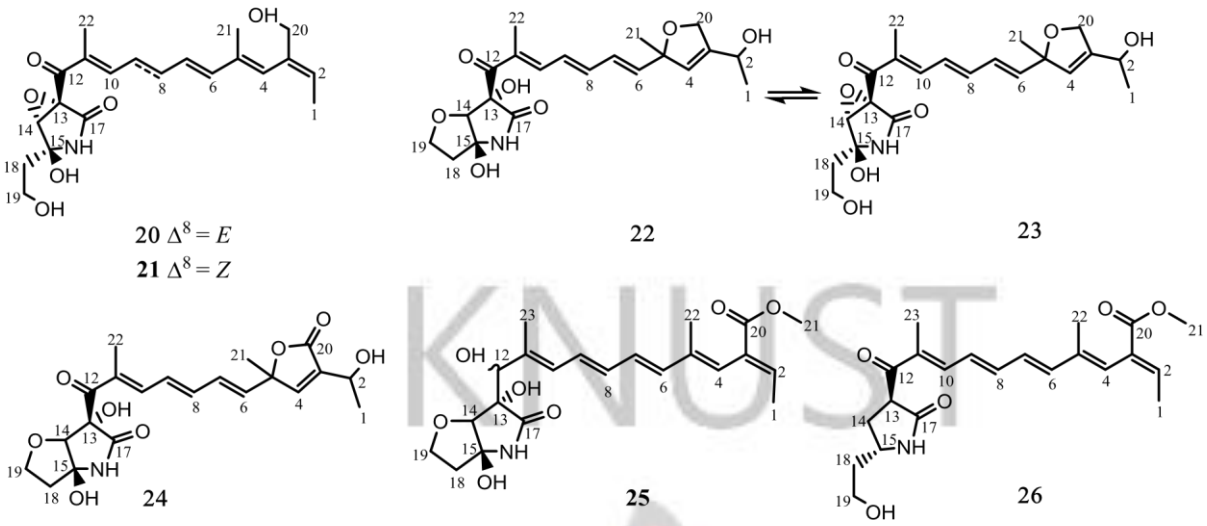


Figure 4.55: Chemical structures of novel metabolites from the endophytic fungus.

Isolated in parallel were five known compounds namely, NG–391/NG–393 (**27**/**28**), (+)–(S)–solaniol (**29**), 2,3–dihydro–5–hydroxy–8–methoxy–2,4–dimethylnaphtho[1,2–b]furan–6,9–dione (**30**) and N_b–acetyltryptamine (3**1**).

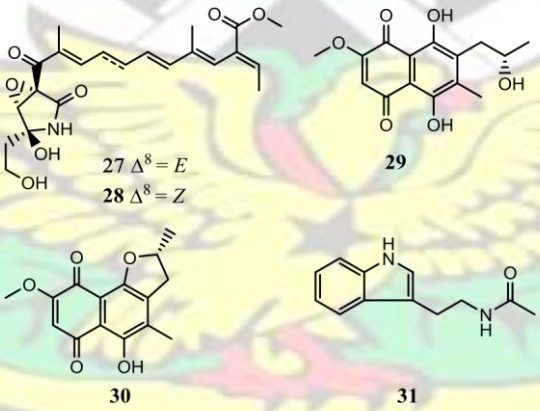


Figure 4.56: Chemical structures of known metabolites from the endophytic fungus.

4.2.1 Structure elucidation of 7–desmethyl fusarin C–20/21 (new compounds)

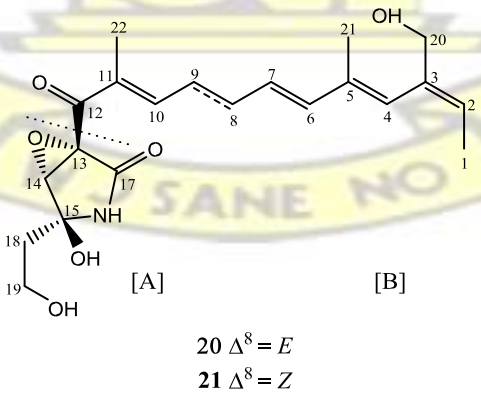


Figure 4.57: Chemical structures of compounds **20**/**21**.

Compounds **20/21** were isolated as yellow amorphous solid and the molecular formula was assigned as $C_{21}H_{27}O_6N$ by HRESI–MS spectrum (Appendix 119) showing a quasi–molecular ion peak at *m/z* 390.1911 $[M + H]^+$ (cald. for 390.1909) with nine double–bond equivalent (DBE). HRESI–MS/MS spectrum (Appendix 120) showed fragment ions at *m/z* 301.1433 $[M + H–C_3H_7O_2N]^+$, *m/z* 372.1804 $[M + H–H_2O]^+$, *m/z* 354.1701 $[M + H–2H_2O]^+$. Integration of the proton signals in the ^{1}H NMR spectrum (Table 4.20 and Appendix 121) revealed compounds **20**/**21** were a mixture of closely related compounds. Analysis of the ^{13}C NMR spectrum (Table 4.20 and Appendix 122) revealed various duplicate signals at δ_C 125.2/125.3 (C–2), δ_C 133.0/132.9 (C–4), δ_C 192.0/192.9 (C–12), δ_C 63.9/63.8 (C–13), δ_C 65.5/65.7 (C– 14), δ_C 86.1/86.6 (C–15), δ_C 172.8/172.6 (C–17), δ_C 38.8/38.5 (C–18), δ_C 58.6/58.7 (C–19), further suggesting the presence of a mixture of closely related compounds. The ^{1}H NMR spectrum was similar to that of the reported 7–desmethyl fusarin C analogues NG–391/NG– 393 (**27**/**28**). The observed differences were the appearance of a signal of methylene protons at δ_H 3.92 (2H, s, H–20), the absence of methoxy proton signal, and the upfield chemical shift of H–2 to δ_H 5.60 (1H, q, *J* = 6.6, 13.2 Hz, H–2). The observation of only two carbonyl signals at δ_C 192.0/192.9 (C–12) and δ_C 172.8/172.6 in the ^{13}C spectrum of **20**/**21** explained the nine DBE compared to ten DBE in **27**/**28**. The two different chemical shifts recorded at δ_H 7.86 (1H, d, *J* = 12, H–10) and δ_H 7.39 (1H, d, *J* = 10.8, H–10) indicated a mixture of 8*E* and 8*Z* isomers similar to that of **27**/**28**. HMBC correlations observed from H–2 to δ_C 67.3 (C– 20), δ_C 133.0 (C–4) and H–20 to C–2, δ_C 139.4 (C–3) and C–4 revealed the partial structure [B]. Comprehensive analysis of the COSY, HSQC and HMBC data affirmed the planar structures of **20**/**21**, which are reduced derivatives of **27**/**28**, consisting of epoxide and γlactam moieties. The experimental electronic circular dichroism (ECD) spectra of **20**/**21** and **27**/**28** (Figure 4.59) were similar, both exhibiting negative Cotton effect (CE) at 238 nm.

Additionally, compounds **20**/**21** and **27**/**28** gave positive specific optical rotation values. Since the partial structure [B] does not contribute to the stereogenicity of the whole molecule, the relative configuration of **20**/**21** was unequivocally determined as shown in the chemical structure (Figure 4.57). Compounds **20**/**21** could be intermediate metabolites in the biosynthesis of **27**/**28**.

KNUST

Table 4.20: NMR spectral data for Compounds **20**/**21** in CD_3OD (see Appendix 121–125)

	20		**21**			
Position	δH[a] multi. (*J* in Hz)	δC[b]	δH[a] multi. (*J* in Hz)	δC[b]	COSY[a]	HMBC[a]
1	1.48, m	15.5	1.48, m	15.5	2	2, 3
2	5.60, q (13.2, 6.6,)	125.2	5.60, q (13.2, 6.6)	125.3	1	1, 4, 20
3		139.4		139.4		
4	6.01, s	133.0	6.01, s	132.9		2, 3, 6, 20, 21
5		139.2		139.2		
6	6.55, m	145.0	6.55, m	145.0	7	4, 7, 8, 21
7	6.48, m	129.3	6.95, m	124.6	6, 8	5, 9

8	6.70, m	145.2	6.46, m	141.3	7, 9	7, 10
9	6.63, m	128.8	6.34, m	124.4	8, 10	7, 11
10	7.39, d (10.8)	146.3	7.86, d (12.0)	140.0	9	8, 12, 22
11		134.8		135.4		
12		192.0		192.9		
13		63.9		63.8		
14	4.04, s	65.5	4.12, s	65.7		12, 13, 15, 17
15		86.1		86.6		
17		172.8		172.6		
18	2.03, m	38.8	2.03, m	38.5	19	14, 15, 19
19	3.73, m	58.6	3.73, m	58.7	18	15, 18
20	3.92, s	67.3	3.92, s	67.3		2, 3, 4
21	1.75, s	14.7	1.70, s	15.2		4, 5, 6
22	1.84, s	11.5	1.86, s	11.2		10, 11, 12

[a]Recorded at 600 MHz; [b]Recorded at 150 MHz

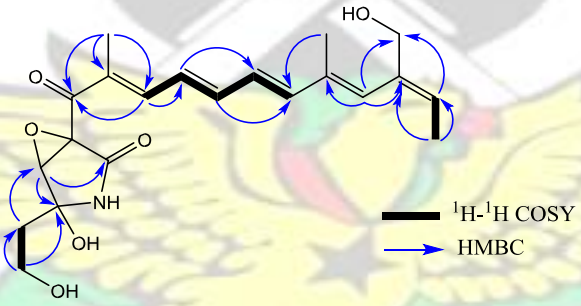


Figure 4.58: Selected HMBC and COSY correlations of compounds **20/21**.

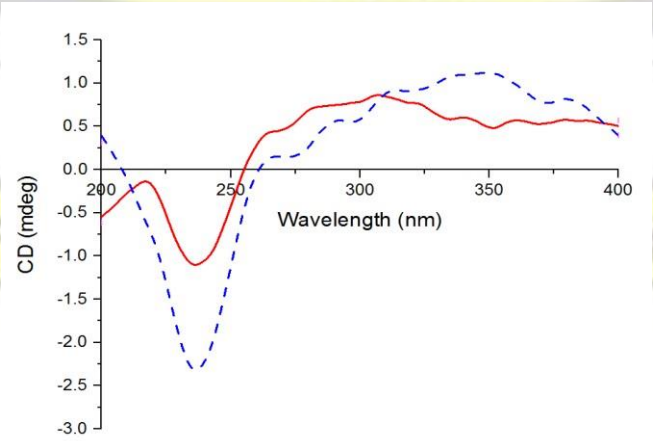


Figure 4.59: Experimental ECD spectrum of **20**/**21** (red continuous curve) and **27**/**28** (blue dashed curve)

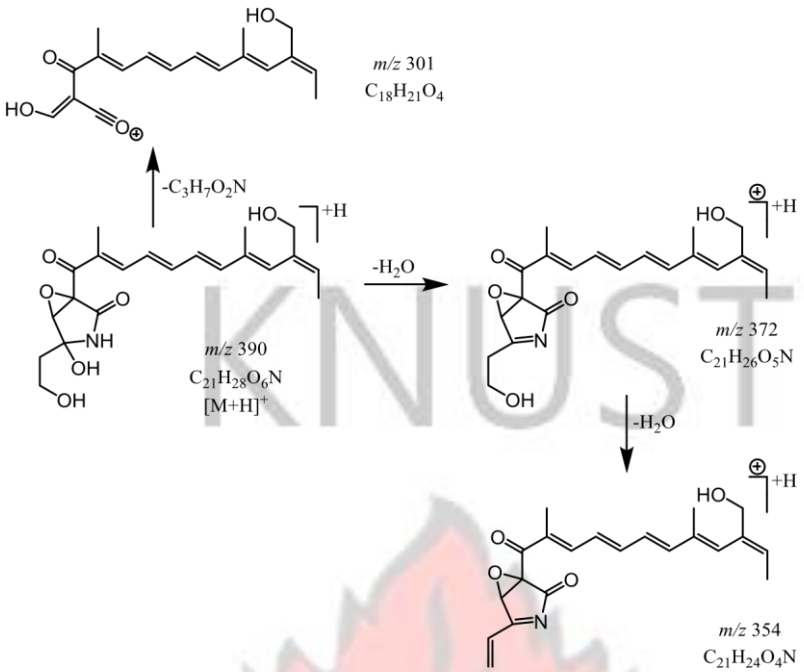


Figure 4.60: Proposed collision–induced mass spectral fragmentation pattern of compounds **20**/**21** in positive ESI mode.

7–desmethyl fusarin C–20/**21**: Yellow amorphous solid; $[\alpha]^{20}_{D}$ + 11 (*c* 0.1, MeOH); LC–UV [MeOH–H_2O (0.1% HCOOH)] λ_{max} 380 nm; IR (solid) ν_{max} 3334, 1637, 636 cm^{-1}; CD spectrum (0.1 mg/mL, MeOH), 213 ($\Delta\varepsilon$ –0.01), 238 ($\Delta\varepsilon$ –0.14), 307 ($\Delta\varepsilon$ +0.12); ^{1}H NMR (CD_3OH, 600 MHz) and ^{13}C NMR (CD_3OH, 150 MHz), see Table 4.20; positive HRESI–MS *m/z* 390.1911 $[M + H]^+$ (cald. for $C_{21}H_{28}O_6N$, 390.1909), *m/z* 372.1806 $[M + H–H_2O]^+$ (cald. for $C_{21}H_{26}O_5N$, 372.1803), *m/z* 412.1731 $[M + Na]^+$ (cald. for $C_{21}H_{27}O_6NNa$, 412.1728).

4.2.2 Structure elucidation of 7–desmethyl fusarin C–22/23 (new compounds)

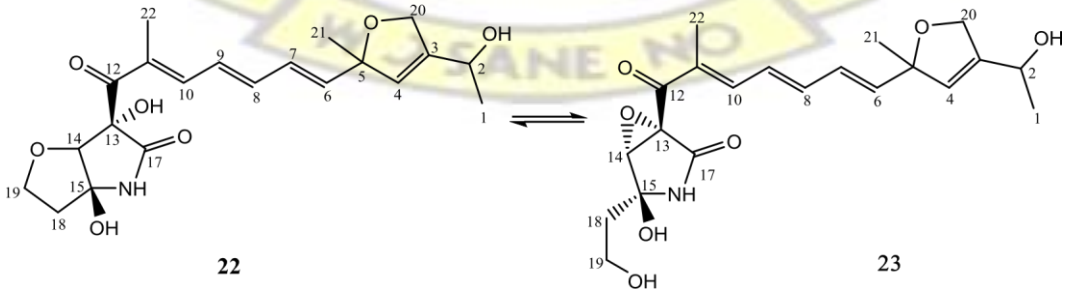


Figure 4.61: Chemical structures of compounds **22**/**23**.

Compounds **22**/**23** were obtained as yellow amorphous solid. The molecular formula was determined to be $C_{21}H_{27}O_7N$ based on the quasi–molecular ion peak at *m/z* 406.1860 $[M + H]^+$ (cald. for 406.1859) in the HRESI–MS spectrum (Appendix 126). HRESI–MS/MS profile showed fragment ions at *m/z* 344.1488 $[M + H–C_2H_6O_2]^+$, *m/z* 388.1756 $[M + H–H_2O]^+$, *m/z* 370.1647 $[M + H–2H_2O]^+$, *m/z* 326.1384 $[M + H–C_2H_6O_2–H_2O]^+$. The ^{1}H NMR spectrum (Table 4.21 and Appendix 128) revealed proton signals typical of 7–desmethyl analogues of fusarin C (Krasnoff *et al*., 2006; Bashyal *et al*., 2007). Surprisingly, the ^{13}C NMR and HSQC indicated the presence of more than the twenty–one carbon signals. HMBC cross peaks from δ_H 4.16 (1H, s, H–14) to δ_C 87.5 (C–13), δ_C 95.7 (C–15), δ_C 176.7 (C–17) and δ_C 69.8 (C–19) suggested the presence of a furanopyrrolidone moiety. Further HMBC cross peaks from δ_H 4.03 (1H, s, H–14) to δ_C 192.2 (C–12), δ_C 86.2 (C–15) and δ_C 172.6 (C–17) revealed the existence of a 2–pyrrolidone moiety. Thus, compounds **22**/**23** had different partial structures [A] but shared the same partial structures [B]. The presence of the HMBC cross peaks from δ_H 4.30 (1H, q, J = 6.6, 12.6 Hz, H–2) to δ_C 22.8 (C–1), δ_C 145.8 (C–3), δ_C 127.1 (C–4) and δ_C 75.0 (C–20); from δ_H 5.52 (1H, s, H–4) to C–2, C–3, δ_C 91.4 (C–5) and C–20; from [δ_H 4.58 (1H, s, H–20a), δ 4.60 (1H, s, 20b)] to C–3, C–4 and C–5; from δ_H 1.29 (3H, s, H–21) to C–4, C–5, and C–6, suggested the presence of a dihydrofuran ring moiety constituted the partial structure [B]. The dihydrofuran ring system was confirmed by NOESY correlations between H–1 and H–4/H–20; H–2 and H–4/H–20; H–4 and H–21/H–6 (Figure 4.62). The configuration of the unsaturated alkyl chain was established to be all of *E* geometry on the basis of the large coupling constant ($J_{6\text{-}7}$ = 15.0) and NOESY correlations. The planar structures of **22**/**23** as a mixture were unequivocally established as shown in Figure 4.61.

KNUST

Table 4.21: NMR spectral data for Compounds **22**/**23** in CD_3OD (see Appendix 128–132)

	22		**23**			
Position	δH^a multi. (*J* in Hz)	δC^b	δH^a multi. (*J* in Hz)	δC^b	COSY[a]	HMBC[a]
1	1.20, m	22.8	1.21, m	22.8	2	2, 3
2	4.30, q (12.6, 6.6)	65.2	4.30, q (12.6, 6.6)	65.2	1	1, 3, 4, 20
3		145.8		145.8		
4	5.52, s	127.1	5.52, s	126.9		2, 3, 5, 20
5		91.4		91.4		
6	5.93, d (15.0)	142.9	5.99, d (15.0)	144.6	7	4, 5, 8, 21
7	6.32, dd (15.0, 10.2)	128.9	6.32, dd (15.0, 10.2)	128.9	6, 8	5, 8, 9
8	6.54, m	141.8	6.52, m	144.1	7, 9	9, 10

9	6.62, m	129.7	6.61, m	129.2	8, 10	10, 11
10	7.33, d (9.6)	143.2	7.33, d (9.6)	145.9	9	8, 11, 12, 22
11		135.1		135.5		
12		200.6		192.2		
13		87.5		63.9		
14	4.16, s	93.7	4.03, s	65.6		12, 13, 15, 17, 19
15		95.7		86.2		
17		176.7		172.6		
18	a. 2.02, m b. 2.06, m	40.0	a. 1.89, m b. 1.93, m	38.9	19	14, 15, 19
19	a. 3.60, m b. 3.81, m	69.8	a. 3.71, m b. 3.74, m	58.6	18	14, 15,18
20	a. 4.58, s b. 4.60, s	75.0	a. 4.54, s b. 4.57, s	75.1		3, 4, 5
21	1.29, s	26.7	1.29, s	26.7		4, 5, 6
22	1.82, s	12.7	1.84, s	11.6		10, 11, 12

[a]Recorded at 600 MHz; [b]Recorded at 150 MHz

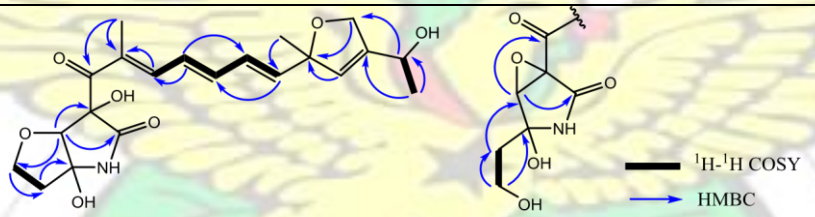


Figure 4.62: Selected HMBC and COSY correlations of compounds **22/23**.

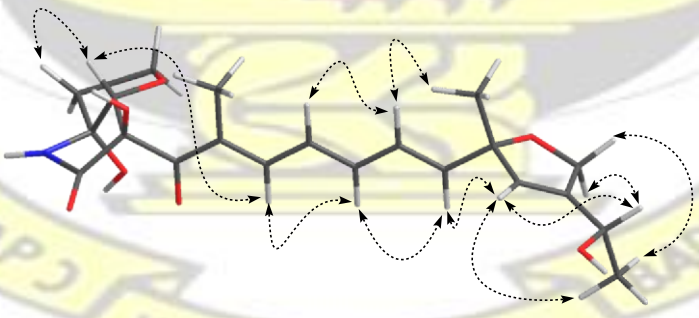


Figure 4.63: Key NOESY correlations of **22**

7–desmethyl fusarin C–22/23: Yellow amorphous solid; $[\alpha]^{20}_{D}$ – 19 (*c* 0.1, MeOH); LC–UV [MeOH–H_2O (0.1% HCOOH)] λ_{max} 332 nm; IR (solid) ν_{max} 3338, 3324, 2360, 1637, 1634, 1094, 1088, 661 cm^{-1}; CD spectrum (0.1 mg/mL, MeOH), 215 ($\Delta\varepsilon$ –0.01), 240 ($\Delta\varepsilon$ –0.20),

260 ($\Delta\varepsilon$ +0.03), 310 ($\Delta\varepsilon$ –0.13), 360 ($\Delta\varepsilon$ +0.11); ^{1}H NMR (CD_3OH, 600 MHz) and ^{13}C NMR (CD_3OH, 150 MHz), see Table 4.21; positive HRESI–MS *m/z* 406.1860 $[M + H]^+$ (cald. for $C_{21}H_{28}O_7N$, 406.1859), *m/z* 388.1755 $[M + H–H_2O]^+$ (cald. for $C_{21}H_{26}O_6N$, 388.1754), *m/z* 370.1649 $[M + H–2H_2O]^+$ (cald. for $C_{21}H_{24}O_5N$, 370.1649), *m/z* 428.1680 $[M + Na]^+$ (cald. for $C_{21}H_{27}O_7NNa$, 428.1679).

4.2.3 Structure elucidation of 7–desmethyl fusarin C–24 (new compound)

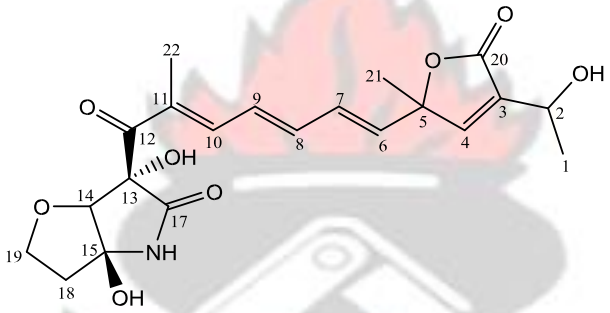


Figure 4.64: Chemical structure of compound **24**.

Compound **24** was isolated as yellow amorphous solid with a molecular formula of $C_{21}H_{25}O_8N$ assigned based on the pseudo–molecular ion peak at *m/z* 420.1656 $[M + H]^+$ (cald. for 420.1654) in the HRESI–MS spectrum (Appendix 135). The HRESI–MS/MS spectrum, gave fragment ions at *m/z* 402.1549 $[M + H–H_2O]^+$, *m/z* 384.1444 $[M + H–2H_2O]^+$, *m/z* 366.1336 $[M + H–3H_2O]^+$ suggesting the presence of three hydroxyl groups. In the ^{1}H NMR spectrum (Table 4.22 and Appendix 137), signals of three nonequivalent methyls were observed at δ_H 1.82 (3H, s, H–3), δ_H 1.47 (3H, s, H–21) and δ_H 1.26 (3H, m, H–1). Chemical shift of two olefinic protons showing overlapping signals at δ_H 7.29 (2H, d, *J* = 1.4 Hz, H–4/10) were observed. In addition, two methine protons at δ_H 4.40 (1H, qd, *J* = 13.3, 7 Hz, H– 2) and δ_H 4.15 (1H, s, H–14); two methylene protons at [δ_H 3.77 (1H, m, H–19a), δ_H 3.82 (1H, m, H–19b)] and [δ_H 2.04 (1H, m, H–18a), δ_H 2.05 (1H, m, H–18b)] were observed. The ^{1}H and ^{13}C NMR spectra were comparable to that of compound **22** but for the presence of a carbonyl

functionality at δ_C 173.6 (C–20) and the absence of methylene protons connected to C–20. Analysis of HMBC cross peaks from H–2 to δ_C 138.3 (C–3), δ_C 153.4 (C–4) and C–20; from H–4 to C–3, δ_C 87.6 (C–5) and C–20; from H–21 to C–4, C–5 and δ_C 135.9 (C–6) affirmed the presence of a γ–lactone ring system constituting partial structure [B]. NOESY correlations between H–1 and H–4; H–4 and δ_H 5.88 (1H, d, J = 15.4 Hz, H–6); H–6 and δ_H 6.52 (1H, dd, J = 10.5, 14.7 Hz, H–8); H–8 and H–10; δ_H 6.64 (1H, m, H–9) and H–22 (Figure 4.66); together with the large coupling constants ($J_{6\text{-}7}$ = 15.4 Hz and $J_{8\text{-}9}$ = 14.7) suggested *E* geometry for all the four olefinic bonds. The planar structure of **24** was unambiguosly elucidated as shown in Figure 4.64.

Table 4.22: NMR spectral data for Compounds **24** in CD_3OD (see Appendix 137–141)

Position	δ_H[a] multi. (J in Hz)	δ_C[b]	COSY[a]	HMBC[a]
1	1.26, m	22.5	2	2, 3
2	4.40, qd (13.3, 7.0)	63.9	1	1, 3, 4, 20
3		138.3		
4	7.29*, d (1.4)	153.4		2, 3, 5, 20
5		87.6		
6	5.88, d (15.4)	135.9	7	4, 5, 8, 21
7	6.41, dd (15.4, 11.2)	132.2	6, 8	5, 9
8	6.52, dd (14.7, 10.5)	140.2	7, 9	6, 9, 10
9	6.64, m	131.5	8, 10	7, 8, 10, 11

10		7.29*, d (1.4)	142.4	9	8, 12, 22		
11		136.3					
12		200.7					
13		87.5					
14		4.15, s	93.7	13, 15, 17, 19			
15		95.7					
17		176.6					
18	a. 2.04, m b. 2.05, m		40.0	19	14, 15, 19		
19	a. 3.77, m b. 3.82, m		69.8	18	14, 15		
20		173.6					
21		1.47, s	24.6	4, 5, 6 22 10, 11, 12		1.82, s	12.8

[a]Recorded at 700 MHz; [b]Recorded at 176 MHz; *Overlapped signals

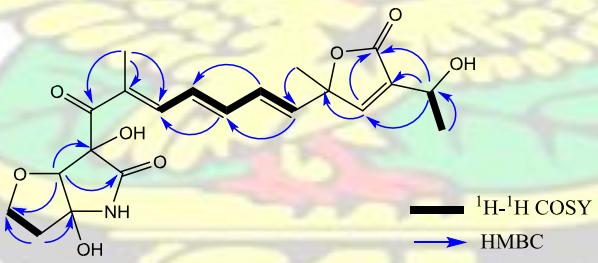


Figure 4.65: Selected HMBC and COSY correlations of compounds **24**.

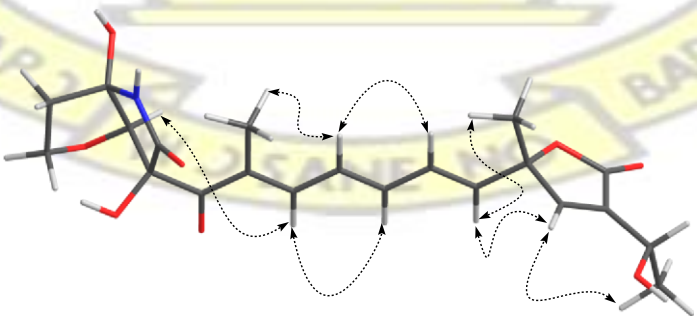


Figure 4.66: Key NOESY correlations of **24**.

7–desmethyl fusarin C–24: Yellow amorphous solid; $[\alpha]^{20}_{D}$ – 3 (*c* 0.1, MeOH); LC–UV [MeOH–H_2O (0.1% HCOOH)] λ_{max} 326 nm; IR (solid) ν_{max} 3324, 1634, 1095 cm^{-1}; CD spectrum (1.0 mg/mL, MeOH), 236 ($\Delta\varepsilon$ –0.09), 306 ($\Delta\varepsilon$ –0.03), 360 ($\Delta\varepsilon$ +0.03); ^{1}H NMR (CD_3OH, 700 MHz) and ^{13}C NMR (CD_3OH, 176 MHz), see Table 4.22; positive HRESI–MS *m/z* 420.1656 $[M + H]^+$ (cald. for $C_{21}H_{26}O_8N$, 420.1654), *m/z* 402.1551 $[M + H–H_2O]^+$ (cald. for $C_{21}H_{24}O_7N$, 402.1549), *m/z* 384.1445 $[M + H–2H_2O]^+$ (cald. for $C_{21}H_{22}O_6N$, 384.1443), *m/z* 442.1475 $[M + Na]^+$ (cald. for $C_{21}H_{25}O_8NNa$, 442.1474).

4.2.4 Structure elucidation of 7–desmethyl fusarin C–25 (new compound)

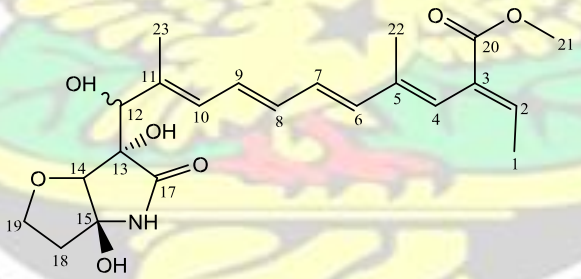


Figure 4.67: Chemical structure of compound **25**.

Compound **25** was pale yellow amorphous solid with molecular formula $C_{22}H_{29}O_7N$ based on the pseudo–molecular ion peak at *m/z* 420.2017 $[M + H]^+$ (cald. for 420.2017) with nine DBE in the HRESI–MS spectrum (Appendix 144). The HRESI–MS/MS spectrum (Appendix 145), in positive mode, exhibited fragments at *m/z* 402.1907 $[M + H–H_2O]^+$, *m/z* 388.1751 $[M + H–CH_3OH]^+$, *m/z* 384.1801 $[M + H–2H_2O]^+$, *m/z* 370.1646 [M + H–H_2O–CH_3OH]+. Detailed

study of the ^{1}H and ^{13}C NMR spectra and comparing to reported data suggested compound **25** was a furanopyrrolidone derivative closely related to the reported 13α–hydroxylucilactaene (Bashyal *et al*., 2007). The ^{1}H NMR spectrum (Table 4.23 and Appendix 146) revealed the presence of three methyl protons at δ_H 1.81 (3H, d, *J* = 3.6 Hz, H–23), δ_H 1.71 (3H, dd, *J* = 1.2, 7.2 Hz, H–1) and δ_H 1.65 (3H, d, *J* = 1.2 Hz, H–22); one methoxy group at δ_H 3.72 (3H, s, H–21); two sets of methylene protons, each showing different chemical shifts, at [δ_H 4.19 (1H, tm, H–19b), δ_H 4.02 (1H, m, H–19a)] and [δ_H 2.49 (1H, m, H–18b), δ_H 2.41 (1H, m, H– 18a)]; two methine protons at δ_H 4.33 (1H, br s, H–12) and δ_H 4.07 (1H, d, *J* = 2.4 Hz, H–14). The remaining signals are those of the various olefinic protons. The stereochemistry of the unsaturated alkyl chain was determined to be all *E* configurations based on NOESY cross peaks (Figure 4.69) between δ_H 6.05 (1H, s, H–4) and δ_H 6.37 (1H, m, H–6); δ_H 6.32 (1H, m, H–7) and δ_H 6.48 (1H, m, H–9); δ_H 6.35 (1H, m, H–8) and δ_H 6.31 (1H, m, H–10). Analysis of HMBC correlations from H–12 to δ_C 126.5 (C–10), δ_C 86.1 (C–14), δ_C 174.0 (C–17) and δ_C 13.8 (C–23) affirmed δ_C 90.4 (C–12) was substituted by a hydroxyl group and not a carbonyl group as noted in the reported 13α–hydroxylucilactaene. Compound **25** may plausibly share the same biosynthetic origin as **20**/**21** and **22**/**23**; thus, the furanopyrrolidone system should have similar relative configuration as the 2–pyrrolidone ring system in **20**/**21** and **22**. The configuration of the hydroxyl group at C–12 was unsuccessfully determined on the basis of the NOESY data. The planar structure of **25** was elucidated as shown in Figure 4.67 based on the detailed analyses of the COSY, HSQC, HMBC and NOESY data.

KNUST

Table 4.23: NMR spectral data for compound **25** in $CDCl_3$ (see Appendix 146–150)

Position	δ_H[a] multi. (*J* in Hz)	δ_{Cb}	COSY[a]	HMBC[a]
1	1.71, dd (7.2, 1.2)	15.9	2	2, 3
2	6.93, qd (7.2, 0.6)	139.9	1	1, 3, 4, 20
3		130.6		
4	6.05, s	124.7		2, 5, 6, 20, 22
5		138.3		
6	6.37, m	136.8	7	4, 5, 7, 8, 22
7	6.32, m	133.9	6, 8	5, 9
8	6.35, m	129.3	7, 9	6, 7
9	6.48, m	128.4	8, 10	7, 8, 10
10	6.31, m	126.5	9	9, 11, 12, 23
11		131.9		
12	4.33, br s	90.4		10, 11, 13, 14, 17, 23
13		83.1		

14	4.07, d (2.4)	86.1		12, 13, 17, 19
15		112.9		
17		174.0		
18	a. 2.41, m b. 2.49, m	39.1	19	14, 15, 19
19	a. 4.02, m b. 4.19, tm	69.8	18	14, 15, 18
20		167.9		
21	3.72, s	51.9		20
22	1.65, d (1.2)	14.3		4, 5, 6
23	1.81, d (3.6)	13.8		10, 11, 12

[a]Recorded at 600 MHz; [b]Recorded at 150 MHz

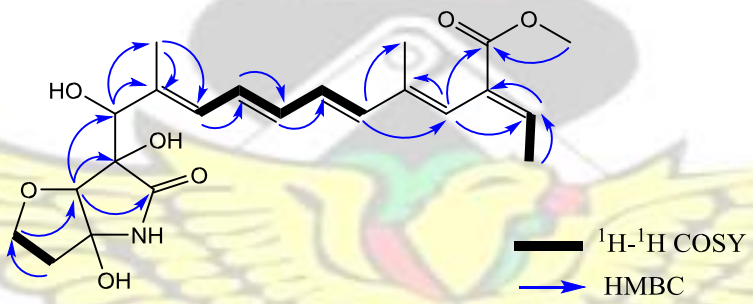


Figure 4.68: Selected HMBC and COSY correlations of compound **25**.

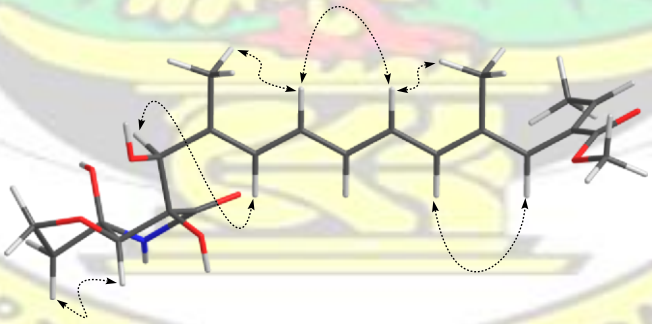


Figure 4.69: Key NOESY correlations of compound **25**.

KNUST

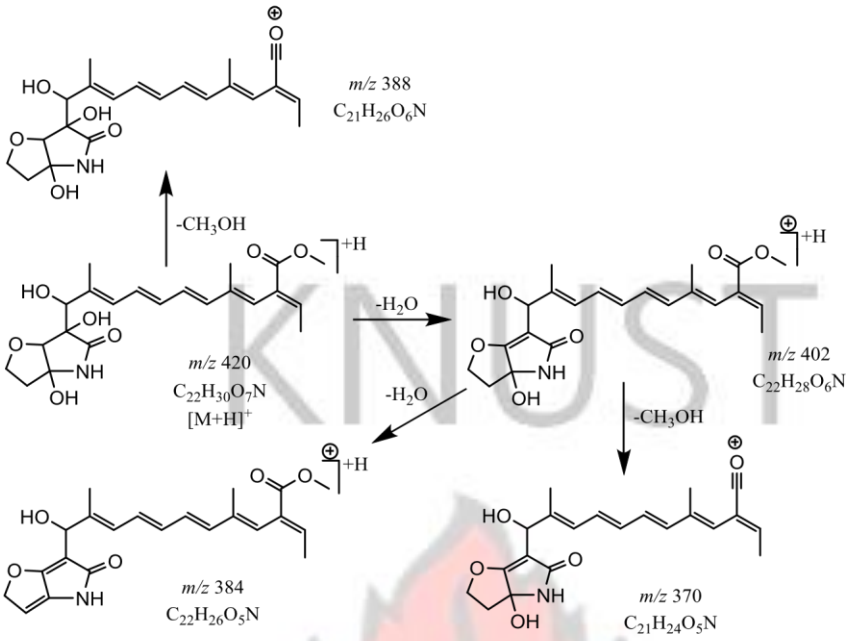


Figure 4.70: Proposed collision–induced mass spectral fragmentation pattern of compound **25** in positive ESI mode.

7–desmethyl fusarin C–25: Pale yellow amorphous solid; $[\alpha]^{20}_{D}$ – 18 (*c* 0.1, MeOH); LC– UV [MeOH–H_2O (0.1% HCOOH)] λ_{max} 216 nm and 326 nm; IR (film) ν_{max} 3334, 1634, 1096, 610 cm^{-1}; CD spectrum (1.0 mg/mL, MeOH), 209 ($\Delta\varepsilon$ +0.05), 253 ($\Delta\varepsilon$ –0.04), 356 ($\Delta\varepsilon$ +0.01); ^{1}H NMR ($CDCl_3$, 600 MHz) and ^{13}C NMR ($CDCl_3$, 150 MHz), see Table 4.23; positive HRESI–MS *m/z* 420.2017 $[M + H]^+$ (cald. for $C_{22}H_{30}O_7N$, 420.2017), *m/z* 402.1911 $[M + H–H_2O]^+$ (cald. for $C_{22}H_{28}O_6N$, 402.1910), *m/z* 384.1805 $[M + H–2H_2O]^+$ (cald. for $C_{22}H_{26}O_5N$, 384.1805), *m/z* 442.1836 $[M + Na]^+$ (cald. for $C_{22}H_{29}O_7NNa$, 442.1836).

4.2.5 Structure elucidation of 7–desmethyl fusarin C–26 (new compound)

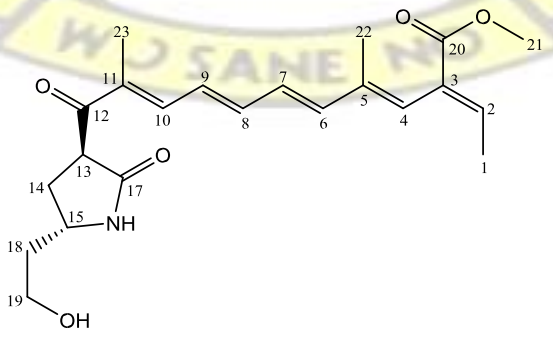


Figure 4.71: Chemical structure of compound **26**.

Compound **26** was obtained as yellow amorphous solid with a molecular formula of $C_{22}H_{29}O_5N$ based on the quasi–molecular ion peak at *m/z* 388.2118 $[M + H]^+$ (cald. for 388.2116) as shown in the HRESI–MS spectrum (Appendix 153) with nine DBEs. HRESI–MS/MS spectrum exhibited, in positive mode, fragment ions at *m/z* 356.1854 $[M + H–CH_3OH]^+$, *m/z* 370.2010 $[M + H–H_2O]^+$, *m/z* 338.1747 $[M + H–CH_3OH–H_2O]^+$ suggesting the presence of one hydroxyl group and a methoxy group. The ^1H NMR spectrum (Table 4.24 and Appendix 155) was similar to that of compound **20** except for the appearance of methine proton signals at δ_H 4.18 (1H, m, H–13) and δ_H 3.98 (1H, m, H–15); methylene proton signals at [δ_H 2.66 (1H, m, H–14a), δ_H 2.61 (1H, m, H–14b)]. This suggested the substitution pattern of the 2–pyrrolidone moiety was different from that of compound **20**. On the basis of the large coupling constants (J_{6-7} = 15.4 and J_{8-9} = 13.0), the configurations of the unsaturated alkyl chain (C–6, C–7, C–8, C–9) were established as all of *E* geometry. Thus the planar structure of **26** was unambiguously elucidated, after detailed analyses of the COSY, HSQC and HMBC data, as shown in Figure 4.71.

Table 4.24: NMR spectral data for compound **26** in $CDCl_3$ (see Appendix 155–159)

Position	δ_H[a] multi. (*J* in Hz)	δ_C[b]	COSY[a]	HMBC[a]
1	1.71, dd (7.2, 1.2)	15.9	2	2, 3
2	6.93, qd (7.2, 0.6)	139.9	1	1, 3, 4, 20
3		130.6		
4	6.05, s	124.7		2, 5, 6, 20, 22
5		138.3		
6	6.37, m	136.8	7	4, 5, 7, 8, 22
7	6.32, m	133.9	6, 8	5, 9
8	6.35, m	129.3	7, 9	6, 7
9	6.48, m	128.4	8, 10	7, 8, 10
10	6.31, m	126.5	9	9, 11, 12, 23

11		131.9		
12	4.33, br s	90.4		10, 11, 13, 14, 17, 23
13		83.1		
14	4.07, d (2.4)	86.1		12, 13, 17, 19
15		112.9		
17		174.0		
18	a. 2.41, m b. 2.49, m	39.1	19	14, 15, 19
19	a. 4.02, m b. 4.19, tm	69.8	18	14, 15, 18
20		167.9		
21	3.72, s	51.9		20
22	1.65, d (1.2)	14.3		4, 5, 6
23	1.81, d (3.6)	13.8		10, 11, 12

[a]Recorded at 700 MHz; [b]Recorded at 176 MHz

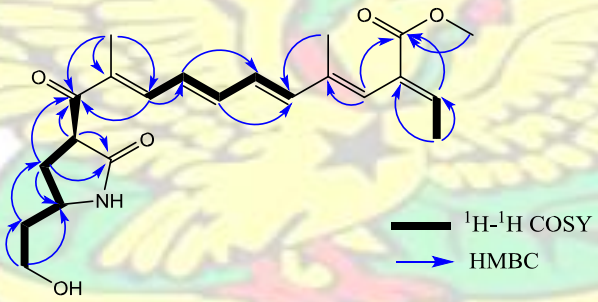


Figure 4.72: Selected HMBC and COSY correlations of compound **26**.

KNUST

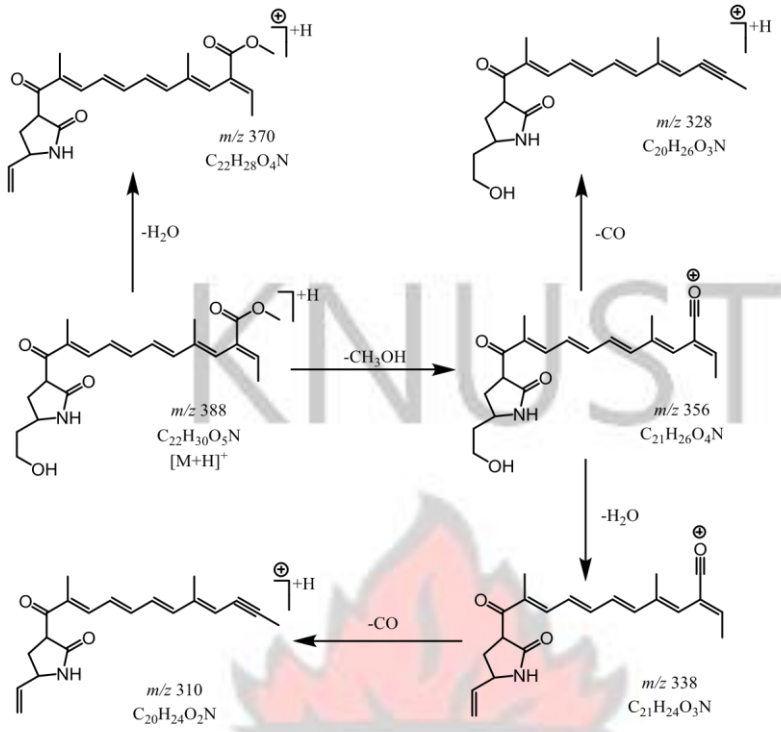


Figure 4.73: Proposed collision–induced mass spectral fragmentation pattern of compound **26** in positive ESI mode.

7–desmethyl fusarin C–26: Yellow amorphous solid; $[\alpha]^{20}_{D}$ – 3 (*c* 0.1, MeOH); LC–UV [MeOH–H_2O (0.1% HCOOH)] λ_{max} 360 nm; IR (film) ν_{max} 3392, 2978, 1701, 1388, 1254, 1066, 610 cm^{-1}; CD spectrum (0.1 mg/mL, MeOH), 225 ($\Delta\varepsilon$ +0.11); ^1H NMR ($CDCl_3$, 700 MHz) and ^{13}C NMR ($CDCl_3$, 176 MHz), see Table 4.24; positive HRESI–MS *m/z* 388.2118 $[M + H]^+$ (cald. for $C_{22}H_{30}O_5N$, 388.2116), *m/z* 410.1938 $[M + Na]^+$ (cald. for $C_{22}H_{29}O_5NNa$, 410.1936).

4.2.6 Structure elucidation of NG–391/NG–393 (27/28, known compounds)

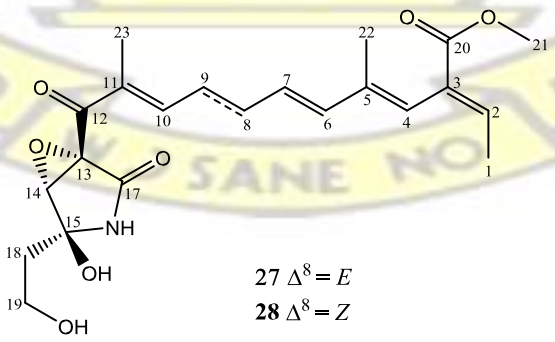


Figure 4.74: Chemical structure of compounds **27/28**.

Compounds **27**/**28** were obtained as a yellowish mixture of compounds. The molecular formula of $C_{22}H_{28}O_7N$ as determined by HRESI–MS spectrum (Appendix 161) showing a quasi-molecular ion peak at *m/z* 418.1859 $[M + H]^+$ (cald. for 418.1860). HRESI–MS/MS profile produced fragment ions at *m/z* 329.1381 $[M + H–C_3H_7O_2N]^+$, *m/z* 400.1751 $[M + H– H_2O]^+$, *m/z* 386.1594 $[M + H–CH_3OH]^+$, *m/z* 368.1489 $[M + H–CH_2–2H_2O]^+$. Integration of the proton signals in the ^{1}H NMR spectrum (Table 4.25 and Appendix 163), similar to **20**/**21** suggested a mixture of two compounds. The ^{13}C NMR spectrum (Table 4.25 and Appendix 164), similarly, revealed many duplicate signals. The notable differences, compared to **20**/**21**, were the presence of methoxy protons at δ_H 3.67 (3H, s, H–21), the presence of an additional ketone group at δ_C 169.3 (C–20) and the absence of methylene protons at C–20. Detailed analysis of the 1D and 2D NMR data, the structures of **27**/**28** were elucidated as a mixture of NG–391 and NG–393 which have been reported to as potent S9–dependent mutagenic mycotoxins (Krasnoff *et al*., 2006).

Table 4.25: NMR spectral data for Compounds **27**/**28** in CD_3OD (see Appendix 163–167)

	27		**28**			
Position	δH[a] multi. (*J* in Hz)	δC[b]	δH[a] multi. (*J* in Hz)	δC[b]	COSY[a]	HMBC[a]
1	1.70, m	16.3	1.70, m	16.3	2	2, 3
2	6.92, q (14.0, 7.0)	141.8	6.92, q (14.0, 7.0)	141.9	1	1, 3, 4, 20
3		132.1		132.0		
4	6.17, s	128.9	6.17, s	128.9		2, 5, 6, 20, 22
5		140.4		140.4		
6	6.53, m	142.2	6.53, m	142.2	7	4, 5, 7, 8, 22
7	6.55, m	130.3	6.91, m	125.5	6, 8	5, 6, 8, 9

8	6.75, m	144.8	6.52, m	141.0	7, 9	6, 7, 9, 10
9	6.77, m	129.5	6.44, t (11.5)	125.0	8, 10	7, 8, 10, 11
10	7.44, d (9.0)	146.1	7.90, d (11.5)	139.9	9	8, 9, 11, 12, 23
11		135.8		135.2		
12		192.2		192.0		
13		64.0		63.9		
14	4.09, s	65.9	4.16, s	65.8		13, 15, 17, 18
15		86.7		86.2		
17		172.8		172.6		
18	2.00, m	38.6	2.00, m	38.9	19	14, 15, 19
19	3.80, m	58.7	3.80, m	58.7	18	15, 18
20		169.3		169.4		
21	3.67, s	52.7	3.67, s	52.7		20
22	1.71, s	14.8	1.70, s	15.2		4, 5, 6
23	1.91, s	11.7	1.91, s	11.3		10, 11, 12

[a]Recorded at 500 MHz; [b]Recorded at 125 MHz

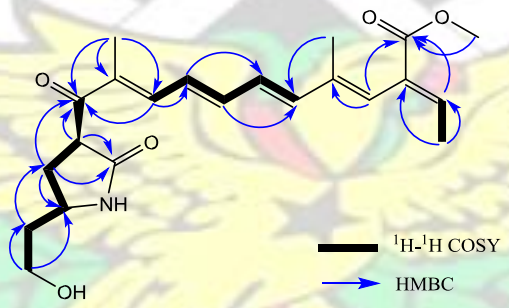
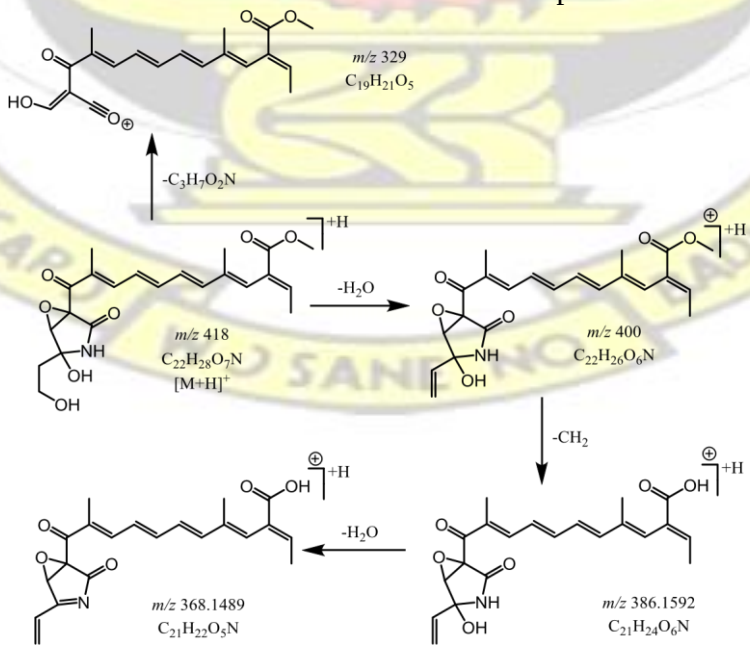


Figure 4.75: Selected HMBC and COSY correlations of compounds **27**/**28**.



KNUST

Figure 4.76: Proposed collision-induced mass spectral fragmentation pattern of compound **27**/**28** in positive ESI mode.

Compounds **27**/**28**: Yellow amorphous solid; $[\alpha]^{20}_{D}$ + 49 (*c* 0.1, MeOH); LC–UV [MeOH– H_2O (0.1% HCOOH)] λ_{max} 374 nm; IR (film) ν_{max} 3319, 1635, 1077, 1015, 595 cm^{-1}; CD spectrum (0.1 mg/mL, MeOH), 216 ($\Delta\varepsilon$ –0.01), 238 ($\Delta\varepsilon$ –0.03), 309 ($\Delta\varepsilon$ +0.13), 350 ($\Delta\varepsilon$ +0.02); ^{1}H NMR (CD_3OH, 500 MHz) and ^{13}C NMR (CD_3OH, 125 MHz), see Table 4.25; positive HRESI–MS *m/z* 418.1859 $[M + H]^+$ (cald. for $C_{22}H_{28}O_7N$, 418.1860), *m/z* 400.1753 $[M + H–H_2O]^+$ (cald. for $C_{22}H_{26}O_6N$, 400.1750), *m/z* 440.1678 $[M + Na]^+$ (cald. for $C_{22}H_{27}O_7NNa$, 440.1676).

4.2.7 Structure elucidation of (+)–(S)–Solaniol (29, known compound)

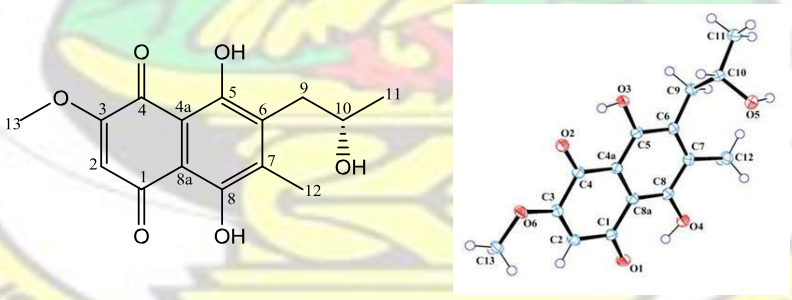


Figure 4.77: Planar and X-ray crystal structures of compound **29**.

Compound **29** was isolated as red amorphous solid with the molecular formula $C_{15}H_{16}O_6$ based on the pseudo-molecular ion peak at *m/z* 293.1023 $[M + H]^+$ (cald. for 293.1020) in the HRESI–MS spectrum (Appendix 168). The HRESI–MS/MS fragmentation, in positive mode, showed two fragments at *m/z* 275.0919 $[M + H–H_2O]^+$ and *m/z* 249.0760 $[M + H–C_3H_4O]^+$. The ^{1}H

NMR spectrum (Table 4.26 and Appendix 170) was similar to that of the known naphthoquinone javanicin (Hashimoto *et al*., 2009) with the exception of an additional methine proton signal at δ_H 4.13 (1H, q, *J* = 6, 12.5 Hz, H–10). This results from the reduction of the ketone group at C–10 in javanicin to a secondary alcohol in **29**. Further signals shown were two chelated hydroxyl protons at δ_H 13.31 (1H, s, 5–OH) and δ_H 13.04 (1H, s, 8–OH); a methine proton at δ_H 6.18 (1H, s, H–2), a typical methoxy proton signal at δ_H 3.91 (3H, s, H– 13), methylene protons at δ_H 2.94 (1H, d, *J* = 2 Hz, H–9b) and δ_H 2.93 (1H, br s, H–9a); an aromatic methyl proton at δ_H 2.33 (3H, s, H–12) and a doublet methyl proton at δ_H 1.31 (3H, d, *J* = 6 Hz, H–11) from coupling with H-10. The ^{13}C NMR spectrum (Table 4.26 and Appendix 171) revealed the presence of two carbonyls at δ_C 184.2 (C–1) and δ_C 177.8 (C–4); seven aromatic quaternary carbons at δ_C 106.6 (C–3), δ_C 109.5 (C–4a), δ_C 162.3 (C–5), δ_C 138.3 (C–6), δ_C 142.2 (C–7), δ_C 160.5 (C–8) and δ_C 107.9 (C–8a); a methine carbon at δ_C 109.6 (C–2); a 2–hydroxypropyl unit at δ_C 36.0 (C–9), δ_C 67.8 (C–10), δ_C 24.0 (C–11); a methoxy carbon at δ_C 56.7 (C–13) and an aromatic methyl carbon at δ_C 13.0 (C–12). The connection of the 2–hydroxypropyl unit to the naphthoquinone nucleus was confirmed at C–6 based on the HMBC correlations of H–9 with C–5, C–6, C–7 and H–10 with C–6. The methoxy moiety was assigned at C–3 on the basis of an HMBC correlation of the methoxy protons H–13 with C–3 and further confirmed by 1D NOESY correlation (Appendix 175) between H–2 and H–13. The structure of **29**, after comparing the 1D and 2D spectral data to reported literature was successfully elucidated as (+)–solaninol (Arsenault, 1968; Hashimoto *et al*., 2009; Trisuwan *et al*., 2010). To establish the absolute configuration of solaniol (**29**), red needle crystals were recovered after recrystallization in acetone. A single crystal was analyzed by X–ray crystallography and the X–ray structure confirmed the planar structure of solaniol (**29)**. Based on the reasonable value of

the Flack parameter, x = –0.07 (14), the absolute configuration was determined as 10S and the relative configuration was as shown in Figure 4.77.

Table 4.26: NMR spectral data for compound **29** in $CDCl_3$ (see Appendix 170–174)

Position	δ_H[a] multi. (*J* in Hz)	δ_C[b]	COSY[a]	HMBC[a]	
1		184.2			
2		6.18, s	109.6	1, 3, 4, 8a	
3		106.6			
4		177.8			
4a		109.5			
5		162.3			
6		138.3			
7		142.2			
8		160.5			
8a		107.9			
9		a. 2.93, br s (2.0)	36.0	10	5, 6, 7, 10, 11 b. 2.94, d
10		4.13, q (12.5, 6.0)	67.8	9, 11	6, 9, 11
11		1.31, d (6.0)	24.0	10	9, 10
12		2.33, s	13.0	6, 7, 8	
13		3.91, s	56.7	3	
5-OH	13.31*				
8-OH	13.04*				

[a]Recorded at 500 MHz; [b]Recorded at 125 MHz; *Interchangeable

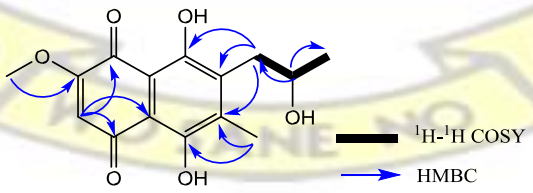


Figure 4.78: Selected HMBC and COSY correlations of compound **29**.

Compound **29**: Red amorphous solid; $[\alpha]^{20}_D$ + 44 (*c* 0.1, MeOH); LC–UV [MeOH–H_2O

(0.1% HCOOH)] λ_{max} 222 nm; ^{1}H NMR ($CDCl_3$, 500 MHz) and ^{13}C NMR ($CDCl_3$, 125 MHz), see Table 4.26; positive HRESI–MS *m/z* 293.1023 $[M + H]^+$ (cald. for $C_{15}H_{17}O_6$, 293.1020), *m/z* 275.0917 $[M + H–H_2O]^+$ (cald. for $C_{15}H_{15}O_5$, 275.0916), *m/z* 315.0843 $[M + Na]^+$ (cald. for $C_{15}H_{16}O_6Na$, 315.0842).

X–ray crystal data of solaniol (29): Red needle crystals, monoclinic crystal system; crystal size 0.051 x 0.069 x 0.547 mm^3, unit cell dimensions *a* = 16.1377(10) Å, *b* = 4.7293(2) Å, *c* = 34.365(3) Å, Volume 2619.6(3) $Å^3$; *Z* = 8, *T* = 100(2) K, μ(Cu Kα) = 0.976 mm^{-1}, D_{calc} = 1.487 g/cm^3; 19410 reflections collected with θ angel ranged from 3.87 to 75.00°; 5307 independent reflections (R(int) = 0.0308). R1 = 0.0427, wR2 = 0.1081 (all data); Flack parameter = –0.07(14). Crystallographic data of **10** was deposited in the Cambridge Crystallographic Data Centre with supplementary publication number CCDC 1487779.

Copies of the data can be acquired, free of charge, from Cambridge Crystallographic Data Centre, 12 Union Road, Cambridge CB2 1EZ, UK by fax: +44(0)1223 336033 or e-mail: deposit@ccdc.cam.ac.uk.

4.2.8 Structure elucidation of 2,3–dihydro–5–hydroxy–8–methoxy–2,4–dimethylnaphtho[1,2–b]furan–6,9–dione (30, known compound)

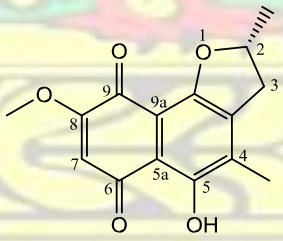


Figure 4.79: Chemical structure of compound **30**.

Compound **30** was isolated as red amorphous solid and the molecular formula was assigned as $C_{15}H_{14}O_5$ based on the ion *m/z* 275.0916 $[M + H]^+$ (cald. for 275.0914) in the HRESI–MS

spectrum (Appendix 176) with nine DBE compared to **29**. HRESI–MS/MS fragmentation afforded a key fragment at *m/z* 257.0809 $[M + H–H_2O]^+$ together with other ions at *m/z* 260.0679 $[M + H–CH_3]^+$, *m/z* 243.0652 $[M + H–CH_3OH]^+$. Analysis of the ^1H NMR spectrum (Table 4.27 and Appendix 178) revealed an olefinic proton at δ_H 6.04 (1H, s, H–7), a methine proton at δ_H 5.17 (1H, q, *J* = 14.7 Hz, 6.3, H–2), methoxy protons at δ_H 3.85 (3H, s, H–3), methylene protons at [δ_H 3.28 (1H, dd, *J* = 16.8, 8.4 Hz, H–3a), δ_H 2.74 (1H, dd, *J* = 17.5, 7.0 Hz, H–3b)] and two sets of methyl protons at δ_H 2.22 (3H, s, 4–Me) and δ_H 1.53 (3H, d, *J* = 6.3 Hz, 2–Me). Based on the 1D and 2D NMR, the structure of **30** was unequivocally elucidated as the reported 2,3–dihydro–5–hydroxy–8–methoxy–2,4–dimethylnaphtho[1,2– b]furan–6,9–dione (Tatum *et al*., 1989).

Table 4.27: NMR spectral data for compound **30** in $CDCl_3$ (see Appendix 178–182)

Position	δ_H[a] multi. (*J* in Hz)	δ_C[b]	COSY[a]	HMBC[a]
1a		154.9*		
2		6.17, q (14.7, 6.3)	82.0	3, 2-Me 1a, 3, 3a, 2-Me
3	a. 3.28, dd (16.8, 8.4) b. 2.74, dd (17.5, 7.0)	35.5	2	1a, 2, 4, 2-Me
3a		139.0		
4		133.7		
5		157.0*		
5a		110.3		
6		190.0		
7		6.04, s	108.8	6, 9, 5a
8		161.4		

9		177.2		
9a		108.9		
2-Me	1.53, d (6.3)	22.0	2	2, 3
4-Me	2.22, s	13.2		4, 5, 3a
8-MeO	3.85, s	56.5		8
5-OH	13.48			

[a]Recorded at 700 MHz; [b]Recorded at 176 MHz; [*]Interchangeable

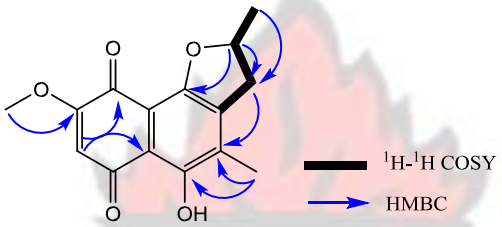


Figure 4.80: Selected HMBC and COSY correlations of compound **30**.

Compound **30**: Red amorphous solid; LC–UV [MeOH–H_2O (0.1% HCOOH)] λ_{max} 224 nm; ^{1}H NMR ($CDCl_3$, 700 MHz) and ^{13}C NMR ($CDCl_3$, 176 MHz), see Table 4.27; positive HRESI–MS *m/z* 275.0916 $[M + H]^+$ (cald. for $C_{15}H_{15}O_5$, 275.0914), *m/z* 297.0735 $[M + Na]^+$ (cald. for $C_{15}H_{14}O_5Na$, 297.0734).

4.2.9 Structure elucidation of N_b–acetyltryptamine (31, known compound)

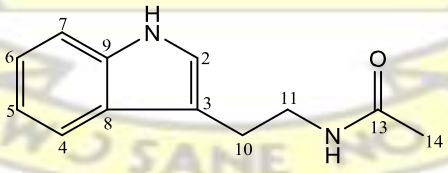


Figure 4.81: Chemical structure of compound **31**.

Compound **31** was obtained a violet amorphous solid and the molecular formula was assigned as $C_{12}H_{14}ON_2$ based on the pseudo–molecular ion peak at *m/z* 203.1181 $[M + H]^+$ (cald. for 203.1179) in the HRESI–MS spectrum (Table 4.28 and Appendix 183). The HRESI–MS/MS, in positive mode, showed a key fragment at *m/z* 144.0804 $[M + H–C_2H_5ON]^+$. The ^1H NMR spectrum (Table 4.28 and Appendix 185) revealed the presence of six downfield proton signals which indicated a monosubstituted indole skeleton. The indole skeleton protons included an olefinic doublet signal at δ_H 7.01 (1H, d, *J* = 1.8 Hz, H–2), a broad singlet signal at *δ* 8.31 (1H, br s, H–1) is attributed to the indoyl N–H proton. The broadening of the H–1 signal is due to the quadrupole broadening effect of nitrogen (Williams and Fleming, 1980).

The other signals of the indole skeleton were aromatic protons at δ_H 7.11 (1H, t, *J* = 7.8 Hz, H–5), δ_H 7.19 (1H, t, *J* = 8.4 Hz, H–6), δ_H 7.36 (1H, d, *J* = 8.4 Hz, H–7) and δ_H 7.58 (1H, d, *J* = 7.8 Hz, H–4). The above signals suggested substitution at the indoyl position 3. The side chain signals observed included one methyl group signal at δ_H 1.90 (1H, s, H–14), two methylene groups at δ_H 2.95 (2H, t, *J* = 6.6 Hz, H–10) and δ_H 3.58 (2H, q, *J* = 6.6, 13.2 Hz, H–11) which appeared as a quadruplet due to coupling with H–10 and δ_H 5.60 (1H, br s, H– 12). The ^{13}C NMR (Table 4.28 and Appendix 186) and HSQC (Appendix 188) spectra showed δ_C 112.8 (C–3), δ_C 127.3 (C–8) and δ_C 136.4 (C–9) were quaternary carbons. The presence of HMBC correlations from H-2 to C–3, C–8, C–9, δ_C 25.2 (C–10) and from H–10 to δ_C 122.1 (C–2), C–3, C–8, δ_C 39.8 (C–11) confirmed substitution of the indole skeleton at C–3. The structure of compound **31**, after comparing the ^1H and ^{13}C NMR data to reported literature, was elucidated as N_b–acetyltryptamine (Wang *et al.*, 2014).

Table 4.28: NMR spectral data for compound **31** in $CDCl_3$ (see Appendix 185–189)

Position	δ_H[a] multi. (*J* in Hz)	δ_{Cb}	COSY[a]	HMBC[a]
1	8.31, br s		2	2, 3, 8, 9
2	7.01, d (1.8)	122.1	1	3, 8, 9
3		112.8		

4	7.58, d (7.8)	118.6	5	3, 6, 8, 9
5	7.11, t (7.8)	119.4	4	4, 6, 7, 8, 9
6	7.19, t (8.4)	122.2	7	4, 7, 9
7	7.36, d (8.4)	111.3	6	5, 8
8		127.3		
9		136.4		
10	2.95, t (6.6)	25.2	11	2, 3, 8, 11
11	3.58, q (13.2, 6.6)	39.8	10, 12	3, 10, 13
12	5.60, br s		11	11, 13
13		170.2		
14	1.90, s	23.3	13	

[a]Recorded at 700 MHz; [b]Recorded at 176 MHz

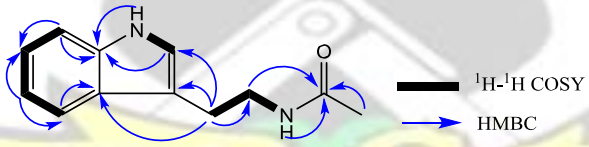


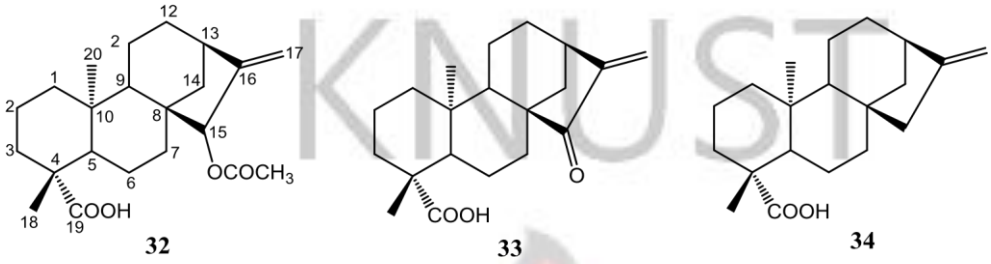
Figure 4.82: Selected HMBC and COSY correlations of compound **31**.

Compound **31**: Violet amorphous solid; LC–UV [MeOH–H_2O (0.1% HCOOH)] λ_{max} 230 nm and 280 nm; ^{1}H NMR ($CDCl_3$, 600 MHz) and ^{13}C NMR ($CDCl_3$, 150 MHz), see Table 4.28; positive HRESI–MS *m/z* 203.1181 $[M + H]^+$ (cald. for $C_{12}H_{15}ON_2$, 203.1179), *m/z* 225.0999 $[M + Na]^+$ (cald. for $C_{12}H_{14}ON_2Na$, 225.0996).

4.3 Imaging and Characterization studies on the fruits of *X. aethiopica* 4.3.1 MALDI–HRMS imaging and HPLC–HRESI–MS^n characterization of kaurane diterpenoids (32–34) in the fruits of *Xylopia aethiopica* (Dunal) A. Rich (Annonaceae)

The spatial distribution of three kaurane diterpenes namely, xylopic acid (**32**), ent–kaur–16–en–19–oic acid (**33**) and 15–oxo–ent–kaur–16–en–19–oic acid (**34**) (Figure 4.83), in the fruits of *X. aethiopica* were visualized by MALDI–HRMS imaging techniques, using isolated xylopic

acid as the reference standard. The selected diterpenes were identified and characterized by HPLC–HRESI–MS^n analysis. Based on the information obtained from the HRESI–MS^n spectra, the fragmentation pathways of the compounds were plausibly proposed.



32 33 34

Figure 4.83: Chemical structures of compounds **32**–**34**

4.3.1.1 MALDI–HRMS imaging of compounds 32–34

The isolated xylopic acid (**32**), used as reference standard, was analyzed by employing various matrices to select the best matrix that afforded better ionization. α–cyano–4– hdroxycinnamic acid (HCCA) emerged as the matrix that afforded satisfactory results. The MALDI–HRMS spectra of xylopic acid (**32**) revealed a low affinity for the molecular ion at *m/z* 361.2374 $[M + H]^+$. However, a high intensity was observed for the precursor ions at *m/z* 301.2163 $[M + H–OCOCH_3]^+$ and *m/z* 399.1932 $[M + K]^+$. The sodium adduct at *m/z* 383.2193 $[M + Na]^+$ gave unsatisfactory results and hence was not considered.

Fresh fruits of *X. aethiopica* were used for the imaging investigation. The transverse sections of the fruit were cut and fixed onto the surface of glass slides. The matrix was sprayed onto the fixed tissues and the target compounds were imaged in positive ionization mode. The ions adopted for the imaging of **32** in the fruit tissue, were *m/z* 301.2166 $[M + H–OCOCH_3]^+$ and *m/z* 399.1932 $[M + K]^+$. Analysis of the IMS spectra showed **32** was mainly localized in the pericarp region of the fruit (Figure 4.84b, c). Only trace amount of xylopic acid (**1**) was visualized in the seed (middle area).

Ent–kaur–16–en–19–oic acid **(33)** was visualized based on the molecular ion peak at *m/z* 317.2111 $[M + H]^+$ (Figure 4.84d) and the more intense potassium adduct ion at *m/z* 355.1670 $[M + K]^+$ (Figure 4.84e). Similar to **32**, **33** was located mainly in the pericarp region of the fruit with trace amount in the seed. The molecular ion peak at *m/z* 303.2319 $[M + H]^+$ was employed in visualizing 15–oxo–ent–kaur–16–en–19–oic acid (**34**). The intensity of the molecular ion was low (Figure 4.84f). The sodium and potassium adducts of **34** were not detected in the MALDI–HRMS spectrum. **34** was located in the pericarp region of the fruit with no trace in the seed.

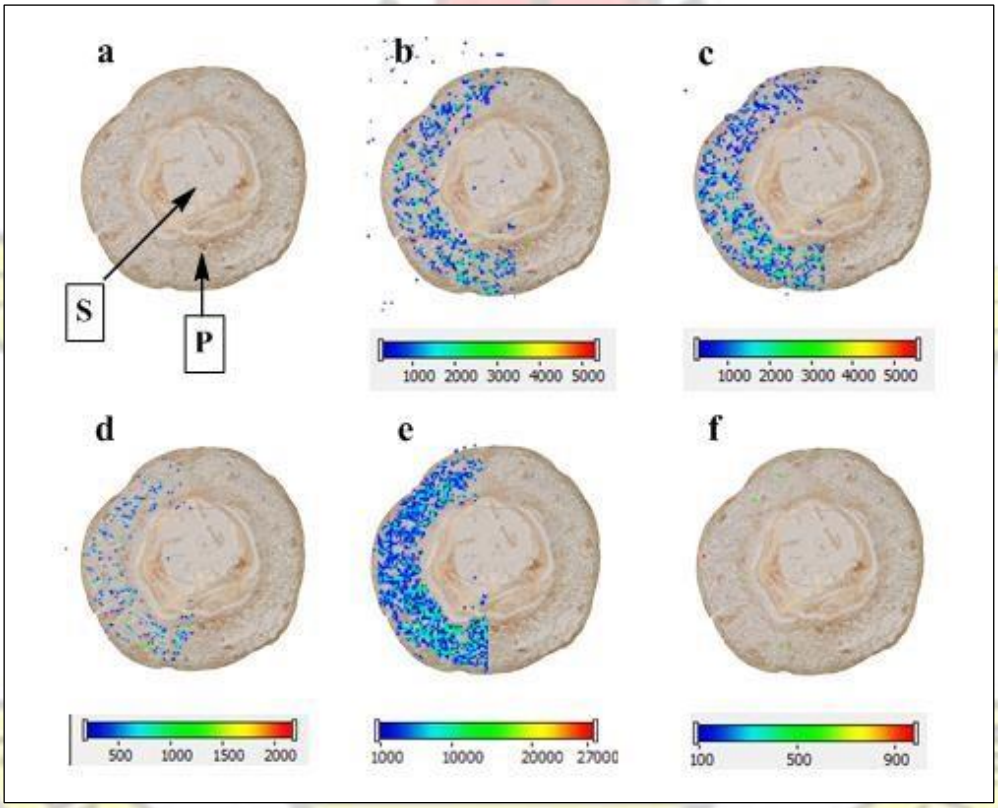
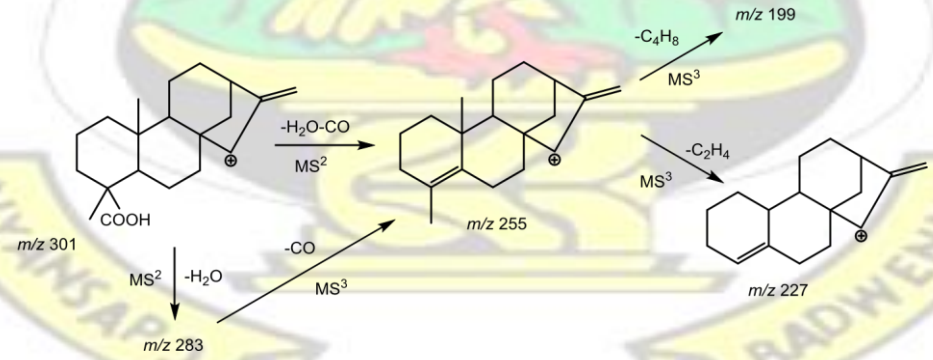


Figure 4.84: Localization of target compounds by MALDI–HRMS imagining in *X. aethiopica*. **a** Optical image of the transverse section of *X. aethiopica* fruit (P, pericarp; S, seed). **b** Localization of xylopic acid (*m/z* 301.216; $[M + H–OCOCH_3]^+$). **c** Localization of xylopic acid (*m/z* 399.193; $[M + K]^+$). **d** Localization of ent–kaur–16–en–19–oic acid (*m/z* 317.211; $[M + H]^+$). **e** Localization of ent–kaur–16–en–19–oic acid (*m/z* 355.167; $[M + K]^+$). **f** Localization of 15–oxo–ent–kaur–16–en–19–oic acid (*m/z* 303.231; $[M + H]^+$).

4.3.2 HPLC–HRESI–MS^n characterization of compounds 32–34

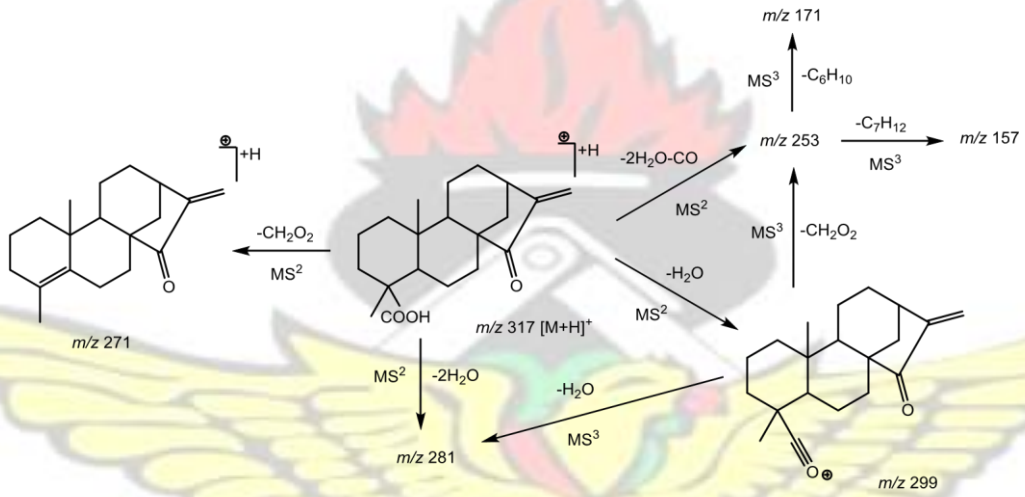
The HRESI–MS spectrum of xylopic acid (**32**) (Appendix 190) showed a base peak at *m/z* 301.2163 $[M + H–OCOCH_3]^+$ together with two additional peaks at *m/z* 383.2193 $[M + Na]^+$ and *m/z* 361.2374 $[M + H]^+$. Owing to the low intensity of the molecular ion peak, the ion at *m/z* 301.2163 $[M + H–OCOCH_3]^+$ was adopted as the precursor ion to study the MS^n fragmentation pattern of **32**. The HRESI–MS^2 spectrum of the precursor ion at *m/z* 301.2166 (Appendix 191), revealed a key ion signal at *m/z* 255 corresponding to subsequent losses of H_2O and CO groups. Additionally, a competing minor ion at *m/z* 283 was observed, which was produced after a loss of a molecular of H_2O. The MS^3 spectrum of the ion at *m/z* 255 (Appendix 192) gave a prominent fragment ion at *m/z* 199 as a result of the loss of C_4H_8. MS^3 spectrum of the precursor ion at *m/z* 283 (Appendix 193) afforded the fragment ion at *m/z* 255 as the abundant ion and a competing ion at *m/z* 265 after respective losses of CO and H_2O. The fragmentation pathway of **32** was proposed (Scheme 2), based on the precursor ion at *m/z* 301.2163 $[M + H–OCOCH_3]^+$.



Scheme 2: Proposed HRESI–MS^n fragmentation pathway of **32** based on the precursor ion at *m/z* 301 $[M + H–OCOCH_3]^+$.

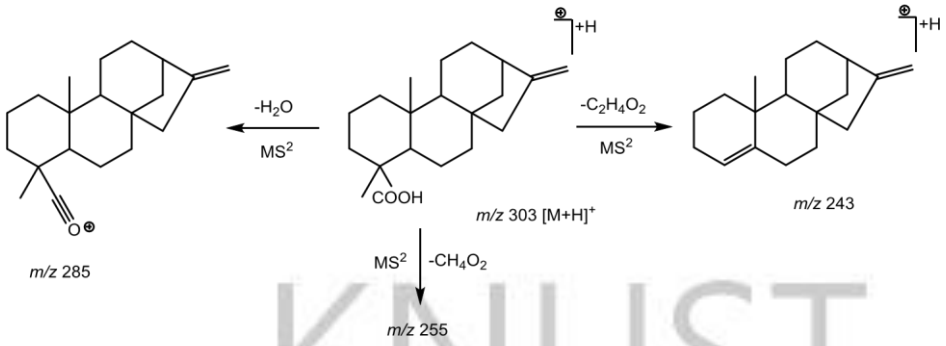
The HRESI–MS^2 spectrum of the protonated molecular ion of **33** (Appendix 194), revealed a principal ion peak at *m/z* 299 which was formed after a loss of H_2O from the carboxylic acid

group at C–19. In addition, ions at *m/z* 253 after losses of $2H_2O$ and CO; *m/z* 271 after a loss of CH_2O_2; *m/z* 281 after loss of two molecules of H_2O were observed. MS^3 analysis of the base ion at *m/z* 299 (Appendix 195) produced a key fragment ion at *m/z* 253 resulting from the loss of CH_2O_2 and an additional fragment ion at *m/z* 281 after loss of H_2O. MS^3 spectrum of the ion at *m/z* 253 (Appendix 196) showed two predominant ions at *m/z* 171 and *m/z* 157 which were formed after losses of C_6H_{10} and C_7H_{12} respectively. The proposed fragmentation pathway of **33** based on the fragment information was as shown in scheme 3.



Scheme 3: Proposed HRESI–MS^n fragmentation pathway of **33**

Similar to **32** and **33**, the HRESI–MS^2 spectrum of the protonated molecular ion of **34** (Appendix 197) gave a characteristic fragment ion at *m/z* 285, formed after the loss of H_2O from the carboxylic acid group. Subsequent losses of $C_2H_4O_2$ and CH_4O_2 afforded fragment ions at *m/z* 243 and *m/z* 255 respectively. The proposed collision-induced mass spectral fragmentation mechanism of **34** was as shown in scheme 4.



Scheme 4: Proposed HRESI–MS^n fragmentation pathway of **34**.

KNUST

4.4 Biological activities

4.4.1 DPPH free radical scavenging assay

Regiafuran A–C (**1**–**3**), mulberrofuran Y (**4**), moracin O (**6**), sanggenon C (**7**), kuwanol E (**8**), chalcomoracin (**9**), 6–prenylated–3,7,5,4′–tetrahydroxy–2′–methoxyflavonol (**12**) and 5,7,4′–trihydroxy–2′–methoxyflavanone (**17**) isolated from the stem bark of *C. regia* were evaluated for their free radical scavenging activities. Table 4.29 shows the IC_{50} values of the tested compounds compared to the reference standard, trolox. Regiafuran A and B, mulberrofuran Y, kuwanol E and 5,7,4′–trihydroxy–2′–methoxyflavanone exhibited pronounced free radical scavenging properties. 5,7,4′–trihydroxy–2′–methoxyflavanone demonstrated the most activity with an IC_{50} of 1.8 μg/mL. A structure–activity relationship analysis of the active and inactive compounds revealed the free radical scavenging activity of regiafuran A reduced when the alcohol functional group at C–6 was converted to a methoxy group in regiafuran B. This suggested that oxygen functionality at C–6 is essential or needed for activity and the activity is unambiguously potentiated when the oxygen functionality is a free hydroxyl moiety. This notion is further observed from the activities of regiafuran C, mulberrofuan Y, moracin O, kuwanol E and chalocomoracin. A comparison of the activities of regiafuran C and mulberrofuran Y, and regiafuran A and regiafuran B, indicated a significant reduction in activity when a geranyl moiety is attached to C–5. The reduction in activity is nonetheless insignificant

when the geranyl moiety is attached to C–4. 6–prenylated–3,7,5,4′– tetrahydroxy–2′–methoxyflavonol, a 6–prenylated derivative of 3,7,5,4′–tetrahydroxy–2′– methoxyflavonol demonstrated more activity than 3,7,5,4′–tetrahydroxy–2′–methoxyflavonol whose activity has previously been reported as 3.31 μg/mL (Gonda *et al*., 2000). This showed that activity is enhanced with an isoprenyl moiety at C–6. Kuwanol E exhibited high activity similar to regiafuran A with an IC_{50} of 2.1 μg/mL, but this activity significantly reduced when the oxygen functionality at C–2 was changed to a furan ring in chalcomoracin. These results disclose not only the scientific basis for the traditional use of *C. regia* in the treatment of burns and wounds, but the potential of 2–arylbenzofuran derivatives as lead compounds in the synthesis of more potent anti–oxidants (Kyekyeku *et al*., 2016).

Table 4.29: Free radical scavenging effects of tested compounds (**1–4**, **6–9**, **12**, **17**)

Compound	**1**	**2**	**3**	**4**	**6**	**7**	**8**	**9**	**12**	**17**	Trolox[a]
IC_{50} (µg/ml)[b]	1.9	2.4	4.9	2.2	3.0	112.8	2.1	4.1	2.8	1.8	1.1

[a]Reference standard; [b]All values are in µg/ml and derived from experiments in triplicate

4.4.2 Anti–inflammatory assay

The potential anti–inflammatory activities of compounds regiafuran A–C (**1**–**3**), chlorophorin (**10**), isochlorophorin (**11**), 6–prenylated–3,7,5,4′–tetrahydroxy–2′–methoxyflavonol (**12**) and 5,7,4′–trihydroxy–2′–methoxyflavanone (**17**) isolated from the stem bark of *C. regia*, were evaluated employing a Parameter PGE_2 forward sequential competitive enzyme immunoassay (R&D Systems Europe Ltd., Abingdon, United Kingdom) method using cortisone as the reference standard. None of the tested compounds exhibited any anti–inflammatory activity (Kyekyeku *et al*., 2016).

4.4.3 Antibacterial assay and possible ecological role of endophytic fungus JK10

The antibacterial activities of the crude extract and the isolated compounds **20**–**28** from the endophytic fungus JK10 were investigated against two Gram negative bacteria, the environmental strain of *Escherichia coli* and *Acinetobacter* sp. BD4, a typical soil bacterium. In addition, the activities of the crude extract and the isolated compounds were evaluated against the clinically relevant bacterium *Staphylococcus aureus* (Gram–positive) and *Bacillus subtilis* (Gram–positive). Streptomycin and gentamicin were employed as the reference standards. Table 4.30 shows the minimum inhibitory concentrations (MIC) of the tested compounds against the four bacteria. 7–desmethyl fusarin C–22/23 and 7–desmethyl fusarin C–25, as well as the crude extract demonstrated remarkable activity at concentrations of 10.0 μg/mL against the soil bacterium *Acinetobacter* sp. BD4 similar to the reference standard streptomycin. The activity of the crude extract against this soil bacterium could be attributed to 7–desmethyl fusarin C–22/23 and 7–desmethyl fusarin C–25 since they exhibited the same MIC values as the crude extract. All the tested compounds and, as expected, the crude extract demonstrated activity against the environmental strain of *E. coli*, with 7–desmethyl fusarin C–24 and 7–desmethyl fusarin C–26 demonstrating the highest activity at concentrations of 5.0 μg/mL. The endophytic fungus could therefore play a very important ecological role in the plant.

Endophytic microorganisms co–evolve a myriad of characteristic traits for existing and functioning in their specific ecological niches (Kusari *et al*., 2012). These evolved characteristic traits with plants involve production of precursors, quorum sensing molecules, secretion of antimicrobial chemical defense molecules among others (Kusari *et al*., 2013; Kusari *et al*., 2015a; Li *et al*., 2015). 7–desmethyl fusarin C–22/23 and 7–desmethyl fusarin C–25 exhibited high activity against *Acinetobacter* sp. which is a soil bacterium and typically inhabit the rhizosphere. The rhizosphere is a hotspot for a wide range of microbial interactions (Li *et al*., 2014). It can therefore be proposed that the endophytic fungus, which was isolated from the

roots, contributes a chemical–mediated defense to the host plant against invading specific soil and environmental bacterial pathogens. The results obtained from this study provide further evidence of the existence of a unique cost–benefit endophyte–plant association (Kusari *et al*., 2012). None of the tested compounds demonstrated any activity against *S. aureus* and *B. subtilis* suggesting the tested compounds are not suitable lead compounds for synthesis of potent antibiotics for treating infections in humans caused by these organisms.

Tab 4.30: Minimum inhibitory concentrations (MIC) of compounds **20□28** and the crude extract (**CrE**) against Gram–positive and Gram–negative bacteria compared to standard references (streptomycin and gentamicin).[a]

Organism (DSMZ no.)	**20**/**21**	**22**/**23**	**24**	**25**	**26**	**27**/**28**	**CrE**	streptomycin	gentamicin
Staphylococcus aureus (DSM 799)	>10.0	>10.0	>10.0	>10.0	>10.0	>10.0	>10.0	5.0	1.0
Escherichia coli (DSM 1116)	10.0	10.0	5.0	10.0	5.0	10.0	5.0	1.0	1.0
Bacillus subtilis (DSM 1088)	>10.0	>10.0	10.0	>10.0	>10.0	>10.0	>10.0	5.0	1.0
Acinetobacter sp. (DSM 586)	>10.0	10.0	>10.0	10.0	>10.0	>10.0	10.0	10.0	5.0

[a]All values are in μg/mL and derived from experiments in triplicate.

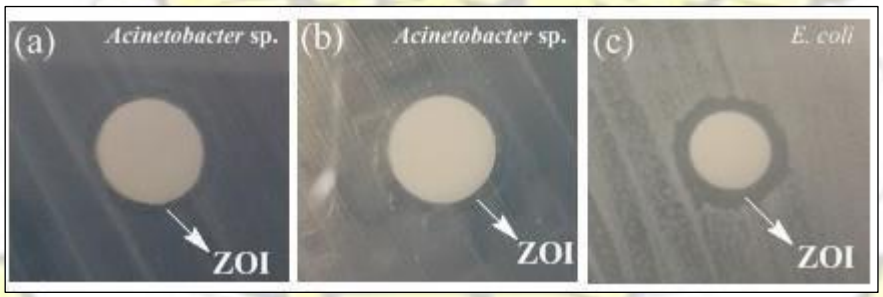


Figure 4.85: Observed ZOIs of compounds **22**/**23** (a, 10 μg/mL), **25** (b, 10 μg/mL) against *Acinetobacter* sp and compound **24** against *E. coli* (c, 5 μg/mL).

KNUST

CHAPTER 5 CONCLUSIONS AND RECOMMENDATIONS

5.1 CONCLUSIONS

Secondary metabolites from *Chlorophora regia*

The aim of this study was to isolate, characterize and evaluate the biological activities of the secondary metabolites from the Ghanaian medicinal plant *C. regia* and the endophytic community harbored in the plant. Extensive phytochemical screening of the stem bark of *C. regia*, afforded the isolation and characterization of nineteen compounds including three new 2–arylbenzofuran derivatives, regiafuran A–C (**1**–**3**), together with three known 2–arylbenzofuran derivatives, mulberrofuran Y (**4**), moracin N (**5**) and moracin O (**6**). Also isolated were three known Diels–Alder adducts sanggenon C (**7**), kuwanol E (**8**) and chalcomoracin (**9**). In addition, two known stilbene derivatives chlorophorin (**10**) and isochlorophorin (**11**) were successfully isolated. One new flavonoid, 6–prenylated–3,5,7,4′–tetrahydroxy–2′–methoxyflavonol (**12**) together with seven known flavonoids, gancaonin P (**13**), 3,5,7,4′–tetrahydroxy–2′–methoxyflavonol (**14**), quercetin (**15**), kaempferol (**16**) and three known flavanones, 5,7,4′–trihydroxy–2′–methoxyflavanone (**17**), 5,7,3′,5′–tetrahydroxyflavanone (**18**) and naringenin (**19**) were isolated. A possible biosynthetic pathway for compound **12** was proposed on the basis of the biosynthesis of flavonols. This constitutes the first report of isochlorophorin (**11**), gancaonin P (**13**), 3,5,7,4′–tetrahydroxy– 2′–methoxyflavonol (**14**), 5,7,4′–trihydroxy–2′–methoxyflavanone (**17**) and 5,7,3′,5′–tetrahydroxyflavanone (**18**) in the genus *Chlorophora*. Regiafuran A and B, mulberrofuran Y,

kuwanol E and 5,7,4′–trihydroxy–2′–methoxyflavanone demonstrated significant free radical scavenging properties compared to the reference standard trolox. The tested compounds, did not show any anti-inflammatory activity using a PGE_2 (prostaglandin E_2) competitive enzyme immunoassay.

Secondary metabolites from endophytic fungus, JK10

The unidentified endophytic fungus, JK10, was isolated from the root tissues of *C. regia*. The endophytic strain was pre–screened under axenic conditions for important secondary metabolites using the OSMAC approach. Large–scale fermentation was then carried out on solid rice media and the mycelia extracted with ethylacetate. Comprehensive investigation resulted in the isolation and characterization of twelve compounds including seven new 7–desmethyl derivatives of fusarin C (**20**–**26**) and five known compounds, NG–391/NG–393 (**27**/**28**), (+)–(S)–solaniol (**29**), 2,3–dihydro–5–hydroxy–8–methoxy–2,4–dimethylnaphtho[1,2–b]furan–6,9–dione (**30**) and N_b–acetyltryptamine (3**1**). The antibacterial activity of the isolated compounds **20**–**28** and the crude extract were evaluated against two Gram–negative bacteria and two Gram–positive bacteria. 7–desmethyl fusarin C–22/23 and 7–desmethyl fusarin C–25 exhibited remarkable activity at concentrations of 10.0 μg/mL against the soil bacterium *Acinetobacter* sp. BD4 compared to the reference standard streptomycin. All the compounds tested demonstrated activity against the environmental strain of *E. coli*, with 7–desmethyl fusarin C–24 and 7–desmethyl fusarin C–26 giving the highest activity at concentrations of 5.0 μg/mL. Herein, it could be proposed that the endophytic fungus, whose origin is from the roots, contributes a chemical–mediated defensive mechanism to the host plant against invading specific soil and environmental bacterial pathogens. This gives credence to long held notion of the existence of a unique cost–benefit endophyte–plant association (Kusari *et al*., 2012). The absolute configuration of solaniol (**29**) was established for the first time by X–ray diffraction analysis of a single crystal, based on the reasonable value of the Flack parameter, x = –0.07 (14), to be 10S.

Altogether, thirty–one compounds were successfully isolated and characterized from the stem bark of *C. regia* and the endophytic fungus, JK10, harbored in the root. Out of these, eleven were new compounds.

MALDI–HRMS imaging and HPLC–HRESI–MS^n characterization of kaurane diterpenoids in the fruits of *Xylopia aethiopica*

The spatial distribution of three kaurane diterpenes including xylopic acid (**32**), ent–kaur–16–en–19–oic acid (**33**) and 15–oxo–ent–kaur–16–en–19–oic acid (**34**), in the fruits of *X. aethiopica* were visualized using MALDI–HRMS imaging techniques. The selected compounds were identified and characterized by HPLC–HRESI–MS^n analyses. The distributions of all the studied compounds were predominantly in the pericarp region of the fruit with non–detectable levels in the seed.

5.2 RECOMMENDATIONS

The following recommendations are proposed for the purposes of future work;

- Phytochemical screening of the other parts of *C. regia* to investigate their phytochemical composition. This would provide useful information of the diversity of secondary metabolites produced by the plant.
- Further in vitro assays should be carried out to investigate the mechanism of action of compounds 7–desmethyl fusarin C–22/23 and 7–desmethyl fusarin C–25 against *Acinetobactor* sp.
- Evaluation of the cytotoxicity profile of the 7-desmethyl derivatives of fusarin C (**2028**) due to their significant antibacterial activities in order to ascertain their suitability in the humans for treating *Acinetobactor* sp. infections.

REFERENCES

1. Abbiw, D. K. (**1990**). *Useful plants of Ghana: West African uses of wild and cultivated plants*, Intermediate Technology Publications and The Royal Botanic Gardens K. E. W. **6**, 4792.

2. Abraham, E. and Newton, G. (**1961**). The structure of cephalosporin C. *Biochemical Journal*, **79**, 377.

3. Adaramoye, O. A., Sarkar, J., Singh, N., Meena, S., Changkija, B., Yadav, P. P., Kanojiya, S. and Sinha, S. (**2011**). Antiproliferative action of *Xylopia aethiopica* fruit extract on human cervical cancer cells. *Phytotherapy Research*, **25**, 1558-1563.

4. Ameyaw, E. O., Woode, E., Boakye-Gyasi, E., Abotsi, W. K., Kyekyeku, J. O. and Adosraku, R. K. (**2014**). Anti-allodynic and anti-hyperalgesic effects of an ethanolic extract and xylopic acid from the fruits of *Xylopia aethiopica* in murine models of neuropathic pain. *Pharmacognosy research*, **6**, 172.

5. Antolovich, M., Prenzler, P. D., Patsalides, E., Mcdonald, S. and Robards, K. (**2002**). Methods for testing antioxidant activity. *Analyst*, **127**, 183-198.

6. Apak, R., Güçlü, K., Özyürek, M. and Karademir, S. E. (**2004**). Novel total antioxidant capacity index for dietary polyphenols and vitamins C and E, using their cupric ion reducing capability in the presence of neocuproine: CUPRAC method. *Journal of Agricultural and Food Chemistry*, **52**, 7970-7981.

7. Arsenault, G. (**1968**). Fungal metabolites—III: Quinones from *fusarium solani* D2 purple and structure of (+)-solaniol2. *Tetrahedron*, **24**, 4745-4749.

8. Asekun, O. and Adeniyi, B. (**2004**). Antimicrobial and cytotoxic activities of the fruit essential oil of *Xylopia aethiopica* from Nigeria. *Fitoterapia*, **75**, 368-370.

9. Balick, M. J. and Cox, P. A. (**1996**). *Plants, people, and culture: the science of ethnobotany*, Scientific American Library, **73**, 25-61.

10. Balkwill, F. and Mantovani, A. (**2001**). Inflammation and cancer: back to Virchow? *The lancet*, **357**, 539-545.

11. Balunas, M. J. and Kinghorn, A. D. (**2005**). Drug discovery from medicinal plants. *Life sciences*, **78**, 431-441.

12. Barnes, P. J., Belvisi, M. G., Mak, J. C., Haddad, E.-B. and O'Connor, B. (**1995**). Tiotropium bromide (Ba 679 BR), a novel long-acting muscarinic antagonist for the treatment of obstructive airways disease. *Life sciences,* **56**, 853-859.

13. Bary, A. (**1866**). *Morphologie und physiologie der pilze, flechten und myxomyceten*, W. Engelmann.

14. Bashyal, B. P., Faeth, S. H. and Gunatilaka, A. (**2007**). 13-alpha-hydroxylucilactaene and other metabolites of an endophytic strain of *Fusarium acuminatum*. *Natural Product Communications*, **2**, 547-550.

15. Bedane, K. G., Kusari, S., Eckelmann, D., Masesane, I. B., Spiteller, M. and Majinda, R. R. (**2015**). Erylivingstone A–C with antioxidant and antibacterial activities from *Erythrina livingstoniana*. *Fitoterapia,* **105**, 113-118.

16. Benzie, I. F. and Strain, J. (**1996**). The ferric reducing ability of plasma (FRAP) as a measure of ―antioxidant power‖: the FRAP assay. *Analytical biochemistry,* **239**, 7076.

17. Boakye-Yiadom, K., Fiagbe, N. and Ayim, J. (**1977**). Antimicrobial properties of some West African medicinal plants iv. Antimicrobial activity of xylopic acid and other constituente of the fruits of *Xylopia aethiopica* (Annonaceae). *Lloydia,* **40**, 543.

18. Bondet, V., Brand-Williams, W. and Berset, C. (**1997**). Kinetics and mechanisms of antioxidant activity using the DPPH. free radical method. *LWT-Food Science and Technology*, **30**, 609-615.

19. Brand-Williams, W., Cuvelier, M.-E. and Berset, C. (**1995**). Use of a free radical method to evaluate antioxidant activity. *LWT-Food science and Technology,* **28**, 2530.

20. Butler, M. S. (**2004**). The role of natural product chemistry in drug discovery. *Journal of natural products,* **67**, 2141-2153.

21. Cao, G., Alessio, H. M. and Cutler, R. G. (**1993**). Oxygen-radical absorbance capacity assay for antioxidants. *Free Radical Biology and Medicine*, **14**, 303-311.

22. Chen, Z., Bertin, R. and Froldi, G. (**2013**). EC50 estimation of antioxidant activity in DPPH assay using several statistical programs. *Food chemistry,* **138**, 414-420.

23. Chevion, S., Roberts, M. A. and Chevion, M. (**2000**). The use of cyclic voltammetry for the evaluation of antioxidant capacity. *Free Radical Biology and Medicine,* **28**, 860-870.

24. Christensen, L. P., Lam, J. and Sigsgaard, T. (**1988**). A novel stilbene from the wood of *Chlorophora excelsa*. *Phytochemistry,* **27**, 3014-3016.

25. Cioffi, G., Escobar, L. M., Braca, A. and De Tommasi, N. (**2003**). Antioxidant Chalcone Glycosides and Flavanones from *Maclura (Chlorophora) tinctoria*. *Journal of natural products,* **66**, 1061-1064.

26. Coussens, L. M. and Werb, Z. (**2002**). Inflammation and cancer. *Nature,* **420**, 860867.

27. Cuyckens, F. and Claeys, M. (**2004**). Mass spectrometry in the structural analysis of flavonoids. *Journal of Mass Spectrometry,* **39**, 1-15.

28. Désiré, S., Nkwengoua, E., Ngantchou, I., Nyasse, B., Denier, C., Hannaert, V., Shaker, K. H. and Schneider, B. (**2013**). Xylopioxyde and other bioactive kauranediterpenes from *Xylopia aethiopica* Dunal (Annonaceae). *Journal of Applied Pharmaceutical Science,* **3**, 13.

29. Dewick, P. M. (**2002**). *Medicinal natural products: a biosynthetic approach*, John Wiley & Sons.

30. Dinarello, C. A. (**2010**). Anti-inflammatory agents: present and future. *Cell,* **140**, 935950.

31. Ekong, D. and Ogan, A. (**1968**). Chemistry of the constituents of *Xylopia aethiopica*. The structure of xylopic acid, a new diterpene acid. *Journal of the Chemical Society C: Organic*, 311-312.

32. Esquenazi, E., Yang, Y.-L., Watrous, J., Gerwick, W. H. and Dorrestein, P. C. (**2009**). Imaging mass spectrometry of natural products. *Natural product reports,* **26**, 15211534.

33. Farrugia, L. J. (**2012**). WinGX and ORTEP for Windows: an update. *Journal of Applied Crystallography*, **45**, 849-854.

34. Fenn, J. B., Mann, M., Meng, C. K., Wong, S. F. and Whitehouse, C. M. (**1989**). Electrospray ionization for mass spectrometry of large biomolecules. *Science,* **246**, 6471.

35. Ferrari, F., Delle Monache, F., Compagnone, R., Suarez, A. and Tillett, S. (**1998**). Constituents of *Morus multicaulis* roots. *Fitoterapia,* **69**, 554-555.

36. Fukai, T., Wang, Q.-H., Takayama, M. and Nomura, T. (**1990**). Structures of five new prenylated flavonoids, gancaonins L, M, N, O, and P from aerial parts of *Glycyrrhiza uralensis*. *Heterocycles,* **31**, 373-382.

37. Busia K. (editor), Ghana Herbal Pharmacopoeia. (**2007**). Edited by Busia K. Science and Technology Policy Research Institute (STEPRI). *Accra, Ghana*. 239–242

38. Gil, M. I., Tomás-Barberán, F. A., Hess-Pierce, B., Holcroft, D. M. and Kader, A. A. (**2000**). Antioxidant activity of pomegranate juice and its relationship with phenolic composition and processing. *Journal of Agricultural and Food chemistry*, **48**, 45814589.

39. Glass, C. K., Saijo, K., Winner, B., Marchetto, M. C. and Gage, F. H. (**2010**). Mechanisms underlying inflammation in neurodegeneration. *Cell,* **140**, 918-934.

40. Glazer, A. N. (**1989**). Phycoerythrin fluorescence-based assay for reactive oxygen species. *Methods in enzymology*, **186**, 161-168.

41. Gonda, R., Takeda, T. and Akiyama, T. (**2000**). Studies on the Constituents of *Anaxagorea luzonensis* A. Gray. *Chemical and pharmaceutical bulletin,* **48**, 12191222.

42. Gordaliza, M., Garcia, P., Del Corral, J. M., Castro, M. and Gomez-Zurita, M. (**2004**). Podophyllotoxin: distribution, sources, applications and new cytotoxic derivatives. *Toxicon,* **44**, 441-459.

43. Graul, A. I. (**2001**). The year‘s new drugs. *Drug News Perspect,* **14**, 12-31.

44. Groweiss, A., Cardellina, J. H. and Boyd, M. R. (2000). HIV-Inhibitory prenylated xanthones and flavones from *Maclura tinctoria. Journal of Natural Products*, **63**, 1537-1539.

45. Guérin, P. (**1898**). Sur la présence d‘un champignon dans l‘ivraie. *J. Botanique,* **12**, 230-238.

46. Hano, Y., Nomura, T. and Ueda, S. (**1989**). Two new Diels-Alder type adducts, mulberrofuran T and kuwanol E, from callus tissues of *Morus alba* L. *Heterocycles,* **29**, 2035-2041.

47. Hashimoto, J., Motohashi, K., Sakamoto, K., Hashimoto, S., Yamanouchi, M., Tanaka, H., Takahashi, T., Takagi, M. and Shin-Ya, K. (**2009**). Screening and evaluation of new inhibitors of hepatic glucose production. *The Journal of antibiotics,* **62**, 625-629.

48. Hashmi, M. A., Khan, A., Ayub, K. and Farooq, U. (**2014**). Spectroscopic and density functional theory studies of 5,7,3′,5′-tetrahydroxyflavanone from the leaves of *Olea ferruginea*. *Spectrochimica Acta Part A: Molecular and Biomolecular Spectroscopy,* **128**, 225-230.

49. Hevesi, B., Houghton, P., Habtemariam, S. and Kéry, Á. (**2009**). Antioxidant and antiinflammatory effect of *Epilobium parviflorum* Schreb. *Phytotherapy Research,* **23**, 719-724.

50. Hillenkamp, F., Unsöld, E., Kaufmann, R. & Nitsche, R. (**1975a**). A high-sensitivity laser microprobe mass analyzer. *Applied physics,* **8**, 341-348.

51. Hillenkamp, F., Unsöld, E., Kaufmann, R. and Nitsche, R. (**1975b**). Laser microprobe mass analysis of organic materials. *Nature*, **256**, 119-120.

52. Hirohata, M., Ono, K. and Yamada, M. (**2008**). Non-steroidal anti-inflammatory drugs as anti-amyloidogenic compounds. *Current pharmaceutical design*, **14**, 3280-3294.

53. Hotamisligil, G. S. (**2006**). Inflammation and metabolic disorders. *Nature*, **444**, 860867.

54. Hutchison, M., Lewer, P. and Macmillan, J. (**1984**). Carbon-13 nuclear magnetic resonance spectra of eighteen derivatives of ent-kaur-16-en-19-oic acid. *Journal of the Chemical Society, Perkin Transactions 1*, 2363-2366.

55. Igwe, S., Afonne, J. & GhasI, S. (**2003**). Ocular dynamics of systemic aqueous extracts of *Xylopia aethiopica* (African guinea pepper) seeds on visually active volunteers. *Journal of ethnopharmacology,* **86**, 139-142.

56. Jacobs, D. I., Snoeijer, W., Hallard, D. and Verpoorte, R. (**2004**). The Catharanthus alkaloids: pharmacognosy and biotechnology. *Current medicinal chemistry,* **11**, 607628.

57. Karas, M. and Hillenkamp, F. (**1988**). Laser desorption ionization of proteins with molecular masses exceeding 10,000 daltons. *Analytical chemistry,* **60**, 2299-2301.

58. Karioti, A., Hadjipavlou-Litina, D., Mensah, M. L., Fleischer, T. C. and Skaltsa, H. (**2004**). Composition and antioxidant activity of the essential oils of *Xylopia aethiopica* (Dun) A. Rich.(Annonaceae) leaves, stem bark, root bark, and fresh and dried fruits, growing in Ghana. *Journal of agricultural and food chemistry,* **52**, 80948098.

59. Kim, Y.-W. and Byzova, T. V. (**2014**). Oxidative stress in angiogenesis and vascular disease. *Blood,* **123**, 625-631.

60. Koes, R. E., Quattrocchio, F. and Mol, J. N. (**1994**). The flavonoid biosynthetic pathway in plants: function and evolution. *BioEssays*, **16**, 123-132.

61. Krasnoff, S. B., Sommers, C. H., Moon, Y.-S., Donzelli, B. G., Vandenberg, J. D., Churchill, A. C. and Gibson, D. M. (**2006**). Production of mutagenic

metabolites by *Metarhizium anisopliae*. *Journal of agricultural and food chemistry,* **54**, 7083-7088.

62. Krishnaiah, D., Sarbatly, R. and Nithyanandam, R. (**2011**). A review of the antioxidant potential of medicinal plant species. *Food and bioproducts processing,* **89**, 217-233.

63. Kusari, P., Kusari, S., Spiteller, M. and Kayser, O. (**2015a**). Implications of endophyte-plant crosstalk in light of quorum responses for plant biotechnology. *Applied microbiology and biotechnology,* **99**, 5383-5390.

64. Kusari, S., Hertweck, C. and Spiteller, M. (**2012**). Chemical ecology of endophytic fungi: origins of secondary metabolites. *Chemistry & biology*, **19**, 792-798.

65. Kusari, S., Lamsh ft, M., Kusari, P., Gottfried, S., Z hlke, S., Louven, K., Hentschel, U., Kayser, O. and Spiteller, M. (**2014**). Endophytes are hidden producers of maytansine in *Putterlickia* roots. *Journal of natural products,* **77**, 2577-2584.

66. Kusari, S., Lamshöft, M., Zühlke, S. and Spiteller, M. (**2008**). An endophytic fungus from *Hypericum perforatum* that produces hypericin. *Journal of Natural Products,* **71**, 159-162.

67. Kusari, S., Pandey, S. P. and Spiteller, M. (**2013**). Untapped mutualistic paradigms linking host plant and endophytic fungal production of similar bioactive secondary metabolites. *Phytochemistry,* **91**, 81-87.

68. Kusari, S., Sezgin, S., Nigutova, K., Cellarova, E. and Spiteller, M. (**2015b**). Spatial chemo-profiling of hypericin and related phytochemicals in *Hypericum* species using MALDI-HRMS imaging. *Analytical and bioanalytical chemistry,* **407**, 4779-4791.

69. Kusari, S. and Spiteller, M. (**2012**). Metabolomics of endophytic fungi producing associated plant secondary metabolites: progress, challenges and opportunities, INTECH Open Access Publisher, 241-266.

70. Kusari, S., Z hlke, S. and Spiteller, M. (**2009**). An endophytic fungus from *Camptotheca acuminata* that produces camptothecin and analogues. *Journal of Natural Products,* **72**, 2-7.

71. Kyekyeku, J. O., Kusari, S., Adosraku, R. K., Zühlke, S. and Spiteller, M. (**2016**). Prenylated 2-arylbenzofuran derivatives with potent antioxidant properties from *Chlorophora regia* (Moraceae). *Fitoterapia,* **108**, 41-47.

72. Lajide, L., Escoubas, P. and Mizutani, J. (**1995**). Termite antifeedant activity in *Xylopia aethiopica*. *Phytochemistry*, **40**, 1105-1112.

73. Lee, J. C., Yang, X., Schwartz, M., Strobel, G. and Clardy, J. (**1995**). The relationship between an endangered North American tree and an endophytic fungus. *Chemistry & biology*, **2**, 721-727.

74. Li, C., Johnson, R. P. and Porco, J. A. (**2003**). Total synthesis of the quinone epoxide dimer (+)-torreyanic acid: Application of a biomimetic oxidation/electrocyclization/Diels-Alder dimerization cascade 1. *Journal of the American Chemical Society*, **125**, 5095-5106.

75. Li, G., Kusari, S., Kusari, P., Kayser, O. and Spiteller, M. (**2015**). Endophytic *Diaporthe* sp. LG23 produces a potent antibacterial tetracyclic triterpenoid. *Journal of Natural Products*, **78**, 2128-2132.

76. Li, G., Kusari, S., Lamsh ft, M., Sch ffler, A., Laatsch, H. and Spiteller, M. (**2014**). Antibacterial secondary metabolites from an endophytic fungus, *Eupenicillium* sp. LG41. *Journal of natural products*, **77**, 2335-2341.

77. Li, J., Strobel, G., Harper, J., Lobkovsky, E. and Clardy, J. (**2000**). Cryptocin, a potent tetramic acid antimycotic from the endophytic fungus *Cryptosporiopsis* cf. *quercina*. *Organic letters*, **2**, 767-770.

78. Li, X.-C., Joshi, A. S., Elsohly, H. N., Khan, S. I., Jacob, M. R., Zhang, Z., Khan, I. A., Ferreira, D., Walker, L. A. and Broedel, S. E. (**2002**). Fatty acid synthase inhibitors from plants: isolation, structure elucidation, and SAR studies. *Journal of Natural Products*, **65**, 1909-1914.

79. Lötsch, J. and Geisslinger, G. (**2001**). Morphine-6-Glucuronide. *Clinical pharmacokinetics*, **40**, 485-499.

80. Louppe, D., Oteng-Amoako, A., Brink, M., Lemmens, R., Oyen, L. and Cobbinah, J. (**2008**). Plant Resources of Tropical Africa 7 (1). *Timbers 1*, PROTA foundation, Backhuys Publishers, Leiden, Netherlands, 365-366.

81. Ma, Y., Li, Q., Van Den Heuvel, H. and Claeys, M. (**1997**). Characterization of flavone and flavonol aglycones by collision_induced dissociation tandem mass spectrometry. *Rapid Communications in Mass Spectrometry*, **11**, 1357-1364.

82. Magassouba, F., Diallo, A., Kouyaté, M., Mara, F., Mara, O., Bangoura, O., Camara,
A., Traoré, S., Diallo, A. and Zaoro, M. (**2007**). Ethnobotanical survey and antibacterial activity of some plants used in Guinean traditional medicine. *Journal of ethnopharmacology*, **114**, 44-53.

83. Maneechai, S., De-Eknamkul, W., Umehara, K., Noguchi, H. and Likhitwitayawuid, K. (**2012**). Flavonoid and stilbenoid production in callus cultures of *Artocarpus lakoocha*. *Phytochemistry*, **81**, 42-49.

84. Mantovani, A., Allavena, P., Sica, A. and Balkwill, F. (**2008**). Cancer-related inflammation. *Nature,* **454**, 436-444.

85. Markham, K., Ternai, B., Stanley, R., Geiger, H. and Mabry, T. (**1978**). Carbon-13 NMR studies of flavonoids—III: Naturally occurring flavonoid glycosides and their acylated derivatives. *Tetrahedron,* **34**, 1389-1397.

86. Medzhitov, R. (**2008**). Origin and physiological roles of inflammation. *Nature,* **454**, 428-435.

87. Miller, N. J., Rice-Evans, C., Davies, M. J., Gopinathan, V. and Milner, A. (**1993**). A novel method for measuring antioxidant capacity and its application to monitoring the antioxidant status in premature neonates. *Clinical science (*London, England: 1979), **84**, 407-412.

88. Minn, J., Daly, W., Negulescu, I., Mcmurtrey, K. and Schultz, T. (**1996**). Antioxidant properties of the hydrophobic stilbenol chlorophorin. *Journal of Agricultural and Food Chemistry,* **44**, 2946-2947.

89. Mireku, E. A., Kusari, S., Eckelmann, D., Mensah, A. Y., Talontsi, F. M. and Spiteller, M. (**2015**). Anti-inflammatory tirucallane triterpenoids from *Anopyxis klaineana* Pierre (Engl.),(Rhizophoraceae). *Fitoterapia,* **106**, 84-91.

90. Moein, M. R., Moein, S. and Ahmadizadeh, S. (**2008**). Radical scavenging and reducing power of *Salvia mirzayanii* subfractions. *Molecules,* **13**, 2804-2813.

91. Mundy, C. and Kirkpatrick, P. (**2004**). Tiotropium bromide. *Nature Reviews Drug Discovery,* **3**, 643-644.

92. Naik, R., Harmalkar, D. S., Xu, X., Jang, K. and Lee, K. (**2015**). Bioactive benzofuran derivatives: Moracins A–Z in medicinal chemistry. *European journal of medicinal chemistry,* **90**, 379-393.

93. Newman, D. J., Cragg, G. M. and Snader, K. M. (**2000**). The influence of natural products upon drug discovery. *Natural product reports,* **17**, 215-234.

94. Newman, D. J., Cragg, G. M. and Snader, K. M. (**2003**). Natural products as sources of new drugs over the period 1981-2002. *Journal of natural products,* **66**, 1022-1037.

95. Newton, G. and Abraham, E. (**1956**). Isolation of cephalosporin C, a penicillin-like antibiotic containing D-α-aminoadipic acid. *Biochemical Journal,* **62**, 651.

96. Nimse, S. B. and Pal, D. (**2015**). Free radicals, natural antioxidants, and their reaction mechanisms. *RSC Advances,* **5**, 27986-28006.

97. Nwozo, S. O., Orojobi, B. F. and Adaramoye, O. A. (**2011**). Hypolipidemic and antioxidant potentials of *Xylopia aethiopica* seed extract in hypercholesterolemic rats. *Journal of medicinal food*, **14**, 114-119.

98. Oberlies, N. H. and Kroll, D. J. (**2004**). Camptothecin and Taxol: Historic Achievements in Natural Products Research. *Journal of Natural Products*, **67**, 129135.

99. Padayachee, T. and Odhav, B. (**2013**). Antimicrobial activity of plant phenols from *Chlorophora excelsa* and *Virgilia oroboides*. *African Journal of Biotechnology*, **12**, 17.

100. Pal, D. and Nimse, S. (**2006**). Screening of the Antioxidant Activity of *Hydrilkr verticillata* Plant. Asian Journal of Chemistry, **18**, 3004-3008.

101. Pan, M.-H., Lai, C.-S., Dushenkov, S. and Ho, C.-T. (**2009**). Modulation of inflammatory genes by natural dietary bioactive compounds. *Journal of agricultural and food chemistry*, **57**, 4467-4477.

102. Prior, R. L., Wu, X. and Schaich, K. (**2005**). Standardized methods for the determination of antioxidant capacity and phenolics in foods and dietary supplements. *Journal of agricultural and food chemistry*, **53**, 4290-4302.

103. Ridker, P. M. and Silvertown, J. D. (**2008**). Inflammation, C-reactive protein, and atherothrombosis. *Journal of periodontology*, **79**, 1544-1551.

104. Römpp, A. and Spengler, B. (**2013**). Mass spectrometry imaging with high resolution in mass and space. *Histochemistry and cell biology*, **139**, 759-783.

105. Royer, M., Herbette, G., Eparvier, V., Beauchêne, J., Thibaut, B. and Stien, D. (**2010**). Secondary metabolites of *Bagassa guianensis* Aubl. wood: a study of the chemotaxonomy of the Moraceae family. *Phytochemistry*, **71**, 1708-1713.

106. Samuelsson, G. (**1992**). Drugs of natural origin: a textbook of pharmacognosy, Stockholm: Swedish Pharmaceutical Press 320p. ISBN.

107. Sheldrick, G. M. (**2008**). A short history of SHELX. *Acta Crystallographica Section A: Foundations of Crystallography*, **64**, 112-122.

108. Sheldrick, G. M. (**2015**). Crystal structure refinement with SHELXL. *Acta Crystallographica Section C: Structural Chemistry*, **71**, 3-8.

109. Shi, Y.-Q., Fukai, T., Sakagami, H., Chang, W.-J., Yang, P.-Q., Wang, F.-P. and Nomura, T. (**2001**). Cytotoxic Flavonoids with Isoprenoid Groups from *Morus mongolica*. *Journal of Natural Products*, **64**, 181-188.

110. Shimizu, K., Yasutake, S. and Kondo, R. (**2003**). A new stilbene with tyrosinase inhibitory activity from *Chlorophora excelsa*. *Chemical and pharmaceutical bulletin*, **51**, 318-319.

111. Sies, H. (**1997**). Oxidative stress: oxidants and antioxidants. *Experimental physiology*, **82**, 291-295.

112. Silva, E. C. C. D., Muniz, M. P., Nunomura, R. D. C. S., Nunomura, S. M. and Zilse, G. A. C. (**2013**). Phenolic constituents and antioxidant activity of geopropolis from two species of amazonian stingless bees. *Quimica Nova*, **36**, 628-633.

113. Somova, L., Shode, F., Moodley, K. and Govender, Y. (**2001**). Cardiovascular and diuretic activity of kaurene derivatives of *Xylopia aethiopica* and *Alepidea amatymbica*. *Journal of ethnopharmacology*, **77**, 165-174.

114. Spengler, B., Hubert, M. and Kaufmann, R. (**1994**). MALDI ion imaging and biological ion imaging with a new scanning UV-laser microprobe. *In:* Proceedings of the 42nd Annual Conference on Mass Spectrometry and Allied Topics, 1041.

115. Stone, J. K., Bacon, C. W. and White, J. (**2000**). An overview of endophytic microbes: endophytism defined. *Microbial endophytes*, **3**, 29-33.

116. Strobel, G., Daisy, B., Castillo, U. and Harper, J. (**2004**). Natural products from endophytic microorganisms⊥. *Journal of Natural products*, **67**, 257-268.

117. Strobel, G., Stierle, A., Stierle, D. and Hess, W. (**1993**). Taxomyces andreanae, a proposed new taxon for a bulbilliferous hyphomycete associated with Pacific yew (*Taxus brevifolia*). *Mycotaxon*, **47**, 71-80.

118. Strobel, G. A., Miller, R. V., Martinez-Miller, C., Condron, M. M., Teplow, D. B. and Hess, W. (**1999**). Cryptocandin, a potent antimycotic from the endophytic fungus *Cryptosporiopsis* cf. *quercina*. *Microbiology*, **145**, 1919-1926.

119. Takasugi, M., Nagao, S., Masamune, T., Shirata, A. and TakahashI, K. (**1980**). Chalcomoracin, a natural Diels-Alder adduct from diseased mulberry. *Chemistry Letters*, 1573-1576.

120. Tatum, J. H., Baker, R. A. and Berry, R. E. (**1989**). Metabolites of *Fusarium solani*. *Phytochemistry*, **28**, 283-284.

121. Trisuwan, K., Khamthong, N., Rukachaisirikul, V., Phongpaichit, S., Preedanon, S. and Sakayaroj, J. (**2010**). Anthraquinone, cyclopentanone, and naphthoquinone derivatives from the sea fan-derived fungi *Fusarium* spp. PSU-F14 and PSU-F135. *Journal of natural products*, **73**, 1507-1511.

122. Tsao, R., Yang, R. and Young, J. C. (**2003**). Antioxidant isoflavones in osage orange, *Maclura pomifera* (Raf.) Schneid. *Journal of Agricultural and Food Chemistry*, **51**, 6445-6451.

123. Tsimogiannis, D., Samiotaki, M., Panayotou, G. and Oreopoulou, V. (**2007**). Characterization of flavonoid subgroups and hydroxy substitution by HPLC-MS/MS. *Molecules*, **12**, 593-606.

124. Turnbull, J. J., Nakajima, J.-I., Welford, R. W., Yamazaki, M., Saito, K. and Schofield, C. J. (**2004**). Mechanistic studies on three 2-oxoglutarate-dependent oxygenases of flavonoid biosynthesis anthocyanidin synthase, flavonol synthase, and flavanone 3β-hydroxylase. *Journal of Biological Chemistry*, **279**, 1206-1216.

125. Van Agtmael, M. A., Eggelte, T. A. and Van Boxtel, C. J. (**1999**). Artemisinin drugs in the treatment of malaria: from medicinal herb to registered medication. *Trends in Pharmacological Sciences*, **20**, 199-205.

126. Wall, M. E. and Wani, M. C. (**1996**). Camptothecin and taxol: from discovery to clinic. *Journal of ethnopharmacology*, **51**, 239-254.

127. Wang, H., Liu, T. and Xin, Z. (**2014**). A new glucitol from an endophytic fungus *Fusarium equiseti* Salicorn 8. *European Food Research and Technology*, **239**, 365-376.

128. Wang, W.-X., Kusari, S., Sezgin, S., Lamshöft, M., Kusari, P., Kayser, O. and Spiteller, M. (**2015**). Hexacyclopeptides secreted by an endophytic fungus *Fusarium solani* N06 act as crosstalk molecules in Narcissus tazetta. *Applied microbiology and biotechnology*, **99**, 7651-7662.

129. WHO (**2002**). WHO traditional medicine strategy 2002-2005.

130. Wikler, M. A. (**2006**). Performance standards for antimicrobial susceptibility testing: Sixteenth informational supplement, Clinical and Laboratory Standards Institute.

131. Williams, D. H. and Fleming, I. (**1980**). Spectroscopic methods in organic chemistry, McGraw-Hill.

132. Wollenweber, E. and Roitman, J. N. (**1991**). New frond exudate flavonoids from Cheilanthoid Ferns. *Zeitschrift für Naturforschung C*, **46**, 325-330.

133. Woode, E., Ameyaw, E., Ainooson, G., Abotsi, W., Gyasi, E. and Kyekyeku, J. (**2013**). Analgesic effects of an ethanol extract of the fruits of *Xylopia aethiopica* and xylopic acid in murine models of pain: Possible mechanism (s). *Pharmacologia*, **4**, 285-300.

134. Woode, E., Ameyaw, E. O., Boakye-Gyasi, E. and Abotsi, W. K. (**2012**).

Analgesic effects of an ethanol extract of the fruits of *Xylopia aethiopica* (Dunal) A. Rich (Annonaceae) and the major constituent, xylopic acid in murine models. *Journal of Pharmacy and BioAllied Sciences*, **4**, 291.

135. Wu, S.-J., Leu, Y.-L., Chen, C.-H., Chao, C.-H., Shen, D.-Y., Chan, H.-H., Lee, E.-J., Wu, T.-S., Wang, Y.-H. and Shen, Y.-C. (**2010**). Camphoratins A− J, potent cytotoxic and anti-inflammatory triterpenoids from the fruiting body of *Taiwanofungus camphoratus*. *Journal of natural products*, **73**, 1756-1762.

136. Yang, Z., Wang, Y., Wang, Y. and Zhang, Y. (**2012**). Bioassay-guided screening and isolation of α-glucosidase and tyrosinase inhibitors from leaves of Morus alba. *Food chemistry*, **131**, 617-625.

137. Zelov , H., Han kov , ., erm kov , ., mejkal, K., Dal Acqua, S., Babula, P., Cva ka, J. and Ho ek, J. (**2014**). Evaluation of anti-inflammatory activity of prenylated substances isolated from *Morus alba* and *Morus nigra*. *Journal of natural products*, **77**, 1297-1303.

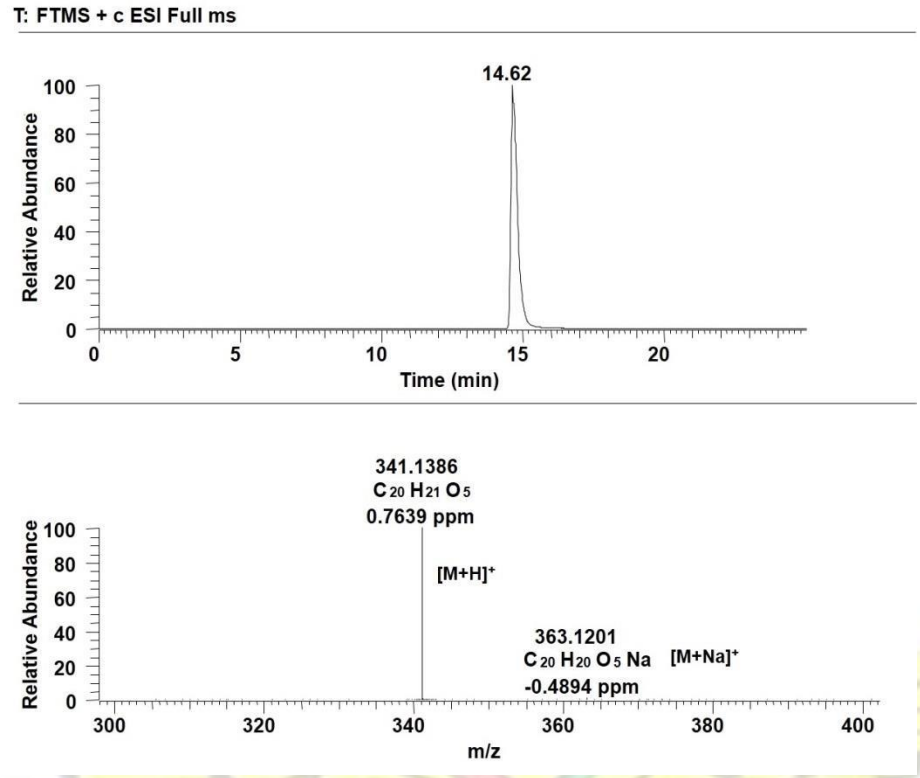
138. Zhou G, Yang X, Jiang Y, Tu P. (**2013**). Flavanoids and xanthones isolated from *Arenaria serpyllifolia* L., *Journal of Chinese Pharmaceutical. Sciences*, **22**, 286– 288.

139. Zou, W., Meng, J., Lu, H., Chen, G., Shi, G., Zhang, T. and Tan, R. (**2000**). Metabolites of *Colletotrichum gloeosporioides*, an endophytic fungus in *Artemisia mongolica*. *Journal of Natural Products*, **63**, 1529-1530.

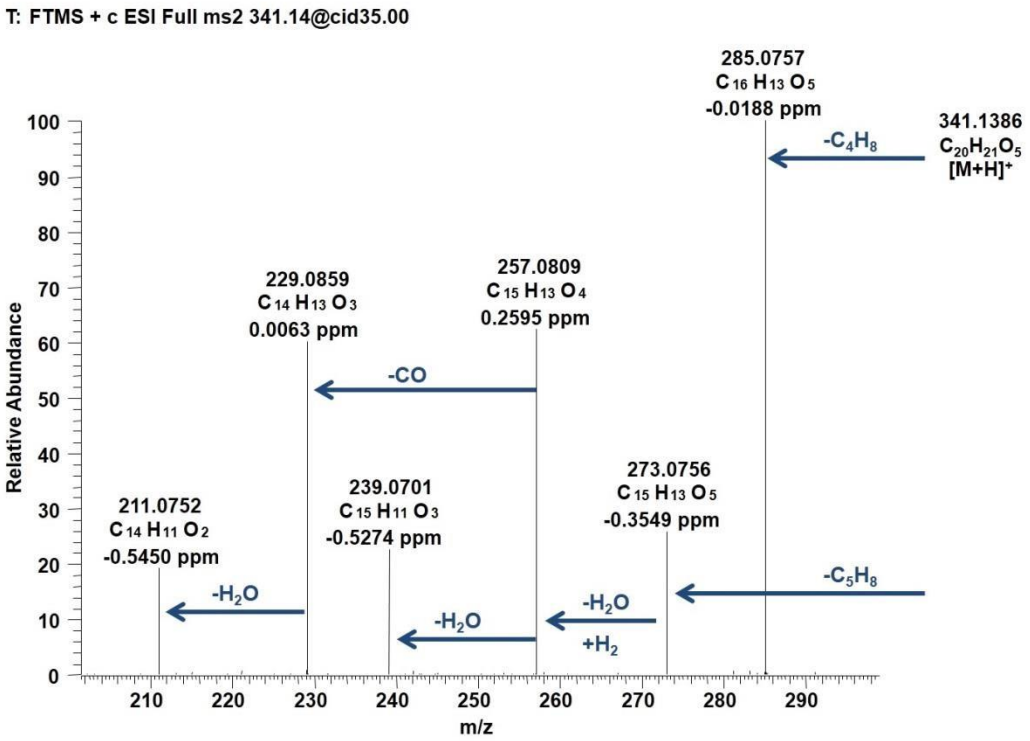
KNUST

APPENDICES

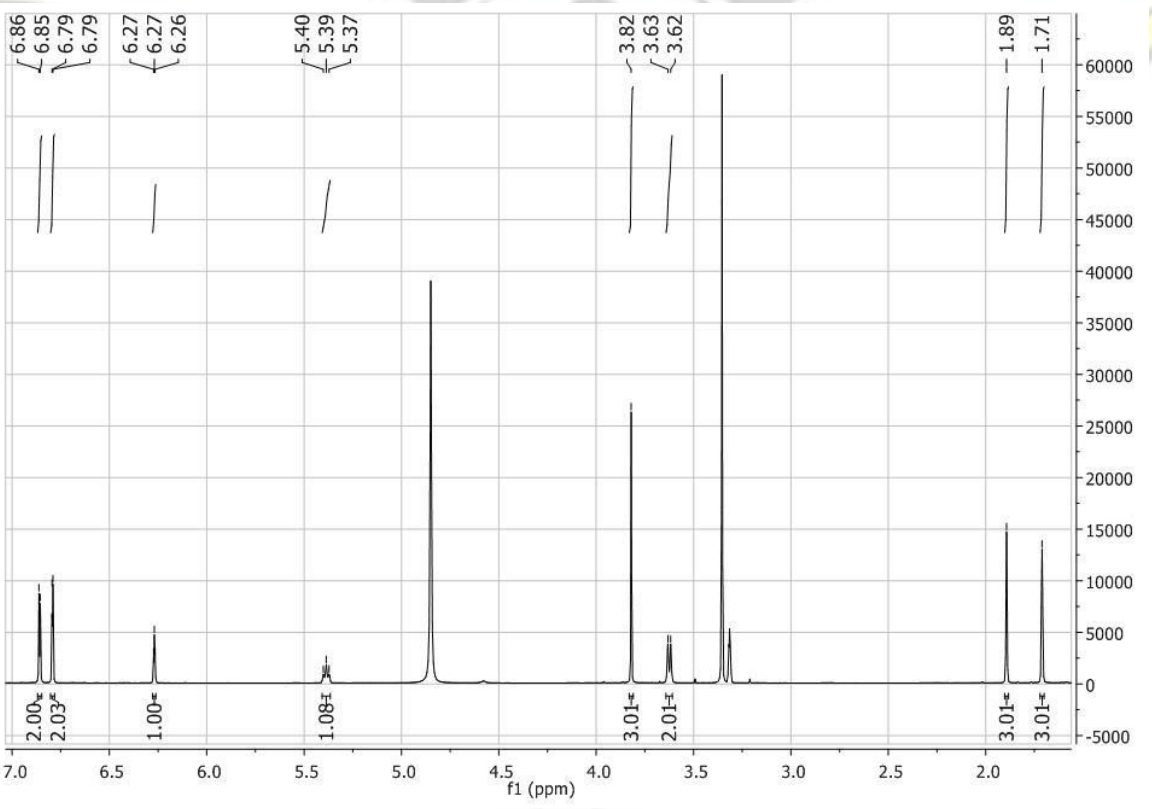
MS, NMR spectra and additional figures



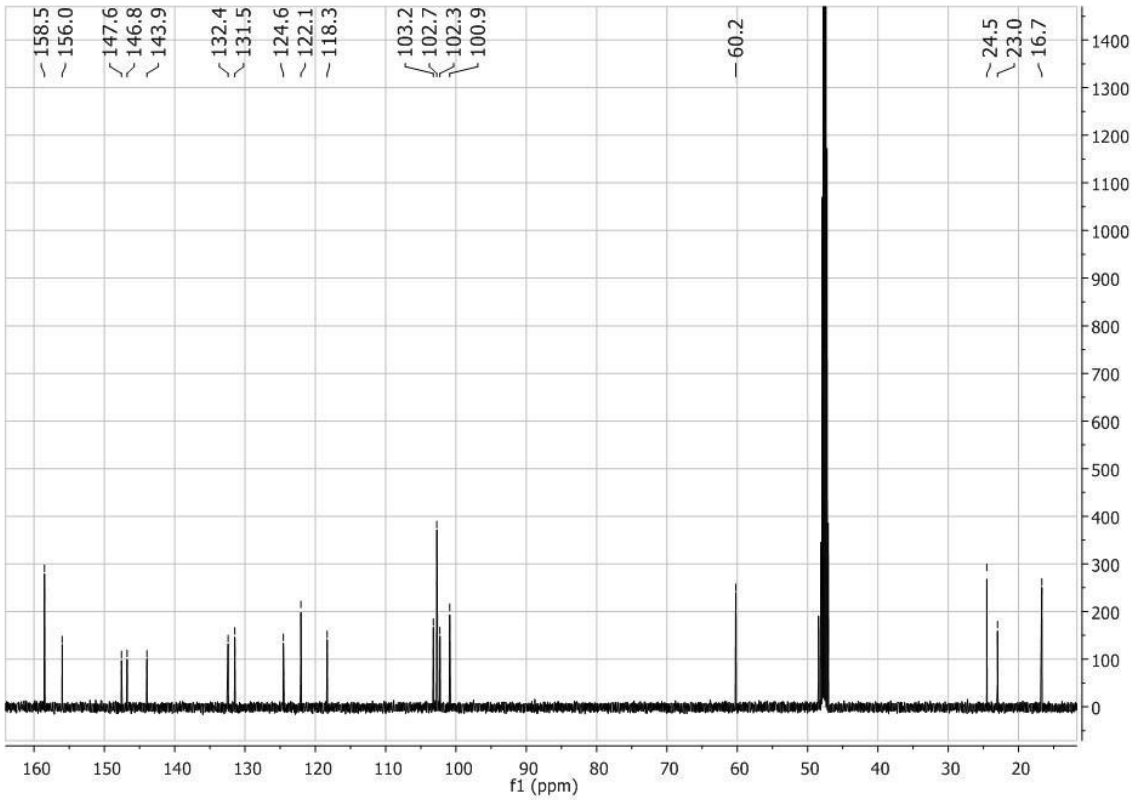
Appendix 1: Positive HRESI–MS spectrum of compound **1**



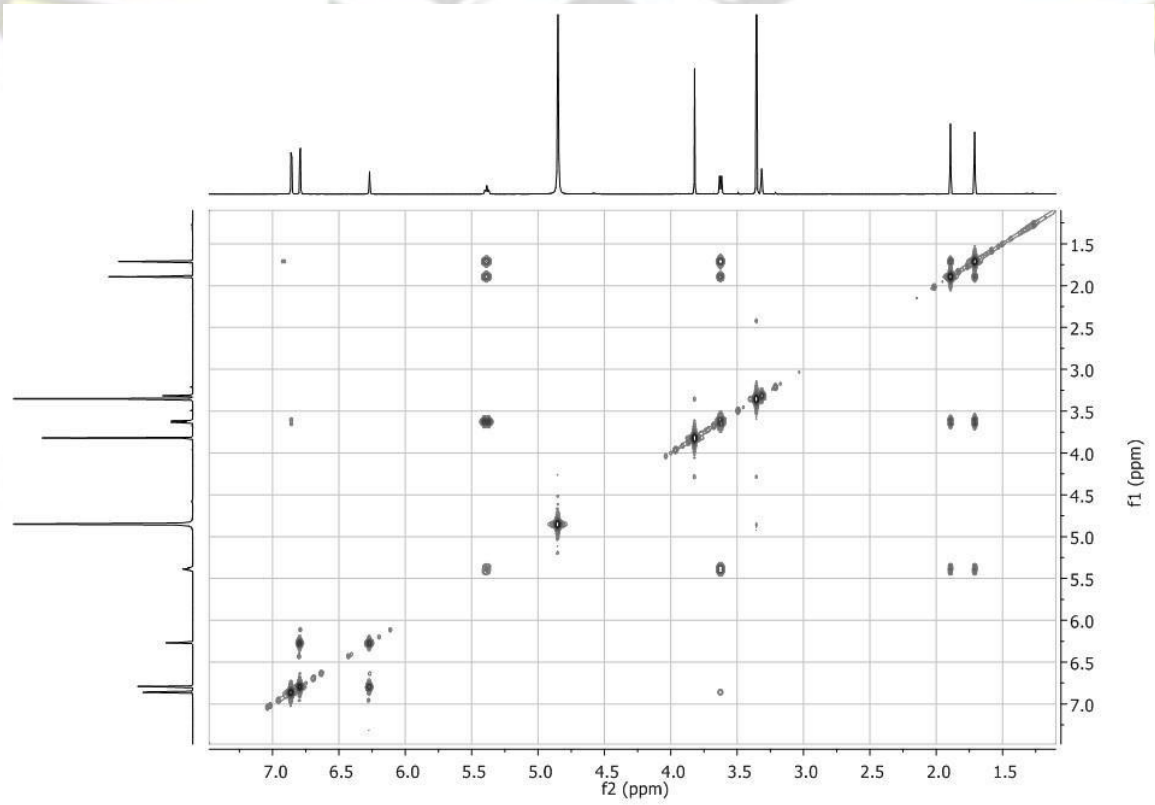
Appendix 2: Positive HRESI–MS/MS spectrum of compound **1**



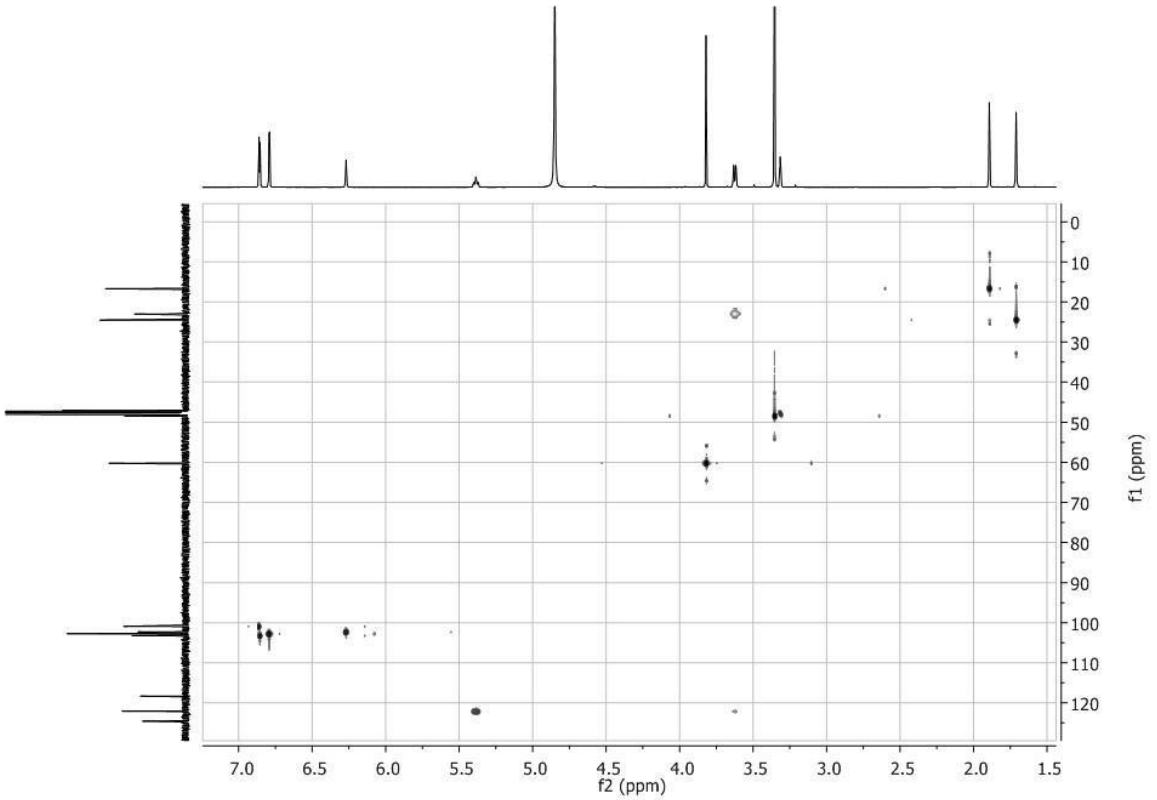
Appendix 3: ^{1}H NMR spectrum (CD_3OD, 500 MHz) of compound **1**.



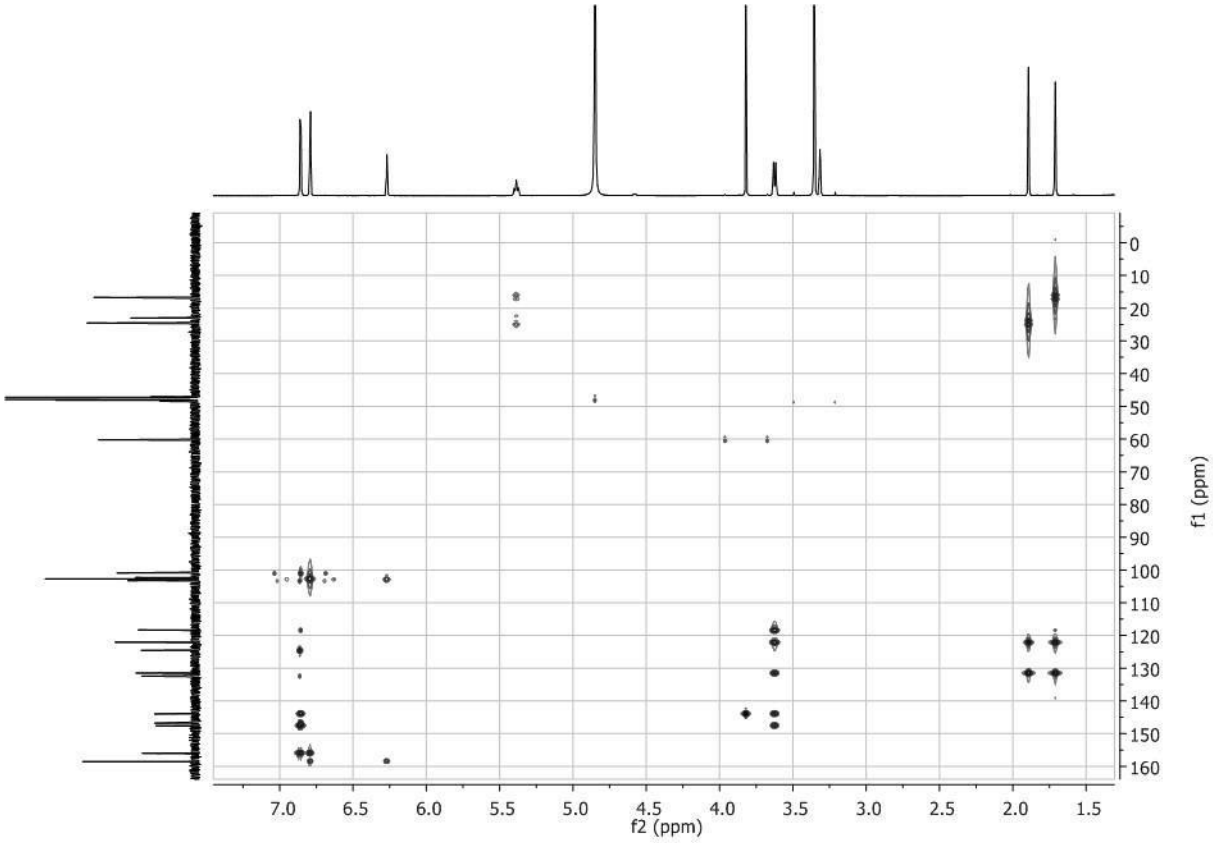
Appendix 4: ^{13}C NMR spectrum (CD_3OD, 125 MHz) of compound **1**.



Appendix 5: $^{1}H–^{1}H$ COSY NMR spectrum (CD_3OD) of compound **1**.

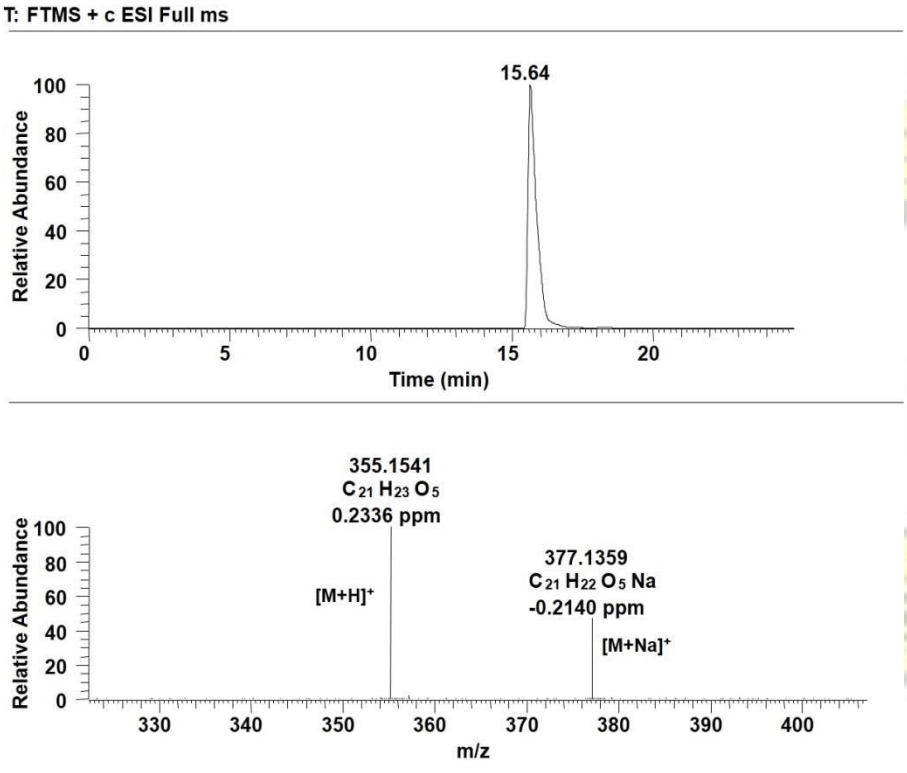


Appendix 6: HSQC NMR spectrum (CD_3OD) of compound **1**.

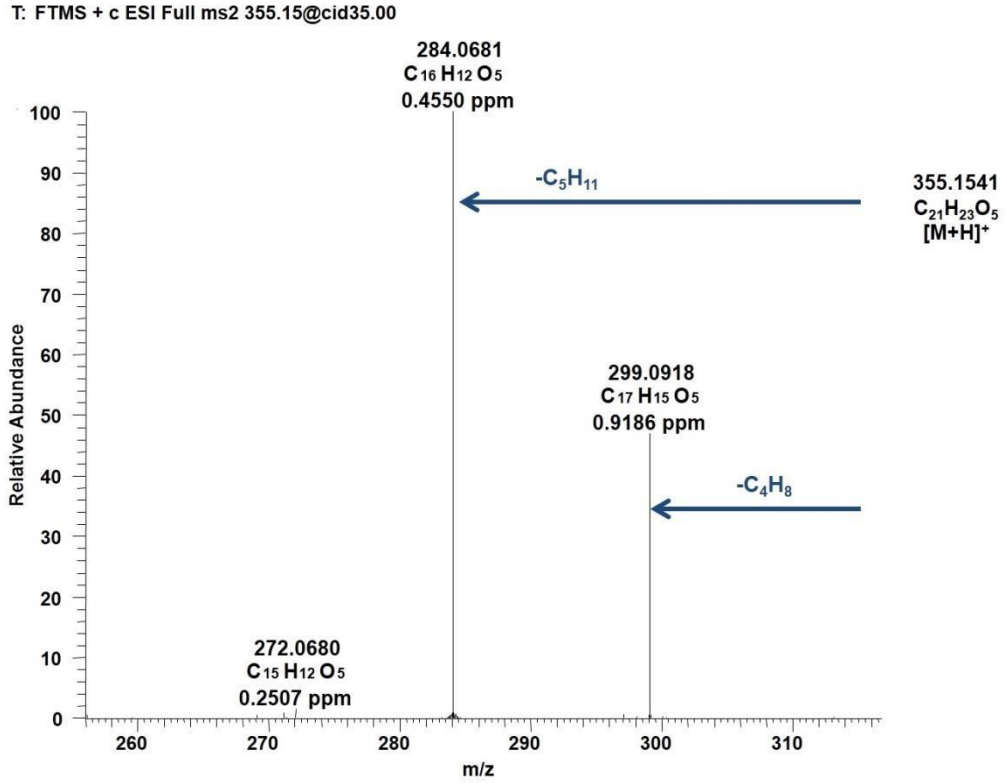


Appendix 7: HMBC NMR spectrum (CD_3OD) of compound **1**.

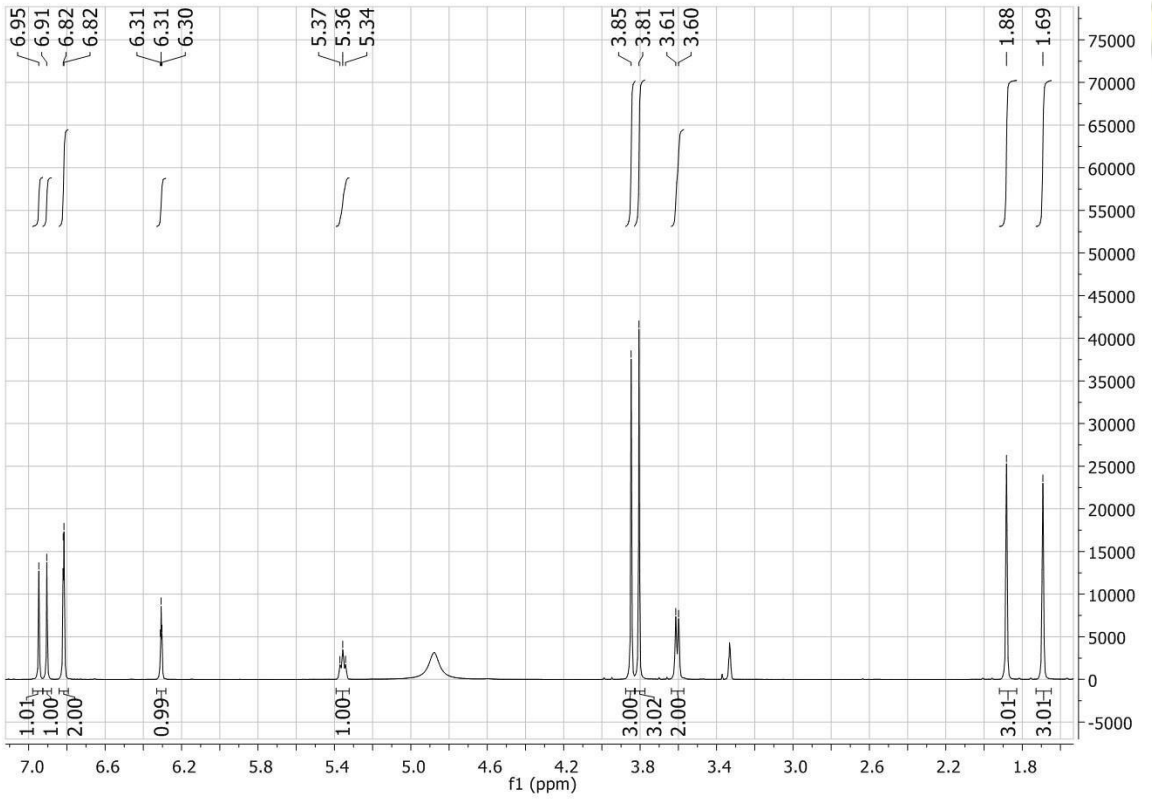
KNUST



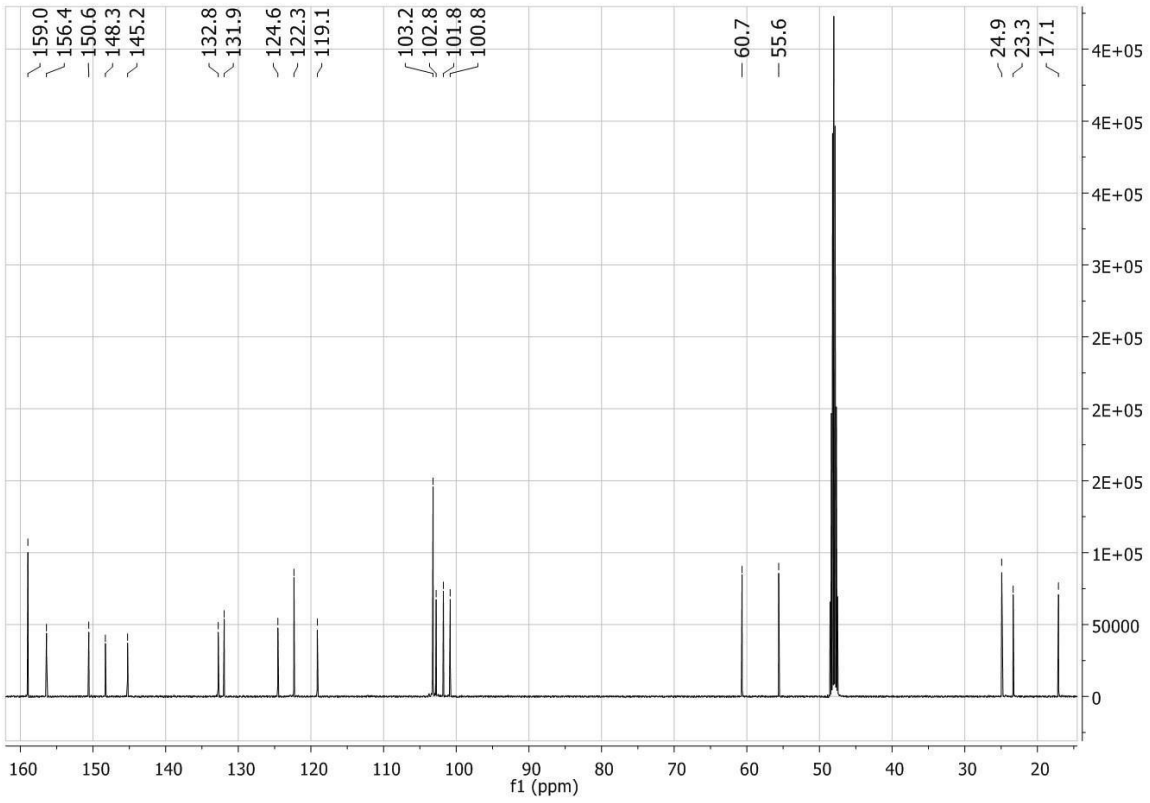
Appendix 8: Positive HRESI–MS spectrum of compound **2**



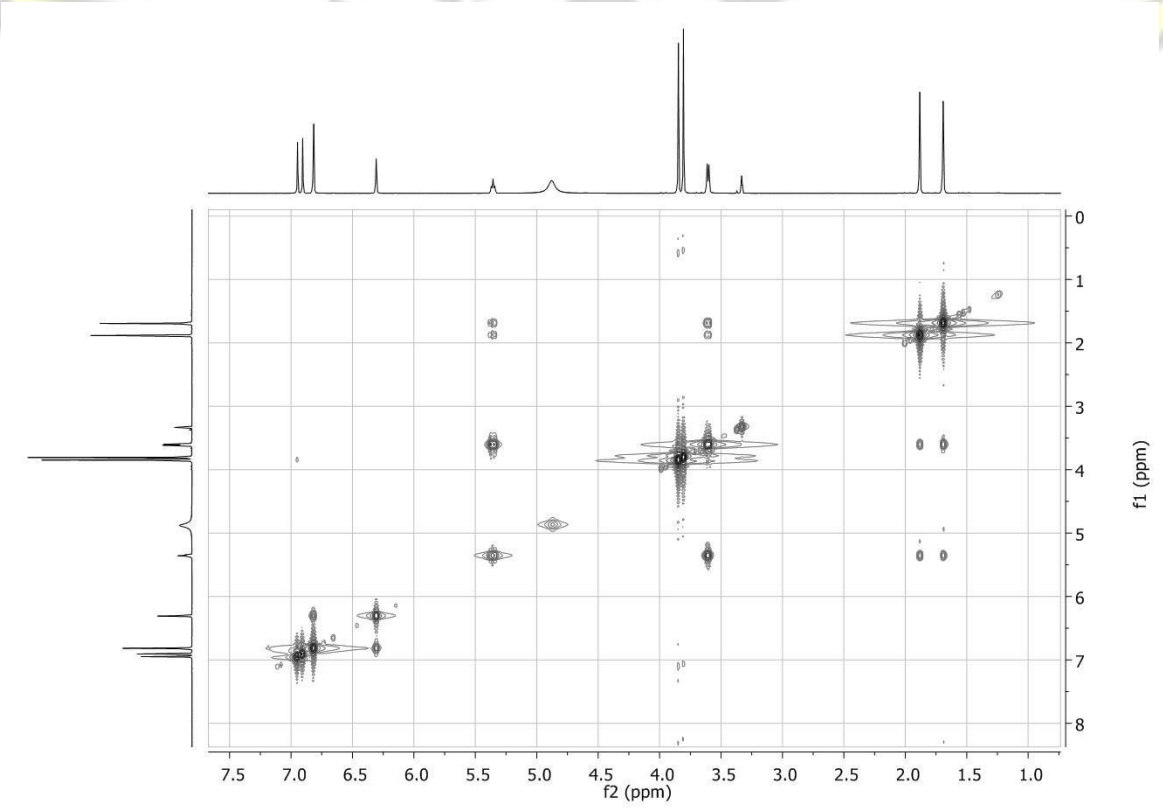
Appendix 9: Positive HRESI–MS/MS spectrum of compound **2**



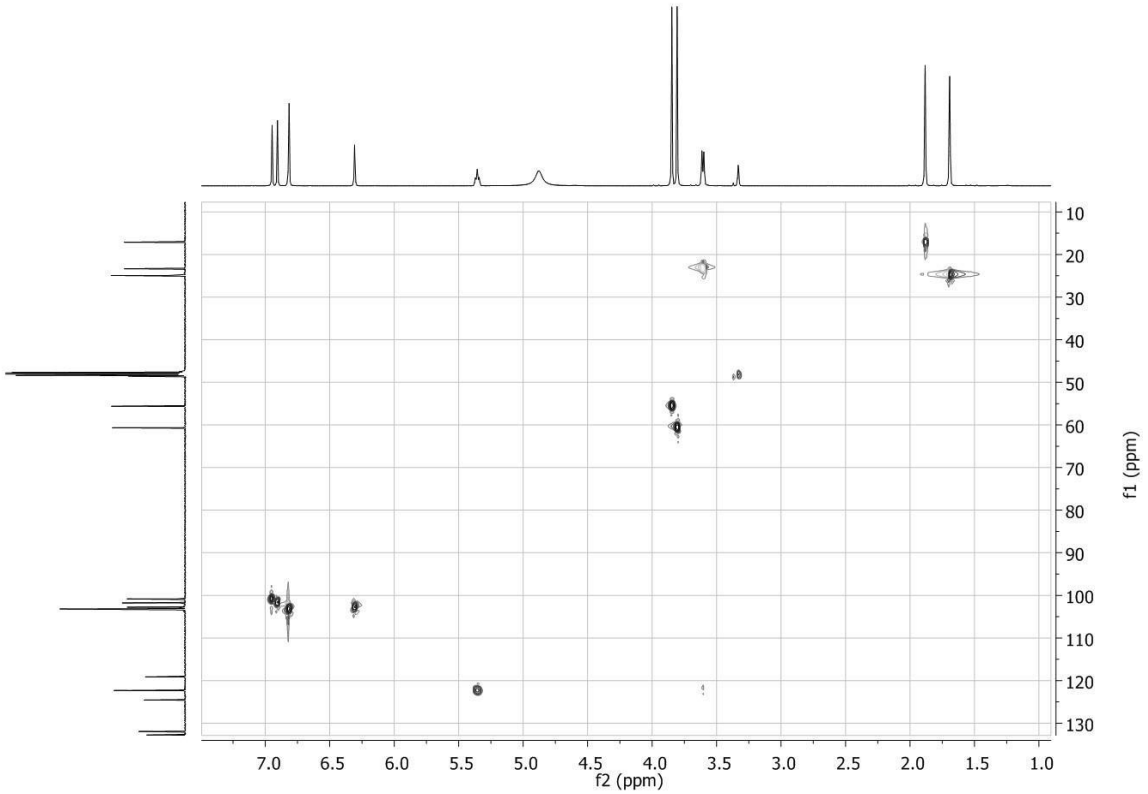
Appendix 10: ^{1}H NMR spectrum (CD_3OD, 500 MHz) of compound **2**.



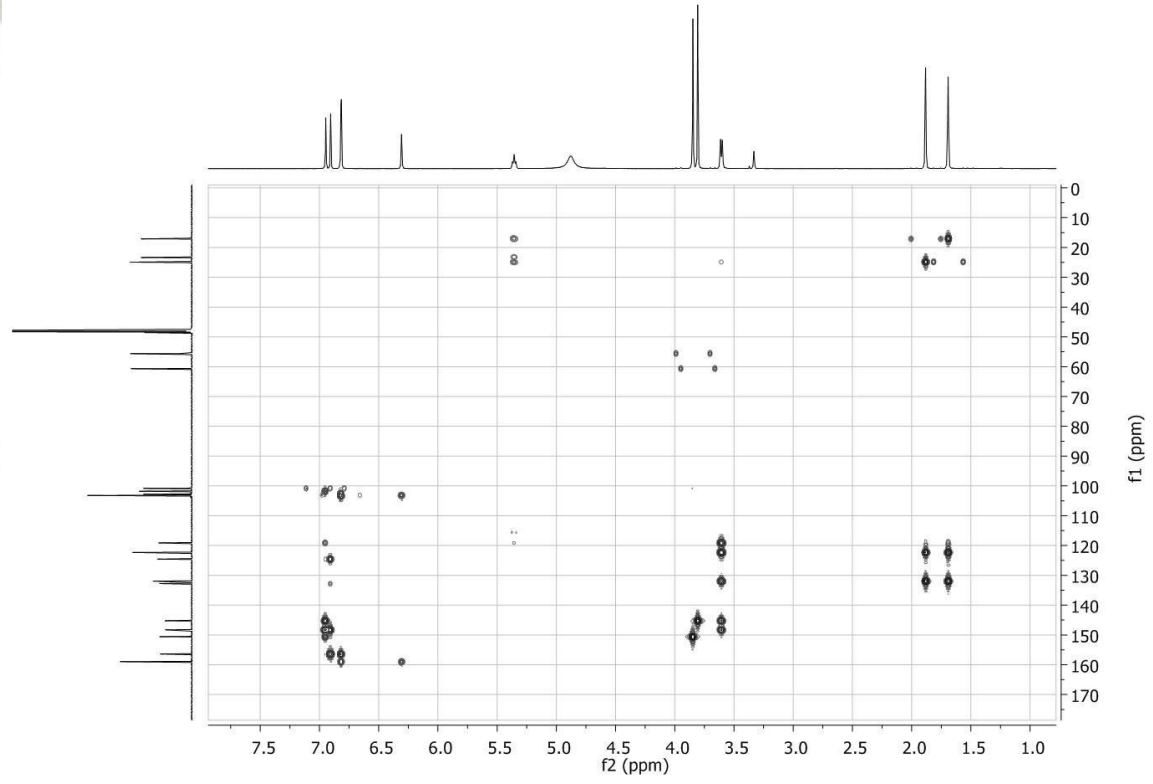
Appendix 11: ^{13}C NMR spectrum (CD_3OD, 125 MHz) of compound **2**.



Appendix 12: $^{1}H–^{1}H$ COSY NMR spectrum (CD_3OD) of compound **2**.

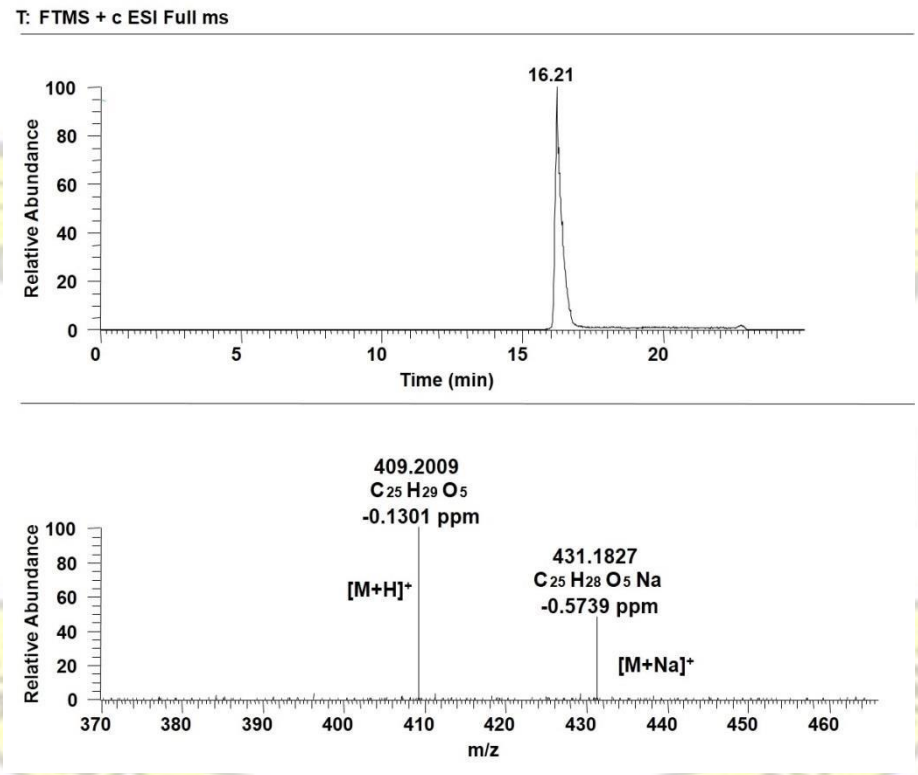


Appendix 13: HSQC NMR spectrum (CD_3OD) of compound **2**.

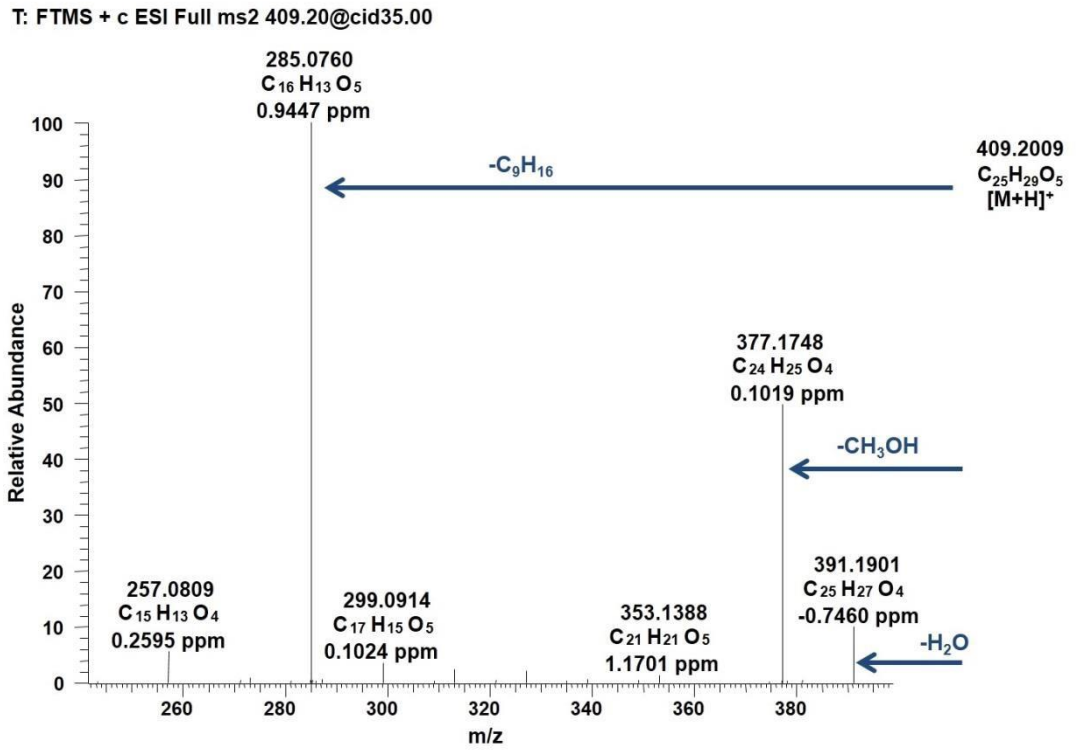


Appendix 14: HMBC NMR spectrum (CD_3OD) of compound **2**.

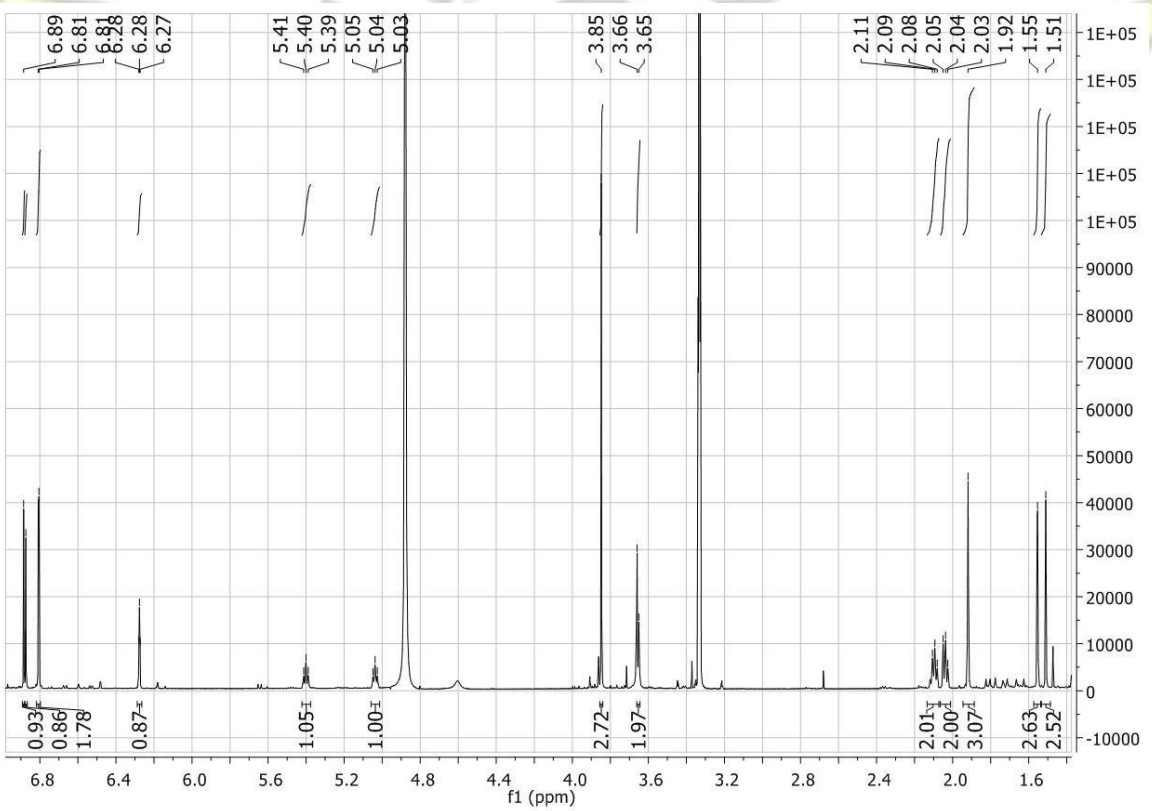
KNUST



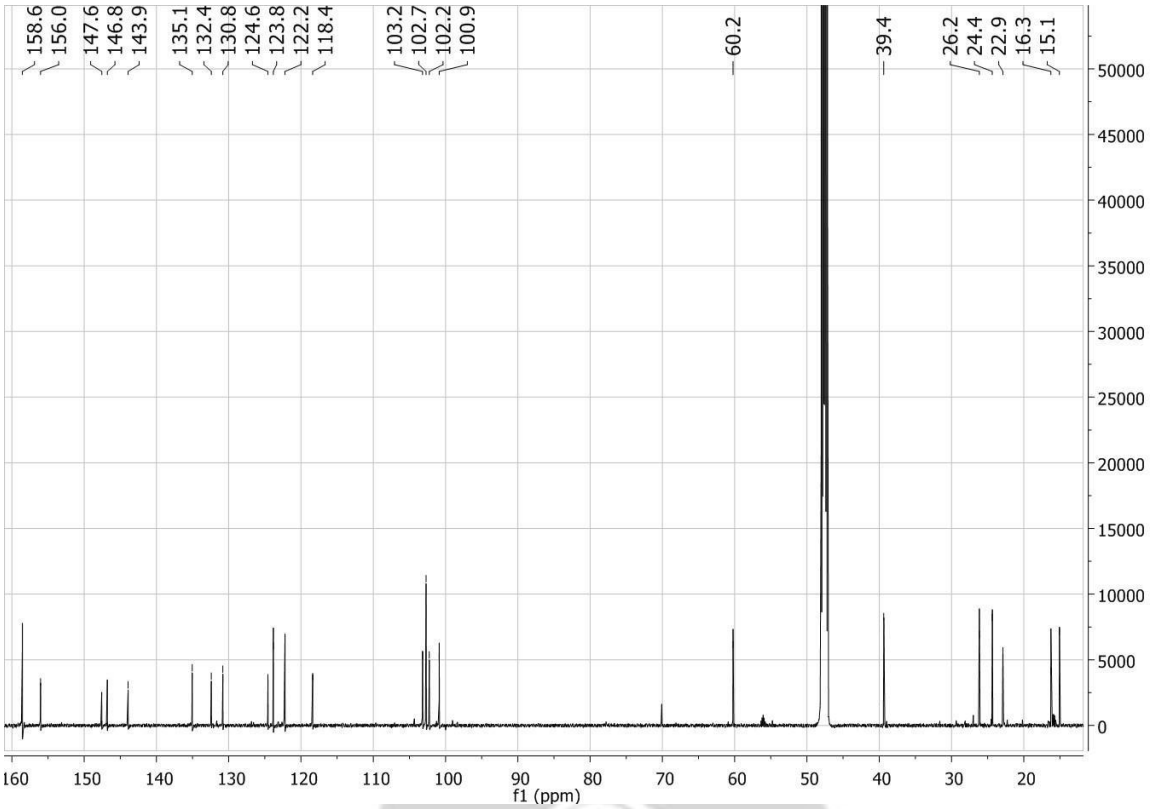
Appendix 15: Positive HRESI–MS spectrum of compound **3**



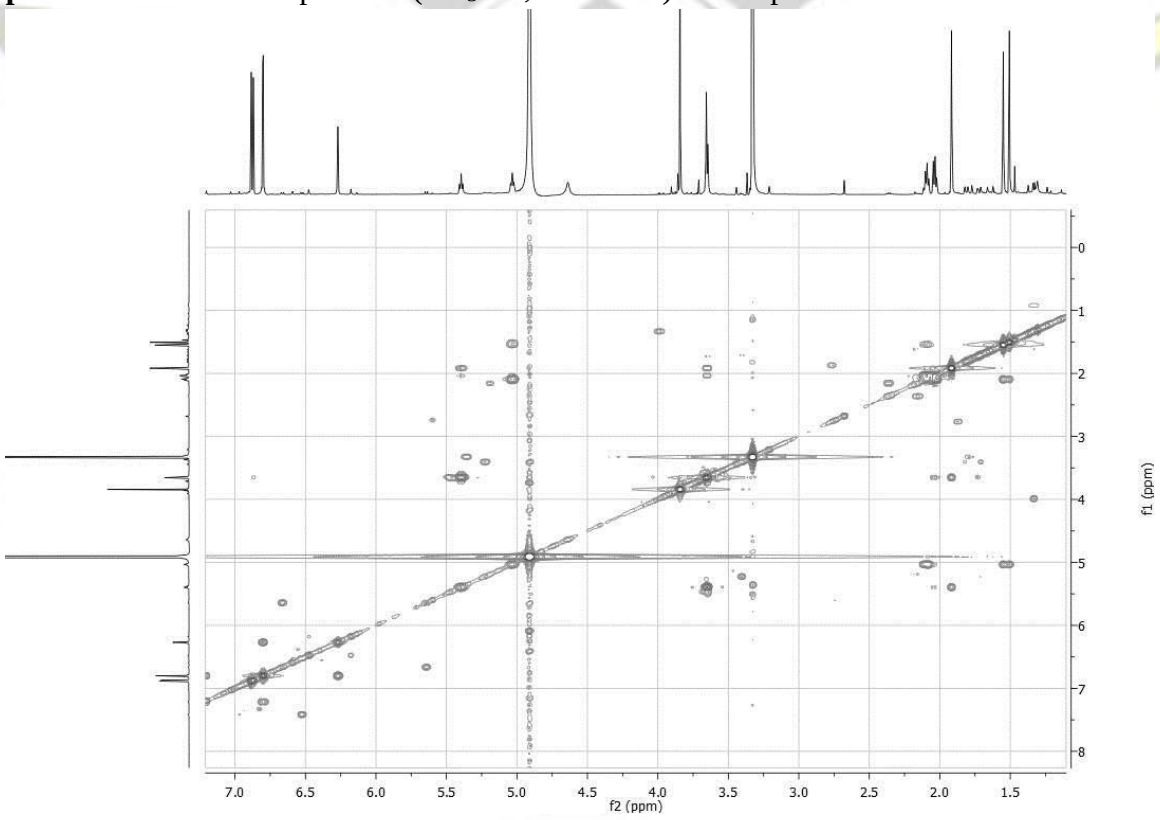
Appendix 16: Positive HRESI–MS/MS spectrum of compound **3**



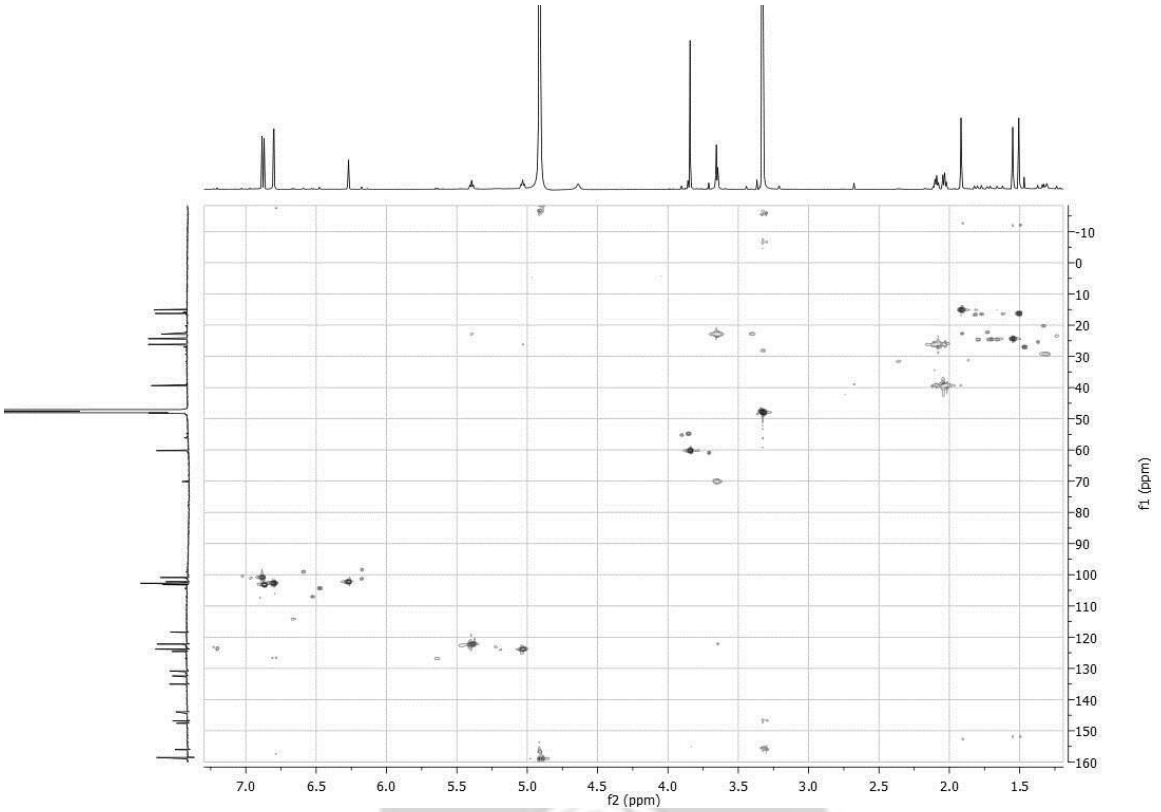
Appendix 17: ^{1}H NMR spectrum (CD_3OD, 600 MHz) of compound **3**.



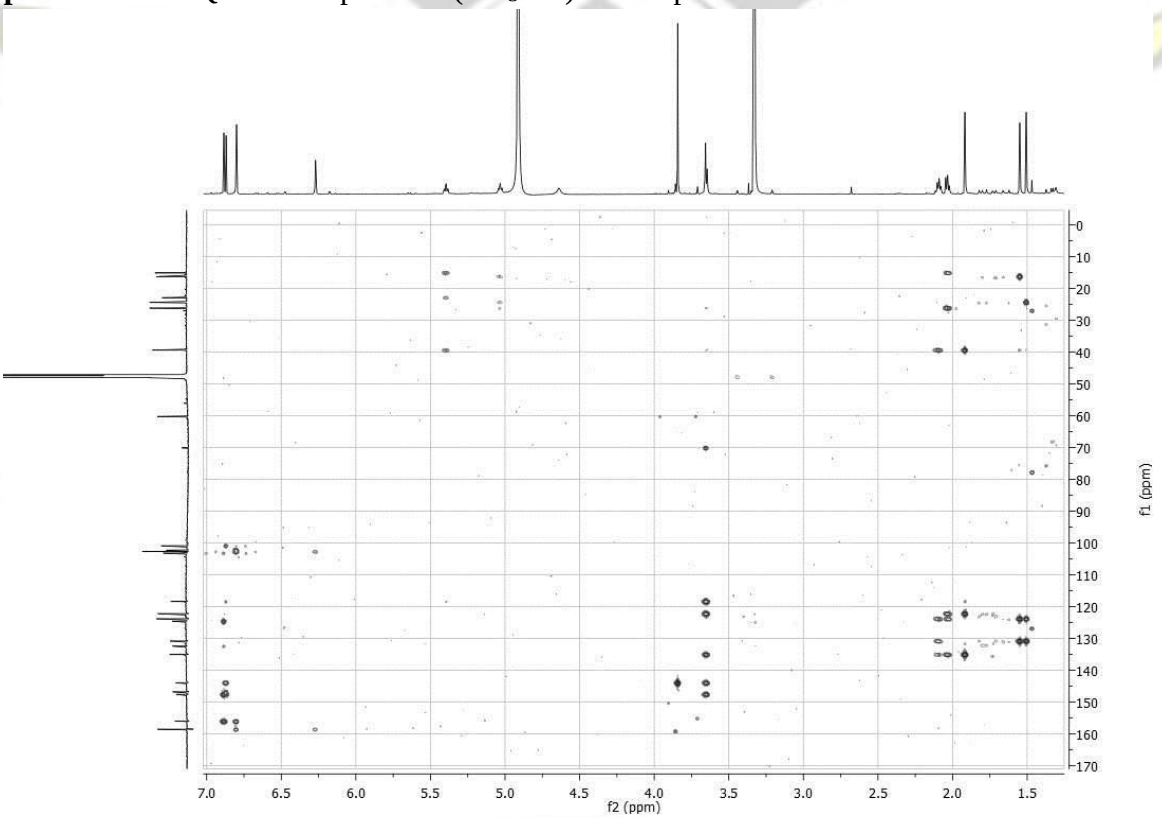
Appendix 18: ^{13}C NMR spectrum (CD_3OD, 150 MHz) of compound **3**.



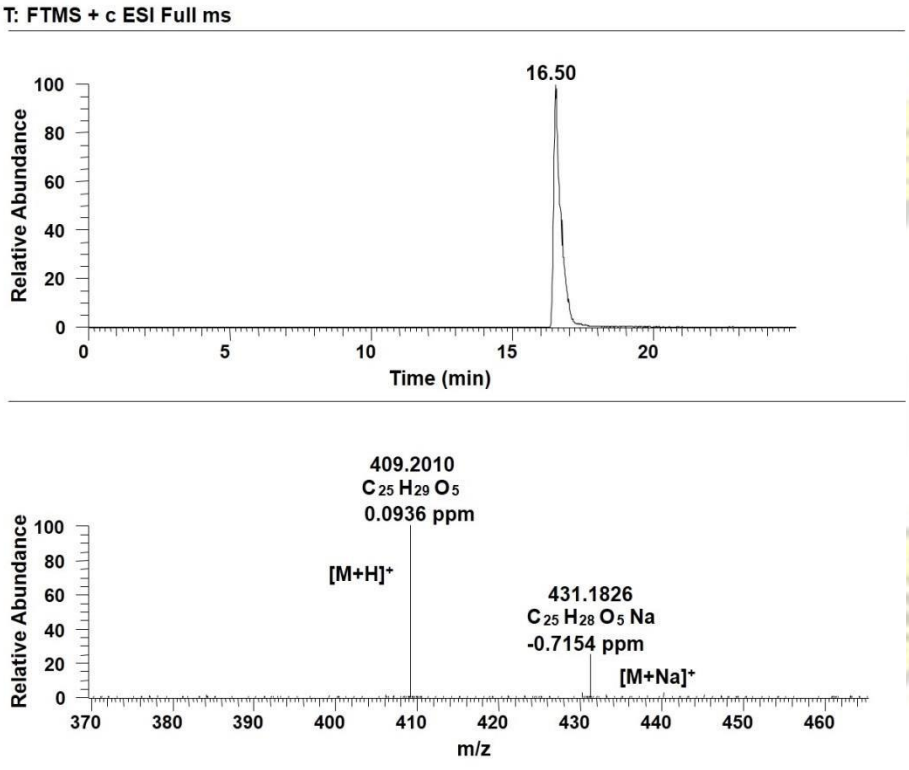
Appendix 19: $^{1}H–^{1}H$ COSY NMR spectrum (CD_3OD) of compound **3**.



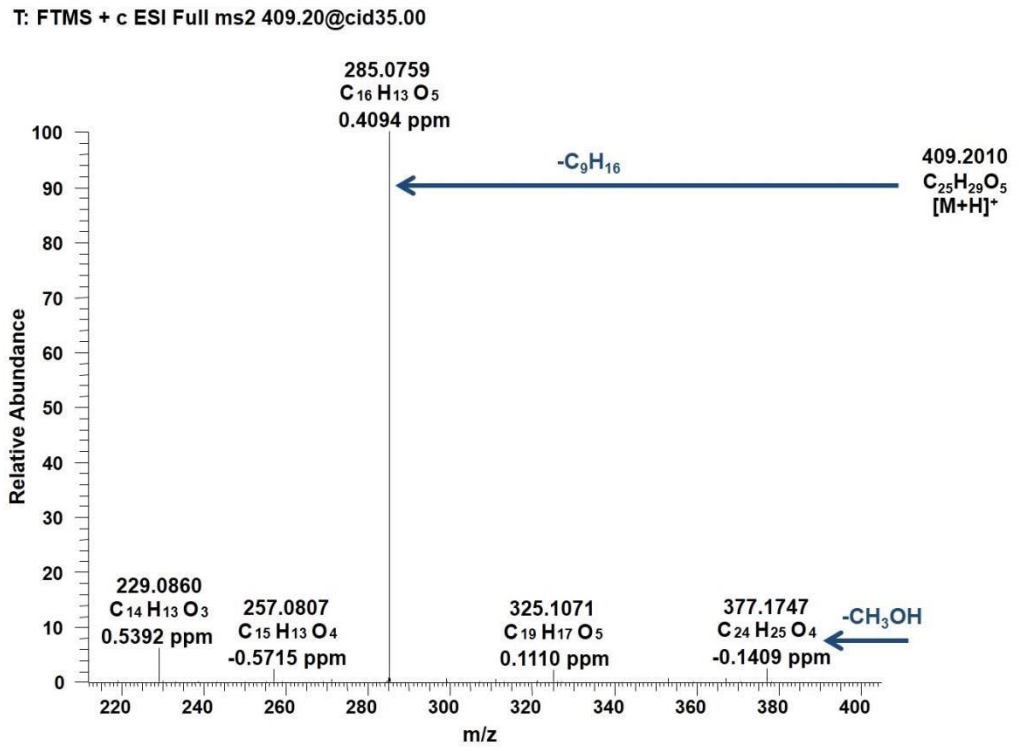
Appendix 20: HSQC NMR spectrum (CD_3OD) of compound **3**.



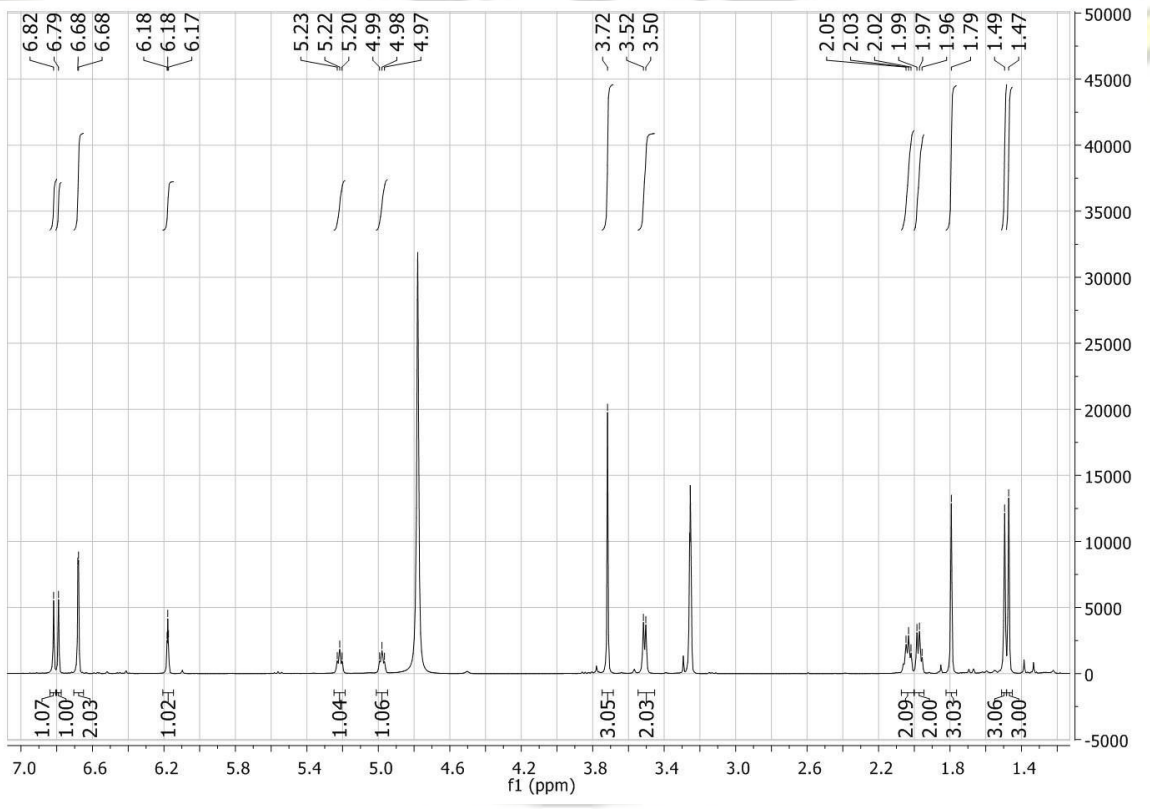
Appendix 21: HMBC NMR spectrum (CD_3OD) of compound **3**.



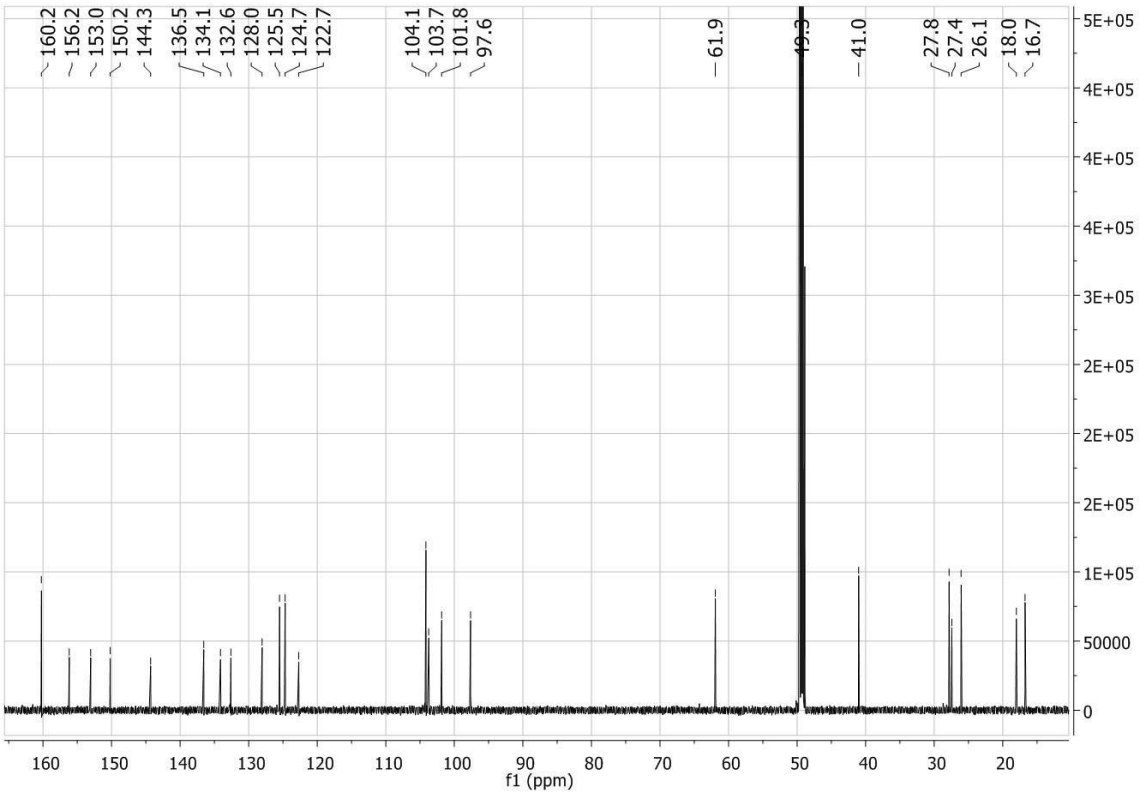
Appendix 22: Positive HRESI–MS spectrum of compound **4**



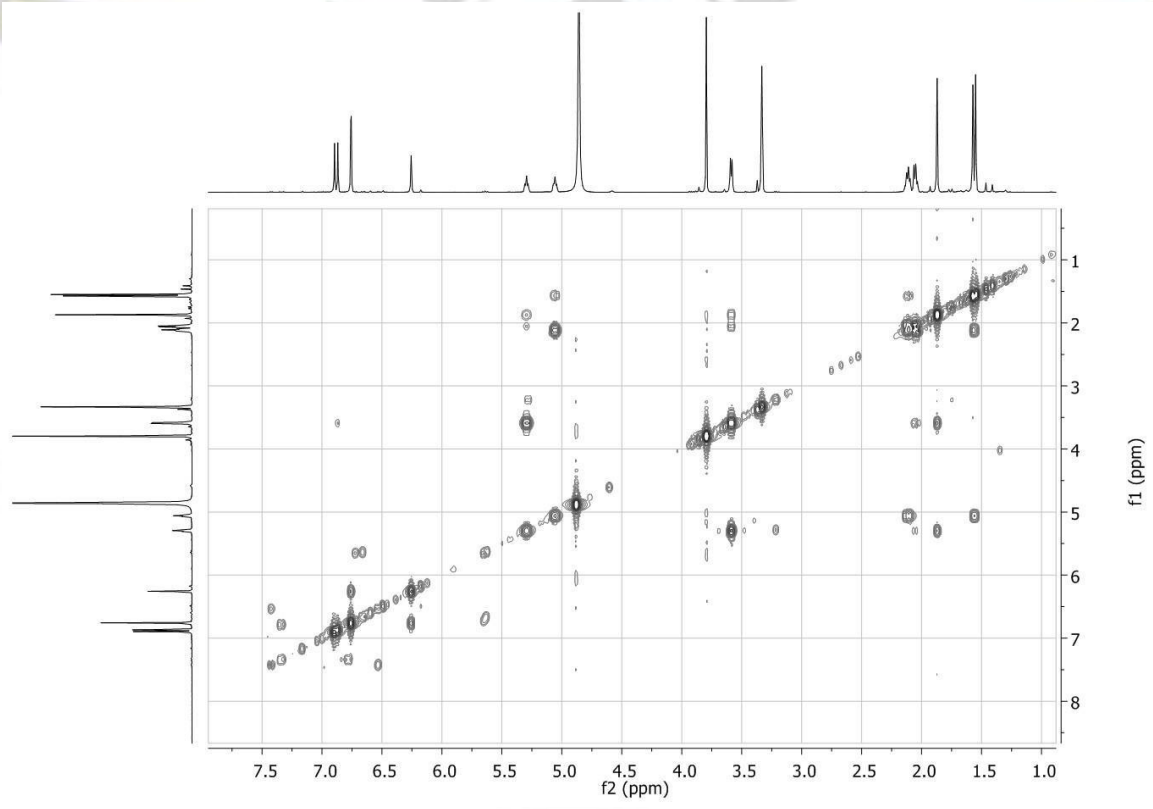
Appendix 23: Positive HRESI–MS/MS spectrum of compound **4**



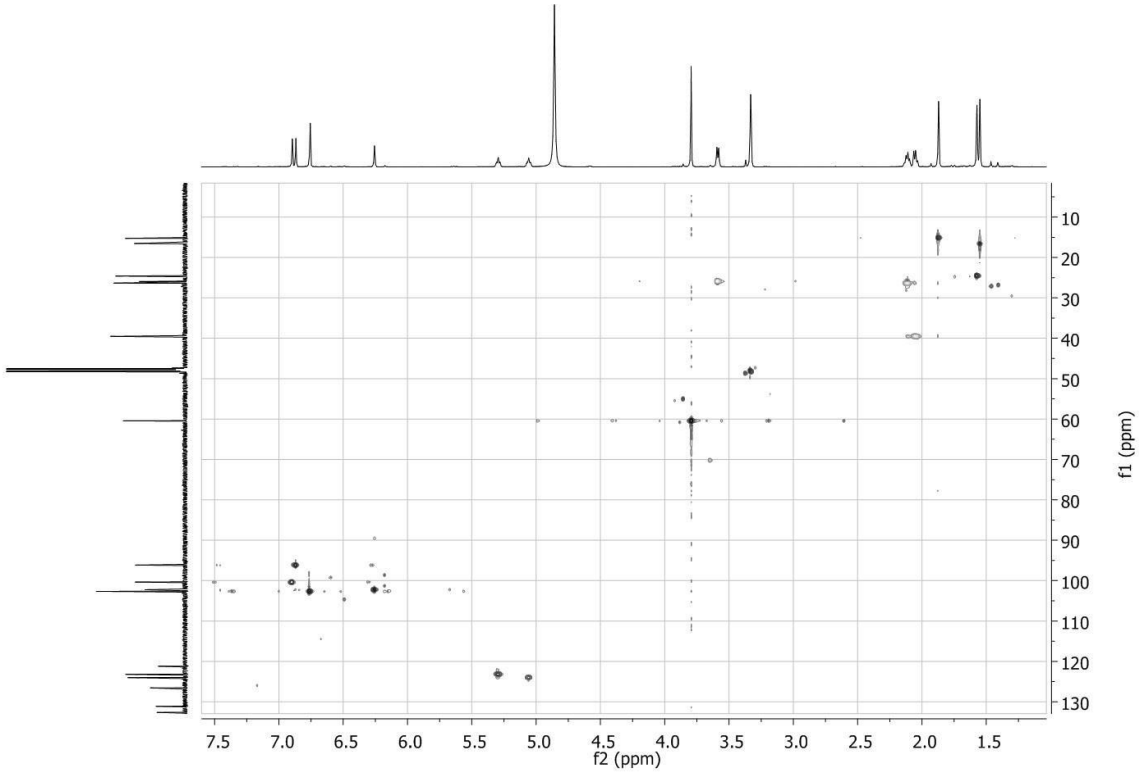
Appendix 24: ^{1}H NMR spectrum (CD_3OD, 600 MHz) of compound **4**.



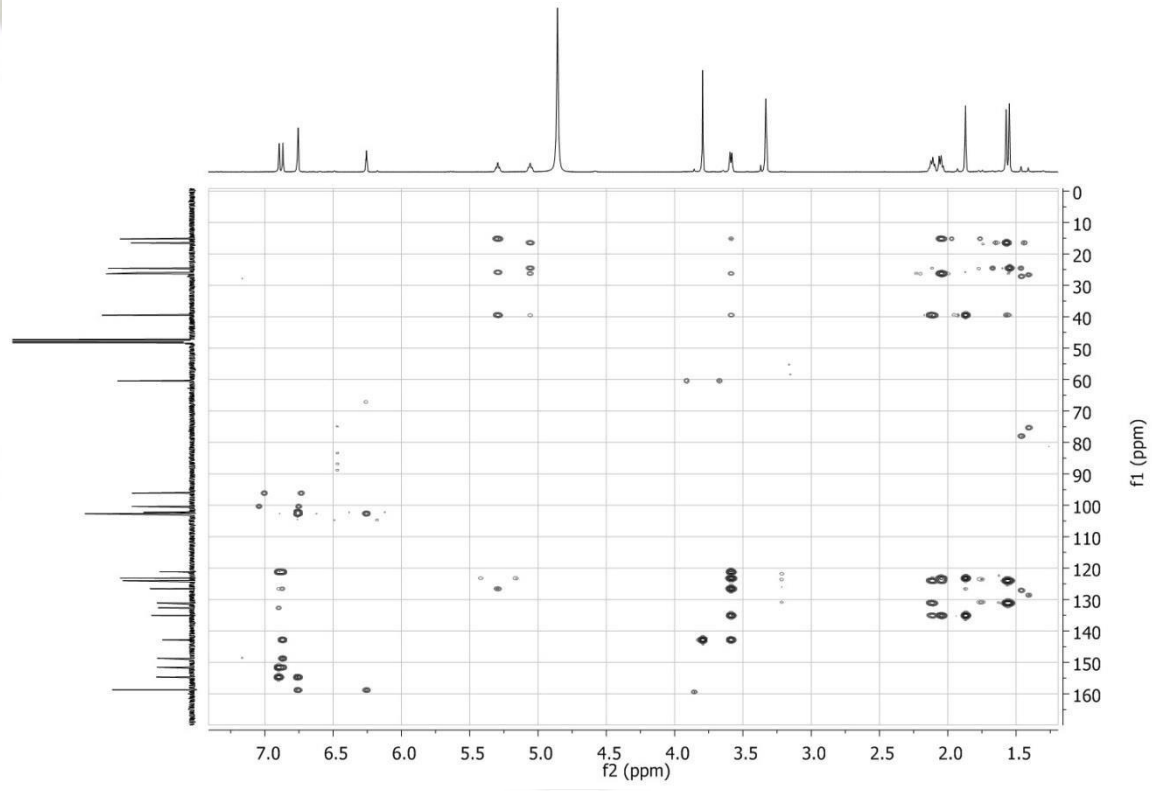
Appendix 25: ^{13}C NMR spectrum (CD_3OD, 150 MHz) of compound **4**.



Appendix 26: $^{1}H–^{1}H$ COSY NMR spectrum (CD_3OD) of compound **4**.

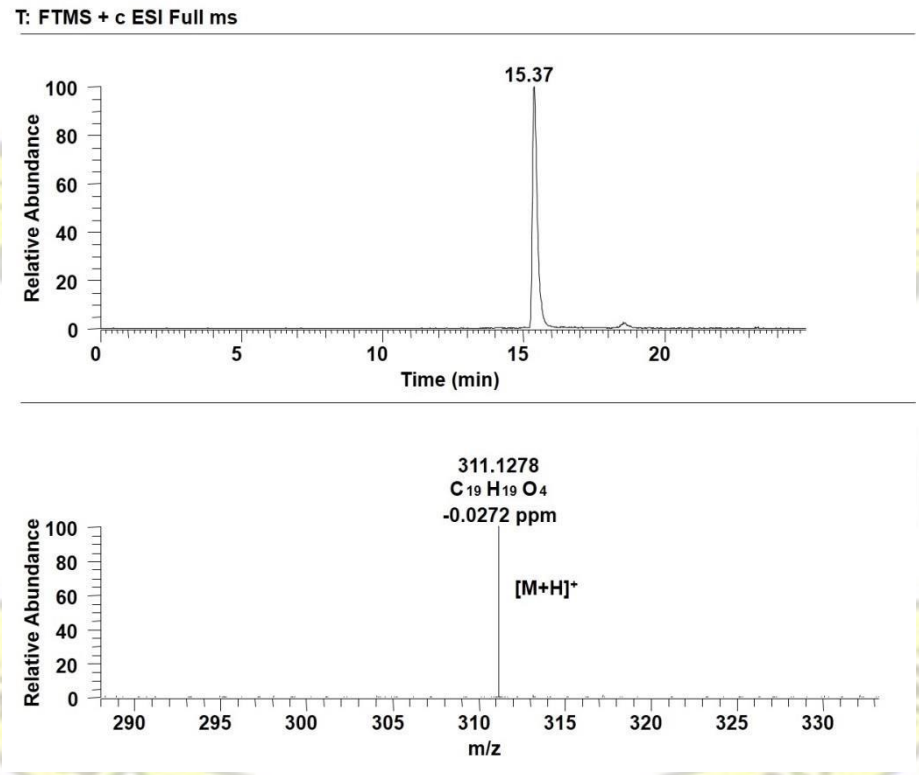


Appendix 27: HSQC NMR spectrum (CD_3OD) of compound **4**.

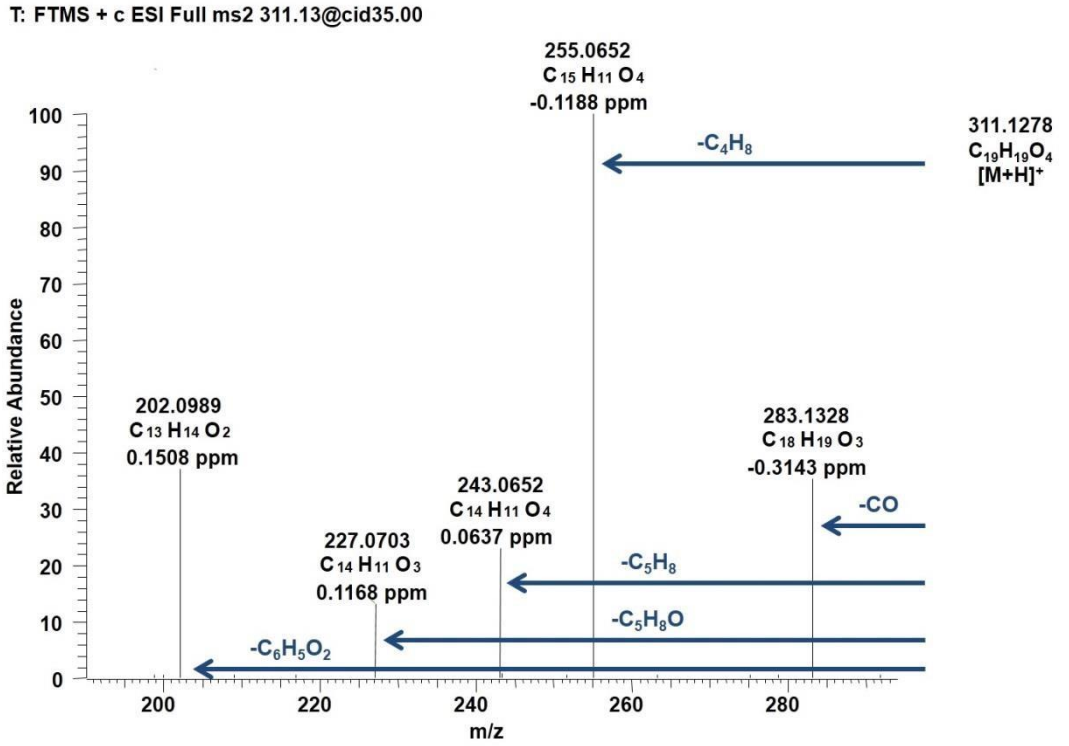


Appendix 28: HMBC NMR spectrum (CD_3OD) of compound **4**.

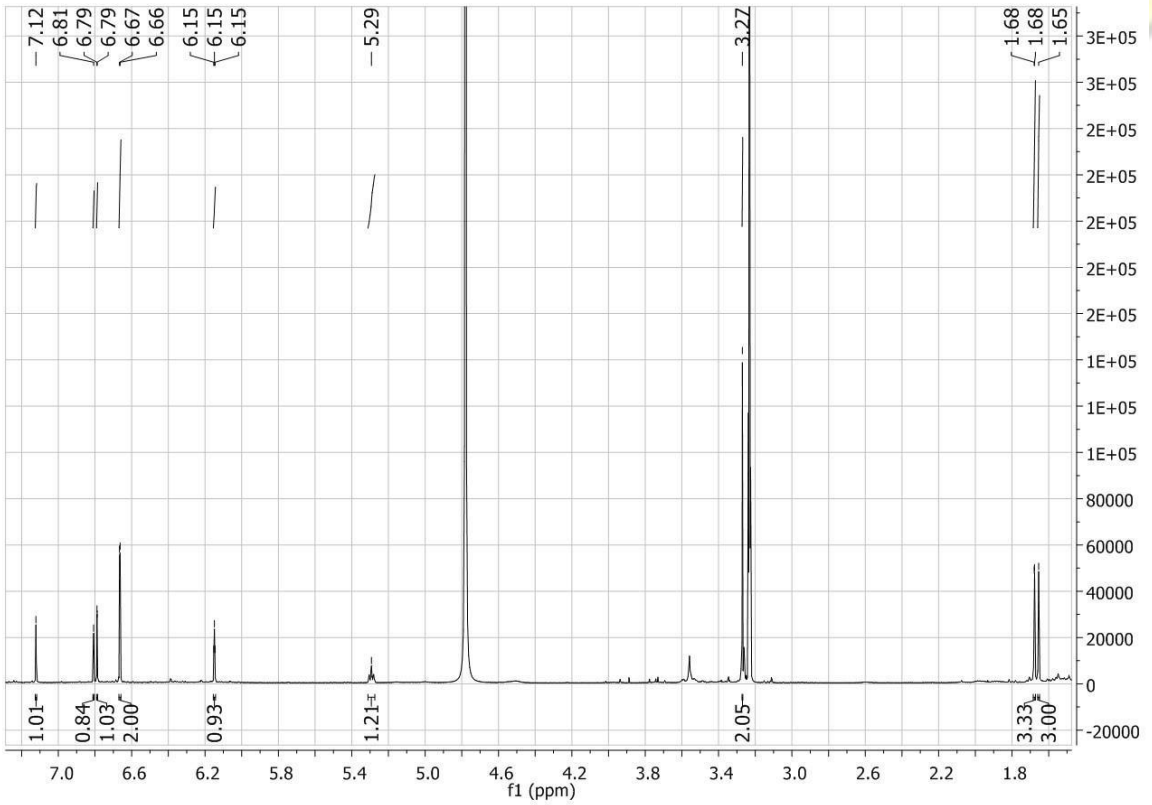
KNUST



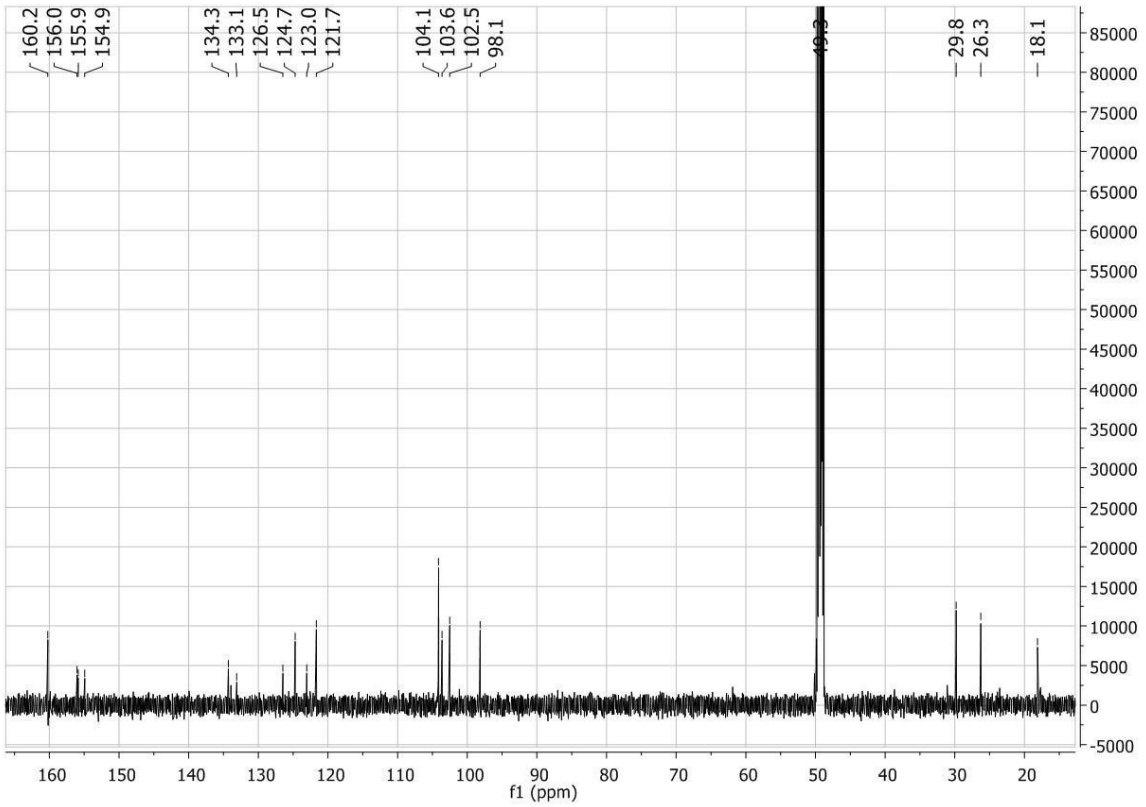
Appendix 29: Positive HRESI–MS spectrum of compound **5**



Appendix 30: Positive HRESI–MS/MS spectrum of compound **5**

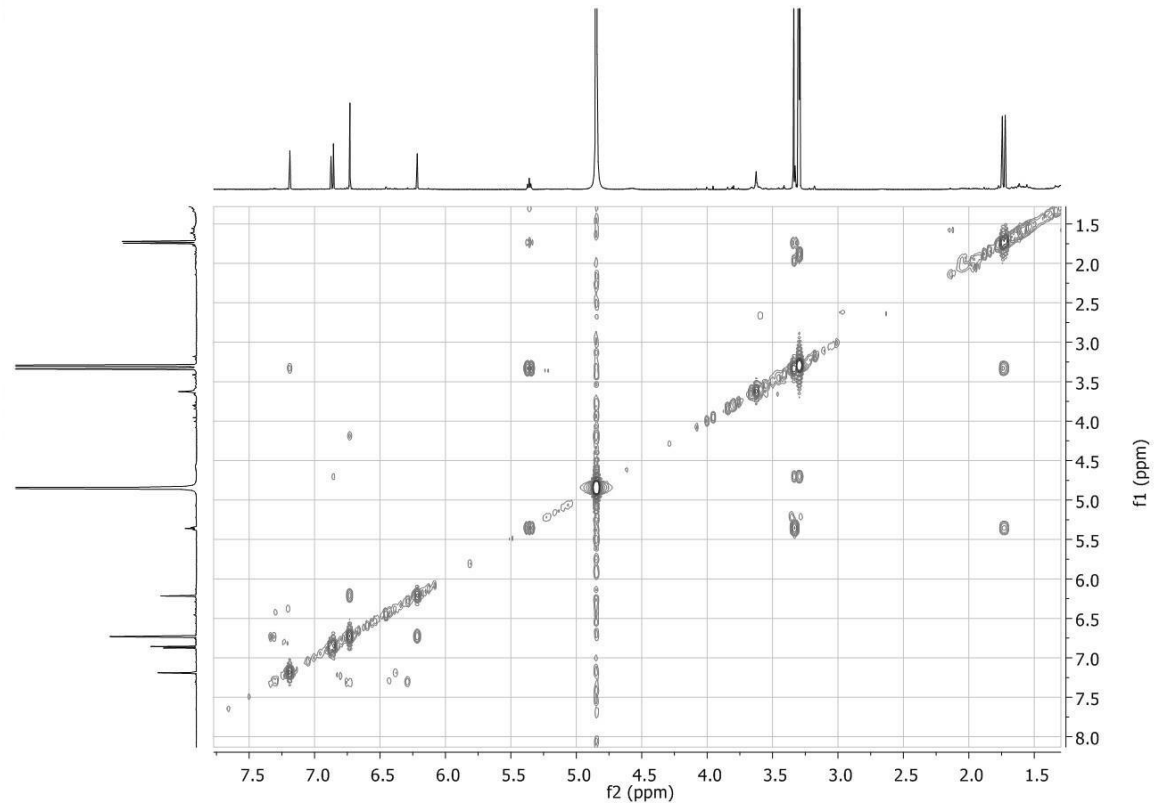


Appendix 31: ^{1}H NMR spectrum (CD_3OD, 600 MHz) of compound **5**.

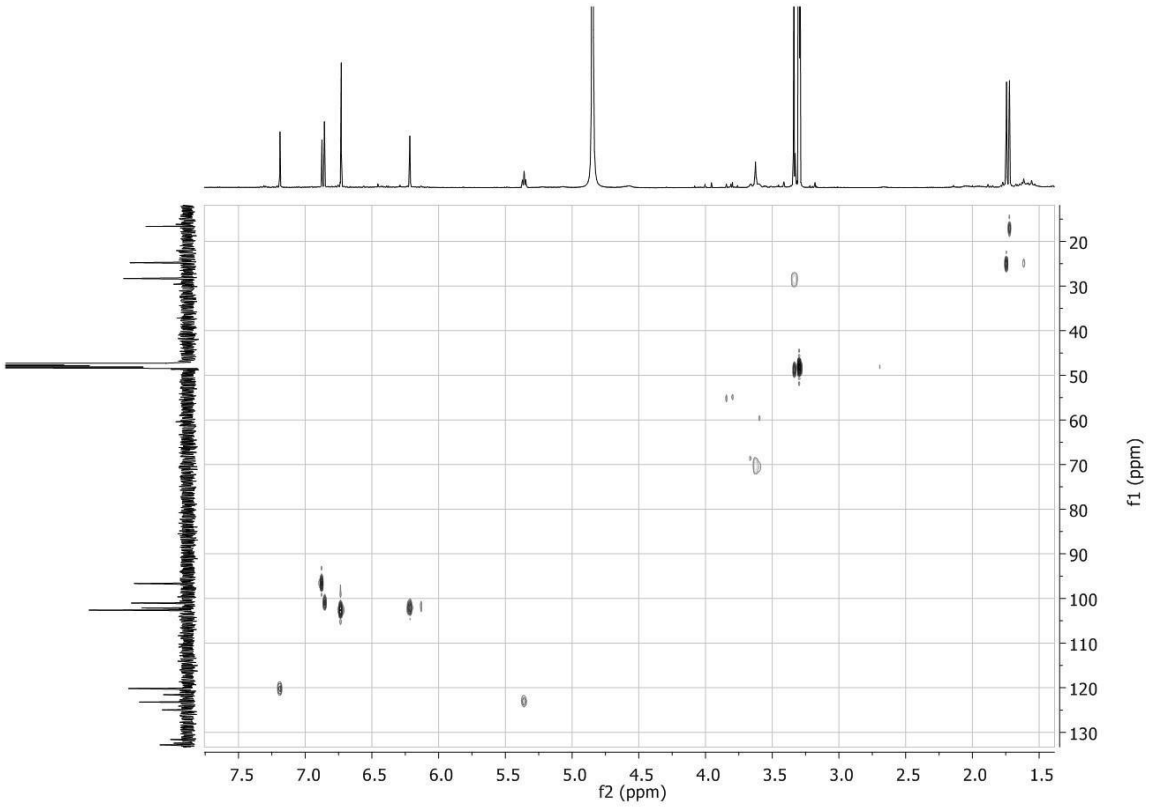


^{13}C NMR spectrum (CD_3OD, 150 MHz) of compound **5**.

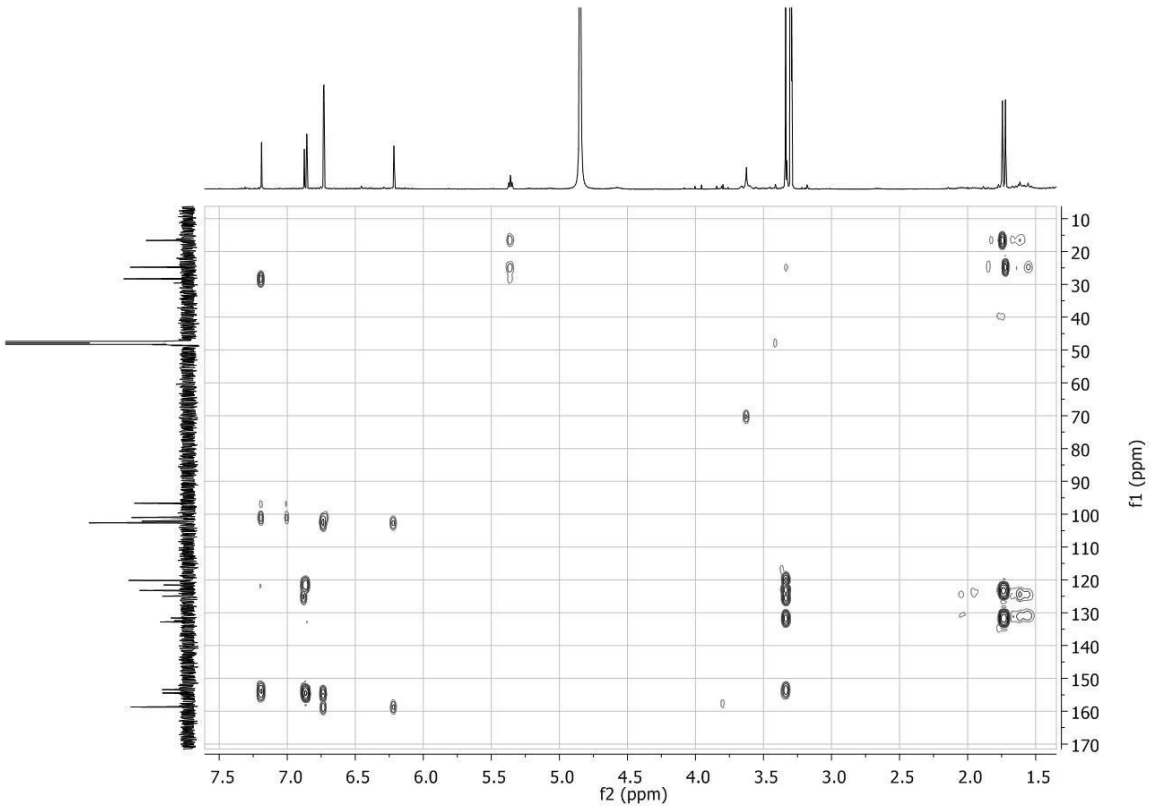
Appendix 32:



Appendix 33: ^{1}H–^{1}H COSY NMR spectrum (in CD_3OD) of compound **5**.

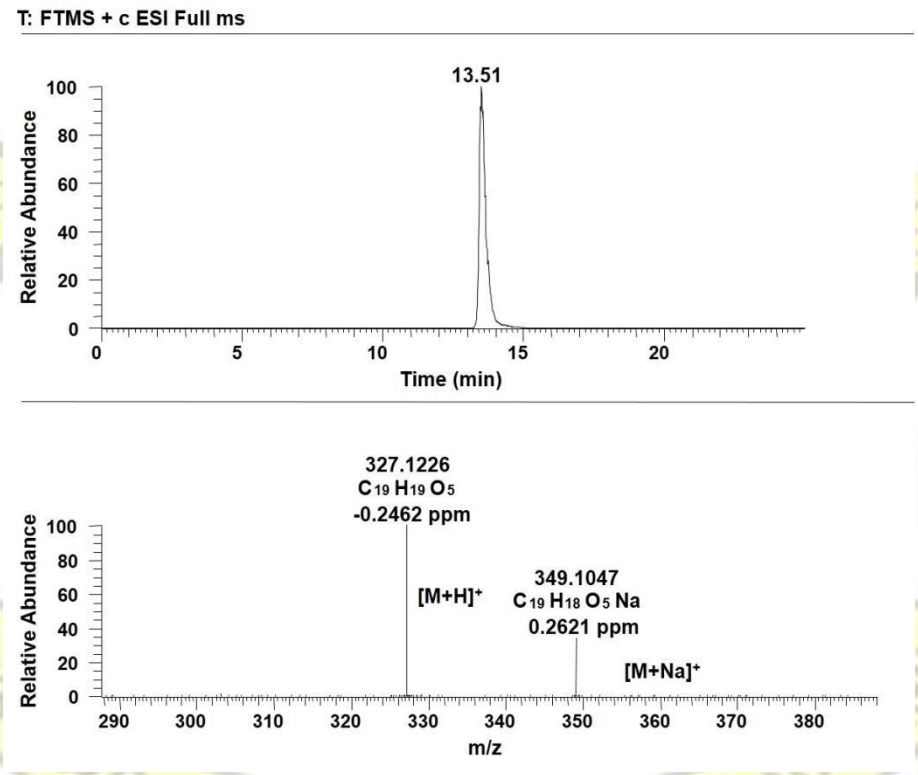


Appendix 34: HSQC NMR spectrum (CD_3OD) of compound **5**.

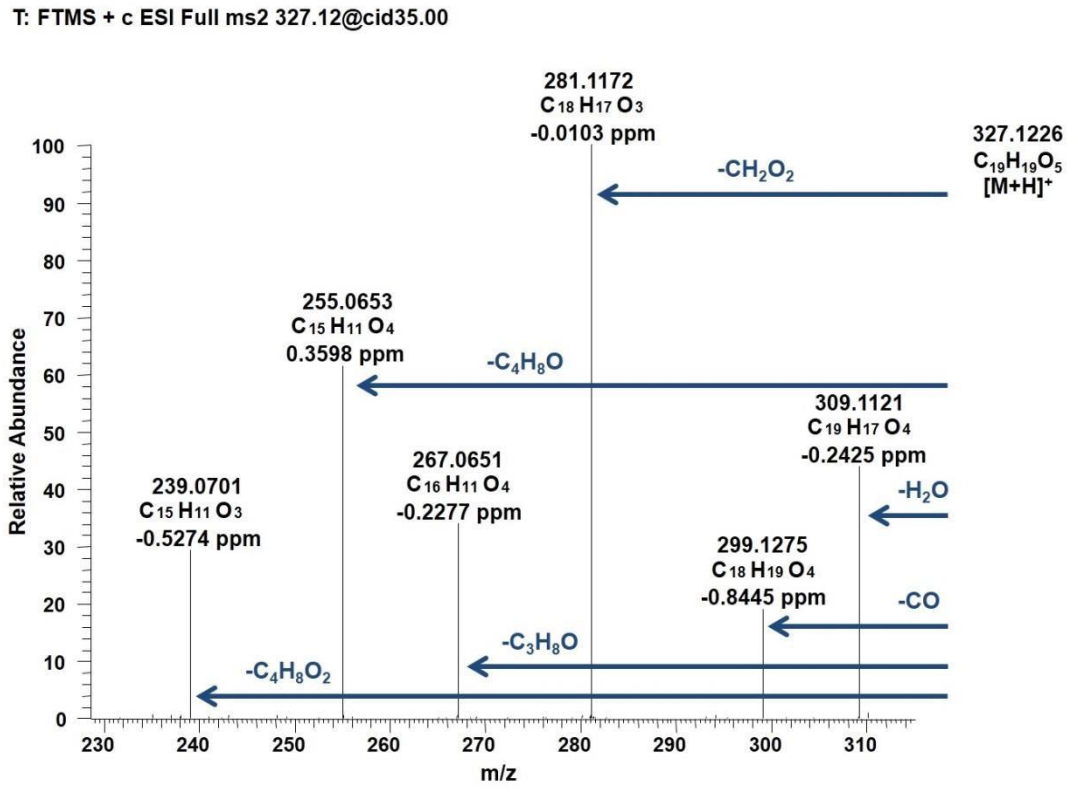


Appendix 35: HMBC NMR spectrum (CD_3OD) of compound **5**.

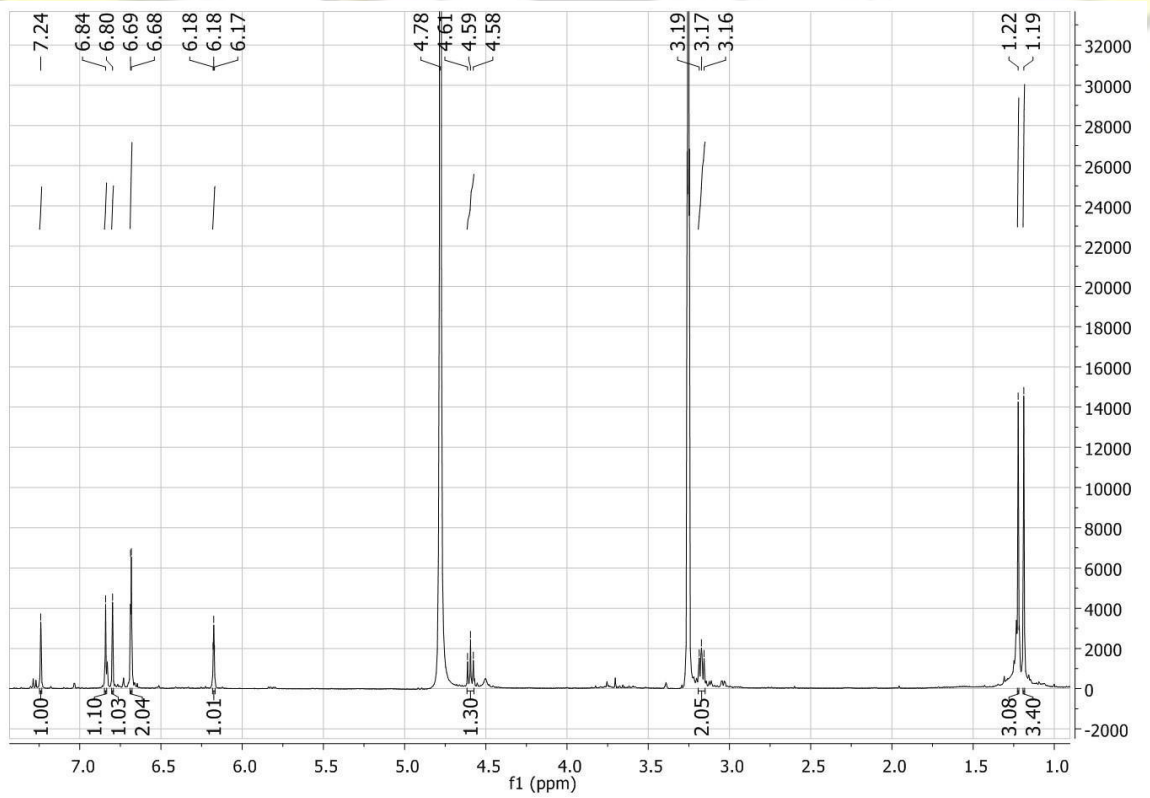
KNUST



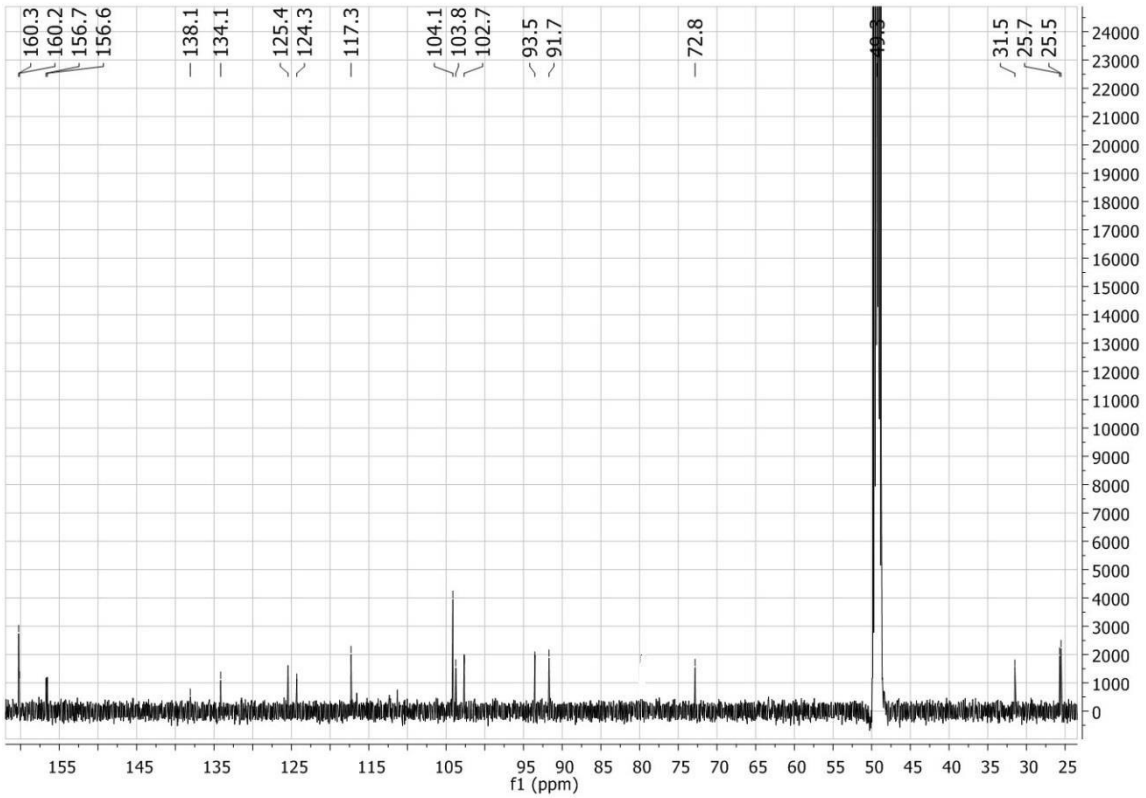
Appendix 36: Positive HRESI–MS spectrum of compound **6**



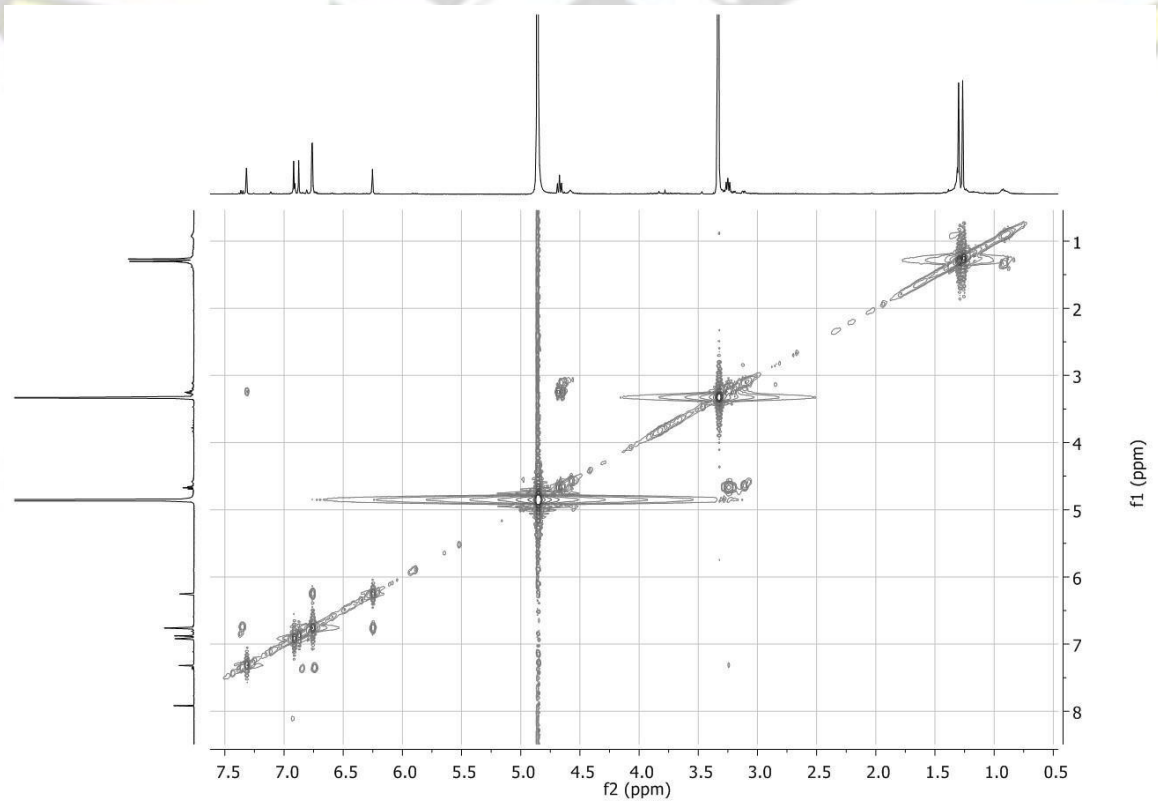
Appendix 37: Positive HRESI–MS/MS spectrum of compound **6**



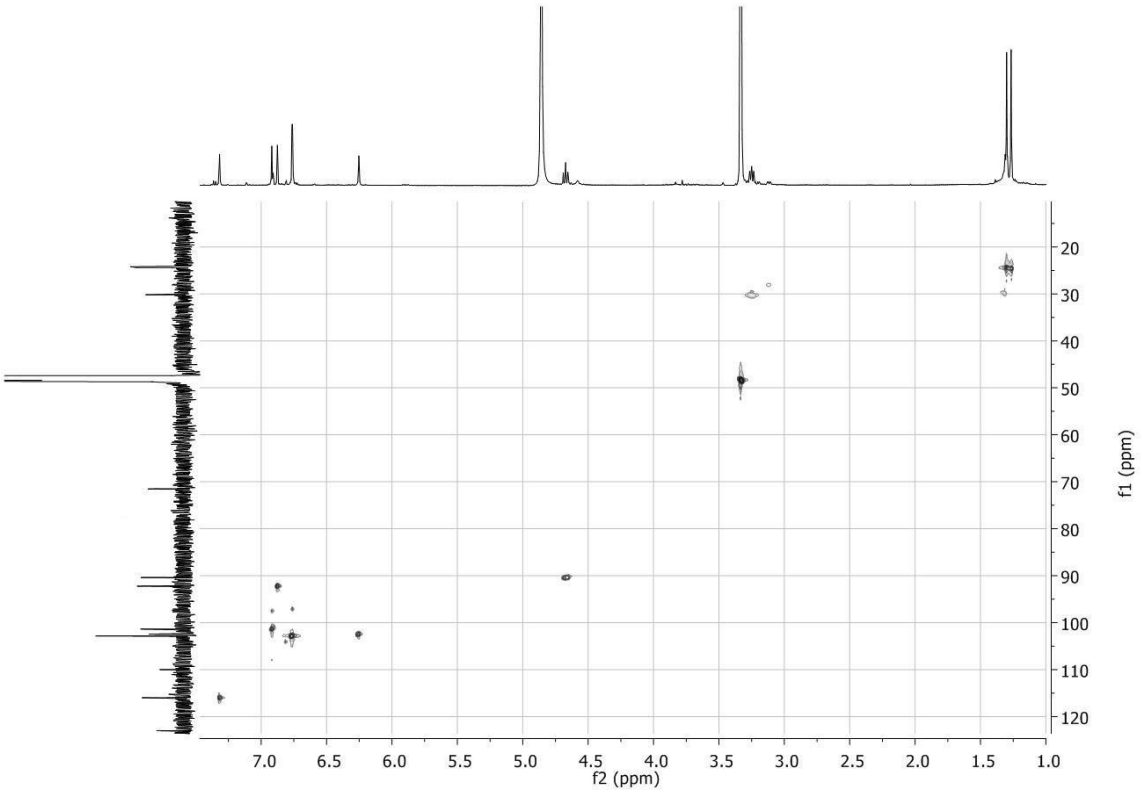
Appendix 38: ^{1}H NMR spectrum (CD_3OD, 500 MHz) of compound **6**



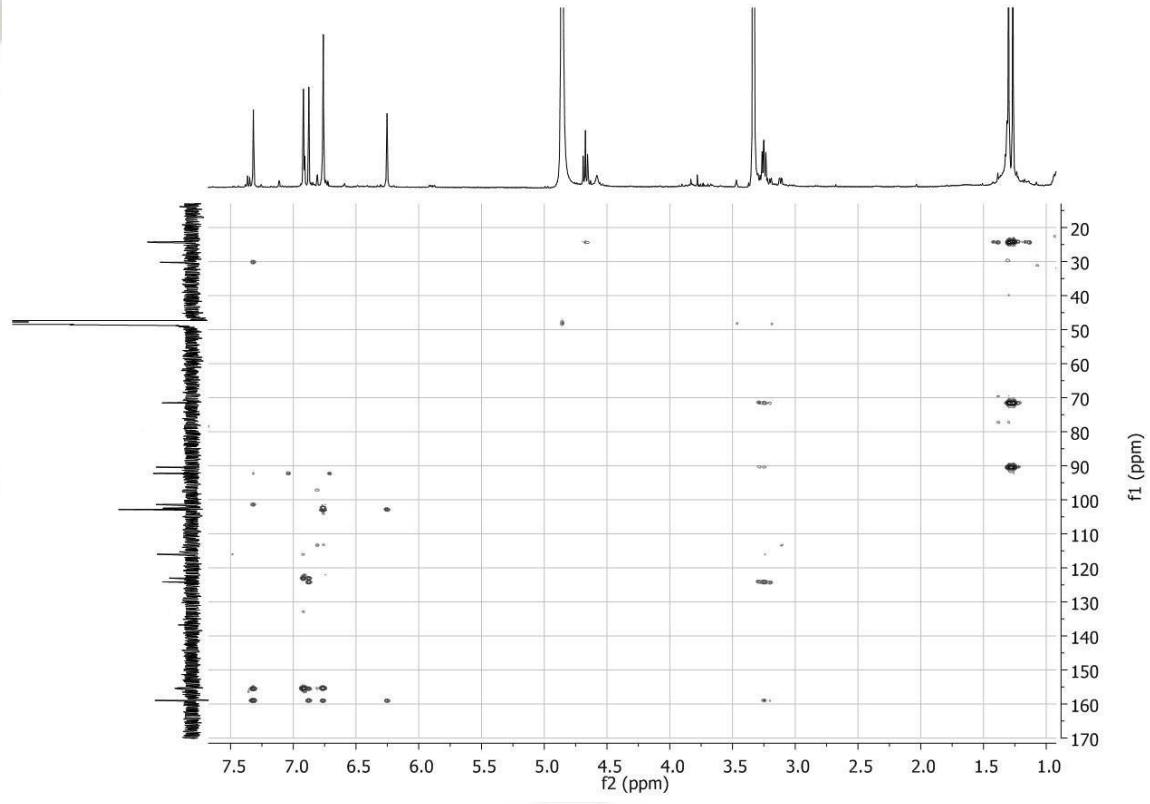
Appendix 39: ^{13}C NMR spectrum (CD_3OD, 125 MHz) of compound **6**



Appendix 40: $^{1}H–^{1}H$ COSY NMR spectrum (CD_3OD) of compound **6**.

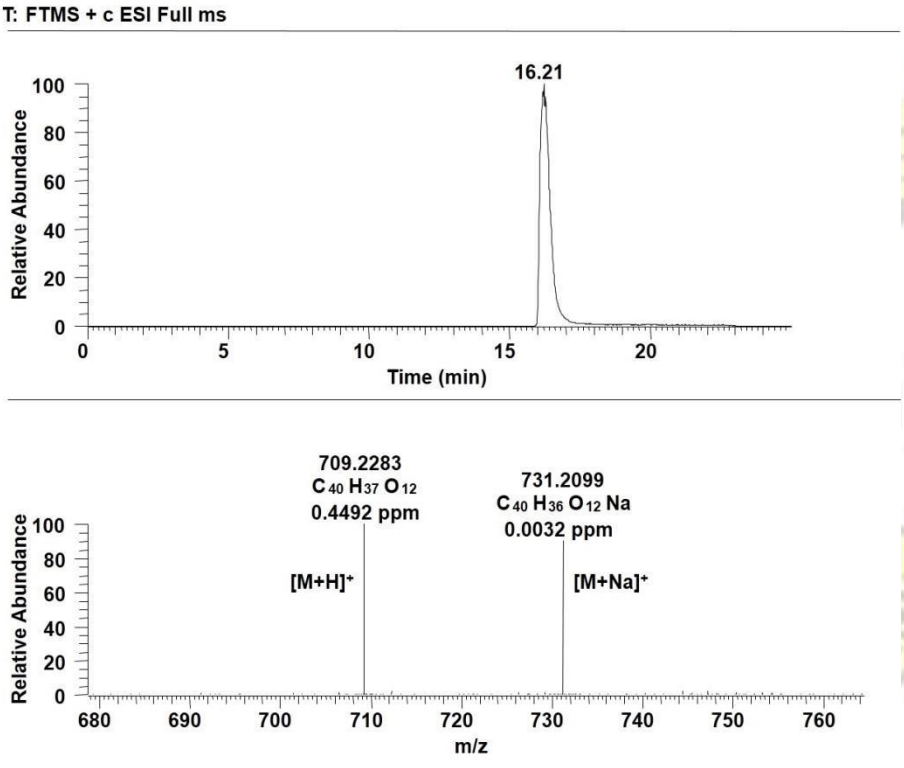


Appendix 41: HSQC NMR spectrum (CD_3OD) of compound **6**

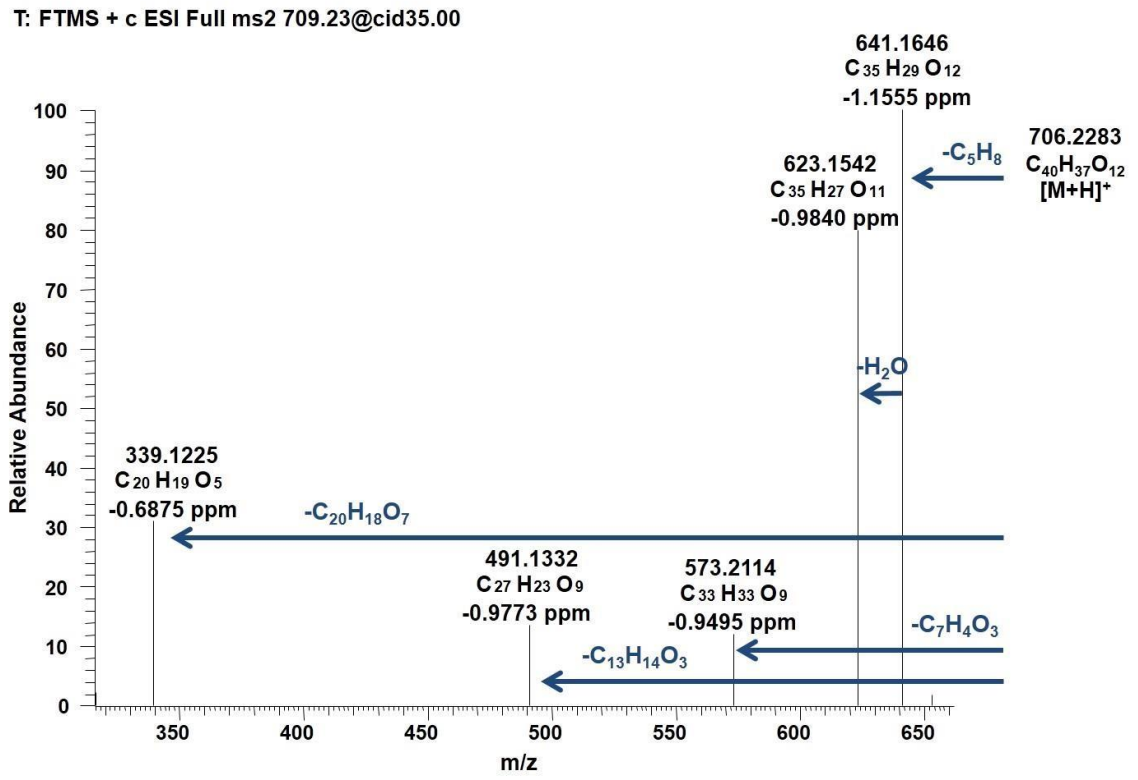


Appendix 42: HMBC NMR spectrum (CD_3OD) of compound **6**.

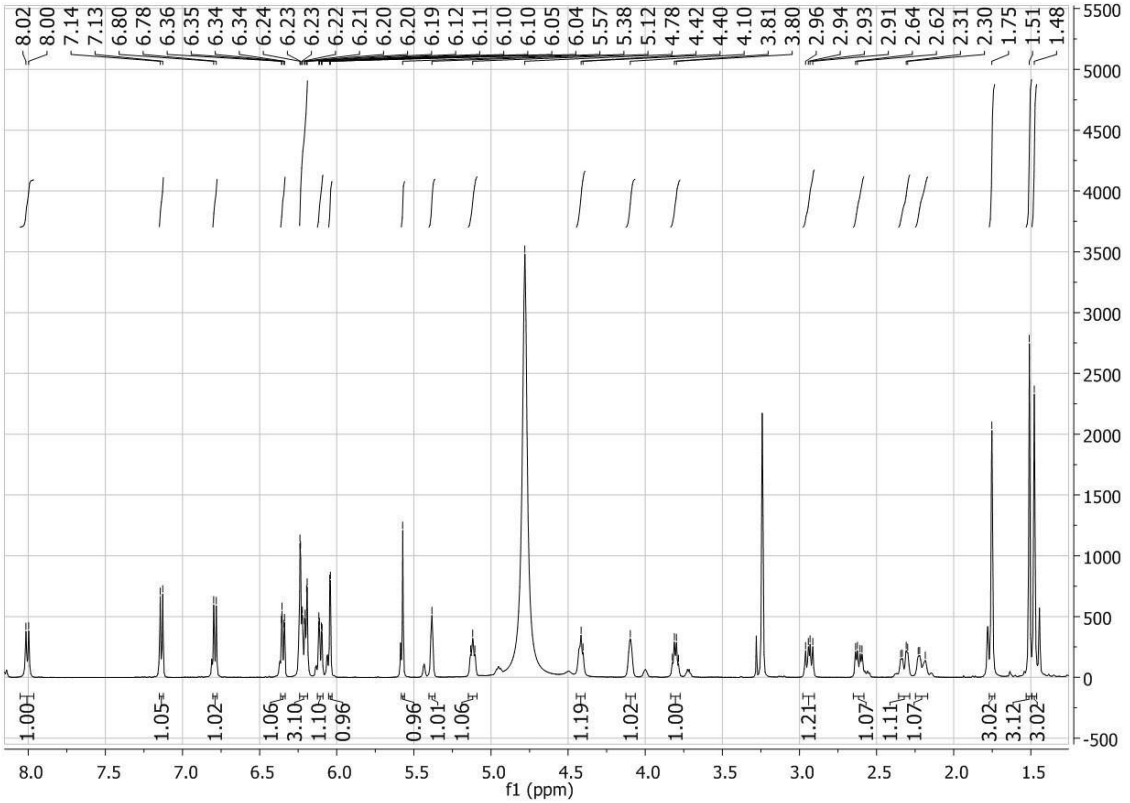
KNUST



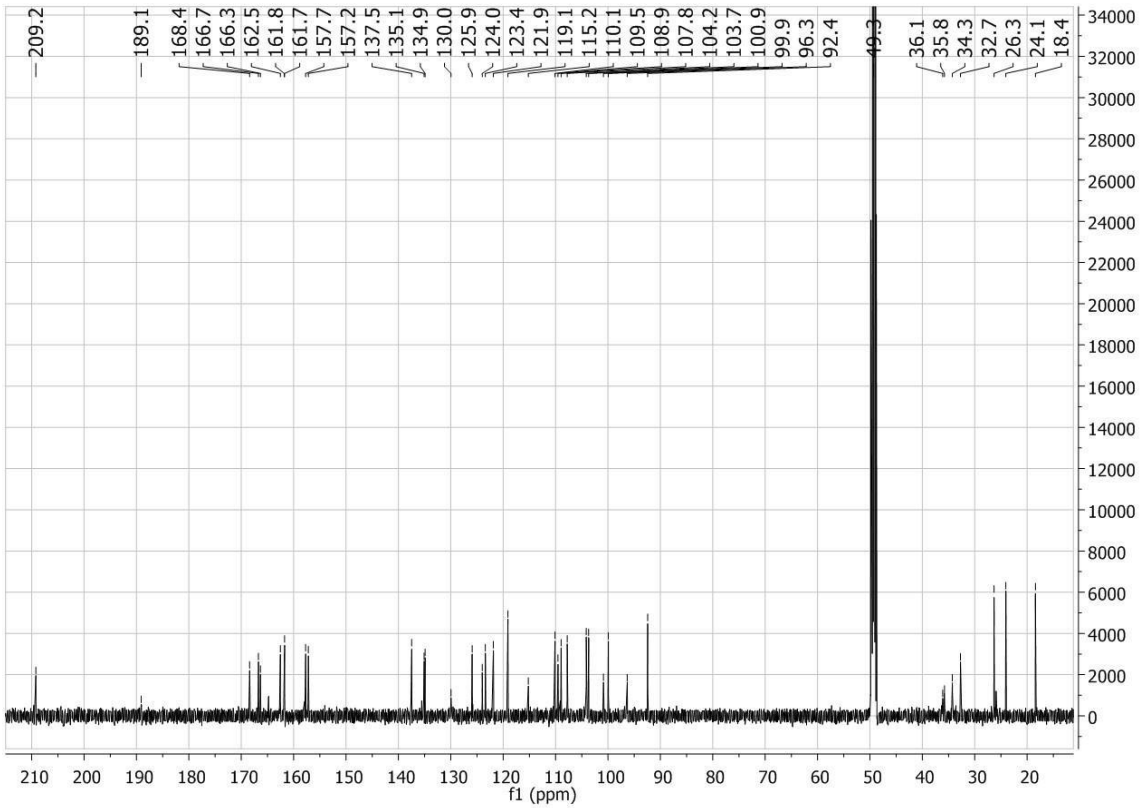
Appendix 43: Positive HRESI–MS spectrum of compound **7**



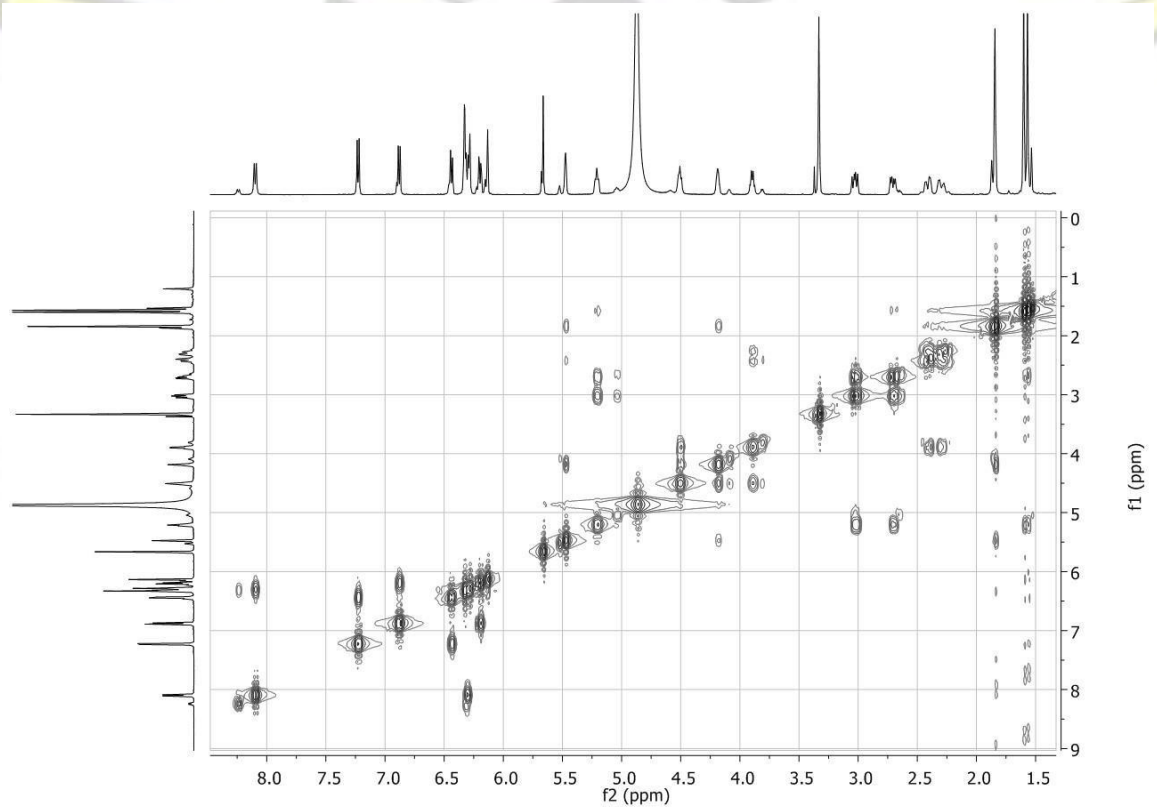
Appendix 44: Positive HRESI–MS/MS spectrum of compound **7**



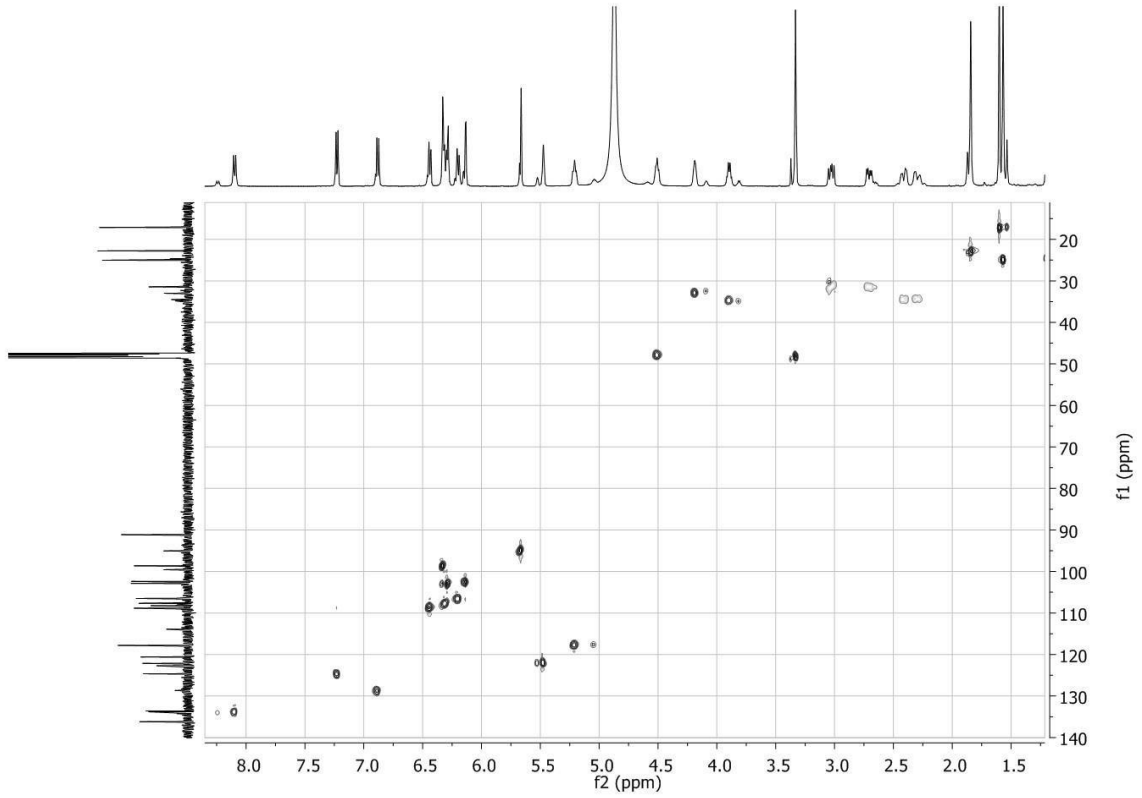
Appendix 45: ^{1}H NMR spectrum (CD_3OD, 500 MHz) of compound **7**



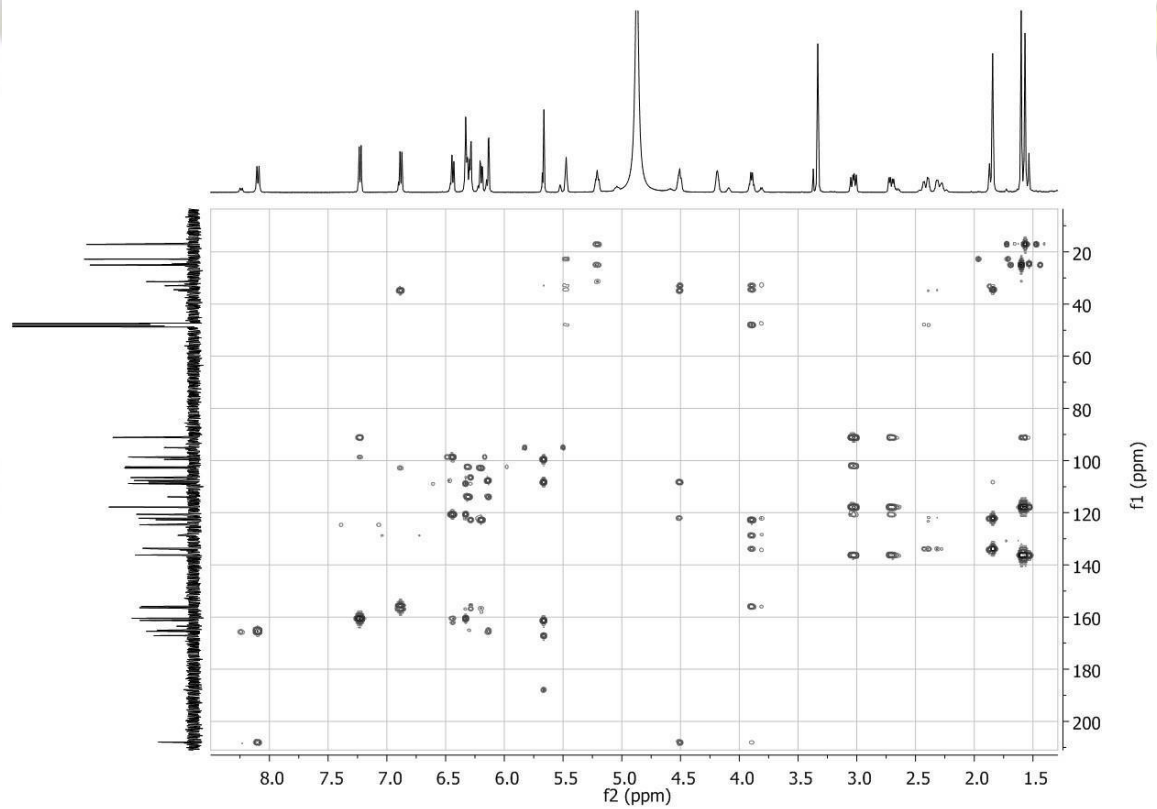
Appendix 46: ^{13}C NMR spectrum (CD_3OD, 125 MHz) of compound **7**



Appendix 47: $^{1}H–^{1}H$ COSY NMR spectrum (CD_3OD) of compound **7**



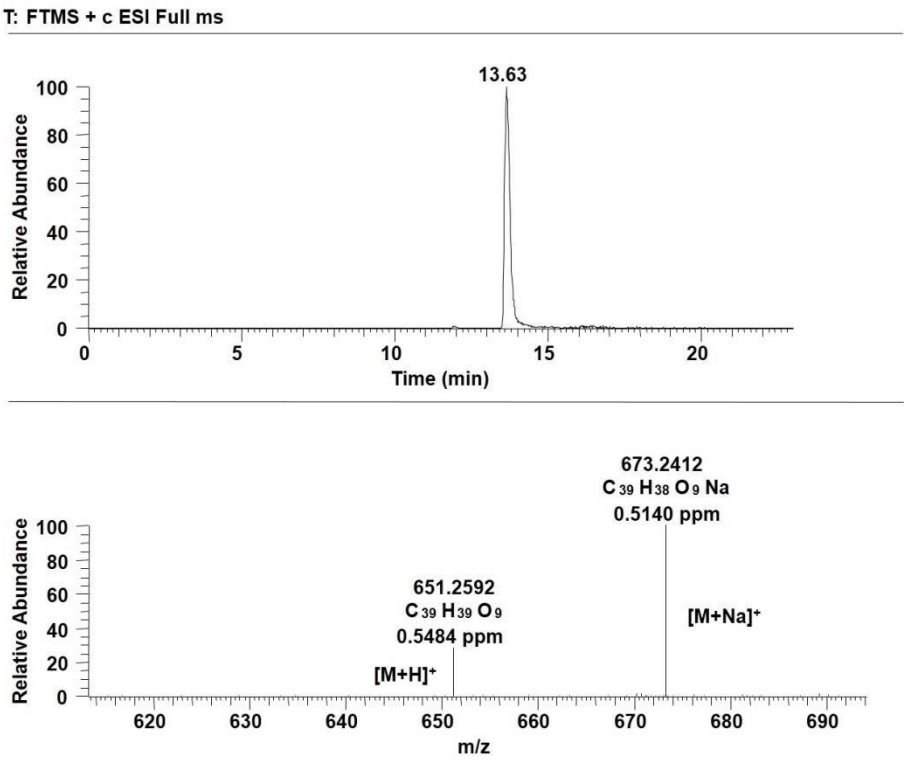
Appendix 48: HSQC NMR spectrum (CD_3OD) of compound **7**



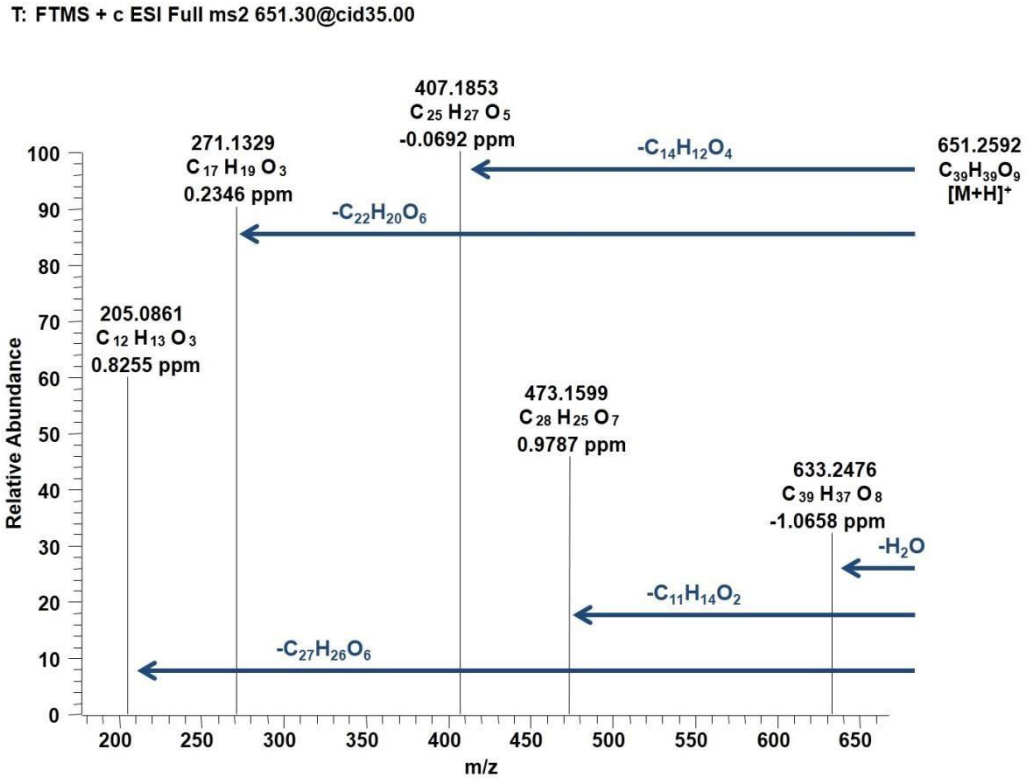
Appendix 49: HMBC NMR spectrum (CD_3OD) of compound **7**

KNUST

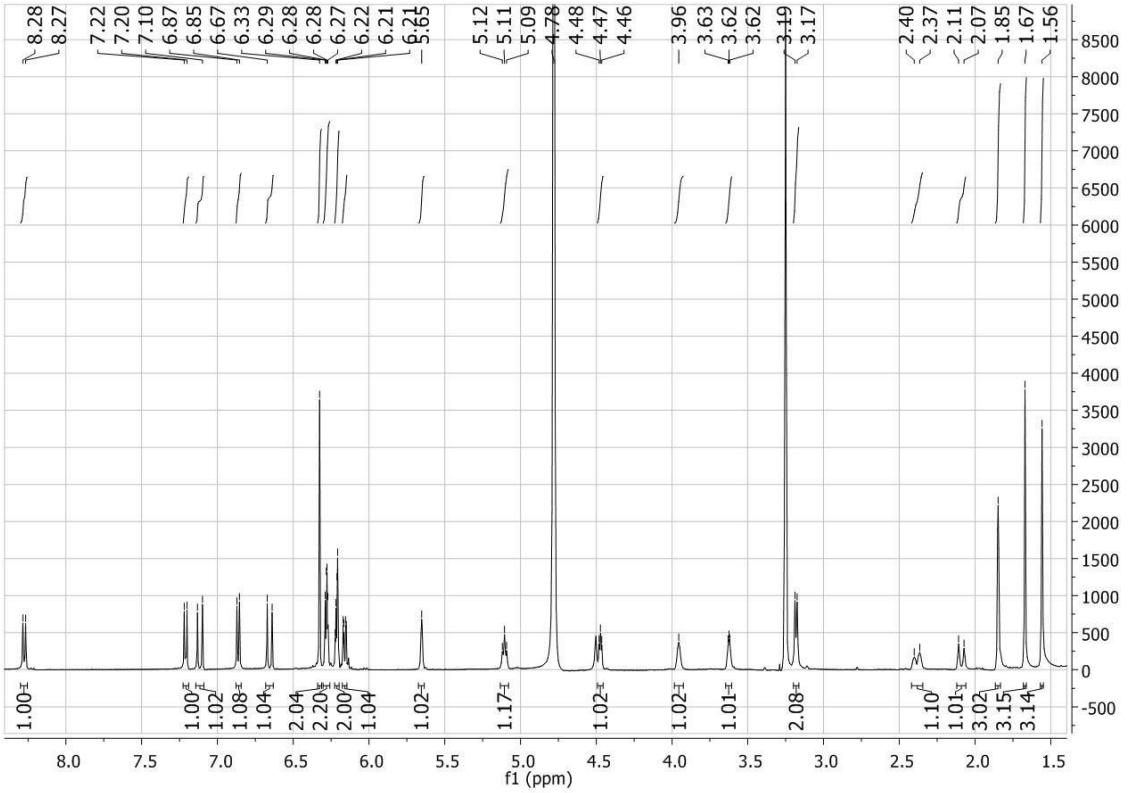




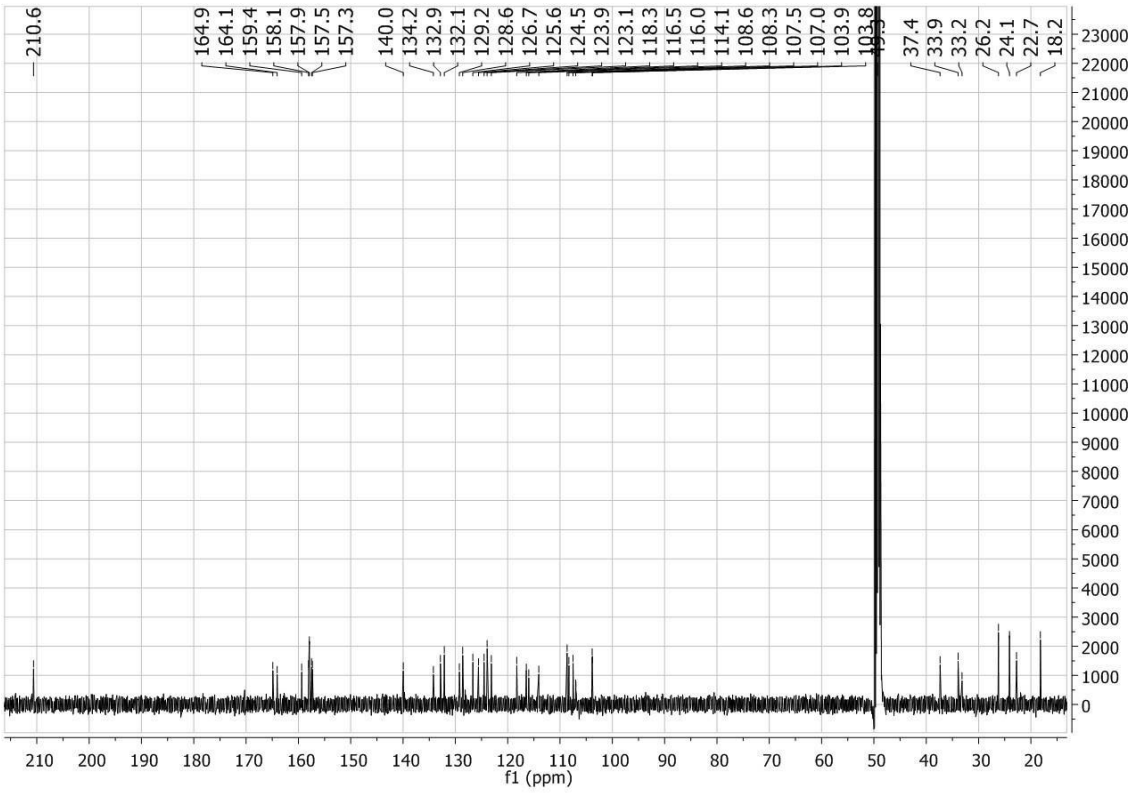
Appendix 50: Positive HRESI–MS spectrum of compound **8**



51: Positive HRESI–MS/MS spectrum of compound **8**

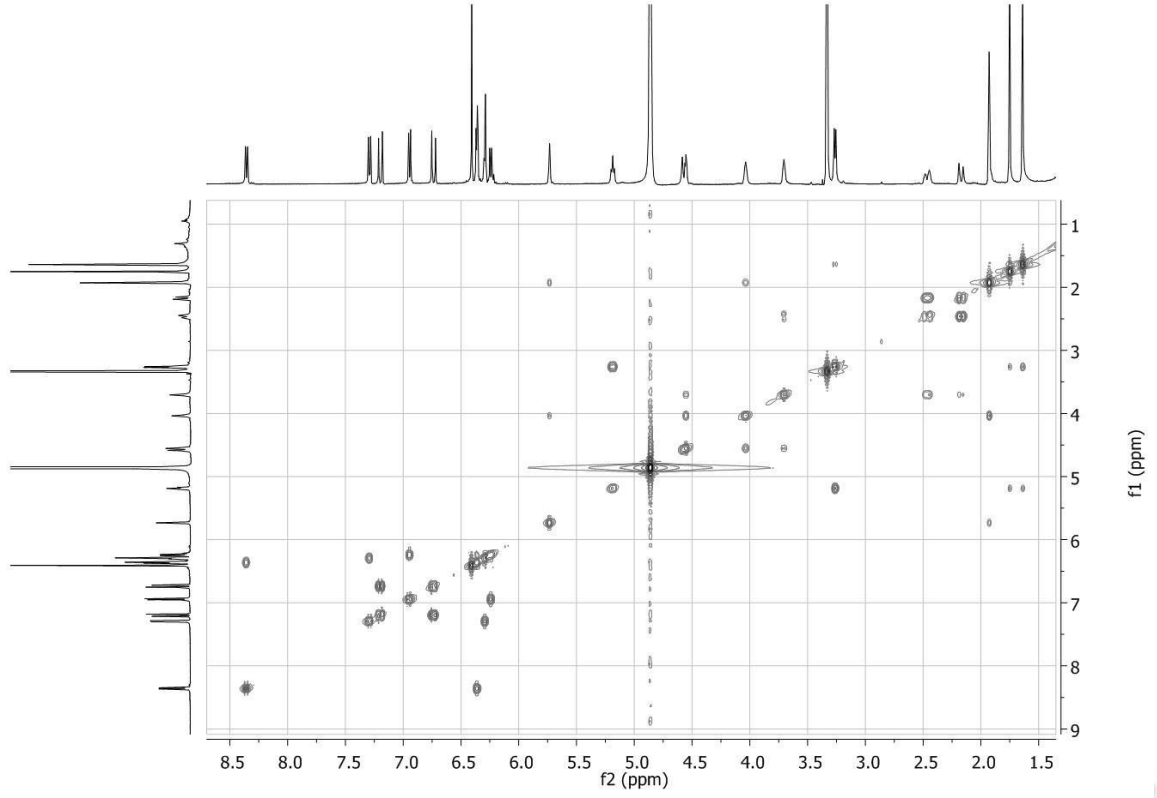


Appendix 52: ^{1}H NMR spectrum (CD_3OD, 500 MHz) of compound **8**

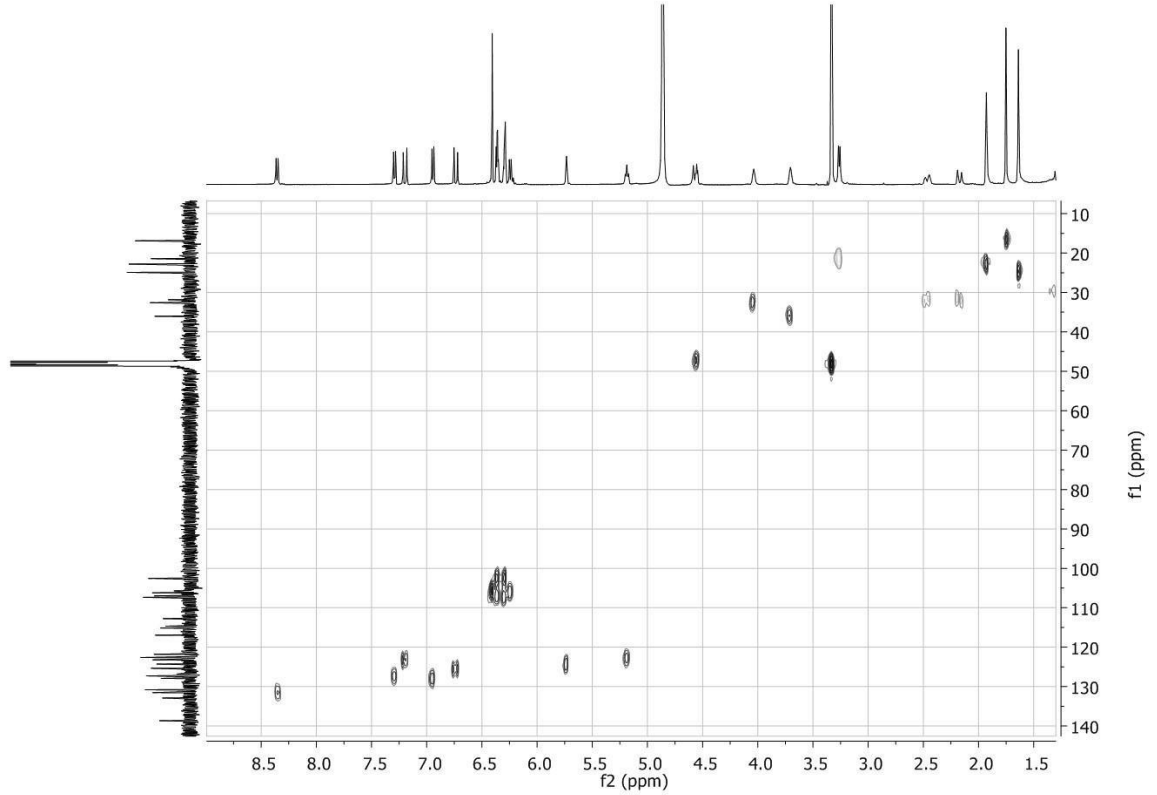


Appendix

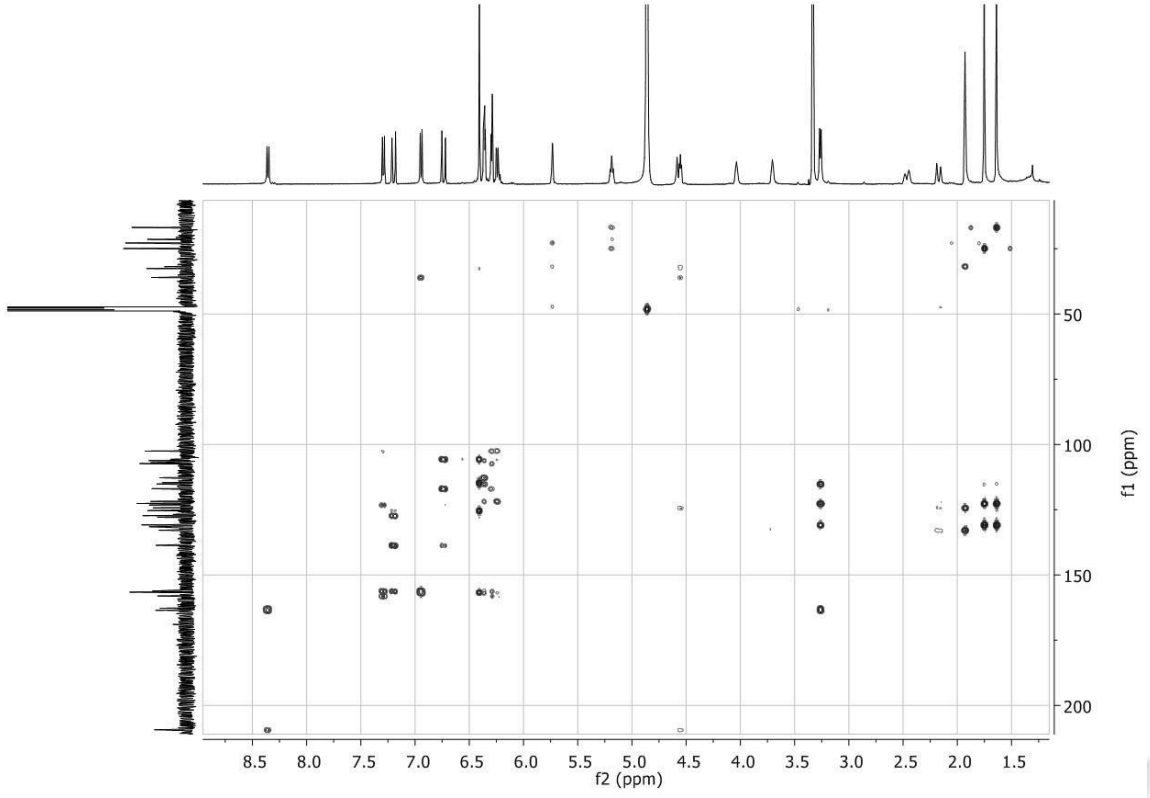
Appendix 53: ^{13}C NMR spectrum (CD_3OD, 125 MHz) of compound **8**



Appendix 54: $^{1}H–^{1}H$ COSY NMR spectrum (CD_3OD) of compound **8**



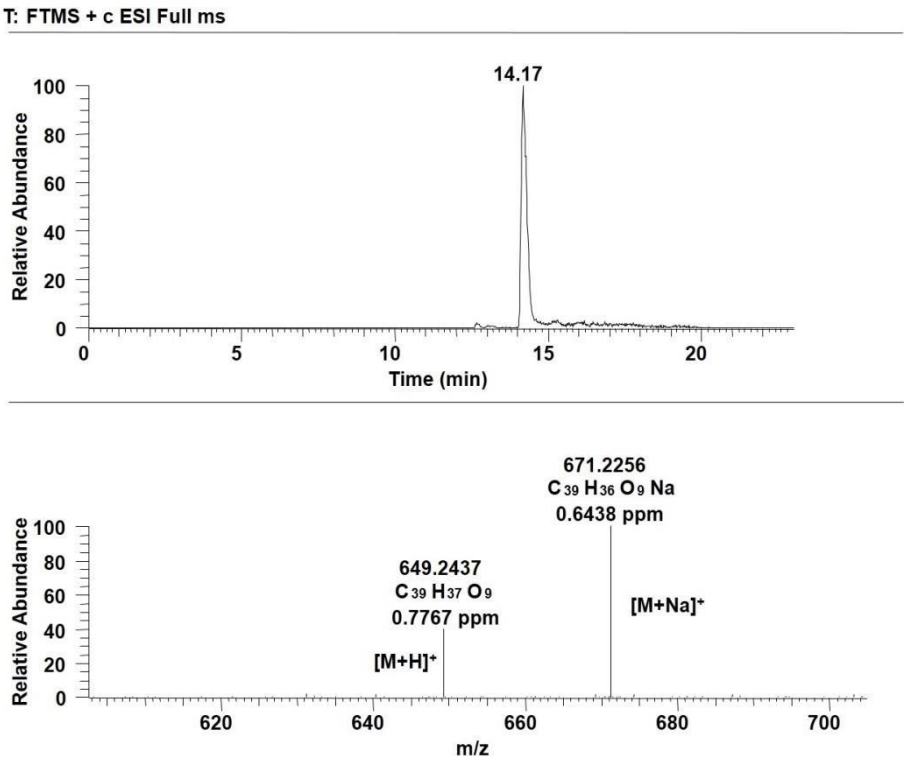
55: HSQC NMR spectrum (CD_3OD) of compound **8**



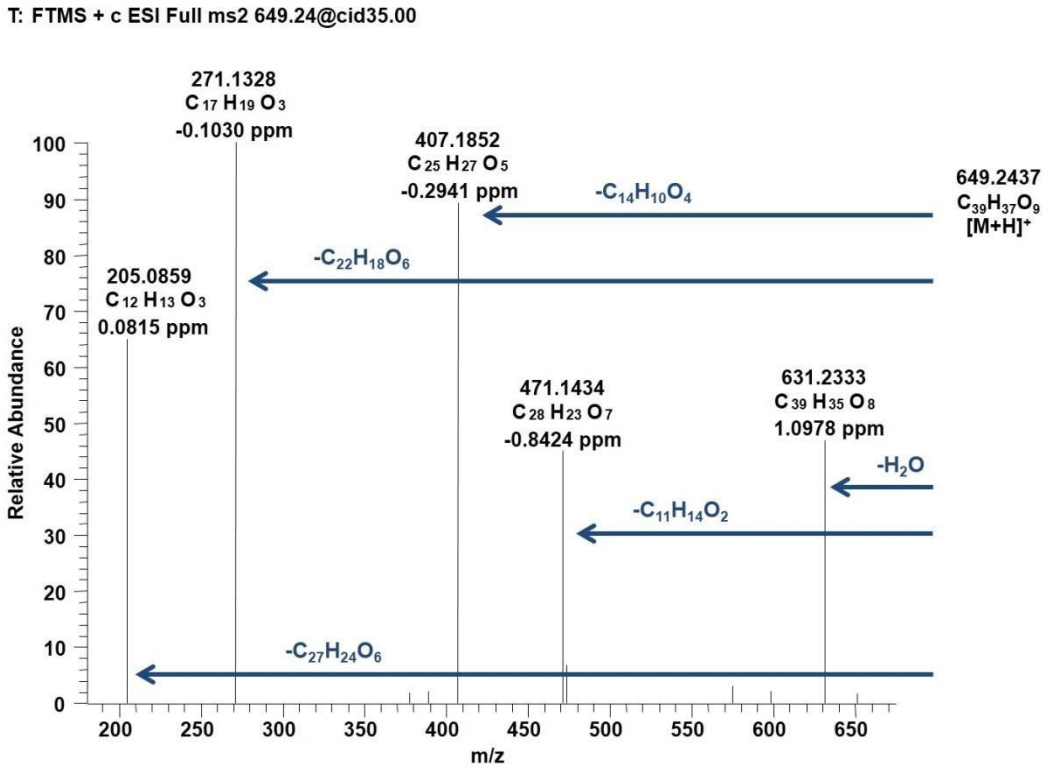
Appendix 56: HMBC NMR spectrum (CD_3OD) of compound **8**

NYANSAPƆ WƆSANE NO BADWENMA

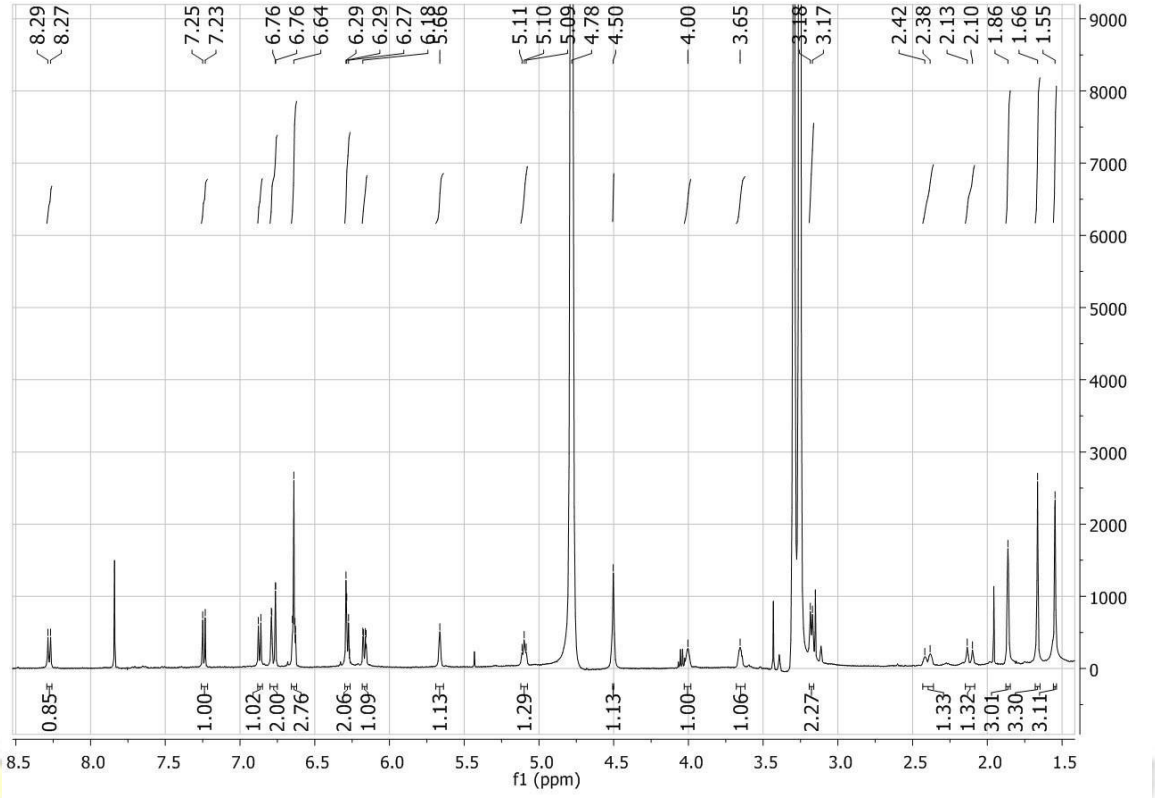
Appendix



Appendix 57: Positive HRESI–MS spectrum of compound **9**

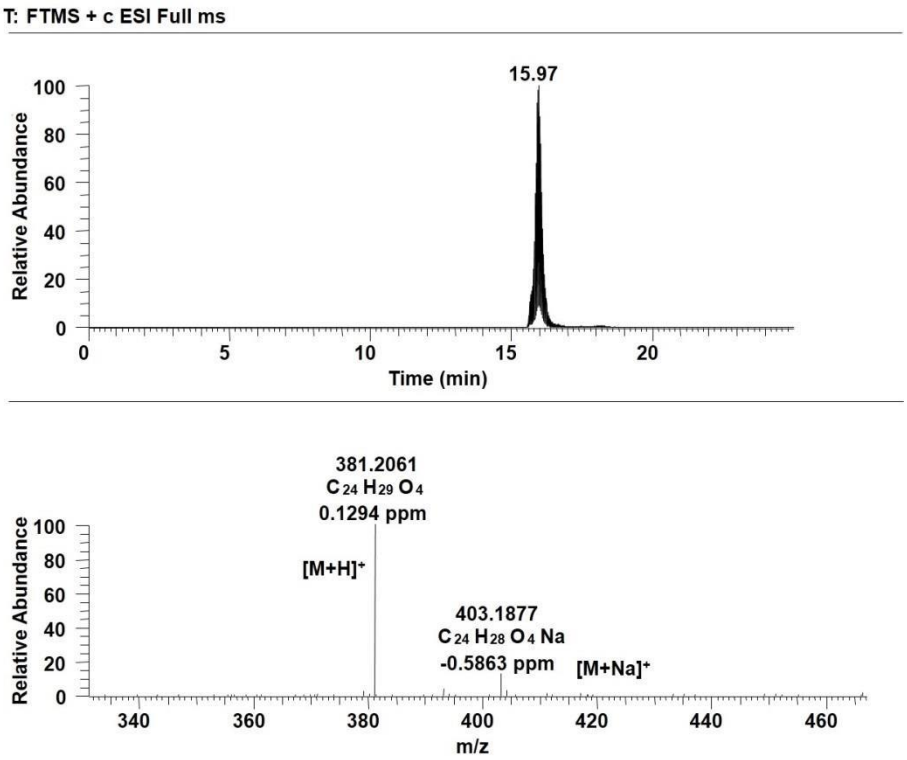


58: Positive HRESI–MS/MS spectrum of compound **9**

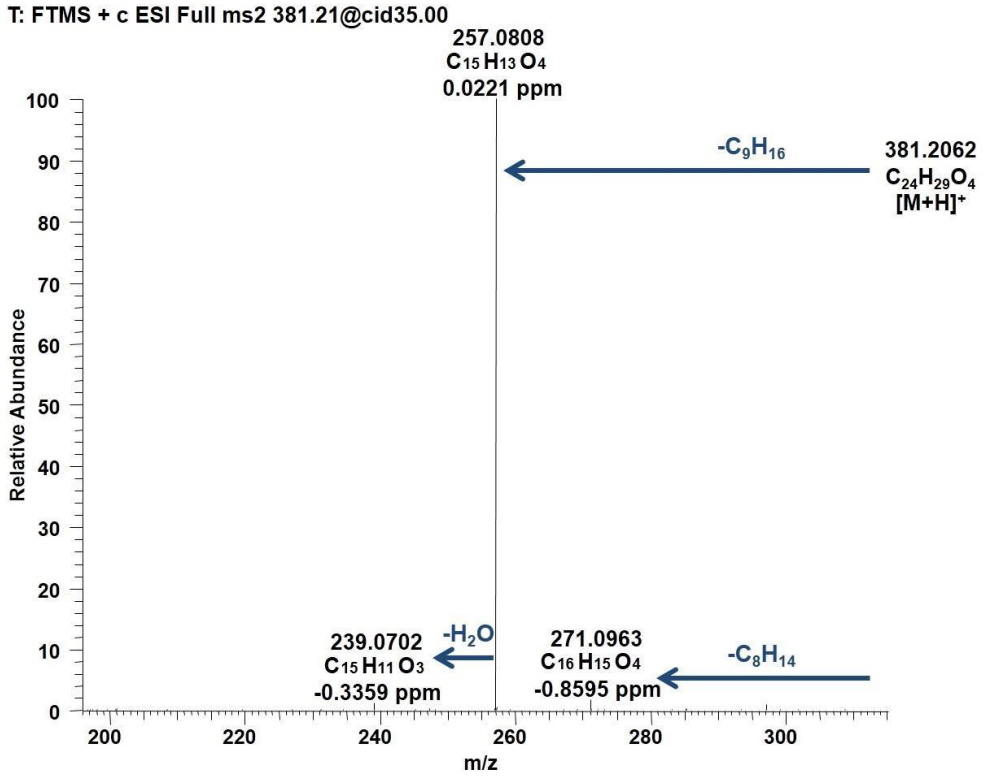


Appendix 59: ^{1}H NMR spectrum (CD_3OD, 500 MHz) of compound **9**

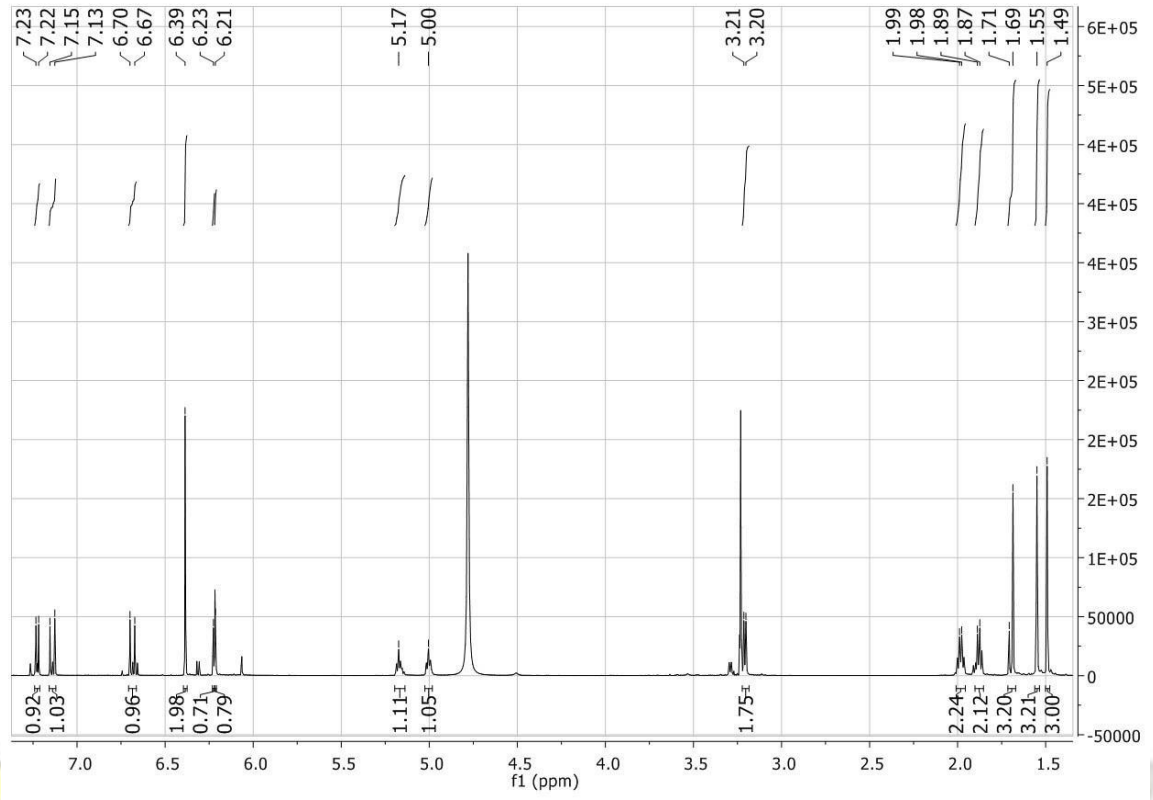
Appendix



Appendix 60: Positive HRESI–MS spectrum of compound **10**

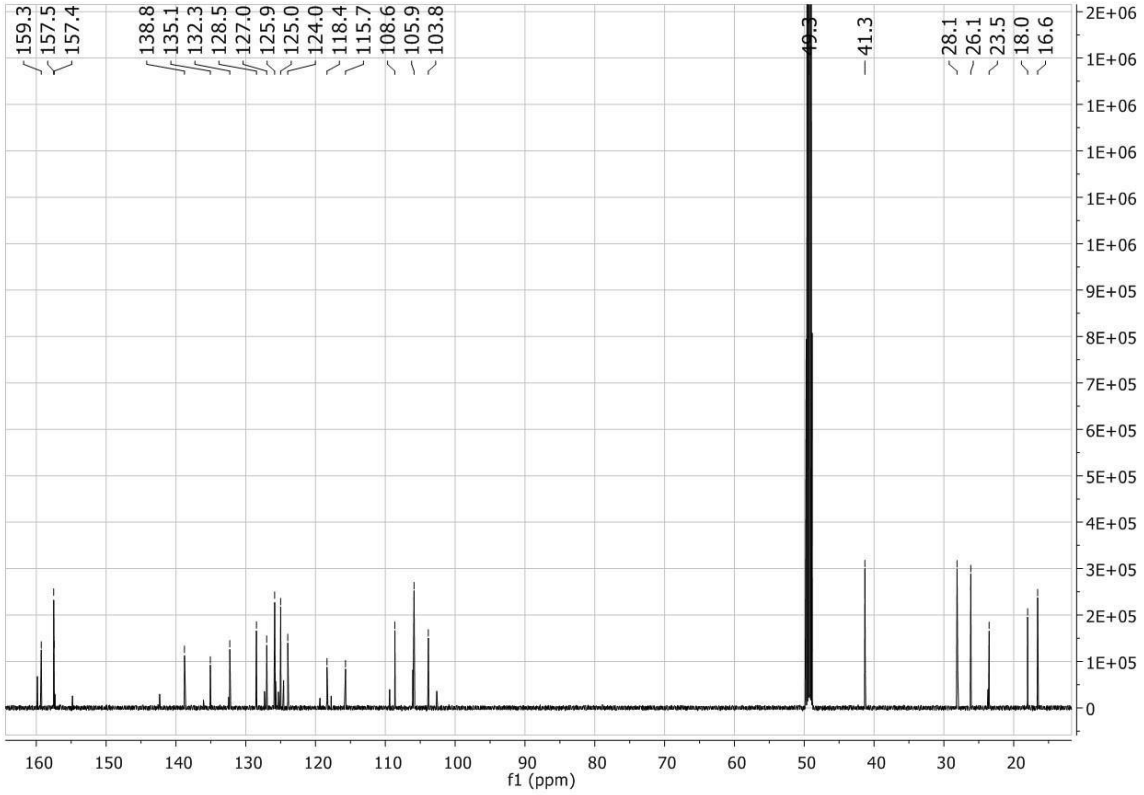


61: Positive HRESI–MS/MS spectrum of compound **10**



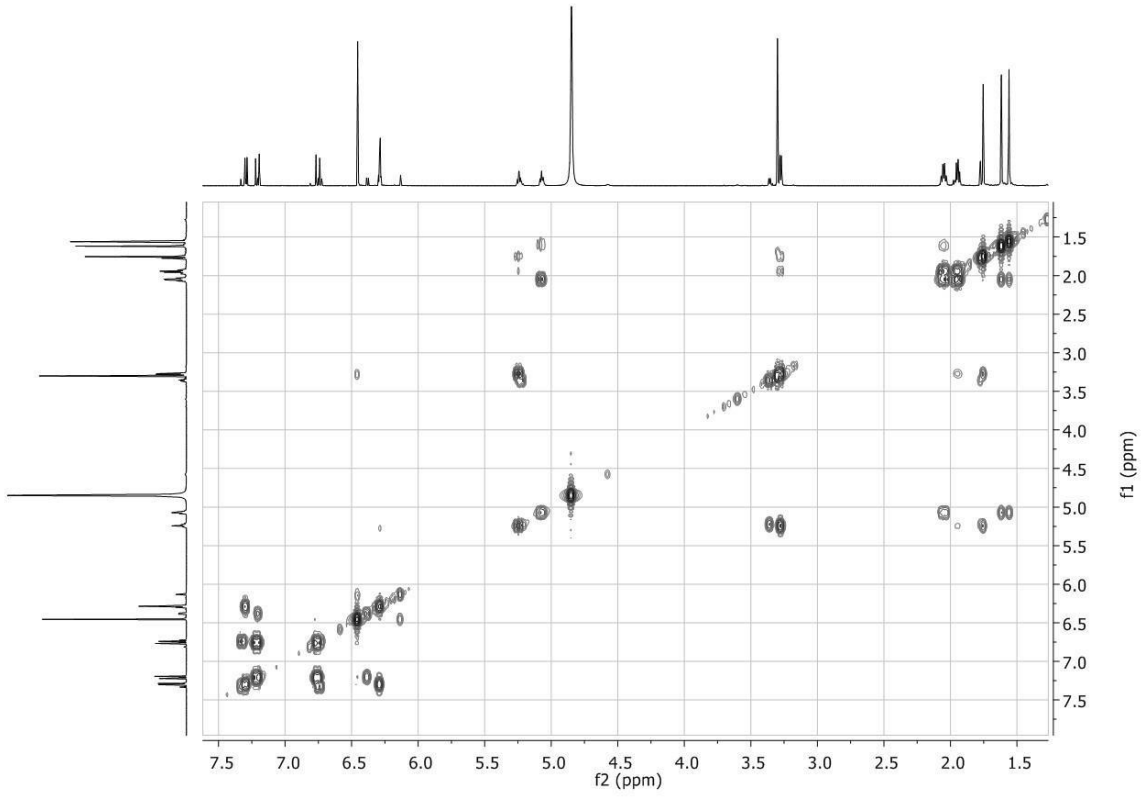
Appendix 62: ^{1}H NMR spectrum (CD_3OD, 600 MHz) of compound **10**

Appendix

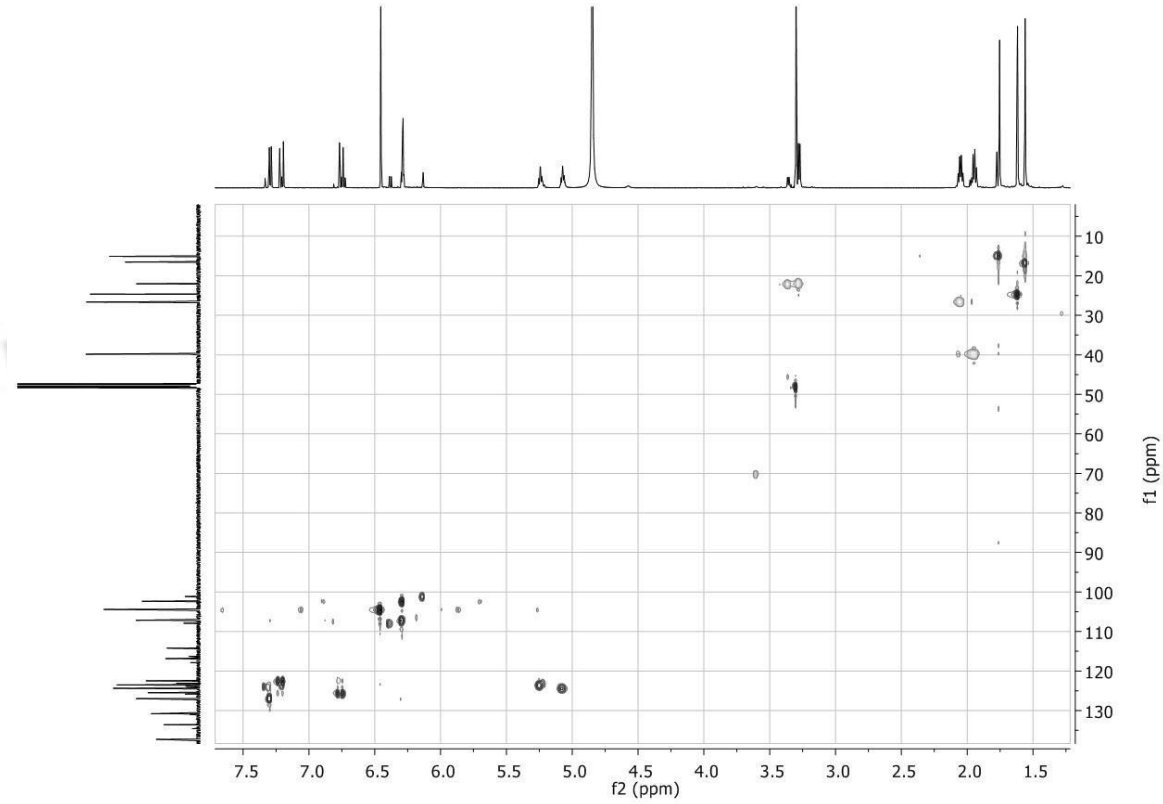


Appendix 63: ^{1}H NMR spectrum (CD_3OD, 150 MHz) of compound **10**

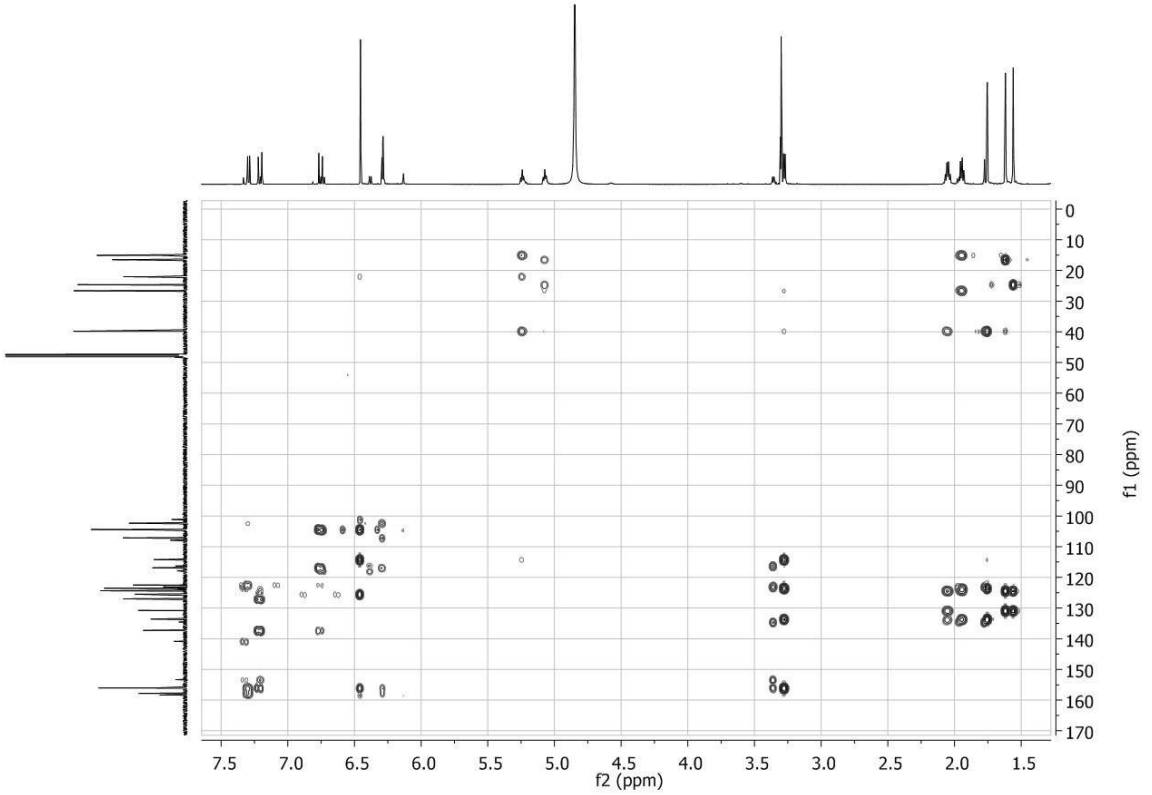
NYANSAPƆ WƆ SANE NO BADWENMA



Appendix 64: $^{1}H–^{1}H$ COSY NMR spectrum (CD_3OD) of compound **10**

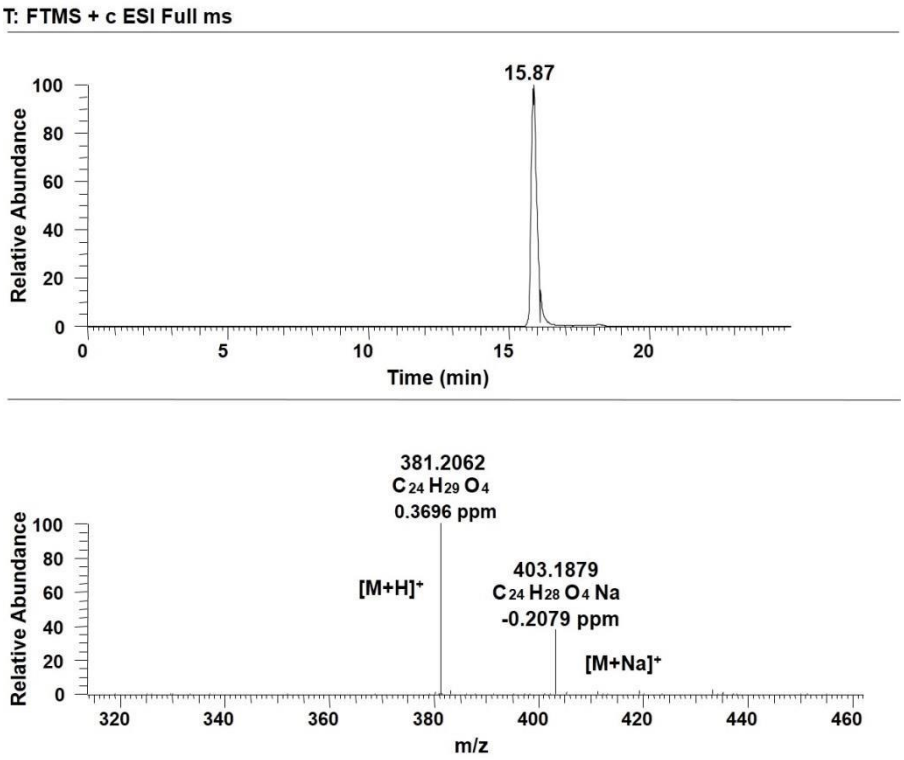


Appendix 65: HSQC NMR spectrum (CD_3OD) of compound **10**

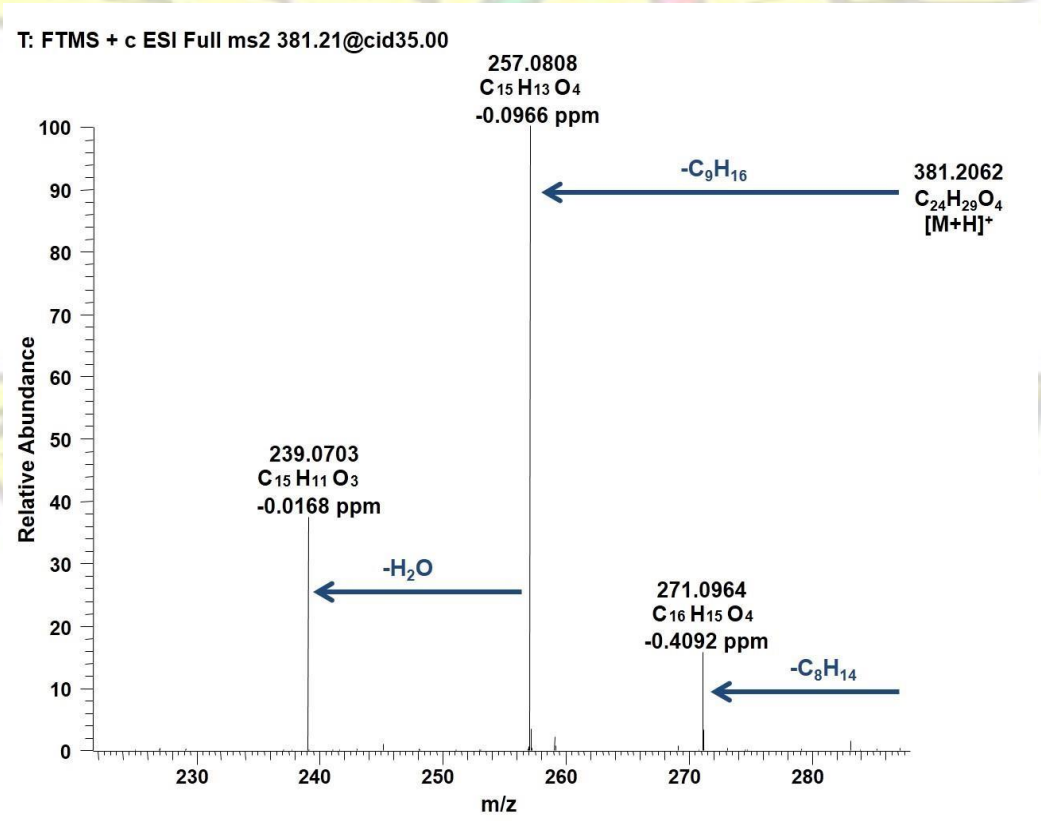


Appendix 66: HMBC NMR spectrum (CD_3OD) of compound **10**

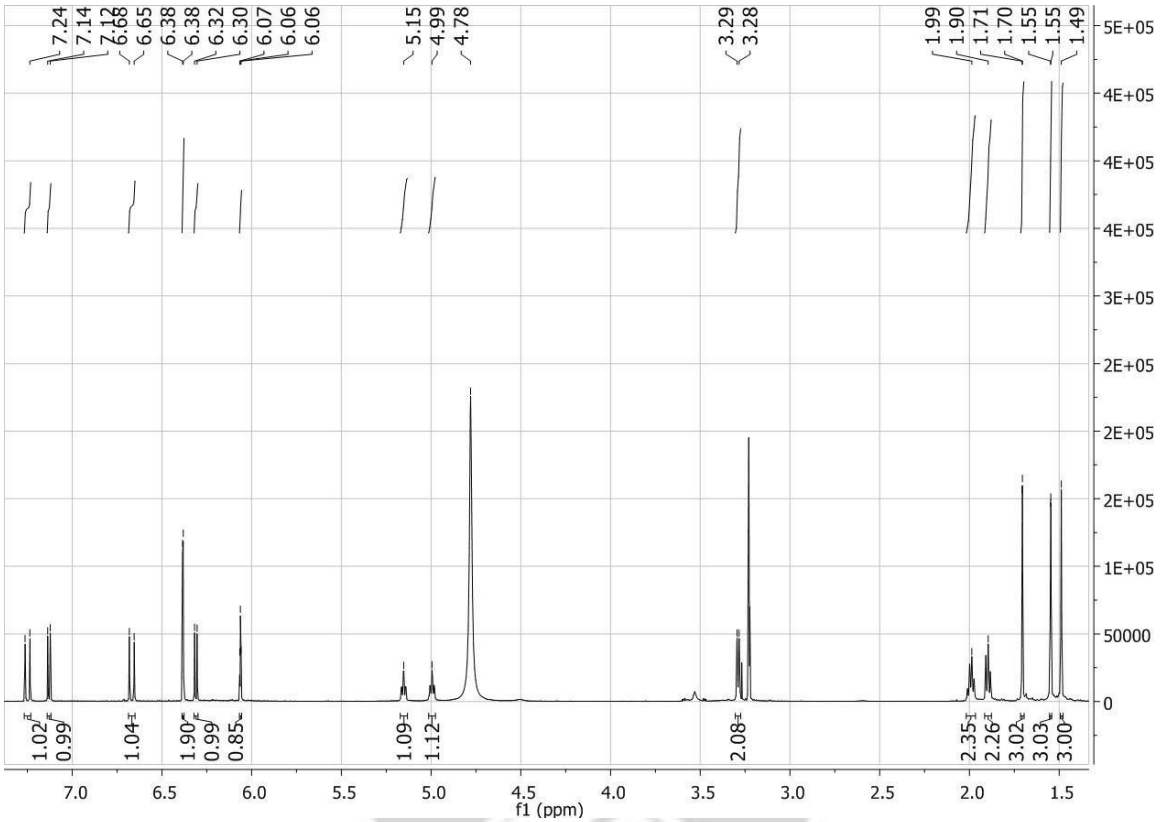
NYANSAPƆ WƆSANE NO BADWENMA



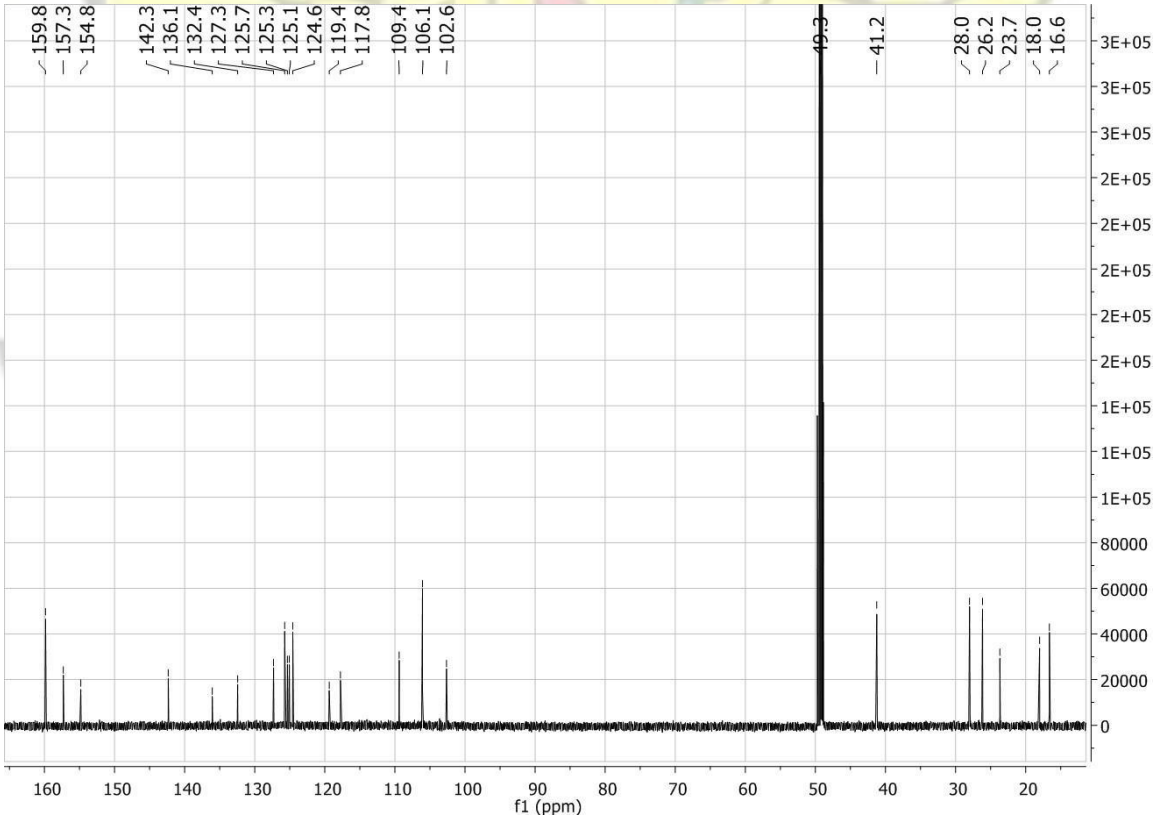
Appendix 67: Positive HRESI–MS spectrum of compound **11**



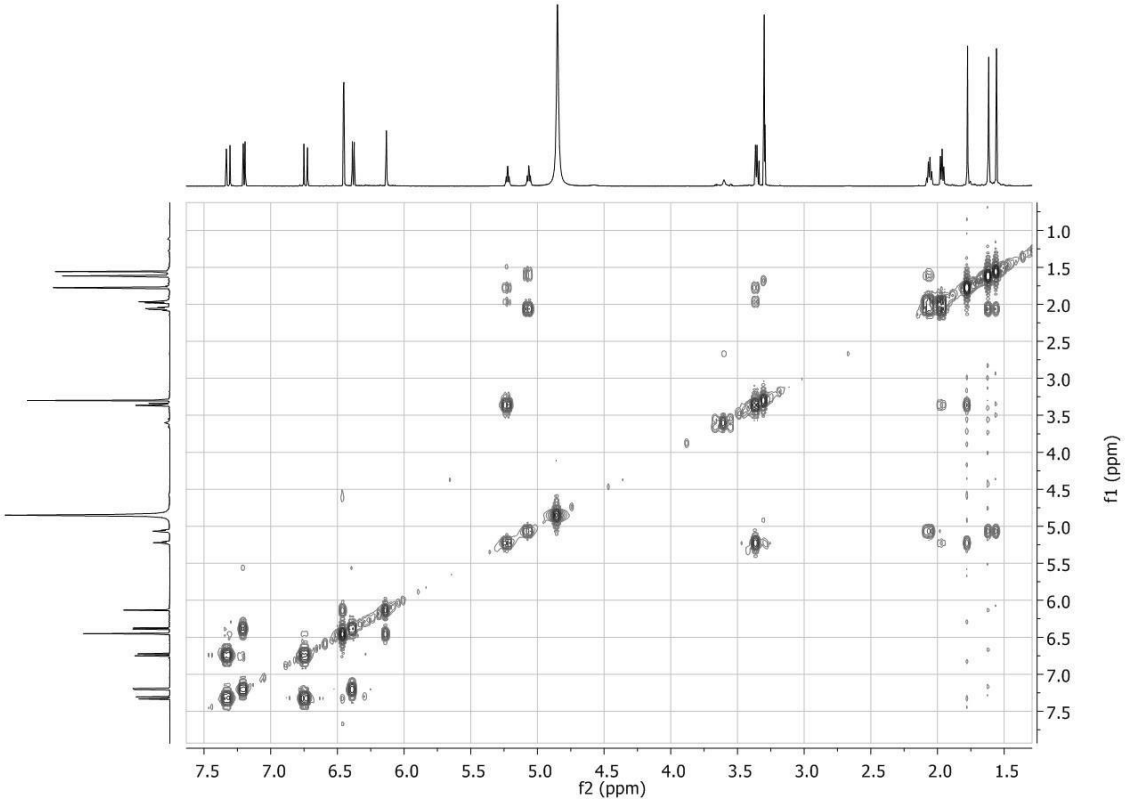
Appendix 68: Positive HRESI–MS/MS spectrum of compound **11**



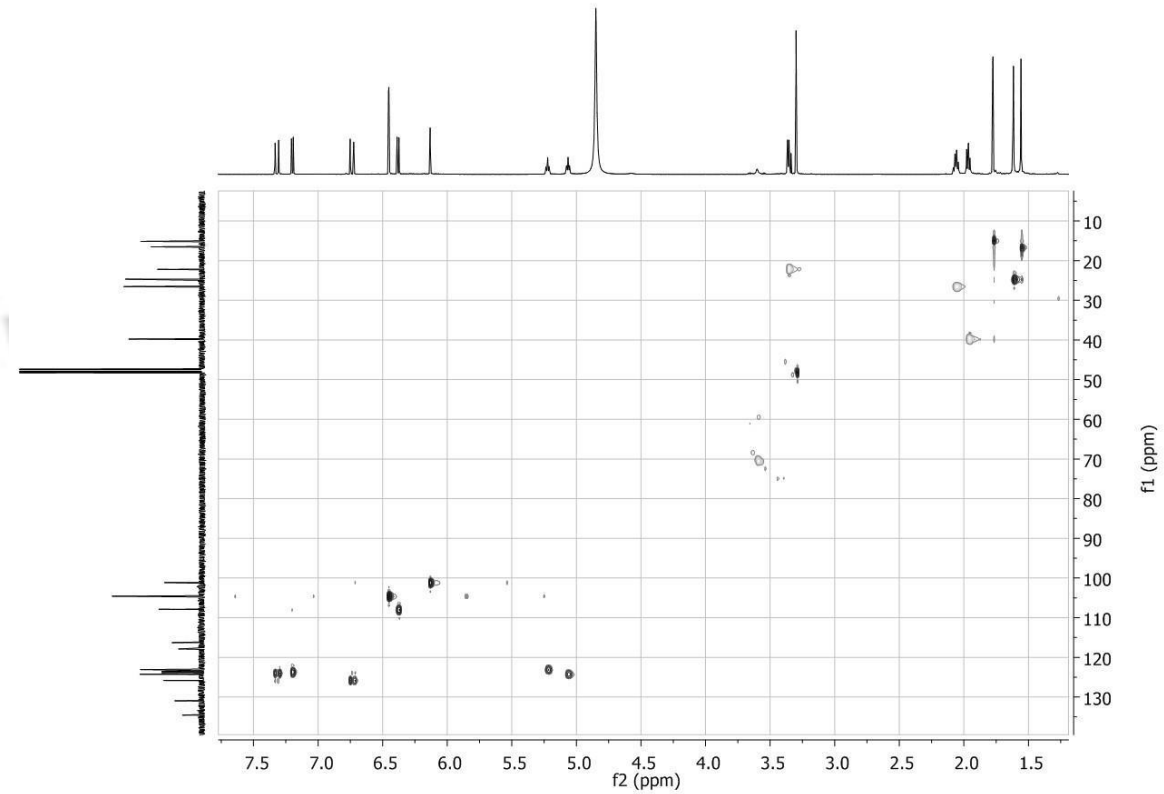
Appendix 69: ^{1}H NMR spectrum (CD_3OD, 600 MHz) of compound **11**



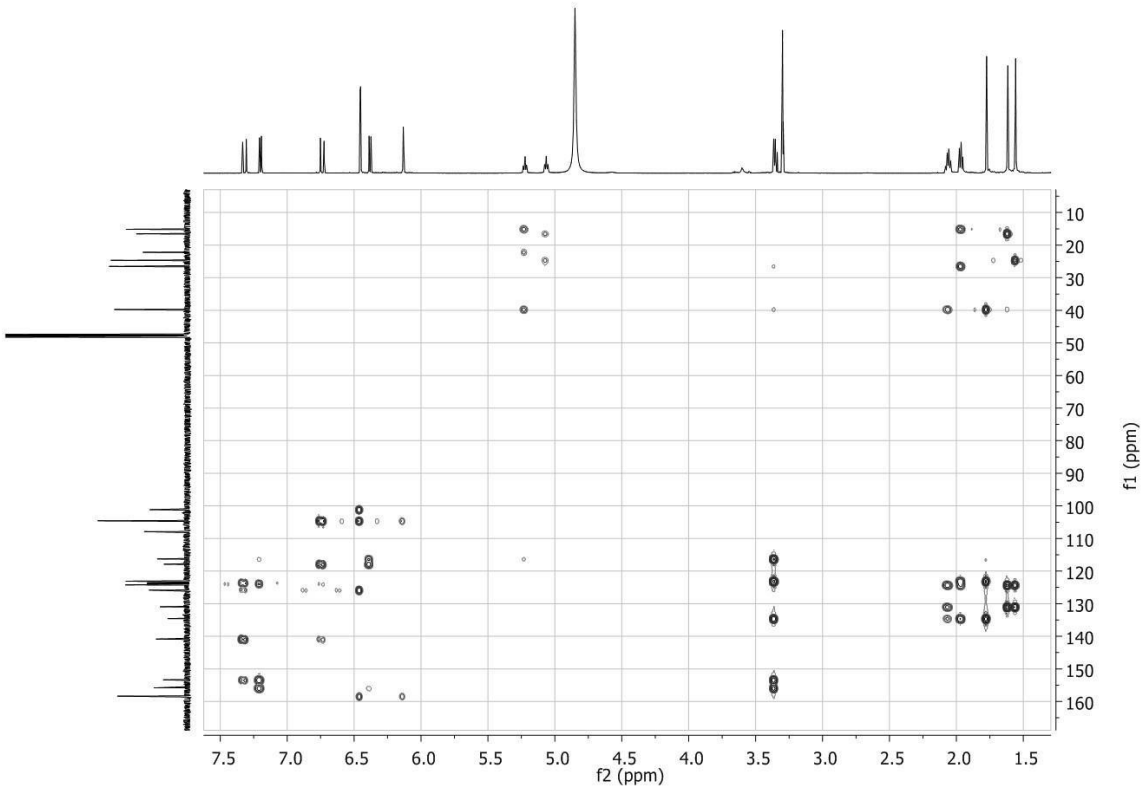
Appendix 70: ^{1}H NMR spectrum (CD_3OD, 150 MHz) of compound **11**



Appendix 71: $^{1}H–^{1}H$ COSY NMR spectrum (CD_3OD) of compound **11**

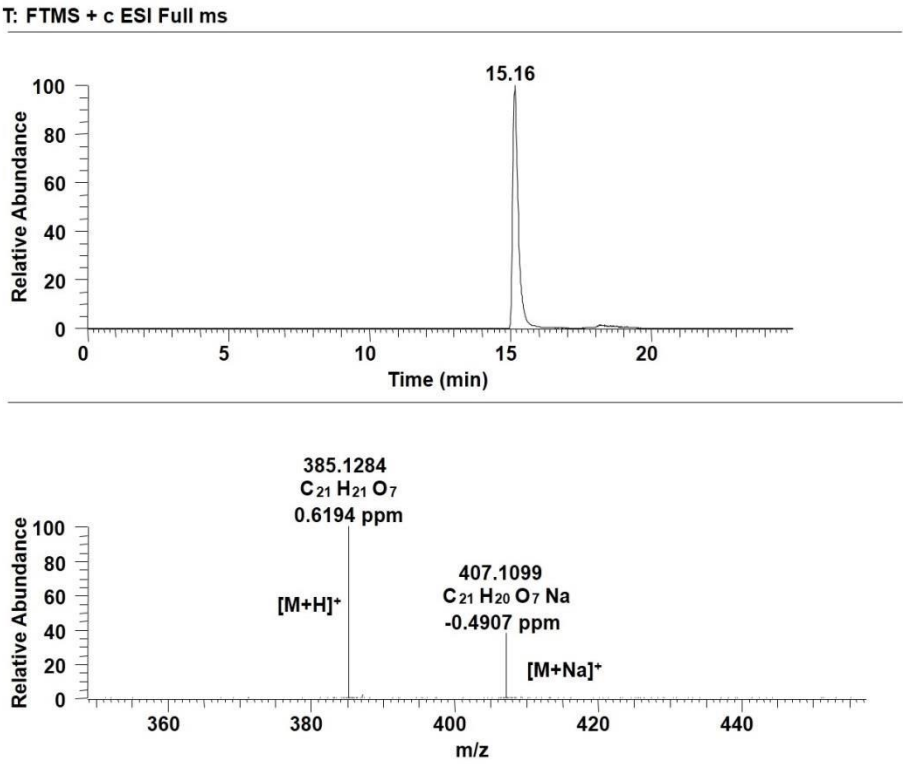


Appendix 72: HSQC NMR spectrum (CD_3OD) of compound **11**

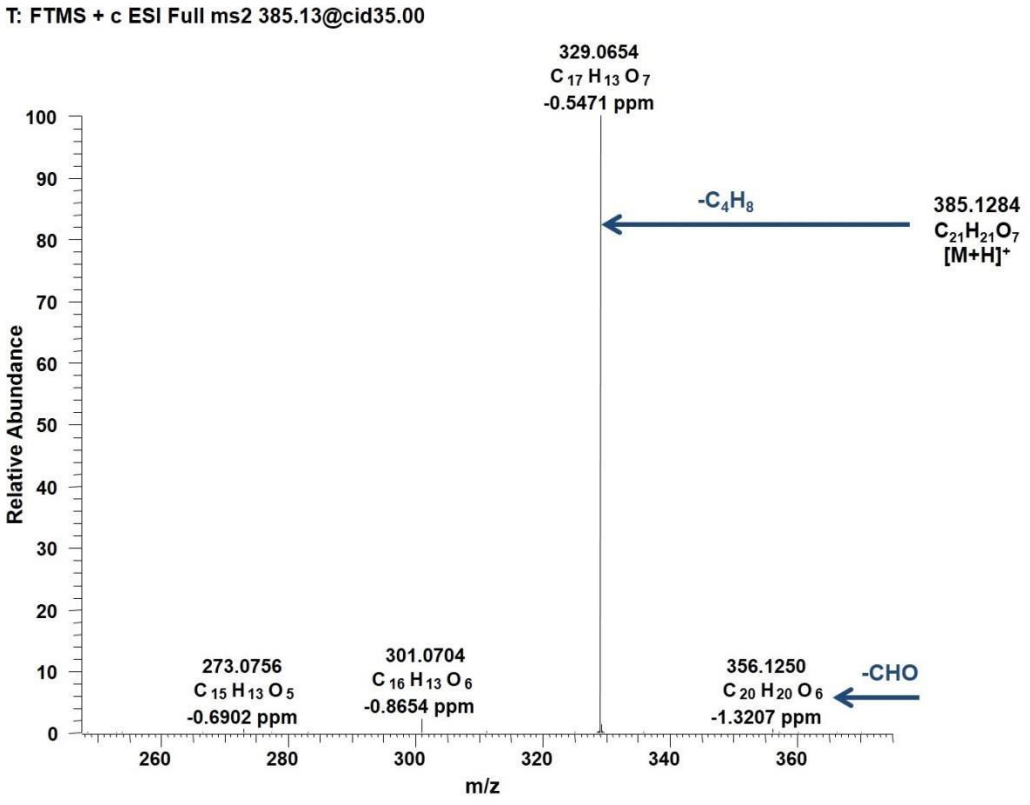


Appendix 73: HMBC NMR spectrum (CD_3OD) of compound **11**

NYANSAPƆ WƆSANE NO BADWENMA

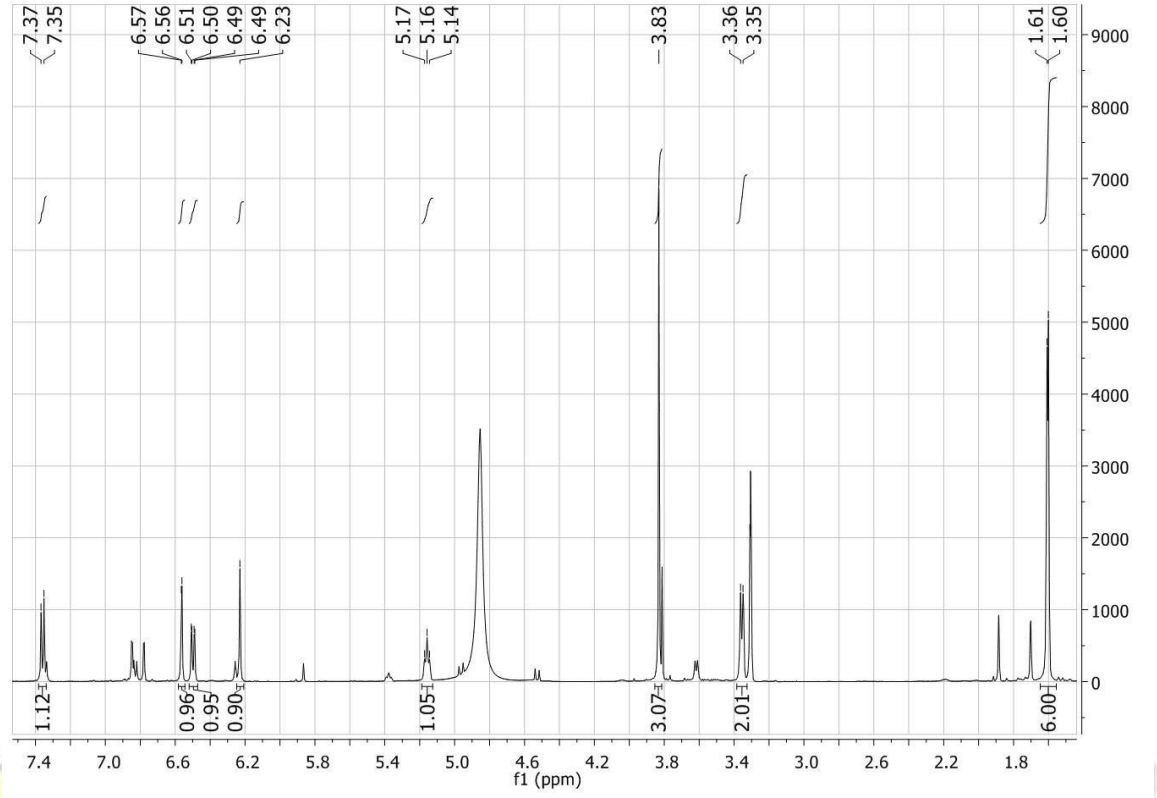


Appendix 74: Positive HRESI–MS spectrum of compound **12**



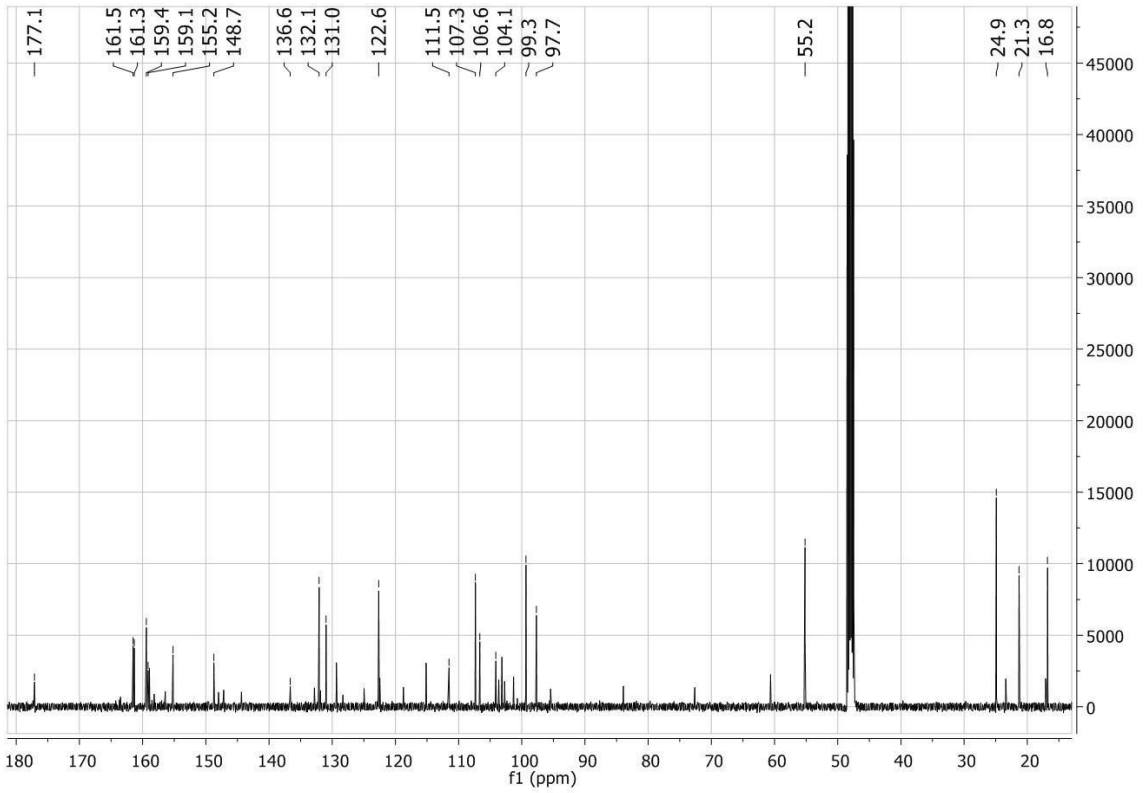
Appendix

75: Positive HRESI–MS/MS spectrum of compound **12**

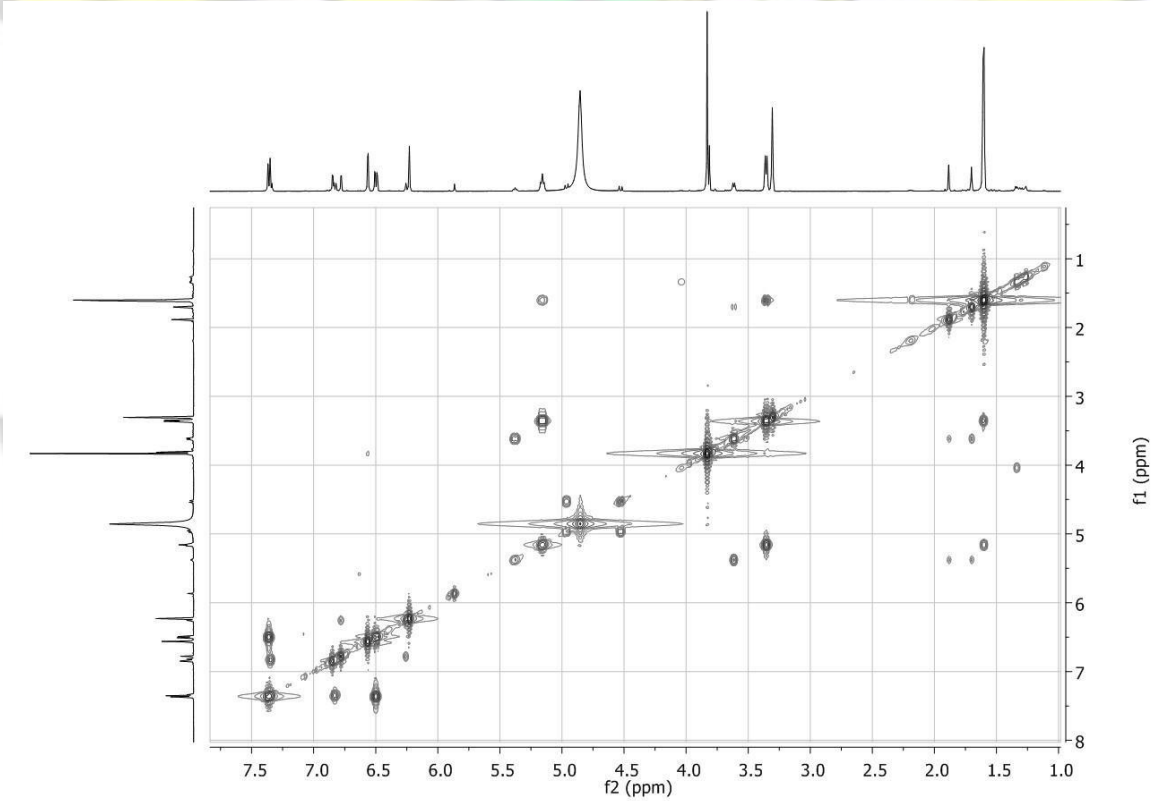


Appendix 76: ^{1}H NMR spectrum (CD_3OD, 500 MHz) of compound **12**.

Appendix

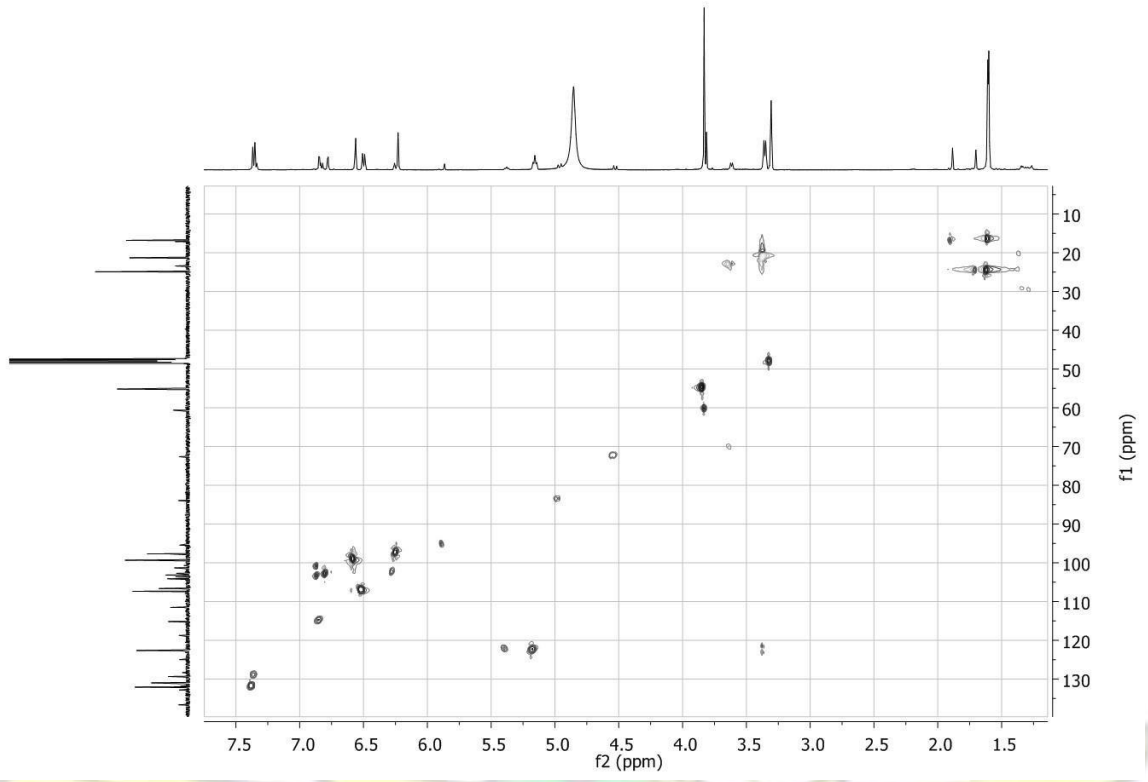


77: ^{13}C NMR spectrum (CD_3OD, 125 MHz) of compound **12**.



Appendix 78: $^{1}H–^{1}H$ COSY NMR spectrum (CD_3OD) of compound **12**.

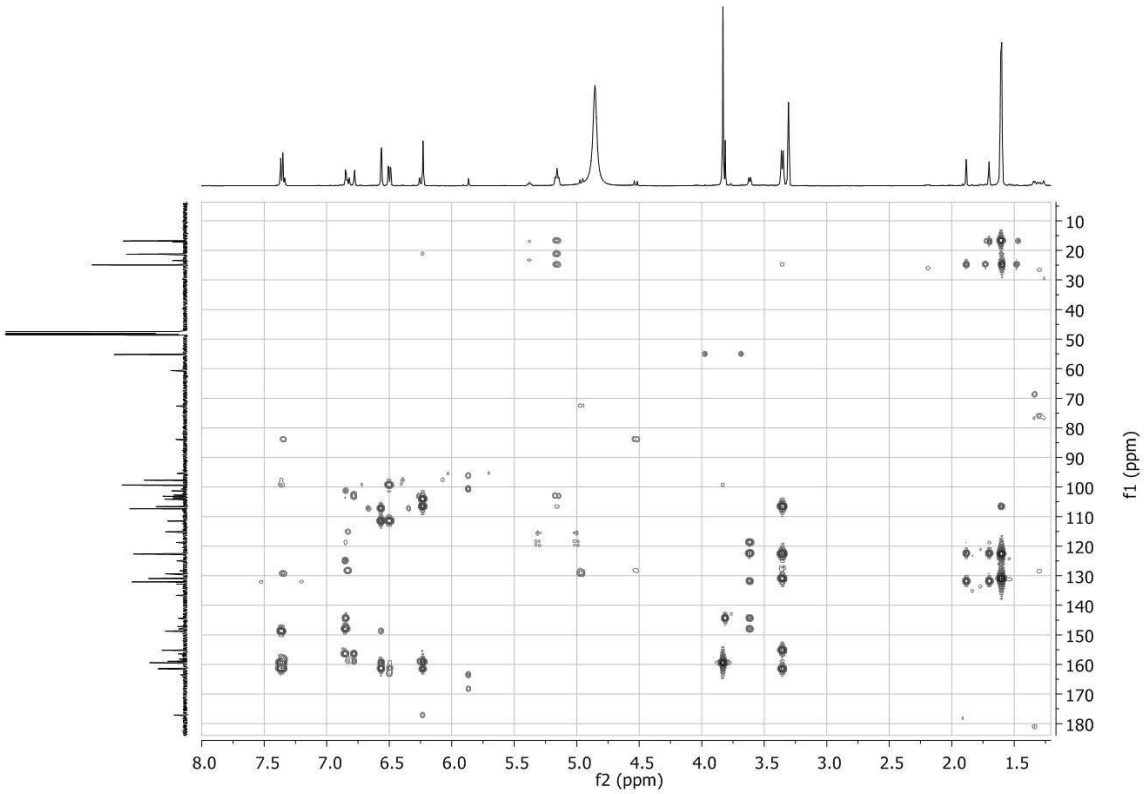
Appendix



79: HSQC NMR spectrum (CD_3OD) of compound **12.**

NYANSAPƆ WƆ SANE NO BADWENMA

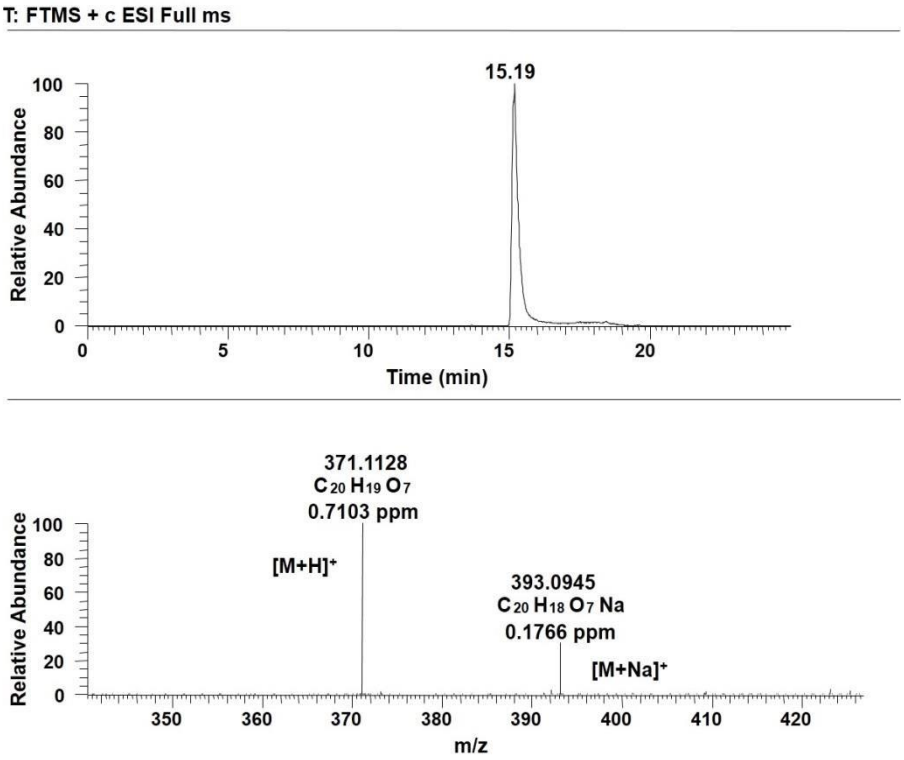
Appendix



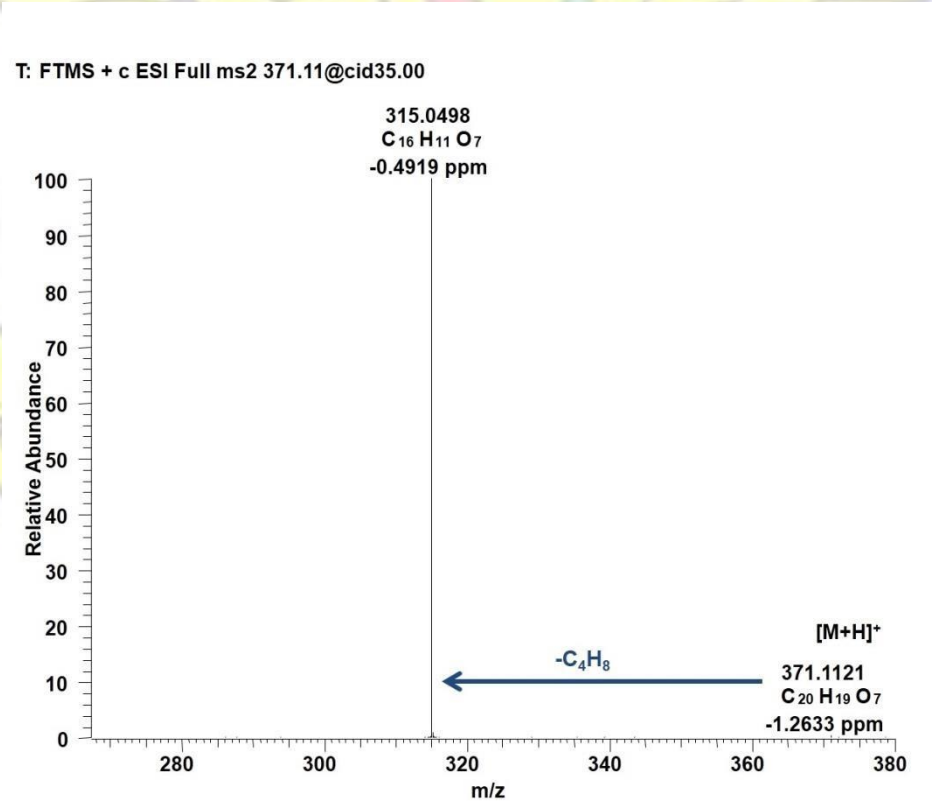
Appendix 80: HMBC NMR spectrum (CD_3OD) of compound **12**.

NYANSAPƆ WƆSANE NO BADWENMA

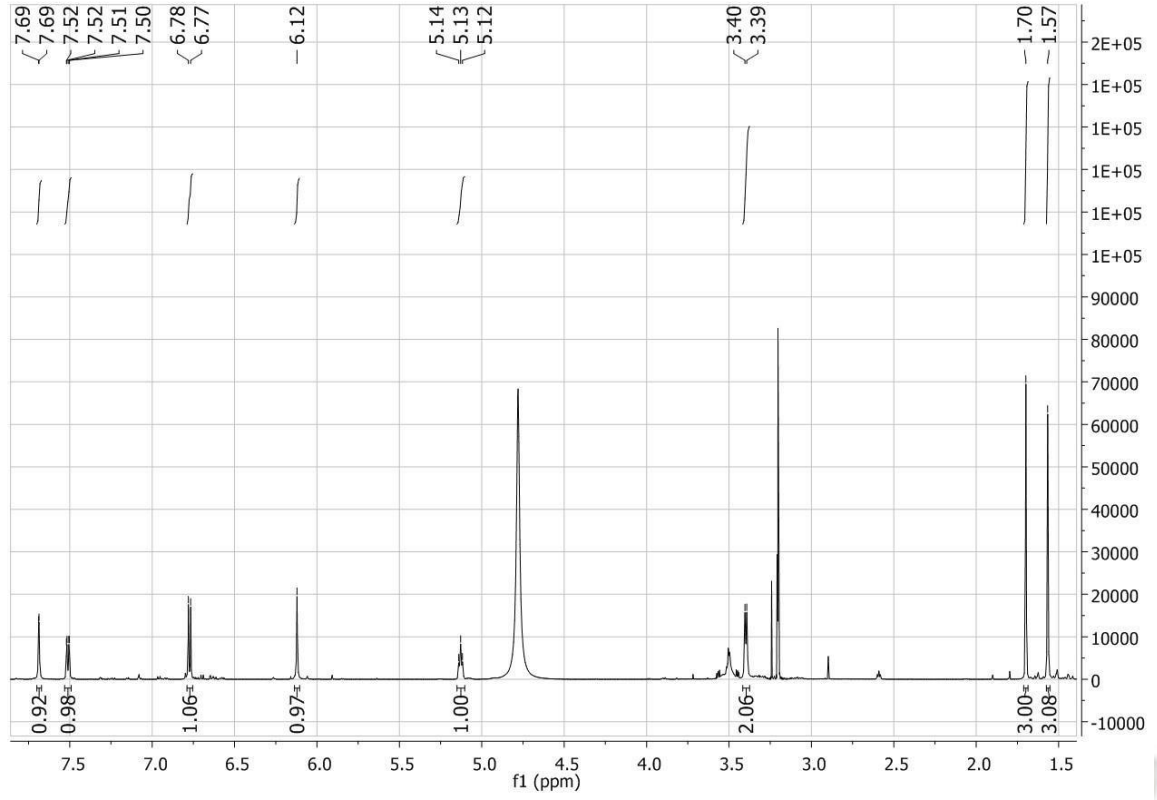
Appendix



Appendix 81: Positive HRESI–MS spectrum of compound **13**

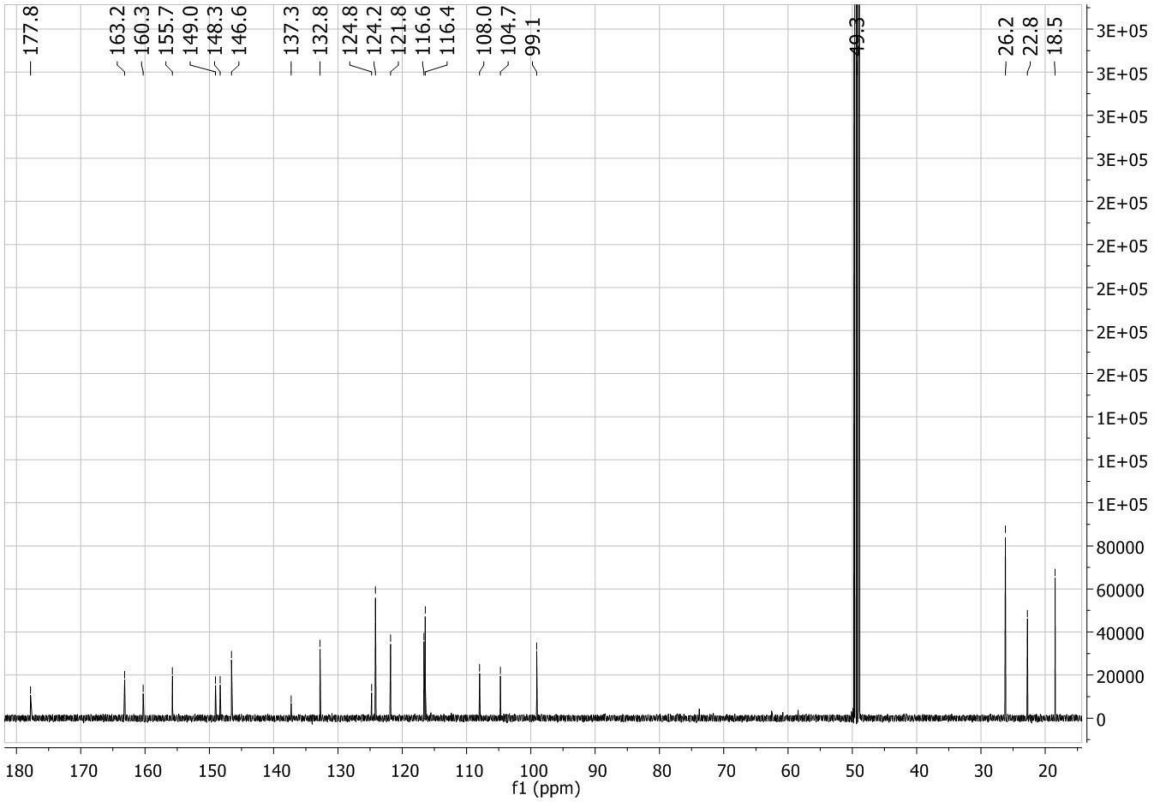


82: Positive HRESI–MS/MS spectrum of compound **13**

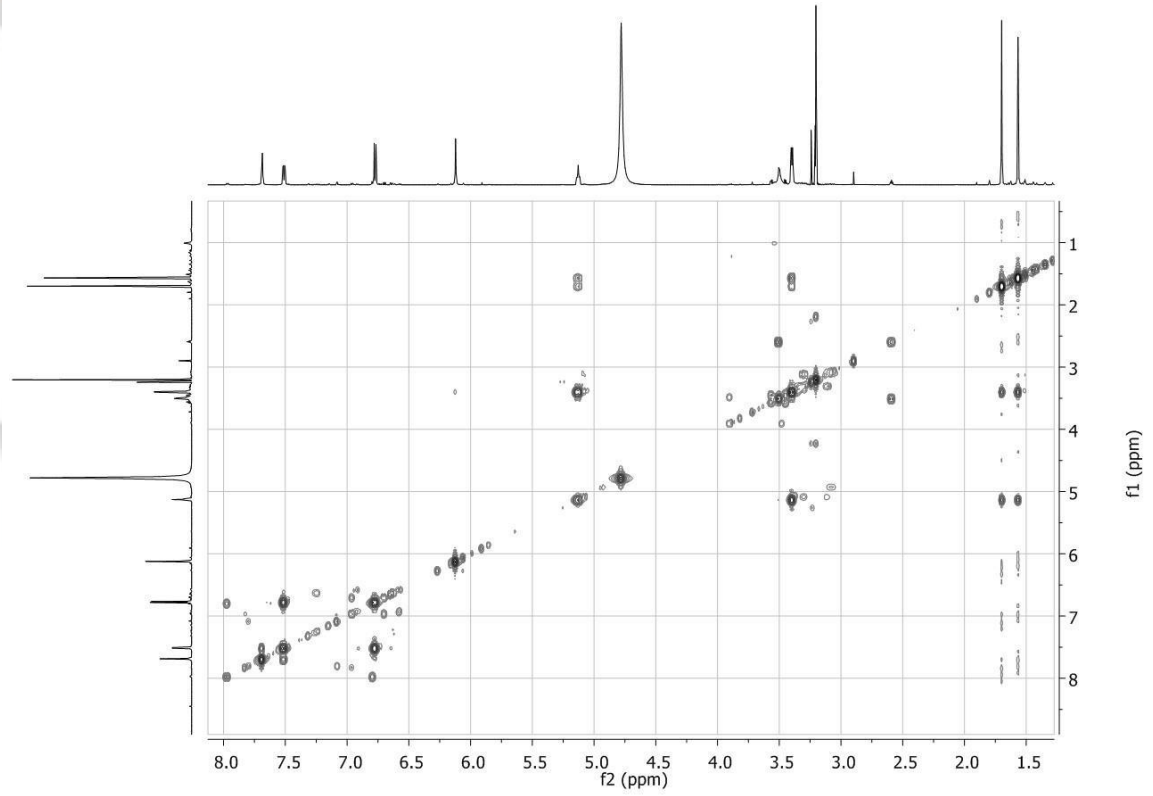


Appendix 83: ^{1}H NMR spectrum (CD_3OD, 600 MHz) of compound **13**

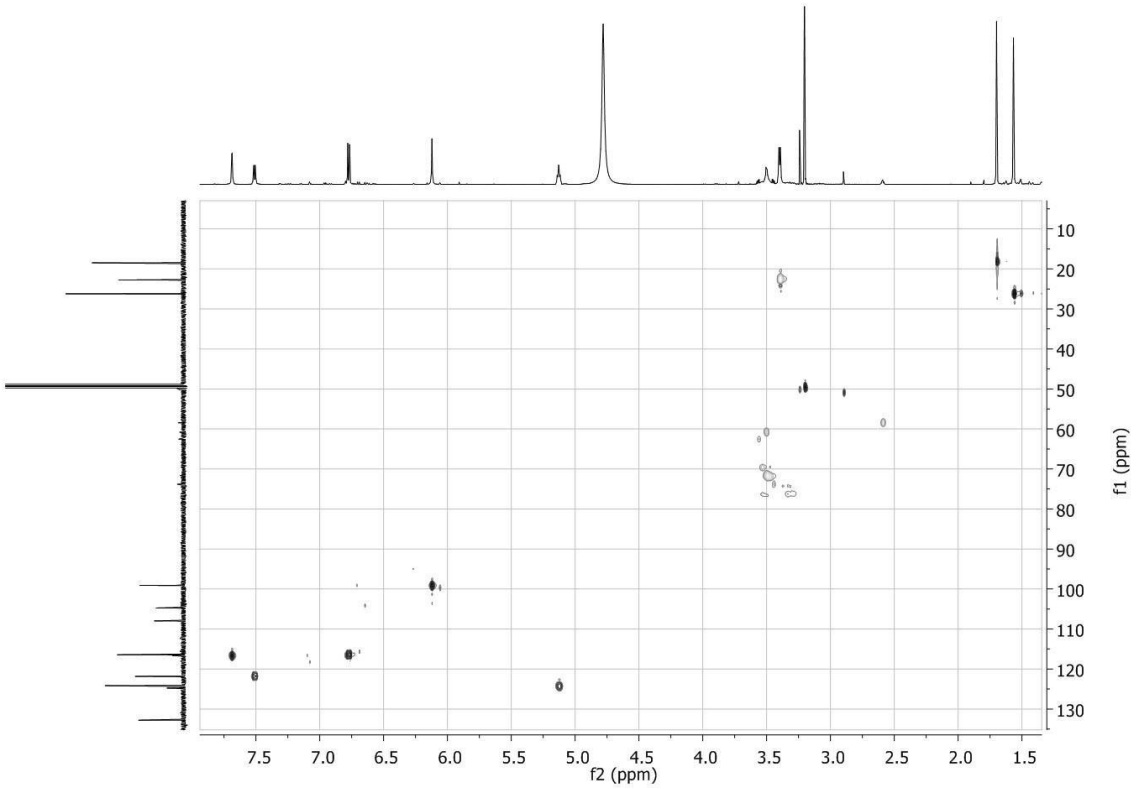
Appendix



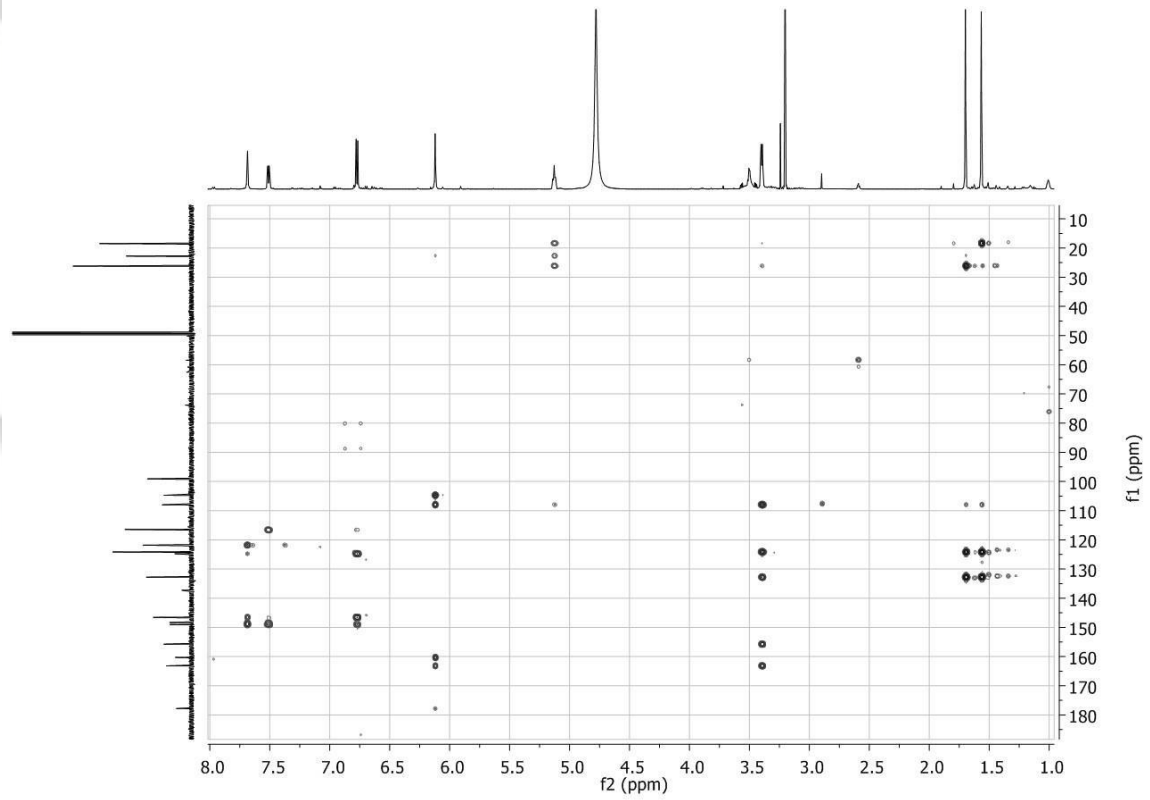
Appendix 84: ^{13}C NMR spectrum (CD_3OD, 150 MHz) of compound **13**



Appendix 85: $^{1}H–^{1}H$ COSY NMR spectrum (CD_3OD) of compound **13**



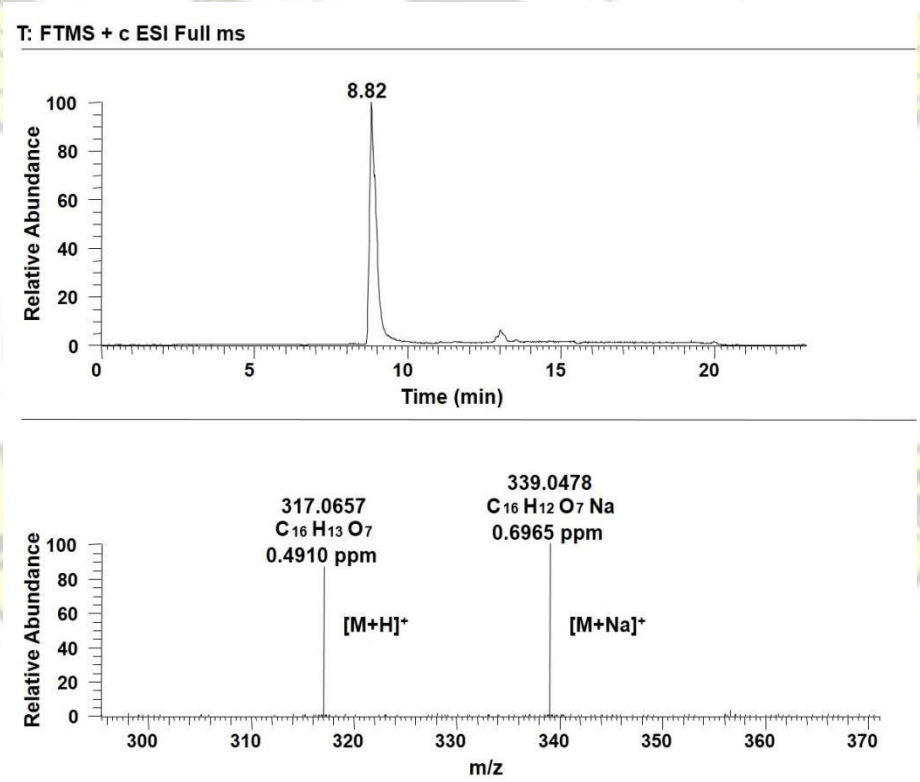
86: HSQC NMR spectrum (CD_3OD) of compound **13**



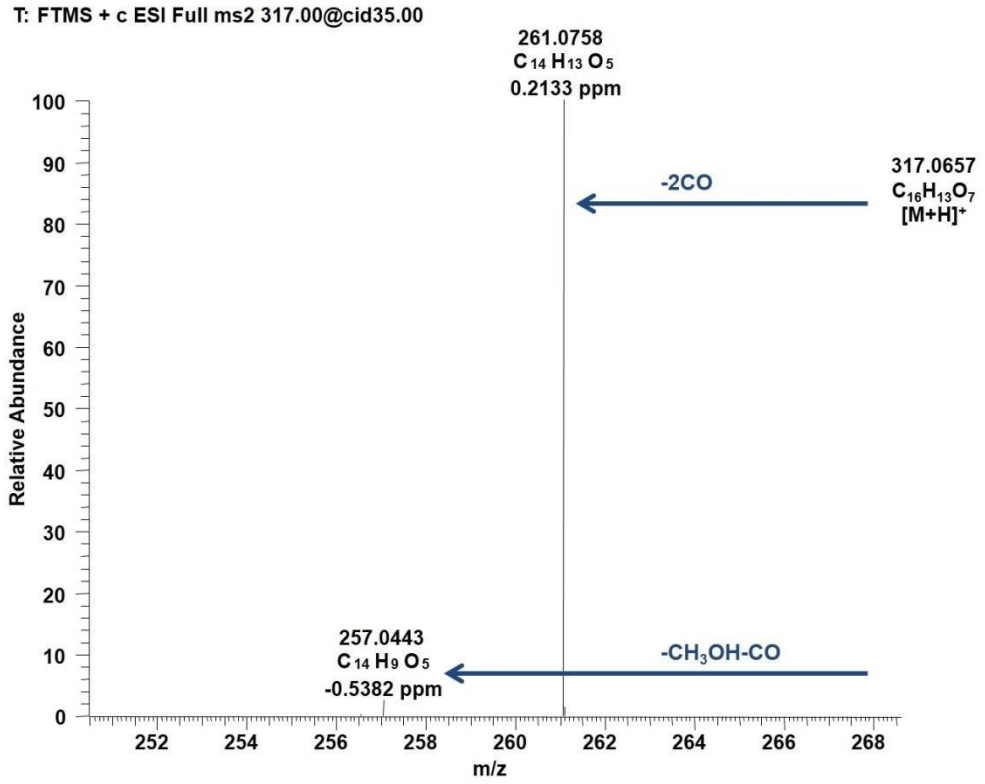
Appendix 87: HMBC NMR spectrum (CD_3OD) of compound **13**

Appendix

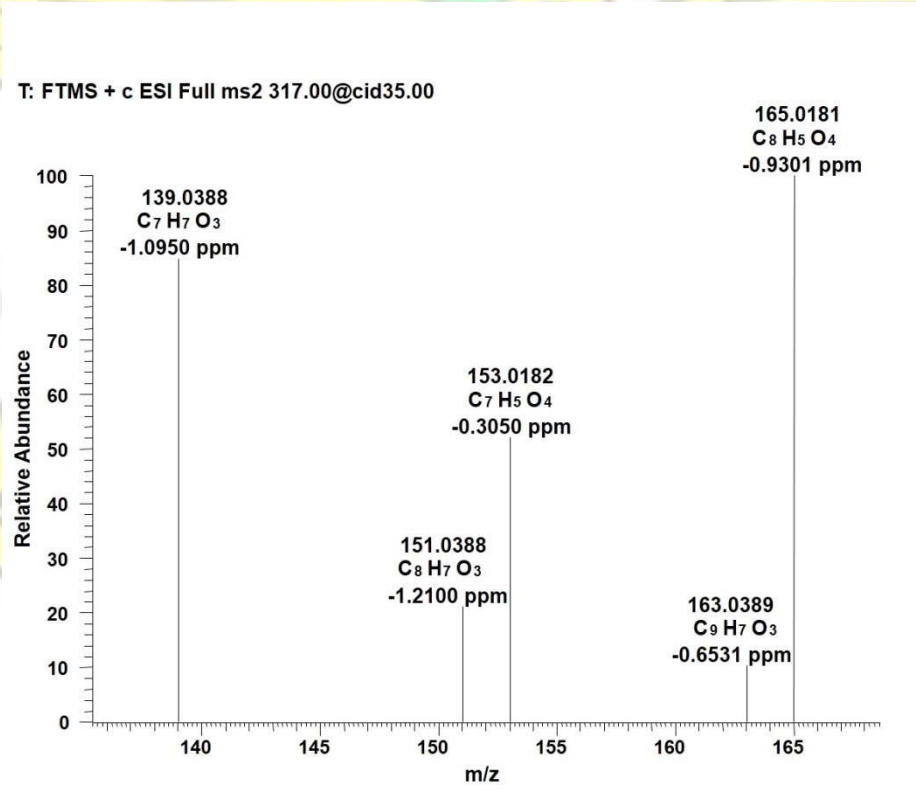
KNUST



Appendix 88: Positive HRESI–MS spectrum of compound **14**

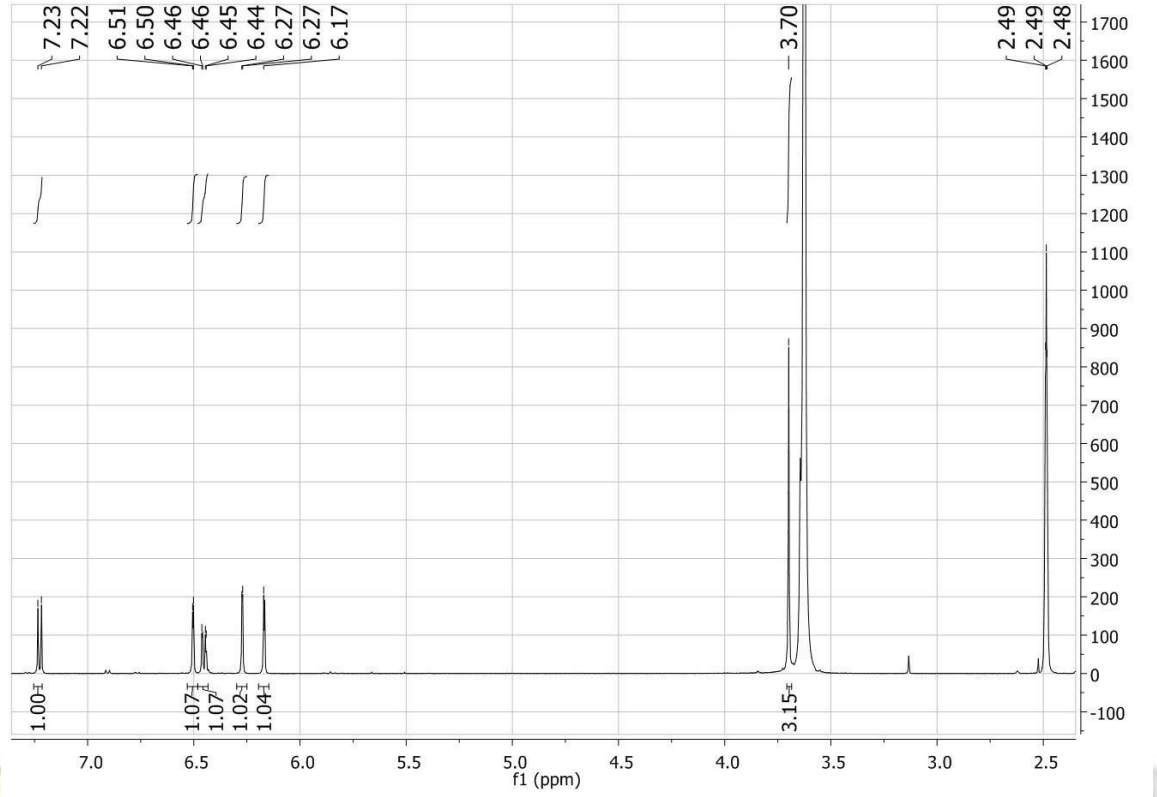


89: Positive HRESI–MS/MS spectrum of compound **14**



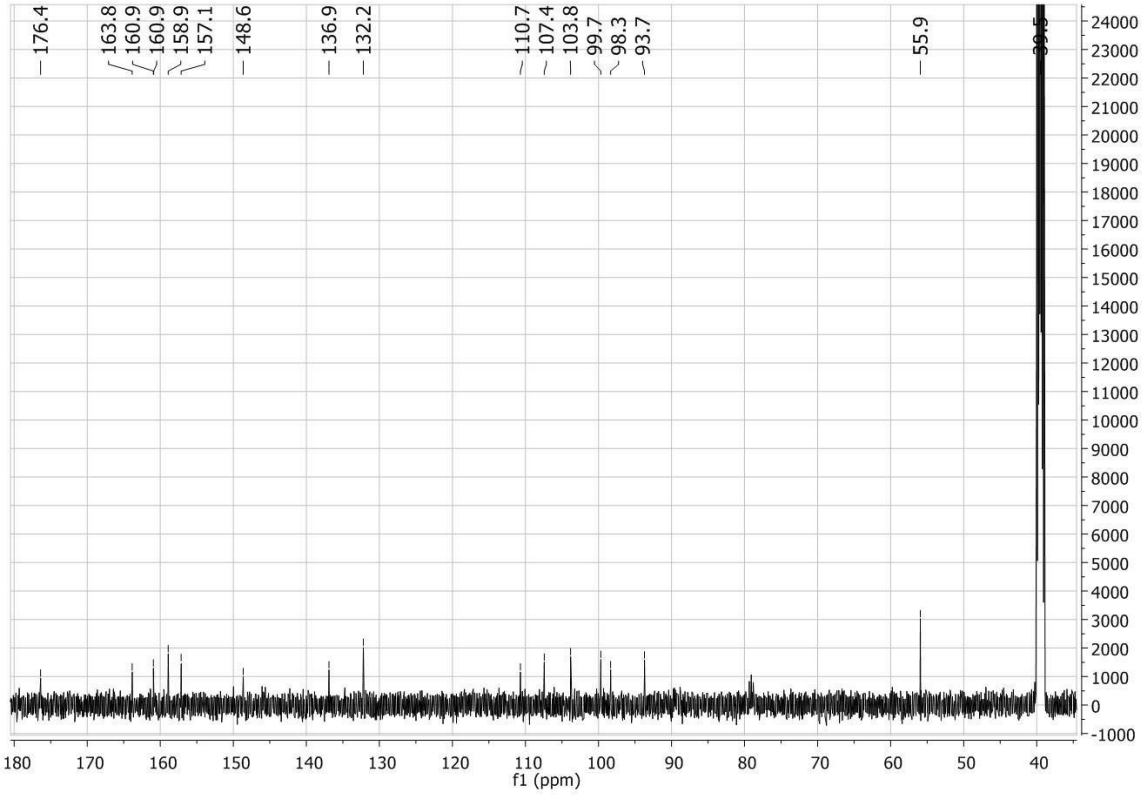
Appendix 90: Positive HRESI–MS/MS (RDA fragments) spectrum of compound **14**

Appendix

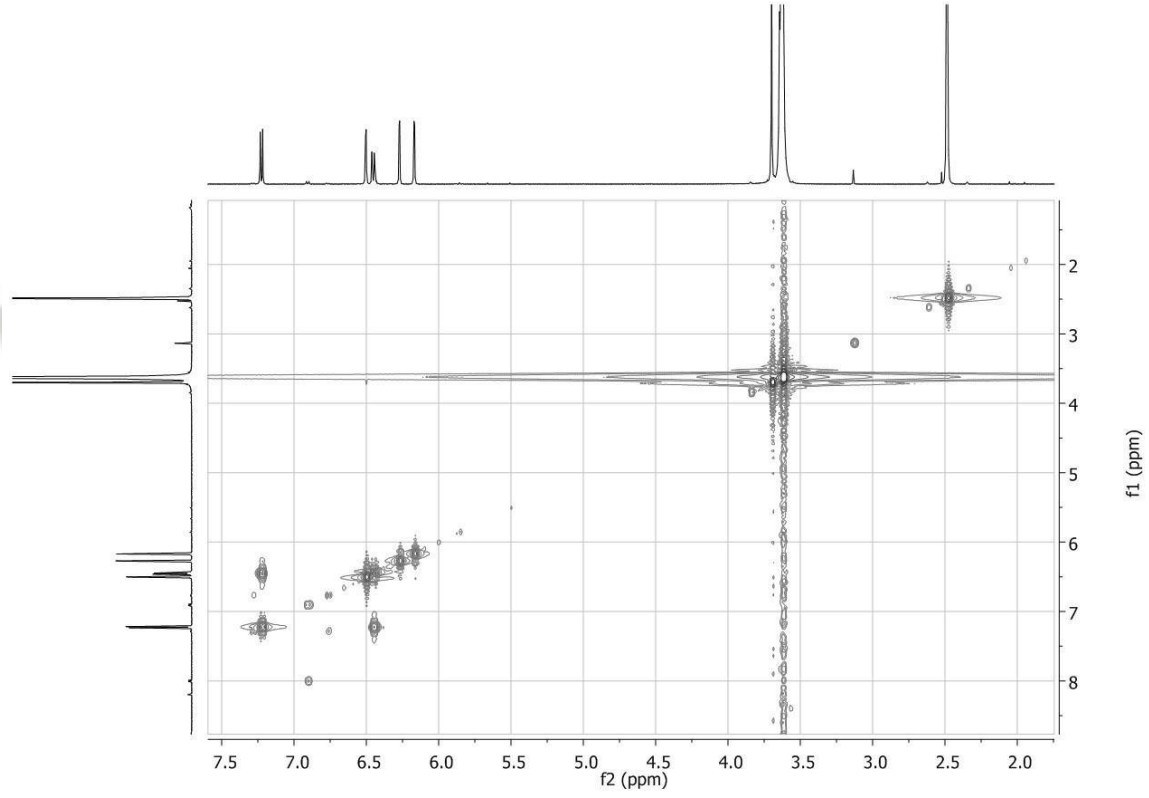


Appendix 91: ^{1}H NMR spectrum (DMSO–d_6, 500 MHz) of compound **14**

NYANSAPƆ W ƆSANE NO BADWENMA

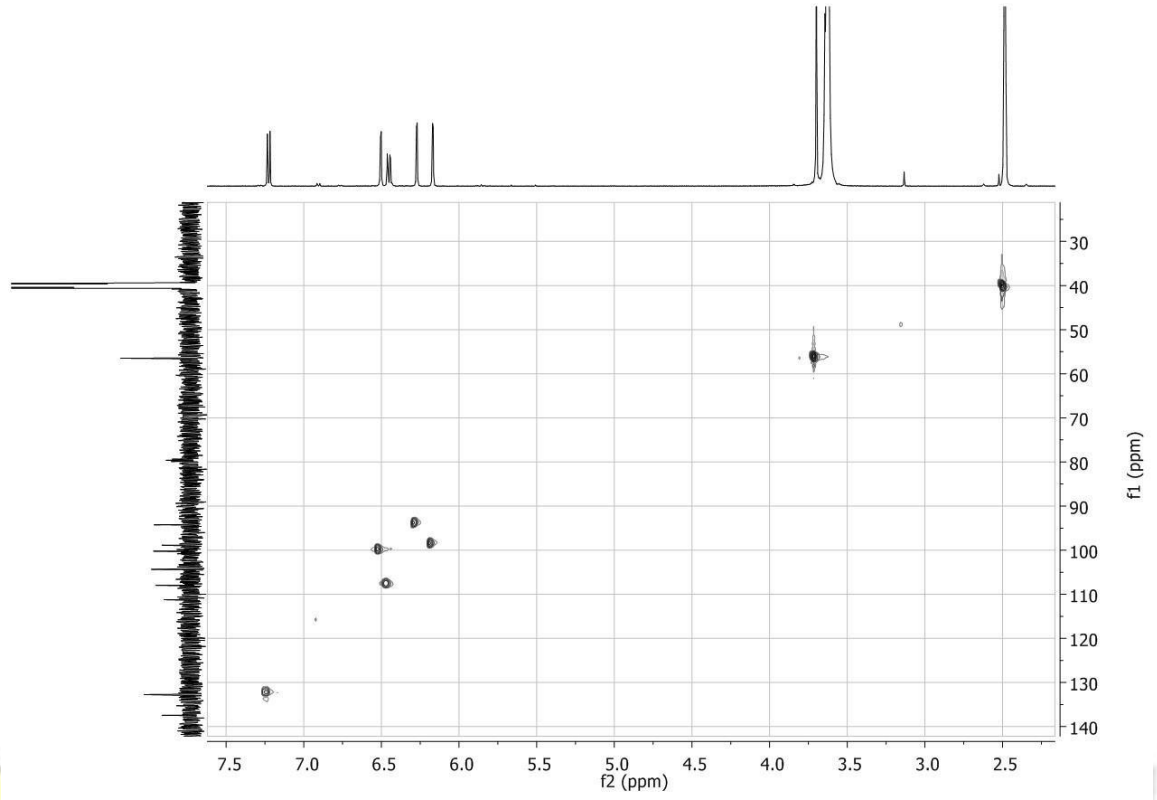


Appendix 92: ^{13}C NMR spectrum (DMSO–d_6, 125 MHz) of compound **14**



Appendix

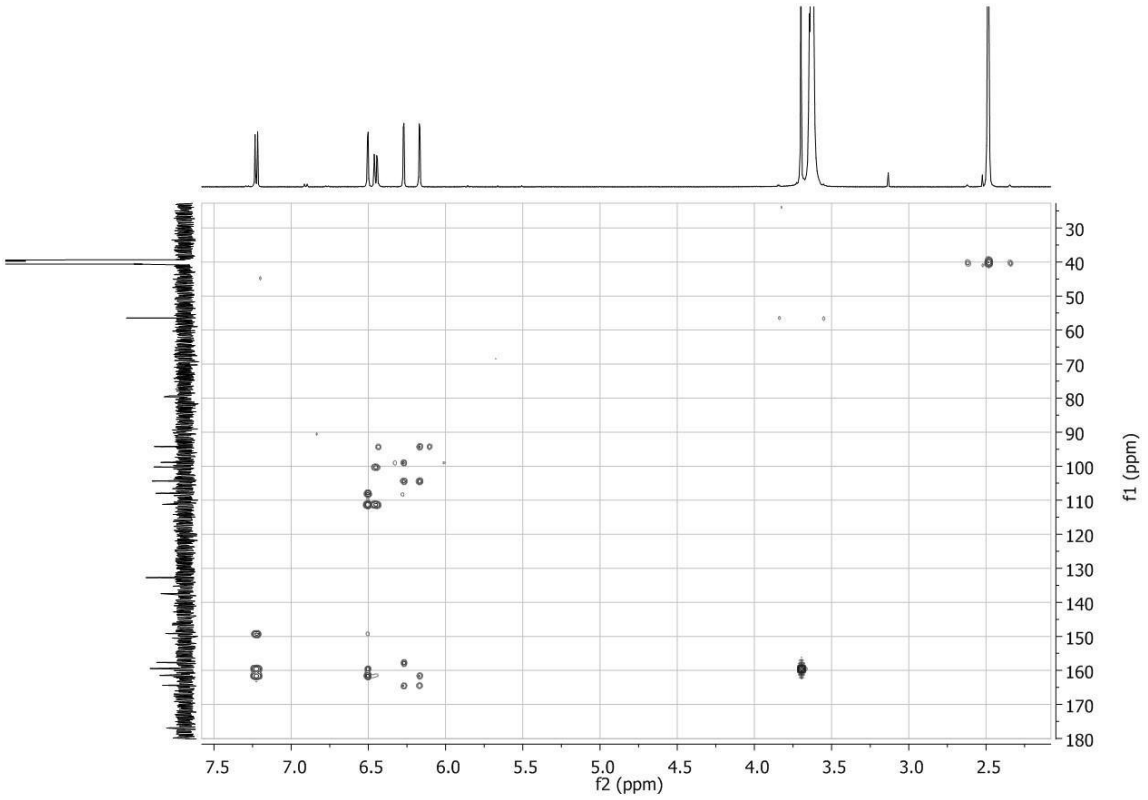
93: $^{1}H–^{1}H$ COSY NMR spectrum (DMSO–d_6) of compound **14**



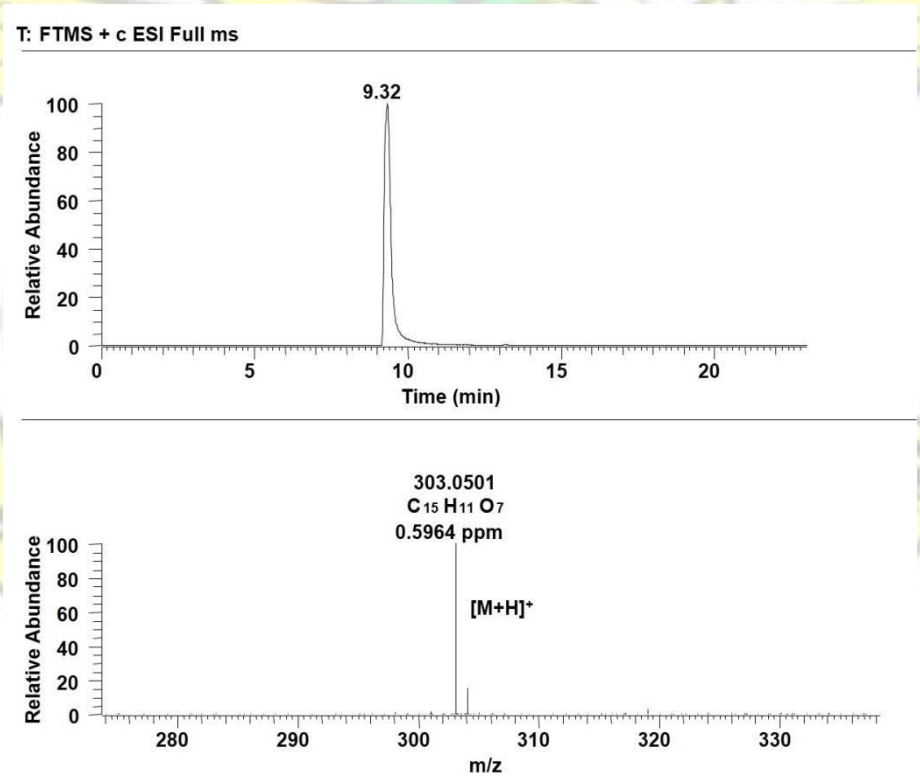
Appendix 94: HSQC NMR spectrum (DMSO–d_6) of compound **14**

NYANSAPƆ WƆ SANE NO BADWENMA

Appendix

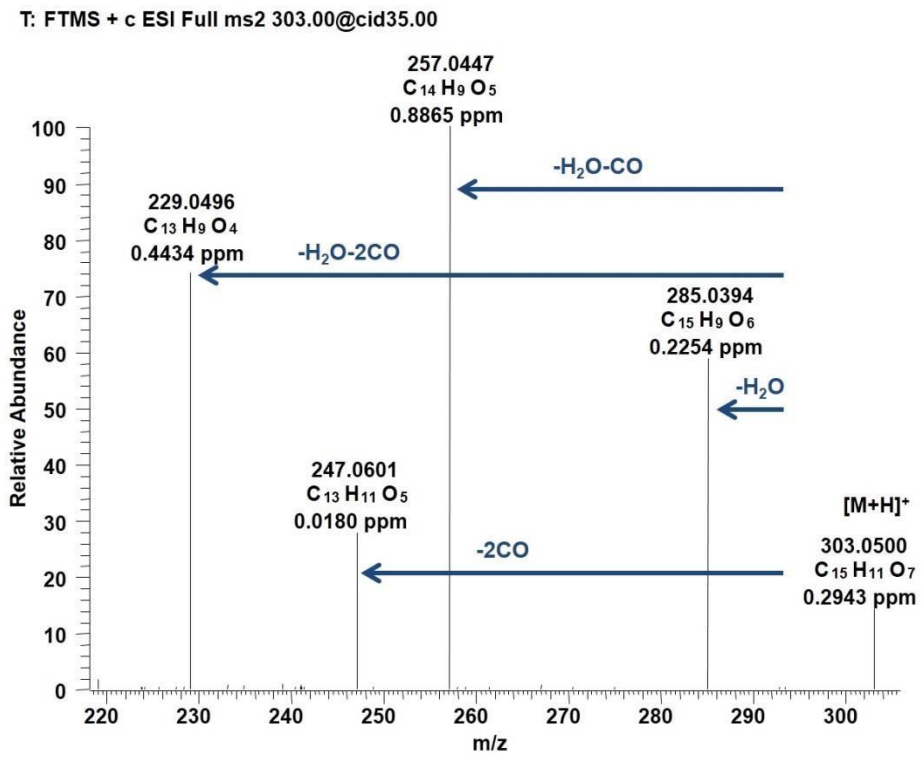


95: HMBC NMR spectrum (DMSO–d_6) of compound **14**



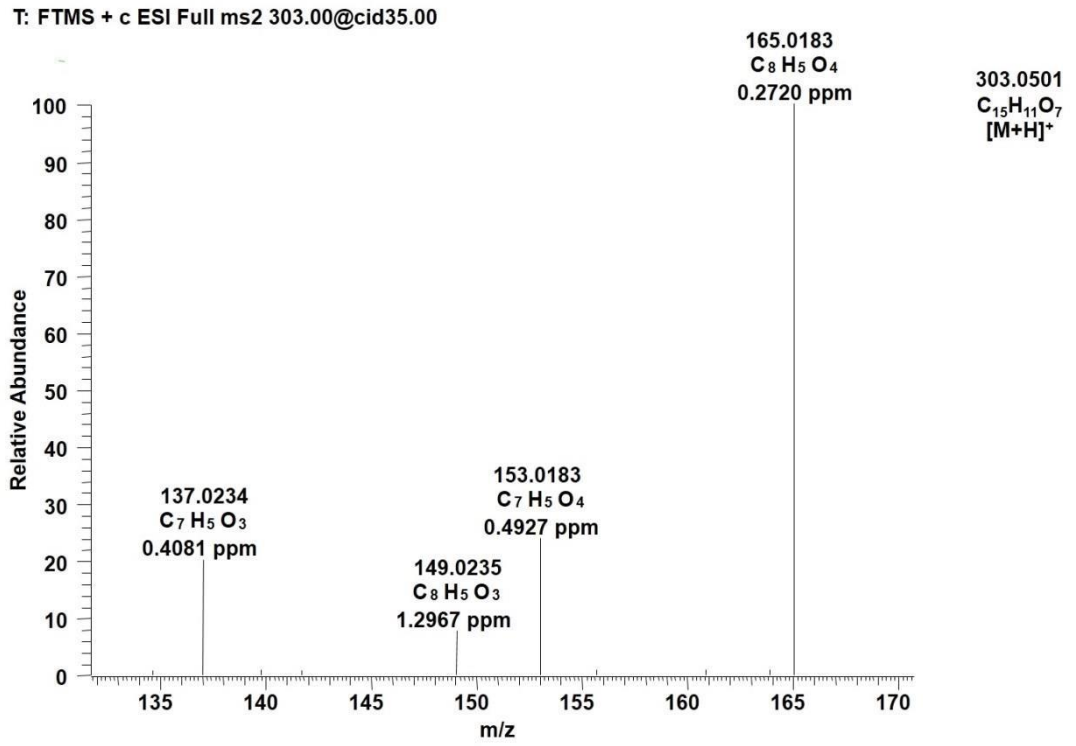
Appendix 96: Positive HRESI–MS spectrum of compound **15**

Appendix

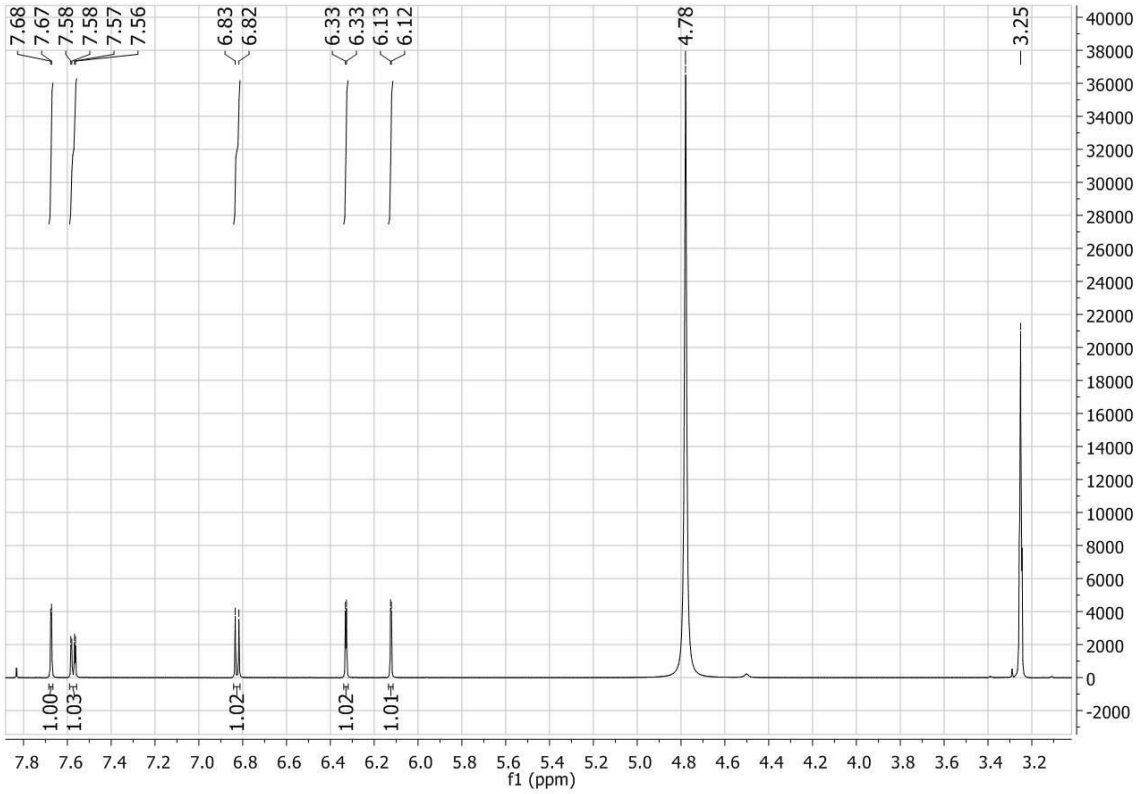


97: Positive HRESI–MS/MS spectrum of compound **15**

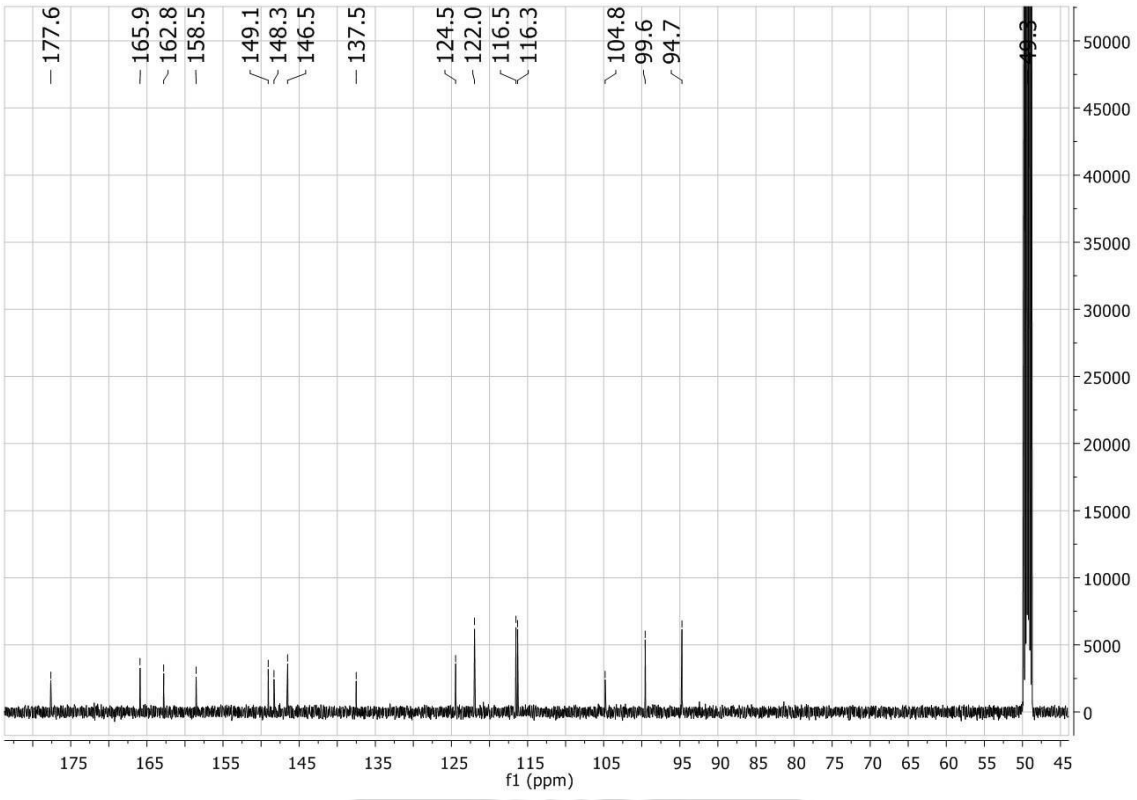
Appendix



Appendix 98: Positive HRESI–MS/MS (RDA fragments) spectrum of compound **15**

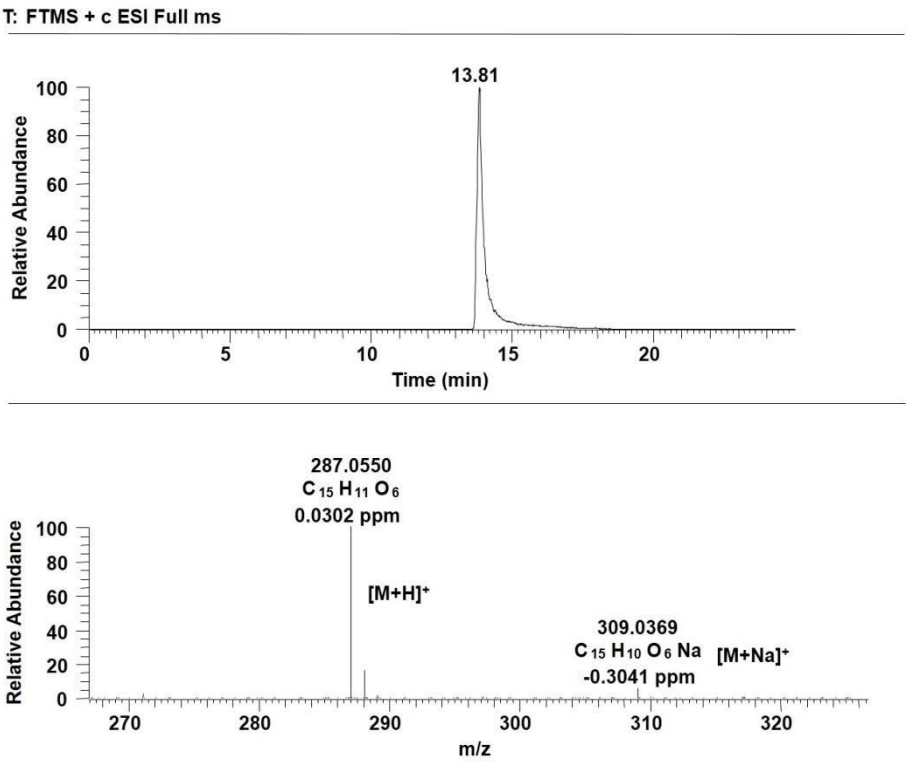


Appendix 99: ^{1}H NMR spectrum (CD_3OD, 500 MHz) of compound **15**

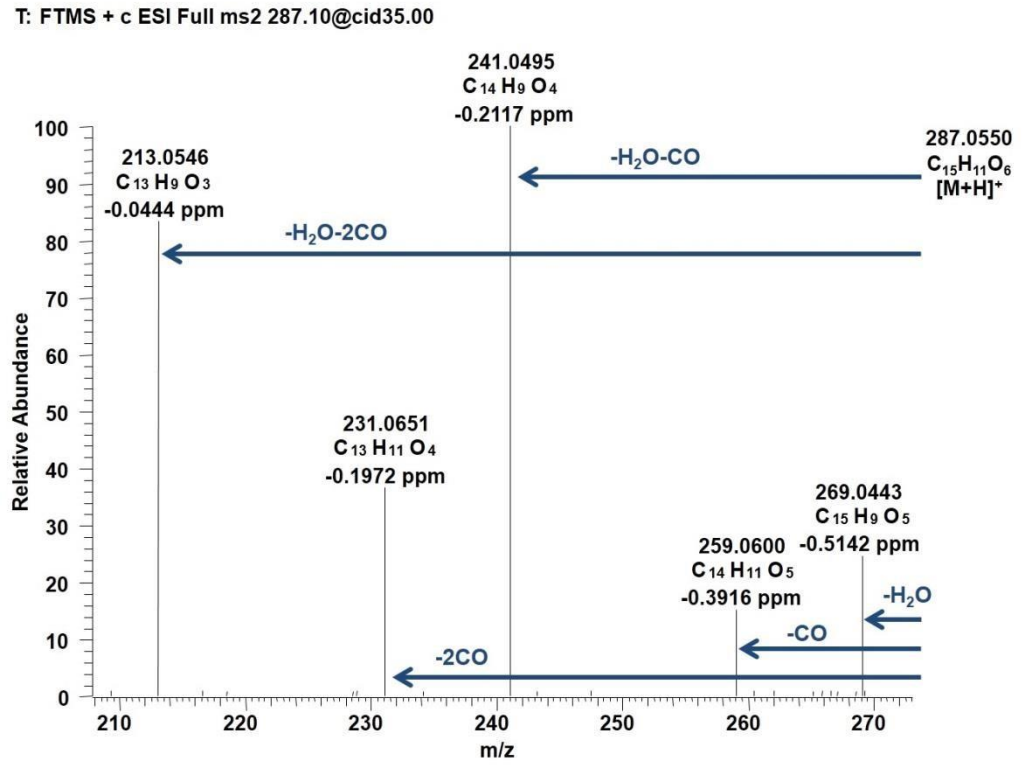


Appendix 100: ^{13}C NMR spectrum (CD_3OD, 125 MHz) of compound **15**

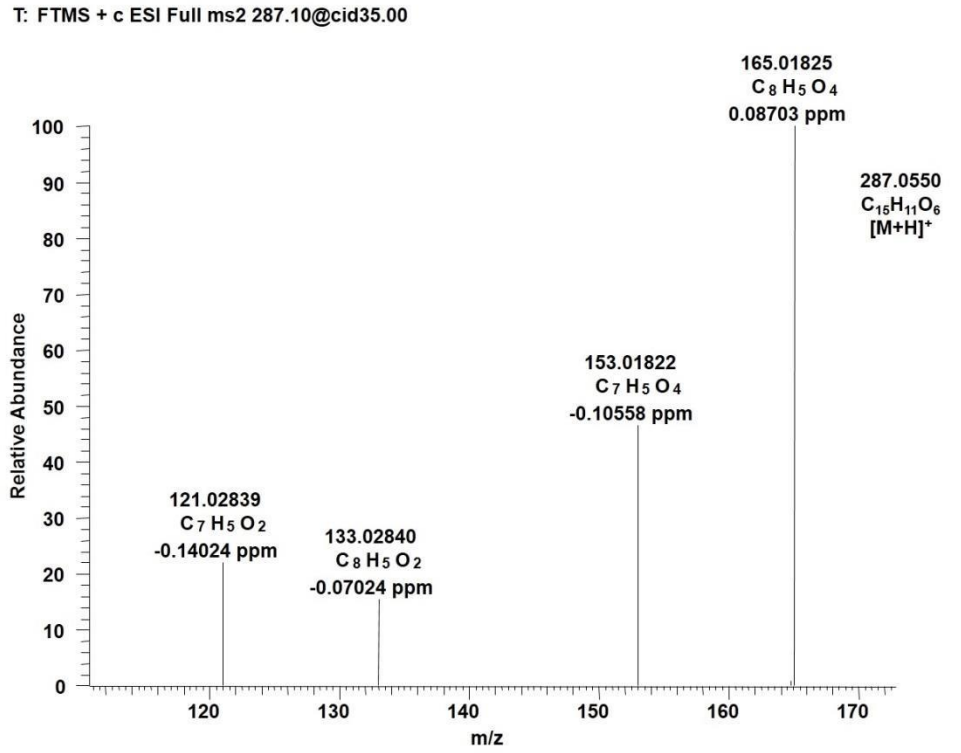
NYANSAPƆ W Ɔ SANE NO BADWENMA



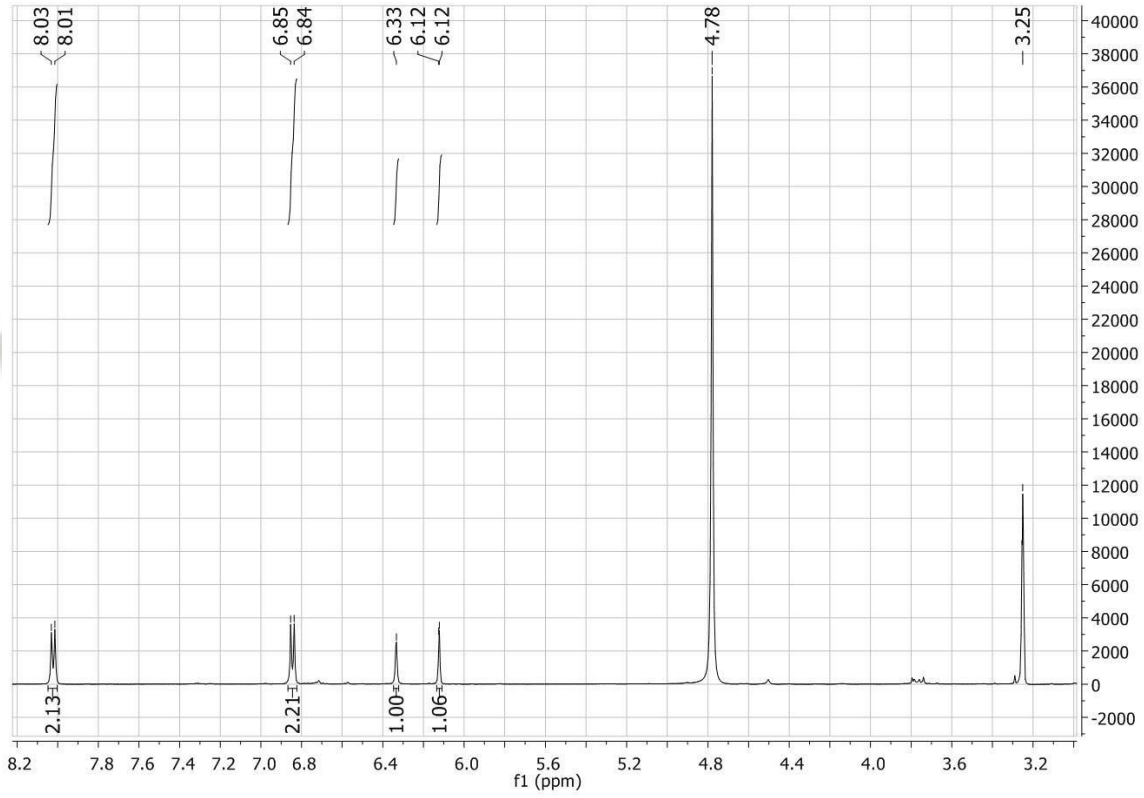
Appendix 101: Positive HRESI–MS spectrum of compound **16**



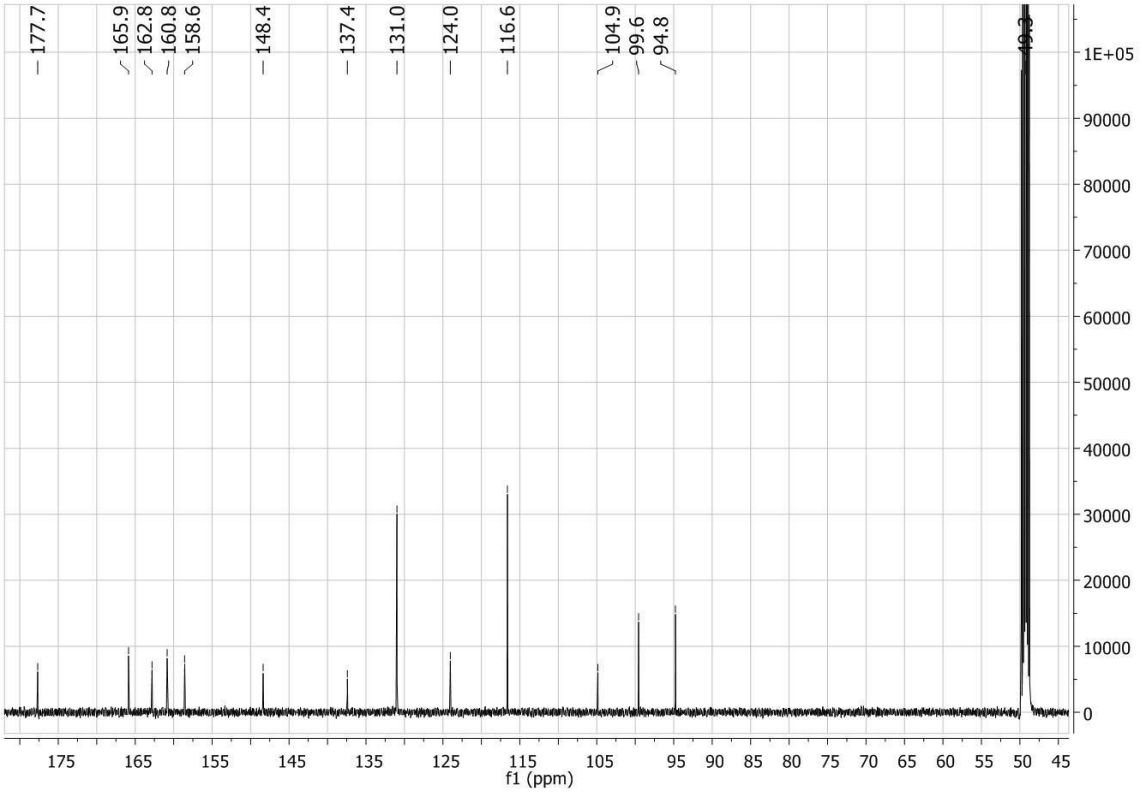
Appendix 102: Positive HRESI–MS/MS spectrum of compound **16**



Appendix 103: Positive HRESI–MS/MS (RDA fragments) spectrum of compound **16**



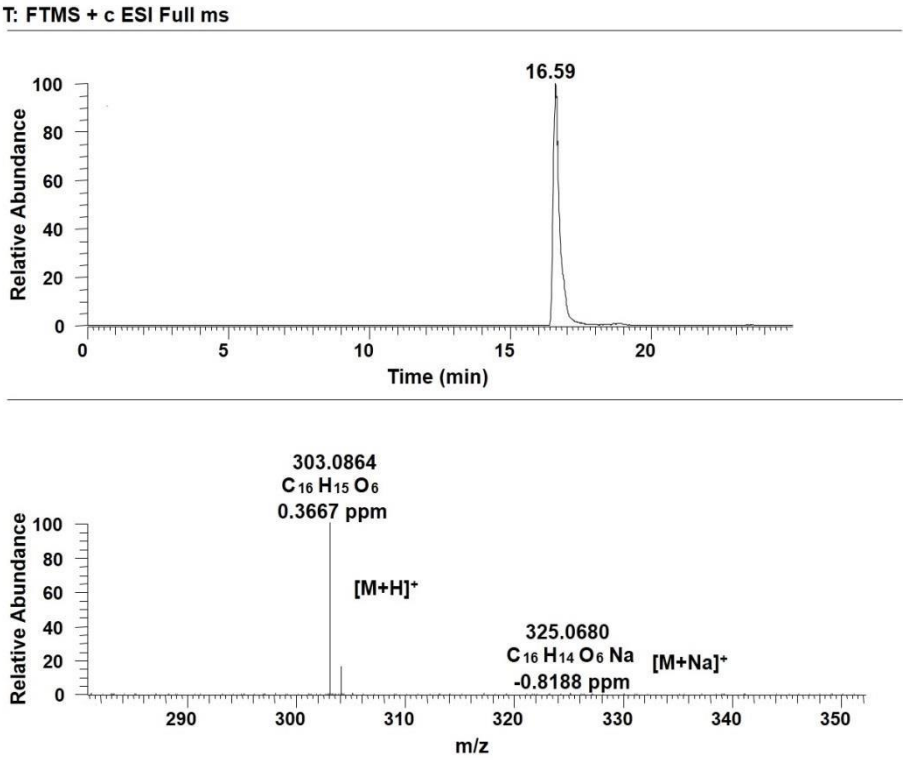
104: ^{1}H NMR spectrum (CD_3OD, 500 MHz) of compound **16**



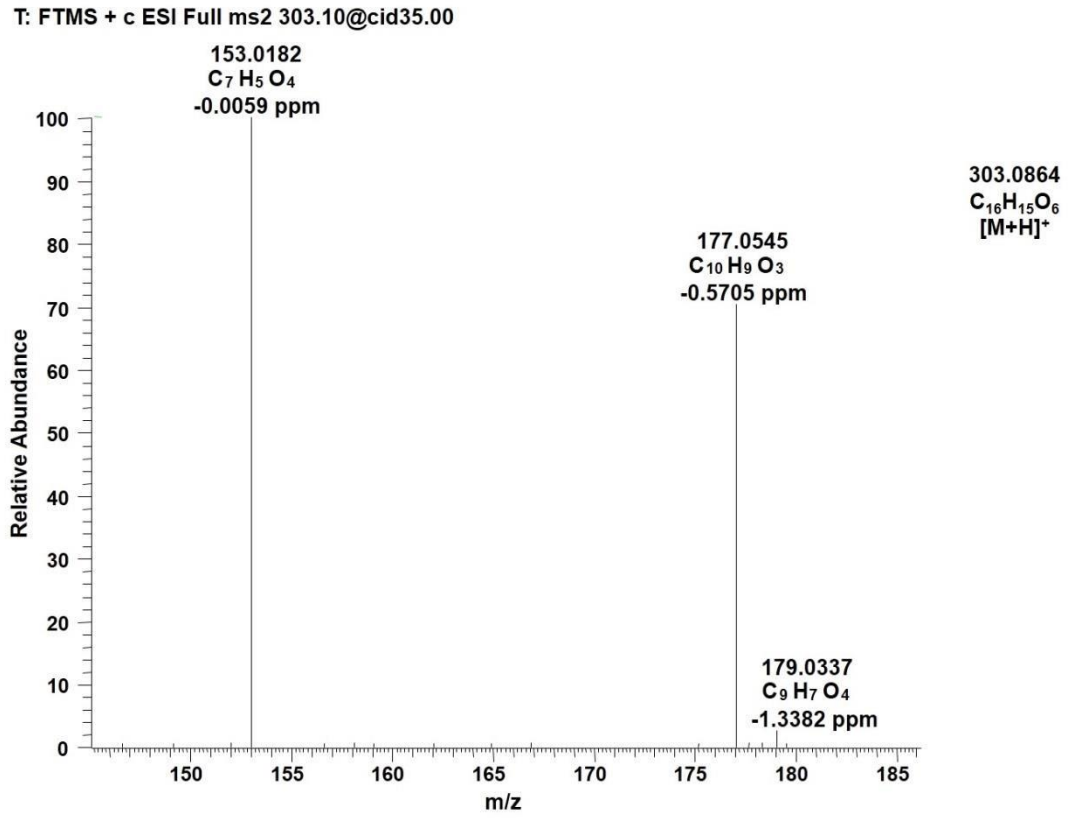
Appendix 105: ^{13}C NMR spectrum (CD_3OD, 125 MHz) of compound **16**

NYANSAPƆ WƆ SANE NO BADWENMA

Appendix



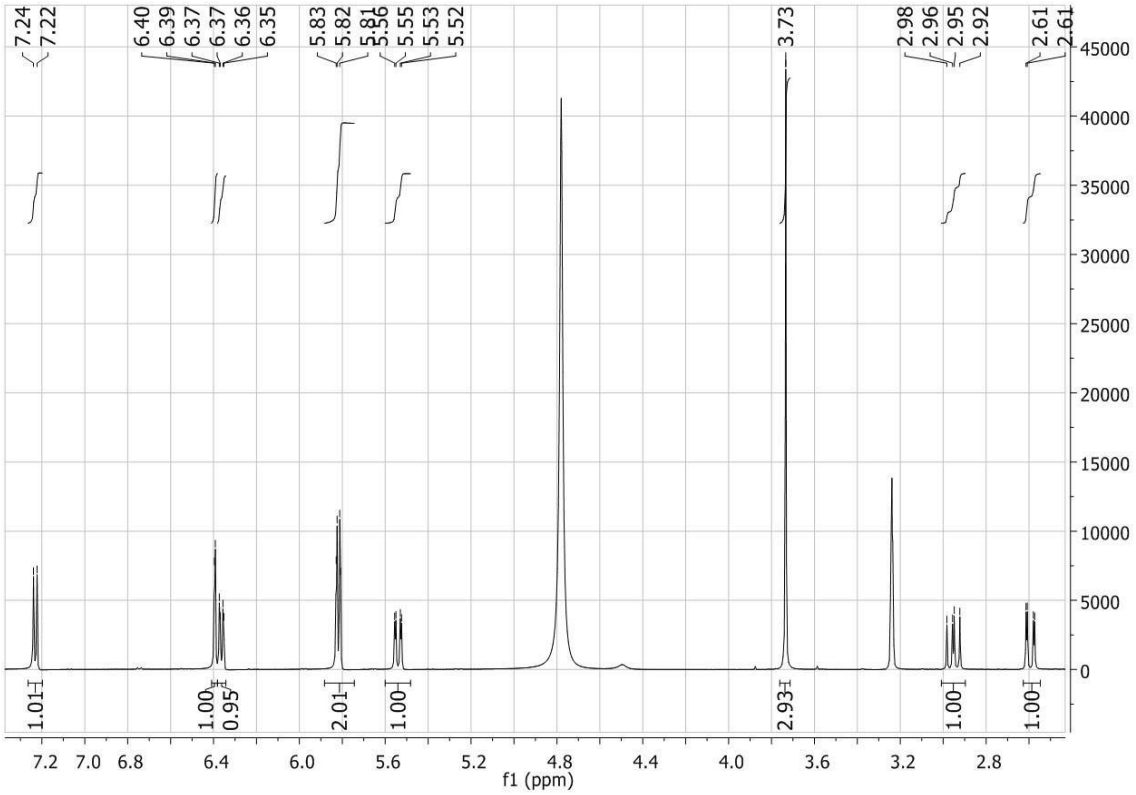
Appendix 106: Positive HRESI–MS spectrum of compound **17**



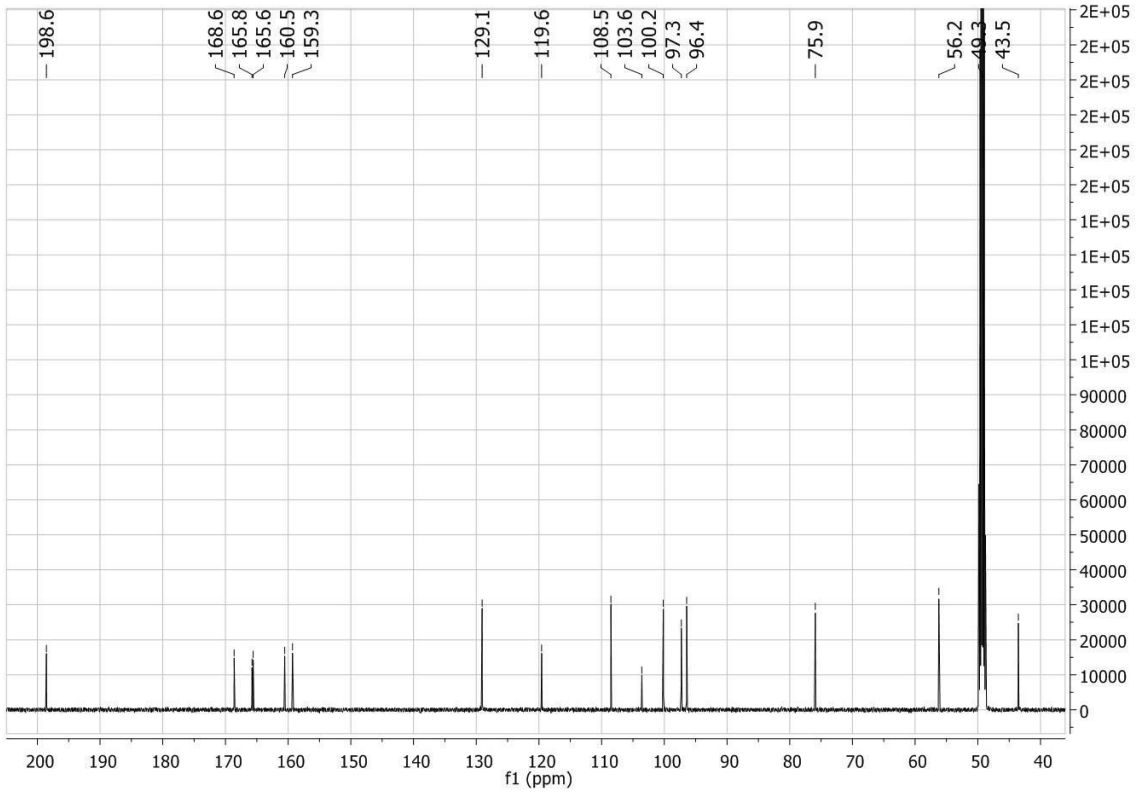
107: Positive HRESI–MS/MS (RDA fragments) spectrum of compound **17**

KNUST

Appendix

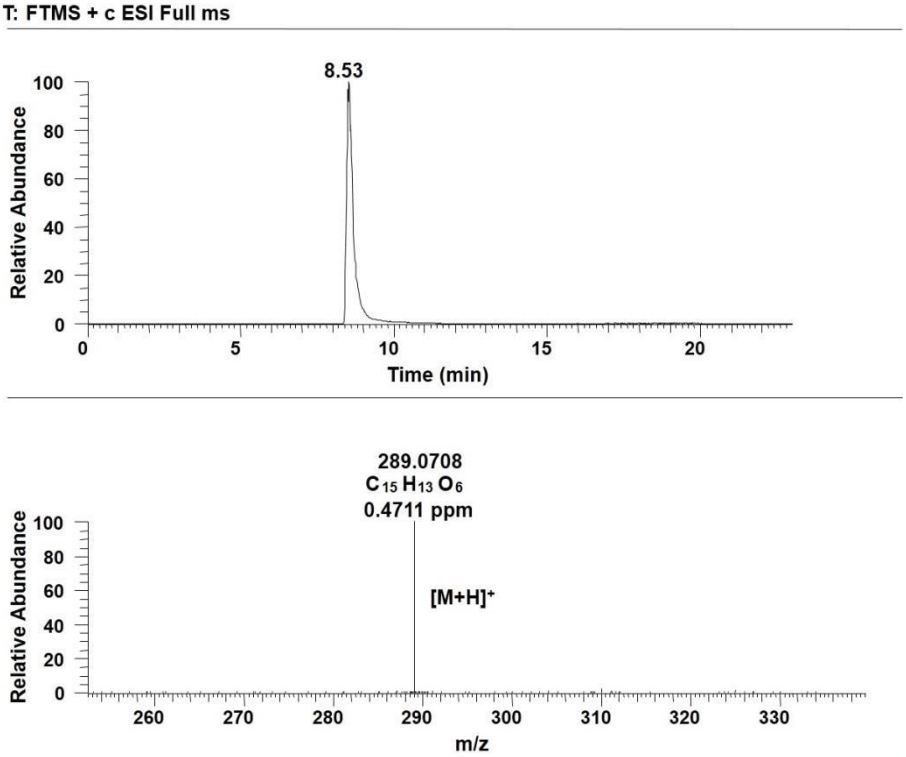


Appendix 108: ^{1}H NMR spectrum (CD_3OD, 500 MHz) of compound **17**

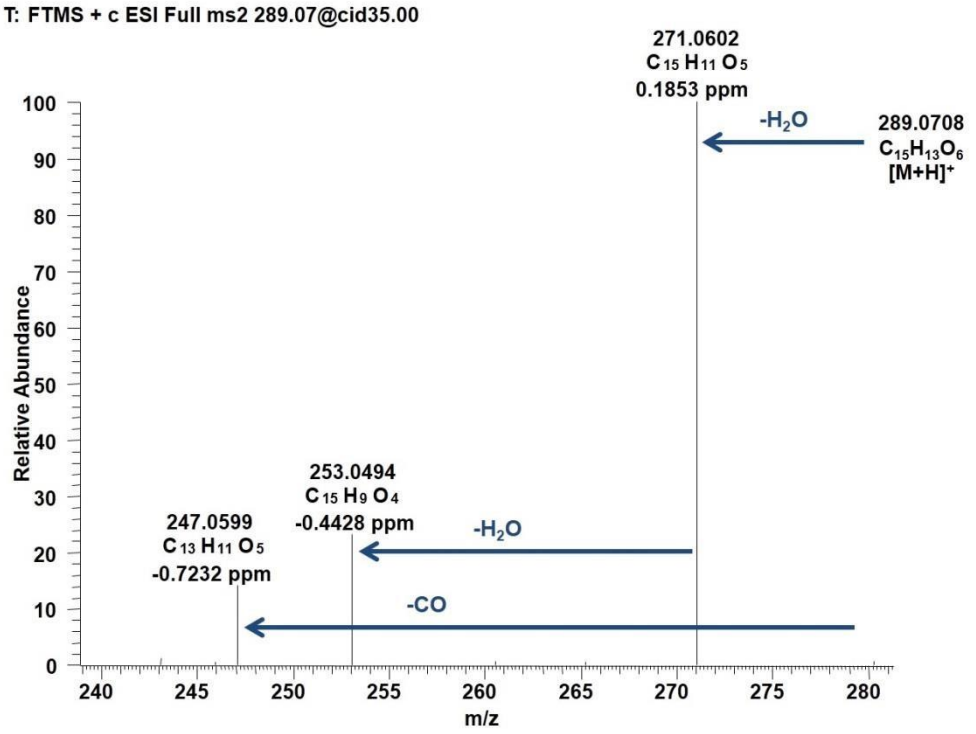


Appendix

109: ^{13}C NMR spectrum (CD_3OD, 125 MHz) of compound **17**

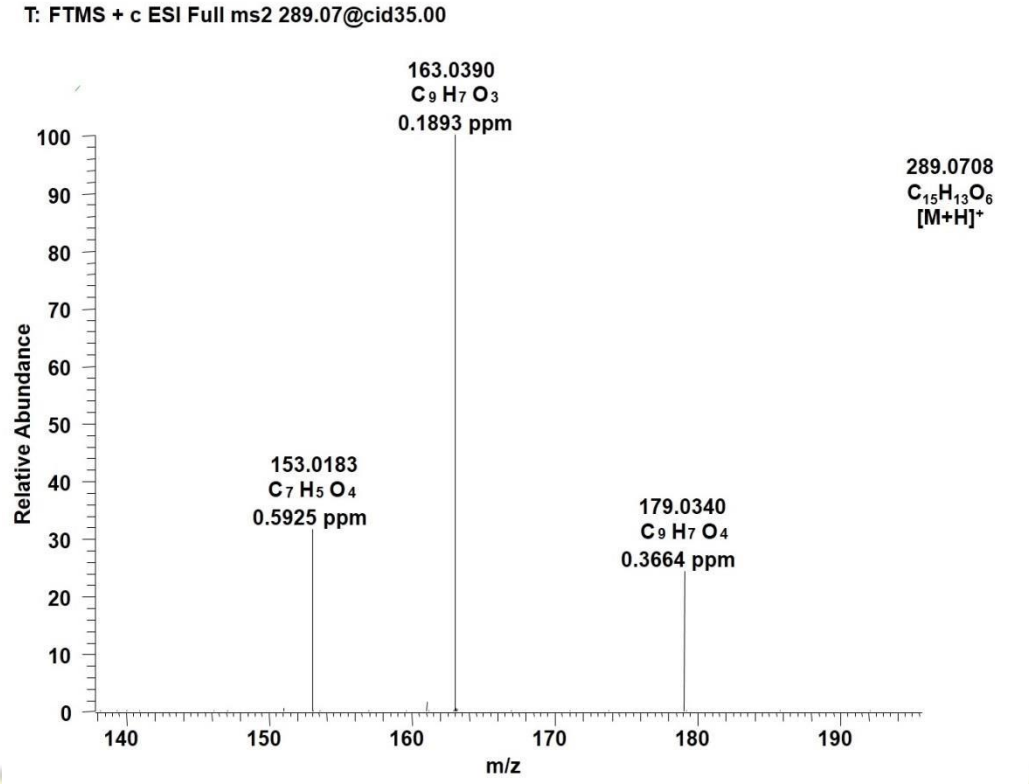


Appendix 110: Positive HRESI–MS spectrum of compound **18**

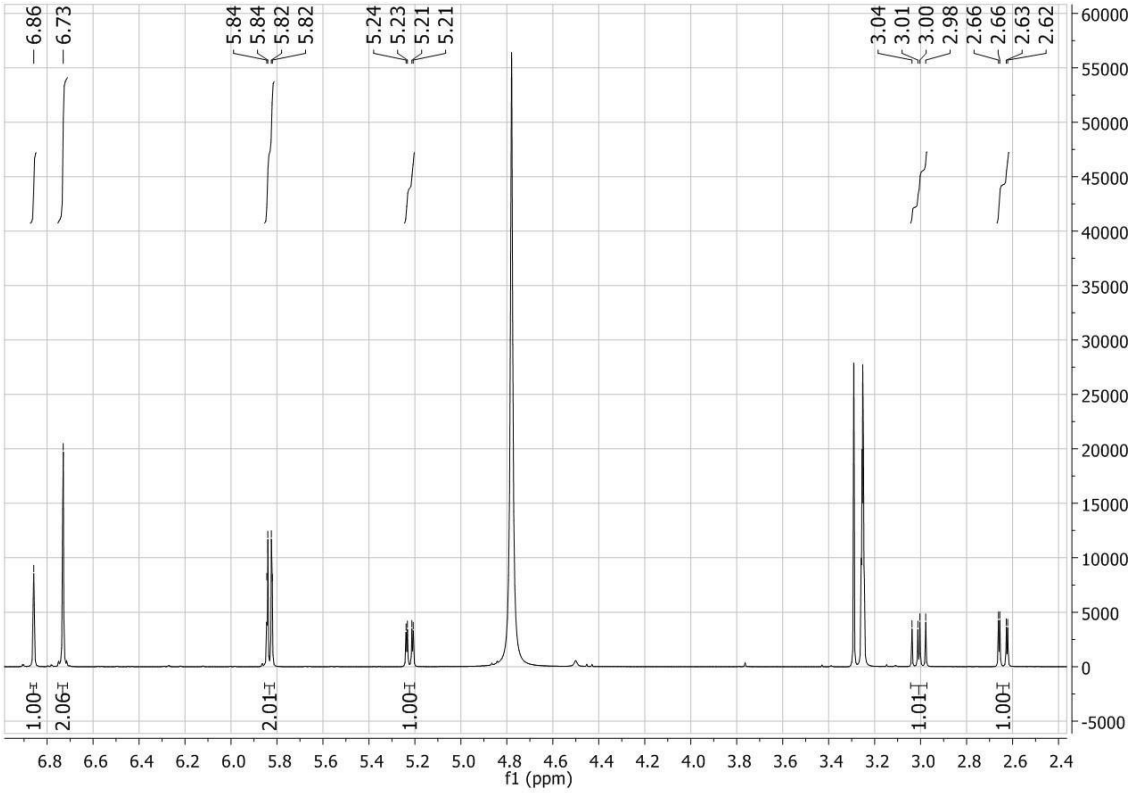


Appendix

111: Positive HRESI–MS/MS spectrum of compound **18**



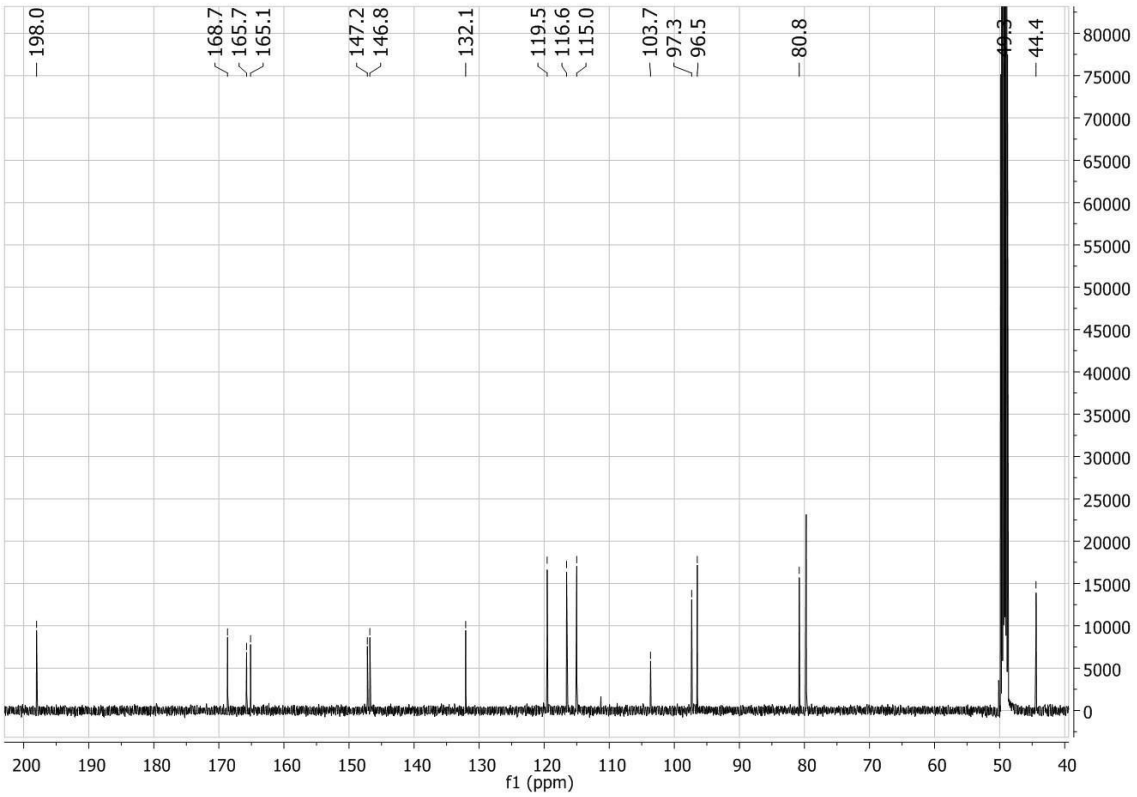
Appendix 112: Positive HRESI–MS/MS (RDA fragments) spectrum of compound **18**



Appendix 113: ^{1}H NMR spectrum (CD_3OD, 500 MHz) of compound **18**

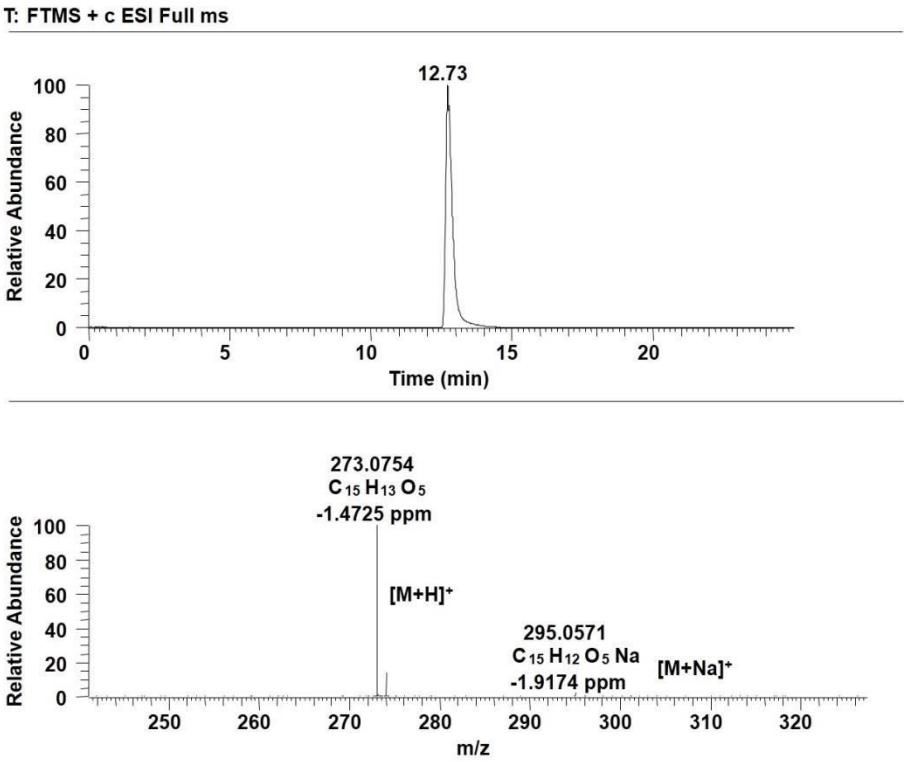
KNUST



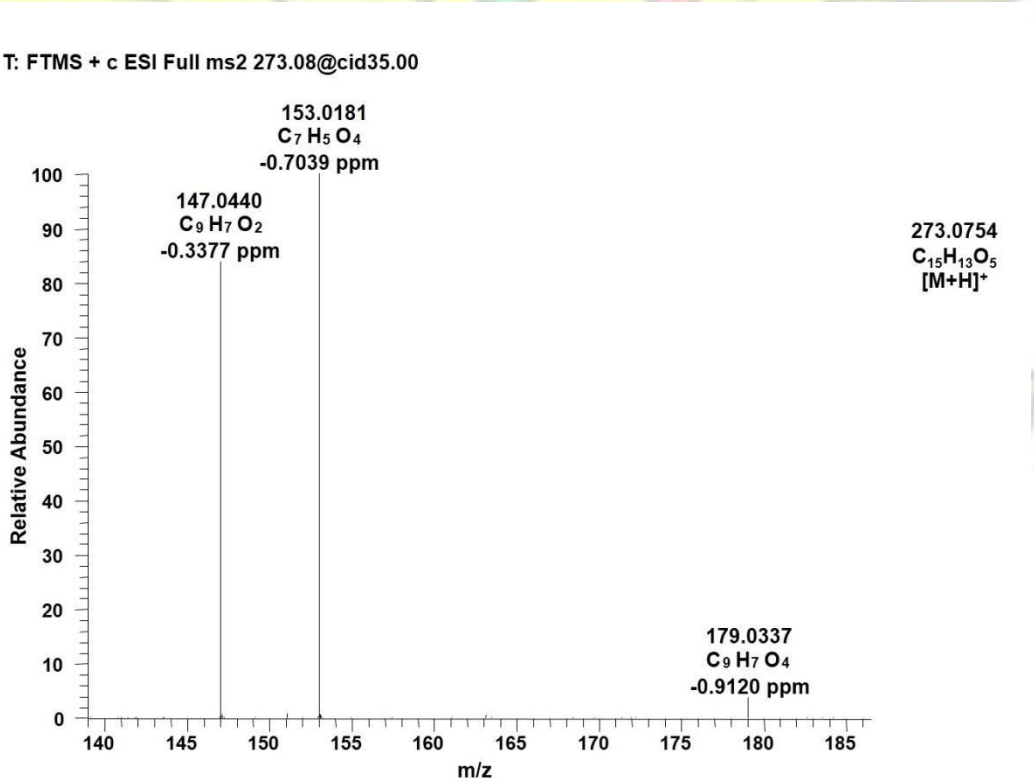


Appendix 114: ^{13}C NMR spectrum (CD_3OD, 125 MHz) of compound **18**

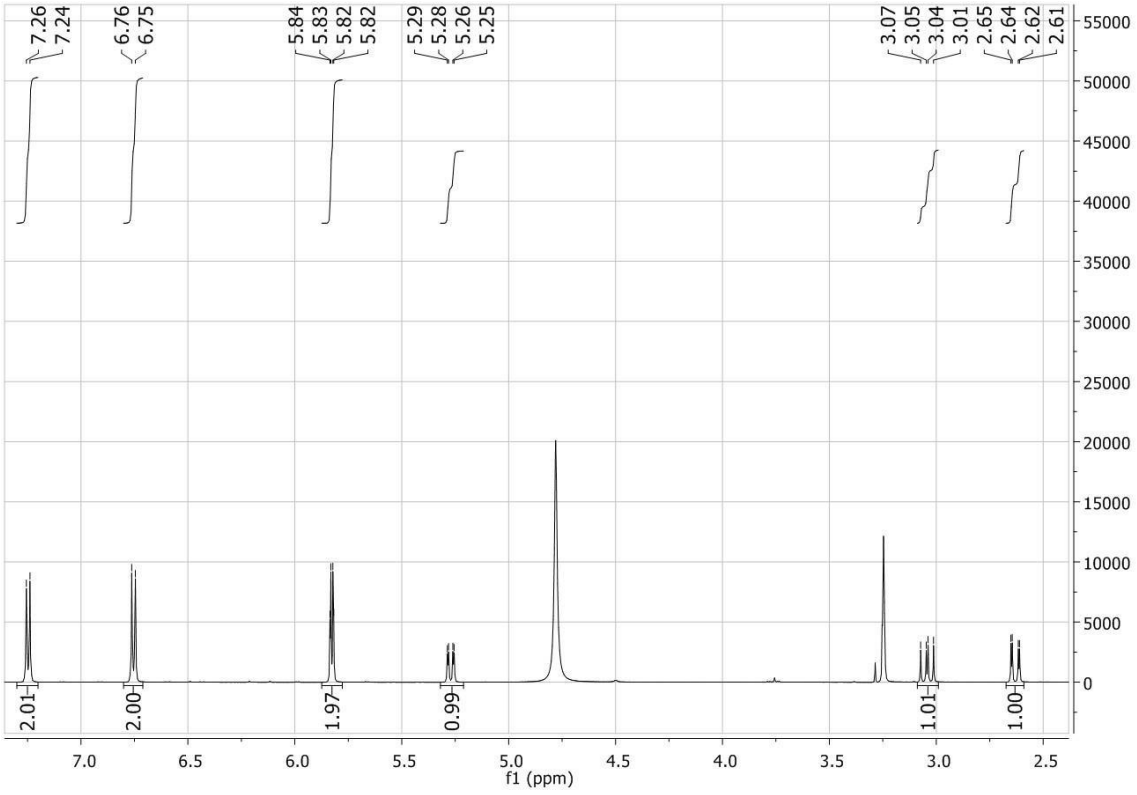
NYANSAPƆ WƆ SANE NO BADWENMA



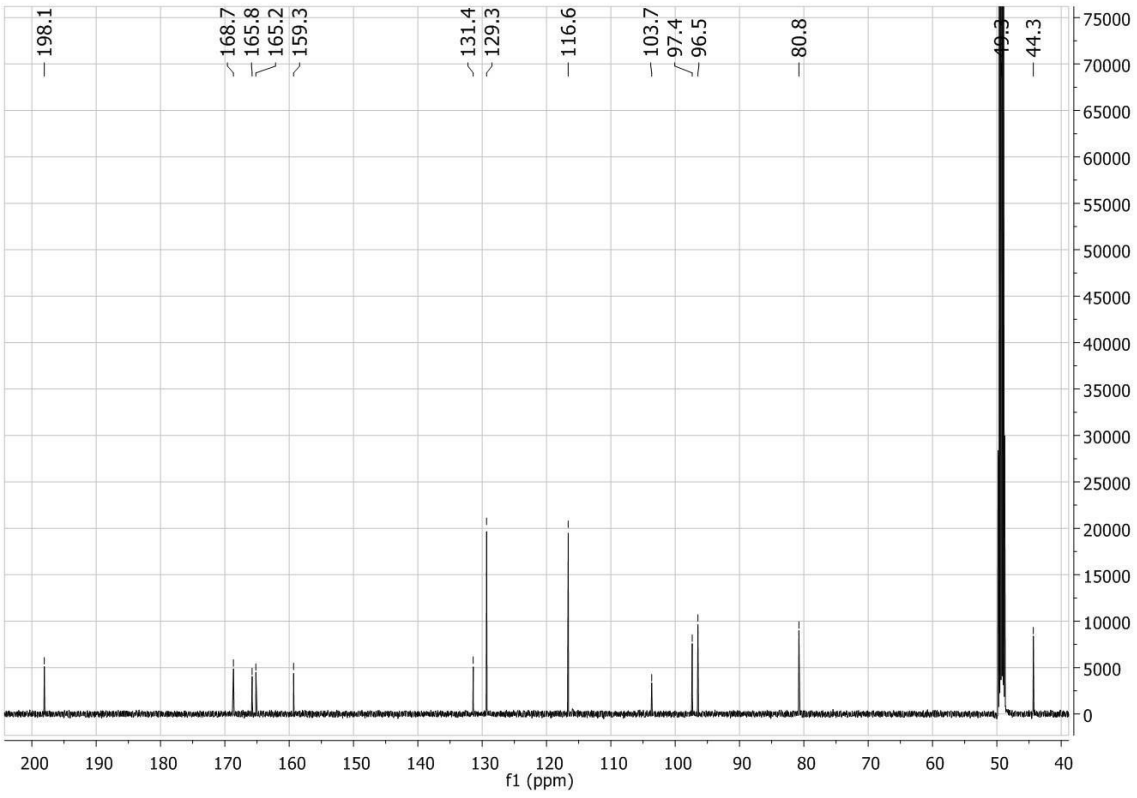
Appendix 115: Positive HRESI–MS spectrum of compound **19**



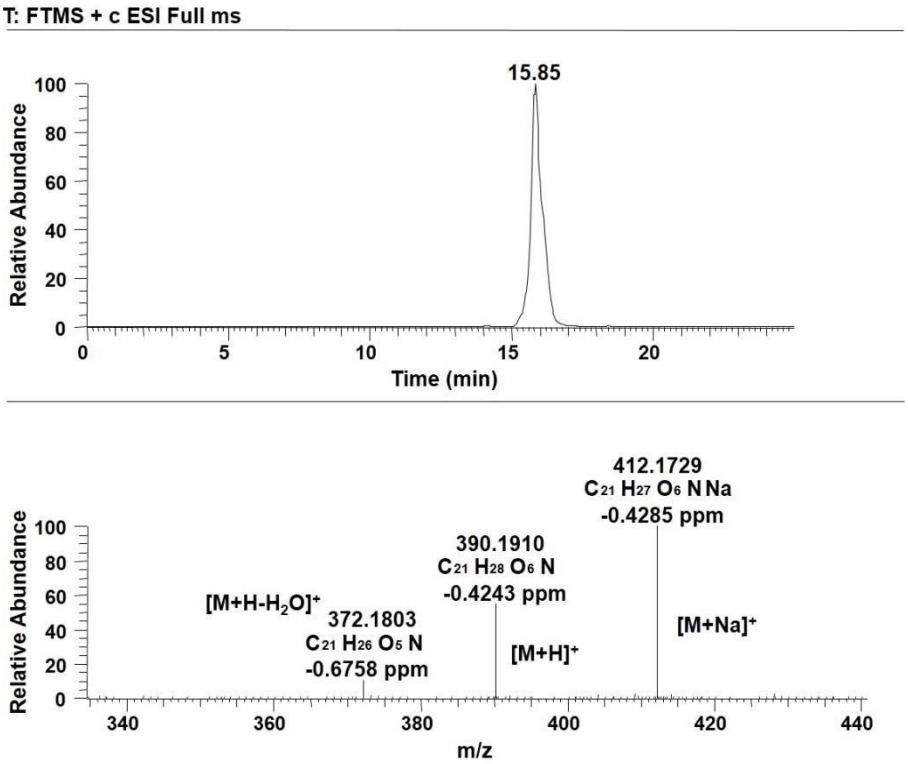
Appendix 116: Positive HRESI–MS/MS (RDA fragments) spectrum of compound **19**



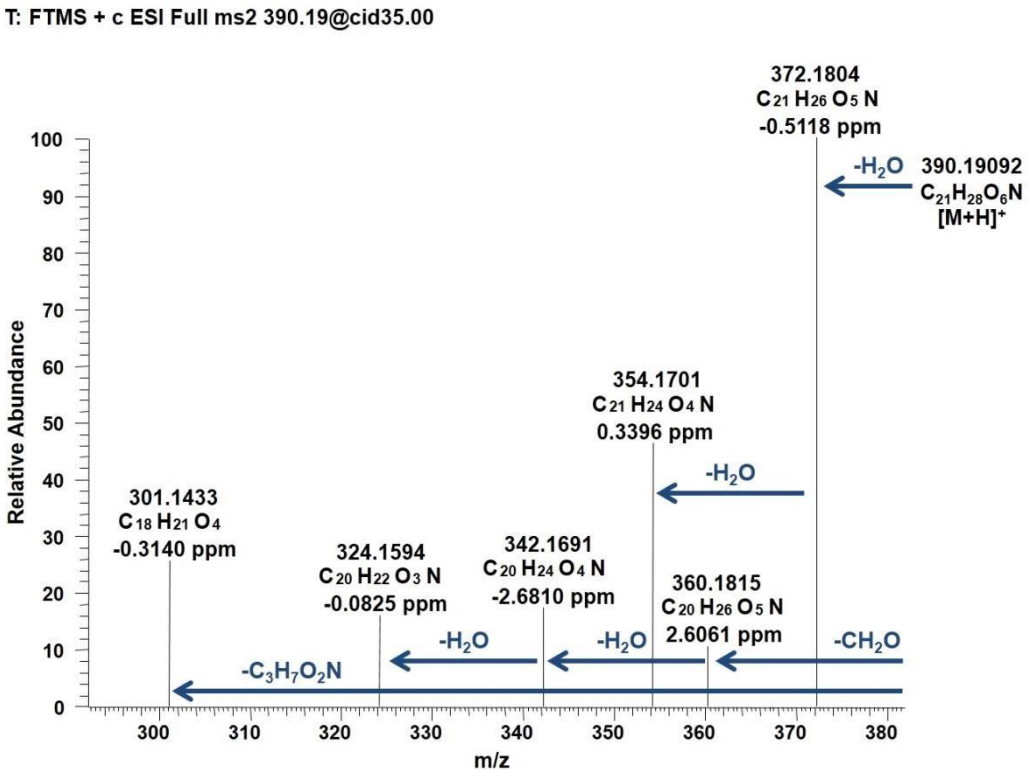
Appendix 117: ^{1}H NMR spectrum (CD_3OD, 500 MHz) of compound **19**



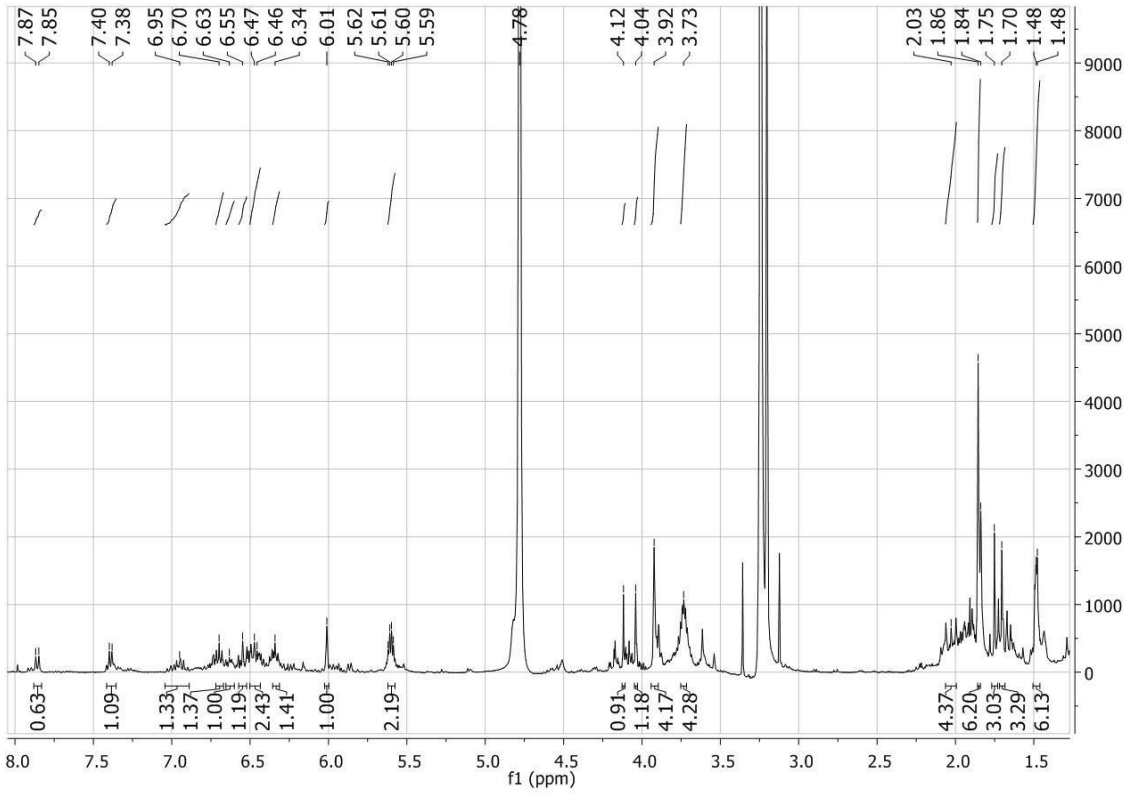
Appendix 118: ^{13}C NMR spectrum (CD_3OD, 125 MHz) of compound **19**



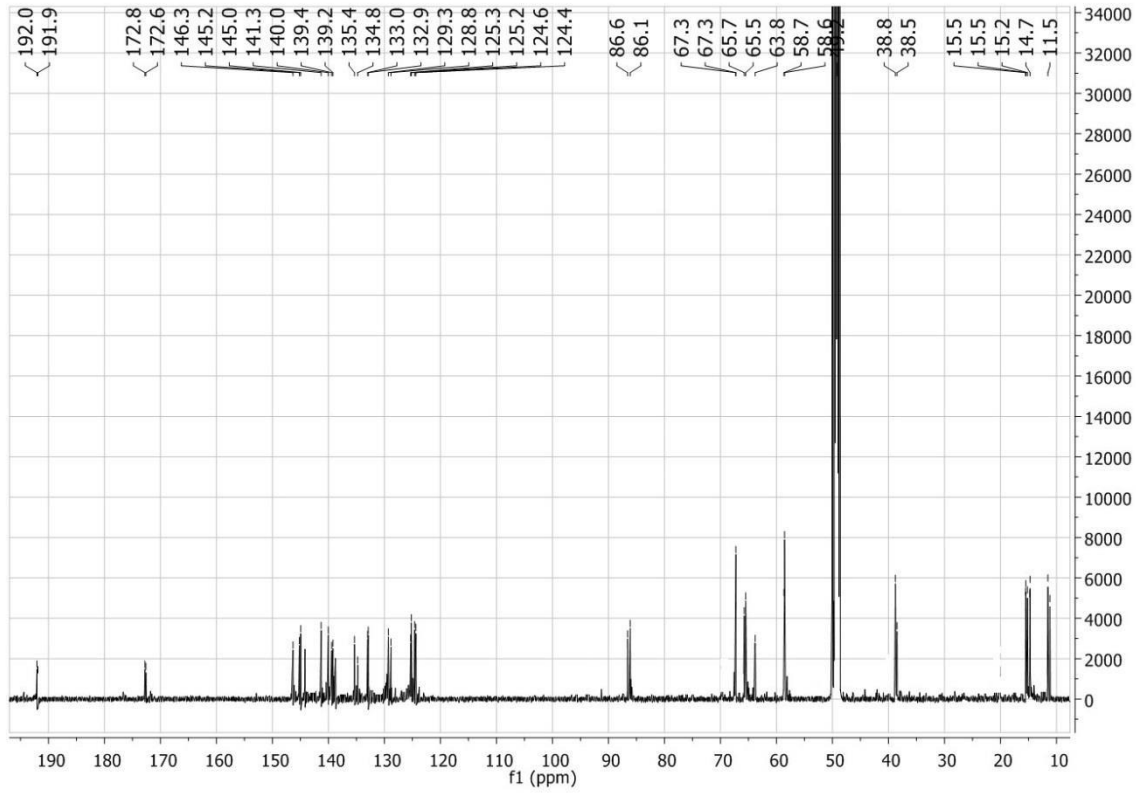
Appendix 119: Positive HRESI–MS spectrum of compounds **20**/**21**



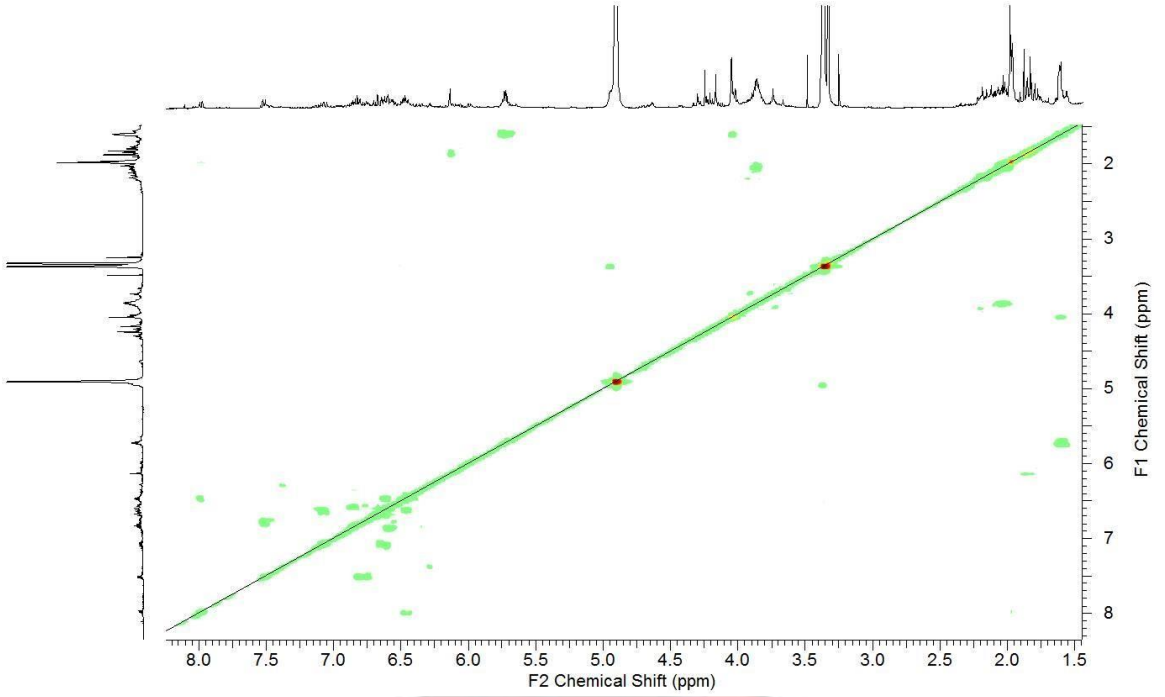
Appendix 120: Positive HRESI–MS/MS spectrum of compounds **20**/**21**



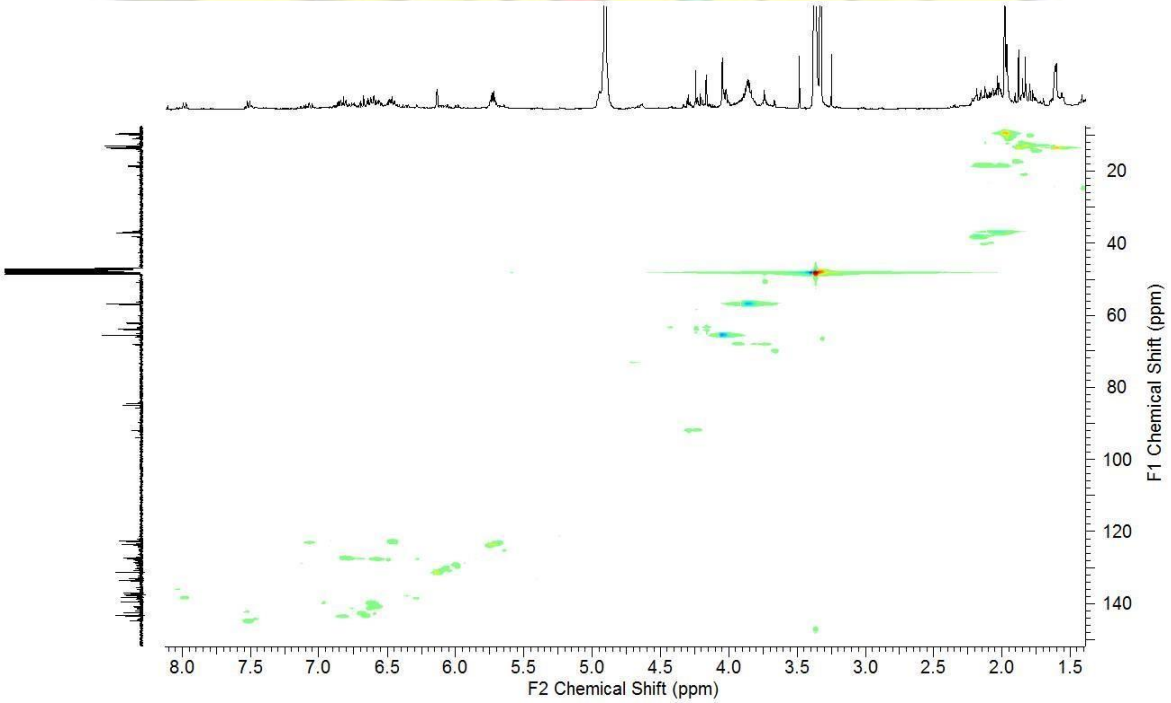
Appendix 121: ^{1}H NMR spectrum (CD_3OD, 600 MHz) of compounds **20**/**21**



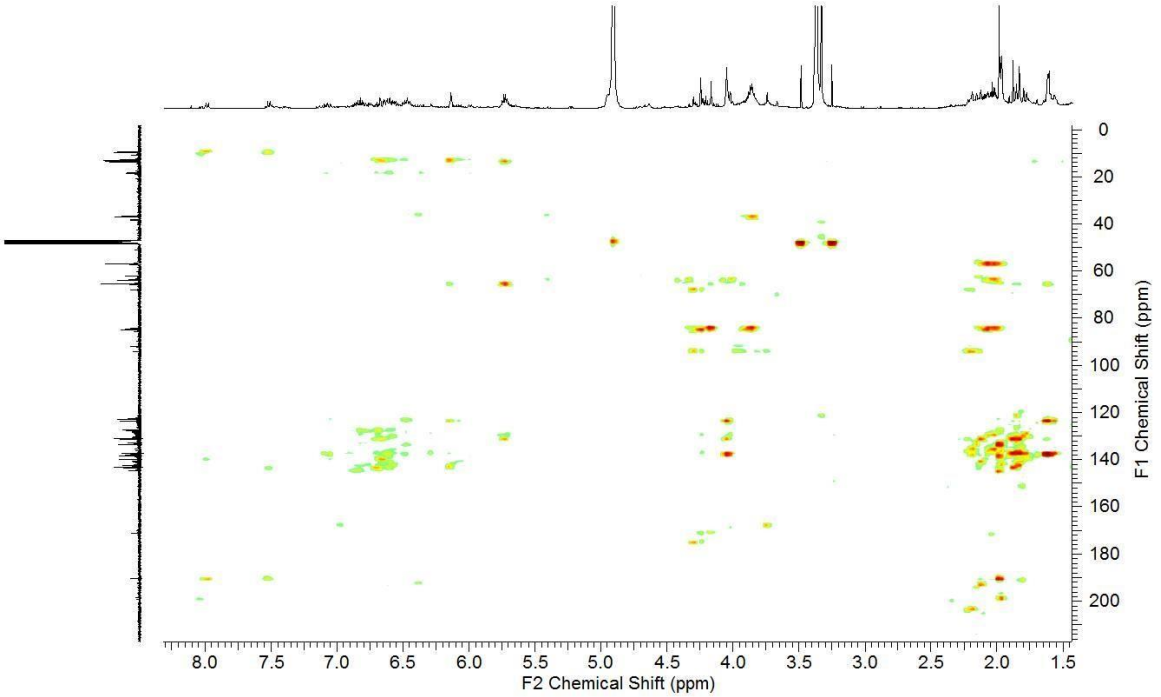
Appendix 122: ^{13}C NMR spectrum (CD_3OD, 150 MHz) of compounds **20**/**21**



Appendix 123: $^{1}H–^{1}H$ COSY NMR spectrum (CD_3OD) of compounds **20**/**21**

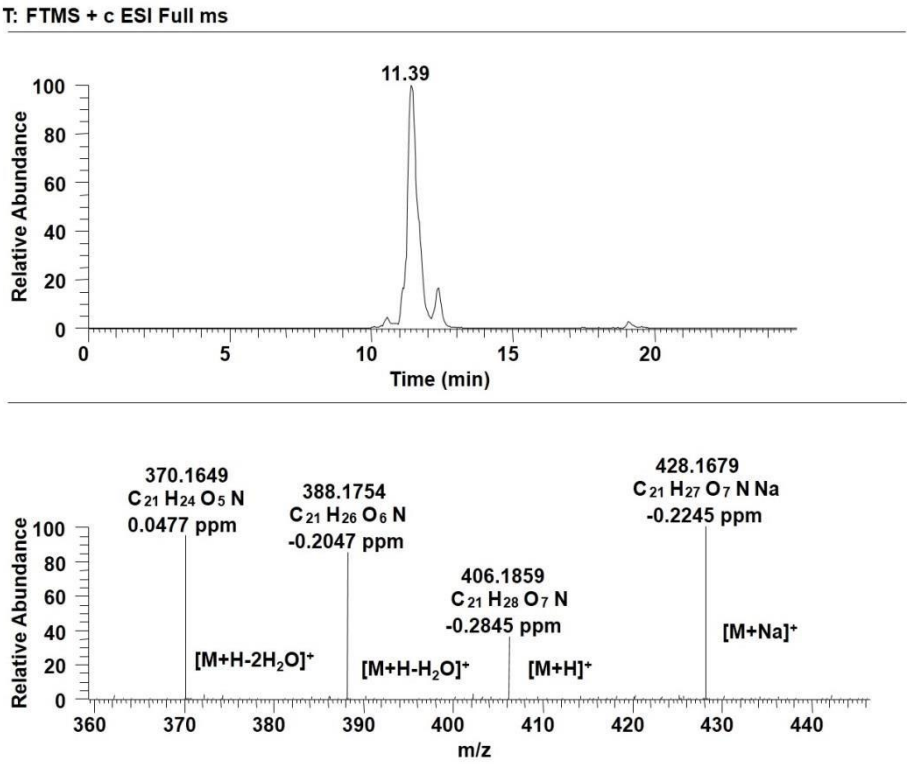


Appendix 124: HSQC NMR spectrum (CD_3OD) of compounds **20**/**21**

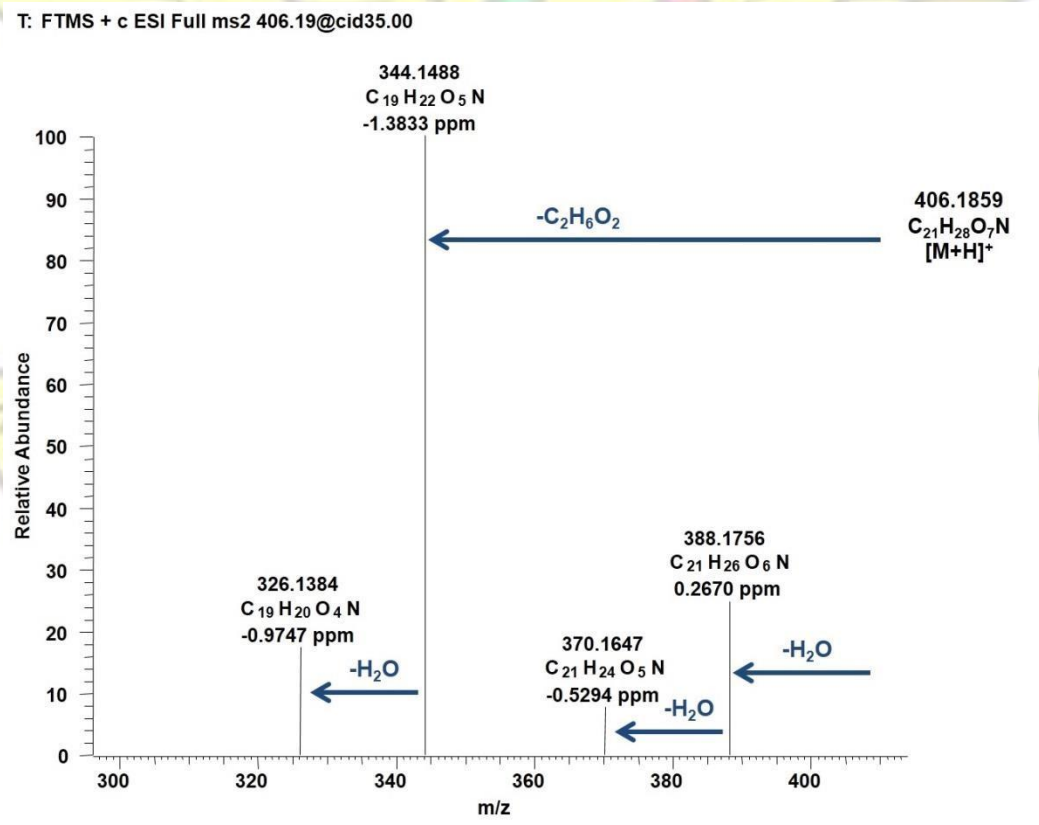


Appendix 125: HMBC NMR spectrum (CD_3OD) of compounds **20**/**21**

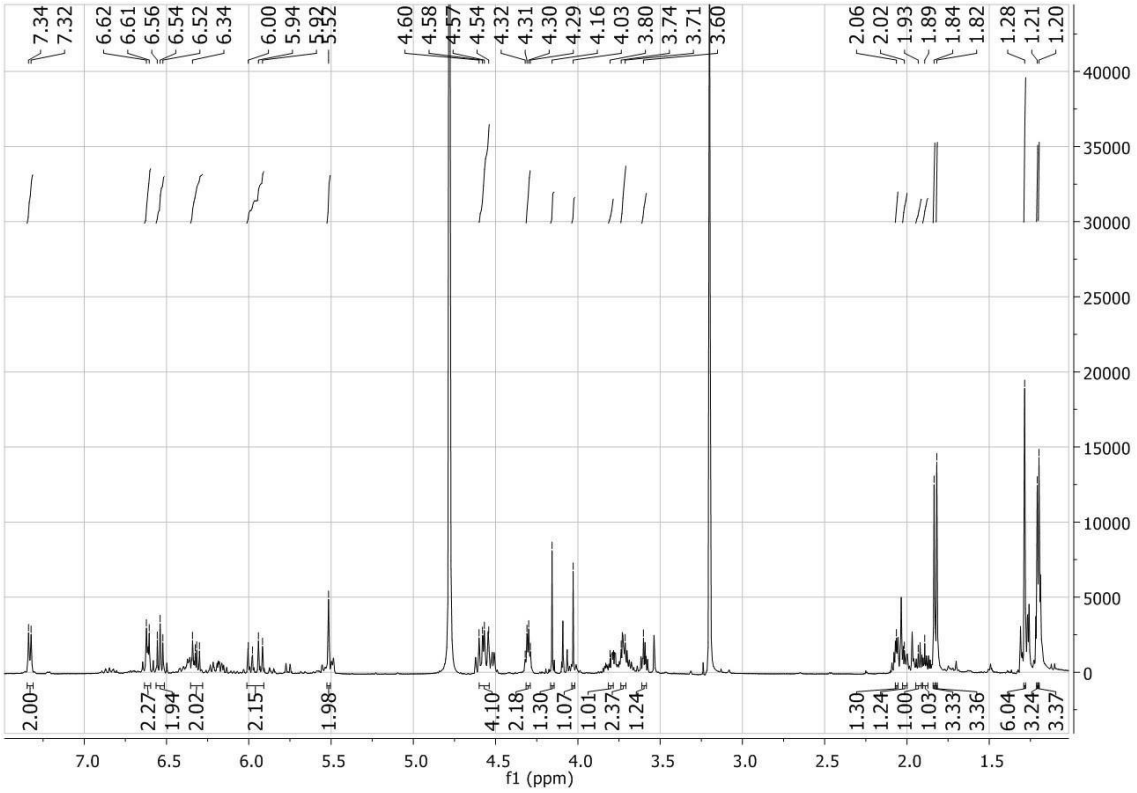
NYANSAPƆ WƆ SANE NO BADWENMA



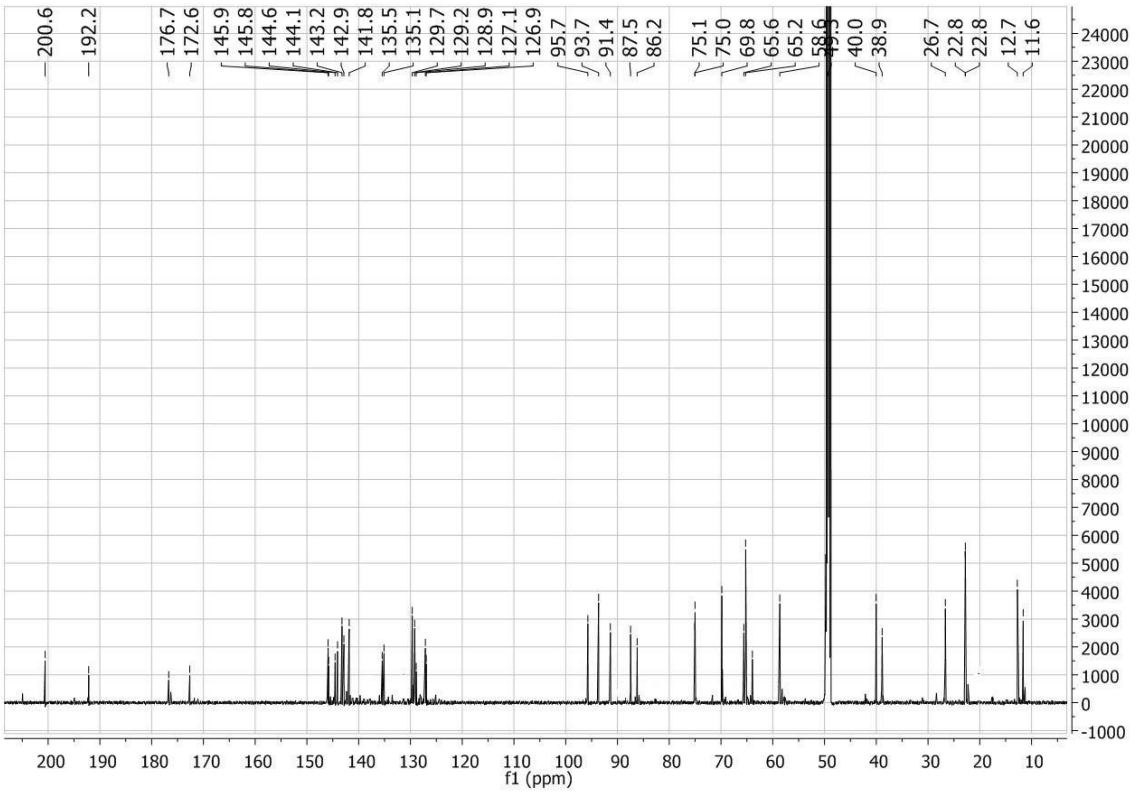
Appendix 126: Positive HRESI–MS spectrum of compounds **22**/**23**



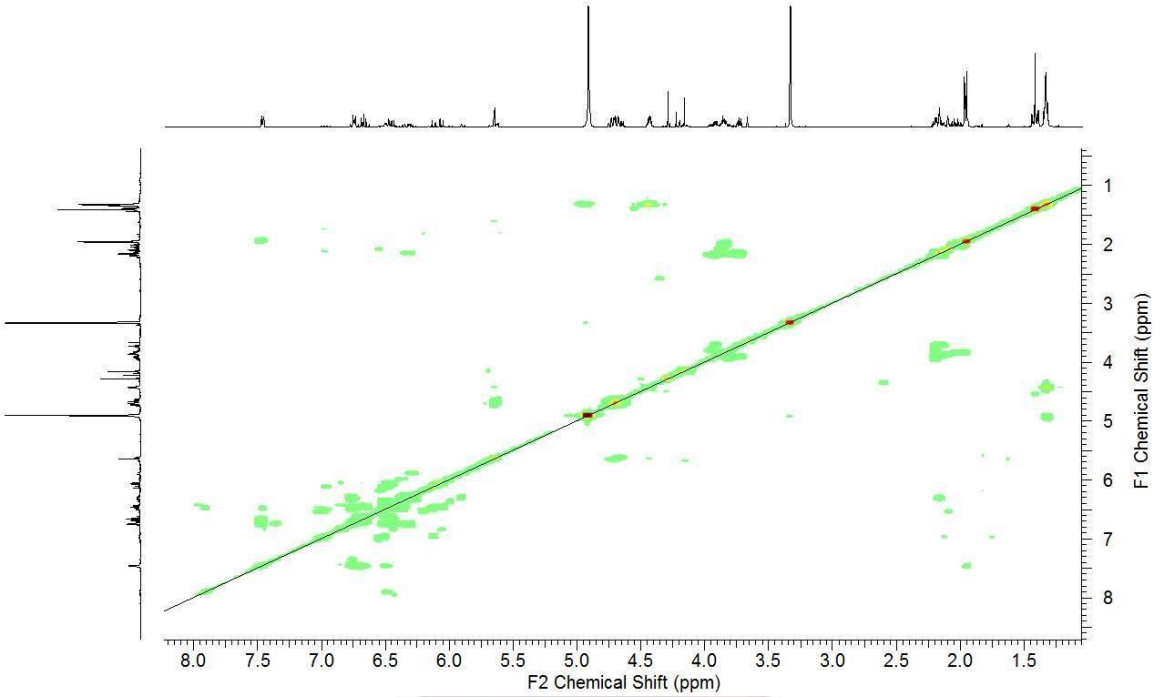
Appendix 127: Positive HRESI–MS/MS spectrum of compounds **22**/**23**



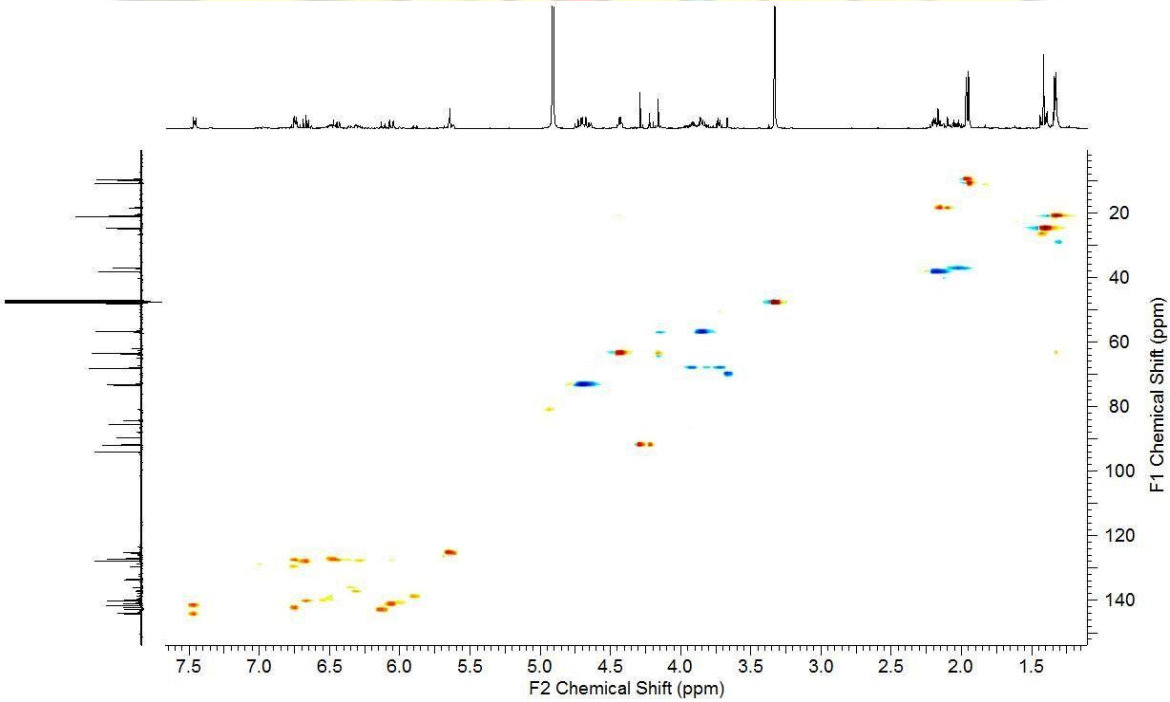
Appendix 128: ^{1}H NMR spectrum (CD_3OD, 600 MHz) of compounds **22**/**23**



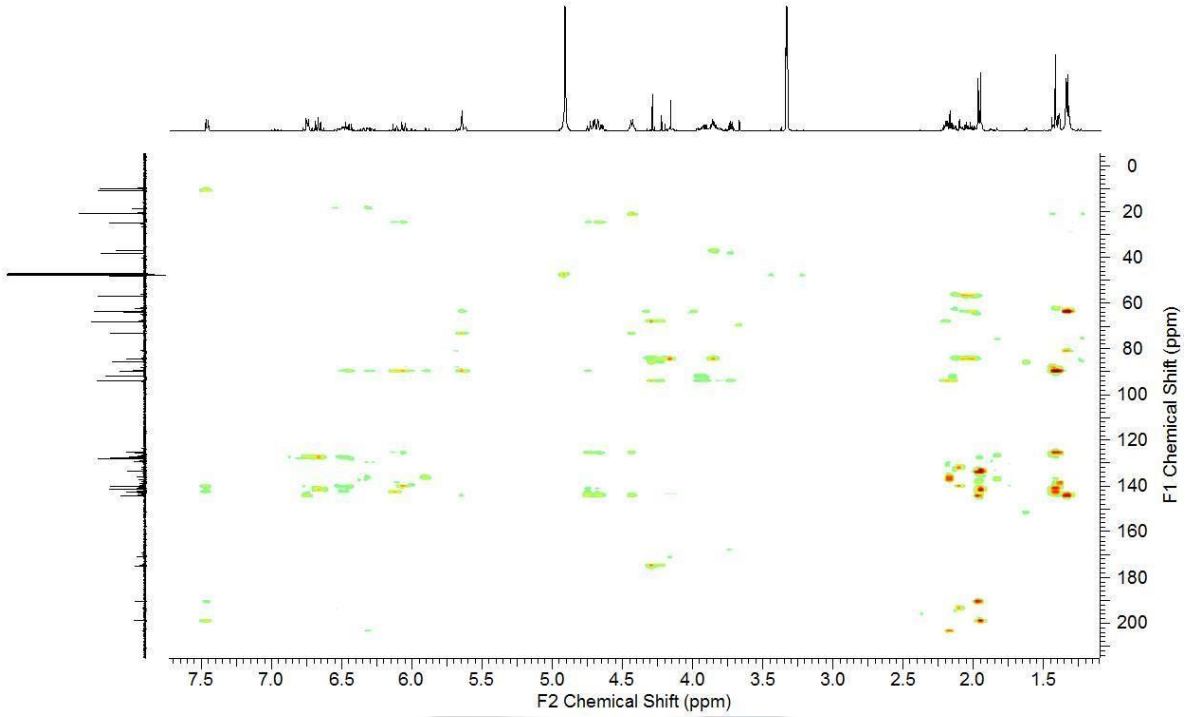
Appendix 129: ^{13}C NMR spectrum (CD_3OD, 150 MHz) of compounds **22**/**23**



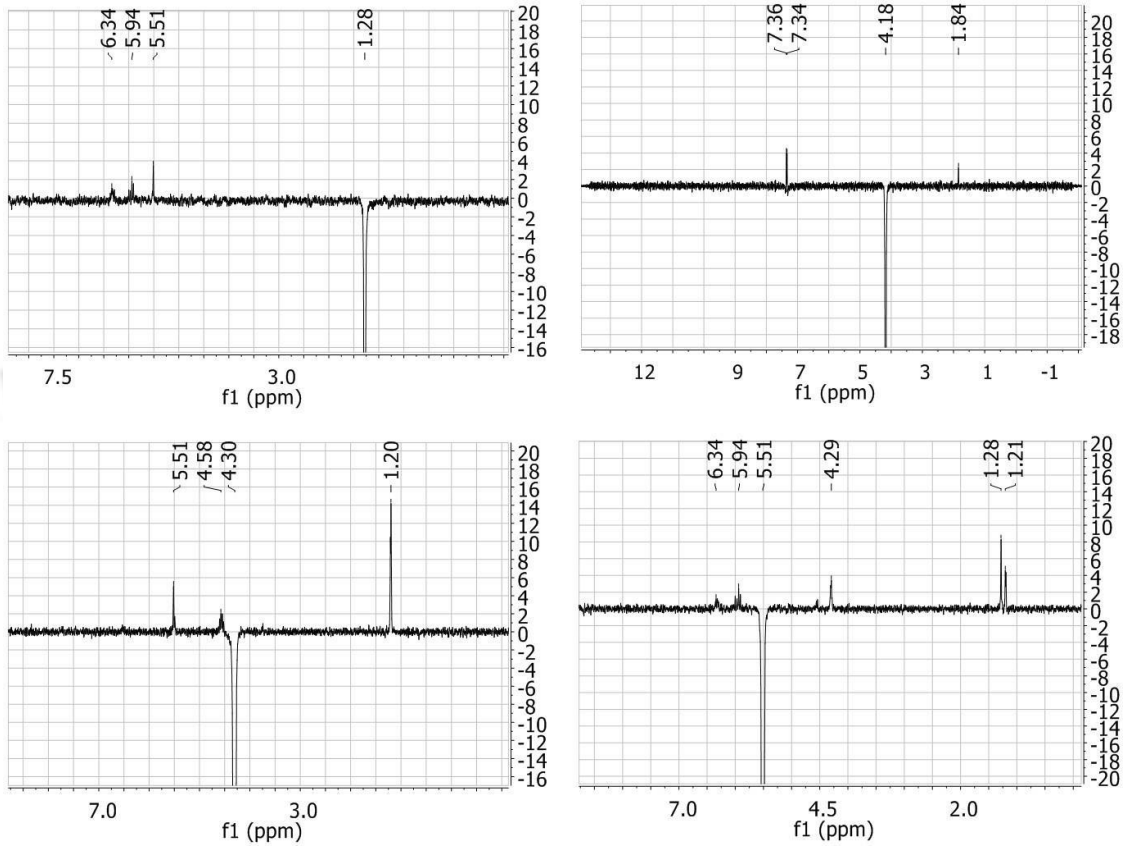
Appendix 130: $^{1}H–^{1}H$ COSY NMR spectrum (CD_3OD) of compounds **22**/**23**



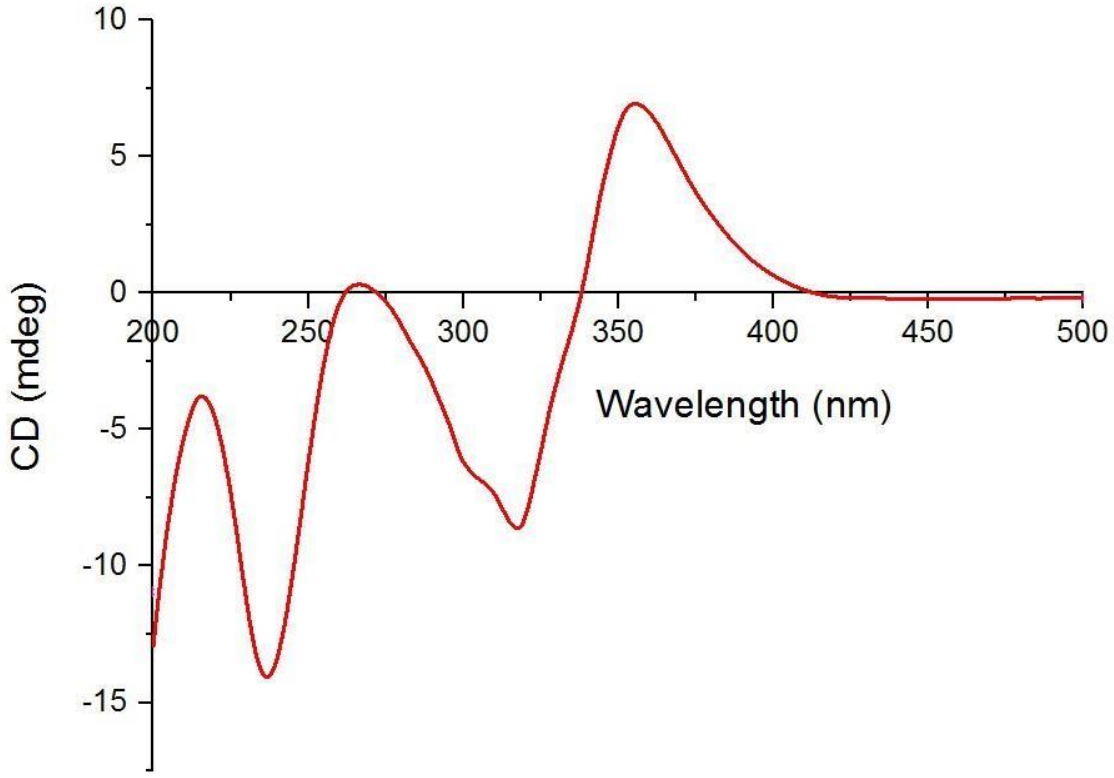
Appendix 131: HSQC NMR spectrum (CD_3OD) of compounds **22**/**23**



Appendix 132: HMBC NMR spectrum (CD_3OD) of compounds **22**/**23**

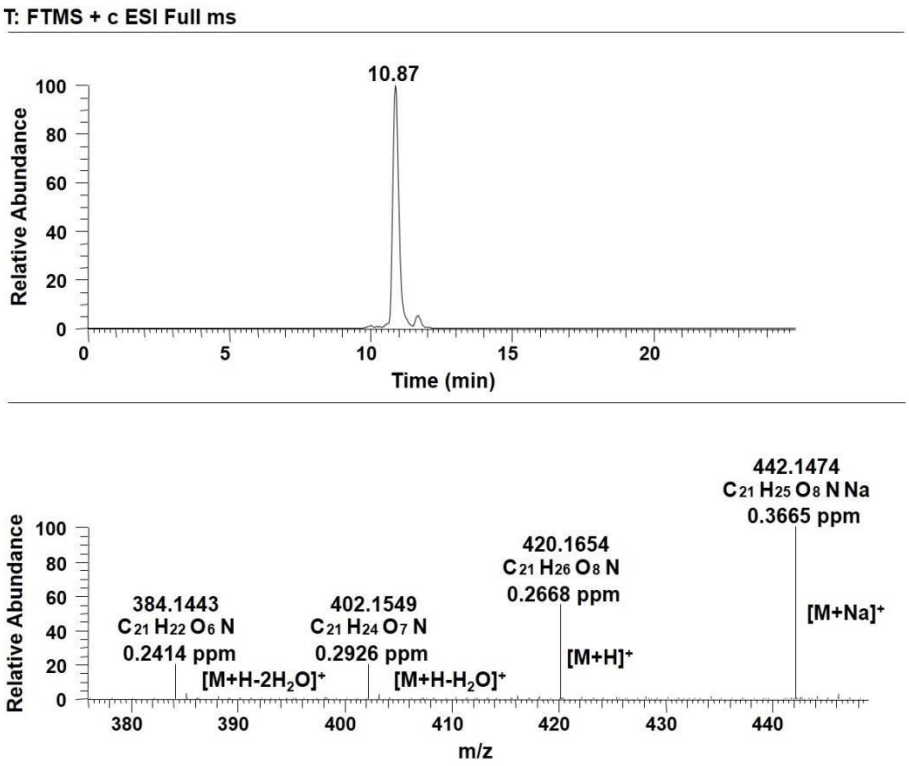


Appendix 133: 1D NOESY NMR spectrum (CD_3OD) of compounds **22**/**23**

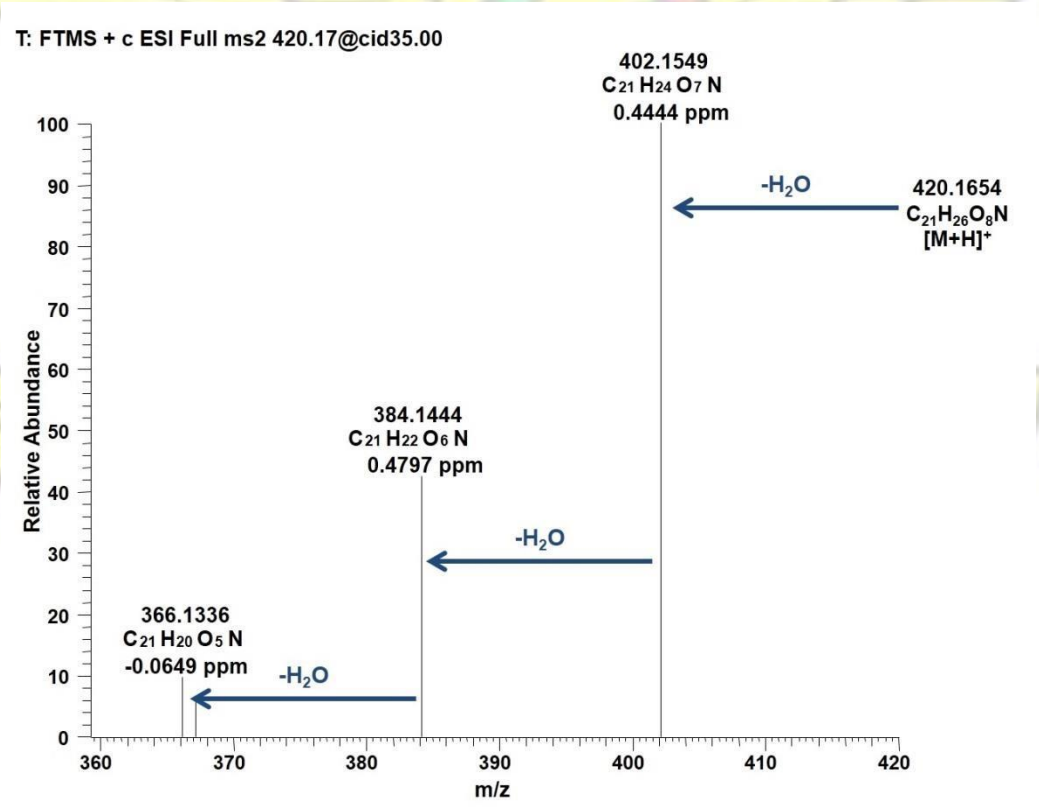


Appendix 134: Experimental electronic circular dichroism (ECD) spectrum (1.0 mg/mL, MeOH) of compounds **22**/**23**

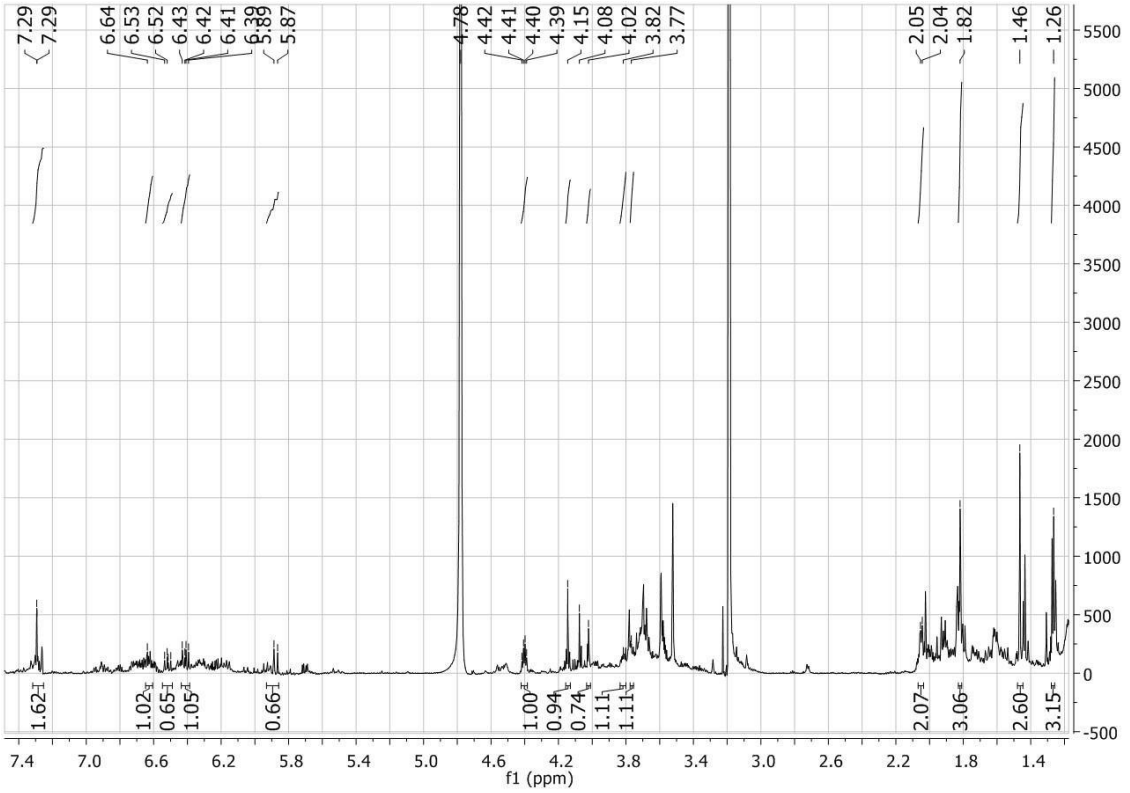
NYANSAPƆ W ƆSANE NO BADWENMA



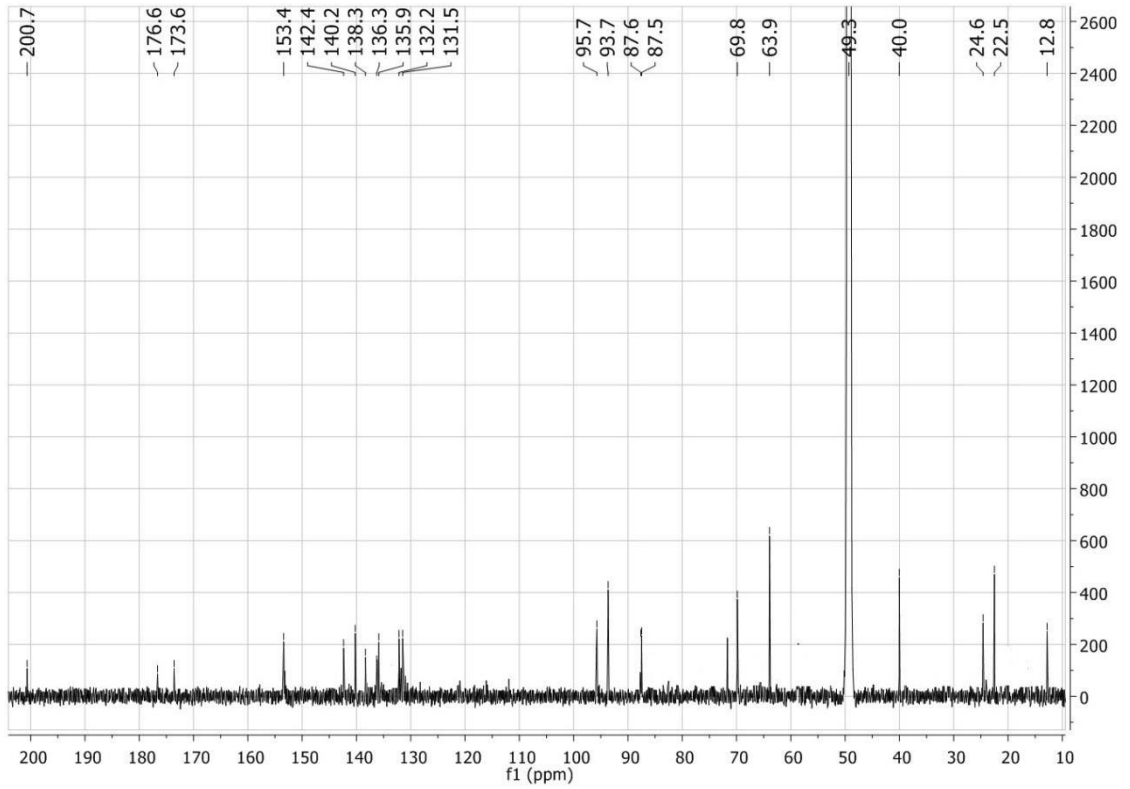
Appendix 135: Positive HRESI–MS spectrum of compound **24**



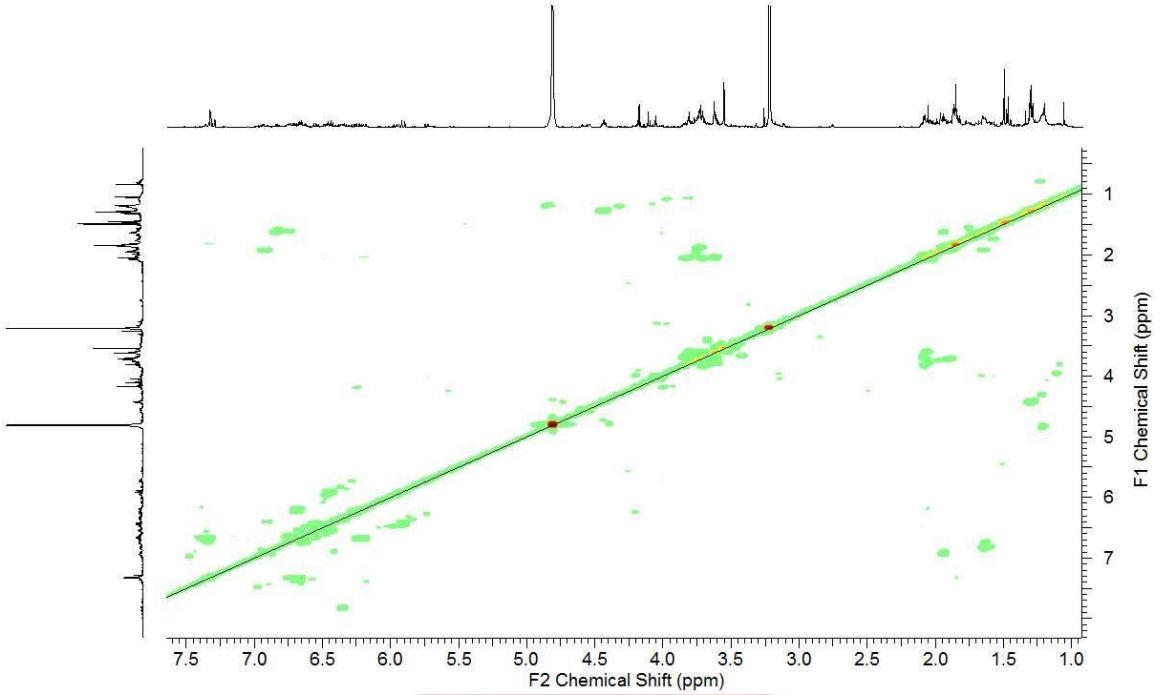
Appendix 136: Positive HRESI–MS/MS spectrum of compound **24**



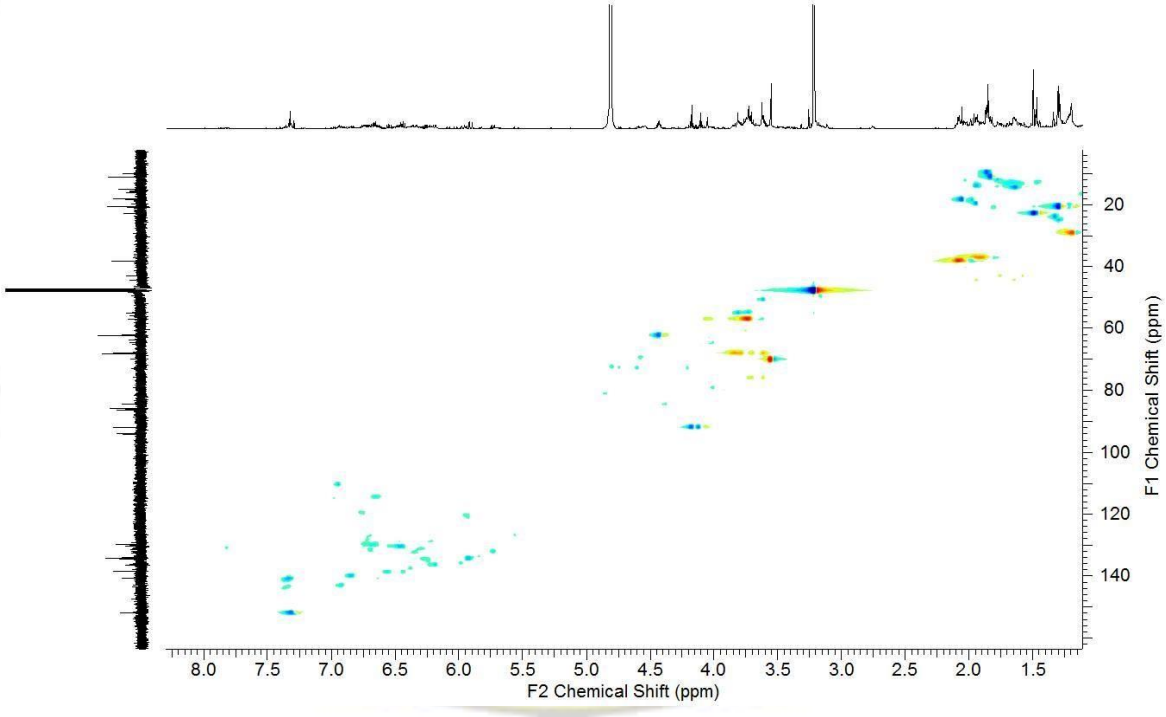
Appendix 137: ^{1}H NMR spectrum (CD_3OD, 700 MHz) of compound **24**



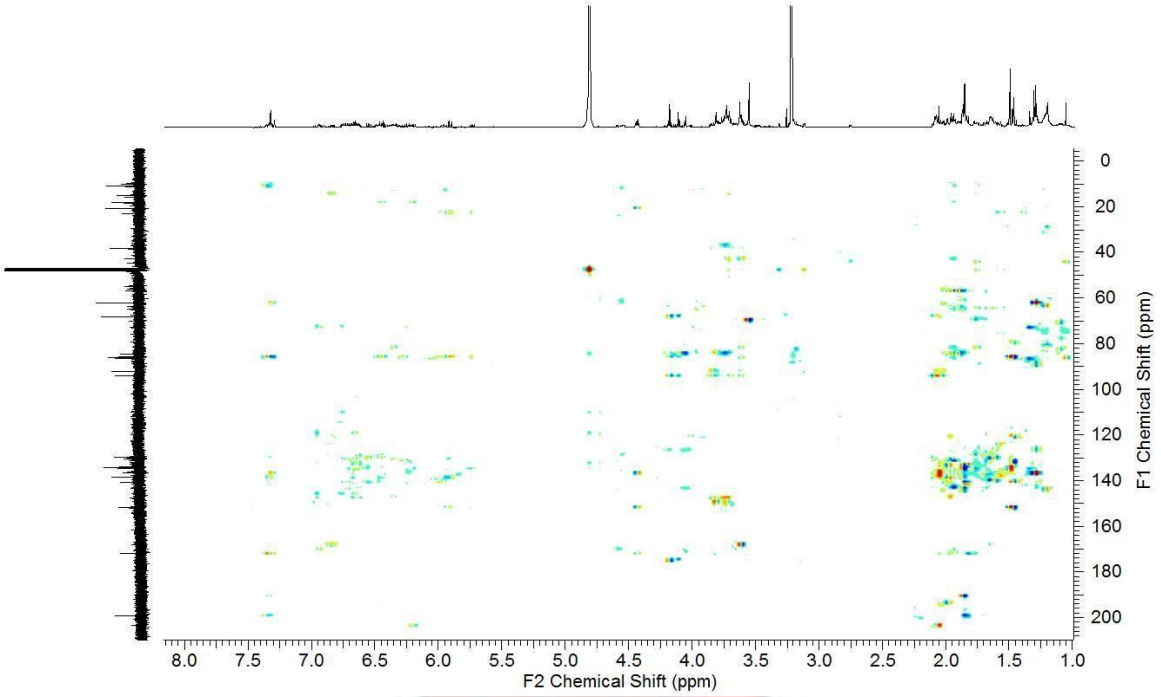
Appendix 138: ^{13}C NMR spectrum (CD_3OD, 176 MHz) of compound **24**



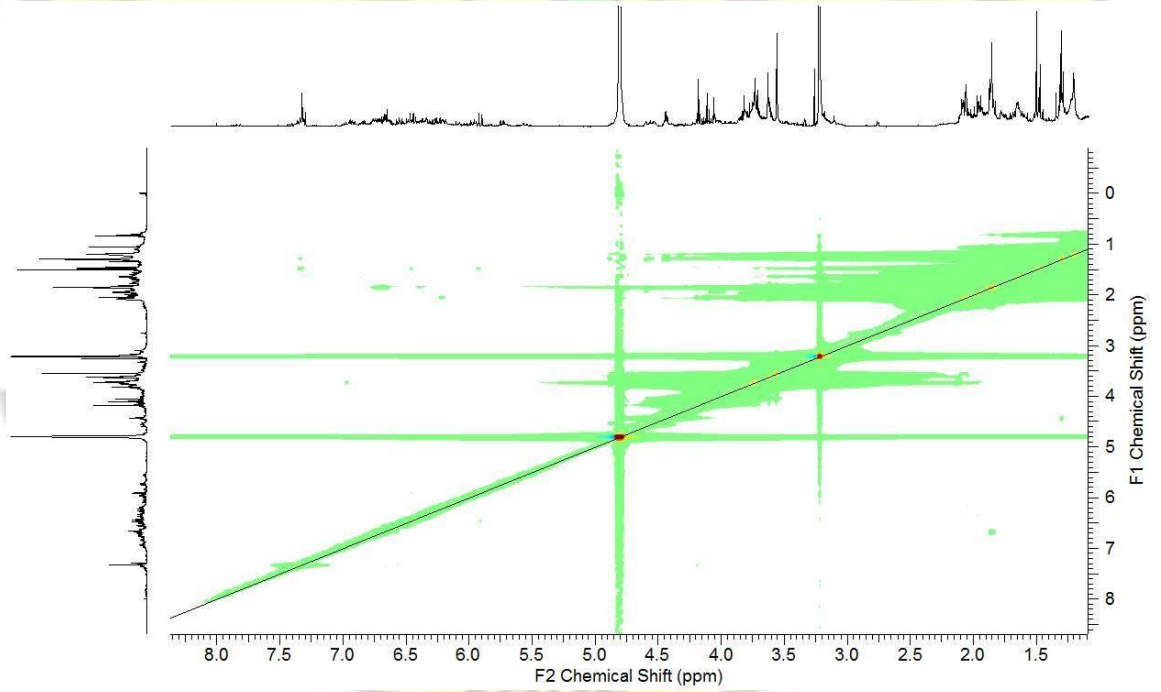
Appendix 139: $^{1}H–^{1}H$ COSY NMR spectrum (CD_3OD) of compound **24**



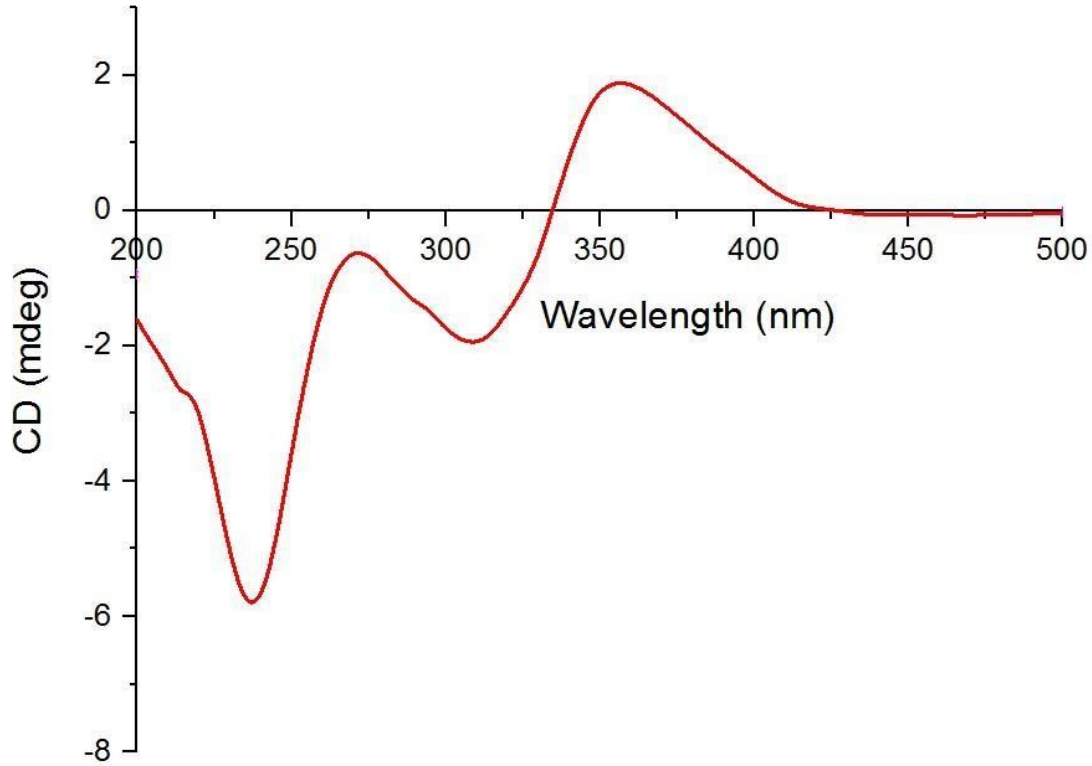
Appendix 140: HSQC NMR spectrum (CD_3OD) of compound **24**



Appendix 141: HMBC NMR spectrum (CD_3OD) of compound **24**

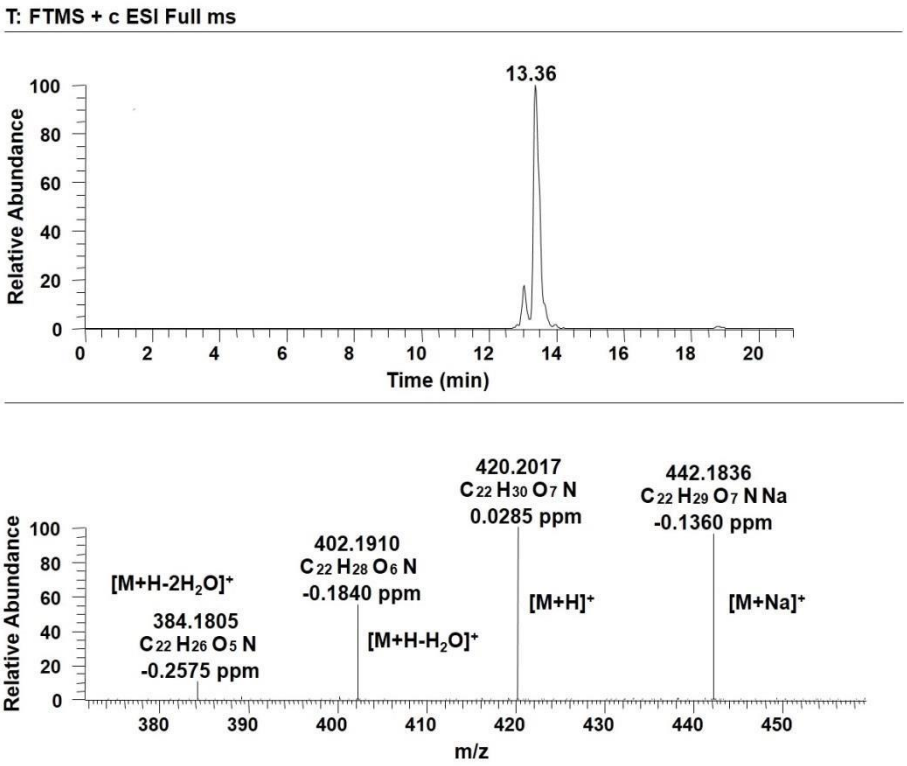


Appendix 142: NOESY NMR spectrum (CD_3OD) of compound **24**

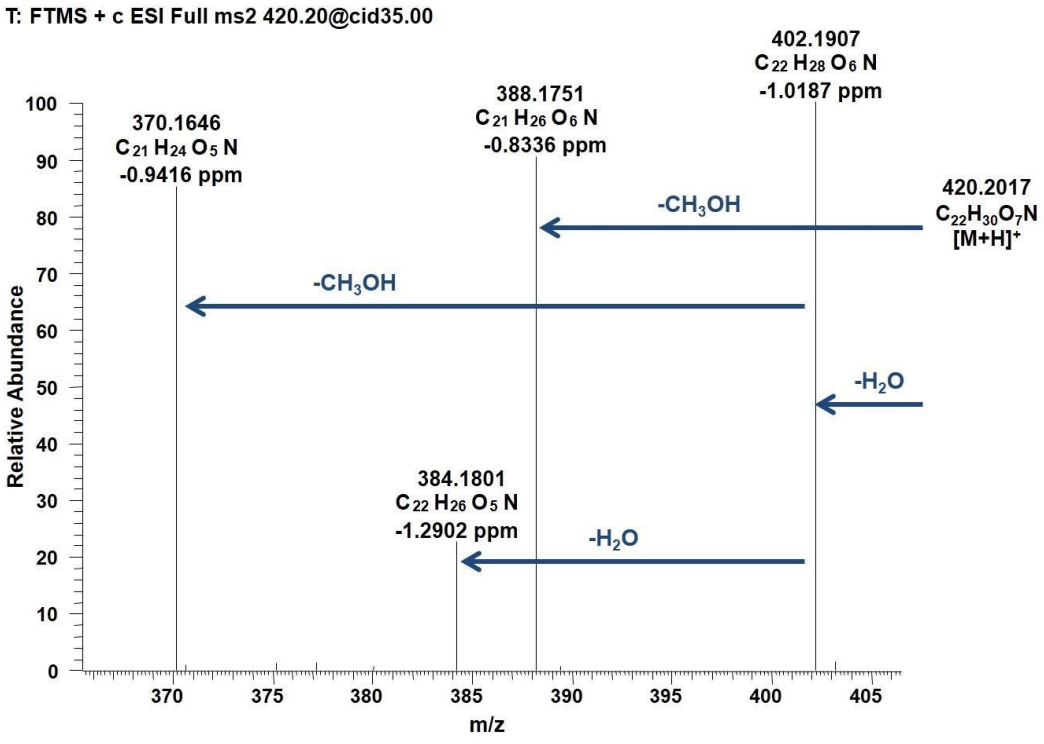


Appendix 143: Experimental electronic circular dichroism (ECD) spectrum (1.0 mg/mL, MeOH) of compound **24**

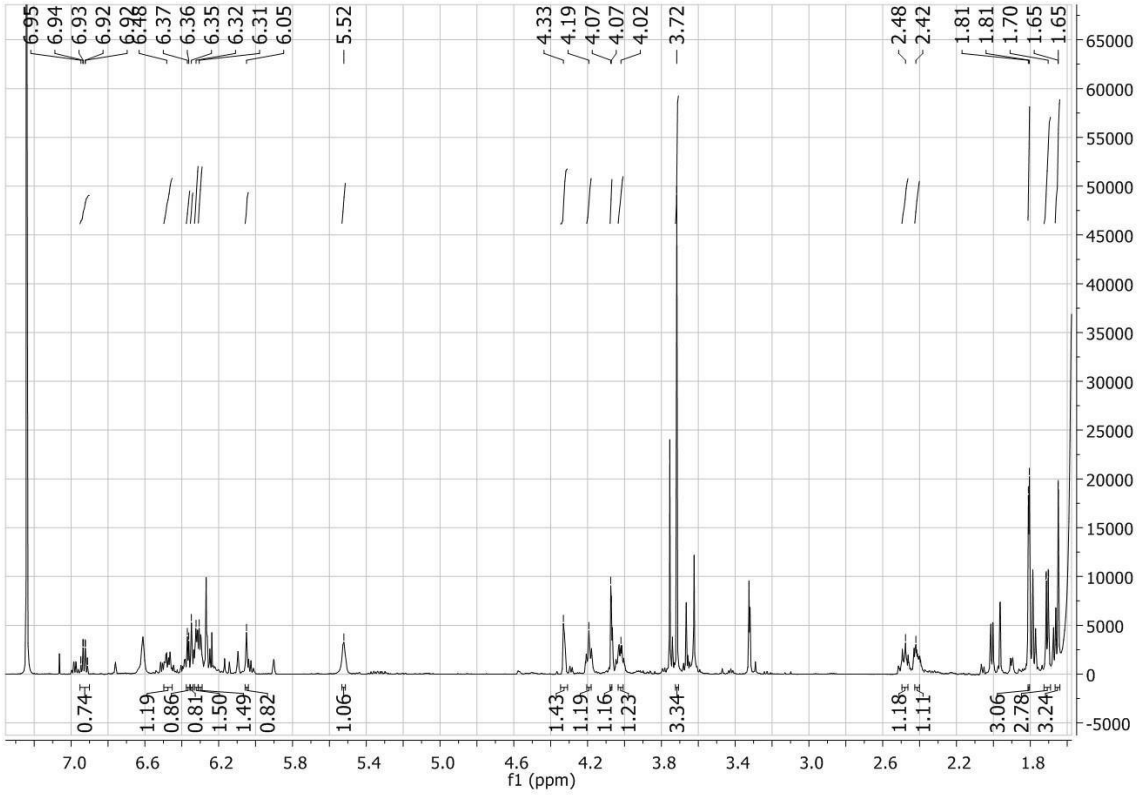
NYANSAPƆ W ƆSANE NO BADWENMA



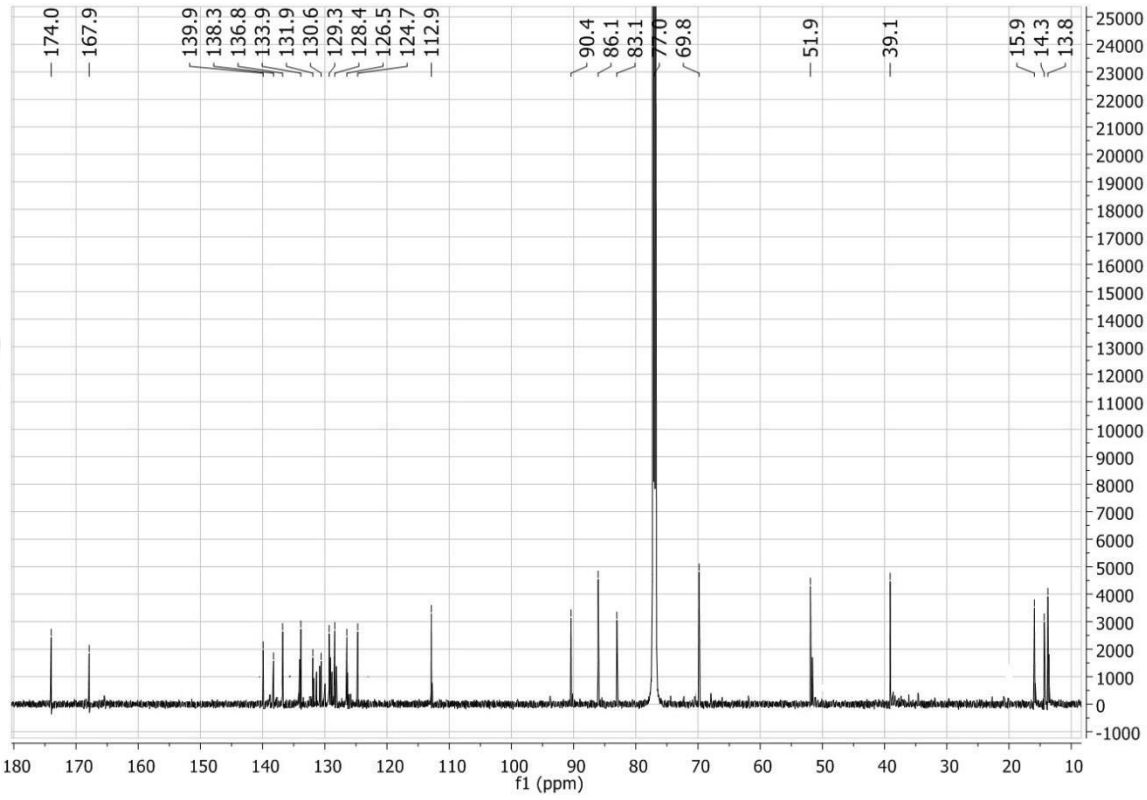
Appendix 144: Positive HRESI–MS spectrum of compound **25**



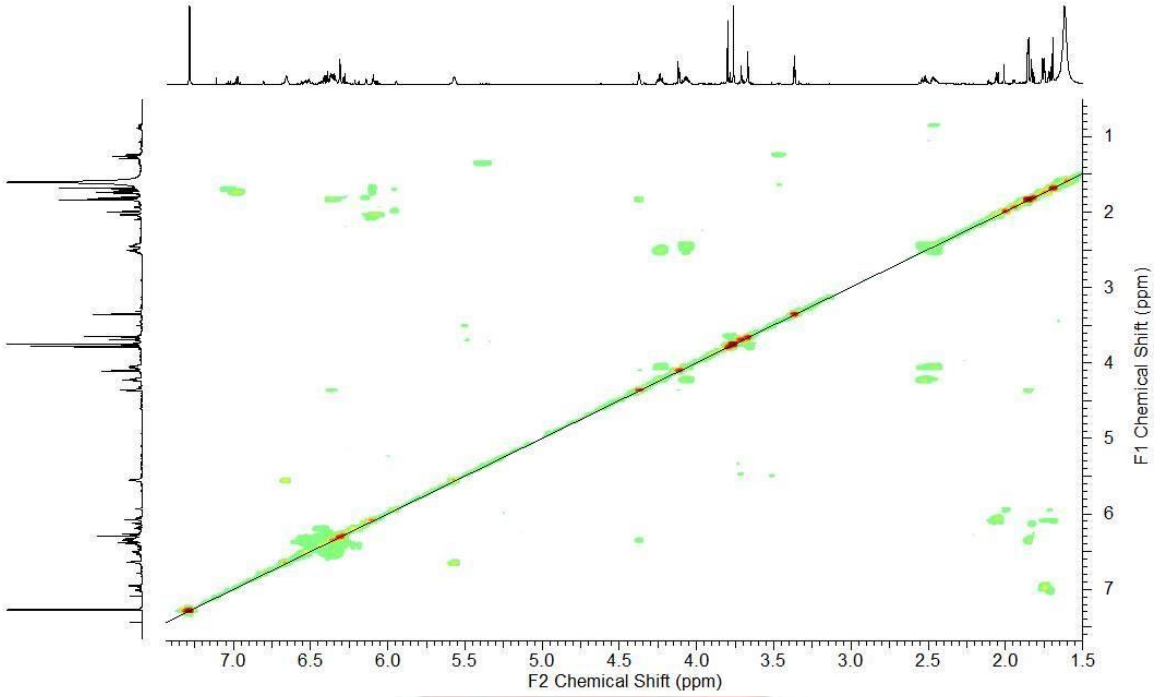
Appendix 145: Positive HRESI–MS/MS spectrum of compound **25**



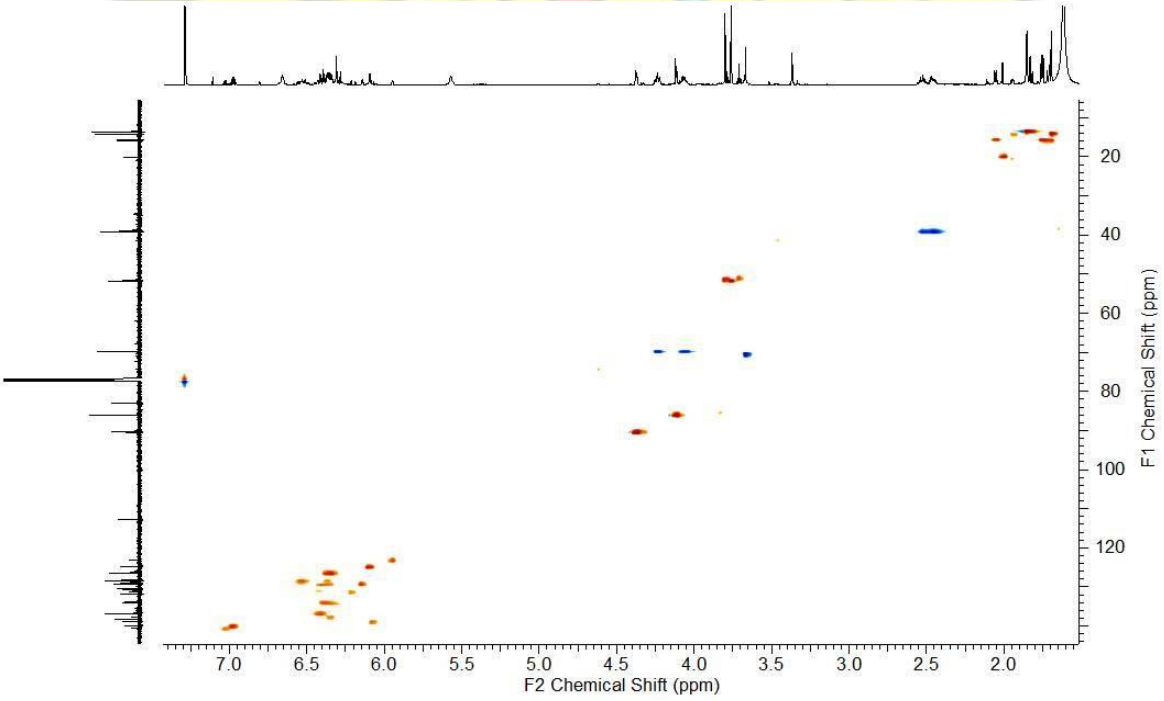
Appendix 146: ^{1}H NMR spectrum ($CDCl_3$, 600 MHz) of compound **25**



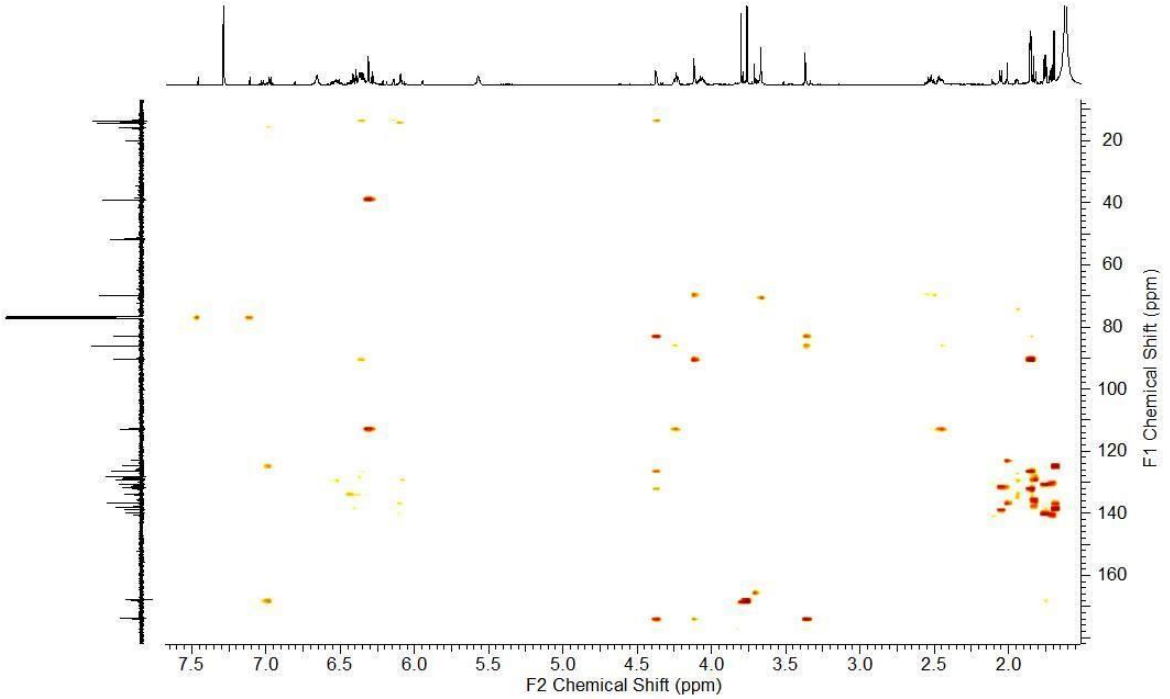
Appendix 147: ^{13}C NMR spectrum ($CDCl_3$, 150 MHz) of compound **25**



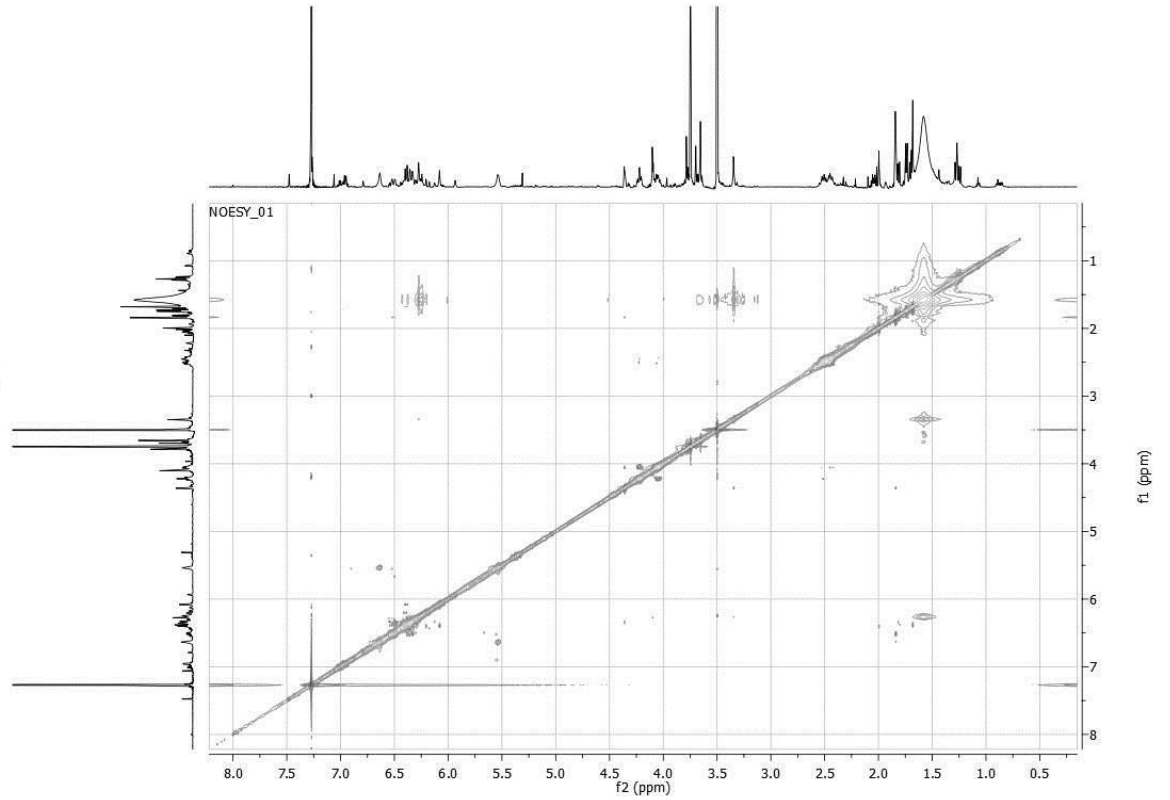
Appendix 148: $^{1}H–^{1}H$ COSY NMR spectrum ($CDCl_3$) of compound **25**



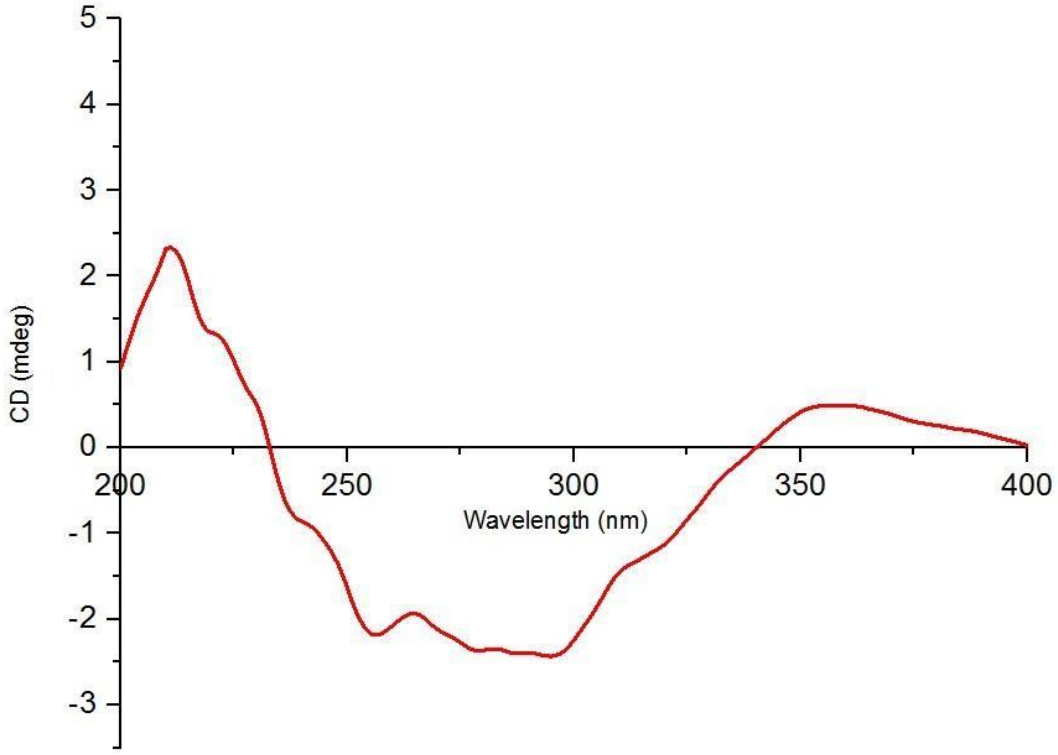
Appendix 149: HSQC NMR spectrum ($CDCl_3$) of compound **25**



Appendix 150: HMBC NMR spectrum ($CDCl_3$) of compound **25**

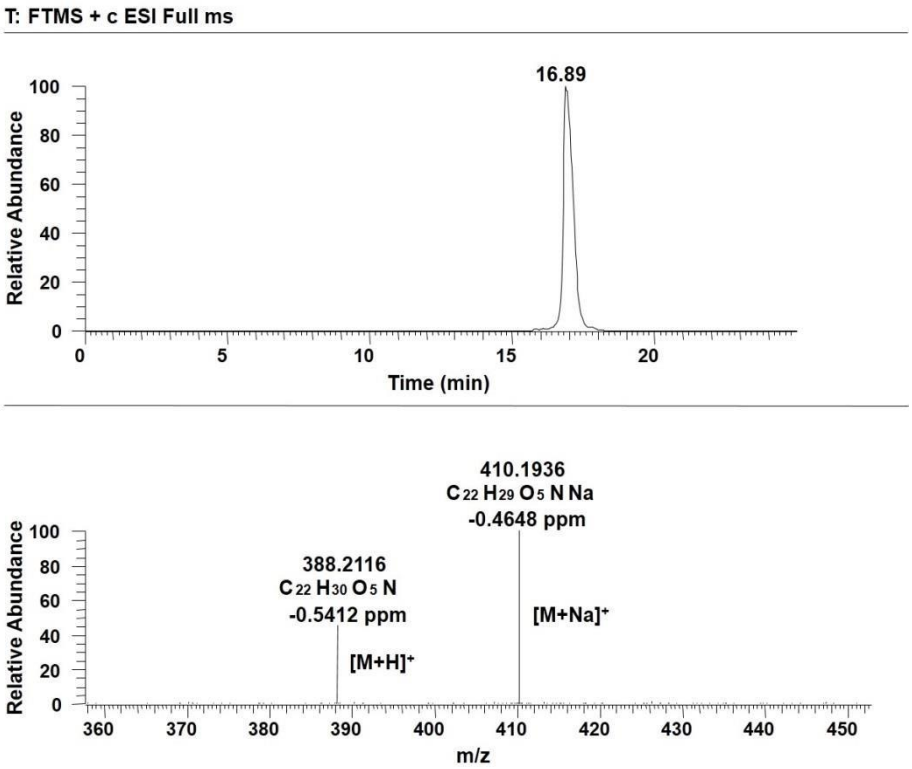


Appendix 151: NOESY NMR spectrum ($CDCl_3$) of compound **25**

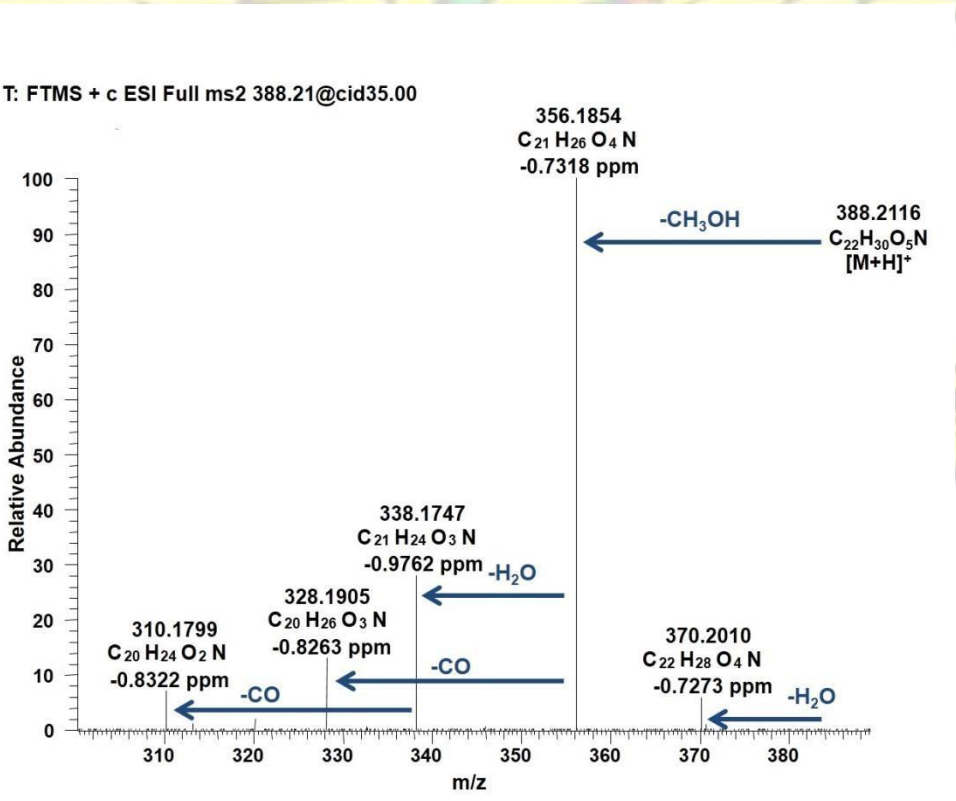


Appendix 152: Experimental electronic circular dichroism (ECD) spectrum (1.0 mg/mL, MeOH) of compound **25**

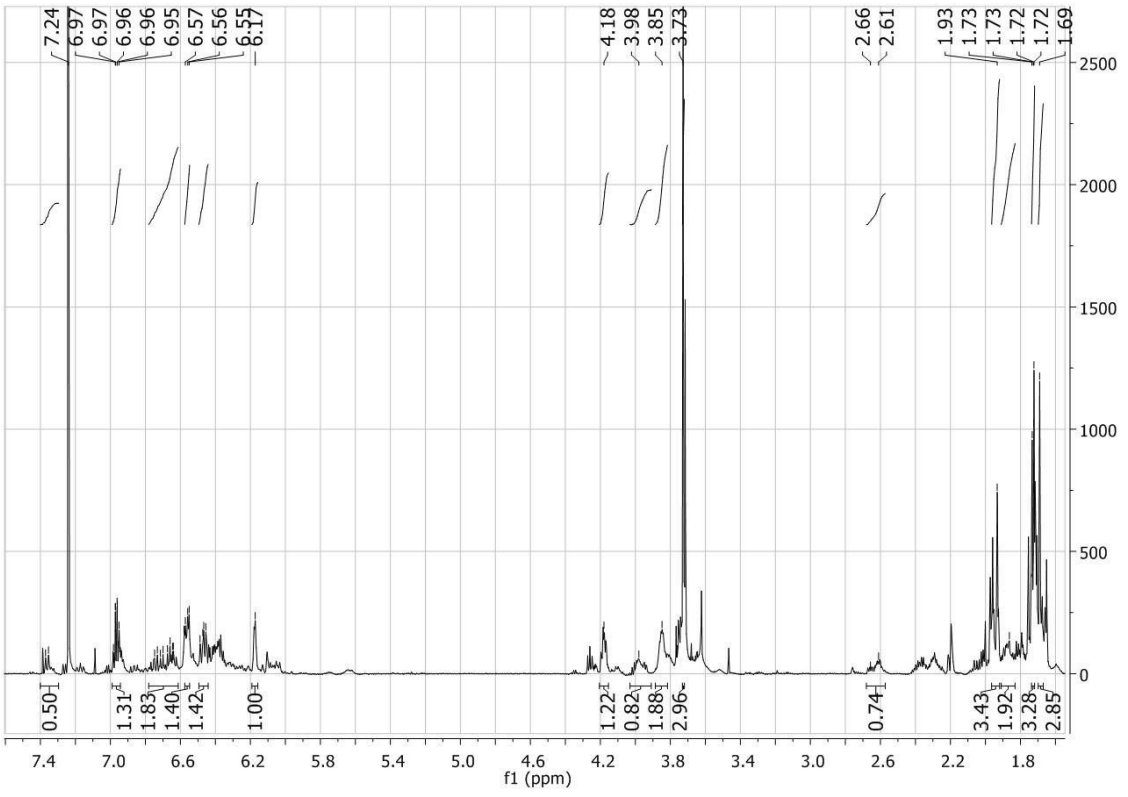
NYANSAPƆ W ƆSANE NO BADWENMA



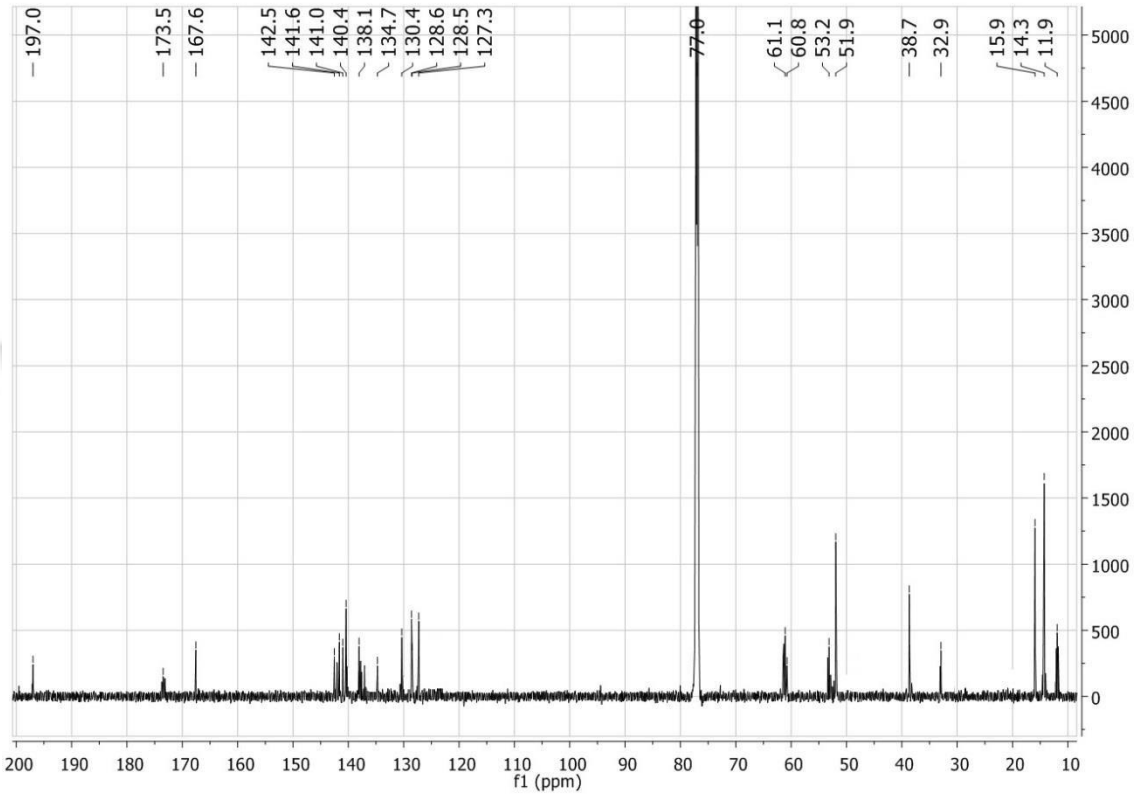
Appendix 153: Positive HRESI–MS spectrum of compound **26**



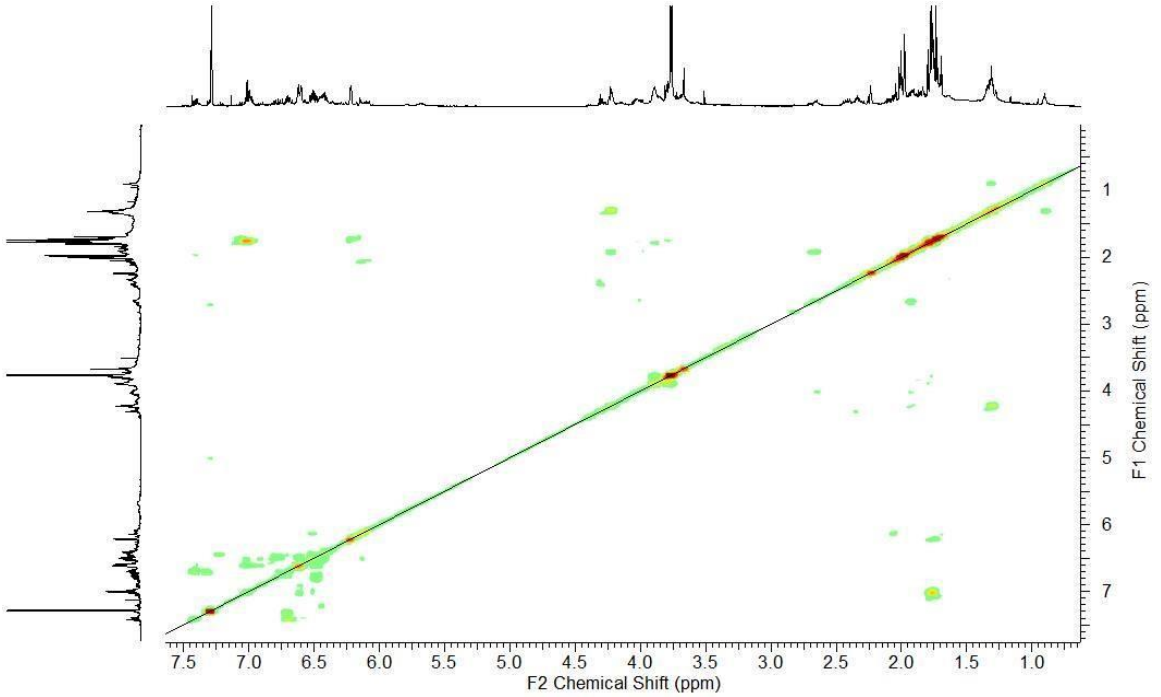
Appendix 154: Positive HRESI–MS/MS spectrum of compound **26**



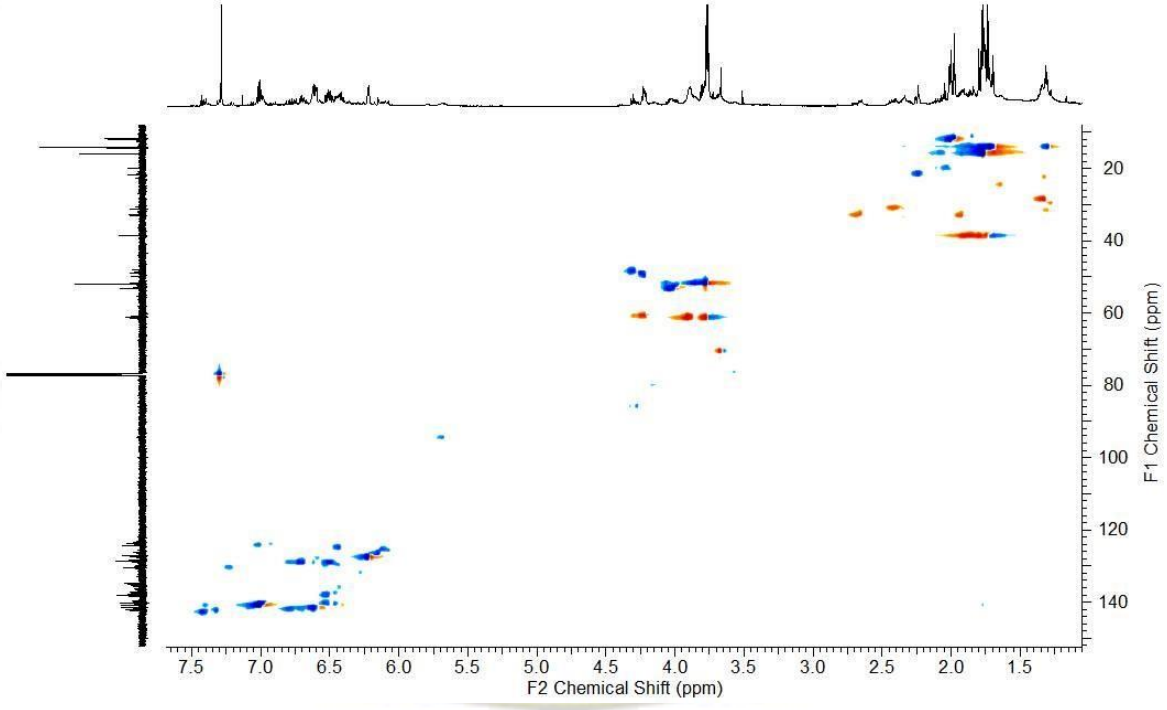
Appendix 155: ^{1}H NMR spectrum ($CDCl_3$, 700 MHz) of compound **26**



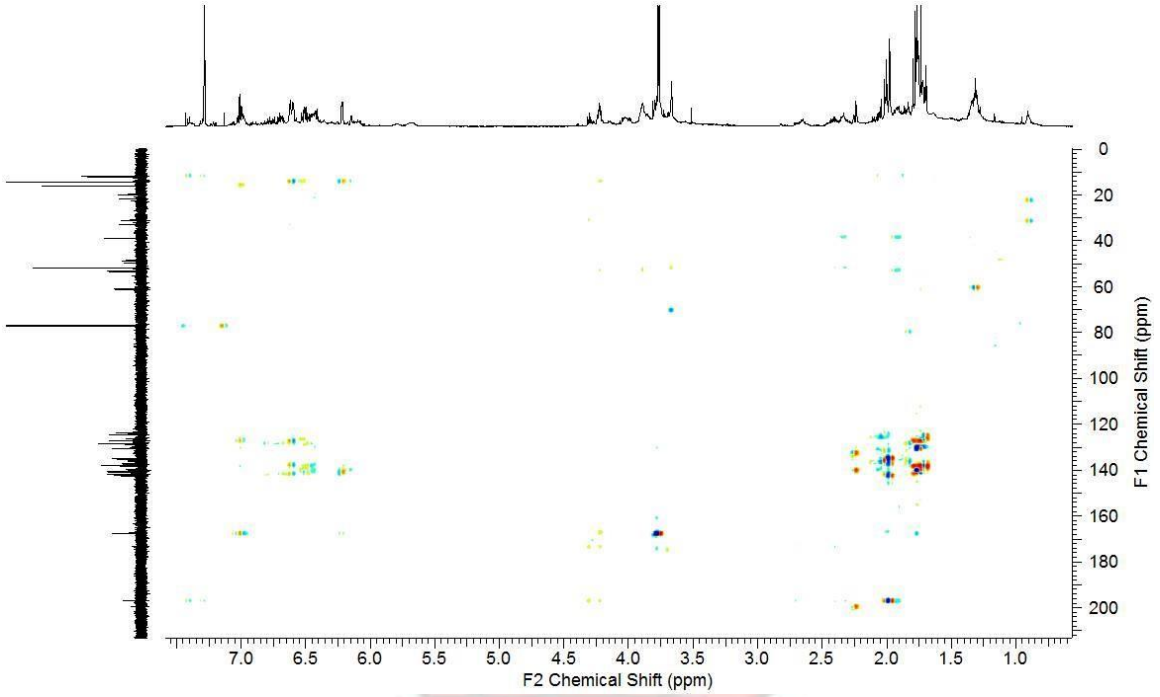
Appendix 156: ^{13}C NMR spectrum ($CDCl_3$, 176 MHz) of compound **26**



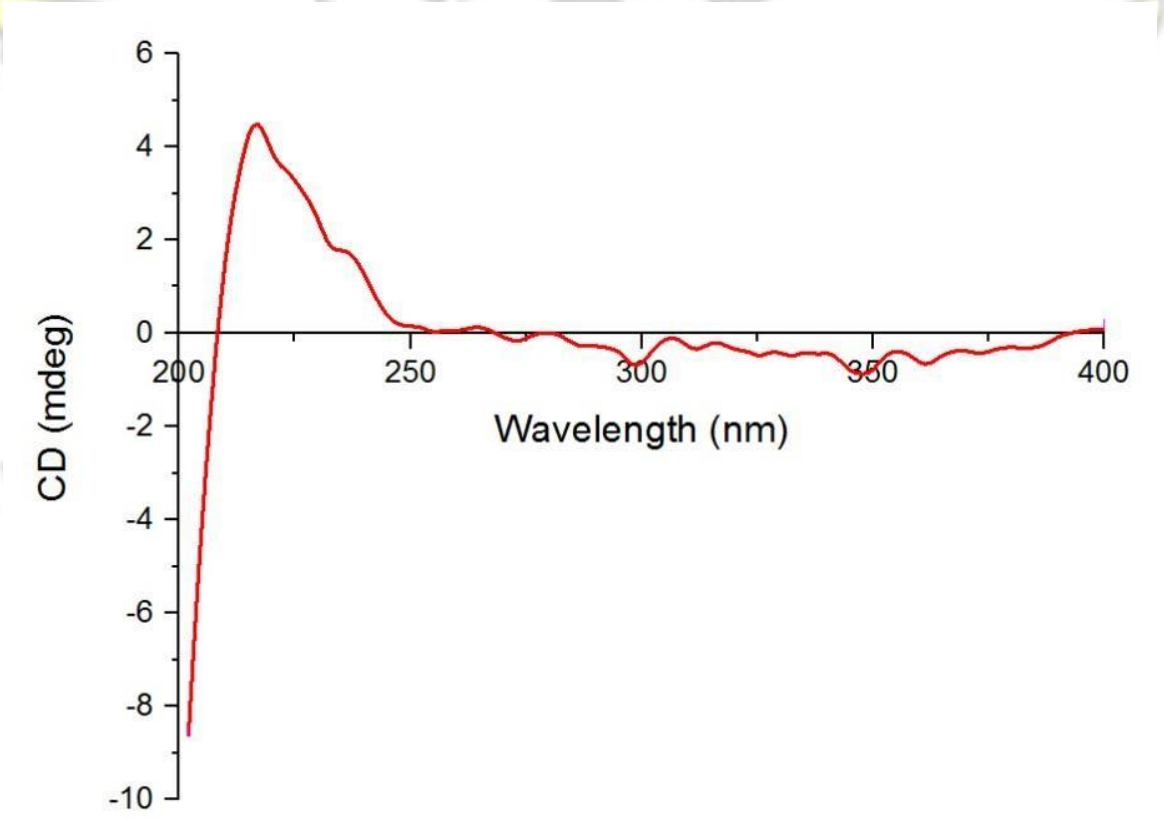
Appendix 157: $^{1}H–^{1}H$ COSY NMR spectrum ($CDCl_3$) of compound **26**



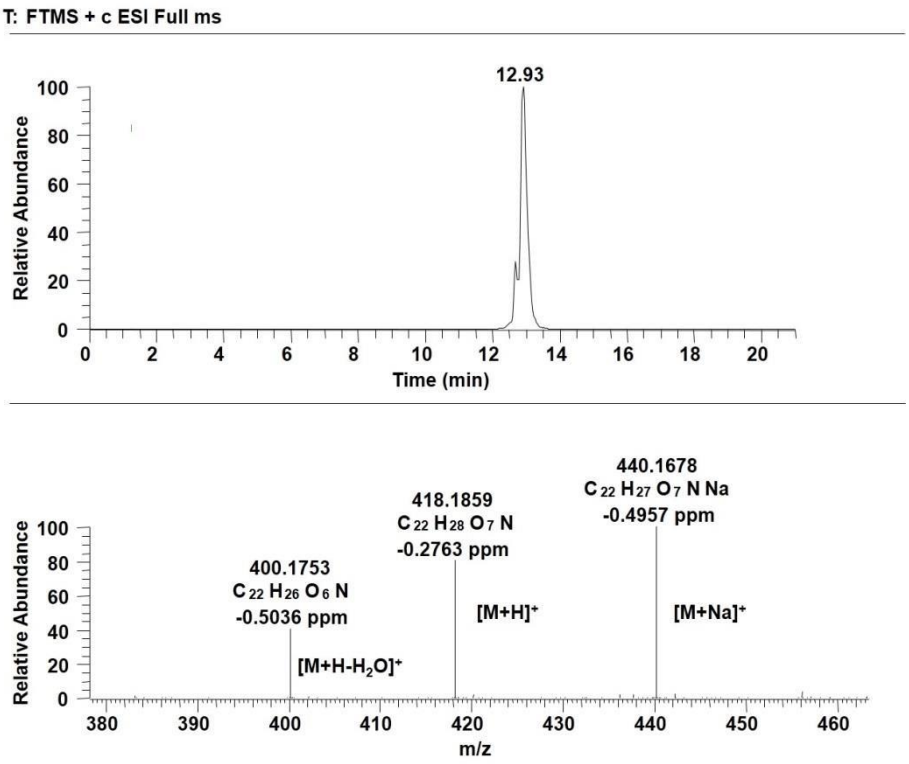
Appendix 158: HSQC NMR spectrum ($CDCl_3$) of compound **26**



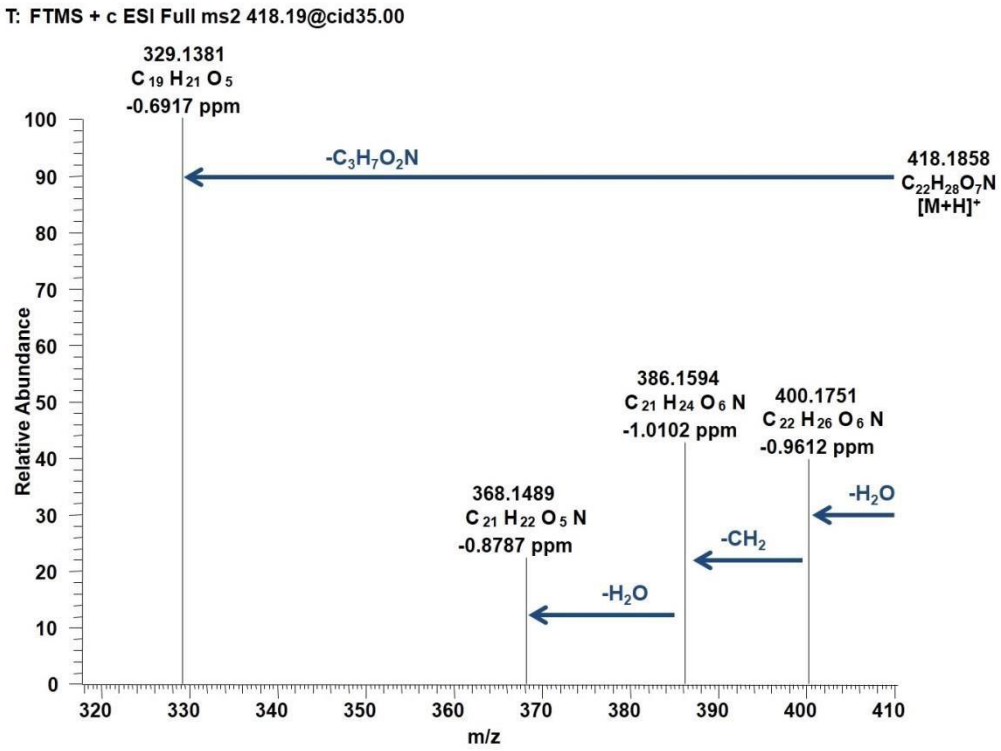
Appendix 159: HMBC NMR spectrum ($CDCl_3$) of compound **26**



Appendix 160: Experimental electronic circular dichroism (ECD) spectrum (1.0 mg/mL, MeOH) of compound **26**

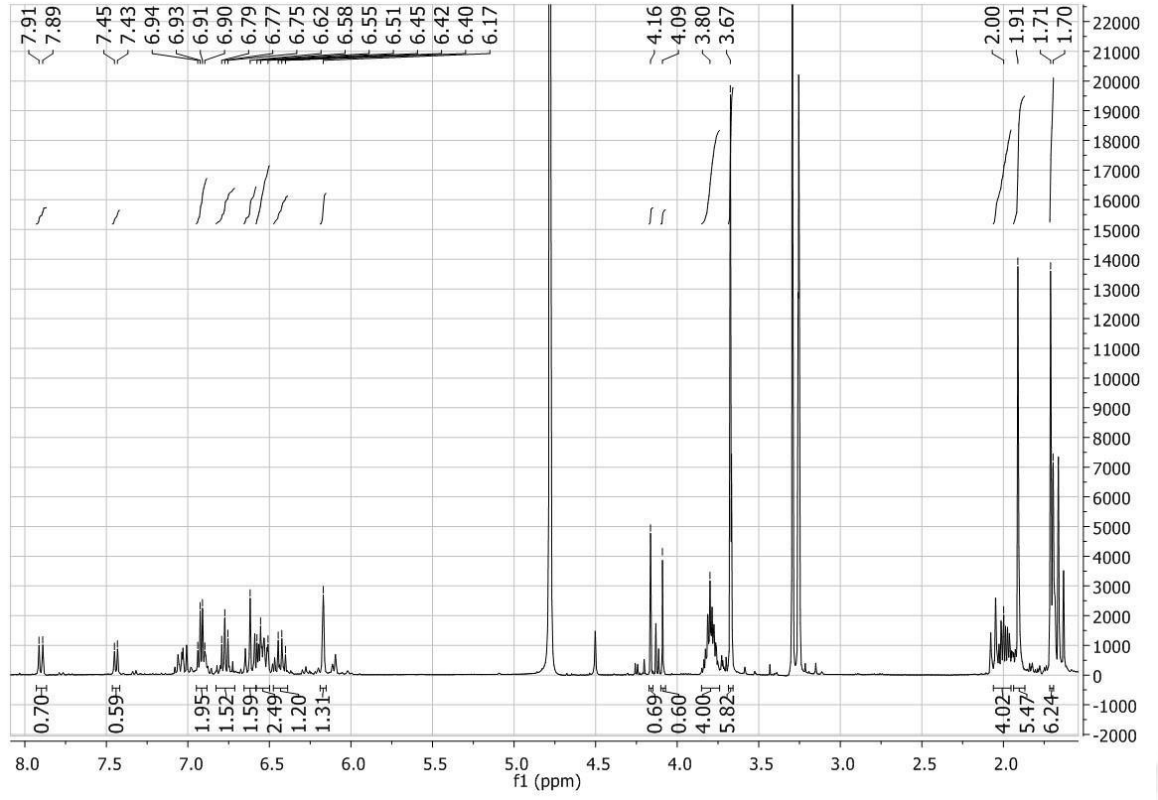


Appendix 161: Positive HRESI–MS spectrum of compound **27**/**28**



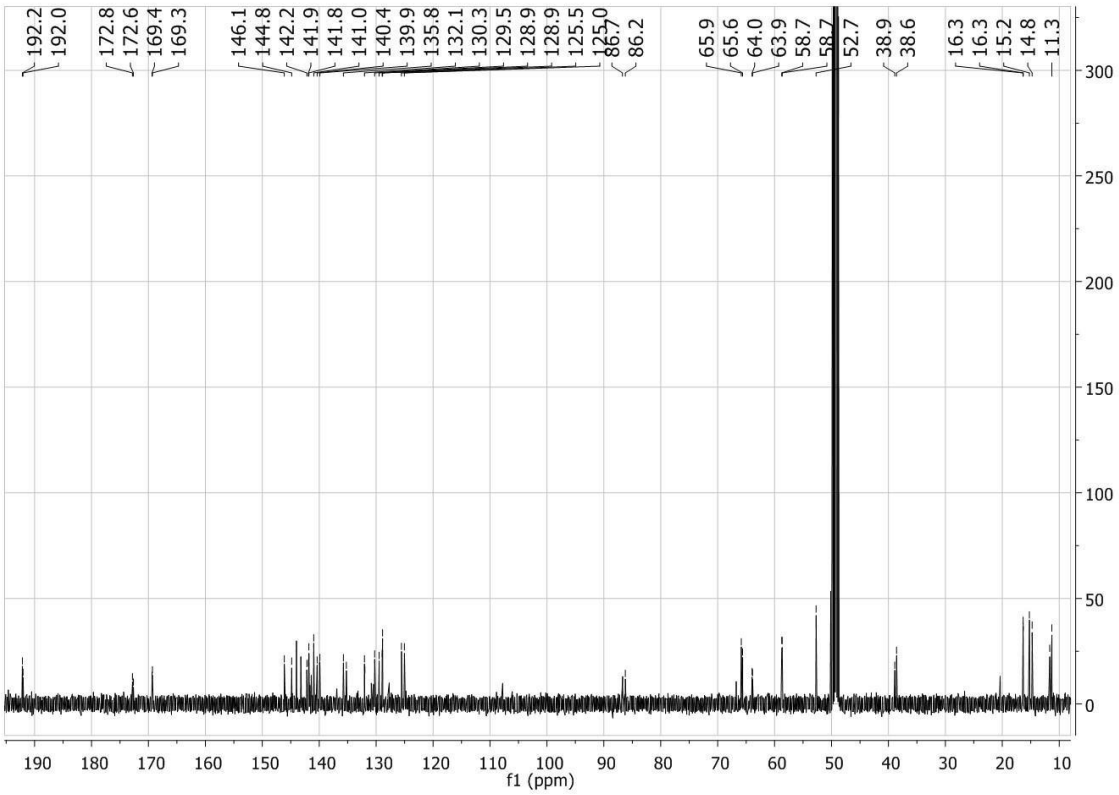
Appendix

162: Positive HRESI–MS/MS spectrum of compound **27**/**28**

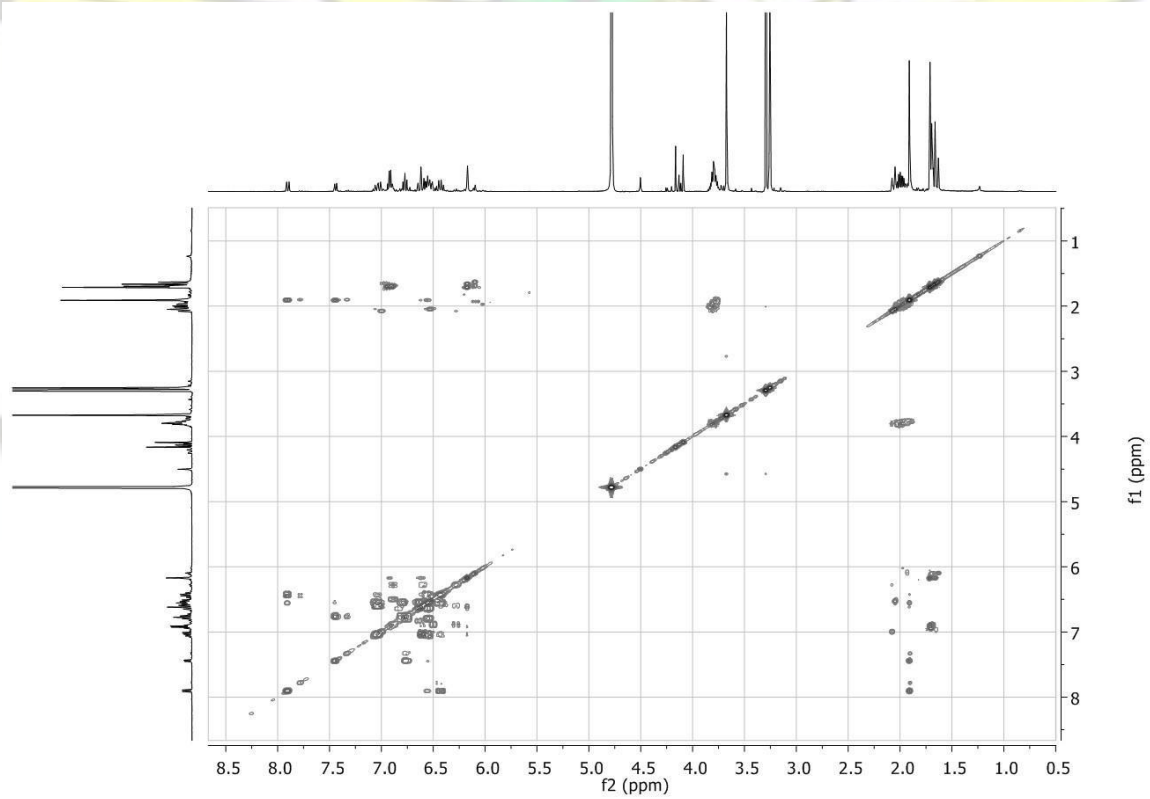


Appendix 163: ^{1}H NMR spectrum (CD_3OD, 500 MHz) of compound **27**/**28**

Appendix

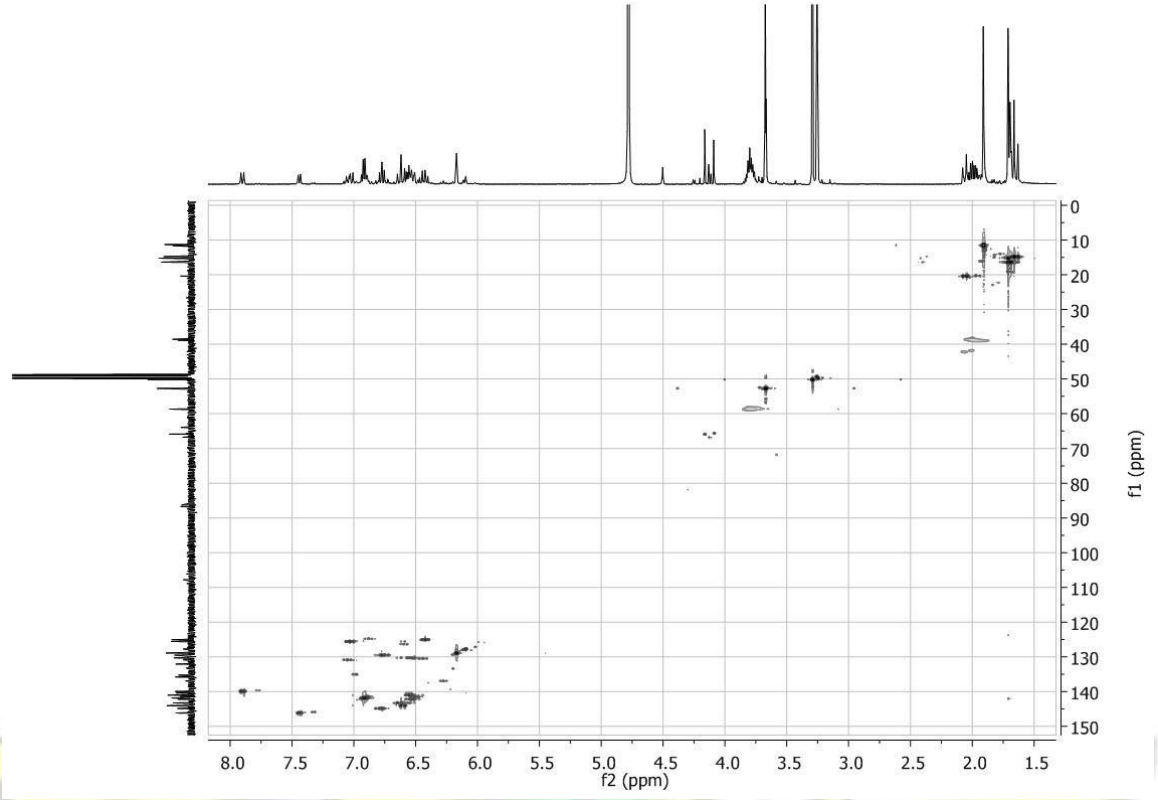


164: ^{13}C NMR spectrum (CD_3OD, 150 MHz) of compound **27**/**28**



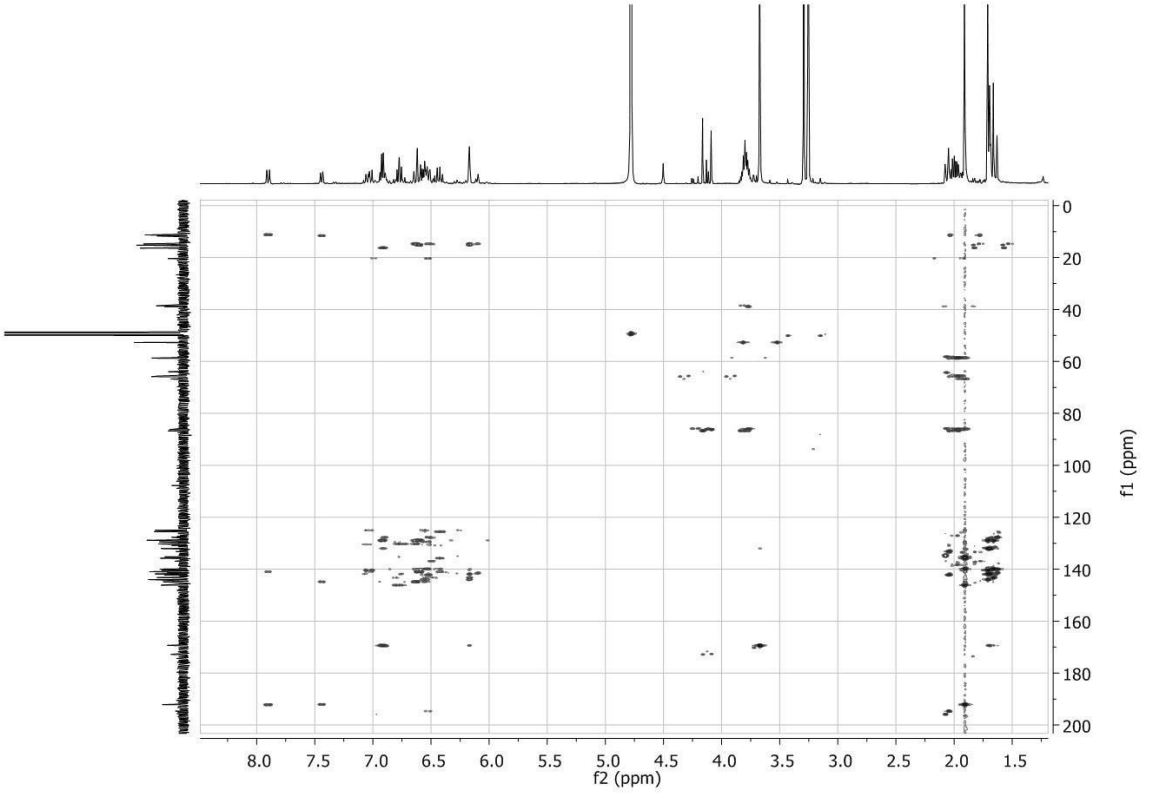
Appendix 165: ^{1}H–^{1}H COSY NMR spectrum (CD_3OD) of compound **27**/**28**

Appendix



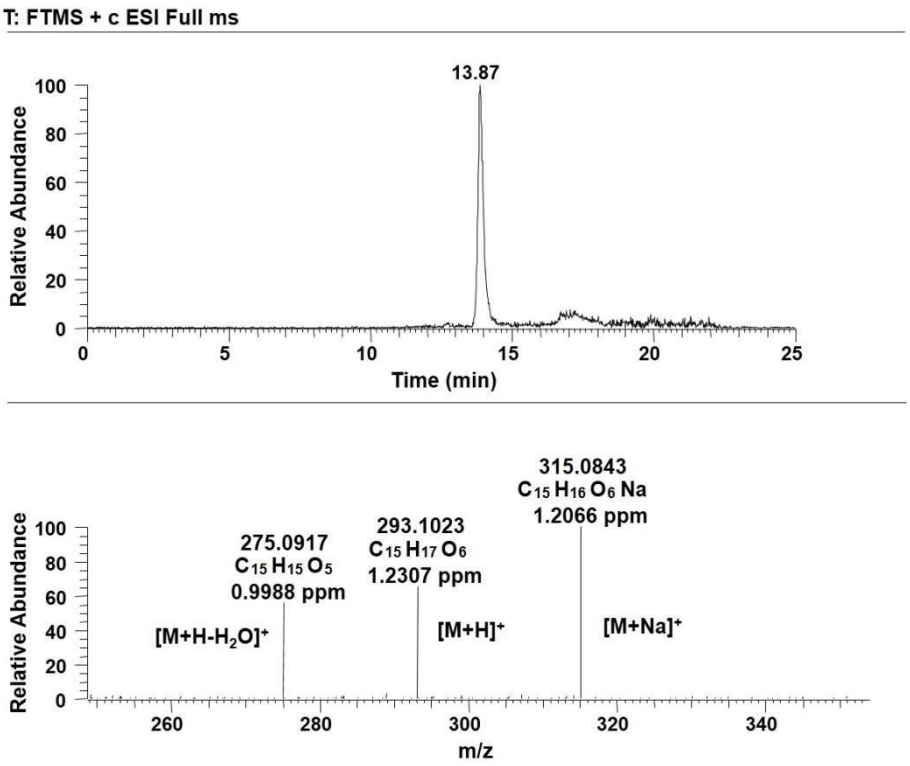
166: HSQC NMR spectrum (CD_3OD) of compound **27**/**28**

Appendix

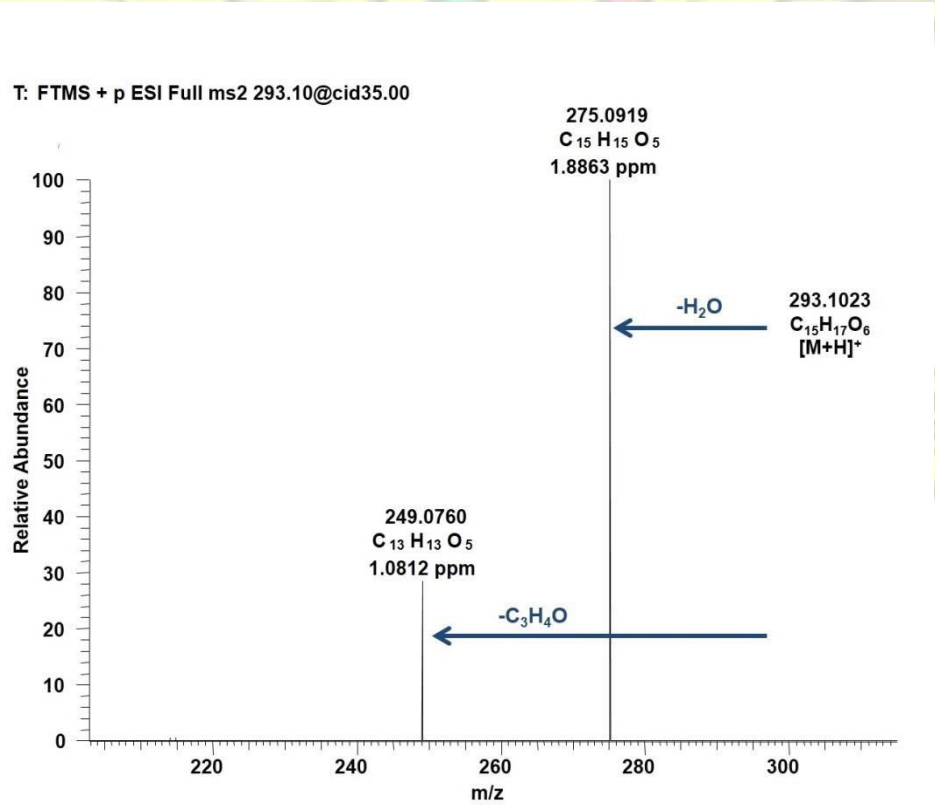


Appendix 167: HMBC NMR spectrum (CD_3OD) of compound **27**/**28**

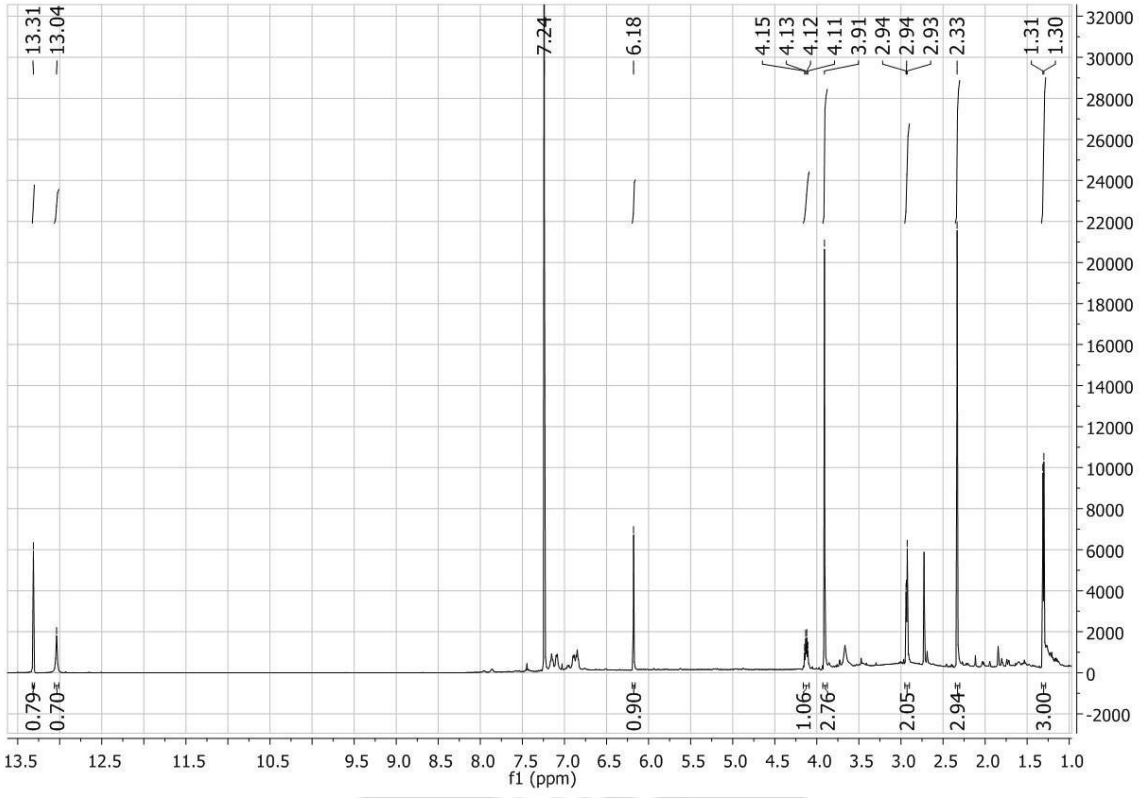
NYANSAPƆ W Ɔ SANE NO BADWENMA



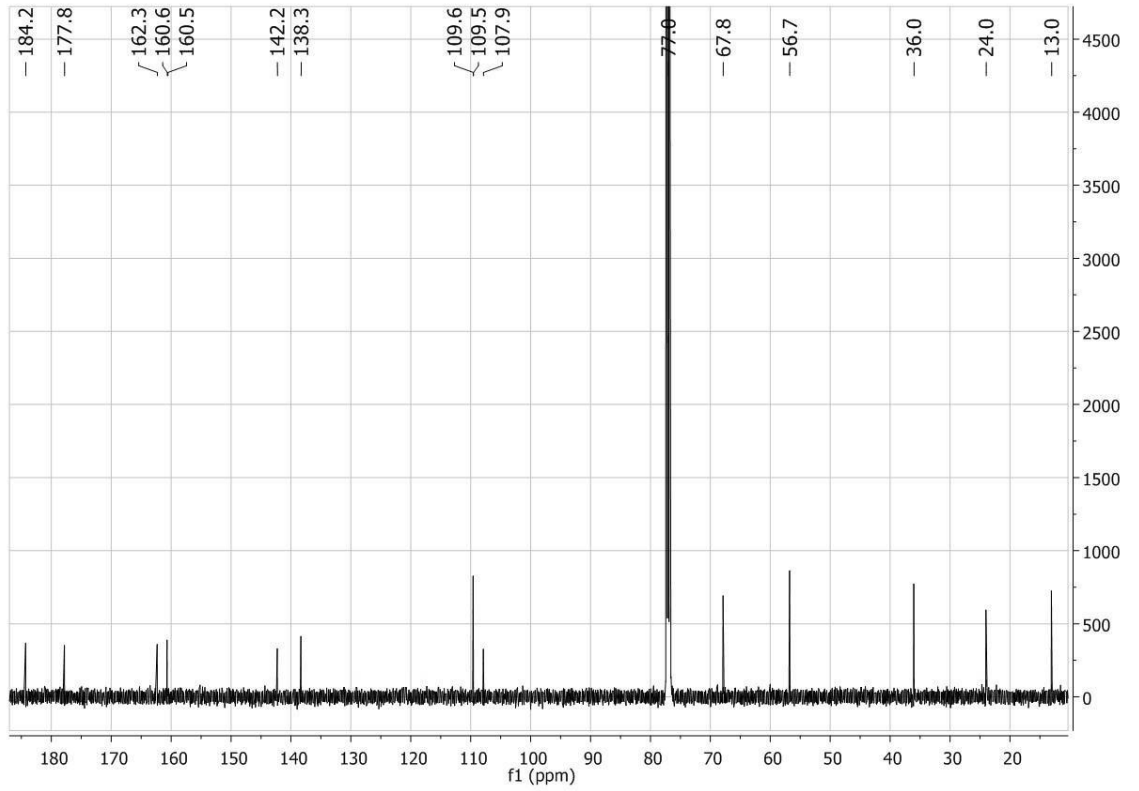
Appendix 168: Positive HRESI–MS spectrum of compound **29**



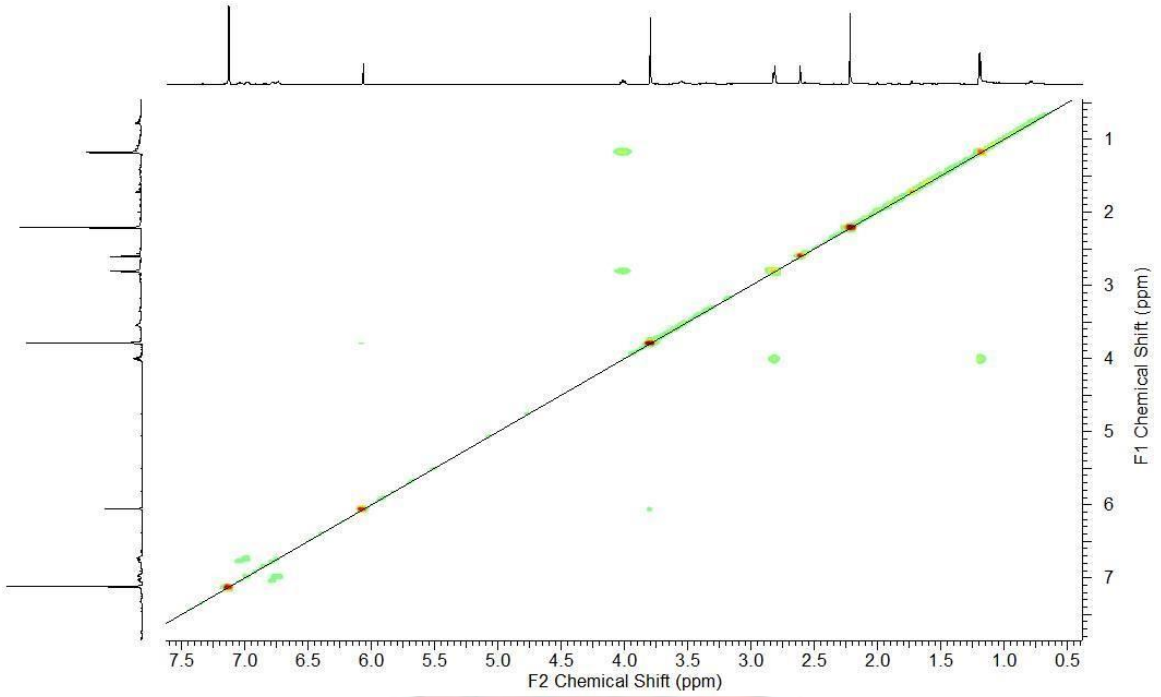
Appendix 169: Positive HRESI–MS/MS spectrum of compound **29**



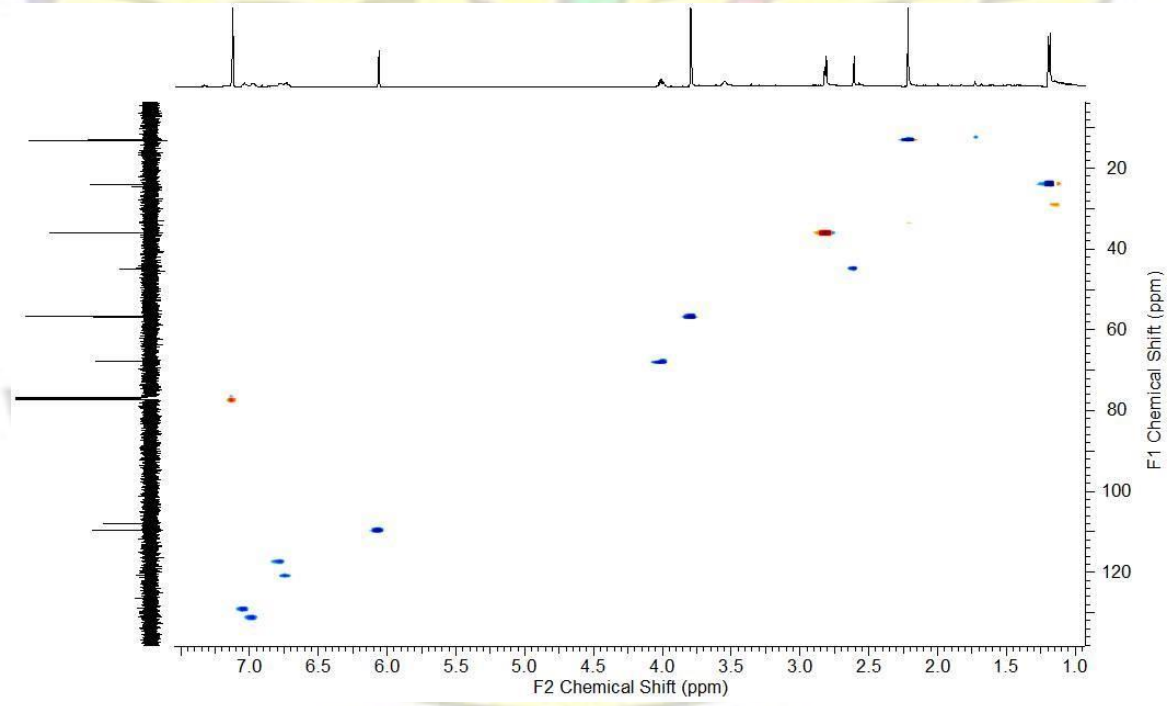
Appendix 170: ^{1}H NMR spectrum ($CDCl_3$, 500 MHz) of compound **29**



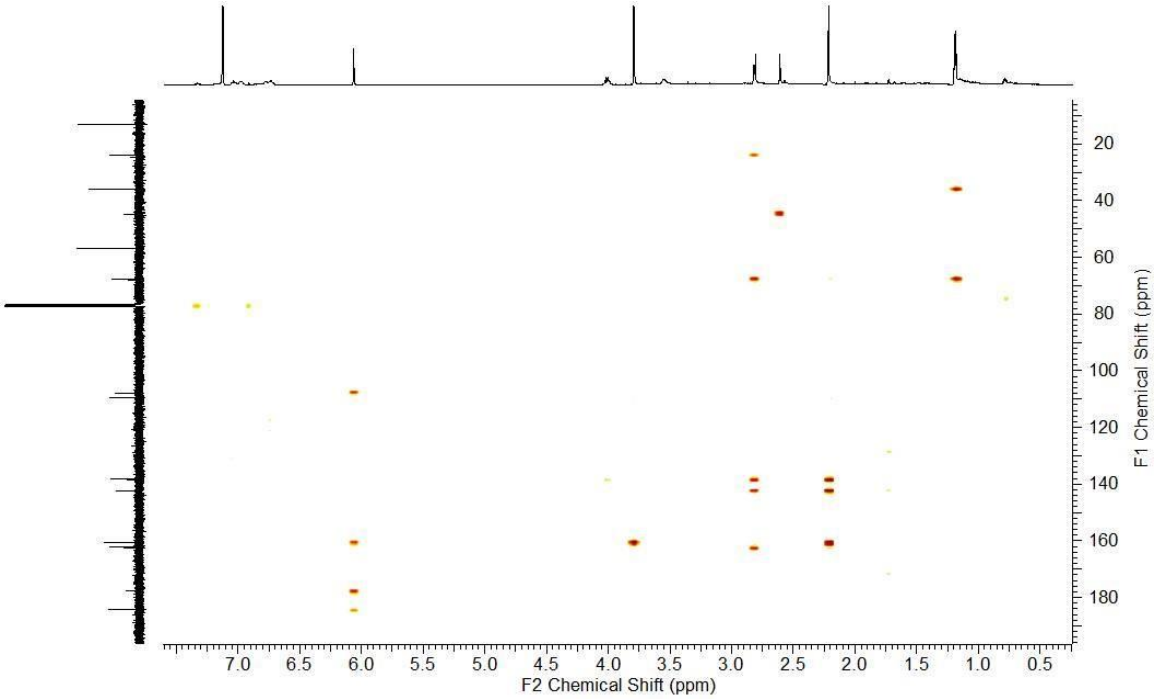
Appendix 171: ^{13}C NMR spectrum ($CDCl_3$, 125 MHz) of compound **29**



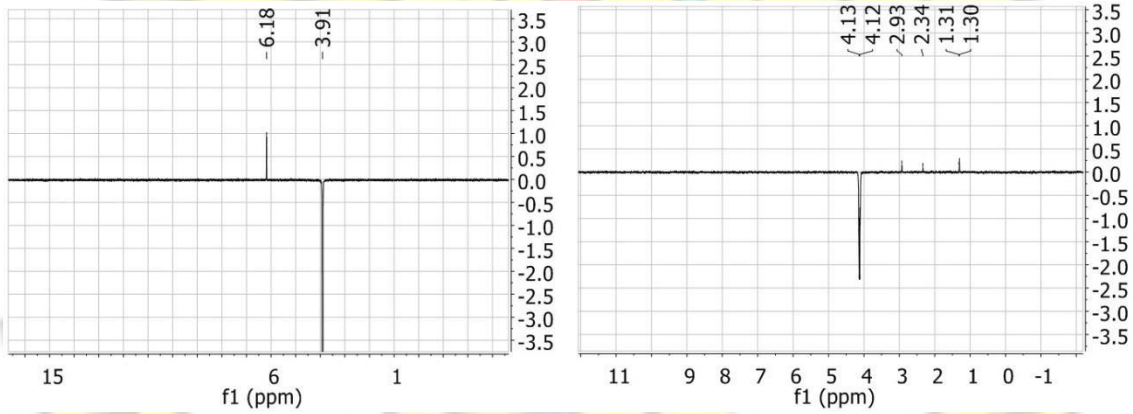
Appendix 172: $^{1}H–^{1}H$ COSY NMR spectrum ($CDCl_3$) of compound **29**



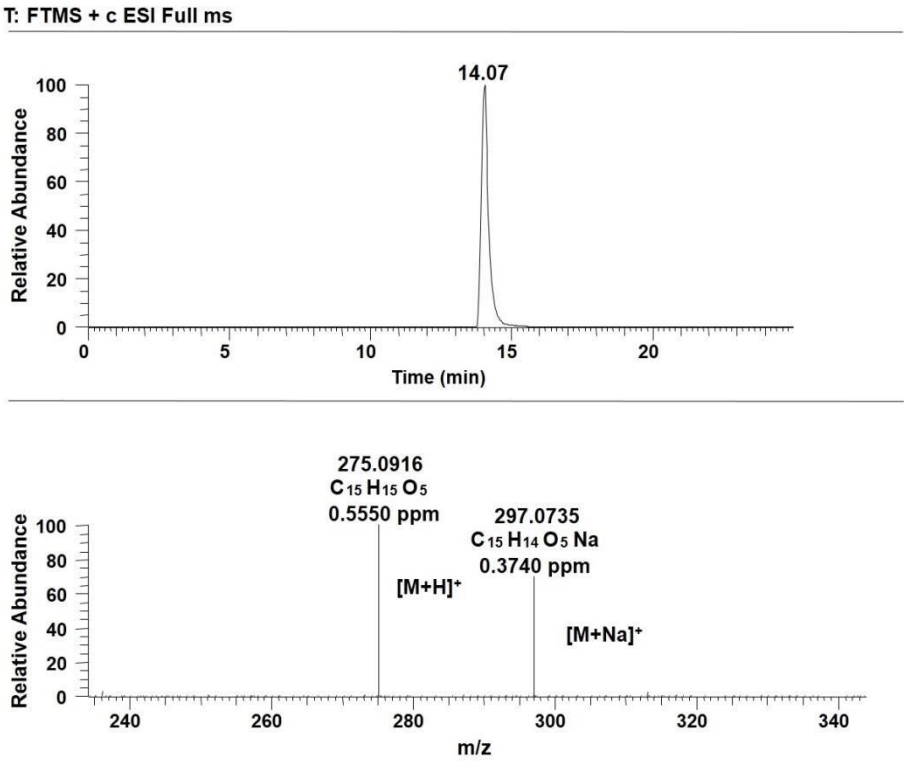
Appendix 173: HSQC NMR spectrum ($CDCl_3$) of compound **29**



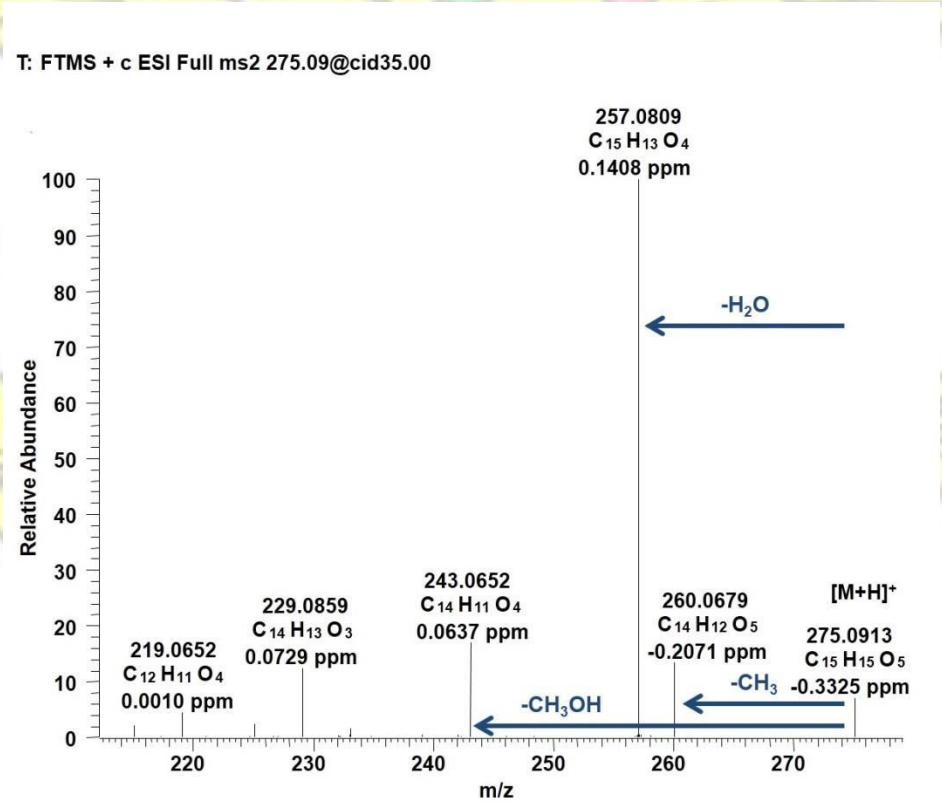
Appendix 174: HMBC NMR spectrum ($CDCl_3$) of compound **29**



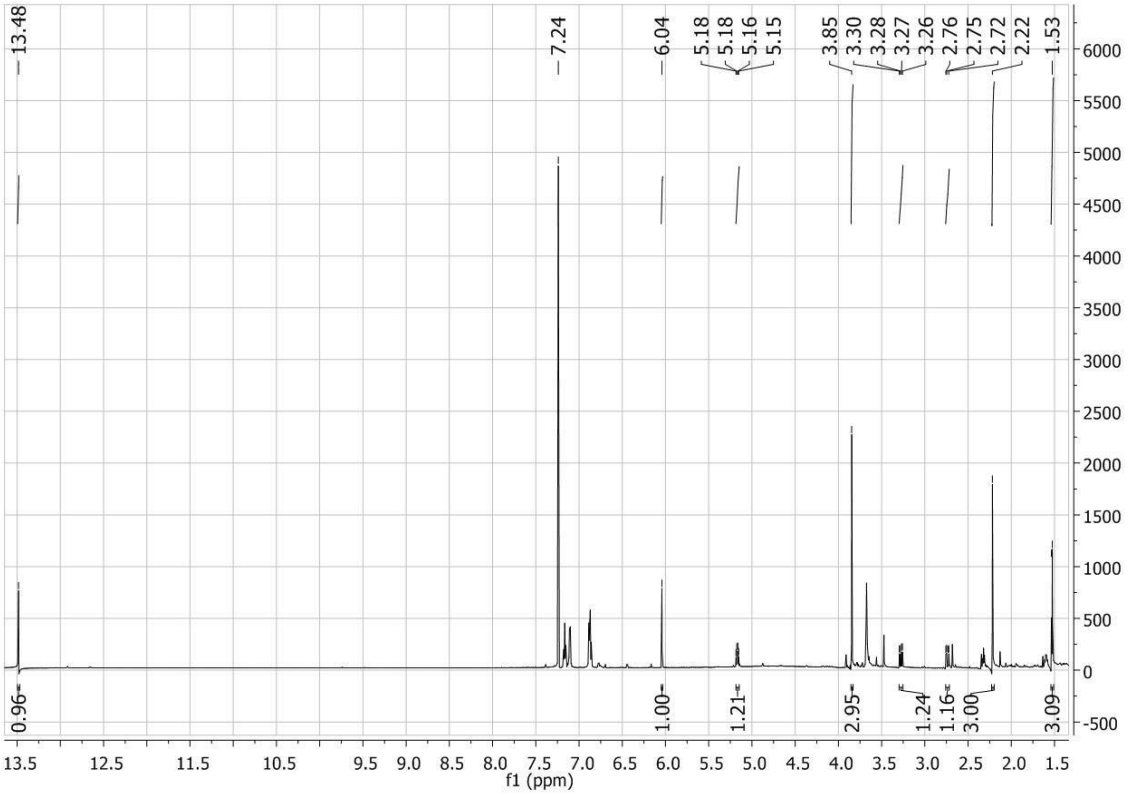
Appendix 175: 1D NOESY NMR spectrum ($CDCl_3$) of compound **29**



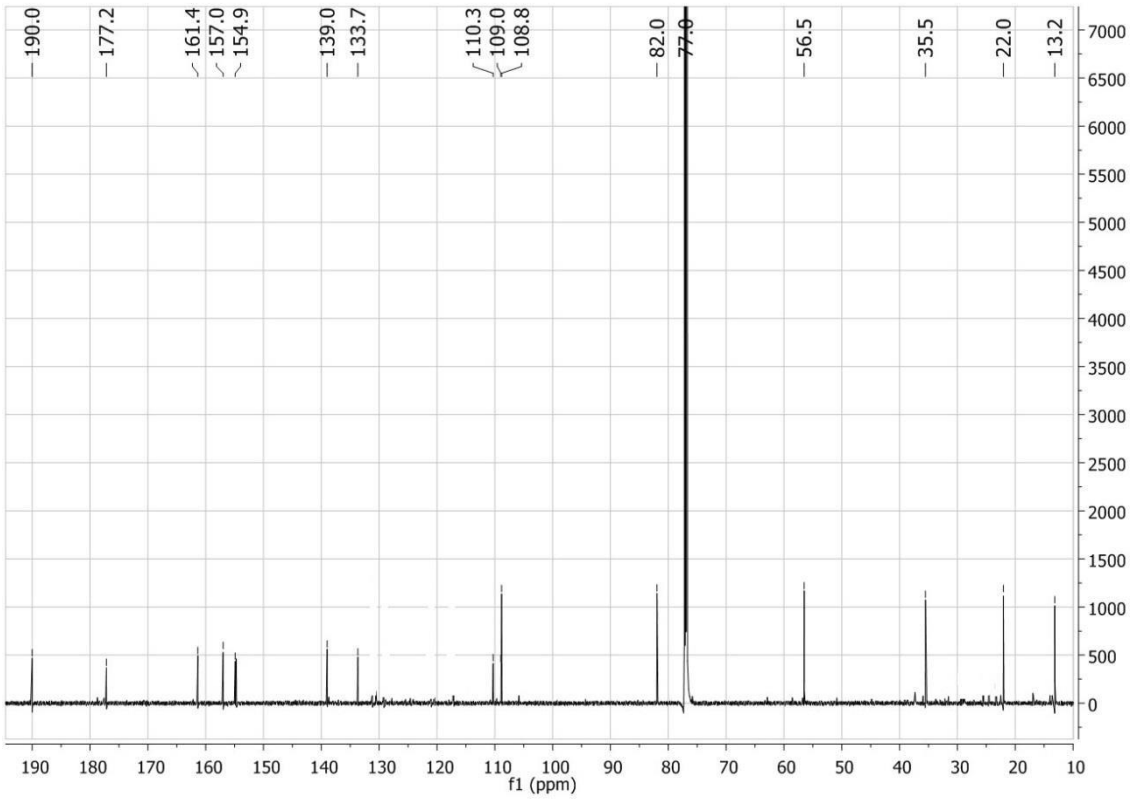
Appendix 176: Positive HRESI–MS spectrum of compound **30**



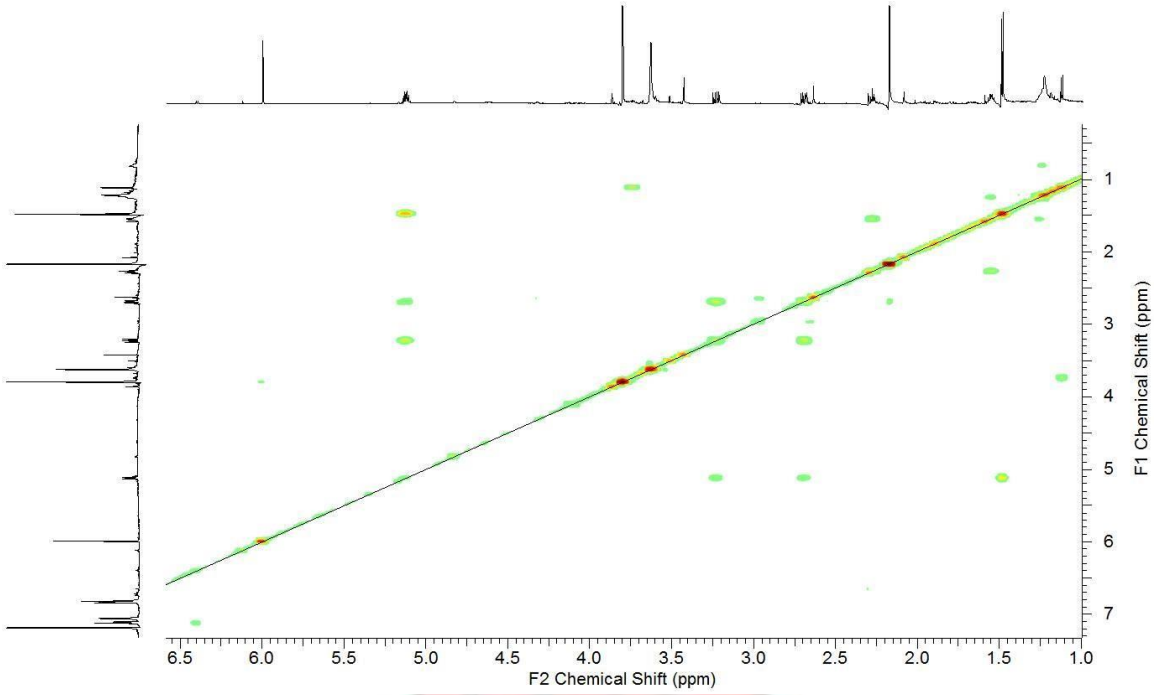
Appendix 177: Positive HRESI–MS/MS spectrum of compound **30**



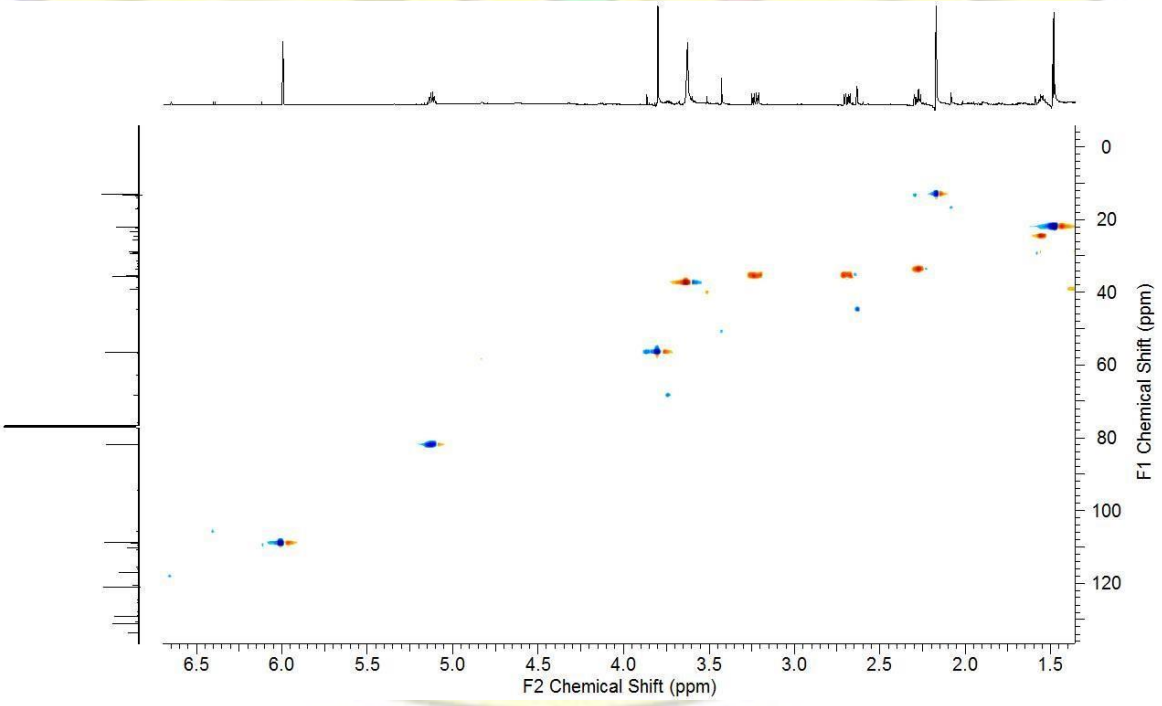
Appendix 178: ^{1}H NMR spectrum ($CDCl_3$, 700 MHz) of compound **30**



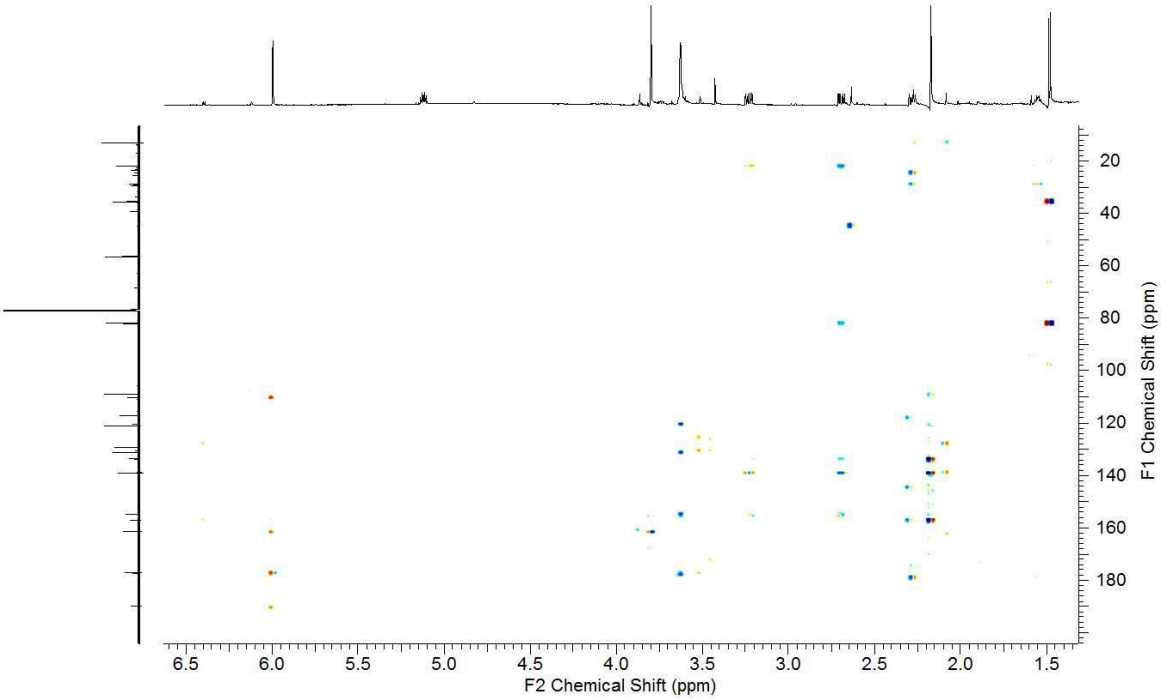
Appendix 179: ^{13}C NMR spectrum ($CDCl_3$, 176 MHz) of compound **30**



Appendix 180: ^{1}H–^{1}H COSY NMR spectrum ($CDCl_3$) of compound **30**

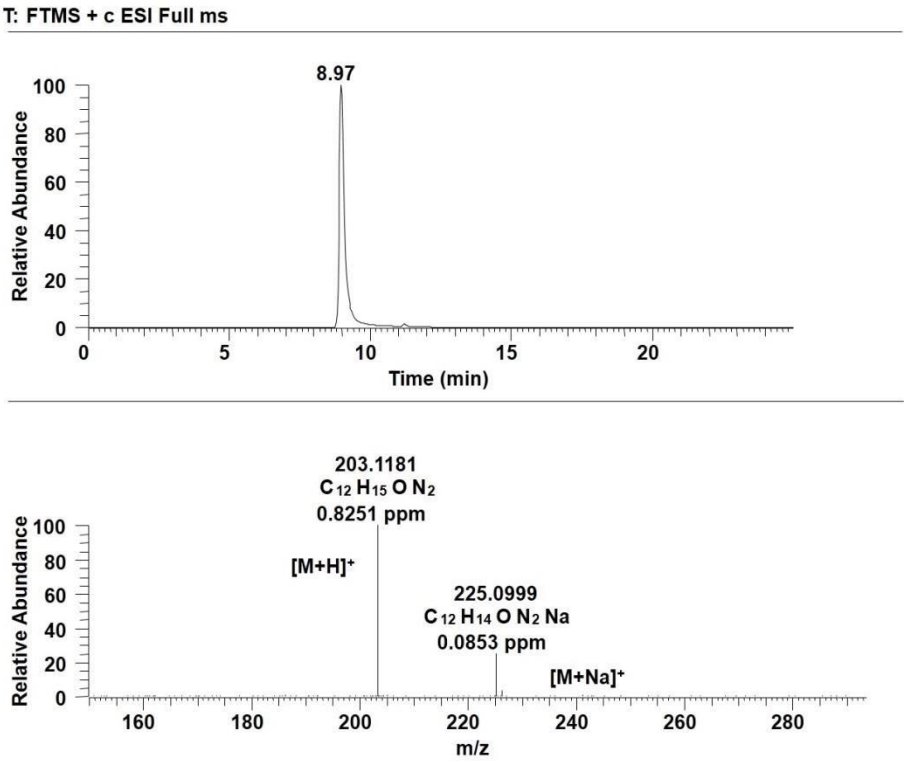


Appendix 181: HSQC NMR spectrum ($CDCl_3$) of compound **30**

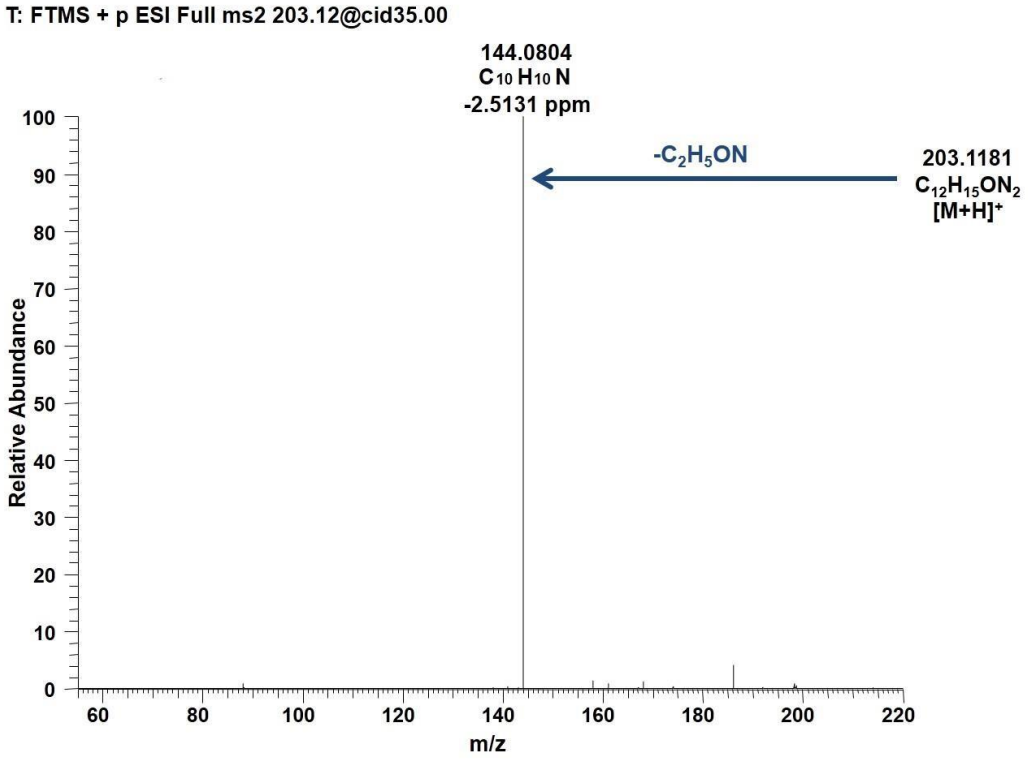


Appendix 182: HMBC NMR spectrum ($CDCl_3$) of compound **30**

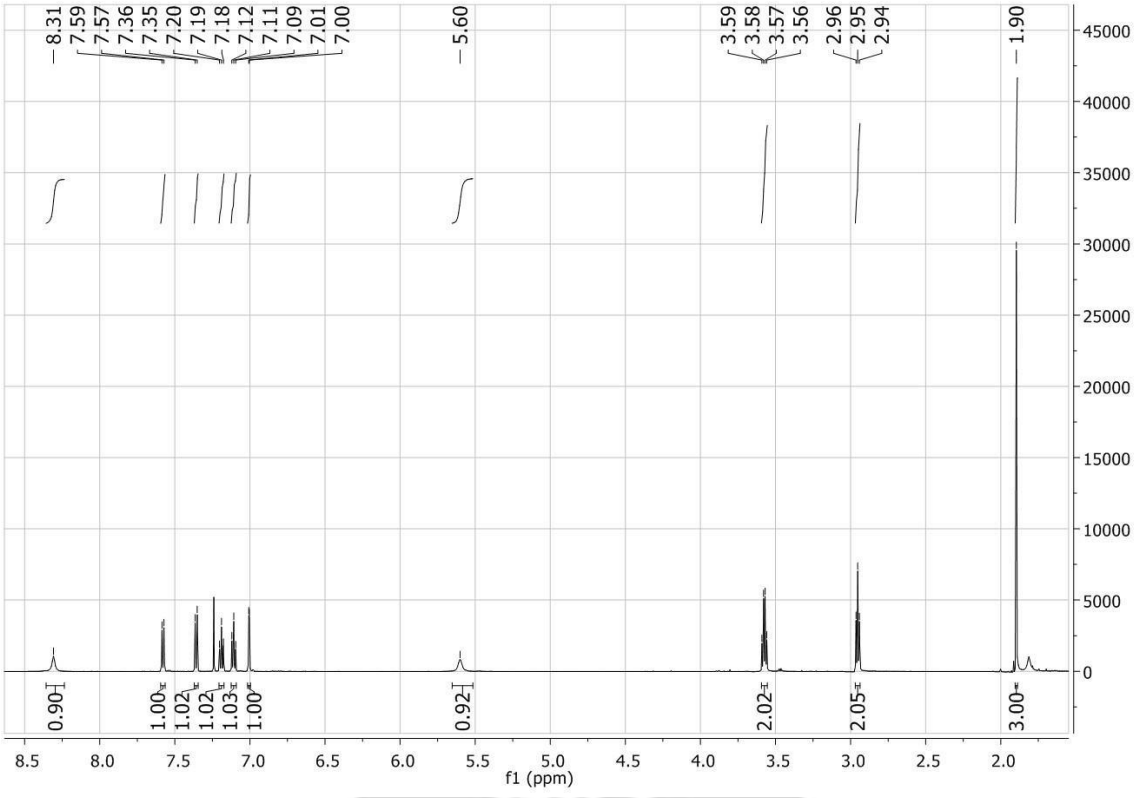
NYANSAPƆ W Ɔ SANE NO BADWENMA



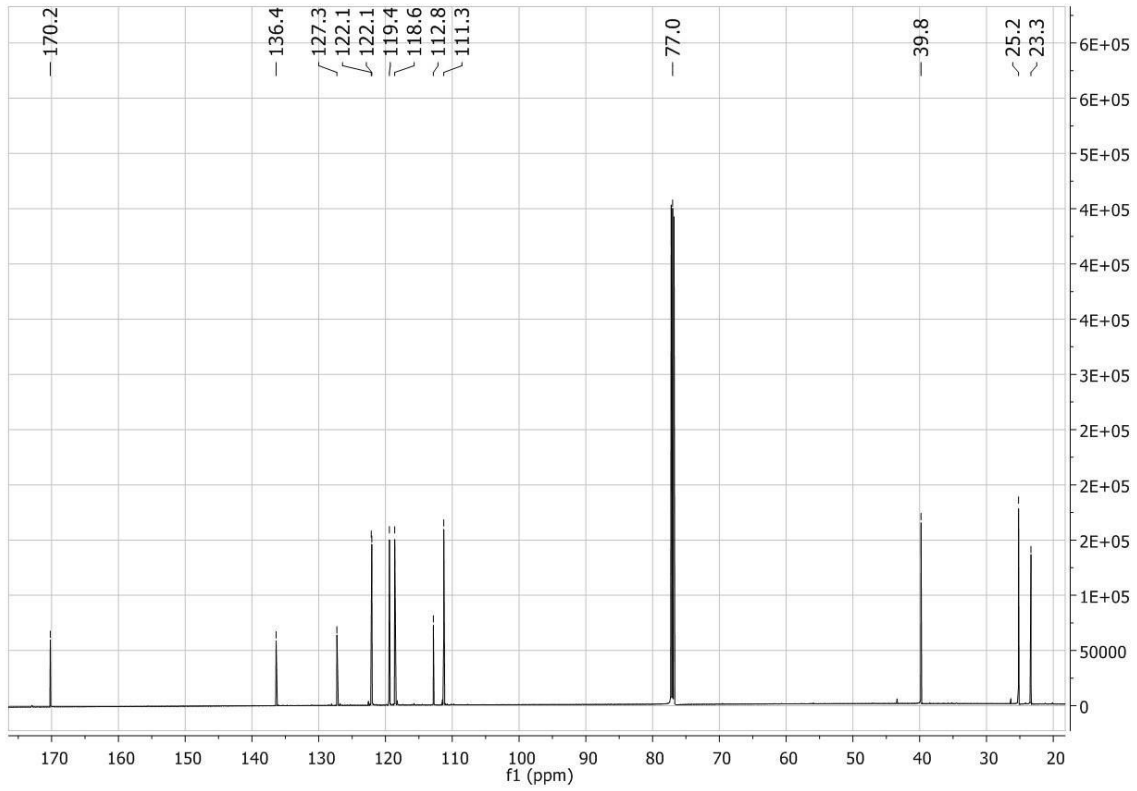
Appendix 183: Positive HRESI–MS spectrum of compound **31**



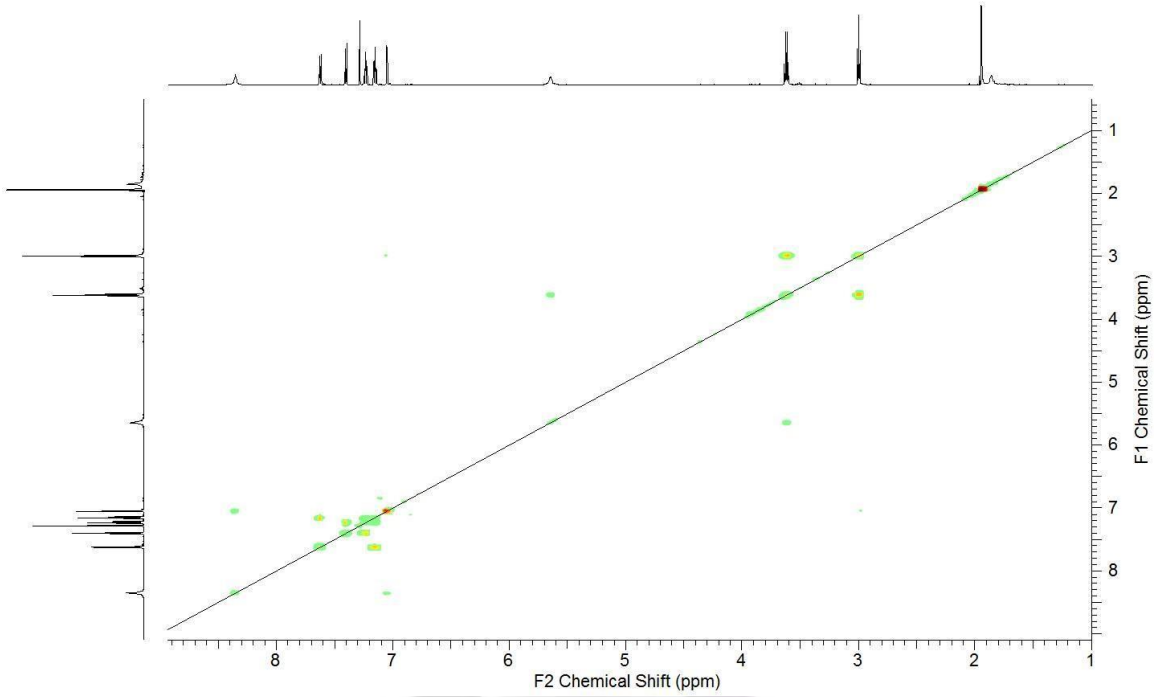
Appendix 184: Positive HRESI–MS/MS spectrum of compound **31**



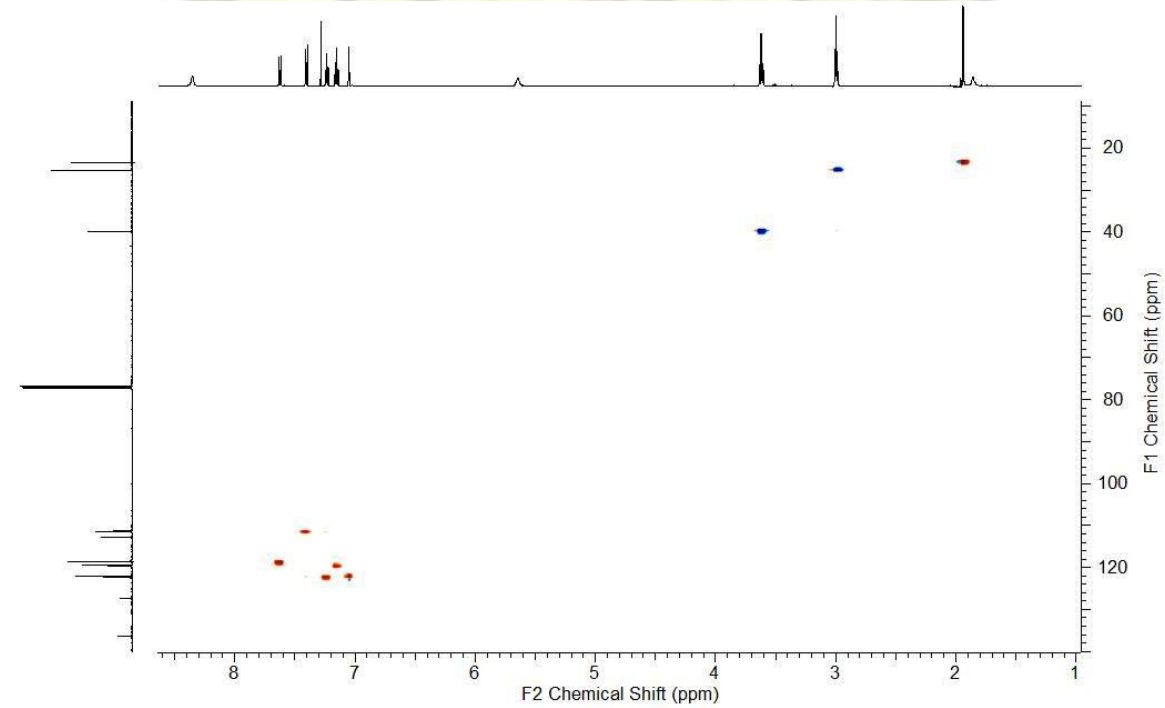
Appendix 185: ^{1}H NMR spectrum ($CDCl_3$, 600 MHz) of compound **31**



Appendix 186: ^{13}C NMR spectrum ($CDCl_3$, 150 MHz) of compound **31**

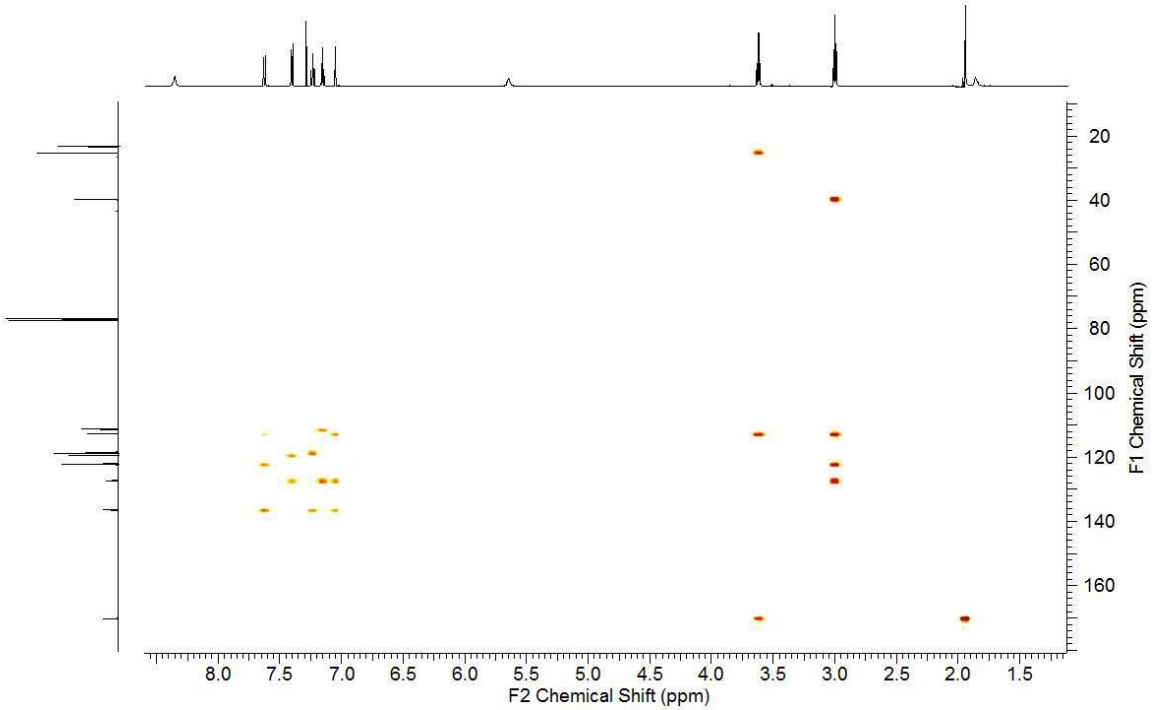


Appendix 187: $^{1}H–^{1}H$ COSY NMR spectrum ($CDCl_3$) of compound **31**



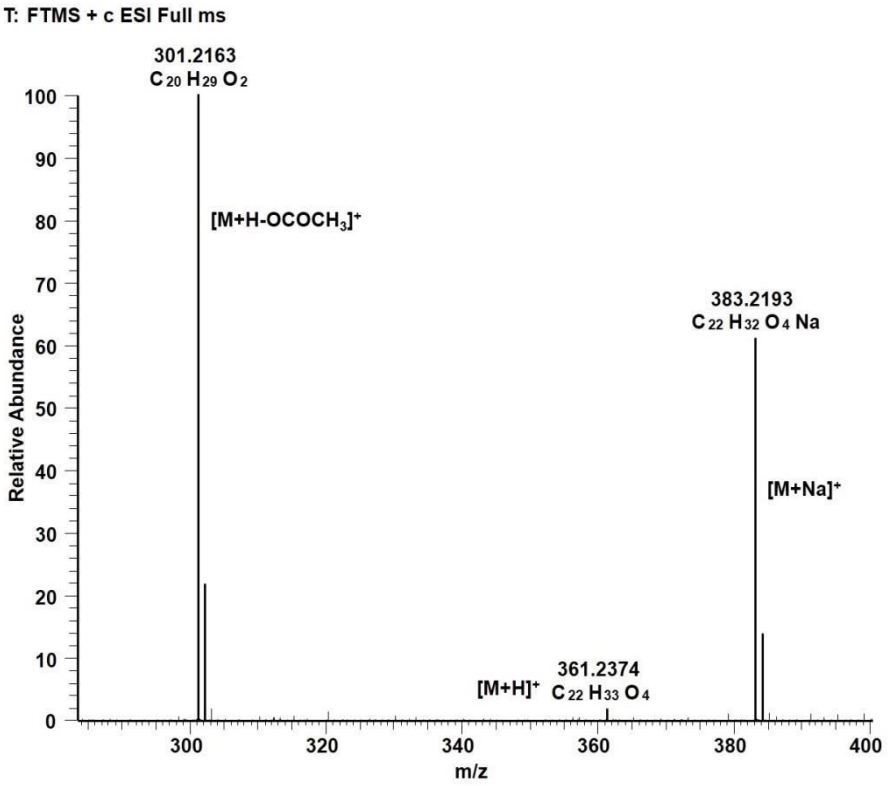
188: HSQC NMR spectrum ($CDCl_3$) of compound **31**

Appendix

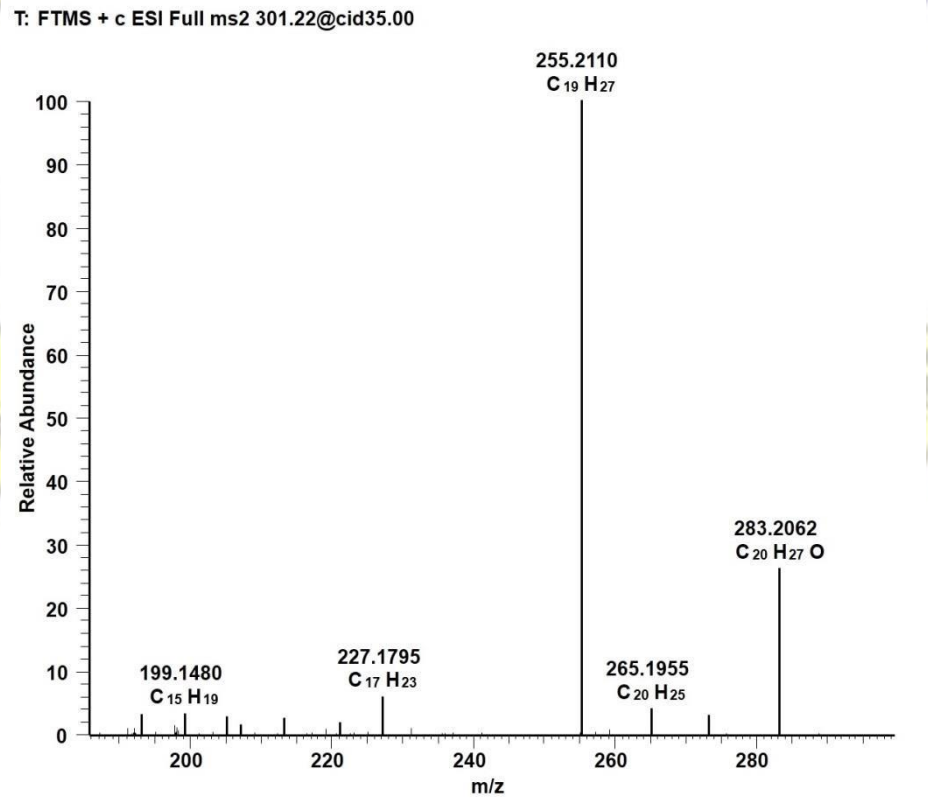


Appendix 189: HMBC NMR spectrum ($CDCl_3$) of compound **31**

NYANSAPƆ W Ɔ SANE NO BADWENMA

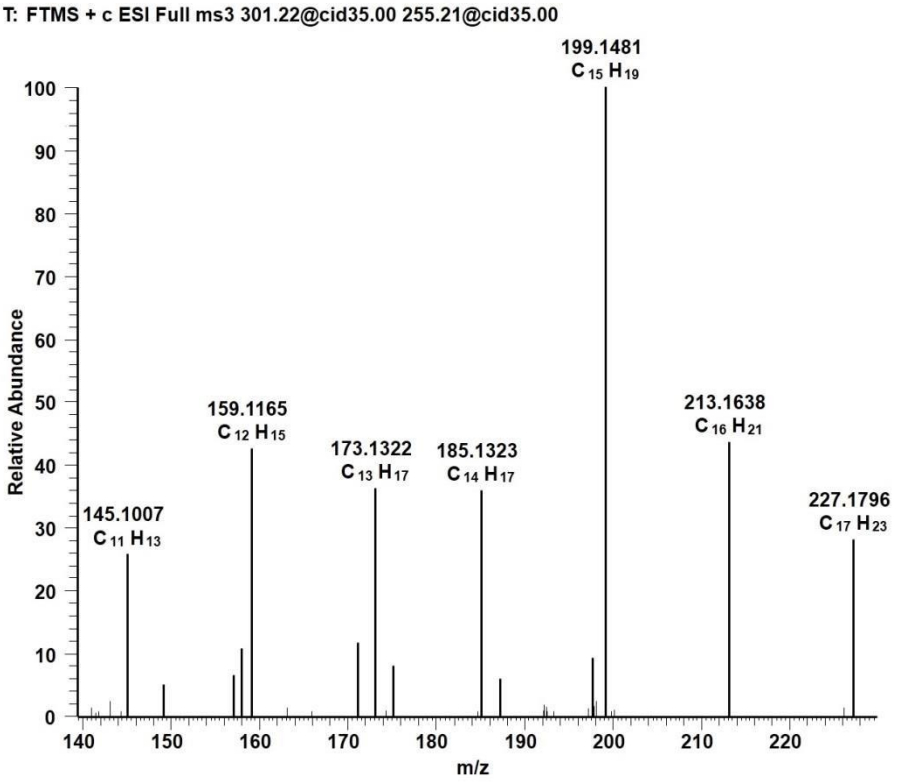


Appendix 190: Positive HRESI–MS spectrum of compound **32**

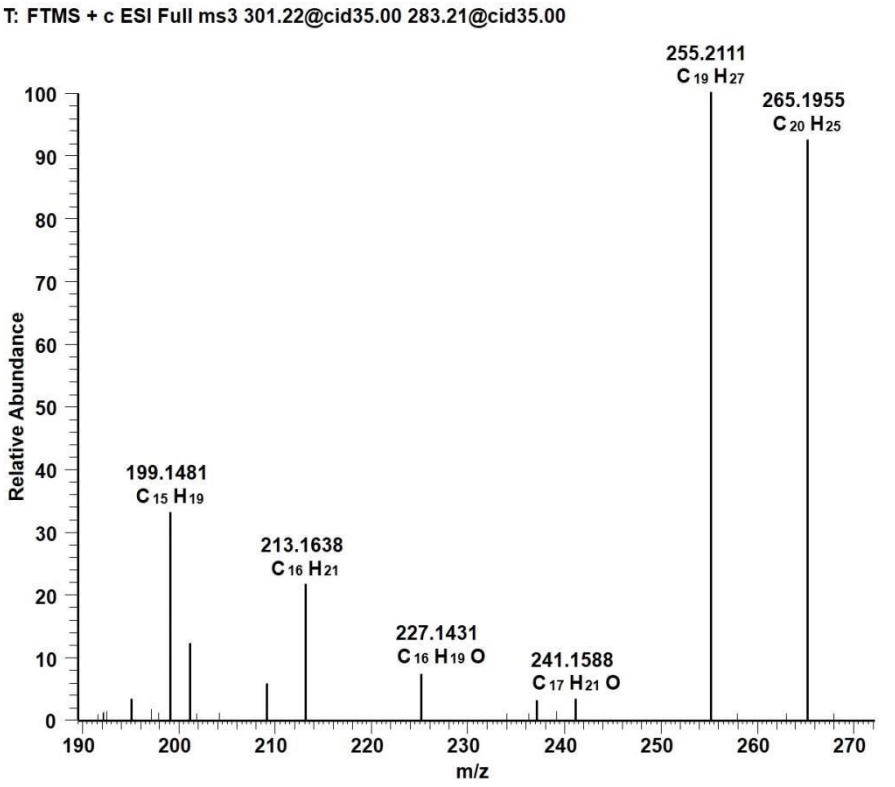


Appendix

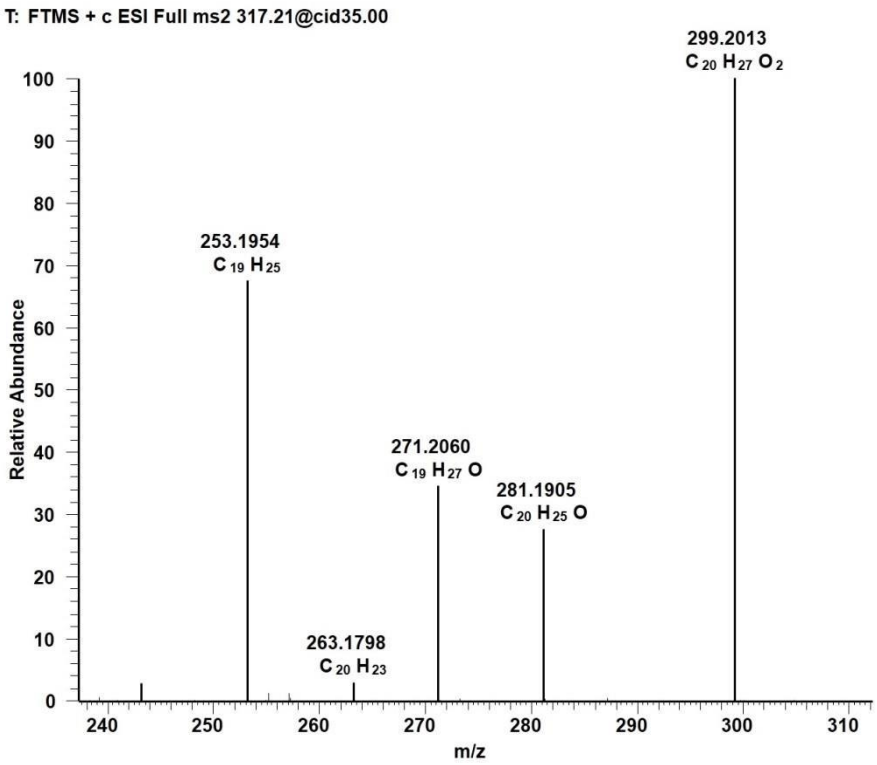
191: Positive HRESI–MS/MS spectrum at *m/z* 301 of compound **32**



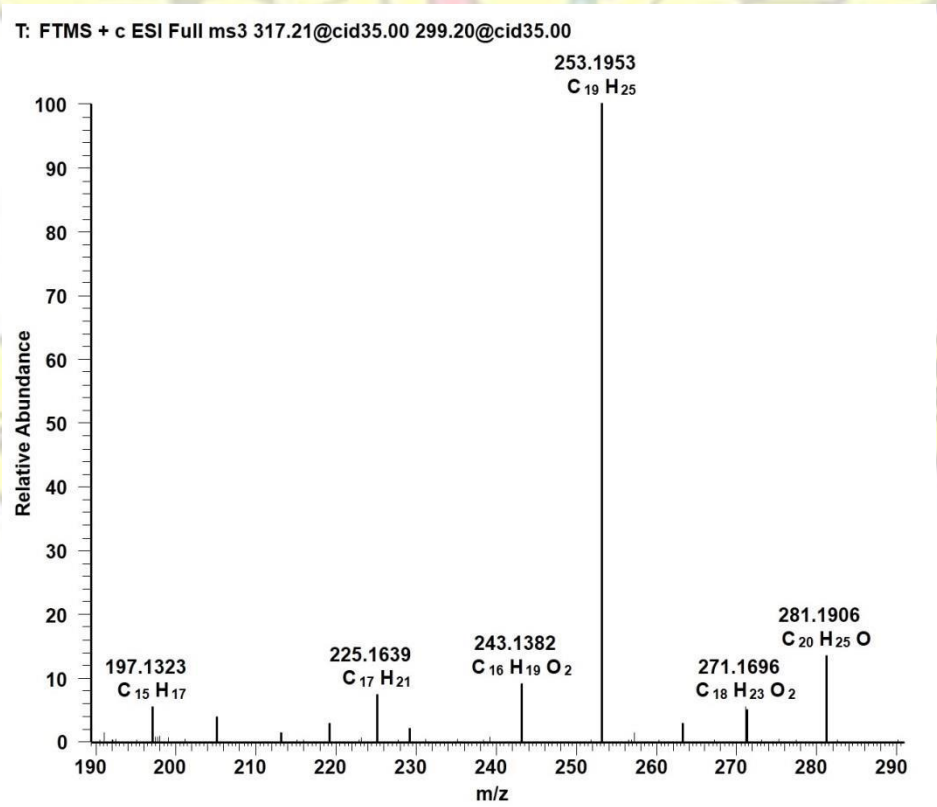
Appendix 192: Positive HRESI–MS^3 spectrum at *m/z* 255 of compound **32**



Appendix 193: Positive HRESI–MS^3 spectrum at *m/z* 283 of compound **32**

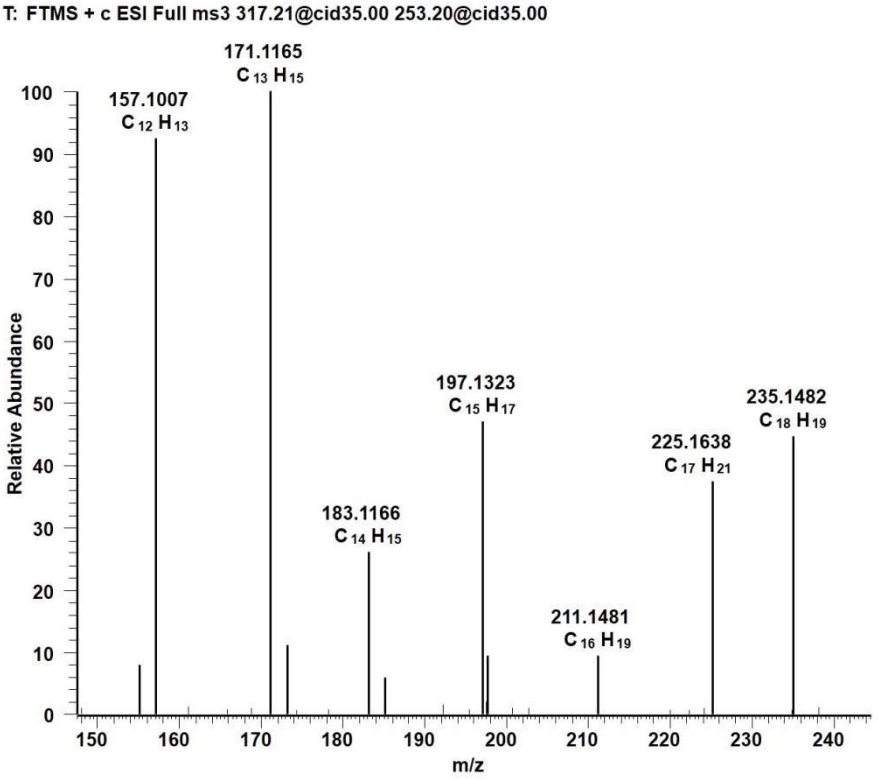


Appendix 194: Positive HRESI–MS/MS spectrum of compound **33**

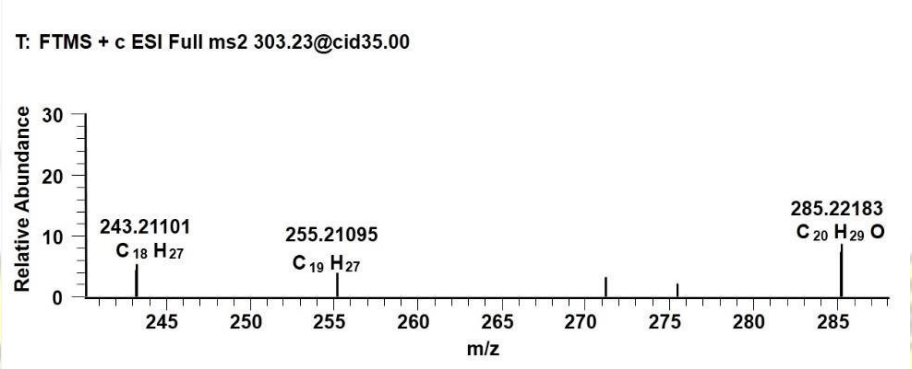


Appendix

195: Positive HRESI–MS^3 spectrum at *m/z* 299 of compound **33**



Appendix 196: Positive HRESI–MS^3 spectrum at *m/z* 253 of compound **33**



Appendix 197: Positive HRESI–MS/MS spectrum of compound **34**